

A Mass Movement Classification for the southern Drakensberg, South Africa

Devlyn Hardwick

A thesis submitted to the Faculty of Science, University of the Witwatersrand,
in fulfillment of the requirements for the degree of Doctor of Philosophy

Johannesburg, 2012

Declaration

I declare that this thesis is my own, unaided work. It is being submitted for the Degree of Doctor of Philosophy in the University of the Witwatersrand, Johannesburg. It has not been submitted before for any degree in any other University.

A handwritten signature in black ink, appearing to read "#ARONICK". The signature is stylized with a large, sweeping initial stroke.

(Signature of candidate)

_____ day of _____ 2012

Abstract

A variety of mass movement landforms occur in the southern Drakensberg, South Africa, and whilst a number of studies on individual landforms have been conducted, regional scale assessments of the Ukhahlamba Drakensberg Transfrontier Park have been relatively limited. Mass movement has been defined as the downward and outward movement of slope-forming material under the influence of a transporting agent such as water, air, ice or snow (Goudie, 2004). This includes landforms such as landslides, debris flows, terracettes, solifluction lobes and rockfall. Although two landslide risk assessments have been conducted in the region, one was site specific and focussed on shallow, translational slides (Bijker, 2001), whilst the other was at a much larger regional scale and focused on large palaeo-mass movements (Singh, 2008).

Numerous international mass movement classifications have been developed over the years, and one of the primary aims of this research is to develop a classification for mass movement landforms within a southern African context. A number of mass movement landforms were identified, measured and mapped in the field to acquire a better understanding of how the landforms originate. This classification was then further adapted to facilitate the identification of mass movement landforms from orthophotos. Aerial photo interpretation techniques were used to map three terrace-type mass movement landforms and four shear-type mass movement landforms in the Garden Castle State Forest of the Ukhahlamba Drakensberg Transfrontier Park.

A further level of detail was added to the classification by ascribing environmental conditions to the different landform types. A Geographic Information System was used to collate and generate spatial information which could be added to the landforms in the mass movement inventory. These were

then analysed using univariate and multivariate statistical modelling. Histograms, as well as an area-weighted frequency distribution, were used to describe the landforms and then hierarchical partitioning was used to identify the environmental variables associated with each type of landform. One main environmental variable was identified for each type of mass movement. Logistic regression was then used to create probability maps for each type of landform. An average of 30% of the study area has a medium to very high likelihood of developing mass movements, although this percentage varies for each type, whilst rock movement deposits are predicted to occupy more than 80% of the study area. Gradient, altitude and lithology were selected most frequently by the statistical models as influencing landform distribution, whilst distance to a rock exposure had the strongest influence on the location of rock movement deposits. Aspect was selected least frequently by hierarchical partitioning which raises questions about the influence of aspect on valley asymmetry. Various models have been developed which describe slope development in the Drakensberg with reference to slope aspect, however the results of this study suggest that other environmental factors may be more important and that slope development is a complex process.

Acknowledgements

This has been a very long time in the making and I would like to say thank you to all the people who have helped me along the way. Special thanks go to my supervisor, Prof. Stefan Grab for giving me the intellectual freedom and support to pursue this topic, as well as for providing funds to visit the site. Thanks also to my little girl for understanding when mommy was busy. The biggest thank you possible has to go to my parents for all the love and support a person could ever wish for and more. And to my husband, for cheering me on when I almost gave up.

Acknowledgement for the provision of funds which made this research possible is made to the University of the Witwatersrand, the Council for Scientific and Industrial Research and the National Research Foundation.

Contents

A MASS MOVEMENT CLASSIFICATION FOR THE SOUTHERN DRakensBERG, SOUTH AFRICA	1
DECLARATION.....	2
ABSTRACT.....	3
ACKNOWLEDGEMENTS.....	5
CONTENTS	6
FIGURES.....	9
TABLES.....	15
1 INTRODUCTION	18
1.1 MASS MOVEMENT: RELEVANCE WITHIN A SOUTHERN AFRICAN CONTEXT.....	18
1.2 AIMS AND OBJECTIVES.....	26
1.3 PROJECT SUMMARY.....	28
2 MASS MOVEMENT CLASSIFICATIONS AND CHARACTERIZATIONS.....	29
2.1 INTRODUCTION.....	29
2.2 CLASSIFICATION THEORY	29
2.3 DEFINING MASS MOVEMENT.....	33
2.4 TECHNIQUES FOR THE CLASSIFICATION AND CHARACTERIZATION OF MASS MOVEMENTS	
36	
2.4.1 <i>Climate as a conditioning factor</i>	36
2.4.2 <i>Climatic regimes</i>	38
2.4.3 <i>Triggering mechanisms</i>	39
2.4.4 <i>Age, state and rate of mass movement activity</i>	41
2.4.5 <i>Movement</i>	45
2.4.6 <i>Morphometry</i>	48
2.4.7 <i>Geographic, geologic and spatial homogeneity</i>	51
2.4.8 <i>Nature of the displaced material</i>	54
2.4.9 <i>Geotechnics</i>	58
2.4.10 <i>Summary</i>	60
2.5 MASS MOVEMENT TYPES	60
2.5.1 <i>Falls</i>	61
2.5.2 <i>Topples</i>	63
2.5.3 <i>Slides</i>	65
2.5.4 <i>Flows</i>	68
2.6 CONDITIONING AND TRIGGERING FACTORS OF MASS MOVEMENTS	73
2.6.1 <i>Factors that increase shear stress</i>	73
2.6.2 <i>Factors that reduce shear strength</i>	74
2.6.3 <i>Triggering events</i>	75
2.7 DEVELOPING A CLASSIFICATION FOR MASS MOVEMENTS IN THE SOUTHERN DRakensBERG	77
3 MASS MOVEMENT MODELING WITH GIS	81
3.1 INTRODUCTION.....	81
3.2 APPROACHES TOWARDS MODELING MASS MOVEMENTS	82
3.2.1 <i>Mass movement inventories and the heuristic approach</i>	82
3.2.2 <i>Statistical models</i>	84

3.2.3	<i>Deterministic models</i>	86
3.2.4	<i>The importance of mapping units</i>	88
3.3	GEOGRAPHIC INFORMATION SYSTEMS FOR HAZARD ZONATION.....	91
3.3.1	<i>Application and derivation of digital elevation models</i>	96
3.3.2	<i>Aerial Photograph Interpretation</i>	98
4	ENVIRONMENTAL SETTING OF THE UDP	104
4.1	INTRODUCTION.....	104
4.2	GEOLOGY AND GEOMORPHOLOGY.....	107
4.2.1	<i>The Drakensberg Group</i>	108
4.2.2	<i>The Clarens Formation</i>	109
4.2.3	<i>The Elliot Formation</i>	110
4.2.4	<i>The Molteno Formation</i>	111
4.2.5	<i>The Tarkastad Subgroup</i>	111
4.2.6	<i>Strength properties of the Karoo Supergroup</i>	112
4.2.7	<i>Geomorphological evolution</i>	114
4.3	CLIMATE.....	118
4.4	VEGETATION.....	119
4.5	SOILS.....	121
4.6	ANTHROPOGENIC ACTIVITIES.....	122
4.6.1	<i>Fires</i>	122
4.6.2	<i>Footpaths</i>	122
5	METHODOLOGY	124
5.1	INTRODUCTION.....	124
5.2	FIELDWORK METHODS.....	124
5.2.1	<i>Field survey</i>	125
5.2.2	<i>Geomorphological field maps</i>	127
5.3	DESKTOP METHODS.....	127
5.3.1	<i>Generating a digital elevation model</i>	128
5.3.2	<i>Comparison of the KZN DEM and TTR DEM</i>	129
5.3.3	<i>Photogrammetric techniques for DEM generation</i>	132
5.4	ENVIRONMENTAL VARIABLES.....	133
5.5	THE MASS MOVEMENT INVENTORY.....	146
5.6	STATISTICAL ANALYSES.....	149
5.6.1	<i>Multivariate techniques: logistic regression, hierarchical partitioning and CLT</i> 149	
5.6.2	<i>Univariate statistics: histograms and the InfoVal</i>	152
5.6.3	<i>Probability mapping</i>	155
5.6.4	<i>Spatial Point pattern analysis</i>	155
6	FIELD-BASED ASSESSMENT OF MASS MOVEMENT LANDFORMS IN THE SOUTHERN DRAKENSBERG	160
6.1	INTRODUCTION.....	160
6.2	SITE A: SLIDE, NGWANGWANE RIVER.....	163
6.3	SITE B: SLIDE, NGWANGWANE RIVER.....	168
6.4	SITE C: SLIDE, NGWANGWANE RIVER.....	171
6.5	SITE D: INCISED FLOW, NGWANGWANE RIVER.....	174
6.6	SITE E: SLIDE.....	178
6.7	SITE F: SLIDE.....	179
6.8	SITE G: SURFICIAL FLOW.....	182
6.9	SITE H: SURFICIAL FLOWS.....	186
6.10	SITE I: SLIDE, BUSHMAN'S RIVER.....	188

6.11	SITE J: SLIDE, BUSHMAN’S RIVER	190
6.12	SITE K: LANDSLIDE COMPLEX, BUSHMAN’S RIVER	193
6.13	SITE L: SLIDE, BUSHMAN’S RIVER	197
6.14	SITE M: INCISED FLOW OR COLLAPSED SOIL PIPE?	199
6.15	SECONDARY MASS MOVEMENT FEATURES	202
6.16	CONCLUSION	202
7	GIS-BASED ASSESSMENT OF MASS MOVEMENT LANDFORMS IN THE SOUTHERN DRAKENSBERG	204
7.1	INTRODUCTION.....	204
7.2	TERRACE-TYPE 1: TERRACETTES.....	204
7.3	TERRACE-TYPE 2: SOLIFLUCTION LOBES	221
7.4	TERRACE-TYPE 3: TERRACES	239
7.5	SHEAR-TYPE 1: SHEAR SCARS.....	256
7.6	SHEAR-TYPE 2: INCISED FLOWS.....	272
7.7	SHEAR-TYPE 3: SURFICIAL FLOWS.....	286
7.8	SHEAR-TYPE 4: SHEET SLIDES	302
7.9	COMPARISON OF THE MASS MOVEMENT LANDFORMS OBSERVED IN THE GCSF.....	314
7.10	ROCK MOVEMENT DEPOSITS	322
8	CONCLUSION.....	346
8.1	METHODOLOGICAL CONSIDERATIONS	346
8.2	GEOMORPHOLOGICAL CONSIDERATIONS	349
8.3	CONTRIBUTION TO INTERNATIONAL AND LOCAL MASS MOVEMENT STUDIES.....	350
9	REFERENCES:.....	353

Figures

FIGURE 1.1 MAP OF LANDSLIDE SUSCEPTIBLE ZONES (AFTER PAIGE-GREEN AND LEYLAND, 2009).....	24
FIGURE 2.1 METHOD FOR ALLOCATING ELEMENTS TO CLASSES.....	32
FIGURE 2.2 CLIMATIC INFLUENCE ON MASS MOVEMENT FORM (SHARPE, 1938).....	38
FIGURE 2.3 SHARPE’S CLASSIFICATION OF MASS MOVEMENT PHENOMENA (SHARPE, 1938).....	57
FIGURE 2.4 CROSS-SECTION SHOWING INTERNAL DEFORMATION DUE TO TENSIONAL FISSURING. COLLUVIAL MATERIAL IS DEPOSITED IN THE CRACKS AND MAY REDUCE THE STRENGTH PROPERTIES OF THE SURROUNDING ROCK BY CHEMICAL AND MECHANICAL WEATHERING.	62
FIGURE 2.5 AN EXAMPLE OF A FALL CAUSED BY BASAL UNDERCUTTING ALONG A CLIFF FACE. BASAL UNDERCUTTING IS DUE TO WAVE ACTION ALTHOUGH A SIMILAR PROCESS MAY BE EXPECTED ALONG STREAMS AND ABOVE SOIL PIPES (AFTER FLAGEOLLET AND WEBBER, 1996).....	63
FIGURE 2.6 DIFFERENT MECHANISMS OF TOPPLING ACTION. FIGURE A SHOWS THE FORWARD ROTATION OF A ROCK MASS THAT HAS BECOME SEPARATED ALONG A JOINT. FIGURE B SHOWS THE BACKWARD ROTATION OF A ROCK MASS THAT HAS TILTED DUE TO A DEEP-SEATED ROTATIONAL SLIDE AT ITS BASE (AFTER CRUDEN AND VARNES, 1996).....	64
FIGURE 2.7 EXAMPLE OF A ROTATIONAL SLIDE.	67
FIGURE 2.8 EXAMPLE OF A TRANSLATIONAL SLIDE.	68
FIGURE 2.9 AN EXAMPLE OF A SURFICIAL FLOW. MATERIAL BEGINS DEPOSITING WITHIN THE TRANSPORT ZONE.	70
FIGURE 2.10 AN EXAMPLE OF AN INCISED FLOW, WITH MATERIAL BEING REMOVED FROM THE SLOPE IN THE TRANSPORT ZONE. ROOT DEPTH IS USUALLY UP TO TENS OF CENTIMETRES.	71
FIGURE 2.11 SOME HYPOTHETICAL MECHANISMS OF TERRACETTE FORMATION. (A) AN EXAMPLE OF CREEP FLOW ASSOCIATED WITH SOLIFLUCTION. THE SOIL BECOMES SATURATED, LOSES COHESION AND FLOWS DOWNSLOPE. (B) AN EXAMPLE OF TERRACETTE FORMATION AS A RESULT OF TRANSLATIONAL SLIDING. (C) AN EXAMPLE OF TERRACETTE FORMATION WHERE EACH STEP REPRESENTS A SMALL ROTATIONAL SLIDE (AFTER BIELECKI AND MUELLER, 2002).	72
FIGURE 3.1 FLOW DIAGRAM SHOWING HOW A TRAINING SITE IS DEVELOPED AND REFINED USING NEURAL NETWORKS TO DETERMINE MASS MOVEMENT SUSCEPTIBILITY (LEE ET AL., 2003).	85
FIGURE 3.2 AN EXAMPLE OF A HYDROLOGICAL-SLOPE STABILITY MODEL. WATER TABLE HEIGHT IS TRANSLATED INTO PORE-PRESSURE IN THE INFINITE SLOPE EQUATION (CASADEI ET AL., 2003).....	88
FIGURE 3.3 AN EXAMPLE OF HOW SOIL MECHANICAL RESPONSE UNITS ARE CREATED AND USED TO COMPUTE THE SUSCEPTIBILITY MAP (MÖLLER ET AL., 2001).	90
FIGURE 3.4 A GIS-BASED CONCEPTUAL SYSTEM INTEGRATED WITH DATA MINING FOR MASS MOVEMENT HAZARD ASSESSMENT (HUABIN ET AL., 2005).....	92
FIGURE 3.5 THE MASKING EFFECTS OF RELIEF AND VEGETATION ON AERIAL PHOTOGRAPHS (BRARDINONI ET AL., 2003).	102
FIGURE 4.1 THE UKHAHLAMBA DRAKENSBERG TRANSFRONTIER PARK IS LOCATED ALONG THE EASTERN BORDER OF LESOTHO. THE GARDEN CASTLE STATE FOREST IS HIGHLIGHTED IN PINK	105
FIGURE 4.2 THE GARDEN CASTLE STATE FOREST. THE AREA IN FULL COLOUR REPRESENTS THE CATCHMENTS SURVEYED IN THE FIELD, WHILST THE MASKED AREA REPRESENTS THAT SURVEYED USING API.	106
FIGURE 4.3 THE TOPOGRAPHIC AND GEOLOGICAL ZONES OF THE DRAKENSBERG (AFTER HUMPHREYS, 1971 (BIJKER, 2001)).	107
FIGURE 4.4 SCHEMATIC PROFILE OF THE DRAKENSBERG SHOWING THE APPROXIMATE ALTITUDE FOR EACH LITHOLOGICAL UNIT (AFTER BIJKER, 2001).	108
FIGURE 4.5 FAILURE IN ROCKS AND SOILS OF INTERCALCATED LAYERS.	113

FIGURE 5.1 FLOW DIAGRAM ILLUSTRATING THE DESKTOP METHOD.	128
FIGURE 5.2 A) SPOT HEIGHTS (M A.S.L.) SHOWING NO OUTLIERS. B) CONTOUR HEIGHTS (M A.S.L.) SHOWING OUTLIERS.	130
FIGURE 5.3 A) EXAMPLES OF ERROR CREATED DURING THE SCAN DIGITIZING BETWEEN MAP SHEETS AND B) THE CORRECTED CONTOURS.	131
FIGURE 5.4 VECTOR DATA OF DRAINAGE LINES AND THE BUFFERED RASTER USED FOR THE STATISTICAL ANALYSES.	135
FIGURE 5.5 VECTOR DATA OF FOOTPATHS AND THE BUFFERED RASTER USED FOR THE STATISTICAL ANALYSES.	136
FIGURE 5.6 VECTOR DATA OF ROCK EXPOSURES AND THE BUFFERED RASTER USED FOR THE STATISTICAL ANALYSES.	137
FIGURE 5.7 LITHOLOGY OF THE SOUTHERN DRAKENSBERG AND ALTITUDINAL CLASSES FROM THE TTR DEM.	139
FIGURE 5.8 ALTITUDE RASTER IN THE BACKGROUND AND CLASSED ALTITUDINAL VALUES IN THE FOREGROUND.	140
FIGURE 5.9 ASPECT ACCORDING TO CARDINAL DIRECTIONS. THE TWO VALUES FOR NORTH (0- 22.5 AND 337.5-360) ARE EQUIVALENT.	142
FIGURE 5.10 GRADIENT IN DEGREES.	143
FIGURE 5.11 THE HYPOTHETICAL LANDSCAPE MODEL (AFTER AYALEW AND YAMAGISHI, 2004).	144
FIGURE 5.12 A COMPOSITE RASTER OF THE FOUR LANDSCAPE UNITS PRESENT IN THE SOUTHERN DRAKENSBERG, DERIVED AFTER AYALEW AND YAMAGISHI'S (2004) NINE-UNIT LANDSCAPE MODEL.	145
FIGURE 5.13 FLOW DIAGRAM OF THE PROCESS USED FOR GENERATING THE STRATIFIED SAMPLES OF THE ROCK MOVEMENT POINT DATA.	159
FIGURE 6.1 IDEALISED BLOCK DIAGRAM OF A LANDSLIDE SHOWING THE TERMINOLOGY USED TO DESCRIBE THE COMPONENTS OF THE SLIDE (AFTER VARNES, 1978).	160
FIGURE 6.2 LOCATIONS OF SITES WHICH WERE MEASURED IN THE FIELD IN RELATION TO THE GCSF.	161
FIGURE 6.3 OBLIQUE PHOTOGRAPH OF SITE A SHOWING MAIN SCARP AND THE TRANSPORT AND DEPOSITIONAL ZONES.	164
FIGURE 6.4 (A) THE CONTACT BETWEEN THE COLLUVIUM AND MUDSTONE AND (B) A TENSION CRACK AT THE CROWN OF THE SLIDE SCAR WHICH HAS DEVELOPED INTO A SOIL PILLAR.	165
FIGURE 6.5 GEOMORPHOLOGICAL MAP OF THE COMPLEX MASS MOVEMENT FEATURE AT SITE A.	166
FIGURE 6.6 OBLIQUE VIEW OF SITE A USING GOOGLE EARTH (2009). TWO POSSIBLE PALAEO- MASS MOVEMENT FEATURES CAN BE OBSERVED. NOTE THE HUMMOCKY TERRAIN ON THE SURROUNDING SLOPES.	167
FIGURE 6.7 OBLIQUE PHOTOGRAPH OF SITE B SHOWING THE MAIN SCARP AND ZONES OF ACTIVITY.	169
FIGURE 6.8 PHOTOGRAPH OF THE DEPLETION ZONE SHOWING THE TWO LITHOLOGICAL UNITS AND SEEPAGE ZONES. THE SCRUB VEGETATION CONSISTS MOSTLY OF <i>LYCOPodium CLAVATUM</i>	169
FIGURE 6.9 GEOMORPHOLOGICAL MAP OF THE ROCKFALL AND TRANSLATIONAL SLIDE AT SITE B.	171
FIGURE 6.10 OBLIQUE PHOTOGRAPH OF SITE C SHOWING THE SHEAR SCAR AND ZONES OF MOVEMENT.	172
FIGURE 6.11 GEOMORPHOLOGICAL MAP OF THE TRANSLATIONAL SLIDE SITE C.	173
FIGURE 6.12 GOOGLE EARTH (2009) IMAGE OF SITE B AND C SHOWING PLANATION SURFACES ABOVE EACH SITE AND THE POSITION OF THE NGWANGWANE RIVER. RIVER TERRACES WHICH MAY INDICATE PREVIOUS POSITIONS OF THE RIVER ARE REPRESENTED BY THE DASHED BLUE LINE.	174
FIGURE 6.13 OBLIQUE PHOTOGRAPH OF THE SLIDE AT SITE B. THE SLIDE IS CHARACTERISED BY A FLOW TRACK WHICH IS TRANSPORTING SEDIMENT DOWNSTREAM TO THE RIVER.	175

FIGURE 6.14 GEOMORPHOLOGICAL MAP OF THE INCISED FLOW AT SITE D.	176
FIGURE 6.15 (A) PROFILE OF THE MAIN SCARP. (B) ANGULAR MATERIAL THAT IS BEING TRANSPORTED IN THE FLOW CHANNEL.	177
FIGURE 6.16 TRANSLATIONAL SLIDE OCCURRING AT SITE E. SITES F,G AND H CAN BE SEEN IN THE BACKGROUND.	178
FIGURE 6.17 GEOMORPHOLOGICAL MAP OF THE TRANSLATIONAL SLIDE AT SITE E.	179
FIGURE 6.18 OBLIQUE PHOTOGRAPH OF SITE F SHOWING THE MAIN SCARP AND ZONE OF DEPOSITION. DASHED WHITE LINES INDICATE WHERE SLOPE GRADIENT DECREASES TO CREATE LOCAL TOPOGRAPHIC TERRACES.	180
FIGURE 6.19 GEOMORPHOLOGICAL MAP OF THE TRANSLATIONAL SLIDE AT SITE F.	181
FIGURE 6.20 OBLIQUE PHOTOGRAPH OF SITE G SHOWING THE SHEAR SURFACE AND THE MAIN FLOW PATH. THE LEVEES ARE SHOWN AS DASHED LINES. THE FOOT OF THE DEPOSITIONAL FAN IS NOT VISIBLE.....	183
FIGURE 6.21 GEOMORPHOLOGICAL MAP OF THE SURFICIAL FLOW AT SITE G.....	184
FIGURE 6.22 THE FLOW DEPOSIT AT SITE G INDICATING (A), HOW THE FLOW SPREAD AROUND GRASS TUSsockS AND (B), HOW VEGETATION CREATED A CAST THAT MOULDED THE SHAPE OF THE DEPOSIT.	185
FIGURE 6.23 VEGETATION WAS FLATTENED AS THE DISPLACED MATERIAL FLOWED OVER IT. (B) DRAINAGE LINES DEVELOPED IN THE MASS AS THE SEDIMENT SETTLED AND THE FLUID DRAINED AWAY.	185
FIGURE 6.24 GEOMORPHOLOGICAL MAP OF THE SURFICIAL FLOWS AT SITE H.	187
FIGURE 6.25 OBLIQUE PHOTOGRAPH OF THE TWO FLOWS AT SITE H SHOWING THE MAIN SCARP AND ZONES OF ACTIVITY.	188
FIGURE 6.26 OBLIQUE PHOTOGRAPH OF THE TRANSLATIONAL SLIDE AT SITE I ON THE BUSHMAN’S RIVER.	189
FIGURE 6.27 GEOMORPHOLOGICAL MAP OF THE TRANSLATIONAL SLIDE AT SITE I.	190
FIGURE 6.28 SITE J DISPLAYING THE MAIN SCARP. NOTE THE EXPOSED BEDROCK JUST BELOW THE SHEAR SURFACE.	191
FIGURE 6.29 (A) VEGETATED ‘ISLANDS’ ON THE SHEAR SURFACE AND (B) THE GRADUAL TRANSITION OF THE CONTACT BETWEEN THE MOBILE SOIL AND WEATHERED SAPROLITE.	191
FIGURE 6.30 GEOMORPHOLOGICAL MAP OF THE TRANSLATIONAL SLIDE AT SITE J.	192
FIGURE 6.31 OBLIQUE PHOTOGRAPH OF SITE K INDICATING A NUMBER OF PRIMARY AND SECONDARY FEATURES.....	194
FIGURE 6.32 OBLIQUE PHOTO OF SITE K1 SHOWING THE MAIN SCARP AND TRANSPORT CHANNEL, SLIDE SCARS IN THE IMMEDIATE VICINITY AND THE LOCATION OF THE BUSHMAN’S RIVER IN RELATION TO THE FOOT OF THE FLOW.	195
FIGURE 6.33 AERIAL PHOTO OF THE SLIDE/FLOW AT SITE K3 SHOWING SHEAR SCARS, FLOW TRACK AND DEPOSITS OF THE FLOW.	196
FIGURE 6.34 AERIAL PHOTO OF SITE K SHOWING THE HYPOTHETICAL RECONSTRUCTION OF MASS MOVEMENTS EVENTS AND THEIR EFFECT ON THE DRAINAGE PATTERN OF THE BUSHMAN’S RIVER.....	197
FIGURE 6.35 SLIDE/FLOW AT SITE L SHOWING THE MAIN SCARP, FLOW TRACKS AND DEPOSITIONAL FAN.....	198
FIGURE 6.36 GEOMORPHOLOGICAL MAP OF THE SLIDE AT SITE L.	199
FIGURE 6.37 OBLIQUE PHOTOGRAPH OF THE MAIN SCARP, FLOW CHANNEL AND DEPOSITIONAL FAN AT SITE M.....	200
FIGURE 6.38 GEOMORPHOLOGICAL MAP OF THE LANDFORM AT SITE M.	201
FIGURE 7.1 DISTRIBUTION OF TERRACETTES DIGITIZED FROM THE 1: 50 000 ORTHOPHOTOS. ..	205
FIGURE 7.2 FRONT VIEW OF SEVERAL GROUPS OF TERRACETTES (1 – 4) TAKEN IN AUGUST 2005. A-B ARE REFERENCE POINTS SHOWING THE LOCATION OF THE TERRACETTES IN FIGURE 7.3.	207
FIGURE 7.3 PLAN VIEW (A – B) OF THE TERRACETTE GROUPS SHOWN IN FIGURE 6.2 (1 – 4) (GOOGLE EARTH, 2008).	208

FIGURE 7.4 HISTOGRAMS OF THE INDEPENDENT VARIABLES FOR TERRACETTES.....	211
FIGURE 7.5 GRAPH REPRESENTING THE PERCENTAGE CONTRIBUTION OF EACH VARIABLE TO THE LOGIT MODEL. THE TABLE SHOWS THE MEAN AND STANDARD DEVIATIONS FOR EACH CONTRIBUTION.....	215
FIGURE 7.6 PROBABILITY MAPS FOR TERRACETTES USING THE RP1 AND RP2 DATASETS.....	217
FIGURE 7.7 PROBABILITY MAPS FOR TERRACETTES USING THE RP3 AND RP4 DATASETS.....	218
FIGURE 7.8 PROBABILITY MAPS FOR TERRACETTES USING THE RP5 DATASETS.....	219
FIGURE 7.9 SUMMARIZED AND PRUNED CLASSIFICATION TREE FOR TERRACETTE TYPE MASS MOVEMENT FEATURES (<i>F</i> : FREQUENCY, <i>G</i> : GINI COEFFICIENT).....	220
FIGURE 7.10 FRONT VIEW OF SEVERAL FIELDS OF SOLIFLUCTION LOBES. A – LARGE SHEET SLIDE, B – SMALLER SHEET SLIDE, C – TRANSLATIONAL SLIDE ALONG A DRAINAGE LINE.....	223
FIGURE 7.11 PLAN VIEW OF THE SOLIFLUCTION FIELDS AS SHOWN IN FIGURE 7.10 (A – LARGE SHEET SLIDE, B – SMALLER SHEET SLIDE, C – TRANSLATIONAL SLIDE ALONG DRAINAGE LINE) (GOOGLE EARTH, 2009).....	224
FIGURE 7.12 DISTRIBUTION OF SOLIFLUCTION LOBES DIGITIZED FROM THE 1: 50 000 ORTHOPHOTOS.....	225
FIGURE 7.13 HISTOGRAM OF THE INDEPENDENT VARIABLES FOR SOLIFLUCTION LOBES.....	227
FIGURE 7.14 GRAPH REPRESENTING THE PERCENTAGE CONTRIBUTION OF EACH VARIABLE TO THE LOGIT MODEL. THE TABLE SHOWS THE MEAN AND STANDARD DEVIATIONS FOR EACH CONTRIBUTION.....	230
FIGURE 7.15: PROBABILITY MAPS FOR SOLIFLUCTION LOBES USING THE RP1 AND RP2 DATASETS.....	235
FIGURE 7.16: PROBABILITY MAPS FOR SOLIFLUCTION LOBES USING THE RP3 AND RP4 DATASETS.....	236
FIGURE 7.17: PROBABILITY MAPS FOR SOLIFLUCTION LOBES USING THE RP5 DATASET.....	237
FIGURE 7.18: SUMMARIZED AND PRUNED CLASSIFICATION TREE FOR SOLIFLUCTION LOBE FIELDS (<i>F</i> : FREQUENCY, <i>G</i> : GINI COEFFICIENT).....	238
FIGURE 7.19 VIEW OF A TERRACE ON A NORTHEAST-FACING SLOPE ALONG THE BUSHMAN’S RIVER.....	241
FIGURE 7.20 GROUP OF TERRACES LONG THE BUSHMAN’S RIVER. MEASURING TAPE (50 CM) SHOWS THE HEIGHT OF THE STEP.....	241
FIGURE 7.21 AERIAL VIEW OF SEVERAL FIELDS OF TERRACES THAT OCCUR IN THE STUDY AREA. LOCATIONS OF PHOTOS 1-4 ARE PROVIDED IN FIGURE 7.22.....	242
FIGURE 7.22 DISTRIBUTION OF TERRACES DIGITIZED FROM THE 1: 50 000 ORTHOPHOTOS. 1-4 REFERS TO IMAGES IN FIGURE 7.21.....	243
FIGURE 7.23 HISTOGRAMS OF THE INDEPENDENT VARIABLES FOR TERRACE-TYPE MASS MOVEMENT FEATURES.....	245
FIGURE 7.24 GRAPH REPRESENTING THE PERCENTAGE CONTRIBUTION OF EACH VARIABLE TO THE LOGIT MODEL. THE TABLE SHOWS THE MEAN AND STANDARD DEVIATIONS FOR EACH CONTRIBUTION.....	248
FIGURE 7.25 PROBABILITY MAPS FOR TERRACES USING THE RP1 AND RP2 DATASETS.....	251
FIGURE 7.26 PROBABILITY MAPS FOR TERRACES USING THE RP3 AND RP4 DATASETS.....	252
FIGURE 7.27 PROBABILITY MAPS FOR TERRACES USING THE RP5 DATASET.....	253
FIGURE 7.28 SUMMARIZED AND PRUNED CLASSIFICATION TREE FOR TERRACE MASS MOVEMENT FEATURES (<i>F</i> : FREQUENCY, <i>G</i> : GINI COEFFICIENT).....	255
FIGURE 7.29 PHOTOGRAPHS OF SLIDE SCARS ON THE ORTHOPHOTOS AND IN SATELLITE IMAGES (GOOGLE EARTH, 2008). EXAMPLES (IN YELLOW) ARE SIMILAR TO SITE J.....	257
FIGURE 7.30 ORTHOPHOTO OF A SLIDE SCAR ALONG THE BUSHMAN’S RIVER. THE SLIDE SCAR IS OBSCURED IN THE SATELLITE IMAGE DUE TO OROGRAPHIC SHADOW (GOOGLE EARTH, 2008). THE APPEARANCE OF THE SLIDE SCAR IN THE ORTHOPHOTOS IS SIMILAR TO THE SLIDE SCAR AT SITE I.....	257
FIGURE 7.31 DISTRIBUTION OF SLIDE SCARS DIGITIZED FROM THE 1: 50 000 ORTHOPHOTOS....	259
FIGURE 7.32 HISTOGRAMS OF THE INDEPENDENT VARIABLES FOR SHEAR SCARS.....	262

FIGURE 7.33 GRAPH REPRESENTING THE PERCENTAGE CONTRIBUTION OF EACH VARIABLE TO THE LOGIT MODEL. THE TABLE SHOWS THE MEAN AND STANDARD DEVIATIONS FOR EACH CONTRIBUTION.....	266
FIGURE 7.34 PROBABILITY MAPS OF SHEAR SCARS FOR THE RP1 AND RP2 DATASETS.	268
FIGURE 7.35 PROBABILITY MAPS OF SHEAR SCARS FOR THE RP3 AND RP4 DATASETS.	269
FIGURE 7.36 PROBABILITY MAPS OF SHEAR SCARS FOR THE RP5 DATASET.	270
FIGURE 7.37 SUMMARIZED AND PRUNED CLASSIFICATION TREE FOR SHEAR SCARS (<i>F</i> : FREQUENCY, <i>G</i> : GINI COEFFICIENT).	271
FIGURE 7.38 AERIAL VIEW OF SLIDE SCARS WITH INCISED FLOW TRACKS (LOCATIONS OF IMAGES 1-4 ARE SHOWN IN FIGURE 7.39)	273
FIGURE 7.39 DISTRIBUTION OF SHEAR SCARS WITH INCISED FLOW TRACKS DIGITIZED FROM THE 1: 50 000 ORTHOPHOTOS.	274
FIGURE 7.40 HISTOGRAMS OF THE INDEPENDENT VARIABLES FOR INCISED FLOWS.....	276
FIGURE 7.41 GRAPH REPRESENTING THE PERCENTAGE CONTRIBUTION OF EACH VARIABLE TO THE LOGIT MODEL. THE TABLE SHOWS THE MEAN AND STANDARD DEVIATIONS FOR EACH CONTRIBUTION.	279
FIGURE 7.42 PROBABILITY MAPS FOR INCISED FLOWS FOR THE RP1 AND RP2 DATASETS.	282
FIGURE 7.43 PROBABILITY MAPS FOR INCISED FLOWS FOR THE RP3 AND RP4 DATASETS.	283
FIGURE 7.44 PROBABILITY MAPS FOR INCISED FLOWS FOR THE RP5 DATASET.	284
FIGURE 7.45 OVERLAY OF THE PREDICTION SURFACE PRODUCED USING RP1 ONTO THE ORTHOPHOTOS. AREAS PREDICTED AS MEDIUM TO VERY HIGH PROBABILITY OCCUR IN SHADOWS (BLACK AREAS) CAUSED BY HIGH RELIEF AND FLYING ANGLE.	284
FIGURE 7.46 SUMMARIZED AND PRUNED CLASSIFICATION TREE FOR SLIDE SCARS WITH INCISED FLOW TRACKS (<i>F</i> : FREQUENCY: GINI COEFFICIENT).	285
FIGURE 7.47 DISTRIBUTION OF SLIDE SCARS WITH SURFICIAL DEPOSITS DIGITIZED FROM THE 1: 50 000 ORTHOPHOTOS.....	287
FIGURE 7.48 AN EXAMPLE OF A LEVEE ASSOCIATED WITH THE SURFICIAL FLOW AT SITE G. LARGER MATERIAL AND VEGETATION HAS BEEN PUSHED TO THE OUTER FLANK OF THE LEVEE.....	288
FIGURE 7.49 AERIAL VIEW OF SLIDE SCARS WITH SURFICIAL DEPOSITS (LOCATION OF 1-2 IS SHOWN IN FIGURE 7.47). NOTE HOW THE SLIDES GENERALLY OCCUR BELOW A ROCK EXPOSURE (BLACK LINES) AND HOW THE DEPOSIT FLOWS ONTO THE PLANATION SURFACES BELOW.	290
FIGURE 7.50 HISTOGRAMS OF THE INDEPENDENT VARIABLES FOR SURFICIAL FLOWS.....	291
FIGURE 7.51 GRAPH REPRESENTING THE PERCENTAGE CONTRIBUTION OF EACH VARIABLE TO THE LOGIT MODEL. THE TABLE SHOWS THE MEAN AND STANDARD DEVIATIONS FOR EACH CONTRIBUTION.	295
FIGURE 7.52 PREDICTION MAPS OF SURFICIAL FLOWS FOR THE RP1 AND RP2 DATASETS.....	298
FIGURE 7.53 PREDICTION MAPS OF SURFICIAL FLOWS FOR THE RP3 AND RP4 DATASETS.....	299
FIGURE 7.54 PREDICTION MAPS OF SURFICIAL FLOWS FOR THE RP5 DATASET.....	300
FIGURE 7.55 SUMMARIZED AND PRUNED CLASSIFICATION TREE FOR SURFICIAL FLOWS (<i>F</i> : FREQUENCY, <i>G</i> : GINI COEFFICIENT).	301
FIGURE 7.56 AERIAL VIEWS OF SHEET SLIDES WITHIN THE SOLIFLUCTION LOBE FILEDS (LOCATIONS OF A AND B ARE SHOWN IN FIGURE 7.57). A INSET-OBLIQUE PHOTOGRAPH OF TWO SHEET SLIDES, ARROWS INDICATE LOCATION IN A.	303
FIGURE 7.57 DISTRIBUTION OF SHEET SLIDES DIGITIZED FROM THE 1:50 000 ORTHOPHOTOS. DISTRIBUTION IS CONFINED TO AREAS WHERE SOLIFLUCTION OCCURS.	305
FIGURE 7.58 HISTOGRAMS OF THE INDEPENDENT VARIABLES FOR SHEET SLIDES.	306
FIGURE 7.59 GRAPH REPRESENTING THE PERCENTAGE CONTRIBUTION OF EACH VARIABLE TO THE LOGIT MODEL. THE TABLE SHOWS THE MEAN AND STANDARD DEVIATIONS FOR EACH CONTRIBUTION.	308
FIGURE 7.60 PROBABILITY MAPS FOR THE RANDOM POINT 1 AND RANDOM POINT 2 MODELS...	310
FIGURE 7.61 PROBABILITY MAPS FOR THE RANDOM POINT 3 AND RANDOM POINT 4 MODELS...	311
FIGURE 7.62 PROBABILITY MAPS FOR RANDOM POINT DATASET 5.....	312

FIGURE 7.63 SUMMARIZED AND PRUNED CLASSIFICATION TREE FOR SHEET SLIDES (<i>F</i> : FREQUENCY, <i>G</i> : GINI COEFFICIENT).	313
FIGURE 7.64 ROCKFALL DEPOSITS IN THE GCSF. ROCK MOVEMENT TYPES INCLUDE TOPPLING AND FALLING.....	323
FIGURE 7.65 KERNEL DENSITY. DENSITY CLASSIFIED USING THE STANDARD DEVIATION.	325
FIGURE 7.66 POINT DENSITY. DENSITY CLASSIFIED USING THE STANDARD DEVIATION.	326
FIGURE 7.67: A COMPARISON OF THE AFFECT OF CELL SIZE ON THE KERNEL DENSITY FUNCTION, SEARCH RADIUS IS 100M. A: 25M, B: 10M.....	327
FIGURE 7.68: A COMPARISON OF THE AFFECT OF THE SIZE OF THE SEARCH RADIUS ON THE KERNEL DENSITY FUNCTION, CELL SIZE IS 10M. A: 100M, B: 25M.....	327
FIGURE 7.69 EXPONENTIAL INCREASE IN THE NUMBER OF POINTS WHICH ARE UNIQUE TO THE CLASS INTERVAL IN WHICH THEY OCCUR.....	329
FIGURE 7.70 A COMPARISON OF THE POLYGONS CREATED FROM THE KERNEL DENSITY FUNCTION. FIGURE A: CONTOUR INTERVALS OF HIGHER DENSITY, B: CONTOUR INTERVALS OF LOWER DENSITY.	330
FIGURE 7.71 COMPARISON OF THE KERNEL DENSITY (BLACK) AND THE GETIS-ORD G_i^* STATISTIC	331
FIGURE 7.72 CLUSTER AND OUTLIER ANALYSIS (ANSELIN LOCAL MORANS I).	332
FIGURE 7.73 COMPARISON OF THE KERNEL DENSITY FUNCTION FOR THE FULL DATASET, 1%, 5% AND 15%.....	334
FIGURE 7.74 HISTOGRAMS OF THE INDEPENDENT VARIABLES FOR SS01.	335
FIGURE 7.75 HISTOGRAMS OF THE INDEPENDENT VARIABLES FOR SS05.	336
FIGURE 7.76 HISTOGRAMS OF THE INDEPENDENT VARIABLES FOR SS15.	337
FIGURE 7.77 GRAPH REPRESENTING THE PERCENTAGE CONTRIBUTION OF EACH VARIABLE TO THE LOGIT MODEL. THE TABLE SHOWS THE MEAN AND STANDARD DEVIATIONS FOR EACH CONTRIBUTION.....	343
FIGURE 7.78 PROBABILITY MAPS FOR ROCK MOVEMENT DEPOSITS USING SS01.....	344

Tables

TABLE 1.1 A SUMMARY OF THE TYPES AND LOCATIONS OF MASS MOVEMENT ACTIVITIES IN SOUTHERN AFRICA.....	22
TABLE 2.1 EARLY TYPES OF MASS MOVEMENT CLASSIFICATIONS (AFTER SHARPE, 1938).	34
TABLE 2.2 CRITERIA USED FOR CLASSIFYING MASS MOVEMENTS ACCORDING TO PRESERVATION OF MORPHOLOGY AND CHRONOLOGICAL SEQUENCE (AFTER GONZÁLEZ-DÍEZ ET AL., 1999).	42
TABLE 2.3 A TEMPORAL CLASSIFICATION OF MASS MOVEMENT ACTIVITY (AFTER FLAGEOLLET, 1996).....	44
TABLE 2.4 SUMMARISED MASS MOVEMENT CLASSIFICATION BY HUTCHINSON (1988).....	46
TABLE 2.5 CLASSIFICATION DEVELOPED BY VARNES (1978).....	55
TABLE 2.6 THE CLASSIFICATION PROPOSED FOR MASS MOVEMENTS IN THE SOUTHERN DRAKENSBERG.....	78
TABLE 3.1 ANALYSIS TECHNIQUES IN RELATION TO MAPPING SCALES (AFTER SOETERS AND VAN WESTEN, 1996).	93
TABLE 4.1 EXPECTED RANGES IN ELEVATION FOR EACH LITHOLOGICAL GROUP FOR THE GCSF. AREA IS IN KM ² AND ALL ALTITUDES ARE IN M .A.S.L.	108
TABLE 5.1 FIELD SURVEY FORM USED TO DESCRIBE THE MASS MOVEMENT FEATURES. ITEMS IN GREY WERE NOT ASSESSED IN THE FIELD.	126
TABLE 5.2 TOTAL AND PERCENTAGE LENGTH OF DRAINAGE LINE BY STREAM ORDER.	134
TABLE 5.3 LAYERS REPRESENTING THE ENVIRONMENTAL VARIABLES USED TO COMPARE MASS MOVEMENT TYPES.	146
TABLE 5.4 CLASSIFICATION USED TO CREATE THE MASS MOVEMENT INVENTORY.....	148
TABLE 5.5 THE VARIOUS TECHNIQUES AND THEIR APPLICATIONS FOR STATISTICAL ANALYSIS. NO* REPRESENTS THAT PREDICTIVE MODELLING CAN BE UNDERTAKEN WITH CART BUT THIS REQUIRES FURTHER ANALYSIS. CART WAS NOT USED FOR PREDICTING MASS MOVEMENT DISTRIBUTION FOR THIS STUDY.	154
TABLE 6.1 MORPHOMETRIC MEASUREMENTS WERE OBTAINED IN THE FIELD FOR ALL SITES EXCEPT K. AVERAGE VALUES EXCLUDE SITE M WHICH WAS NOT CLASSIFIED.	162
TABLE 7.1 COMPARISON OF THE FREQUENCY DISTRIBUTIONS AND INFOVAL WEIGHTS FOR TERRACETTES. BOLD INDICATES HIGHEST VALUE IN CATEGORY, COLOUR INDICATES VARIABLE WITH GREATEST FREQUENCY.....	213
TABLE 7.2 THE AIC, BIC AND VARIABLES SELECTED FOR EACH ITERATION. NOTE THAT THE PERCENTAGE OF CORRECTLY PREDICTED TERRACETTES IS SIMILAR FOR EACH MODEL....	216
TABLE 7.3 TOTAL AREA (KM ² AND PERCENT) OF PROBABILITY VALUES FOR EACH ITERATION OF RANDOM POINTS FOR TERRACETTE TYPE MASS MOVEMENTS.....	220
TABLE 7.4 COMPARISON OF THE FREQUENCY DISTRIBUTIONS AND INFOVAL WEIGHTS. BOLD INDICATES HIGHEST VALUE IN EACH CATEGORY, COLOUR INDICATES VARIABLE WITH GREATEST FREQUENCY.....	229
TABLE 7.5 SUMMARY OF THE CONTINGENCY TABLE STATISTICS USED TO COMPARE RELATIONSHIPS BETWEEN TOPOGRAPHIC VARIABLES. TESTS ARE SIGNIFICANT AT THE 95% CONFIDENCE INTERVAL.	230
TABLE 7.6 COMPARISON OF THE PERCENTAGE AREA OF EACH LITHOLOGICAL UNIT TO RANGES IN GRADIENT.....	232
TABLE 7.7 THE AIC, BIC AND VARIABLES SELECTED FOR EACH ITERATION. VARIATIONS IN PREDICTIVE ABILITY ARE CAUSED BY DISSOLVING SOME OF THE CLASSES.	233
TABLE 7.8 SUMMARY OF THE CONTINGENCY TABLE STATISTICS USED TO COMPARE RELATIONSHIPS BETWEEN TOPOGRAPHIC VARIABLES AND DISTANCE TO A ROCK EXPOSURE. TESTS ARE SIGNIFICANT AT THE 95% CONFIDENCE INTERVAL.	233

TABLE 7.9 CROSS-TABULATION OF THE PERCENTAGE AREA OF EACH LITHOLOGICAL CLASS COMPARED TO THE DISTANCE TO A ROCK EXPOSURE (M). HIGHEST PERCENTAGE IS IN BOLD.	234
TABLE 7.10 TOTAL AREA (KM ² AND PERCENT) OF PROBABILITY VALUES FOR EACH ITERATION OF RANDOM POINTS FOR THE SOLIFLUCTION LOBE FIELDS.	238
TABLE 7.11 COMPARISON OF THE FREQUENCY DISTRIBUTIONS AND INFOVAL WEIGHTS. BOLD INDICATES HIGHEST VALUE IN EACH CATEGORY, COLOUR INDICATES VARIABLE WITH THE GREATEST FREQUENCY.	246
TABLE 7.12 THE AIC, BIC AND VARIABLES SELECTED FOR EACH ITERATION. VARIATIONS IN PREDICTIVE ABILITY ARE CAUSED BY DISSOLVING SOME OF THE CLASSES.	249
TABLE 7.13 CROSS-TABULATION OF THE PERCENTAGE AREA OF EACH LITHOLOGICAL CLASS COMPARED TO ALTITUDE (M.A.S.L). HIGHEST PERCENTAGE IS IN BOLD.	249
TABLE 7.14 TOTAL AREA (KM ² AND PERCENT) OF PROBABILITY VALUES FOR EACH ITERATION OF RANDOM POINTS FOR THE TERRACE TYPE MASS MOVEMENT FEATURES.	255
TABLE 7.15 COMPARISON OF THE FREQUENCY DISTRIBUTIONS AND INFOVAL WEIGHTS. BOLD INDICATES HIGHEST VALUE IN CATEGORY, COLOUR INDICATES VARIABLE WITH GREATEST FREQUENCY.	264
TABLE 7.16 THE AIC, BIC AND VARIABLES SELECTED FOR EACH ITERATION. NOTE THAT THE PERCENTAGE OF CORRECTLY PREDICTED TERRACETTES IS SIMILAR FOR EACH MODEL.	267
TABLE 7.17 TOTAL AREA (KM ² AND PERCENT) OF PROBABILITY VALUES FOR EACH ITERATION OF RANDOM POINTS.	271
TABLE 7.18 COMPARISON OF THE FREQUENCY DISTRIBUTIONS AND INFOVAL WEIGHTS. BOLD INDICATES HIGHEST VALUE IN CATEGORY, COLOUR INDICATES VARIABLE WITH GREATEST FREQUENCY.	277
TABLE 7.19 THE AIC, BIC AND VARIABLES SELECTED FOR EACH ITERATION. NOTE THAT THE PERCENTAGE OF CORRECTLY PREDICTED INCISED FLOWS IS SIMILAR FOR EACH MODEL.	280
TABLE 7.20 TOTAL AREA (KM ² AND PERCENT) OF PROBABILITY VALUES FOR EACH ITERATION OF RANDOM POINTS.	285
TABLE 7.21 COMPARISON OF THE NUMBER OF SURFICIAL SCARS IN RELATION TO ROCK EXPOSURES.	292
TABLE 7.22 COMPARISON OF THE FREQUENCY DISTRIBUTIONS AND INFOVAL WEIGHTS. BOLD INDICATES HIGHEST VALUE IN CATEGORY, COLOUR INDICATES VARIABLE WITH GREATEST FREQUENCY.	293
TABLE 7.23 THE AIC, BIC AND VARIABLES SELECTED FOR EACH ITERATION. NOTE THAT THE PERCENTAGE OF CORRECTLY PREDICTED SURFICIAL SLIDES IS RELATIVELY SIMILAR FOR EACH MODEL.	296
TABLE 7.24 TOTAL AREA (KM ² AND PERCENT) OF PROBABILITY VALUES FOR EACH ITERATION OF RANDOM POINTS.	301
TABLE 7.25 COMPARISON OF THE FREQUENCY DISTRIBUTIONS AND INFOVAL WEIGHTS. BOLD INDICATES HIGHEST VALUE IN CATEGORY, COLOUR INDICATES VARIABLE WITH GREATEST FREQUENCY.	307
TABLE 7.26 THE AIC, BIC AND VARIABLES SELECTED FOR EACH ITERATION.	309
TABLE 7.27 TOTAL AREA (KM ² AND PERCENT) OF PROBABILITY VALUES FOR EACH ITERATION OF RANDOM POINTS.	313
TABLE 7.28 COMPARISON OF THE FREQUENCY DISTRIBUTIONS, INFOVAL AND HIERARCHICAL PARTITIONING FOR THE TERRACE-TYPE MASS MOVEMENT FEATURES.	315
TABLE 7.29 LENGTH (KM) AND AREA STATISTICS (KM ²) FOR EACH OF THE MASS MOVEMENT TYPES. SHAX IS THE SHORTEST AXIS OF A BOUNDING RECTANGLE REPRESENTING THE POLYGON OF THE SHAPE AND LOAX IS THE LONGEST AXIS OF THE SAME RECTANGLE.	318
TABLE 7.30 FREQUENCY OF LANDFORMS WITH CR IN RANGE INTERVALS OF 0.2. THE AVERAGE CIRCULARITY RATIO IS ALSO GIVEN.	319
TABLE 7.31 COMPARISON OF THE FREQUENCY DISTRIBUTIONS, INFOVAL AND HIERARCHICAL PARTITIONING FOR THE SHEAR-TYPE MASS MOVEMENT FEATURES.	320

TABLE 7.32 A COMPARISON OF THE NUMBER OF SHEAR SCARS FOR EACH TYPE WHICH ARE WITHIN 5M OF A DRAINAGE LINE AND THE PERCENTAGE OF THOSE SCARS ACCORDING TO STREAM ORDER.	321
TABLE 7.33 DESCRIPTIVE STATISTICS OF THE QUADRATS	324
TABLE 7.34: SUMMARY STATISTICS FOR THE DENSITY VALUES PRODUCED USING THE KERNEL AND POINT DENSITY FUNCTIONS (NUMBER OF EVENTS PER SQUARE KM)	325
TABLE 7.35: DESCRIPTIVE STATISTICS OF THE AREA AND NUMBER OF POINTS ASSOCIATED WITH THE HIGHEST DENSITY CLASS CREATED USING TWO DIFFERENT SEARCH RADII	328
TABLE 7.36 COMPARISON OF THE FREQUENCY DISTRIBUTIONS AND INFOVAL WEIGHTS FOR SS01. BOLD INDICATES HIGHEST VALUE IN CATEGORY, COLOUR INDICATES VARIABLE WITH GREATEST FREQUENCY.....	339
TABLE 7.37 COMPARISON OF THE FREQUENCY DISTRIBUTIONS AND INFOVAL WEIGHTS FOR SS05. BOLD INDICATES HIGHEST VALUE IN CATEGORY, COLOUR INDICATES VARIABLE WITH GREATEST FREQUENCY.....	340
TABLE 7.38 COMPARISON OF THE FREQUENCY DISTRIBUTIONS AND INFOVAL WEIGHTS FOR SS15. BOLD INDICATES HIGHEST VALUE IN CATEGORY, COLOUR INDICATES VARIABLE WITH GREATEST FREQUENCY.....	341
TABLE 7.39 TOTAL AREA (KM ² AND PERCENT) OF PROBABILITY VALUES FOR SS1.	345

1 Introduction

1.1 Mass movement: relevance within a southern African context

Whilst many studies have been undertaken on mass movement over the last century, catastrophic large mass movement events continue to cause human fatalities. In 2007, 395 fatal landslides occurred worldwide resulting in the deaths of more than 3 000 people, whilst in 2003–2006, 4 399 fatal landslides caused an estimated 10 976 deaths (Petley, 2008). In 2008, 67 countries reported landslide events, with an average of four fatalities per event (Kirschbaum et al., 2010). The socio-economic impacts of mass movements are also usually severe; remediation and infrastructure replacement in the United States and Japan was thought to cost between US\$1 and US\$5 billion a year (Schuster, 1996). The most recent estimate of costs for prevention and rehabilitation of mass movements in southern Africa are about US\$ 20 million a year (Paige-Green, 1989), however this is probably an underestimate given that no new approximations have been made (Paige-Green and Leyland, 2009).

Almost 90% of the fatal landslides recorded during 2007 were triggered by intense and prolonged precipitation (Petley, 2008; Kirschbaum et al., 2010) and it is expected that global environmental change will indirectly result in an increasing number of catastrophic mass movements (Trauth et al., 2003; Geertsema et al., 2006; Petley, 2010). Disastrous rainfall-triggered mass movement in southern Africa has been recorded in the Western Cape (Blight et al., 1970) and KwaZulu Natal (Thomas and van Schalkwyk, 1993). If climate change causes an increase in the intensity and frequency of El Niño and ENSO events, more mass movement activity may be expected in such areas in years to come (Dore, 2005). It is therefore important that South African earth scientists

increase their understanding of mass movements, particularly for improving spatial and temporal predictions of their likely future occurrences.

Mass movement has been defined as the downward and outward movement of slope-forming material under the influence of a transporting agent such as water, air, ice or snow (Goudie, 2004). Many definitions and classifications of mass movement have been produced during the last century (see chapter 2) but there is general recognition amongst scientists that the term ‘mass movement’ includes topples, falls, slides, flows and spreads and that the rate of movement can be very slow to very rapid. Accurately classifying mass movement has become increasingly important as communities and insurance companies require precise definitions to reduce risk and prevent disasters (Shroder and Cvercková, 2005).

Mass movements are the result of the combined effect of environmental conditions which reduce the stability of slope material, and trigger mechanisms which initiate movement. Examples of conditioning factors include fluvial/wave incision (Fiorillo, 2003; Ng, 2006; Ouimet et al., 2007), excavation (Göcktürkler et al., 2008), increased load (Glade, 2000), soil erosion (Pradhan et al., 2012), deforestation (García-Ruiz et al., 2010), land-use change (Coelho-Netto et al., 2007; Jakob and Lambert, 2009; Mugagga et al., 2012), and increased pore pressures in weakly structured or clay rich soils (Hürliman et al., 2001; Basile et al., 2003), amongst others. Trigger mechanisms associated with mass movement development include prolonged and/or intense rainfall (Hungr et al., 2001; Wieczorek et al., 2004), snowmelt (Naudet et al., 2008; Kawagoe et al., 2009), changes in water-level associated with increasing or decreasing groundwater depth (Brien and Reid, 2008), volcanic eruptions (Devoli et al., 2007; Harris et al., 2011) and earthquake vibrations (García-Rodríguez et al., 2008; Ayalew et al., 2011).

The impacts of mass movement vary depending on the magnitude of the mass movement event, however impacts are usually described in terms of the effects of mass movement on the urban environment. Risk has been defined in terms of the number of human lives lost, the damage to property and the disruption to economic activities that a particular mass movement causes (Varnes, 1984). Yet, mass movement may strongly affect the natural environment as well. Sediments that are mobilised by mass movement may significantly contribute towards the sediment budget of a drainage system (Korup, 2004; Schwab et al., 2008; Chen, 2009). Other impacts include the damming of rivers by landslides and rock avalanches (Dai et al., 2005; Parvaiz et al., 2012), vegetation removal and land-use change (Restrepo and Alvarez, 2006), altering channel morphology and longitudinal river profiles (Ouimet et al., 2007; Molnar et al., 2010), and changing slope topography (Dunning et al., 2009). In addition, the impacts of a catastrophic mass movement may have a morphogenetic influence for millennia or tens of millennia through the disturbance of other geomorphic processes (Hewitt et al., 2008).

Mass movement research in southern Africa has been relatively limited, and few studies have investigated the nature and distribution of mass movement phenomena at a national or provincial level. The Council for Geoscience has recognized this and is currently engaged in identifying, inventorizing and mapping landslides in the Western Cape, KwaZulu-Natal and Limpopo provinces (Diop et al., 2010). Recently, research has been conducted on mass movements in the province of KwaZulu-Natal, however the types of mass movement investigated were primarily limited to very large palaeo-landslides (Singh, 2008). Most southern African studies have been site-specific in approach and include the Durban area of KwaZulu-Natal (Knight et al., 1977; Garland, 1978; van Schalkwyk and Thomas, 1991; Thomas and van Schalkwyk, 1993; Bell and Maud, 2000), Richard's Bay (Smedley and Nowlan, 1978), Esikhaleni, Eastern Cape (Beckedahl et al., 1988), Du Toit's Kloof,

Western Cape (Boelhouwers et al., 1998; Gupta 2001), the Injusuthi Valley, Drakensberg (Bijker, 2001), the Fish River Catchment, Namibia (Stengel, 2001) and the Vunguvungu Banga Catchment and Rumphi District, Malawi (Msilimba and Holmes, 2005; Dill et al., 2005; Msilimba and Holmes, 2010).

Studies that have mapped the distribution of mass movement types, monitored rates of their development and established the causes of instability have been limited (Beckedahl et al., 1988; Thomas and van Schalkwyk, 1993). The main focus of mass movement research in southern Africa has been on the nature of mass movement deposits, which is used to infer the palaeo-climatic conditions under which such processes could operate (c.f. Boelhouwers, 1991, 1999, 2003; Grab, 1996, 1999, 2000; Hanvey and Marker, 1992; Boelhouwers et al., 1998; Boelhouwers and Sumner, 2003; Lewis, 2005; Mills and Grab, 2005; Temme et al., 2008). Consequently, more emphasis has been placed on using mass movement deposits to provide proxy climatic data than on understanding the features themselves. Table 1.1 provides a summary of the publications that have reported on the types and locations of mass movement activity in southern Africa.

Smaller landslides, which have been active relatively recently, are documented from the Drakensberg (Bijker, 2001) and along the eastern coast of Durban, KwaZulu-Natal (Knight et al., 1977; van Schalkwyk and Thomas, 1991; Bell and Maud, 1995; Bell and Maud, 2000). These shallow translational slides have been related to periods of increased rainfall and occur in Peninsula sandstones (Boelhouwers et al., 1998) and weathered granites in the Western Cape (Gupta, 2001), fragmented shales and mudstones of the Ecca Group in the Eastern Cape (Beckedahl et al., 1988), in Berea red beds in Durban (Bell and Maud, 2000) and in sandstones and mudstones of the Clarens, Elliot, and Molteno Formations and Drakensberg Group in the Ukhahlamba-Drakensberg Park (UDP) (Bijker, 2001).

Author	Type	Location
King (1944)	Terracettes, small slide scars	Drakensberg
Blight et al. (1970)	Slides	Port Elizabeth, Eastern Cape and Bethlehem, Free State
Green and Bloch (1971)	Rockfalls	Ceres and Wolseley, Western Cape
Sparrow (1971)	Solifluction	Lesotho and Drakensberg
Hastenrath and Wilkinson (1973)	Terracettes	Lesotho
Shroder (1976)	Rotational slides, earthflows	Malawi
Knight et al. (1977)	Slides	South Coast and Durban, KwaZulu-Natal
Garland (1978)	Rotational slide	Durban, KwaZulu-Natal
Smedley and Nowlan (1978)	Rotational slide	Richard's Bay, KwaZulu-Natal
Garland (1979)	Shallow slope failure, terracettes	Mooi River Valley, Kamberg
Garland and Humphrey (1980)	Soil creep, shallow slope failures, rockfalls	Drakensberg
Hanvey et al. (1986)	Debris flows	Rhodes, Eastern Cape
Beckedahl et al. (1988)	Mass movement complex (slides, rock falls and soil creep)	Esikhaleni, Eastern Cape
Lewis (1988)	Solifluction	Lesotho, Drakensberg mountains
Verster and van Rooyen (1988)	Terracettes	Long Tom Pass, Mpumalanga and Mike's Pass, Drakensberg
Watson (1988)	Terracettes	Drakensberg
Boelhouwers (1991)	Stepped microrelief (cattle steps and terracettes)	Drakensberg
van Schalkwyk and Thomas (1991)	Slides and flows	KwaZulu-Natal
Hanvey and Marker (1992)	Terracettes	Lesotho
Meiklejohn (1992)	Solifluction lobes, cryoplanation terraces	Drakensberg
Cooper (1993)	Landslides	Mtamvuna estuary, KwaZulu-Natal
Thomas and van Schalkwyk (1993)	Planar slide, rotational slide, flow failure	Southern Drakensberg
Grab (1996)	Debris flows/slides, rock falls/slides	High Drakensberg
Lewis (1996)	Solifluction terraces	Eastern Cape, Drakensberg
Mitchell (1996)	Palaeo-rockfalls	Sehonghong, Lesotho
Stengel (1997)	Fossil landslides	Southern Namibia
Boelhouwers (1998)	Arcuate shaped slip scars and terracettes	Giant's Castle, Drakensberg
Boelhouwers et al. (1998)	Shallow planar slides, deeper rotational slides, debris flows	Du Toit's Kloof, Western Cape
Boelhouwers (1999)	Solifluction, terraces	Matroosberg, Western Cape
Grab (1999)	Mini mud flows	High Drakensberg
Bell and Maud (2000)	Landslides	Durban, KwaZulu-Natal
Boelhouwers et al. (2000)	Debris flows	Marion Island
Grab (2000)	Stone-banked lobes, solifluction	High Drakensberg
Bijker (2001)	Shallow rotational and translational slides	Injusuthi Valley, Drakensberg
Bye and Bell (2001)	Translational slides	Sandsloot, Limpopo
Gupta (2001)	Debris slides, rock falls	Du Toit's Kloof, Western Cape
Shaw et al. (2001)	Debris flows	Cape Point, Western Cape
Stengel (2001)	Large palaeo-rotational landslides	Fish River Catchment, Namibia
Boelhouwers et al. (2002)	Solifluction	Sani Pass, Lesotho
Boelhouwers (2003)	Mass-wasting forms, shallow soil slides, creep and solifluction processes	Lesotho highlands, above and below the Escarpment
Kück and Lewis (2002)	Solifluction, creep, terracettes	Eastern Cape, Drakensberg
Mills and Grab (2005)	Solifluction lobes	Leqooa Valley, southern Drakensberg
Msilimba and Holmes (2005)	Earth and debris flows	Vunguvungu Banga Catchment, Malawi
Singh (2008)	Large palaeo-rotational landslides	KwaZulu-Natal
Terme et al. (2008)	Solifluction	Okhombe valley, KwaZulu-Natal
Mills et al. (2009)	Solifluction lobes, terraces	Lesotho
Msilimba and Holmes (2010)	Landslides	Rumphi District, Malawi

Table 1.1 A summary of the types and locations of mass movement activities in southern Africa.

Solifluction lobes and terracettes have mostly been studied in relation to periglacial activities in the Drakensberg and Lesotho, possibly due to the association between temperature and altitude, as these areas experience regular frost and snow. Solifluction lobes and terracettes have not been included in the

landslide hazard analyses of Bijker (2001) and Singh (2008) as these represent mass movement processes which occur at a much slower rate. Rockfalls in South Africa are most commonly associated with mining activities, where rockfalls and bursts are associated with blasting activities (Esterhuizen and Streuders, 1998), although rockfall activity has been associated with earthquakes in the Ceres Mountains of the Western Cape (Green and Bloch, 1971). Rockfalls in the Drakensberg occur as falling and toppling movements along the horizontally-bedded rock outcrops of the Karoo Supergroup.

The first map of mass movement potential produced for southern Africa was published by Paige-Green (1989) and this map has recently been updated. The analysis ranks lithology, gradient, climate and seismic activity to establish relative risk of landslide activity (Paige-Green and Leyland, 2009) (Figure 1.1). Areas of high susceptibility have a combination of unfavourable lithological, moisture and topographic conditions. Areas of medium to low susceptibility have two or less conditions classified as unfavourable. This type of susceptibility analysis represents a heuristic approach to hazard zonation, referred to as 'qualitative map combination' (Soeters and van Westen, 1996). Garland and Humphrey (1980) used a similar method for erosion susceptibility mapping in the Kamberg area of the Drakensberg, but used variables relating to the morphometric, hydrologic and material conditions specific to the area.

More recently, statistical and deterministic approaches have been used for mass movement studies in the Western Cape (Gupta, 2001) and Drakensberg (Bijker, 2001). Gupta (2001) used a bivariate statistical method to compare the frequency distribution of mass movements to selected environmental conditions, whilst Bijker (2001) used a coupled hydrologic-slope stability model to predict the number of unstable days experienced on north-facing slopes during a 31 year period. Limited work has been undertaken on the effects of mass movement activity in urban areas (Thomas and van Schalkwyk,

1993) and it would seem that most studies have focussed on mass movements in remote mountainous regions of southern Africa. These regions are regarded as high water yield areas which are important for producing and managing water resources and most are demarcated as protected areas.

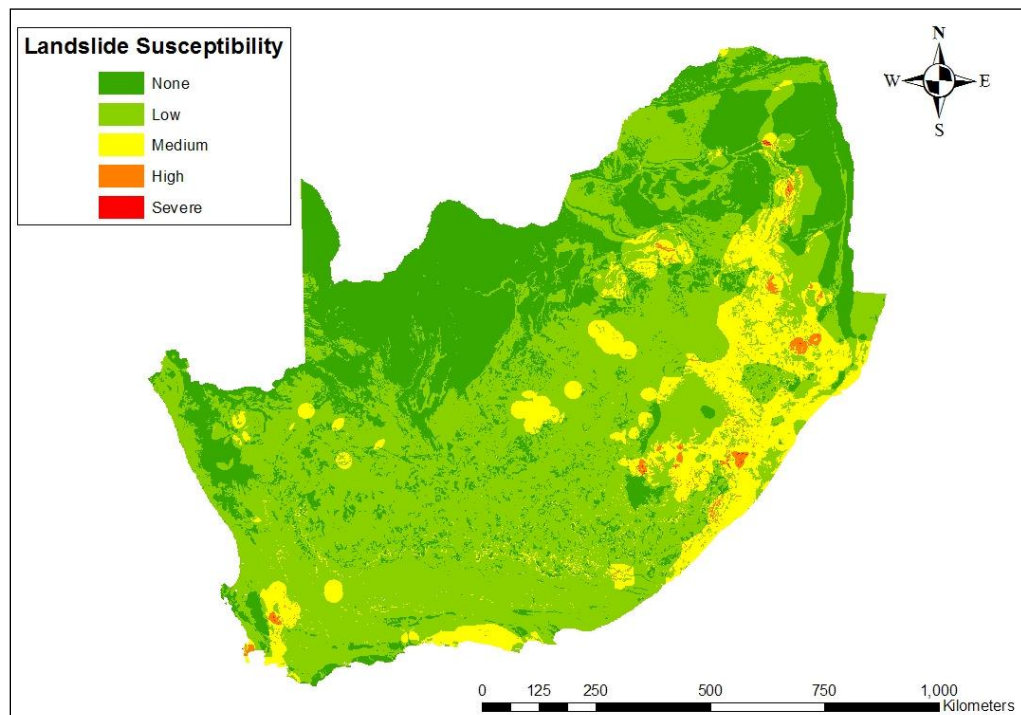


Figure 1.1 Map of landslide susceptible zones (after Paige-Green and Leyland, 2009).

Classifications developed specifically for mass movement features in southern Africa are limited. The morphometric attributes of a number of slides, falls and flows were used to classify a mass movement complex in the Transkei (Beckedahl et al., 1988) using indices developed by Crozier (1973). Mass movements that damaged roads and railways during the ‘Natal floods’ of 1987/88 were classified according to movement type, however mass movements that did not destroy infrastructure were designated as part of the natural erosion cycle and excluded from the classification (Thomas and van Schalkwyk, 1993). Type of material has been used to distinguish between mass

movement forms (Gupta, 2001), whilst the classification developed by Varnes (1978) has also been adopted for the Drakensberg (Bijker, 2001).

The use of Geographic Information Systems (GIS) for modelling and predicting the spatial distribution of mass movement features is widely accepted in the international literature (e.g. Carrara et al., 1991; Guzzetti et al., 2000; Lineback Gritzner et al., 2001; Clerici et al., 2002; Lee et al., 2003; Ayalew et al., 2004; Ermini et al., 2005; Akgun et al., 2008; Dahal et al., 2009; Yalcin, 2008; Bai et al., 2010; Pradhan, 2010; Yalcin et al., 2011; Xu et al., 2012). Although GIS can be used for heuristic, statistical or deterministic modelling approaches, the input data required by the models may be impossible to collect or prohibitively expensive (Lineback Gritzner et al., 2001). In South Africa, the application of GIS in mass movement studies has been limited, possibly due to the lack of quality digital data and the expense of in-field data collection.

A regional landslide hazard analysis which was undertaken in KwaZulu-Natal used lithological and rainfall data and a 90m digital elevation model made available by the Shuttle Radar Topography Mission (SRTM) (Singh, 2008; Singh et al., 2008). Most of the landslides observed in the study are presently inactive large palaeo-landslides and therefore represent slide events which occurred under different climatic conditions. Whilst the methodology adopted is similar to the one used in this dissertation, the scale of the area and the types of mass movement features under investigation are different. A wider range of mass movements are examined in this dissertation, occurring within a smaller study area, at smaller scales, and which have been active more recently than the landslides studied by Singh (2008).

Remote sensing techniques, such as Aerial Photo Interpretation (API), offer a cheaper and quicker approach for regional mass movement feature identification than field-based methods (Brardinoni et al., 2003). The success of

this technique is dependent on the nature and size of the features to be examined, the scale and resolution of the images, and the masking effects of vegetation (Mantovani et al., 1996; Brardinoni et al., 2003; McKean and Roering, 2004; Van Den Eeckhaut et al., 2005). API has been successfully adopted to investigate and map mass movement phenomena in southern Africa (Bijker, 2001; Singh, 2008).

1.2 Aims and Objectives

Singh (2008) produced a landslide hazard map which includes the southern Drakensberg, South Africa, however the resolution of the map is relatively coarse and the analysis does not include all of the types of mass movement which have been observed to occur in the UDP. A site-specific classification has not yet been undertaken, neither have a large variety of environmental factors leading to mass movement activity been assessed. Although producing a mass movement inventory is an important part of the modelling process, an appropriate classification needs to be developed that adequately describes the type of movement within the scale of investigation of the study area.

The aim of this study is to produce a site-specific classification for mass movement features and an inventory of mass movement distribution in the Bushman's Nek region of the southern Drakensberg, South Africa. A Geographic Information System (GIS) is used to predict likely locations for future mass movement development. The environmental variables selected for analyses are altitude, aspect, distance to drainage lines, rock exposures and footpaths, gradient, lithology, and slope unit. These variables were selected as they often appear in landslide and rockfall hazard zonation studies (Nefeslioglu et al., 2008; Pandey et al., 2008) and are relatively easy to generate or are readily available. Inventorying mass movement features is important to conservation managers and land use planners as it provides information about

the types of geomorphological processes occurring in an area which impacts on the kinds of activities which may occur there. The UDP is a popular tourist destination and a proportion of revenue collected by the UDP is returned to the surrounding rural communities (Linde and Grab, 2008). Sustainable use of the UDP is therefore important for water provision, tourism and local economic development.

The UDP is a state owned protected area which is managed by a provincial conservation body called Ezemvelo KwaZulu-Natal Wildlife (KZN Wildlife). The UDP is composed of twelve individual protected areas which total approximately 242,813 ha (Kruger, 2007). Only a small percentage of the UDP is accessed by visitors and most of the human impacts are concentrated along footpaths, at camp sites or at specific destinations, such as waterfalls or rock overhangs (Kruger, 2007). The UDP is thus suited to studies focusing on the environmental, rather than anthropogenic, effects on mass movement. The southernmost extent of the UDP was selected to classify mass movements as a wide variety of landforms were observed in the area, which had not been noted in the northern regions of the UDP, particularly solifluction lobes.

The primary objectives of this project include:

- To review existing mass movement classifications.
- To identify mass movement features for classification in the study area and to produce a mass movement inventory from data collected in the field and by API.
- To produce a digital elevation model for the extraction of topographic data.
- To produce a matrix of data that represent the topographic and geologic variables associated with mass movement activity.
- To identify a frequency-distribution of mass movement types associated with the environmental variables.

- To use statistical techniques to identify rockfall deposits within the UDP.
- To produce mass movement feature distribution and susceptibility zonation maps.
- To develop a classification of mass movement features which is relevant to a southern African context.

1.3 Project Summary

Chapter 2 introduces classification theory and the problems of nomenclature, reviews types of mass movement classifications and types of features, and discusses the triggering and conditioning mechanisms of mass movement. Chapter 3 summarises the different approaches used for landslide and rockfall hazard zonation, discusses the applications of GIS in mass movement studies and the use of API for mass movement feature identification. Chapter 4 describes the vegetation, geology, geomorphology, conservation management practices and general environmental setting of the southern Drakensberg. Chapter 5 outlines the field and desktop methods used for data collection and analysis. Chapter 6 presents each of the mass movement feature types and rock movement deposits, and discusses the results of the frequency distributions, Information Value, logistic regression models and classification trees. Amendments to the classification are suggested and a comparison is made between mass movement types with similar characteristics. Chapter 7 concludes with a discussion on the final classification developed for mass movement features, some comments on the problems associated with the statistical techniques adopted and recommendations for future research.

2 Mass movement classifications and characterizations

2.1 Introduction

The study of mass movements has long interested engineers, urban planners, hydrologists and geomorphologists due to the widespread effects that mass movements have on natural systems and manmade structures. This multidisciplinary attention has resulted in arbitrary and confusing terminology in the literature since each group has developed their own nomenclature. To discuss mass movements in the southern Drakensberg, it is necessary to first introduce the theory of classification, produce an explicit and comprehensive list of definitions used in the literature and define the terminology as it pertains to this dissertation.

This discussion is followed by a review on the various approaches used to distinguish between mass movement types, followed by a description of each type in terms of its style of motion, composition and environmental attributes. Finally, the classification proposed for mass movements in the southern Drakensberg is presented.

2.2 Classification theory

Mass movement classification theory was primarily a conceptual exercise during the 1950's and 1960's. The ubiquitous use of classifications in all branches of science resulted in the inclusion of algebraic reasoning in class-producing decision-making processes from the 1970's onwards. Set theory established the language for algebraic classification (c.f. Enderton, 1977) and pattern recognition introduced statistical techniques for classifying randomly distributed data (c.f. Young and Calvert, 1974). Fuzzy set theory was

introduced in the 1980's to account for sets that could not be properly represented by clearly defined classes (c.f. Kandel, 1986). More recently, classification theory has been adapted to create programming languages that have application in GIS.

Definitions and classifications order information about the environment. Definitions establish meaning whilst classifications group the data. Both organize data into a comprehensible format that promotes learning and communication. A classification separates data into specially constructed classes using a filter or set of rules. These rules are developed abstractly or by observation, and their application depends on the objectives of the classification (Harvey, 1969). Classification procedures may be used to assign a new object to an existing set of classes, such as in discriminant analysis or pattern recognition, or separate objects into groups that have specific properties (Gordon, 1987).

The diversity of classifications that exist for the same data set is dependent on the rules or properties of the data used in the classifying procedure. This results in classifications that are marginally to vastly different. The accuracy of a classification is difficult to establish due to the contextual nature of the rule forming process, but a set of requirements exists that should be taken into consideration (Gordon, 1987). Firstly, classes should contain data that occur in unique clusters and have internal cohesion and external isolation. Secondly, the classification should have stability and be little affected by small errors or the addition of new objects or variables. The authenticity of a classification can be established by determining its ability to simplify data, predict trends and formulate general hypotheses.

General or natural classifications function as data storage systems and provide a nomenclature for understanding empirical problems (Harvey, 1969). However,

maximizing the data storage capabilities of a classification increases the number of descriptors used and reduces its efficiency for naming things. For example, classifying a mass movement feature as a moderate, reactivated, enlarging, composite, translational earth slide advances our knowledge on the subject but increases the complexity of the classification. Specific or artificial classifications are those that are designed for a special purpose and vary greatly depending on the method and research criteria used. A good example of a general classification for mass movements is that developed by Varnes (1978), whilst a more specific classification has been presented by Hutchinson (1968).

Various methods exist for allocating data to classes (Figure 2.1). Grouping unites elements into sets which combine to make the universal set. Partitioning occurs when the universal set is divided into exhaustive and exclusive subsets (Harvey, 1969). Grouping is an inductive procedure which establishes regularities and relationships between sets. It is useful for classifying data when the relationships between variables are unknown (Harvey, 1969). Classes are not mutually exclusive or exhaustive and all elements can be ascribed to a set even if all the parameters are not met (Young and Calvert, 1974). Groups are also allowed to overlap if similarities occur in the data. However, grouping is entirely dependent on the ability of the data to reflect complex relationships and thus classes may misrepresent the structure of the data set (Gordon, 1987). Poor quality or limited data would result in important criteria being excluded or misinterpreted, especially if processes operate on widely ranging spatial and temporal scales.

Partitioning separates elements into disjoint groups and no element may be included more than once. An element is included in a set only if all the criteria are met (Gordon, 1987). Data may also be organized into a hierarchical structure to summarize the relationships that exist between classes (van Der Eyk et al., 1969). Hierarchical organization assumes that each class is wholly

contained within the class above it and is useful for displaying structure between sets simultaneously. If sets exist that cannot be hierarchically nested, geometrical methods may be used. Objects that are similar to one another are represented by points in a two or three dimensional space. The clustering behaviour of the data will establish how closely the data are related (Gordon, 1987).

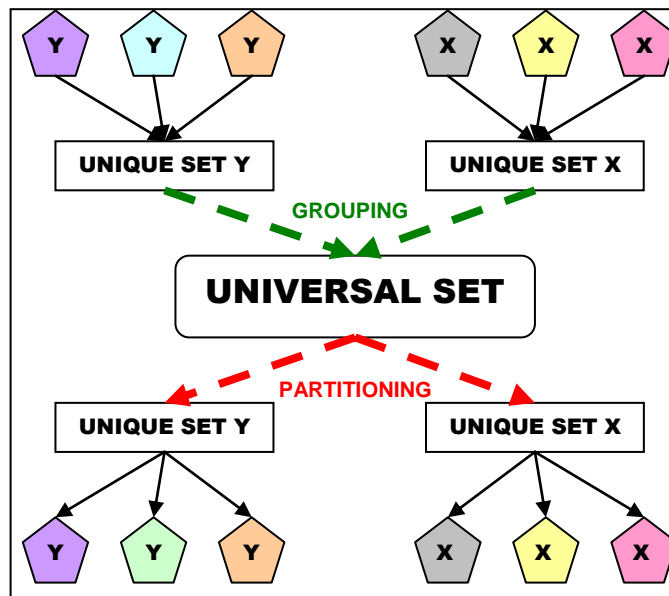


Figure 2.1 Method for allocating elements to classes.

Few contributions have recently been made to classification theory in the form of hypothetical arguments. Emphasis has shifted to more practical applications, and with the advancement of computer science, has seen the introduction of classification theory in programming languages, GIS and statistical algorithms. Statistical techniques such as discriminant analysis and logistic regression are used to distinguish between groups and neural networks and principal components analysis can be used to recognise patterns or identify clusters in large multivariate datasets (Porkess, 2004).

2.3 Defining mass movement

Possibly the earliest definition of mass movement describes the process as the ‘movement of slope materials occurring under the influence of gravity but without the assistance of a transporting medium, such as water, air, ice or snow’ (Penck, 1894, p.471). More recently, Goudie (2004, p.644) has defined mass movement as ‘the downward and outward movement of slope-forming material under the influence of gravity... [and not requiring] a transporting medium such as water, air or ice’. Landslides are defined as the perceptible or comparatively rapid downward movements of slope-forming materials, such as earth, rock or debris (Sharpe, 1938; Cruden, 1991). All terrestrial mass movements are affected by water and/or air and/or ice at some stage during their development, and all occur under the influence of gravity. As mass movements have been observed on Mars and the moons of Jupiter, which display similar morphometric attributes to terrestrial mass movements (Moore et al., 1999; Malin and Edgett, 2000; Harrison and Grimm, 2003; Gerstell et al., 2004; Mangold, 2005), the requirement of gravity in the definitions provided by Penck (1894) and Crozier (1986) is unnecessary. Twidale (1976) and Goudie (2004) overcame this limitation by including the action of material failure and its influence on movement type in their definition of landsliding.

The term ‘landslide’ is often used synonymously with the term ‘mass movement’ (Coates, 1977; Crozier, 1986; Shroder and Cvercková, 2005) which results in the arbitrary exclusion of creep and subsidence from some classifications (c.f. Varnes, 1958; Coates, 1977). Where creep is included, it is defined as a precursor of large mass movements and defined as a type of slide (Zaruba and Mencl, 1969) or flow (Varnes, 1978). Subsidence is generally excluded from most classifications, however Hutchinson (1968) included it to account for the vertical, rather than parallel movement of slope forming materials.

Numerous mass movement classifications and definitions have been developed in the late 19th century (Table 2.1). Emphasis appears to have shifted from generating classifications to refining them (c.f. Allison, 1993, 1994, 1995; Coussot and Meunier, 1996; González-Díez et al., 1999; Hungr et al., 2001; Ayalew and Yamagishi, 2004; Jakob, 2005), although the geophysical community is still engaged in developing a landslide classification at present (Fell et al., 2008). Two additional shifts have been observed in the literature; namely in the early 2000's focus shifted away from classifications to deterministic modelling and hazard mapping, and secondly, there is renewed interest in mass movement types and the possibilities of using statistical modelling to differentiate between them (Alexander, 2008).

Author	Based on	Classes	Description
Baltzer (1875)	Material type and movement type	Four	Later revised to include size of the displaced mass
Heim (1882)	Material type and movement type	Six	Debris slide, rock slide, compound and miscellaneous
Penck (1894)	Movement type	Four	Loose mass movement, landslides, flowage and washing
Molitor (1894)	Cause of movement	Four	Slides caused by too steep slope, slides caused by combination of inclined strata and water, slides caused by water and slides caused by subsidence. Type 1 and 2 have slip surfaces, Type 3 has fluid behavior
Braun (1909)	Movement type and material type	Four	Sliding, flowing, falling and sinking. Further divided according to material
Howe (1909)	Based on Heim (1882)		Includes soil creep and mudflow. Lists slides from artificial cuts and subsidence as miscellaneous
Stiny (1910)	Effect of gravity	Two	Where gravity impacts directly; rock fall and slips; earth falls, slips and creeps and where gravity acts indirectly; movements aided by water, ice and snow
Almagia (1910)	Movement type	Five	Superficial flow, Deep-seated and large flowslips, rockslides and movements along a defined plane, falls due to weathering and falls due to undercutting
Penck (1924)	Coherency of moving mass	Two	Movement of single bodies, which includes all types of falls and movements of accumulative systems; flows that occur on the surface of the earth or those below the vegetation cover
Terzaghi (1925)	Friction type	Two	Dry movements where static movement is fully effective and mush movements where static friction is reduced or eliminated. Includes creep and mudflows but not solifluction
Heim (1932)	Material, movement and water content	Twenty	Includes compound landslides, unfinished landslides, subsequent slides and 'still unknown types of landslides'
Miyabe (1935)	Movement, material and precipitation	Four	Slides of superficial layers of earth's crust, earth and rock flows, slow large earth movements and rock falls

Table 2.1 Early types of mass movement classifications (after Sharpe, 1938).

Reference to the work of Varnes (1958, 1978, 1984) and Dikau et al. (1996) is frequently made in the literature on landslides and mass movement. The

original classification developed by Varnes (1958) was for the American Transportation Research Board, whilst Dikau et al. (1996) developed a classification for the European Community Programme (EPOCH) using terminology conceived by the International Geotechnical Societies' UNESCO Working Party on World Landslide Inventory. A summary of the classifications used before the 1950's is provided by Sharpe (1938) and Hansen (1984). Some of the earliest classifications of mass movement were developed in the late 1880's and were based on the type and size of the material moved (e.g. Baltzer, 1875; Heim, 1882). Fifty years later, underlying geology, prevailing climatic conditions and type of movement were considered better discriminating attributes for developing classifications (e.g. Ladd, 1935; Sharpe, 1938). The role that mass movement has in determining slope morphology was first explored in the 1940's and 1950's, from which the first quantitative classifications were developed. These were based on the morphometric attributes of the mass movement types (Ward, 1945; Popov, 1946; Skempton, 1953) and their failure surfaces (Terzaghi and Peck, 1948).

The defining attributes of mass movement to be used in this dissertation are as follows:

- Mass movement is the downward and outward movement of slope material, with or without the influence of gravity.
- Material must be displaced as a unit; the degree of internal consistency and size of the displaced mass form part of the classification.
- Movement may occur over a wide range of time scales.
- Mass movement occurs under the influence of external agents when thresholds of stability within the mass are exceeded. Although the integrity of slope material may be considered unstable by itself, an external agent causes failure. The factors that create material instability are referred to as conditioning factors and those that cause movement are referred to as initiating factors.

- Mass movement includes falls, topples, spreads, slides and flows. Creep is included in the classification as a subset of flows. Subsidence is included as a subset of falls.
- The objective of using these defining attributes is to adhere to the terminology and structure suggested by Varnes (1978) and Dikau et al. (1996), and to adapt these to reflect the local southern Drakensberg environment, which is similar to the approach adopted by Singh (2008).

2.4 Techniques for the classification and characterization of mass movements

2.4.1 Climate as a conditioning factor

The negative impacts of mass movement on human safety has increased public pressure and prompted mass movement specialists to shift their focus towards better understanding mass movement trigger mechanisms and processes. Over time, there has been a gradual shift from localised to more regional approaches. Although GIS and remote sensing has played an integral role in these developments, Alexander (2008) argues that purely GIS-based analyses are inductive and imprecise. Larger, multidisciplinary teams of geomorphologists, geoscientists and engineers have thus been formed in an attempt to develop nested hierarchical models of the environmental and geophysical attributes of mass movements (e.g. *Inventario dei Fenomeni Franosi in Italia - Inventory of Landslides in Italy*; Colombo et al., 2005).

An investigation of the mass movement literature reveals some important shifts in the focus of mass movement research over time. Firstly, the term landslide is used most often in the literature to describe mass movement phenomena. Secondly, it appears that until the 1990's, no classification or terminology had been internationally accepted. This led to the development of the Multilingual

Landslide Glossary by the International Geotechnical Societies' UNESCO Working Party on World Landslide Inventory and the European Community Programme's (EPOCH) Temporal Occurrence and Forecasting of Landslides in the European Community (Dikau et al., 1996), which are the most commonly used classifications used in mass movement studies.

Mass movement classifications range in complexity from simple, with one discriminating attribute, to complex, with hierarchical and tabular groupings based on two or more factors (Hansen, 1984). Very few simple classifications were developed after the 1950's, as classifications used a main attribute to distinguish between types and secondary factors to delineate subtypes. The most commonly used main attributes or classifiers are type of material and/or type of movement (e.g. Sharpe, 1938; Varnes, 1958, 1978, 1984; Hutchinson, 1988; Cruden and Varnes, 1996; Dikau et al., 1996), morphology of the material moved or the surface of movement (e.g. Skempton, 1953; Blong, 1973a, 1973b; Crozier, 1973), and geotechnical properties (e.g. Anderson and Howes, 1985 and Brooks et al., 1995). Very often, mass movements are defined by their characteristics, which form secondary attributes and subtypes in a classification. Attributes for classifying and characterising mass movements may include the following:

- Climatic regimes
- Triggering mechanisms
- Age, state and rate of mass movement activity
- Movement
- Morphometry
- Geographic location, geology and spatial homogeneity
- Nature of the displaced material
- Geotechnics

2.4.2 Climatic regimes

Mass movement characterisations based on climate recognise the influence that climatic setting and global climate change have on mass movement activity. One of the earliest climate-based mass movement classifications developed by Sharpe (1938), attempted to show how mass movements and fluvial/glacial processes were related to particular prevailing climatic conditions (Figure 2.2). Earthflows could be distinguished from mudflows according to the amount of water available in the environment at the time and represent humid and arid conditions respectively. Solifluction has been distinguished from other slow mass movement processes due to its association with subarctic conditions (i.e. ground freezing), and this convention was later used to separate creep processes into periglacial and non-periglacial types (Twidale, 1976; Hutchinson, 1988).

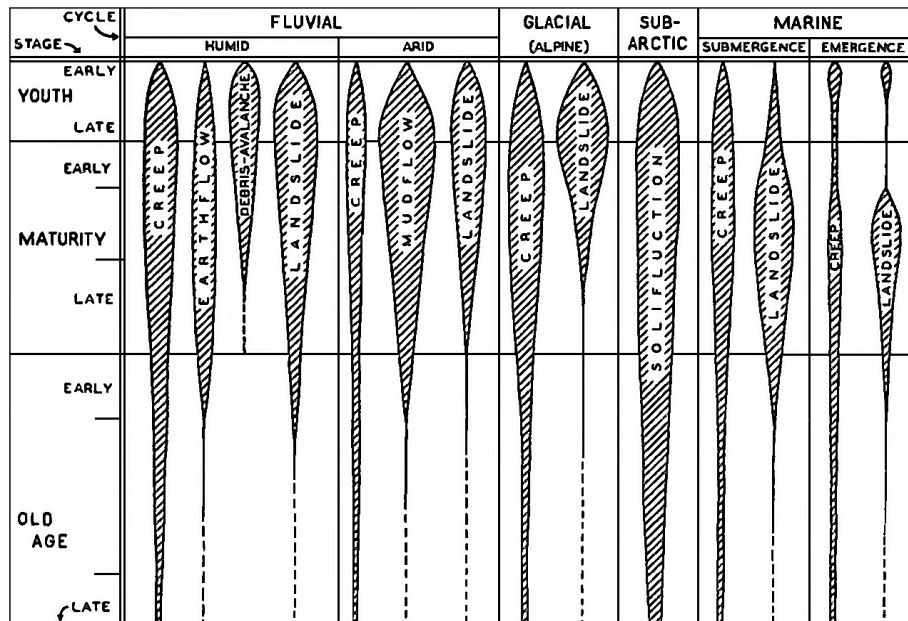


Figure 2.2 Climatic influence on mass movement form (Sharpe, 1938).

Climate change is expected to play a significant role on mass movement activity in the future because climatic conditions determine the availability of moisture. Climate change affects the synoptic origins of rainfall, which determines the frequency and duration of events and consequent antecedent soil

moisture conditions and vegetation cover (Brooks and Richards, 1994; Brooks et al., 1995; Dixon and Brook, 2007; Jakob and Lambert, 2009). Widespread mass movement activity has been associated with shifts in storm-generating mechanisms associated with the Little Ice Age (Lamb, 1982) and previous major glaciations (Owen, 1991). Studies on the effects of global climate change on mass movement activity have established that the late glacial, interglacial and interstadial transitional periods of the Pleistocene provided extreme climatic conditions conducive to the development of slump earthflows, whilst rotational slide blocks were typical occurrences during wetter Holocene periods (Terhorst, 2001).

Linked to the recent study of mass movements in relation to changes in climatic regimes, is the study of large, palaeo-landslides (Pánek et al., 2008), which have also been referred to as ‘giant and very large postglacial landslides’ and ‘prehistoric deep-seated bedrock collapses’ (Hancox and Perrin, 2009). Palaeo-landslide activity has been associated with the terminal phase of the Holocene in the Crimean Mountains, Ukraine (Pánek et al., 2008), with the Middle Holocene in Austria (Prager et al., 2008) and with post glacial recession in New Zealand (Hancox and Perrin, 2009), however these studies suggest that strong earthquake tremors would probably have been the trigger mechanisms leading to failure. Increased slope instability has been associated with moisture balance fluctuations during the Holocene in Italy which suggest that landslides occur more frequently under cold humid conditions than warmer, drier climatic conditions (Borgatti and Soldati, 2010).

2.4.3 Triggering mechanisms

Mass movements develop due to a series of pre-emptive conditions and require a trigger mechanism to overcome a critical stability threshold. Authors have referred to these two states as those that increase shear stress and reduce shear

resistance or shear strength (Terzaghi, 1950; Varnes, 1978). Others refer to these states as preparatory or conditioning factors and triggering factors (Cendrero and Dramis, 1996; Zêzere et al., 1999). Triggering events include high-intensity or long duration rainfalls, and are sometimes associated with hurricanes, earthquakes, volcanic activity, deforestation or logging, fires, snowmelt and tsunamis (Jakob and Lambert, 2009). Trigger events have been used to classify mass movement activity in Taiwan (Lin et al., 2008) and Italy (Guzzetti et al., 2009) so that landslides were classified as ‘event landslides’ if they were initiated by a known trigger, or ‘active landslides’ if movement was initiated between successive years of aerial photographs.

Rainfall duration and intensity are the most commonly used climatic parameters that can be related to mass movement type (Brooks and Richards, 1994; Finlay et al., 1997; Ng and Shi, 1998; Glade, 2000; Hardenbicker and Grunert, 2001; Aleotti, 2004; Wieczorek et al., 2004; Malet et al., 2005; Godt et al., 2006; Wang and Sassa, 2006; Claessens et al., 2007; Guzzetti et al., 2007; Guzzetti et al., 2008; Chang and Chiang, 2009; Li et al., 2011; Martelloni et al., 2011). Falls and shallow slides generally occur during high-intensity rainfall periods, whilst deeper-seated slides are usually triggered by rainfall occurring over an extended period of time (Zêzere et al., 1999; Baeza and Corominas, 2001). In Italy, debris flow initiation is known to occur in conjunction with surface runoff during very intense, typically short duration rainstorms (Berti and Simoni, 2005).

Rainfall thresholds have also been used to identify the nature of movement triggering versus non-triggering events (Crozier, 1997; Glade, 2000), whilst in Australia, multiple-occurrence regional landslide events (MORLEs) have been observed, during which thousands of mass movements occur simultaneously over an extended area (Crozier, 2005). MORLEs are directly related to critical storm rainfall thresholds combined with antecedent moisture conditions

(Crozier, 2005). Whilst a number of local, regional and global rainfall thresholds have been developed (Aleotti, 2004; Godt et al., 2006), a recent study by Guzzetti et al. (2008) found that rainfall thresholds cannot be used to differentiate between shallow landslides and debris flows.

Mass movements have additionally been characterised according to trigger mechanisms such as earthquake activity in Australia (Crozier, 2005), the Himalaya (Barnard et al., 2001), Japan (Fukuoka, 2004; Chigira and Yagi, 2006), the USA (Miles and Keefer, 2009) and China (Yin et al., 2009; Xu et al., 2012). The effects of different forest management approaches in British Columbia have been used to classify different types of landslides (Dhakal and Sidle, 2003) as different types of mass movements can have a variety of influences on vegetation (Marston, 2010). The influence of vegetation on mass movement is particularly important for understanding rockfall runout behaviour as trees can act as natural barriers (Bigot et al., 2009).

2.4.4 Age, state and rate of mass movement activity

Various methods exist for establishing chronologies which can be used to understand the causes of mass movement, generate frequency-magnitude relationships and facilitate hazard prediction and prevention (Lang et al., 1999; Helsen et al., 2002; Corominas and Moya, 2010). For instance, dendro-chronological investigations were carried out in Canada (Harris and McDermid, 1998) and in Germany (Gers et al., 2001), whilst a chronological classification (Table 2.2) was developed in Spain using ^{14}C age determinations of mass movement deposits (González-Díez et al., 1999). The relative frequency and magnitude of rock fall events was established using dendrochronology in the Spanish Pyrenees (Moya et al., 2010). More recent cosmogenic techniques use ^{36}Cl and ^{10}Be to date bedrock exposed after landslide events (Ivy-Ochs et al., 2009; Le Roux et al., 2009). Although lichenometric dating can only be used

for certain rock types (Lang et al., 1999), the method has been successfully used to characterise the relative timing of mass movement events in Scandinavia (Rapp and Nyberg, 1981), central and northwest Europe (van Steijn, 1996), the French Alps (Helsen et al., 2002) and the Polish Carpathians (Bajgier-Kowalska, 2008).

Group	Name	Morphological features	Class	Description
A	Recent	Crown, deposit and micro-morphological features are perfectly preserved. Show signs of recent activity; cracks, terraces, creep, tilted trees, solifluction lobes, boulder accumulations. Have a poorly vegetated surface.	1	Identified from aerial photographs, <25 years old
			2	25-200 years old Fluvial deposits
B	Young	Main crowns are well preserved, minor crowns slightly eroded. Deposits have smoothed surface, depressions show infilling. Surface vegetated with shrubs or trees.	3	200-3000 BP Historical movements, fluvial deposits
			4	3000-5000 BP Fluvial deposits
C	Mature	Main crown eroded, minor crowns not visible, deposits have very smooth surface and rills	5	5000-5500 BP Fluvial deposits
			6	5500-15 000 BP Fluvial and glacial (well preserved cirques)
D	Old	Very eroded crowns and deposits, with rills and gullies	7	15 000-30 000 BP Fluvial and glacial deposits (cirques and moraines)
			8	30 000-50 000 BP fluvial and glacial deposits (poorly preserved cirques)
E	Very old	Main crowns dismantled with deep gullies in the deposits	9	50 000-120 000BP Fluvial deposits
			10	>120 000 BP Fluvial deposits

Table 2.2 Criteria used for classifying mass movements according to preservation of morphology and chronological sequence (after González-Díez et al., 1999).

Hansen (1984) suggests that the state of mass movement activity is a better indicator than the age of movement, because it anticipates the possibility for future reactivation. However, terms such as ‘active’ or ‘dormant’ have a wide variety of interpretations and meanings attached to them (Flageollet, 1996).

Qualitative descriptors of activity, such as ‘relict’, ‘extinct’, ‘fossil’, ‘recent’ and ‘older’, have been used to highlight the progressive development of mass movements (Ohlmacher and Davis, 2003; van Den Eeckhaut et al., 2009; van Den Eeckhaut et al., 2010). Terminology exists for describing the degree of mass movement activity in relation to its development, stabilisation and age. Stages of development have been referred to as ‘initial’, ‘advanced’ or ‘exhausted’, whilst stages of stability include ‘active’, ‘dormant’ and ‘stabilised’ (Zaruba and Mencl, 1969). These have limited application as they represent site-specific attributes that are hypothetically rather than quantitatively derived.

Frequency-magnitude relationships have also been used to determine the return periods of mass movement activity (Table 2.3), as this method may be more universally applicable where mass movements are triggered by seismic events, high magnitude rainfall events or during particular climatic episodes (Ohmori and Hirano, 1988; Flageollet, 1996; Crozier and Glade, 1999; Nyssen et al., 2003; Brardinoni and Church, 2004; Guthrie and Evans, 2004; Katz and Aharonov, 2006; Gabet, 2007; Hungr et al., 2008; Corominas and Moya., 2010; Jakob and Friele, 2010). Most classifications describe the rate of movement in relative rather than absolute terms. Soil creep represents the slowest movement type, whilst falls and topples are the most rapid.

Velocity classes for mass movements were identified by the Working Party for World Landslide Inventory (1994) to determine the impact of speed on structures (Dikau et al., 1996). Movements with an ‘extremely rapid’ velocity of $>3\text{m/s}$ are associated with major destruction of property and loss of human life, whilst movements of ‘rapid velocity’ ($>1.5\text{m/day}$) may enable evacuation, yet buildings and roads are likely to be destroyed. Movements that have a ‘very slow’ to ‘extremely slow’ velocity ($\leq 0.016\text{m/year}$) will not cause damage to solidly built structures (Dikau et al., 1996). Recently, the velocity and areal

extension of Italian mass movement landforms were compared in a matrix to define the intensity of events. The matrix was then used to define the nature of a mass movement hazard, so that a low frequency, low intensity movement is rated as a low hazard, whilst a high frequency, high intensity movement is rated as a high hazard (Colombo et al., 2005).

State of Activity	Type of Activity	Return Period	Period of Last Activity
Inactive- definitely or in long term			Pre-Quaternary (> 2 mil yrs BP)
Stabilized- temporarily or in a predefined period		Long term >1000 yrs	Pleistocene Lower-(700k- 2 mil yrs BP) Middle-(125k-700k yrs BP) Upper-(10k-125k yrs BP)
Dormant- renewal failure	Singular or episodic	Low frequency (100-1000 yrs) Medium frequency (0-100 yrs) High frequency (1-10 yrs)	
Active- as a first time failure at an old or new site or as reactivation	Intermittent- seasonal or non-seasonal or continuous	Very high frequency (< 1 year)	Holocene Ancient-(3000-10 000 yrs BP) Ancient historic-(200- 3000 yrs BP) Recent historic-(1-200 yrs BP) Present

Table 2.3 A temporal classification of mass movement activity (after Flageollet, 1996).

Volumetric diffusion rate has been used to define quasi-continuous and episodic mass movements (Martin, 2000; van Asch et al., 2007). Movements with a diffusion rate of 0.0002 m² per year are classified as ‘slow’ movements, whilst movements diffusing at a rate of 0.1 m² per year have been classified as ‘rapid’ (Martin, 2000). Simpler classifications define ‘rapid’ as movement occurring at a speed of >1.5 m/day and ‘less than rapid’ movement as <1.5m per day (Hungar et al., 2001). Obtaining quantitative measures of velocity is difficult unless specialised equipment is placed at the site and continually monitored.

2.4.5 Movement

Movement type has been a frequently used factor for the classification of mass movements from as early as 1875 (Hansen, 1984). Slides and flows were first distinguished by the presence or absence of a slip surface. Flows were associated with continuous deformation that displayed no evidence of shearing, whilst slides were identified by finite shear (Sharpe, 1938). Although flows may begin as slides and slides may develop into flows, the dominant form of the feature determines its type. Four primary types of mass movement were identified by Sharpe (1938) as slow flowage (soil creep, talus creep, rock creep, rock glacier creep and solifluction), rapid flowage (earthflow, mudflow, and debris avalanche), sliding (slump, debris slide, debris fall, rockslide and rockfall) and subsidence.

Possibly the most widely used classification is that by Varnes (1958), with subsequent improvements being made on the original classification, as new data became available. Although subsidence was excluded in the classification, creep, topples and spreads were consequently added. Movements consisting purely of ice and snow are termed avalanches and are excluded from the classification. Five main groups of movement are identified as falls, topples, slides, spreads and flows (Varnes, 1958). A sixth group represents complex movements, which are combinations of more than two of the five types. Originally, slides were subdivided according to the coherency of the mass, but this was later changed so that the subdivisions were based on the type of slide motion (i.e. rotational or translational), as this was found to have a greater influence on the design of stability methods.

More recently, slope movements have been classified into eight categories and several subdivisions by Hutchinson (1988) (Table 2.4). The categories include rebound, caused by natural or human induced movement, creep, sagging, landslides, flow-like debris movements, topples, falls and complex movements.

Type	Subtype
A. Rebound	1. Human excavation
	2. Naturally eroded valleys
B. Creep	1. Mantle creep: superficial, predominantly seasonal
	2. Mass creep: deep-seated, continuous
	3. Progressive creep, pre-failure creep
	4. Post-failure creep
C. Sagging of mountain slopes	1. Single-sided sagging associated with initial stages of movement
	2. Double-sided sagging associated with the initial stages of double landsliding leading to ridge spreading
	3. T-sagging or sagging associated with multiple toppling
D. Landslides	1. Confined failures
	2. Rotational slips
	3. Compound slides that are non-circular with listric or bi-planar slip surfaces
	4. Translational slides
E. Debris movements of flow-like form	1. Non-glacial mudslides
	2. Periglacial mudslides
	3. Flow slides
	4. Debris flows, rapid flows of wet debris
	5. Sturzstroms, extremely rapid flows of dry debris
F. Topples	1. Bounded by pre-existing discontinuities
	2. Released by tension failure at rear of mass
G. Falls	1. Primary, involves fresh detachment of material
	2. Secondary, involves loose material, detached earlier
H. Complex slope movements	1. Cambering and valley bulging
	2. Block-type slope movements
	3. Abandoned clay cliffs
	4. Landslides becoming mudslides or flows at toe
	5. Slides caused by seepage erosion
	6. Multi-tiered slides
	7. Multi-storied slides

Table 2.4 Summarised mass movement classification by Hutchinson (1988).

Creep is divided into non-periglacial and periglacial type creep, which is an improvement on the classification by Varnes (1958), as it includes all creep processes. The classification is comprehensive but complicated and repetitive so that the subdivisions of slides seem arbitrary, with no clear difference being made between confined slides and rotational, compound and translational

slides. Flow slides are classed under ‘debris movements of flow-like form’, but no clear distinction is made between flow slides and debris flows (Varnes, 1958).

Both Sharpe (1938) and Varnes (1978) understood that mass movement processes occur in relation to one another and that gradations exist between forms. These authors acknowledged that a rigid classification is impractical because it cannot encompass all the nuances of form. As mass movements rarely occur in isolation, combinations of movements identified in the 1958 classification were later reassigned as ‘complex’ (Varnes, 1978). Such complex varieties include ‘rock-fragment flow’, ‘slump-topples’, ‘rock slide-rock fall’ and ‘earth slump-earth flow’ (Varnes, 1978). This revised classification gained wide acceptance and was the most cited classification in the journal *Geomorphology* between 1994 and 2005 (Doyle and Julian, 2005).

In Japan, a third category of movement was added to the Varnes (1978) classification called ‘semi-translational’, to describe translational slides that have a curved shear surface and represent movements that are between translational and rotational (Dahal et al., 2009). In Italy, Varnes’ (1978) classification was modified to include hummocky topography where no landslides are observed, but where morphological, vegetation and geological factors suggested previous slope instability (Galli et al., 2008). Hutchinson’s (1988) classification has been modified to classify mass movements which occur exclusively in peat (Dykes and Warburton, 2007). The adopted terms, such as ‘bog burst’, ‘bogflow’, ‘bogslide’, ‘peat slide’ ‘peaty-debris slide’ and ‘peat flows’ are analogous to the mass movement types described by Cruden and Varnes (1996), Dikau et al. (1996) and Hungr et al. (2001).

Terms relating to the direction and mode of extension of the mass movement have been introduced by a number of authors including Varnes (1978, 1984),

Cruden and Varnes (1996) and Dikau et al. (1996). Movement is progressive if it occurs simultaneously above and below an existing feature, whilst retrogressive movement occurs above a feature. Retrogressive movements may conceal existing mass movements as the displaced material is deposited over depletion and transport zones. Movements advance if extension occurs in the direction of movement, which is usually downslope. Movement is defined as complex if two or more types occur simultaneously, or compound if a combination of shear surfaces overlap. Multiple movements occur if there is repeated movement along the same shear surface and successive movement occurs when multiple movements develop in succession (Varnes, 1978, 1984; Cruden and Varnes, 1996; Dikau et al., 1996).

Keefer (1984) developed a classification for landslide types caused by earthquakes grouped into three categories, namely; I) disrupted slides, falls and avalanches, II) slumps and blockslides and (III) lateral spreads and flows, which were then subdivided according to material type. This classification was successfully adopted in the USA to predict the possibility and areal concentration of earthquake-induced landslides (Miles and Keefer, 2009). A similar classification describes category I as 'rockslide avalanches', category II as 'coherent landslides' and introduced a third category called 'mobilization of valley fill' (Chigira and Yagi, 2006). Another classification based on movement type, developed for periglacial mass movements, identified 'mudflows', 'flowslides/skinflows' and 'detachment slides' as classes which represent a continuum of thaw-induced landslide mechanisms (Harris et al., 2008).

2.4.6 Morphometry

Heim [1932, in Sharp (1938)] was one of the first authors to separate the form of a landslide into three zones in order to accurately describe the nature of the processes occurring within them. An upper region, middle section and zone of deposition were identified, and the geometry or morphometry of these zones

was used to describe mass movement types in later classifications (e.g. Blong, 1973a, 1973b; Crozier, 1973). The morphometric attributes of the deposited material and failure surface were expressed as geometrical measurements and this method demonstrates a shift from qualitative to quantitative classifications of mass movement.

Morphometric attributes were first identified by Skempton (1953), particularly the depth/length ratio, which was used to distinguish between rotational (slumps) and translational (slips) slides. Deviations in the range of depth/length ratios for a particular type are interpreted to indicate subsequent alterations to the mass movement form (Crozier, 1973). More recently, mass movement characterisation has been based on geometric or morphometric attributes (c.f. Baroni et al., 2000; Gerrard and Gardner, 2000; Malamud et al., 2004), which are also used to differentiate between types of flow phenomena (Crozier, 1996; Legros, 2002; Jakob, 2005).

The morphometric attributes identified by Blong (1973a, 1973b) include the slope length, angle, width, area and perimeter of the erosional zone, height of the headwall and volume of the failed mass. Slope angle above the crown and total slope length from the crest of the hillslope to the base of the shear plane are used for determining the percentages of failed mass to total slope area (Blong, 1973a, 1973b). Slides with steep gradients and erosional zones occurring close to the slope base apparently have smaller shear planes and depositional areas. This suggests that shear plane width increases for slides that are not limited in their downslope extent, and that gravity, described by the gradient of the slope, controls the form of the shear plane and nature of the displaced mass. Although some relationships exist between the morphometric attributes, no single attribute can be used to distinguish between landslides (Blong, 1973a, 1973b).

Seven morphometric indices were used to classify 66 landslides in New Zealand, which are based on the depth of the displaced mass, modified depth/length ratios, width, fluidity and rate of displacement (Crozier, 1973). Dilation or spreading of the displaced mass was suggested to be an important descriptor of flows, which become narrower in width with length downslope, and have low tenuity values. Slides have higher displacement values than flows, whilst shallow flows have higher flowage and fluidity values than slides (Crozier (1973). More recently, morphometric attributes obtained from landslide inventories in Italy, Guatemala and the United States were compared to determine frequency-size distributions (Malamud et al., 2004) and morphometric attributes were used in Belgium to identify large, deep-seated landslides (Demoulin and Glade, 2004). A volume-based classification was adopted in China which recognises ‘extreme large-scale’ landslides ($> 1.0 \times 10^8 \text{m}^3$), ‘large-scale’ landslides ($1.0 \times 10^7 - 1.0 \times 10^8 \text{m}^3$) and ‘medium-scale’ landslides [no values given] which are further subdivided according to displaced material (Keqiang et al., 2008).

Although using measured variables provides useful quantitative information, it is often difficult to measure these attributes in the field. Calculating the depth of the shear surface is particularly problematic as subsequent movements may conceal the location of the surface, and the height of the main scarp is not necessarily representative of the true failure surface. Obtaining volumetric measurements is therefore not always possible and measurements need to be inferred. Measuring mass movement area is also problematic because the zone of depletion may not represent the entire shear surface, thus predictions generally underestimate the total area that is affected by mass movement.

More recent morphometric approaches have been developed using synthetic aperture radar (SAR) and light detection and ranging (LIDAR), as well as a variety of airborne and space-borne laser scanners for creating remotely sensed

data (Kääb, 2008). Classifications using remotely sensed data have emerged where field work is limited due to cost or time constraints. Approaches are similar to those used for landcover mapping, and images are classified according to surface roughness and texture elements or transformation properties. Pattern elements and diagnostic features can be used to identify unstable terrain, whilst mass movements can be identified from aerial photographs, depending on the scale of the image (Rib and Liang, 1978; Mantovani et al., 1996). Airborne and ground-based laser scanners produce very detailed Digital Elevation Models (DEMs) of up to 1m resolution that can show the characteristic morphology of different types of movement as disturbed areas exhibit distinctive spectral peaks that are different to that of smooth, unfailed terrain (Bichler et al., 2004; McKean and Roering, 2004; Chigira et al., 2004; Reidel and Walther, 2008)

SAR has been used to monitor movement rates in a variety of geological and altitudinal settings (e.g. Bovenga et al., 2006; Colesanti and Wasowski, 2006; Corsini et al., 2006; Rott and Nagler, 2006; Noferini et al., 2007; Peyret et al., 2008), whilst LIDAR has been used to map and characterise morphometric attributes for mass movement landforms and monitor rates of movement (e.g. Chen et al., 2006; Glenn et al., 2006; Schulz, 2007; van Den Eeckhaut et al., 2007; Dewitte et al., 2008; Avian et al., 2009; Baldo et al., 2009; Kasai et al., 2009; Lan et al., 2010).

2.4.7 Geographic, geologic and spatial homogeneity

Prior to the 1940's, mass movement features were named according to their location (Hansen, 1984). These mass movements were usually localised, singular catastrophic events that occurred in populated areas and studies focussed on determining the cause of failure (Comegna et al., 2007; Floris and Bozzano, 2008). Contemporary research on mass movements is sometimes

limited to a specific feature, such as the Black Ven mudslide in the United Kingdom (Brunsden and Chandler, 1995), the Zymoetz River landslide in Canada (McDougall and Hungr, 2004), the Ca' di Malta landslide in Italy (Mora et al., 2003) and the Super-Sauze earthflow in France (Flageollet et al., 1999, 2000; Malet et al., 2005). Classifications based on location have been used to distinguish between mass movements that occur in mountainous regions with those occurring on ocean floors (Moore and Mathews, 1978), or those occurring at particular altitudes (Hewitt, 1993) and along coastal cliffs (Hutchinson, 1983; Margielewski and Urban, 2003; Brunsden and Lee, 2004).

Terrain units represent another type of geographical characterisation which were originally developed to assist with hazard analysis, particularly for GIS-based assessments. Terrain units may be divided into equal area grid cells or unique polygons that represent areas of homogeneity. 'Hard', 'intermediate' and 'soft' terrain types have been identified, and are based on slope curvature, angle and altitude (Pike, 1988). Rapid debris flows and debris avalanches occur on hard to intermediate terrains, whilst slow seasonal sliding, associated with earth flows and slides, generally occur on intermediate to soft terrains (Pike, 1988). The Hypothetical Nine-Unit Land-Surface Model was used to show how mass movements could be classified according to their occurrence on landforms with particular combinations of vertical (profile) and lateral (plan) curvatures (Dalrymple et al., 1968). A similar approach was used in the Blue Nile Basin to show that rockfalls occur on concave-planar slopes (sloping valleys), whilst slides occur on slopes that are planar-planar (sloping flats), concave-concave (sloping closed basins) and concave-convex (sloping recessing hills) (Ayalew and Yamagishi, 2004). Convex-convex slopes (sloping inflated hills) are suggested to be the most stable form of curvature combinations observed in the Blue Nile Basin area (Ayalew and Yamagishi, 2004).

Another form of terrain unit is the watershed unit which has a distinct topographic boundary. Watershed morphometric attributes and flood data have been used to differentiate between watersheds that experience debris flows, debris floods and flood activity (Wilford et al., 2004). Watershed basins have also been classified according to lithology, soil type, slope gradient, average rainfall and return period in order to compare the morphometric attributes of debris flows (Tiranti et al., 2008). Drainage divides (Carrara et al., 1991), unique polygons (van Westen et al., 2000), Soil Mechanical Response Units (Möller et al., 2001) and Unique Condition Units (Clerici et al., 2002) represent spatially homogenous units that contain combinations of attributes that are associated with mass movement .

Characterisations and classifications based on geographic locality include those that define mass movements according to the geological, lithological or rheological material within which movement occurs. For instance, Schmidt and Beyer (2001) identified that falls in Germany occur on steep Wellenkalk cliffs of marine sedimentary origin composed of shell limestone, whilst flows are limited to clays found at the base of these slopes. In southeast Britain and Canada, mass movements have been characterised according to the stratigraphic structure and dip of mudrocks (Cruden, 1988; Bromhead and Ibsen, 2004). Features are referred to as ‘dip-slope failures’ where the dip of the bedding is steep, whilst failures are referred to as ‘bedding-controlled’ landslides where the sliding surface is controlled by the location and orientation of a single argillaceous bed (Bromhead and Ibsen, 2004).

In Turkey, rotational slides have been recorded in unconsolidated to semi-consolidated clay and mudstone, whilst translational slides have been observed in thin to medium bedded marl (Yesilnacar and Topal, 2005). Variations in the underlying geology and tectonic composition of the slope are also known to influence mass movement types in Italy (Sorriso-Valvo et al., 1999; Caniani et

al., 2008), whilst pyroclastic deposits, weathered tuff, colluvium, and depression fill are the predominant material types in which mass movement occurs in Japan (Chigira et al., 2004; Chigira and Yagi, 2006) and Canada (Sterling and Slaymaker, 2007). However, similar mass movement types may occur in dissimilar geological settings, hence Sharpe's (1938) suggestion that material type is an insufficient classifier.

Mass movement type has been related to biophysical diversity, namely in three areas; site diversity, soil diversity and habitat diversity (Geertsema and Pojar, 2007). The type and magnitude of a mass movement will determine the nature of the biophysical response; for example, large, deep-seated landslides produce more surface expression than shallow translational slides, which in turn affects soil texture and porosity. The effects of mass movement on fluvial systems have also been discussed as rock avalanches may cause damming of river systems, whilst debris flows can create localised turbidity which affects the health of aquatic ecosystems (Montgomery et al., 2003).

2.4.8 Nature of the displaced material

The coherency and content of material displaced by a mass movement are commonly used in classifications of mass movements that progress from slides to flows. Classifications and characterisations can be based on particle size, relative proportion of particle sizes, deformation characteristics, coherency, origin and total air, ice or water content. The classification of Varnes (1978) presents the best example of material type as a secondary classifier (Table 2.5). Materials are separated into bedrock and engineering soils which are subdivided into predominantly coarse and fine grained categories. Bedrock is defined as hard or firm rock that was intact prior to collapse. Engineering soil is described as any transported or residual unconsolidated or loose aggregate of solid particles that occurs in a natural mineral, rock or inorganic composition,

together with any interstitial gas or liquid (Varnes, 1978). A modification of this classification was adopted in China to describe landslides which were classified as ‘rock mass’ and ‘colluvial’ landslides, whilst the rock mass category was further subdivided into ‘bedding’ and ‘dissected’ landslides’ (Keqiang et al., 2008).

Other definitions state that rock is a coherent, consolidated mass, normally of significant proportions and extent, whilst debris consists of material coarser than 2mm and occurs as clasts incorporated into a matrix of assorted materials (Dikau et al., 1996). Material has also been classified using the proportion of sand content to the overall composition of the displaced mass so that where the proportion of sand and finer sized particles is <80%, the mass is debris. Where the mass has >80% sand and finer particles, it is characterised as earth (Hung et al., 2001). The amount of peat in a mass movement can also be used to differentiate between types, especially in areas where peat deposits are extensive (Dykes and Warburton, 2007).

TYPE OF MOVEMENT	TYPE OF MATERIAL				
	BEDROCK		BEDROCK	ENGINEERING SOILS	
				Predominantly coarse	Predominantly fine
Falls			Rock fall	Debris fall	Earth fall
Topples			Rock topple	Debris topple	Earth topple
Slides	Rotational	Few units	Rock slump	Debris slump	Earth slump
	Translational	Many units	Rock block slide	Debris block slide	Earth block slide
Lateral spreads			Rock slide	Debris slide	Earth slide
Flows			Rock spread	Debris spread	Earth spread
			Rock creep	Debris flow	Earth flow
			Deep creep	Soil creep	
Complex	Combination of two or more principle types of movement				

Table 2.5 Classification developed by Varnes (1978).

The state of deformation that a material undergoes has also been used to classify mass movements as the conditions leading to deformation can be determined in a laboratory using a centrifuge (Harris et al., 2008; Khaldoun et al., 2009). Creep is defined as a type of flow rather than slide due to the transitional behaviour of the material from solid to plastic (Scheidegger, 1984). A regional classification for mass movements in Nepal identified different types of mass movements based on the eventual coherency of the deposit (Gerrard and Gardner, 2000). According to Gerrard and Gardner (2000), slumps and rotational slides have a relatively confined and coherent displaced mass, whilst debris slides break up on failure and travel further downslope, often reaching local drainage lines. Material origin has also assisted to differentiate between slope debris flows and gully debris flows (Glade, 2005).

Besides the ambiguous terminology that exists, material type cannot be considered a sufficient classifying attribute (Selby, 1993). Some mass movements, such as debris flows, sort and deposit displaced material during transport, which reduces the proportion of fines in the deposit. Other types of mass movement may incise into slope materials and incorporate material into the deposit, which does not reflect the stability conditions of the displaced material. It has been argued that separate inventories should be made for rockfalls and flows/slides because the physics involved are different (Malamud et al., 2004). This argument is supported by an understanding of the physics of motion. Rockfalls are controlled by fragmentation processes, whilst slides and flows are controlled by slope stability processes. Low-density debris flows or hyper-concentrated stream flows can also be excluded from a mass movement classification because they exhibit flood rather than flow or slide behaviour.

The presence and abundance of water, air and ice in a mass movement has been used to create subdivisions that reflect the gradations of form existing between successive types of mass movement (Sharpe, 1938, Harris and Gustafson, 1988,

1993; Gruber and Haeberli, 2007; Harris et al., 2008; Picarelli et al., 2008). A progression exists between stream flows (which have a high water content, low debris load and occur on low angled slopes), and landslides (which have a low water content, high debris load and occur on moderate to steep slopes) (Sharpe, 1938). Slope wash, sheetfloods, mud and earthflows, and debris avalanches are transitory phases between these two end members and are identified by relative water content (Kov anen and Slaymaker, 2008) (Figure 2.3). Water content has been qualitatively assigned and defined as dry (no visible moisture), moist (contains some water but no free water and may behave as a plastic), wet (enough water to behave as a liquid) and very wet (has enough water to flow as a liquid on low gradients) (Varnes, 1978).

		MOVEMENT		EARTH or ROCK				
		KIND	RATE	ICE			WATER	
				CHIEFLY ICE	EARTH OR ROCK PLUS ICE	EARTH OR ROCK, DRY OR WITH MINOR AMTS OF ICE OR WATER	EARTH OR ROCK PLUS WATER	CHIEFLY WATER
SIDE	FLOW	USUALLY IMPERCEPTIBLE	SLOW TO RAPID	ROCK-CREEP				FLUMAL TRANSPORTATION
				TALUS-CREEP				
FREE	FLOW	PERCEPTIBLE	RAPID	ROCK-GLACIER CRR	SOIL-CREEP		SOLIFLUCTION	
				DEBRIS-AVALANCHE		EARTHFLOW		
WITH	SLIP (LANDSLIDE)	PERCEPTIBLE	SLOW TO RAPID	MUDFLOW <small>SEMIARID, ALPINE, VOLCANIC</small>				
				DEBRIS-AVALANCHE				
NO FREE SIDE	SLIP FLOW	FAST or SLOW	SLOW TO RAPID	SLUMP				
				DEBRIS-SLIDE				
				ROCKSLIDE				
				ROCKFALL				
				SUBSIDENCE				

Figure 2.3 Sharpe's classification of mass movement phenomena (Sharpe, 1938).

Debris flow types have been subdivided into 'muddy debris flows' and 'granular debris flows', based on the water-debris mixture (Cousot and Meunier, 1996). Muddy debris flows are defined as flows in which the fine

fraction is large enough (>10%) for the fine particle-water mixture to form an interstitial fluid, which lubricates grain motions and imposes its behaviour on the mass. Granular debris flows contain enough fine particles for direct grain contacts to influence the movements of the mass (Coussot and Meunier, 1996). Water content, which influences pore pressure dynamics, has also been used to define mass movements (Hungr et al., 2001). ‘Dry sand flow’ is flow that occurs without significant excess pore pressure, whilst ‘sand flow slides’, ‘clay flow slides’ and ‘peat flow’ are associated with excess pore pressures or liquefaction, whilst ‘earth flow’ occurs by plastic deformation (Hungr et al., 2001) . According to Hungr et al. (2001), a ‘debris flow’ is a saturated non-plastic flow, whilst a ‘mud flow’ is a saturated plastic flow and ‘debris floods’ are surging flows of water heavily charged with debris. Centrifuge experiments have been used to compare critical slopes angles in a variety of soils which experience freeze-thaw. This method allowed for the classification of solifluction lobes, mudflows and ‘detachment slides’ based on the behaviour of the failed mass under different conditions (Harris et al., 2008). Mudflows occur in non-cohesive silt, whilst detachment slides occurred in over-consolidated silt-clay.

2.4.9 Geotechnics

Geotechnical properties represent an engineering approach to classification and characterisation of mass movements, based on quantitative measures of the external and internal stability of slope forming materials. Geotechnical properties are usually used in hazard models rather than classifications, because they are determined for a single or generalised type of mass movement activity that occurs under site specific conditions (c.f. Brooks et al., 1995; Chen and Lee, 2004). Consensus on a geotechnical classification of mass movement types has apparently not yet been reached and a working committee has recently been

established by the Joint Technical Committee on Landslides and Engineered Slopes to deal with this (Fell et al., 2008).

Typical methods used to characterise slope stability include ground penetrating radar (GPR) (Sass et al., 2008; Yalcin, 2008), DC electrical resistivity (Perrone et al., 2006; Erginal et al., 2009; Piegari et al., 2009) and seismic reflection and refraction which can produce detailed 3D models of a site up to 80m deep (Bichler et al., 2004). Originally, 2D and 3D spatial imaging was used for shallow geophysical analyses, but 4D (space and time) modelling has since been developed (Jongmans and Garambois, 2007). Borehole data, inclinometers and piezometers are used to locate failure surfaces, calculate displacement rates and measure soil moisture; such data are then used to produce geophysical models. Limit equilibrium slope stability models are then developed to confirm the findings of the geophysical models, a procedure known as ‘back-analysis’ (Ko Ko, 2004).

Geotechnical classifications are most commonly used for characterizing rock masses which may be susceptible to rock fall. Information related to the geology, dip, discontinuity spacing and orientation are most commonly used to calculate a rating which represents the stability of the rock mass (Schweigl et al., 2003). The direct Rock Quality Designation is a measure of the degree of jointing in borehole cores and is described as ‘Very Poor’ (RQD% <25) to ‘Excellent’ (RQD% >90-100), whilst the indirect RQD can be estimated from the number of joints per unit volume (Singh and Goel, 1999). The Rock Mass Rating, originally developed by Bieniawski (1989) has also been used to classify rocks stability and describes rock masses according to the uniaxial compressive strength of intact rock material, RQD, joint or discontinuity spacing, joint condition, ground water conditions and joint orientation (Pantelidis, 2009).

2.4.10 Summary

From the discussion thus far, it is apparent that a wide variety of approaches exist for classifying and characterising mass movements. Ultimately, mass movement categorisations are developed to serve a particular purpose. A classification or categorisation that focuses on rate of movement and the size of the displaced mass is most valuable for urban settings where town planners need to consider mass movement frequency-magnitude relationships in a development context. However, a classification that categorises movements according to type and climatic setting would be more useful for assessing the impacts of climate change. Geotechnical classifications and categorisations are important when detailed information is required by engineers about site-specific conditions, particularly for the rehabilitation or prevention of mass movement activity that could lead to damaged infrastructure or the loss of life. Thus, the quality of a classification needs to be evaluated within the context of the study and its location.

2.5 Mass movement types

The proposed classification is primarily based on movement type and is described by the appearance and morphological form of the mass movement features and the style of movement. Illustrations are used to portray how a feature may appear in the landscape, and alternative terminology is included in the description of a movement type to provide assistance when comparing between classifications (c.f. Dikau et al., 1996). The description is important because it provides information that may be used for feature classification in the field or during API investigation. Only causes and environmental attributes that are characteristic of a type are included in the description, whilst a more general summary of conditioning and trigger mechanisms is presented in section 2.6.

2.5.1 Falls

Falls originate when material detaches from a steeply inclined surface such as coastal cliffs, river banks, escarpments and bedrock outcrops and travels for at least part of its trajectory by free-fall (Margielewski and Urban, 2003). The detached mass may break up, bounce or roll when impacting on the slope below, and a transition exists between bouncing and falling motions so that a short slope inclined at $<76^\circ$ will cause bouncing, whilst long slopes of $<45^\circ$ will generate rolling (Cruden and Varnes, 1996). Movement is usually rapid until the mass reaches the foot of the slope, whilst the distance that the falling material will travel is controlled by the topography of the slope and the presence of obstacles which prevent movement. Falls are characterized as high energy and mobility events which are usually volume limited (Agliardi and Crosta, 2003; Zimmer et al., 2012). Repeated falls from the same area may form a fan shaped cone of debris, or if the displaced material has sufficient velocity, it may be deposited on the opposite side of the valley (Cruden and Varnes, 1996).

Although the mechanics of failure may be different, the surface of separation is similar to the shear surface of a sliding motion (Cruden and Varnes, 1996). Within bedrock, the surface of separation forms along faults, joints and bedding planes, whilst in consolidated soil bodies, undercutting by stream incision creates stress cracks which act in a similar manner to joints and fractures in rock (Figure 2.4). The form of the rupture surface is controlled by the orientation of the joints and faults in the material, and the surface may be planar or wedge-shaped if the joints intersect (Romana, 1988).

The runout distance which rock falls achieve is determined by slope roughness, the volume of the displaced blocks, the energy lost during impacts with the slope and the initial velocity of the fall (Antoniou and Lekkas, 2010). Runout distances can be determined from the observed location of existing displaced

blocks to 3D kinematic models which use a Digital Elevation Model and assuming falling rocks will follow the same path as water (Jaboyedoff and Labiouse, 2011).

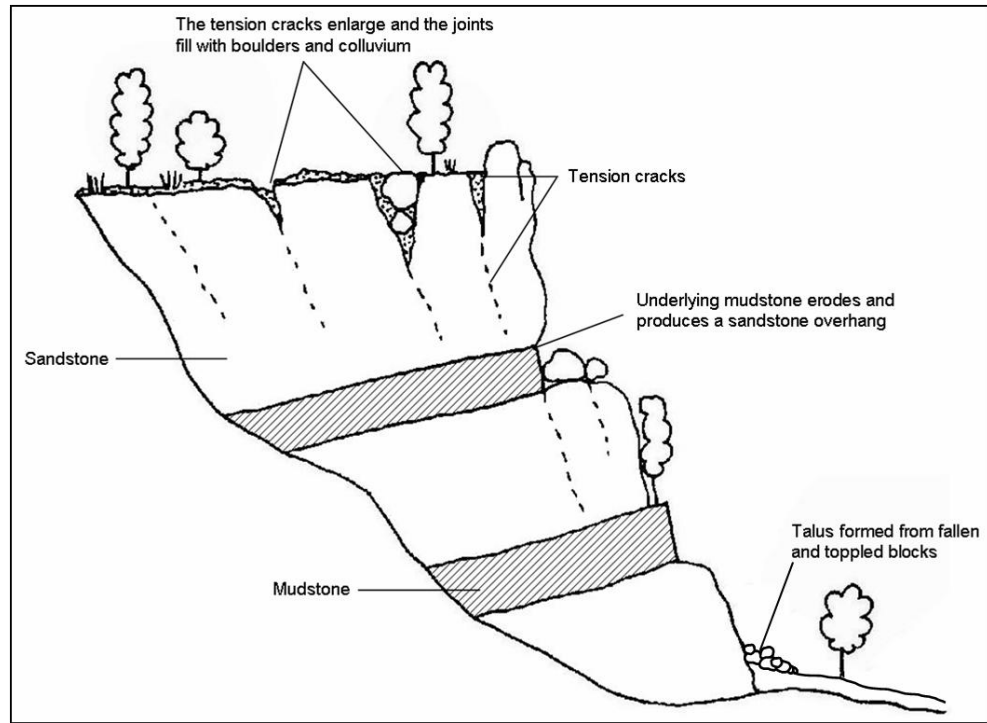


Figure 2.4 Cross-section showing internal deformation due to tensional fissuring. Colluvial material is deposited in the cracks and may reduce the strength properties of the surrounding rock by chemical and mechanical weathering.

Direct causes of falls are due to factors (cryoclastic, thermoclastic or biotic) that widen or enlarge discontinuities or cause mechanical rupture or chemical deterioration (Flageollet and Weber, 1996). Potential fall sites have steep to vertical faces and are common where overhangs, undercuts or cracks occur in the vicinity of the slope face due to stream incision, wave action or weakening of the underlying material (Figures 2.4 and 2.5) (Margielewski and Urban, 2003).

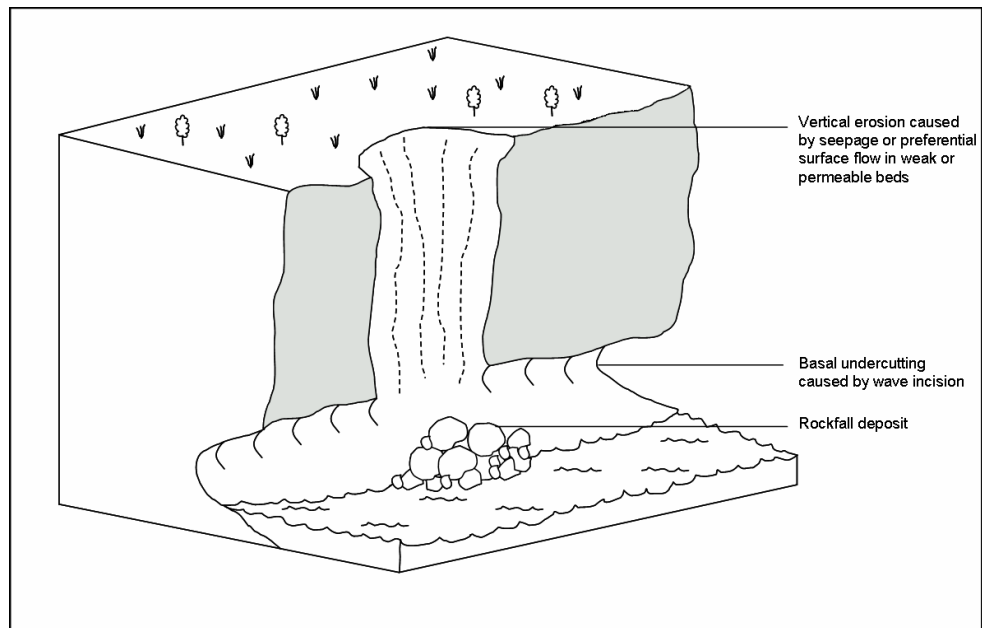


Figure 2.5 An example of a fall caused by basal undercutting along a cliff face. Basal undercutting is due to wave action although a similar process may be expected along streams and above soil pipes (after Flageollet and Webber, 1996).

Falls have been included in the classification proposed for the southern Drakensberg, however the distribution of fall source areas is almost impossible to determine remotely, because rock faces in the UDP are almost vertical. The deposits of rock falls can be easily mapped and heuristic and statistical methods may be adopted to identify clusters of deposited material. Once the deposits have been identified, it is possible to use 3D modeling to trace back the source areas of the deposits (Antoniou and Lekkas, 2010; Pirulli et al., 2011).

2.5.2 Topples

A topple is the movement of a mass about a pivot or hinge on a slope (Varnes, 1978). Movement may result in falling, bouncing, rolling or sliding but the movement tilts before collapsing (Dikau et al., 1996). Toppling may occur in soft rocks, such as schists, limestone caps or thinly bedded sedimentary formations or brittle rocks such as basalt or dolerite. Causes of toppling are the same as those for falls, but include the loss or weakening of elastic underlying

material (Romana, 1988). Topples differ from falls because during toppling, the load is transferred to the base of the detached mass. The height of the vertical face above the slope and the width of the column base are important factors that determine whether a topple will develop into a fall (Figure 2.6).

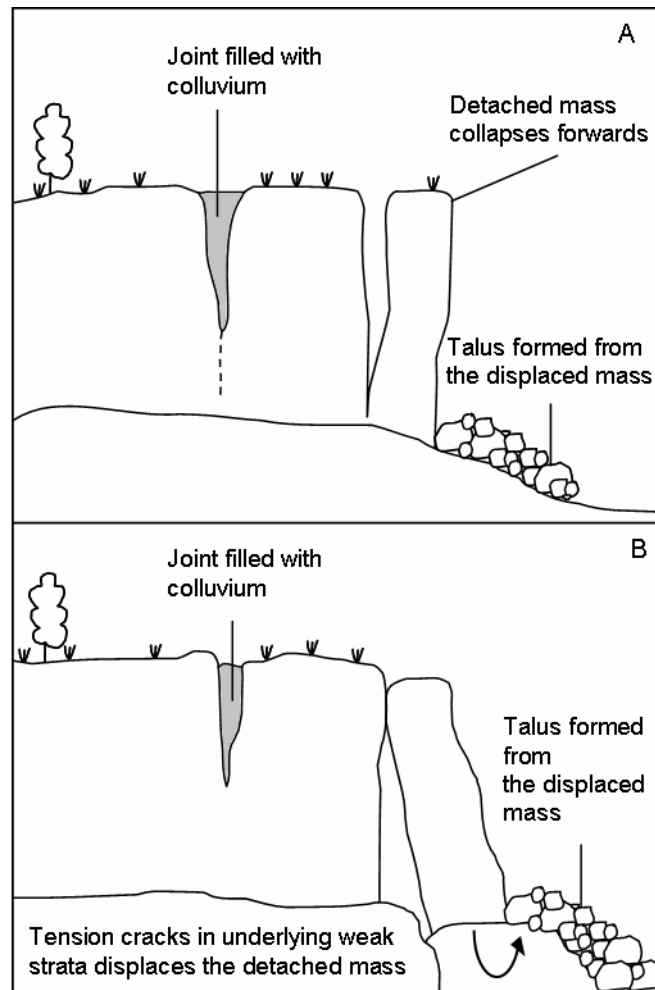


Figure 2.6 Different mechanisms of toppling action. Figure A shows the forward rotation of a rock mass that has become separated along a joint. Figure B shows the backward rotation of a rock mass that has tilted due to a deep-seated rotational slide at its base (after Cruden and Varnes, 1996).

Numerous topples were observed in the study area, however the same problems associated with mapping rockfalls applies. Whilst most topples remain close to the rock face from which they separated, some may roll downslope. It is

therefore difficult to infer from an aerial photo whether the primary type of movement was as a fall or a topple, although it may be possible to identify the source area.

2.5.3 Slides

The slide category represents all movements that occur along a recognisable shear surface. The shear surface is a zone of ductile deformation between two undeformed blocks that have suffered shear displacement, and deformation is non-elastic and permanent (Harris et al., 2008). Slide movements may progress into falls or flows, depending on a number of external and internal factors, such as slope angle, velocity and water content. Consequently, composite and complex movements usually have longer runout lengths than single or multiple slides due to the transmission of kinetic energy within the mass (Legros, 2002). This effect has been illustrated in Ethiopia using the average length-width ratio, which for ancient slides is 2.44 and for complex slide-flows is 5.56 (Nyssen et al., 2003).

The topography of a slide is irregular and hummocky, but over time it will become rounded by weathering (Buma and van Asch, 1996). Sliding produces a disrupted, anomalous drainage pattern when compared to the surrounding slopes, which may delay drainage and increase pore pressure (Varnes, 1984). Ponds and peaty areas may develop behind the displaced mass, whilst slide scarps become susceptible to rill and gully erosion and are sometimes confused with massive forms of sheet erosion (Ayalew and Yamagishi, 2004). Older slides are recognisable by their vegetation pattern, which reflects the hydrological condition of the slide. Light-tolerant, fast growing species will dominate on the shear surface, whilst drought-tolerant, shallow-rooting species will grow on the scarp, and deep-rooting, moisture-tolerant plants will occur at the foot of the slide (Cruden and Varnes, 1996).

Slides may occur in weathered soils, especially those derived from clay, mudrocks and silty clays. The weathered material moves over a shear surface of unweathered or lightly weathered bedrock, a pedological horizon (Baroni et al., 2000) or structural surface (Sorriso-Valvo et al., 1999). The angle at which the material fails may be related to the degree of weathering on the slope, the regolith depth and shear strength of the material (Varnes, 1978). If the slip surface is irregular, the surface expression of the slide may be a series of shallow terraces that have experienced buckling, heaving or wedging (Ibsen, 1994; Sorriso-Valvo et al., 1999). Areas prone to sliding are identified by irregular, wavy contour lines on topographic maps, discontinuous artificial lineaments and closely-spaced curved contour lines that depict scarps.

Rotational slides have a curved, spoon-shaped shear surface and are popularly referred to as slumps and slips (Figure 2.7). A single rotational slide usually experiences little deformation of the displaced mass (Cruden and Varnes, 1996). The rate of displacement will be less wherever hinging occurs in the mass. The length-width ratios of rotational slides are small and depth-length ratios range between 0.15 and 0.33 (Cruden and Varnes, 1996). Rotational slides may occur on slopes between 13°- 28° (Skempton, 1953; Crozier, 1973; Zêzere et al., 1999) and generally occur at greater depths than translational slides. The displaced mass moves almost vertically downward at the head of the slide and the upper surface tilts backward towards the scarp (Cruden and Varnes, 1996). As the mass starts to rotate, it may disaggregate into discrete blocks and terraces. Terrace formation, which is often associated with multiple rotational movements, is caused by tension cracking (Varnes, 1978). The cracks open intermittently and allow the displaced mass to travel a small distance at a time. Each tension crack is discernible by its scar and the surfaces of the terraces are usually vegetated. Terracettes and soil creep have been classified as a form of shallow rotational slide (Varnes, 1958; Buma and van Asch, 1996).

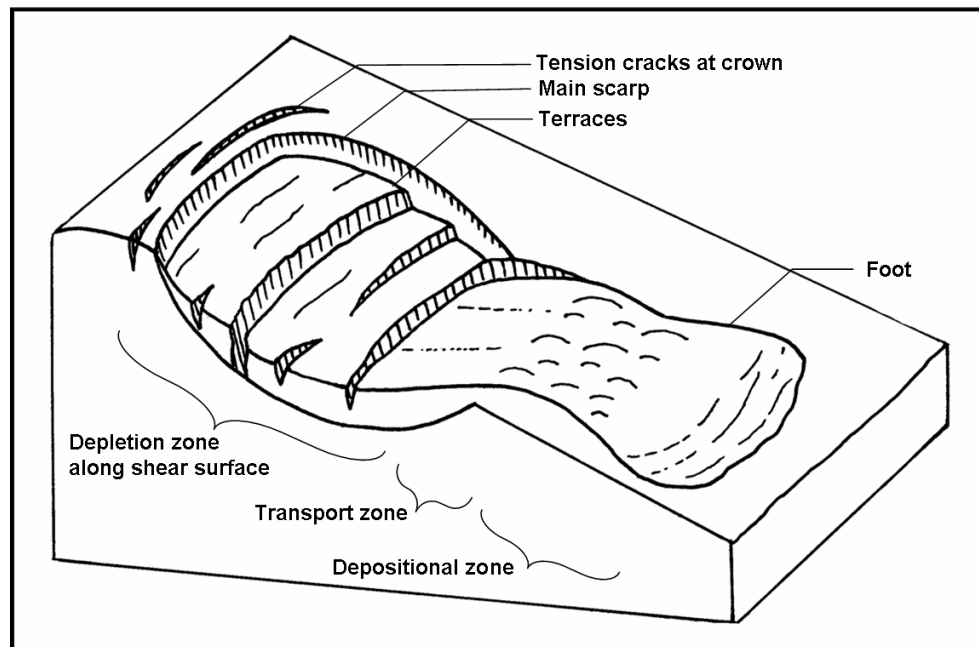


Figure 2.7 Example of a rotational slide.

Translational slides are non-circular failures that have a planar shear surface (Figure 2.8). The scarp of a translational slide is usually pronounced and nearly vertical and may have a crescent or u-shape. Translational slides are roughly rectangular in plan view and movement commonly occurs on low-angled shear surfaces parallel to the surface of the ground. The range of slope angles that failure occurs on is difficult to extract from the literature, as a variety of classifications are used, although slope angles between 11° - 50° have been associated with sliding movements (Zêzere et al., 1999; D'Amato Avanzi et al., 2004). Movements are usually shallow and have length-width ratios of between 0.5 and 1.5m (Corominas, 1996). The mass reaches an equilibrium condition when the bottom of the available slope is reached (Sorriso-Valvo and Gulla, 1996). However, translational slides may continue indefinitely if the conditions that create instability continue (Cruden and Varnes, 1996). With time, the slope will degrade to a lower angle and the shear surface will gradually disappear. The displacement and velocity of a translational slide tends to be higher than

that of a rotational slide due to the nature of the shear surface (Corominas, 1996).

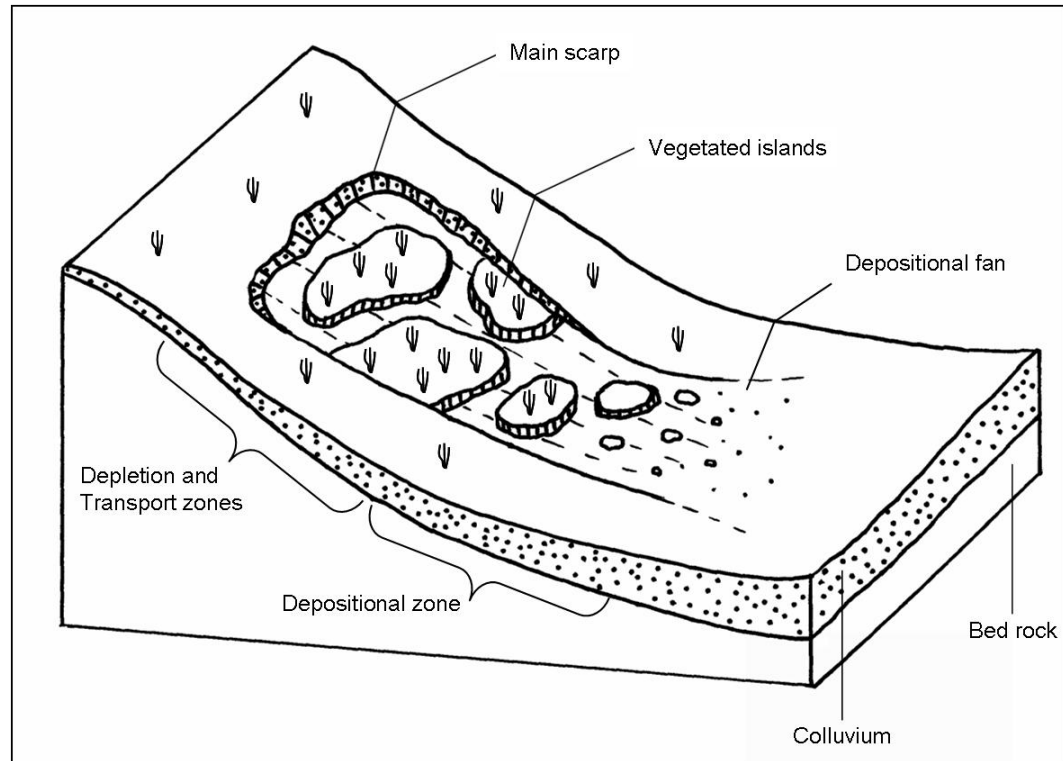


Figure 2.8 Example of a translational slide.

2.5.4 Flows

Flows move as fluid bodies over rigid beds (Hungr et al., 2001), which may be created by the presence of impermeable layers or a permafrost layer. The mechanics of motion in a flow are caused by internal processes of deformation rather than external stresses (Scheidegger, 1984). The material behaviour of a flow ranges from a strong, stiff plastic that forms relatively thick lobes, to a weak fluid with sufficient strength to form fans and levees, and which mould around rigid structures (Crozier, 1996; Msimlimba and Holmes, 2010). Flows are easily divided into a source, transport and deposition zone according to their morphological form. The source area is usually bowl-shaped because it is formed by a combination of tension cracks and slide scars (Blahut et al., 2010).

Flows occur on slopes with a threshold stability angle of 20°, although their presence on slopes between 2° to 41° has been recorded (Matsuoka, 2001; Cascini et al., 2011). In Nepal, 60% of slides occur on slope angles of 20° or less, whilst 60% of flows occur on slopes greater than 20° (Gerrard and Gardner, 2000).

The transport area is characterised by one or many transport channels which commonly follow pre-existing drainage lines and are usually steep, with linear or concave profiles. Track length is dependent on slope length and steepness (Brunsdon and Ibsen, 1996), viscosity (Corominas, 1996), volume (Legros, 2002) and earthquake magnitude where applicable (Sato et al., 2005). Debris from the slope may accumulate along the track periphery to form lateral ridges or levees which form by diminution of discharge, flow abandonment, lateral displacement, channel bank overflow or ground erosion (Corominas, 1996; Hungr et al., 2001; Wilford et al., 2004). Erosion, caused by scouring, may increase the sediment volume carried by the flow, and consequently alter the density of the displaced mass (Montgomery et al., 2009; Martha et al., 2010). The displaced mass will spread across valley floors or benches as the slope angle decreases and laterally-confining margins are removed, with deposition sometimes occurring in waves (Coussot and Meunier, 1996). In the Drakensberg, accumulation lobes form on planation surfaces that represent local base levels. The extent to which the mass is displaced, is an expression of its volume rather than drop height (Legros, 2002).

The accumulation zone generally has a lobe or fan-shape which extends upwards as more material is added. Deposits may have flat platy profiles, bulging, steep nosed profiles or elongated profiles with thicker mid-sections (Baroni et al., 2000). Higher concentrations of large boulders usually occur close to the lobe front, although flows can contain a wide distribution of grain sizes (Coussot and Meunier, 1996). Clasts in the flow deposit may orientate

themselves with their major axis parallel to the direction of flow, transversely as a semi-circle, or randomly depending on sediment concentration (Baroni et al., 2000; Wilford et al., 2004).

Flows in the southern Drakensberg occur as surficial or incised flows (Figure 2.9 and Figure 2.10). During a surficial flow, the displaced material is deposited over the surface of the slope as the flow loses momentum. Vegetation in the transport zone is flattened, whilst the particles in the deposit become finer and the thickness of the deposit decreases with distance downslope. During an incised flow, colluvial material and vegetation is removed within the flow channel, adding to the volume and velocity of the displaced mass.

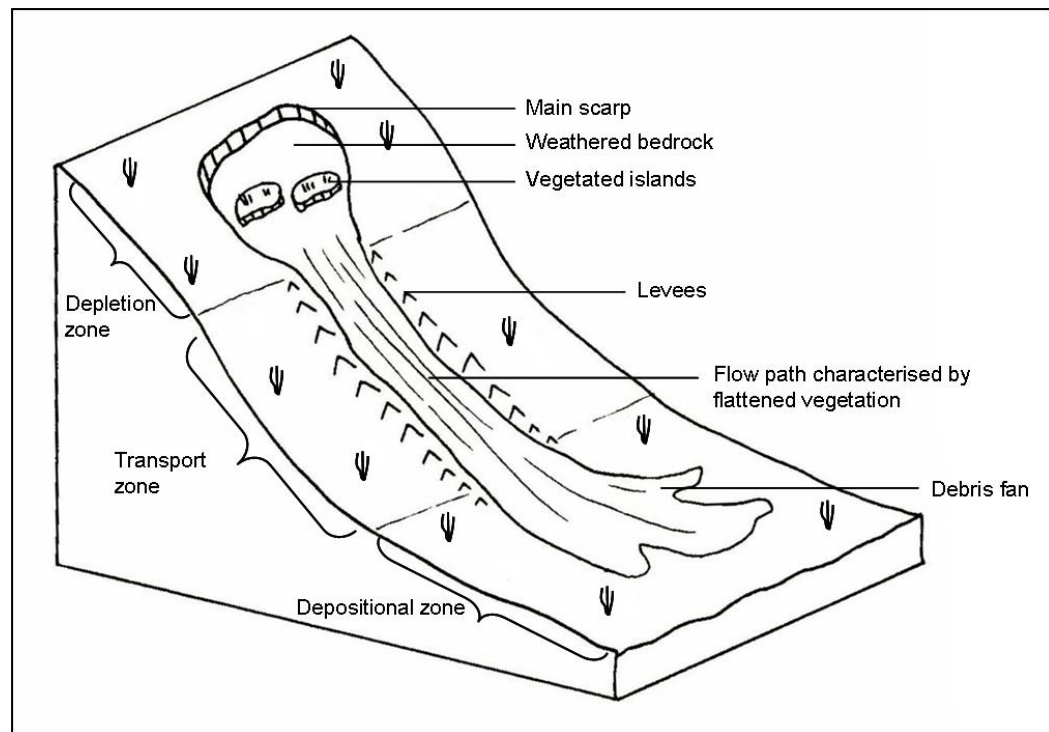


Figure 2.9 An example of a surficial flow. Material begins depositing within the transport zone.

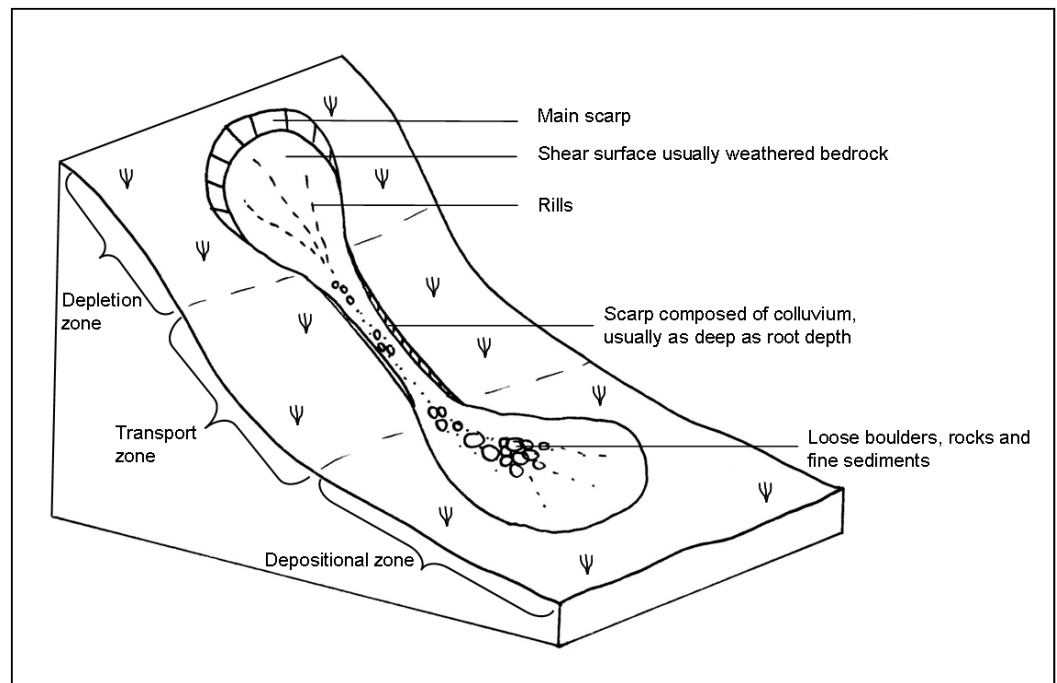


Figure 2.10 An example of an incised flow, with material being removed from the slope in the transport zone. Root depth is usually up to tens of centimetres.

Creep flows have a ‘humped’ profile and wavelike plan view (Scheidegger, 1984). The ‘humps’ are referred to as terracettes, which have a different genesis and morphology to terraces formed by slides (Figure 2.11). Creep flows on vegetated slopes usually occur at the bottom of the root zone and the vegetation may move downslope without being separated from the soil (Scheidegger, 1984; Dhakal and Sidle, 2003). On steeper slopes, where movement is more rapid, surface cracking may occur and result in stepped terracettes that occur intermittently to continuously (Selby, 1993). In Iceland, creep processes acting on plateaus and slopes angled from 2° push sediment onto adjacent slopes and into catchments (Glade, 2005). Consequently, empty sediment storages are continuously refilled and become source zones for channelised and surficial flows (Glade, 2005). Solifluction, which is a type of creep flow, is associated with saturated conditions created by seasonal thawing (Matsuoka, 2001). Permafrost within the active layer may provide a rigid flow surface for seasonally thawed material (Twidale, 1976). Conditioning factors expected to

influence creep processes are mean annual air temperature, mean annual ground temperature, and freeze-thaw dynamics (Matsuoka, 2001).

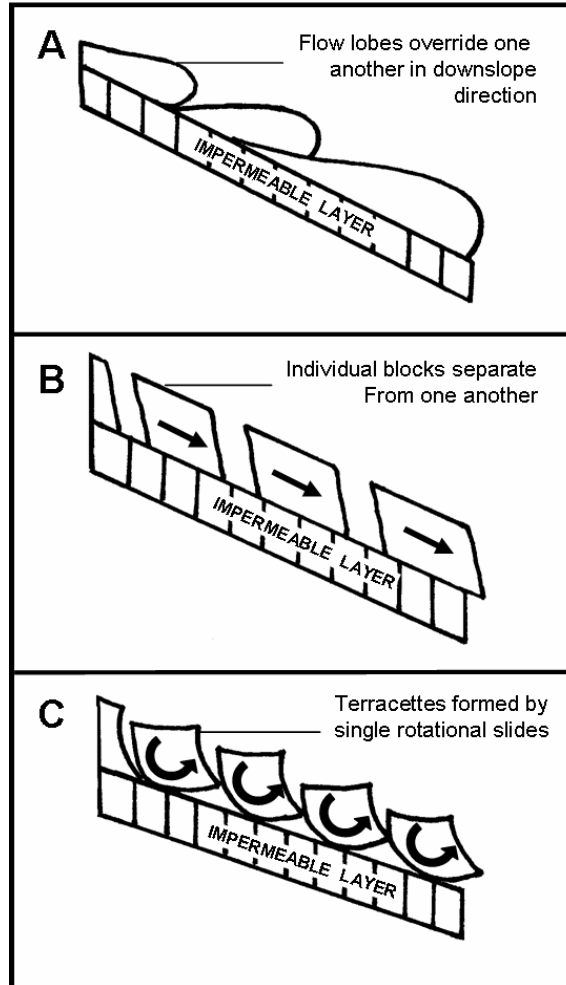


Figure 2.11 Some hypothetical mechanisms of terracette formation. (A) An example of creep flow associated with solifluction. The soil becomes saturated, loses cohesion and flows downslope. (B) An example of terracette formation as a result of translational sliding. (C) An example of terracette formation where each step represents a small rotational slide (after Bielecki and Mueller, 2002).

Flows are sometimes referred to as debris slides (Gerrard and Gardner, 2000), mudslides (Brunsden and Ibsen, 1996), and sagging or creep (Bisci et al., 1996). The term lahar is of Japanese origin and was introduced by Scrivenor in 1929 (Lavigne et al., 2000) to describe flows which occur on the slopes of volcanoes and are composed of volcaniclastic materials (Corominas, 1996).

2.6 Conditioning and triggering factors of mass movements

The processes that result in mass movement consist of a sequence of cause and effect events, thus no mass movement can be attributed to a single definite cause. Rather, a series of preparatory events or conditioning factors exist, which lead to increased shear stress or reduced shear strength (Varnes, 1978; Schmidt and Beyer, 2001). Trigger mechanisms of mass movements are distinct from conditioning factors because they cause an almost immediate response (Wieczorek, 1996). A mass movement will occur when the natural slope exceeds the limit for the balance of the materials composing it or when the strength of the material is less than the shear stress required for equilibrium (Flageollet and Weber, 1996).

As it is difficult to isolate a single cause of mass movement, it is sometimes necessary to evaluate all the potential causes of failure (Duncan and Wright, 2005). Surrogates of conditioning factors can be grouped into categories and substituted into prediction models where the causes of movement are unknown (Rib and Liang, 1978). Topography, which is defined by slope angle, orientation and length, curvature, and elevation, is the most important conditioning or preparatory attribute associated with mass movement activity, whilst increased rainfall is the most common trigger mechanism.

2.6.1 Factors that increase shear stress

Shear stress increases when the support of a slope is removed or if added load occurs at the top of a slope (Cruden and Varnes, 1996), both of which may be achieved naturally or by anthropogenic influences. Lateral support is lost when the toe of a slope is eroded by mass movements, fluvial/wave action, and chemical weathering, which cause slope steepening, falls and topples (Brunsdon and Lee, 2004). Apparently, excavations for cuts, quarries, pits and canals, as

well as drawdown in lakes and dams have the same effect (Duncan and Wright, 2005). Two-thirds of landslides in the Garhwal Himalaya are caused by the removal of lateral support by human activities such as road, footpath and terrace construction (Barnard et al., 2001). Changes in lateral pressure induced by thermal fatigue, hydrostatic expansion, clay hydration and mobilisation of residual stresses also result in increased shear stress conditions (Varnes, 1978). Shear stress may be initiated by transitory stress created by explosions or earthquakes and tectonic activity; whilst uplift may occur on steeper slopes and decrease stability due to renewed stream incision (Cendrero and Dramis, 1996; Cruden and Varnes, 1996).

The addition of material to the slope through mass movements may cause the length and height of the slope to increase. Previously displaced material, precipitation, volcanic activity, increased vegetation and anthropogenic activities are causes for increased load (Glade, 2000). Water introduced by irrigation systems and reservoirs, and melting from glaciers and permafrost due to global warming, may have a greater impact on adding load to a slope than precipitation (Buma, 2000; Duncan and Wright, 2005). Concave slope forms that concentrate surface and subsurface flow (Selby, 1993; Gerrard and Gardner, 2000), rising groundwater levels and percolating surface flow also increase surcharge.

2.6.2 Factors that reduce shear strength

Materials that have inherently weak material characteristics or discontinuities have low strength properties. For example, clays may be naturally weak or may become weak through weathering processes. The initial state of a material is characterised by the composition, texture or lithology of the slope materials (Montgomery et al., 2009), the existence of former mass movements (Zêzere et al., 1999), the presence of discontinuities (Cendrero and Dramis, 1996;

Hencher, 2010), massive beds over weak materials, strata inclined toward a free face and alternating permeable over impermeable beds (Twidale, 1976; Varnes, 1978; Cruden and Varnes, 1996). Changes to the initial state of the material are caused by weathering and physicochemical reactions, which cause clayey materials to soften and hydrate, or alternatively desiccate, crack and disintegrate (Varnes, 1978; Duncan and Wright, 2005). Intergranular pressures between soil particles are destroyed when they become saturated or frozen (Twidale, 1976), which may be caused by precipitation, rising groundwater levels, drainage pattern alteration and ponding (Duncan and Wright, 2005).

Vegetation removal in the form of logging or burning causes slope instability by increasing saturated soil conditions or reducing root support (Baum and Godt, 2010). Land units in Portugal that have short, sparse vegetation had a frequency of 20-51 mass movements/km² over a 37 year period, which was almost double the frequency of those recorded for more vegetated areas (Zêzere et al., 1999). Tree roots provide a mechanism for stabilising shallow soils that are prone to mass movement by anchoring the soil mantle to a more stable substrate such as bedrock or till. Dense networks of fine roots act as a membrane of lateral strength that holds the soil in place (Selby, 1993; Dhakal and Sidle, 2003). Wildfire may produce a hydrophobic soil layer that acts as a shear surface below and parallel to the burnt ground (Wieczorek, 1996).

2.6.3 Triggering events

The most common triggers of mass movements are rainfall, snowmelt, water-level changes, volcanic eruptions and earthquake vibrations (Cendrero and Dramis, 1996; Wieczorek, 1996; Cascini et al., 2011). Long duration, low intensity storms may trigger mass movements if the storms occur after prolonged wet periods (Glade, 2000), however high intensity, short duration storms are most commonly described as movement triggering events (Baroni et

al., 2000). A zone of transition exists between rainfall events that never trigger movement and those that always trigger movement, with the critical failure period being within a few hours of the rainfall peak (Casagli et al., 2006). The probability that mass movement will occur within this zone is given by the combination of rainstorm events, antecedent rainfall and soil moisture conditions, so that dry periods that precede unusually large storms may also be associated with mass movement activity (D'Amato Avanzi et al., 2004; Ayenew and Barbieri, 2005; Baum and Godt; 2010).

Increased precipitation associated with hurricanes may trigger mass movements, as these rainfall events are very intense and of long duration (Malamud et al., 2004). In the Garhwal Himalaya, the 30 largest slides that occurred in March 1999 were the result of intense rainfall events, whilst only two were earthquake induced (Barnard et al., 2001). Mass movement activity has also been related to the ENSO phenomena in Argentina, where more mass movements occur during warm El Nino episodes than during cold periods (La Nina) (Moreiras, 2005).

Rapid melting of snow, glaciers and permafrost caused by increasing air temperatures may also trigger mass movements (Cendrero and Dramis, 1996; Wiczorek, 1996; Ballantyne, 2002). Sudden water-level changes against a slope can trigger mass movements because a pore-water pressure gradient is created, which increases shear stresses within the slope material. Rapid drawdown occurs in dams and on river banks when a river drops after the flood stage or if dam overflow is released (Wiczorek, 1996). Storm waves cause cliff recession because they act as a drawdown mechanism and scour the cliff foot, and a possible critical wave height exists for initiating cliff foot erosion (Brunsden and Lee, 2004).

Volcanic eruptions and earthquake activity produce vibrations that cause liquefaction of cohesionless deposits during which pore-pressures are temporarily raised to produce lahars (Fukuoka et al., 2004). Repetitive vibrations created by tectonic activity promote horizontal and vertical earth accelerations that cause cyclic variations within the slope, increasing the internal stress above its static value and causing unstable conditions (Duncan and Wright, 2005; Sanchez et al., 2010). Not all earthquakes cause mass movements and even earthquakes of similar magnitudes within a study region are not guaranteed to cause uniform mass movements within the affected region. This is due to the influence that conditioning factors, such as aspect, soil moisture, and bedrock lithology have on slope stability (Fukuoka et al., 2004, Wen et al., 2004).

2.7 Developing a classification for mass movements in the southern Drakensberg

For the purpose of creating a classification for this study, certain assumptions have been made regarding terminology, which are explained in detail where appropriate. Type of movement is the primary discriminating factor, whilst the coherency of the displaced material and state and style of activity are used for creating subcategories (Dikau et al., 1996). The environmental attributes which may have caused mass movement are assessed for each type, but are not used as descriptive terms. The types of movement used in this classification are falls, topples, slides and flows and each type of movement is described by the nature of the displaced mass (Table 2.6).

This classification can be used to identify mass movement features in the UDP, however only some aspects were adopted for the API and statistical modelling. Translational slides were easily identified on the aerial photos, in combination with surficial and incised flows. Creep type movements, such as terracettes,

terraces and solifluction lobes were also relatively distinct. Large, palaeo-landslides with rotational shear surfaces were observed in the study area, which have been referred to as ‘deep-seated landslides’ by Sumner and Meiklejohn (2000) and ‘palaeo-landslides’ by Singh (2008).

Material with the behavioural properties of a:	Type of movement	Style of movement
Solid (rocks and boulders, consolidated soil mass)	Fall Displaced material moves down and away from its original position, may freefall, bounce or roll.	Single Movement occurs as a single event.
	Topple Displaced material displays a pivot action and rotates forwards before moving down and away from its original position.	Multiple Repeated events of the same type of motion in the same general location and along the same shear surface.
	Slide Displaced material moves along a shear surface that is easily identifiable as either a: Translational slide: movement is forward and parallel to a planar shear surface, or a Rotational slide: movement is backward and along a curved shear surface.	Composite Two or more types of movement occur simultaneously or as a result of an initial movement.
Plastic (particles of varying sizes, capable of being remoulded)		
Liquid (particles of varying sizes that are cohesionless)	Flow Material moves along a shear surface and parallel to the slope at a velocity dependent on the coherency of the mass. The plastic-liquid limit of the displaced material determines whether the flow occurs as a: Creep flow: displaced material shifts downslope in sheets and has a curved wave-like form. Surficial flow: displaced material flows over the surface of the slope, depositing displaced material as it flows downslope. Incised flow: displaced material has gouging effect on slope material, removing slope material as it flows downslope.	

Table 2.6 The classification proposed for mass movements in the southern Drakensberg.

In this study, palaeo-landslides are considered to be similar to ‘deep-seated slope gravitational deformations’ as defined by Agliardi and Crosta (2003), however they are assumed to have occurred under climatic conditions which no longer exist at present. Palaeo-landslides were therefore not included in the mass movement inventory as renewed movement at this scale is not expected to occur, nor are the variables being sampled representative of the same environmental conditions. Rockfalls are included in this study and are mapped according to the location of the rock movement deposits. Rockfalls and topples in the Drakensberg are assumed to occur almost continuously in response to ongoing rock weathering processes. Thus the deposits may represent rocks that have been displaced singly or as multiple events resulting in deposits that are superimposed on one another over time.

Material type is distinguished according to the internal coherency of the mass after failure has occurred, however it was not possible to identify this remotely given the resolution of the orthophotos. The coherency of the mass could be determined in the field by classifying the state of the displaced mass. Solid material has enough internal consistency to resist forces of shear stress, and displacement will occur along a zone of weakness once the shear strength of the material is overwhelmed with little deformation. Plastic material has enough internal coherency to remain en masse, but has reduced shear strength properties which allows the material to slowly deform in bending or buckling motions. Fluid materials have no internal coherency and low shear strength, and this enables the displaced mass to travel long distances in a short period of time.

Style of movement is a sub-category that allows for the establishment of hierarchical relationships between movement types. Style of movement and rate of movement were not included in the API or statistical modelling as time-series data were not used. Thus, the relationship between mass movement features could not be determined. Single movements are events that occur once,

whilst multiple movements are repeated movements of the same type. Composite movements involve two or more types of movement, which occur as a consequence of an initial movement. Examples are of slides which develop into falls when the material is displaced above a rock exposure, or when the displaced material associated with a slide loses its internal coherency and becomes a flow-type movement.

The proposed classification attempts to address a number of issues. Firstly, differentiating between erosion and mass movement processes has resulted in much confusion; both Sharpe (1938) and Twidale (1976) include particle movement as a form of mass movement, according to which rain-splash detachment and surface runoff should be categorised as mass movement processes. Although it is recognised that particle creep is a form of mass movement, the proposed classification only applies to movements of material occurring as an aggregated mass or body of particles. Secondly, the inclusion of subsidence has been problematic for classifications that focus on the horizontal movement of slope materials. As subsidence and vertical soil pipe collapse commonly occur in the Drakensberg, it is included in the proposed classification as a type of fall but excluded from the API due to the limited scale of the imagery. Thirdly, the classification includes solifluction and creep processes as types of plastic deformation in the flow category. Fourthly, the definition of and argument for the existence of a shear surface is often vague. For the purposes of this classification, slides are distinguishable from falls because they occur along a shear surface (Zaruba and Mencl, 1969), whereas falls occur along a surface of separation (Flageollet and Weber, 1996). Lastly, the classification does not include mass movements of the spread type as the geology of the area is limited enough to exclude forms of this type.

3 Mass movement modeling with GIS

3.1 Introduction

The evolution of GIS-based modelling has been controlled by the development of information technology in general. Three periods of development can be identified in the history of GIS: the 1950s-1970s represent the innovation stage where GIS technology was developed; the 1980s characterise the introduction of general-purpose GIS systems which coincided with the inauguration of the personal computer; and from the 1990s onwards the focus has been on user-orientated approaches (Goodchild, 2000; Malczewski, 2004). GIS in mass movement analysis, particularly in hazard prediction, has advanced from early hand-drawn manual overlays of attributes used during the 1950s and 1960s to advanced 2D and 3D models. Major developments in the applications of GIS for hazard mapping occurred in the 1980s (e.g. Carrara 1983, 1988, 1989; Brabb, 1984; Gupta and Joshi, 1990), with task-specific models being developed as the need for more accurate hazard assessments has increased. Reviews of the methods used to generate hazard maps can be found in Carrara et al. (1995), Soeters and van Westen (1996), Guzzetti et al. (1999), Weirich and Blesius (2007) and Alexander (2008).

A natural hazard has been defined as the probability that a potentially damaging phenomenon will occur within a given area during a given period of time (Varnes, 1984). This definition includes concepts of magnitude, location and frequency and can be used to identify the different types of mass movement hazard zonation techniques that exist. Predictive models identify the location of potentially unstable slopes by assimilating the relevant environmental conditions associated with mass movement development, whilst mass movement inventories describe the locations of previous mass movements (Guzzetti et al., 1999; Varnes, 1984; Huabin et al., 2005; van Westen et al., 2008).

Both approaches can be used to portray spatial information in the form of a map and/or database. The ideal map should indicate the spatial and temporal variations of mass movement type, magnitude, velocity and extent for the specified region. Separate maps should be made for each mass movement type as each motion is associated with unique terrain conditions that pose different threats under similar environmental conditions (Soeters and van Westen, 1996; Guzzetti et al., 1999).

3.2 Approaches towards modeling mass movements

Various approaches exist for mapping, modeling and predicting when and how a mass movement will occur. Choice of approach is determined by the expected applications of the maps, the size of the study area, the resolution of the data and the resources available to carry out the work (Malamud et al., 2004). Mass movement inventories, geomorphological analysis and statistical methods are commonly used for regional studies whilst deterministic methods are employed for more detailed site-specific studies (Baeza and Corominas, 2001; Akgun, 2012). All methods for modeling mass movement are based on three principles. Firstly, mass movements leave discernible morphological features on the landscape that can be identified, classified and mapped in the field or by remote sensing. Secondly, that movement is controlled by mechanical laws that can be determined by empirical, statistical or deterministic methods; and thirdly, that mass movement can be predicted (Guzzetti et al., 1999; Cascini et al., 2011).

3.2.1 Mass movement inventories and the heuristic approach

Mass movement inventories are the simplest form of mass movement hazard maps and show the location and types of mass movements within a region (van Westen et al., 2008; Akgun, 2012). Inventory maps may be combined with maps expressing various terrain parameters, such as topography, geology or

drainage to produce mapping units that are ranked into mass movement susceptibility classes (Casadei et al., 2003). Mass movement inventories are widely used during preliminary site investigations as an aid for selecting appropriate modeling techniques, as direct inputs into statistical models or as calibration and validation datasets for deterministic models (Fernandes et al., 2004). Mass movement inventories may be undertaken after a specific trigger event to determine the type and number of movements that were initiated by the event. However, the inventory will only provide information for the period immediately preceding the data collection process (Casadei et al., 2003; Blahut et al., 2010). Historical inventories represent the sum of one or many mass movement events over time in a region, but the inventories may be incomplete where evidence of mass movement activity is lost due to modification by subsequent mass movements, erosion and vegetation (Malamud et al., 2004).

Heuristic methods use the opinion of an expert who conducts field or aerial photograph investigations to identify unstable areas based on quasi-static variables or unstable events (Fall et al., 2006). The final product is similar to a mass movement inventory map but includes a qualitative description about the stability conditions of the slopes based on professional opinion or based on the frequency of events which occur for a particular range of values (García-Rodríguez et al., 2008). Susceptibility analysis which compares the magnitude and frequency of events to mass movement occurrence is based on the assumption that mass movements are a function of daily rainfall intensity and previous water accumulation conditions, and that mass movement inducing rainfall events can be determined from historical data or intensity-duration graphs (Buma, 2000; Casadei et al., 2003; Godt et al., 2006; Wang and Sassa, 2006). Although the rainfall threshold approach has regional application, it cannot be used to predict the exact location of mass movement activity given the high variability of risk associated with different topographic locations (Casadei et al., 2003).

The heuristic approach is subjective and the quality and reliability of the data are dependent on the skill and experience of the investigator or the type and age of the features under investigation (Carrara et al., 2003; Fall et al., 2006). This results in a serious mismatch between mass movement inventories undertaken by different researchers, particularly when considering the spatial distribution, classification and estimated degree of activity (Carrara et al., 2003; Galli et al., 2008).

3.2.2 Statistical models

Statistical models determine the factors that have historically led to mass movement activity and provide quantitative predictions for areas where similar conditions exist. Bivariate statistical analysis models use selected conditioning factors of mass movement, represented as maps and combine them with a mass movement inventory map (Akgun et al., 2008). Weighting values or rankings are assigned to each condition map based on the frequency distribution of mass movement activity for that particular parameter (Ruff and Czurda, 2008; Blahut et al., 2010). Multivariate statistical analysis models use maps of all possible factors sampled using a predefined mapping unit. The presence or absence of mass movement activity is noted for each unit and the resulting matrix is analysed using generalised linear models, such as logistic regression, as well as discriminant analysis or artificial neural networks (Figure 3.1) (e.g. Busoni et al., 1995; Baeza and Corominas, 2001; Carrara et al., 2003; Lee et al., 2003; Guzzetti et al., 2005; Wang and Sassa, 2006; Greco et al., 2007; García-Rodríguez et al., 2008; Yilmaz, 2009; Bai et al., 2010; van den Eeckhaut et al., 2010; Akgun, 2012). However the use of logistic regression for producing hazard maps has increased noticeably over the last few years (Akgun, 2012).

Complex statistical algorithms are required to process the large amounts of data that make a useful representative sampling population, as the multivariate

approach does not use selective criteria based on professional knowledge (Baeza and Corominas, 2001). Carrara et al. (2003) compared the predictive accuracy of a statistical model to the number of input variables used and found that the accuracy of prediction improved by 11% if 15 extra variables were included in the model. Baeza and Corominas (2001) found that 5 out of 13 variables were sufficient for assessing slope instability, whilst Guzzetti et al. (2005) determined that only 26 out of 46 variables were statistically significant. García-Rodríguez et al. (2008) found that using only two variables produced a statistically robust prediction model. According to Buma (2000), simple models may be sufficient for modelling regional instability conditions as complex models over-parameterise. Statistical approaches are sensitive to the type and quality of factors chosen for susceptibility analysis. Factors are often chosen because the data can be easily gathered using data-capture techniques rather than because they are the most suitable for analysis (Baeza and Corominas, 2001; Akgun, 2012).

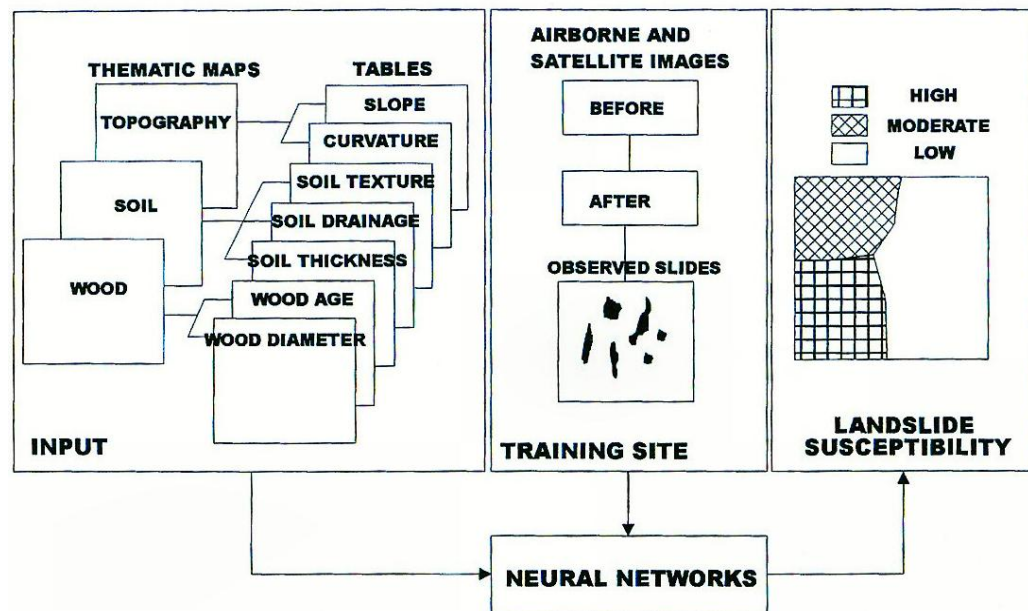


Figure 3.1 Flow diagram showing how a training site is developed and refined using neural networks to determine mass movement susceptibility (Lee et al., 2003).

3.2.3 Deterministic models

Deterministic or black box models are mathematical models that imply understanding of the interactions between triggering mechanisms and conditioning factors (Fernandes et al., 2004). Deterministic models try to represent these relationships with algorithms that model how groundwater fluctuations, antecedent soil water conditions, rainfall thresholds and slope materials react under simulated conditions (Ng and Shi, 1998; Glade, 2000). This approach requires detailed field data and relies on the formulation of a number of assumptions to form the constants and coefficients of the model. The simplest assumption of a hydrological model is that subsurface flow is in a steady state and that changes in pore pressure are controlled by local topography. Estimated pore pressure values are used in an infinite slope equation to determine slope instability. The model SHALSTAB (Shallow-Stability) assumes that the main controlling factor defining the location of mass movements is topography (Fernandes et al., 2004). The distributed Shallow Landslide Analysis Model (dSLAM) (Wu and Sidle, 1995) and the Combined Hydrology and Stability Model (CHASM) (Wilkinson et al., 2002) are hydrological models that incorporate the effects of vegetation and topography on mass movement. Vegetation stabilises shallow soils by providing vertical and lateral support, thus deterministic models try to incorporate the effects of frequent logging, burning and grazing into their simulations (Dhakal and Sidle, 2003).

Soil water models aim to model the relationship between factors affecting pore pressures and soil matrix suction. Soil porosity, permeability, degree of saturation, water content and hydraulic conductivity are some of the variables used to model the effects of rainfall intensity and duration for various soil types (c.f. Ng and Shi, 1998; Chang et al., 2009; Chang and Chiang, 2009; Lee and Ho, 2009; Cascini et al., 2011). However, the conditions that affect soil moisture conditions are spatially and temporally variable at all scales, which

makes developing reliable predictions about the nature and distribution of pore pressures difficult.

Deterministic models incorporate generalised parameters in order to mimic the complexity that exists within natural systems. Adopting a number of assumptions about the shear surface, depth and direction of subsurface flow and internal shear strength of slope materials minimises the number of parameters used in the model (Figure 3.2). However, these assumptions do not necessarily occur under natural conditions so that mass movements that are subject to lateral forces are not easily modelled using deterministic methods (Casadei et al., 2003). Deterministic models are only applicable when geomorphic conditions are homogenous throughout the study area and the types of mass movement are uniform and simple (Dhakal and Sidle, 2003; Fernandes et al., 2004). Deterministic models have a tendency to over-predict areas of instability due to variations in the quality of the input topographic data generated by a GIS (Casadei et al., 2003), and because site-specific data are extrapolated and averaged to apply to larger areas (Dhakal and Sidle, 2003).

In order to run a deterministic model, the study area is divided into discrete one, two or three dimensional units. Two and three dimensional models are represented by a matrix of cells that is vertically and laterally connected so that 'spill-over' effects or antecedent conditions can be incorporated into the model. Factors of safety are calculated for each cell as a ratio of material shear strength to downslope shear stress and simulations are run on each cell to determine how changes to the input variables affect the factors of safety (Brooks et al., 1995; Wilkinson et al., 2002). Variables associated with topography (slope angle and upslope contributing area), precipitation, soil properties (thickness, hydraulic conductivity, density, cohesion and angle of internal friction) and vegetation (tree surcharge, canopy effects, root strength and cohesion) are used to calculate the shear stress and strength inputs. Once the map is developed, it can be

compared to existing inventory maps to determine how accurately the selected input variables predict where unstable areas are likely to occur.

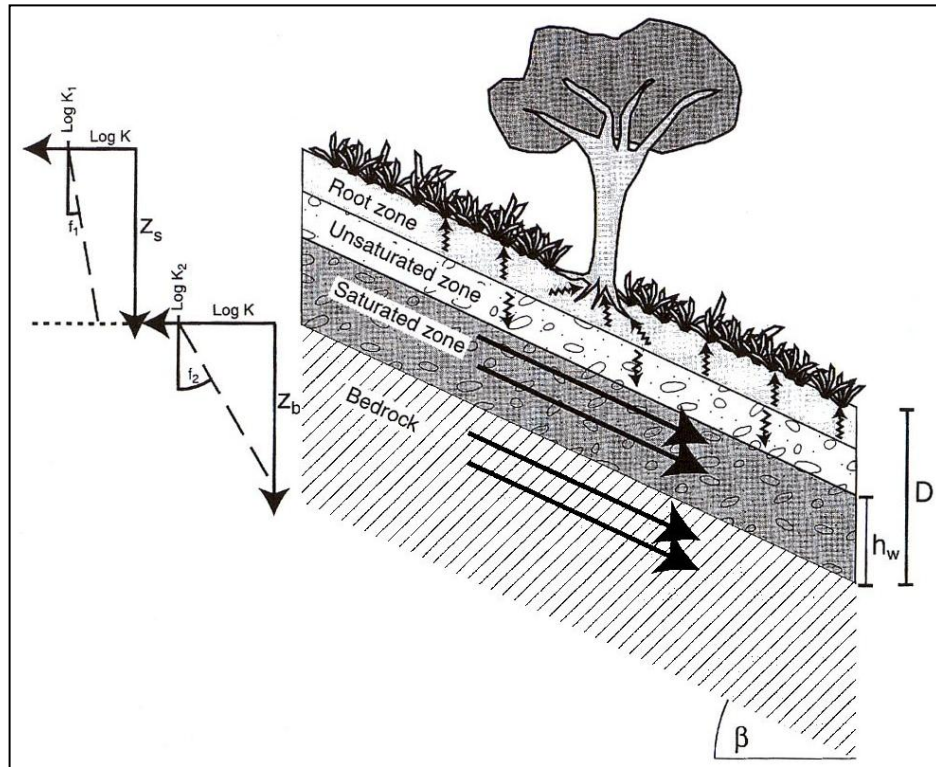


Figure 3.2 An example of a hydrological-slope stability model. Water table height is translated into pore-pressure in the infinite slope equation (Casadei et al., 2003).

3.2.4 The importance of mapping units

Mass movement inventories and statistical and deterministic models require a suitable mapping unit, or model platform, to be identified before the models can be processed. A mapping unit represents a portion of the land surface that contains internally homogeneous ground conditions that differ from adjacent units along identifiable boundaries (Guzzetti et al., 2005). The selection of mapping units is dependent on the type of mass movements to be investigated, the scale of the investigation and the type, quality, resolution and scale of the input data. Grid-cells are most commonly used for raster-based GIS applications that divide the study area into squares of equal area (Gupta and

Joshi, 1990; Clerici et al., 2002; Yesilnacar and Topal, 2005). Each grid cell is assigned a value for the input variables under consideration, or a matrix of raster layers is created where each layer represents a single input variable.

The raster data format is widely used for deterministic and statistical probabilistic models as each cell can be used to represent a number of input variables. However, computational processing time and numerical instability can occur if the number of grid cells used for the analysis is overwhelmingly large (Huabin et al., 2005). This is primarily determined by grid cell resolution and the processing power of the computer. According to Clerici et al. (2002), a study area of 332km² with 5x5m cells can take from 36 minutes to 1.5 hours to process depending on the processor used to run the model.

Terrain units are based on a land-use classification which assumes that processes, forms and materials create geomorphic boundary conditions which can be identified and delineated. The classification process is intrinsically subjective so that different investigators may classify a given region in different ways (Huabin et al., 2005). For instance, Möller et al. (2001) identified Soil Mechanical Response Units (SMRU) (Figure 3.3) to predict mass movement activity in Germany, but found that defining a critical size for a unit was problematic. Unique-condition units are usually made in conjunction with a mass movement inventory map. Each input variable is separated into classes and stored as maps that are sequentially overlain to form a matrix of unique combinations of input variables (Clerici et al., 2002; Ermini et al., 2005; Federici et al., 2007; Conoscenti et al., 2008).

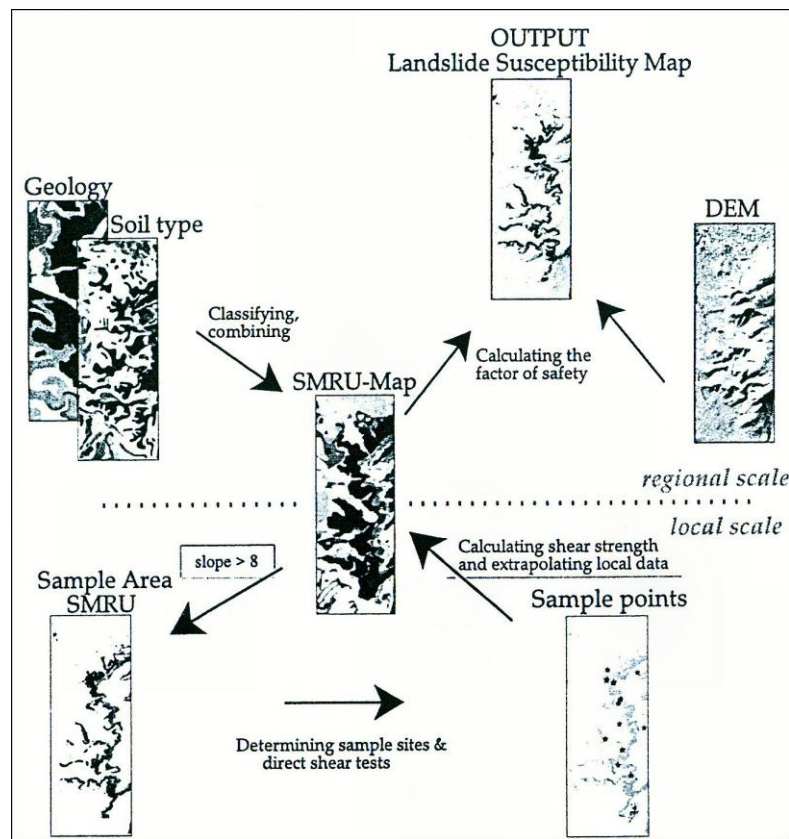


Figure 3.3 An example of how Soil Mechanical Response Units are created and used to compute the susceptibility map (Möller et al., 2001).

Terrain units are used where it is conceptually or operationally difficult to identify boundary conditions. Unique-condition units can be used where the data layers are spatially continuous but linear features or ‘patchy’ datasets present coverage problems (van Westen et al., 2000). If a large number of maps are overlain and each has more than 5 classes, the total number of unique-condition units becomes unmanageable and inaccurate. Further noise is introduced by data errors caused by digitising inaccuracies and problems associated with projections.

Slope-units and topographic-units are derived from digital elevation models and represent areas of homogeneous hydrological behaviour and topographic form (Fall et al., 2006). This approach is conceptually superior to those previously mentioned because it factors in the effects of topography (in terms of slope

angle, aspect and form) and hillslope hydrology (drainage basin delineation at a variety of scales and surface flow characteristics). However, the scale and quality of the digital elevation model determines the quality of the topographic and hydrological outputs (Rowbotham et al., 2005). The outputs cannot be more detailed than the scale of the contours or spot heights used to generate the digital elevation model, and as the algorithms that calculate the outputs use a neighbourhood sampling technique to calculate the values of the surrounding cells, errors can be propagated throughout the output layer.

3.3 Geographic Information Systems for hazard zonation

A Geographic Information System (GIS) is a system of hardware and software that has three main applications, namely data storage and retrieval, data manipulation or modelling, and data display or layout. A GIS is a useful and cost-effective tool for analysing any spatial data that can be combined with heuristic, deterministic and statistical models, as each involves the handling and interpreting of large datasets, complex modelling procedures, and ultimately, the production of maps (Fall et al., 2006). GIS techniques are used to examine spatial and non-spatial relationships using attribute, overlay, neighbourhood and connectivity operations that are included in the software or introduced as user-defined scripts to automate modelling processes (Walsh et al., 1998). For mass movement research, GIS technology has increasingly been used during preliminary site investigations, to derive topographic and hydrologic data and to generate and present hazard maps (Akgun, 2012). Planning a GIS project requires making a number of decisions about the scale, resolution, type and quality of the data to be used, as these decisions will influence how input data are collected in the laboratory and field (Figure 3.4).

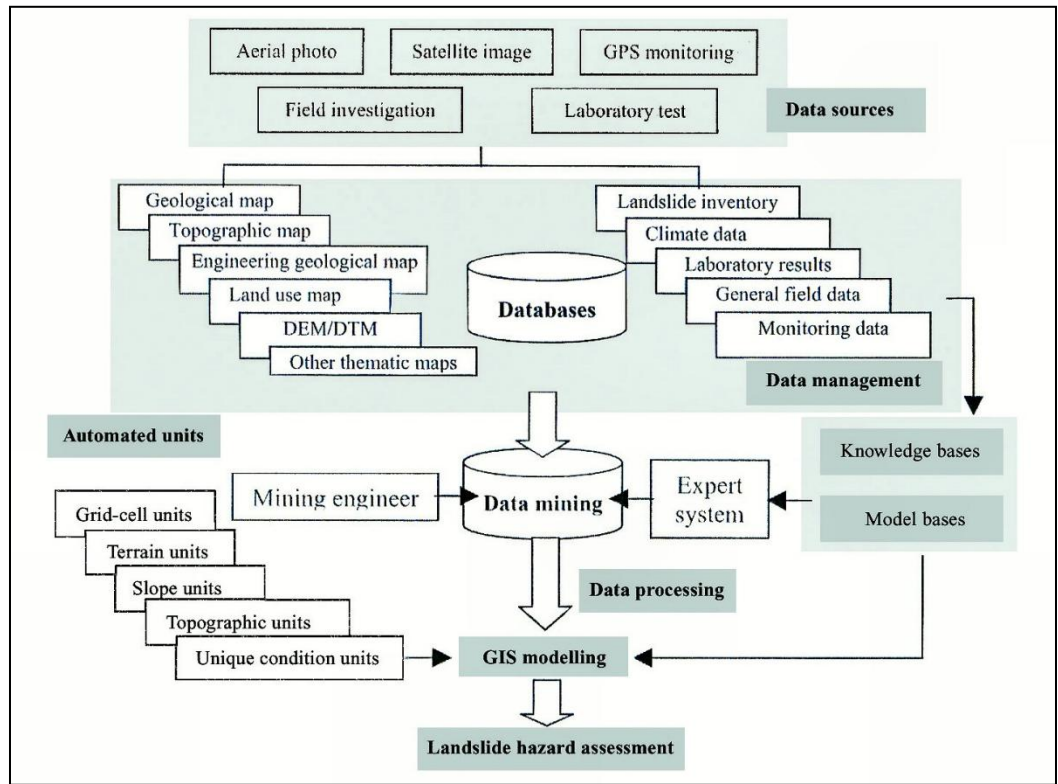


Figure 3.4 A GIS-based conceptual system integrated with data mining for mass movement hazard assessment (Huabin et al., 2005).

Scale, resolution and accuracy are concepts which often cause confusion. Scale is a measure of the amount of reduction between the real world and its graphic representation so that the same objects look different at different scales (Benz et al., 2004). A GIS is essentially ‘scaleless’ because digital data is displayable at any scale, thus scale is important for map annotation and displaying information (Clarke, 1999). Ranges in scales of analysis have been identified for hazard modelling that indicate how data intensive and detailed the investigation will be (Table 3.1). National-scale modelling provides a general indication of problem areas within a country, whilst regional mapping scale is useful for large areas usually greater than 1 000 km², but the level of detail for both is usually low. Medium- and large-scale mapping is the most detailed and the areas under investigation are limited from between a few hundred to tens of square kilometres (Soeters and van Westen, 1996). Range of scale influences

the choice of modelling technique to be used. Heuristic analyses can be undertaken at the regional, medium and large scale, whereas statistical modelling is best applied at a medium scale and deterministic models at the large-scale.

			Recommended scale of use		
Type of Analysis	Technique	Number of Input layers	Regional 1:100 000 to 1:500 000	Medium 1:25 000 to 1:50 000	Large 1:5 000 to 1: 15000
Inventory	Distribution	1	Yes	Yes	Yes
	Activity	6	No	Yes	Yes
	Density	3	Yes	No	No
Heuristic	Landuse classification	3	Yes	Yes	Yes
	Map overlay	12	Yes	Yes	No
Statistical	Bivariate	12	No	Yes	No
	Multivariate	12	No	Yes	No
Deterministic	Safety factor analysis	9	No	No	Yes

Table 3.1 Analysis techniques in relation to mapping scales (after Soeters and van Westen, 1996).

Resolution is a term that is used in relation to raster or grid data and is an expression of the average area dimensions that a pixel covers on the ground (Benz et al., 2004). The representational accuracy of a raster is dependent on the output value of the cells, so that cells with a small output value produce a higher precision grid with more total cells. Although it is possible to increase the number of cells in a grid, it is not possible to improve the level of accuracy. Therefore, if one converts a 30m DEM where each cell represents 30x30m on the ground, to a grid containing 10x10m cells, the resolution of the layer does not improve although the number of cells in the grid increases. Digital elevation models created from contours will have a resolution that is not more detailed than the interval spacing between the contours.

The resolution of a raster is a trade-off between economical constraints and accuracy requirements. An improvement in the capability of GIS and computer-

processing technology, as well as image quality and availability, is reflected in the improvements in the resolution used by investigators. A cell size resolution of 200x200m was considered suitable for predicting mass movement activity thirty years ago (Carrara et al., 1978), whilst contemporary research makes use of 0.5 to 30m grid cells (Lineback Gritzner et al., 2001; Ermini et al., 2005; Tarolli and Tarboton, 2006; Arrowsmith and Zielke, 2009; Bai et al., 2010; Akgun, 2012). This improvement has also occurred with the advent of GPS (Global Positioning System) and automated remote sensing technologies, making it easier to process large datasets and extract high-quality elevation data.

Advanced remote sensing techniques, such as Light Detection and Ranging (LiDAR) and Terrestrial Laser Scanning have been employed to model mass movement features in 3D, which facilitates locating shear zones and accurately quantifying displaced volumes of material (Dunning et al., 2009). Improvements in the resolution of satellite images has resulted in the use of classification algorithms for the automated detection of landslide scars; for instance Borghuis et al. (2007) showed that 63% of landslides that were mapped manually could be detected using image classification techniques.

Accuracy is a measure of how closely the data represent real conditions, and is determined by analyzing data integrity and locational accuracy. Integrity is determined by ascertaining how much information has been lost or whether non-existent features or 'noise' has been introduced, which is usually done by comparing maps to aerial photographs or field work. Error is introduced when vector datasets displaying different parameters that do not share coincident boundaries are overlaid and slivers are created that do not exist in reality. Topological errors are also associated with vector datasets and occur if features do not properly intersect, connect or adjoin, producing dangles or open arcs. Errors of this type are introduced during digitizing but can be avoided if proper snapping settings are employed. Integrity errors may also occur as part of the

classification process and one method of quantifying this type of error is Cohen's Kappa (Foote and Huebner, 1995; Walsh et al., 1998).

Locational accuracy is a statement of uncertainty about the error between a map feature and the true position of the attribute (Foote and Huebner, 1995). A GPS is often used in the field to locate mass movement features and the positional accuracy achieved by a GPS may range from millimetres to metres. Accuracy is improved when differential corrections are made to the readings which are calculated by comparing the known location of a permanent ground receiving station to its satellite coordinates, effectively reducing error by up to 10m (Walsh et al., 1998). Errors in locational accuracy may be increased during the modelling process and a number of tools exist within a GIS, such as cross-validation, to quantify how great the error is.

The format that the data will be modelled in is also of importance when planning a GIS project. Vector data are used to display discrete data that have a discernible boundary or surface extent. Mass movement inventories are composed of polygons that outline the boundary of the scar, track, deposit, or all three zones of a mass movement feature. Vector data can store more information per object than raster data, making them most useful for mass movement inventories. Because the total number of objects in a vector layer is less than the number of cells in a raster of the same extent, vector data are more stable, use less memory and process faster than raster data. Raster data represent continuous data that change incrementally over a spatial or temporal surface, and is the format most commonly used for modelling applications. Most GIS-based mass movement zonation models use vector input layers and convert them to a raster format to facilitate the running of models that include a DEM (e.g. Carrara et al., 1991; Lineback Gritzner et al., 2001; Clerici et al., 2002; Lee et al., 2003; Ohlmacher and Davis, 2003; Yesilnacar and Topal,

2005; Fall et al., 2006; Greco et al., 2007; Nefeslioglu et al., 2008; Yilmaz, 2009; Bai et al., 2010).

3.3.1 Application and derivation of digital elevation models

A digital elevation model (DEM) is a digital and mathematical representation of terrain within a selected area. DEM is a generic concept that refers to the elevation values of the ‘ground’ that sometimes includes the tops of buildings and vegetation. A Digital Terrain Model (DTM) differs from a DEM because it provides information about the actual ground surface elevation. Triangulated Irregular Networks (TINs) are a vector-type DEM that represents a surface as a set of contiguous, non-overlapping triangles with vertices made up of sampling points (Zhou et al., 2003). Heights between vertices form neighbourhoods that can be used to interpolate elevation between sampling points. DEMs have been used to model the runout behaviour of avalanches (Noetzli et al., 2006; Delparte et al., 2008), rock falls (Lan et al., 2007, 2010; Holm and Jakob, 2009); lahars (Huggel et al., 2008) and landslides (Booth et al., 2009; Shroder and Weihs, 2010; Shroder et al., 2011a, b).

DEMs were originally created manually by placing a sampling window or graph paper over a topographic map and deriving the elevations at specified intervals from the closest contour. Later, automated interpolation procedures were introduced such as the Morphology-Dependent Interpolation Procedure (MDIP) that classified a grid-node neighbourhood by exploring the values around the node in eight directions (Carrara et al., 1991; Dikau et al., 1991). At present, DEMs are generated from stereo-pairs of imagery using photogrammetric techniques or by acquiring a large number of 3D sampling points and running a resampling technique that ‘fit’ the data to a particular grid structure. TopoToRaster is a tool within the ArcGIS environment based on the Australian National University DEM (ANUDEM), developed by Hutchinson

(1988, 1989), which uses a multi-resolution iterative finite difference interpolation technique and a combination of vector data layers to generate a DEM (ESRI, 2004). ANUDEM is a superior interpolation technique because it includes the option to enforce drainage so that the risk of propagating errors when further hydrological interpolations are run is reduced because the cells that represent drainage lines are always given lower elevations than the surrounding cells (Kenny and Matthews, 2005). ANUDEM is capable of identifying sinks, or cells of unusually low elevations, which can be removed during the data pre-processing stage.

Primary topographic and hydrological attributes that are produced from a DEM and used as model inputs are generally first and second derivatives of elevation data. Topographic derivatives most commonly used in the literature are altitude, slope, and plan and profile curvature (Lineback Gritzner et al., 2001; Lee et al., 2003; Ohlmacher et al., 2003; Ayalew et al., 2004; Ermini et al., 2005; Yesilnacar and Topal, 2005; van Den Eeckhaut et al., 2010). Aspect is sometimes used, but its statistical significance decreases with distance from the poles so that although it is often generated for mass movement models, it is consequently excluded in the final prediction simulations.

Slope is a graphic representation of the maximum rate of change in value from each cell to its neighbours and represents the steepest downhill slope for a location on a surface (ESRI, 2004). Aspect is a derivative of slope where eight compass directions between 0° and 360° are assigned to each cell. Profile curvature represents the rate of change of slope for each cell in the direction of dipping, and plan curvature shows the bending of the surface perpendicular to the slope direction. Both affect the flow of water in and out of a slope and may therefore be associated with specific types of mass movement (Ayalew et al., 2004; Ayalew and Yamagishi, 2004; Martha et al., 2010).

Hydrological derivatives of a DEM are usually used for regional rather than large scale studies. Typical hydrological attributes that can be determined from a DEM are flow direction, flow accumulation, stream order and watershed delineation. Carrara et al. (1991) modelled flow direction using BACINI1/2, which simulates the overland flow concentration generated by a hypothetical spatially homogeneous rainfall event across a completely impermeable surface. Watershed morphometrics have successfully been used to differentiate between debris flows and hyper-concentrated debris floods in Canada (Wilford et al., 2004).

3.3.2 Aerial Photograph Interpretation

Whilst heuristic methods aim to establish the real causes of mass movements, the scale of slope movements and the complexity of conditions that lead to instability are such that these methods are impractical to use over large areas (Soeters and van Westen, 1996). As mass movements directly affect the surface of the ground, any remote sensing techniques can be used to identify instability (Weirich and Blesius, 2007). Remote sensing includes aerial photography and satellite imagery; yet stereoscopic air-photo interpretation has been the most frequently used tool for mass movement identification, mapping and monitoring until the late 1990's (Mantovani et al., 1996; Metternicht et al., 2005; Roering et al., 2009; Shroder and Weihs, 2010; Shroder et al., 2011a,b).

Mass movement information is extracted from aerial photographs and satellite imagery based on the identification of mass movements and their effects on the morphology, vegetation and drainage conditions of a slope surface (Gupta and Joshi, 1990; Soeters and van Westen, 1996; van Den Eeckhaut et al., 2007; Martha et al., 2010). As each type of movement is associated with different environmental conditions, it is possible to identify areas where mass movements are likely to occur and then verify their existence by field

investigation. It is also possible to use detailed images to identify a signature or pattern for a particular type of movement which will facilitate the identification of those features from less detailed imagery (Metternicht et al., 2005). Sequential aerial photos have successfully been used to determine the effects of climate change on geomorphological form, and time-series analysis has been used to show the rate of movement of single features such as the Black Ven mudslide, or particular rainfall events such as hurricane Mitch (Pallas et al., 2004; Walstra et al., 2007; Brardinoni et al., 2009).

Soeters and van Westen (1996) outlined a number of parameters for the identification of mass movement features by API. Image identification is limited by the quality of the image so that detailed classifications cannot be made based on interpretation alone. Therefore, a simpler classification is usually adopted for the interpretation stage (Mantovani et al., 1996). Falls and topples are identified where very steep slopes ($>50^\circ$) occur, where bedrock is exposed or drainage lines are undercutting a slope (Pallas et al., 2004). Local drainage patterns may be disturbed, which is indicated by abrupt changes in the width and pattern of the river. Deflection of local drainage lines caused by the deposited material may result in undercutting and mass movement on the opposite side of the valley. Deposits of fallen rocks and boulders appear in the image as areas of coarse grain, whilst the surrounding smooth grass-covered slopes are represented by finer spectral grains (Allen et al., 2011).

Slides are identified by their characteristic morphology so that the crown and scarp are easily identified as an abrupt change in slope or as a curved line (Walstra et al., 2007). Irregular morphology on the deposit and a lack of vegetation on the scar creates textural and tonal variations in the images (Gupta and Joshi, 1990; Mantovani et al., 1996; Brardinoni et al., 2009). Poor surface drainage and ponding may occur at the back of the sliding mass and wet zones

or springs are sometimes evident along the toe of the displaced mass as a variation or thickening of vegetation.

Flows have distinct source, transportational and depositional zones that are visible on aerial photographs (Barlow et al., 2009; Blahut et al., 2010). As the source zone is usually caused by sliding or falling motions, the distinguishing attributes of the particular movement type are evident in this zone. The source area and transport route of an incised flow is usually smooth and denuded of vegetation, whereas the flow track of a surficial flow appears denuded because the displaced material has flattened the vegetation and the material has been deposited on top of it. Tonal contrast is generally the same for each type of flow but as surface wash removes the deposit characteristic of a surficial flow, the flow path gradually disappears leaving behind the scar of the original movement. Large blocks of rock may be transported in the displaced mass and these are recognisable as rough or coarse texture (Guzzetti et al., 2008). Creep is characterised by an irregular micromorphology, appearing as ripples and steps on images that are distinct from the smooth slopes of the surrounding terrain (Walsh et al., 2003). The textural differences between terracettes and solifluction lobes are distinct on medium to large scale images due to variations in material type and vegetation.

In South Africa, panchromatic black-and-white stereo imagery is available from the National Geo-Spatial Information (NGI). Aerial photographic coverage in the form of contact prints are available from the 1950's to the present, and the scales of photography range from 1:10 000 to 1:50 000. Colour imagery at 1:10 000 is available for selected parts of the country, whilst spatially referenced digital imagery is only available for images taken during the last twenty years. Orthophotos are available for selected areas at 1:10 000, however it became evident during the data collection process that most of the 1:10 000 images are enlarged versions of the 1: 50 000 images.

Various factors need to be considered before purchasing aerial photographs. Stereo-images require an overlap of 60% in the horizontal and 30% in the vertical to be viewed in 3D. The photos should be taken at a scale that best facilitates feature identification. Mantovani et al., (1996) and Metternicht et al. (2005) suggest that 1:15 000 is the most useful photographic scale. Format is important and where possible, high resolution scans of contact diapositives from the original negatives should be used (Walstra et al., 2007). Obtaining aerial photos is time consuming, often the data format is incorrect and the metadata are lacking, and thus further pre-processing is required.

Errors may be introduced during the image processing stage of an aerial photograph investigation and maps that are digitised from incorrectly georeferenced photos result in erroneous maps. Photos can be corrected to account for relief effects by the process of orthorectification, whereby images are geometrically corrected by factoring in the elevation of the area using a DEM and the focal length, flying height and camera centre (Rocchini, 2004). Orthorectification is often confused with georeferencing, which uses a polynomial function to calculate the difference between a known ground control point and its counterpart on an image. The ground control points act as anchors around which the image is stretched and warped. Root Mean Square Error (RMSE) can be used to quantify this deviation, however it is often incorrectly referred to as an indication of accuracy without referencing the number of ground control points used or the warping technique adopted. Fewer points require more shifting, so the precision of the final product becomes questionable (Rocchini, 2004).

Errors can also be introduced during the interpretative stage of a project. A number of factors may result in discrepancies when different interpreters produce an inventory (Guzzetti et al., 2000; Galli et al., 2008). More than twice as many features were identified per km² by interpreters that had more time,

background information and access to resources than their counterparts. Variable topographic relief is distorted on aerial photographs and can create anomalies, scale differences and relief displacements. Poor scans and image quality reduce the resolution of an aerial photo, making the identification of features difficult. Snow and cloud cover, shadow effects and vegetation can mask geomorphological features (Figure 3.5), resulting in an underestimation of the distribution of mass movement features (Zinck et al., 2001; Brardinoni et al., 2003; van Den Eeckhaut et al., 2005).

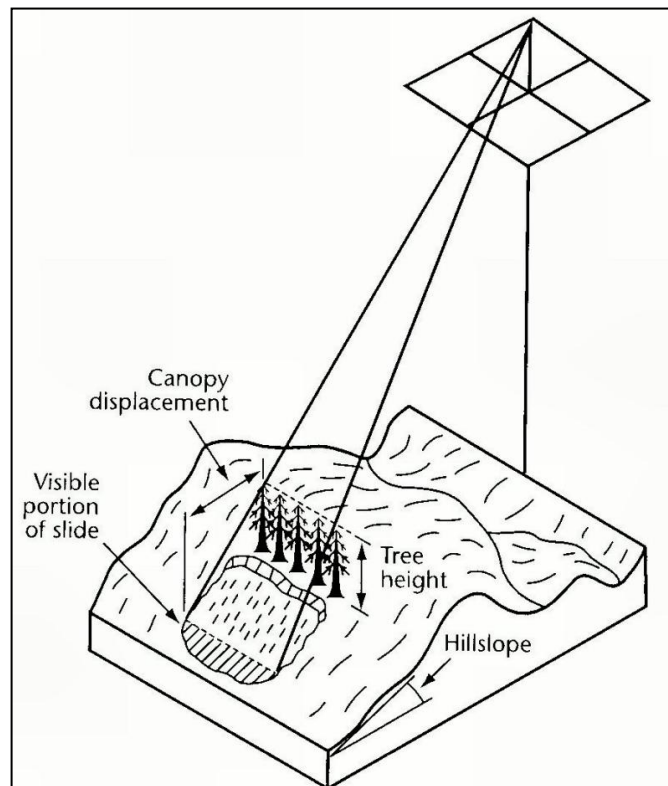


Figure 3.5 The masking effects of relief and vegetation on aerial photographs (Brardinoni et al., 2003).

Improvements in technology have led to the development of relatively sophisticated software for spatial and statistical analyses and these advances have in turn been driven by the increasing need to accurately map, model and predict naturally occurring, complex processes which impact on the safety of

human beings and their property. The Internet has provided access to open-source software programmes, and whilst GIS and API represent user-friendly and powerful tools for the assessment of mass movements, it is important to bear in mind that a map or model is merely a representation of reality.

Maps and models may be incorrect due to the introduction and propagation of errors during data collection and interpolation, or may result from a poorly constructed research design. A number of assumptions are made about the processes and spatial relationships that are modeled in a GIS and these may also skew the final product, producing results that appear more or less significant than can be expected in reality (van Westen et al., 2008; Blahut et al., 2010; Akgun, 2012). The risk is that mass movement models may over- or under-predict mass movement activity. In the former case, policy makers may lose trust in the ability of a model to accurately predict mass movement activity, and may choose to ignore the data due to a perceived lack of robustness. Under-predicting mass movement activity may result on a poorly structured urban design plan which would put human lives in jeopardy. Carrara and Pike (2008) note that even after almost 25 years of progress, GIS-based hazard analysis remains problematic due to the complex nature of mass movements and the deceptive 'ease-of-use' that GIS offers. It is therefore important that where mass movement models are used to predict activity which could impact on human lives and property, that error and accuracy assessments are included in the analysis.

4 Environmental setting of the UDP

4.1 Introduction

The Drakensberg form part of the Great Escarpment of southern Africa which extends from the Eastern Cape through KwaZulu-Natal and into the Free State and Mpumalanga (Figure 4.1). The escarpment represents a crescent-shaped altitudinal divide separating the Lesotho Plateau from the coastal lowlands of South Africa. Peaks on the escarpment reach to over 3 400m a.s.l., the highest being Thaba Ntlenyaba (3 482m a.s.l.), whilst valley floors extend down to about 1 500m a.s.l. The topography of the Drakensberg has been divided into the ‘High’ and ‘Little’ Berg (Figure 4.3). The former is characterised by summit areas (>2 900m a.s.l.) composed of sheer basalt cliffs, which are separated by ledges and steep grass-covered slopes. The Little Berg represents a system of sloping ridges and spurs with asymmetrical V-shaped valleys. Cliffs and minor scarps occur at all altitudes where sandstone faces are exposed.

Aerial photo interpretation was undertaken for the entire Garden Castle State Forest (GCSF) area, which covers approximately 13% (30 766 ha) of the Ukhahlamba Drakensberg Park (UDP). The GCSF is one of 12 Protected Areas of the UDP, and is managed by Ezemvelo KZN Wildlife. Sehlabathebe National Park lies to the southwest of the GCSF and is managed by the government of Lesotho. The UDP, which currently covers about 242 813ha, was originally established in 1903 and has been added to the Ramsar Convention’s List of Wetlands of International Importance in 1997 and declared a World Heritage Site in 2003 (UNEP-WCMC, 2006). Fieldwork and ground truthing was undertaken in the Bushman’s and Ngwanwane valleys, with access obtained through the Bushman’s Nek border post (Figure 4.2).

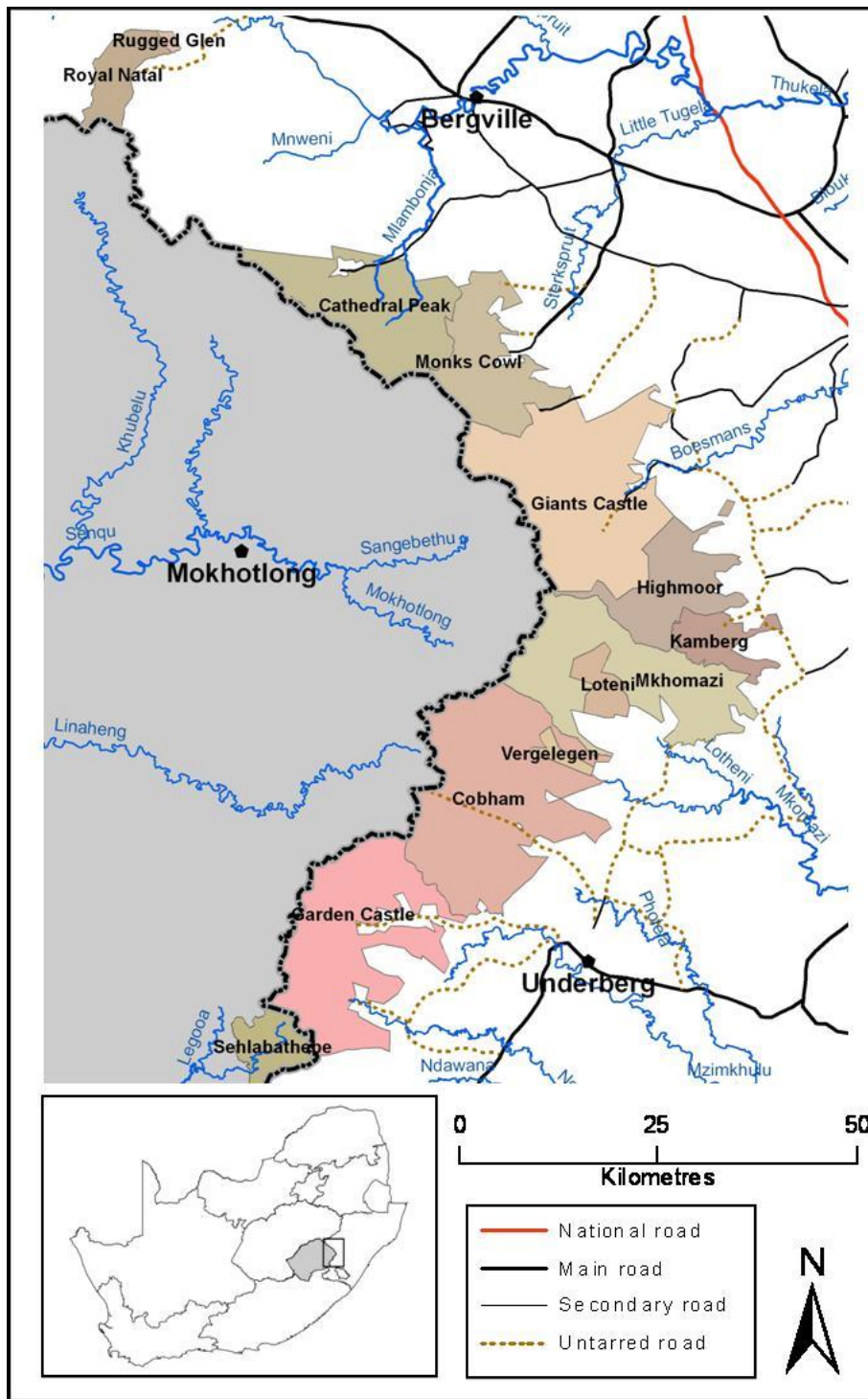


Figure 4.1 The Ukhahlamba Drakensberg Transfrontier Park is located along the eastern border of Lesotho. The Garden Castle State Forest is highlighted in pink

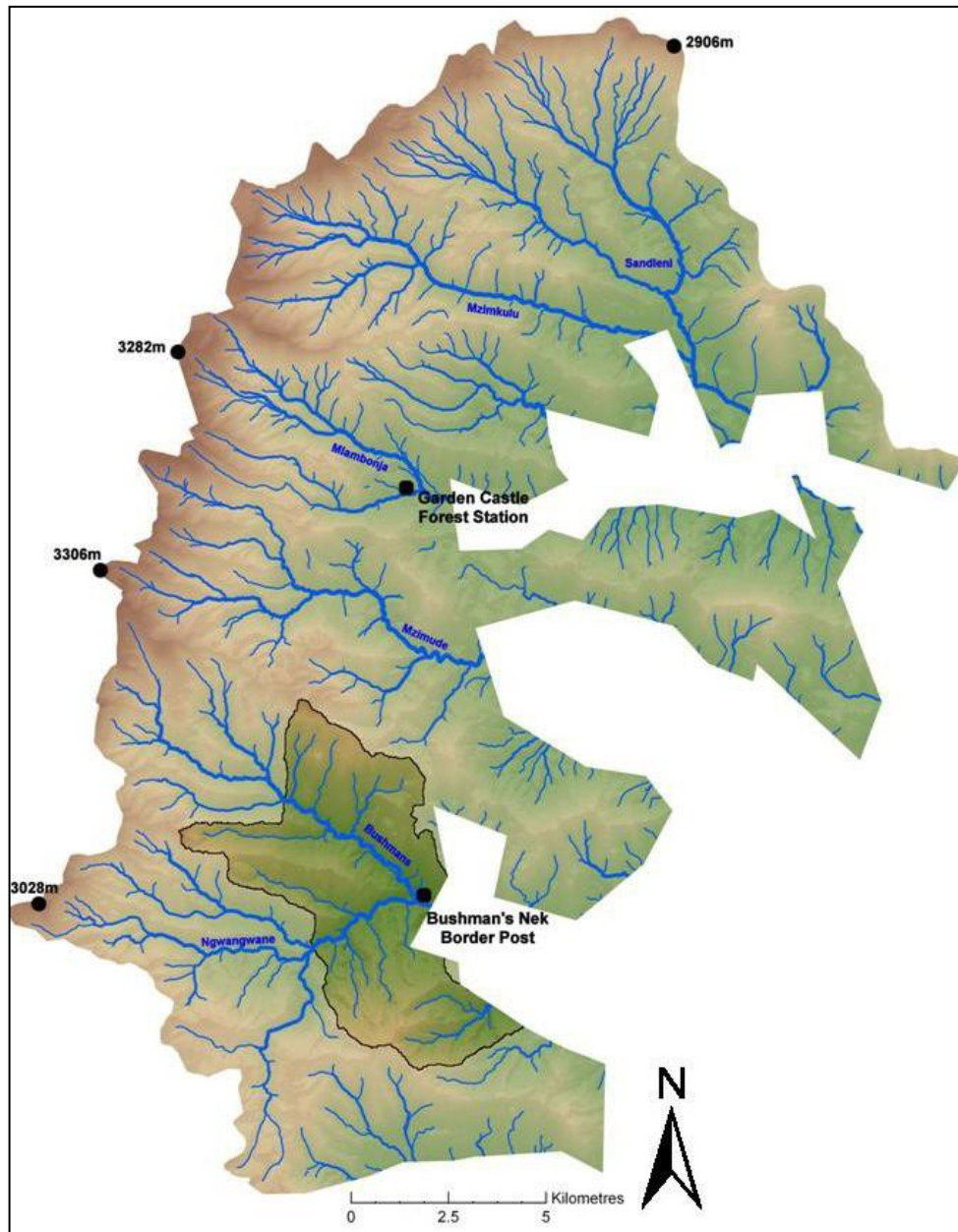


Figure 4.2 The Garden Castle State Forest. The area in full colour represents the catchments surveyed in the field, whilst the masked area represents that surveyed using API.

Management of the UDP is coordinated by the Forest Act No.72 (1968), the Mountain Catchment Areas Act No.63 (1970) and the Natal Regional Planning Commission. A series of multiple-landuse zones were proposed for the UDP as the Wilderness Heart, Landslide Zone, Trail Zone and Drakensberg Threshold

by Humphreys in the seventies (Irwin et al., 1980). The first two zones represent the most environmentally fragile areas and require intensive conservation management and little human interference. The Landslide Zone is demarcated as the area just below the Clarens Formation and is characterised by steeply inclined slopes and shallow soils that are susceptible to erosion (Humphreys, 1971) (Figure 4.3).

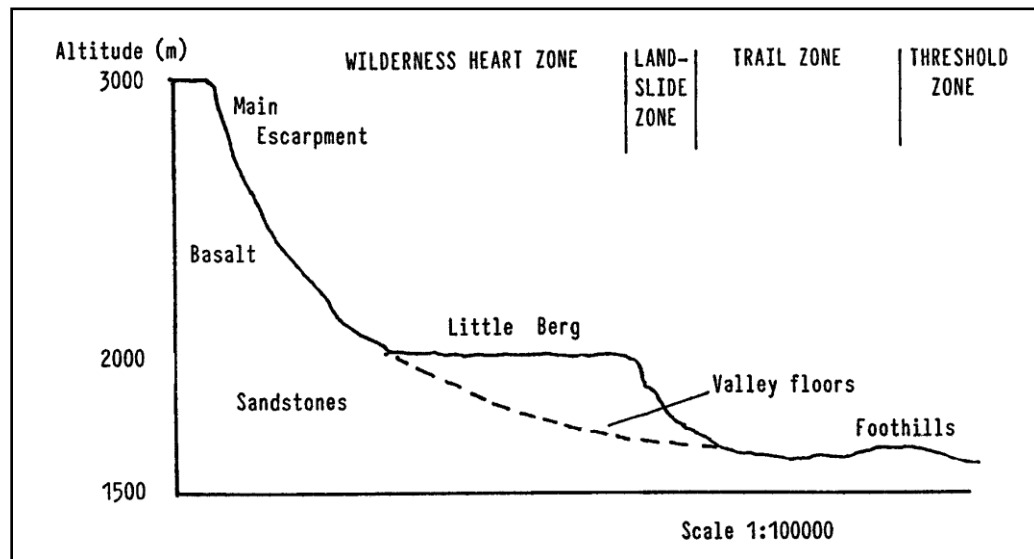


Figure 4.3 The topographic and geological zones of the Drakensberg (after Humphreys, 1971 (Bijker, 2001)).

4.2 Geology and Geomorphology

The stratigraphy of the Drakensberg Mountains forms part of the Karoo Supergroup and is characterised by a sequence of horizontally bedded sedimentary strata overlain by basalt and intruded by a network of dolerite dykes and sills (Figure 4.4). Strata are generally flat-lying or gently dipping towards the south and south-west. Table 4.1 shows the altitudinal ranges of each lithological type, which has been created from the FOCAL STATISTICS tool in ArcGIS and 1:250 000 digital geological data provided by the Council for Geoscience (CGS, 2008).

Lithology	Area (sq. km)	Min altitude	Max altitude	Range	Mean altitude
Drakensberg basalt	57	2129	3279	1150	2608
Clarens	48	1958	2581	623	2273
Elliot	103	1796	2522	726	2115
Molteno	62	1667	2350	683	1925
Tarkastad	86	1528	2133	605	1765
Alluvium	11	1564	1834	270	1687

Table 4.1 Expected ranges in elevation for each lithological group for the GCSF. Area is in km² and all altitudes are in m .a.s.l.

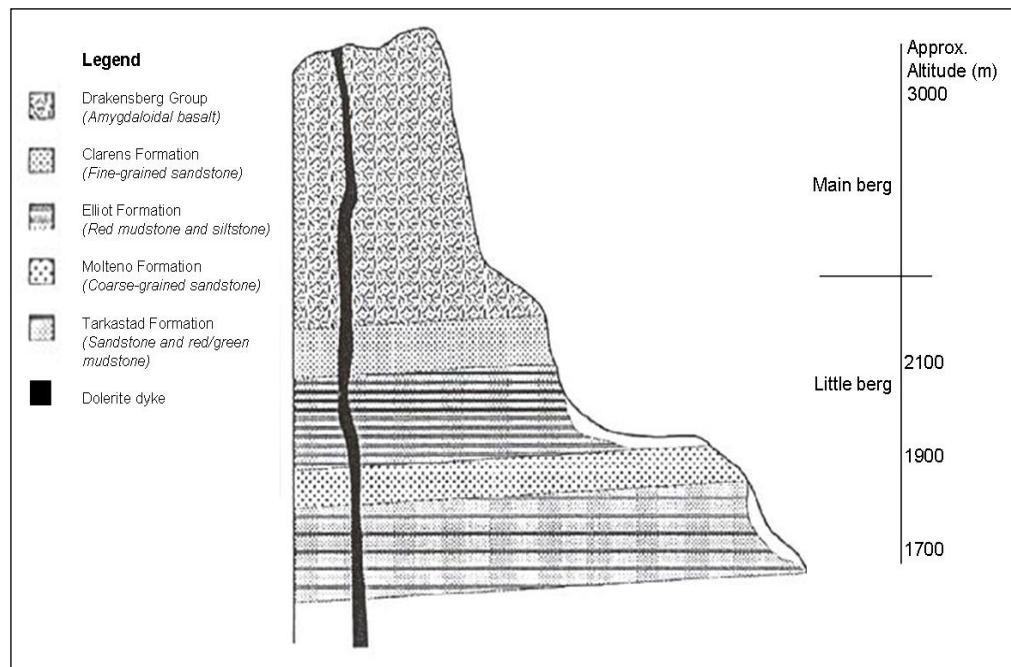


Figure 4.4 Schematic profile of the Drakensberg showing the approximate altitude for each lithological unit (after Bijker, 2001).

4.2.1 The Drakensberg Group

The Drakensberg Group consists of numerous individual basalt and olivine-bearing lava flows that overlie the Clarens Formation and are dark grey to purplish-red in colour (Haughton, 1969). These lava flows most likely occurred about 182 Ma during the rifting associated with the break-up of Gondwanaland (Dingle et al., 1983). The rock mass is not uniform and each zone consists of a basal zone containing pipe amygdales, a central zone of massive basalt and an upper zone of vesicular basalt (King, 1944; Du Toit, 1954; Boelhouwers,

1988a). Basalt that contains amygdales is less resistant to weathering and acts as an aquifer capable of supplying large quantities of water to springs (Dingle et al., 1983). Lava that intruded under pressure into the weaker argillaceous horizons formed sills, whilst lava that cooled and solidified in fissures formed vertical dykes (McCarthy and Rubidge, 2005). A comparison between basalts and sandstones of the Clarens Formation found that the basalts achieved higher temperatures than the sandstones, making them more susceptible to the effects of thermal fatigue (Sumner and Nel, 2006). The Drakensberg is characterised by stepped topography and these terraces represent single lava flows rather than fluvial terraces created during erosion cycles (Grab et al., 2005).

Dolerite is more resistant to erosion than the rocks of the Stormberg Group; with dykes and sills visible on the landscape as linear ridges and flat-topped hills up to 300km from the main Drakensberg basalt outcrop, which suggests that the lavas covered a greater extent than currently (Moore and Blenkinsop, 2006). Due to the mode of intrusion and rapid cooling, dolerite is normally highly jointed and displays a hexagonal to rectangular pattern of vertical joints with a horizontal subset of smaller joints (van Zijl, 2006). Subsequent movements, tectonic activity or shrinkage leads to the formation of slickensided surfaces, although at depth these joints are tightly closed and permit little or no water seepage. Topples commonly occur in dolerite where joint spacing has become widened due to weathering processes (Brink, 1983).

4.2.2 The Clarens Formation

Warming and aridity increased towards the end of the deposition of the Elliot Formation and the rocks of the Clarens Formation attest to desert conditions during the Late Triassic to Early Jurassic (Eriksson, 1983). A large sand sea formed that extended into Zimbabwe, Botswana and Namibia, but sedimentation slowed when the compression of the sediments relaxed, causing

the crust to rupture (Bordy et al., 2005). Large volumes of basaltic lava flowed out over the Clarens desert forming the Drakensberg Group approximately 183 Ma (McCarthy and Rubidge, 2005). The Clarens Formation is composed of pale creamy to white coloured fine sandstones and siltstones that are exposed as pronounced rock scarps and basal undercutting produces caves and overhangs to which its original term, 'Cave Sandstone', is attributable (Visser, 1989). Discolouration occurs where the rocks are exposed to water, particularly at seepage zones (Haughton, 1969). The grains show moderately good sorting, and grain support and shapes are dominantly sub-rounded to sub-angular (Eriksson, 1983). The Clarens Formation is exposed from 1 958 to 2 581m a.s.l. in the GCSF (Table 4.1).

4.2.3 The Elliot Formation

Global warming and the northward drift of Gondwana to warmer latitudes led to increasingly arid conditions in the Late Triassic and is reflected in the rocks of the Elliot Formation, which are floodplain sediments deposited by meandering rivers (Visser and Botha, 1980; Eriksson, 1983; Smith et al., 1993; Bordy et al., 2005). The presence of iron oxide and salt pans indicate that the environment was characterised by seasonally flooded ephemeral pans (McCarthy and Rubidge, 2005). Formerly referred to as the Red Beds, the Elliot Formation is characterised by massive red siltstones and mudstones with occasional lenses of fine to coarse sandstone (Eriksson, 1983; Boelhouwers, 1988a). The red colour is attributable to the presence of iron oxide which coats the grains, and the sandstones are generally yellow to whitish but bleach when exposed as outcrops (Haughton, 1969; Smith et al., 1993). Differences in sorting and grain shapes are attributable to distinct depositional processes rather than being derived from different source materials (Eriksson, 1983). Red to purple argillite is common at the contact zone between the Molteno and Elliot Formations and slopes underlain by the Elliot formation are relatively smooth

due to the absence of resistant sandstone outcrops (Boelhouwers, 1988a; Killick, 1990). The Elliot Formation is exposed from 1 796 to 2 522m a.s.l. in the GCSF (Table 4.1).

4.2.4 The Molteno Formation

The Molteno Formation was deposited under seasonally warm to humid climatic conditions mainly by large perennial rivers with established floodplains during the Middle Triassic (Bordy et al., 2005). The rocks of the Molteno Formation are light coloured, fine to very coarse sandstones that are interbedded with layers of argillaceous sediments and conglomeritic sandstones (Boelhouwers, 1988a; Smith et al., 1993). The sandstones have a sparkling appearance due to the deposition of silica upon the quartz grains which regenerates the crystal faces and the sandstones generally weather to form pitted surfaces (Brink, 1983). The shales and mudstones are grey or blue but become yellow during weathering (Haughton, 1969). The sandstones exhibit various types of cross-bedding and grains are typically rounded to sub-rounded, sometimes sub-angular, and composed of quartz and feldspar (Eriksson, 1983). The argillaceous materials are usually covered by vegetated soil cover and the sandstone forms ledges and terraces (Boelhouwers, 1988a; Killick, 1990). The Molteno Formation thickens towards the southern Drakensberg (King, 1944) and is exposed from 1 667 to 2 350m a.s.l. in the GCSF (Table 4.1).

4.2.5 The Tarkastad Subgroup

The Tarkastad Subgroup represents the uppermost member of the Beaufort Group to crop out in the study area and is exposed from 1 528 to 2 133m a.s.l. in the GCSF (Table 4.1). It is characterised by reddish-brown and greyish-green sandstones, siltstones and mudstones that were deposited in fluvial-deltaic conditions (Dingle et al., 1983). The Tarkastad Subgroup is overlain by the Stormberg Group which is composed of the Molteno, Elliot and Clarens

Formations. The rocks of the Beaufort Group were deposited during the Permian/Triassic by large, northward-flowing, meandering rivers in which sand and mud accumulated. These rivers were replaced by multi-channelled, braided river systems that deposited sand rather than the silts and mud of earlier meandering rivers, possibly as a result of massive vegetation loss, the cause of which is unknown (McCarthy and Rubidge, 2005).

4.2.6 Strength properties of the Karoo Supergroup

Slope instability is largely due to differences in permeability between the arenaceous and argillaceous materials. Sandstone layers are more permeable than mudstones, so moisture accumulates at contact zones and porewater pressures develop at the interface (Sumner et al., 2009). Falls, topples and slides occur in the rocks and residual soils, where two distinct types of failure can be observed (Figure 4.5). In Figure 4.5a, increased moisture results in increased weathering at the contact between layers and pores in the sandstones, which become wider and larger until the material disintegrates (Meiklejohn, 1997). Disintegration is most common in sandstones comprising more than 50% quartz, which is typical of the Clarens Formation, as the Molteno and Elliot Formations contain silica which acts as a cementing agent (Brink, 1983).

The underlying mudstone becomes exposed and weathers quickly so that the sandstone loses basal support and eventually collapses (Boelhouwers, 1988a). Alternatively, on slopes covered by residual soils, clay minerals leach from the overlying sandstone and become deposited as a stratum of clayey sand on top of the mudstone (Figure 4.5b). The presence of montmorillonite makes the material extensively slickensided until the colluvial material collapses and sliding occurs, with the new sandstone exposed at the base of the outcrop (Blight et al., 1970).

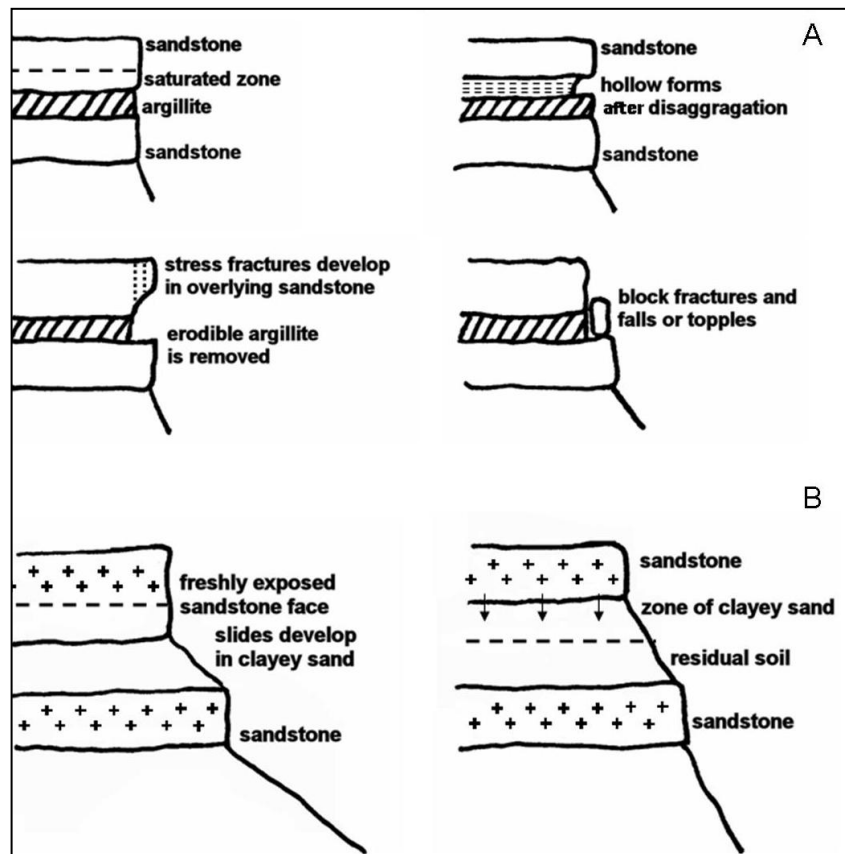


Figure 4.5 Failure in rocks and soils of intercalated layers.

Sandstones weather non-uniformly so that dense layers may be underlain by less competent layers, and the assumption that residual soils become less weathered with depth and more competent does not apply to residual sandstone soils (Brink, 1983). Van Rooy and van Schalkwyk (1993) note that mudrocks of the Karoo Supergroup rapidly deteriorate when exposed. An unusual property of residual soils of the Clarens and Molteno Formations is that although they are composed of predominantly kaolinite clay particles, which has a non-expanding lattice structure, excessive shrinking and swelling has been observed with changes in moisture content (Roper, 1969). Slope stability conditions are also affected by dolerite intrusions as contact metamorphism and shattering reduce the stability of the slope as a whole. Seepage may occur along intrusions and faults which increases localised moisture conditions and

weathering (Brink, 1983). Moon and Selby (1982) noted that sandstone and dolerite slopes fall within the strength equilibrium envelope, whereas argillaceous slopes do not.

4.2.7 Geomorphological evolution

A number of theories have been put forward to describe the origin and development of the escarpment prior to the work of Partridge and Maud (1987). Suess (1904) attributed the development of the escarpment to extensive faulting and down-tilting along the eastern coast but this theory was later contested by Penck (1908) and King (1944) who suggested that the scarp was erosional in origin. The existence of bevelled surfaces and rejuvenated streams was interpreted to be caused by periods of erosion and uplift, which formed planation surfaces and caused stream incision. King (1982) identified five periods of uplift and four planation surfaces in the Drakensberg, whereas Partridge and Maud (1987) identified two periods of uplift and three periods of erosion. This discrepancy may be due to scale, as King's (1982) model is based on regional evidence, particular to the Drakensberg, whilst that of Partridge and Maud (1987) applies to southern Africa as a whole (Boelhouwers, 1988a).

Rift faulting during the early Cretaceous, caused by the rising of a mantle plume beneath Gondwana, forced the crust to rise and become weakened and resulted in the break-up of the continent. The escarpment represents one of the zones of fracture that developed, created by the high absolute elevation (about 2 000m) of southern Africa at the time (McCarthy and Rubidge, 2005). A period of accelerated denudation occurred in the Late Cretaceous (from 91 ± 2 to 69 ± 3 Myr) which involved the removal of around 3 km of crustal section at a mean rate of about 95 m/Myr (Brown et al., 2002). Most of the inland retreat of the escarpment is thought to have occurred during this period and extensive planation surfaces were formed throughout the subcontinent (Partridge and

Maud, 1987). Moderate uplift of between 150-300m occurred at the end of the early Miocene, causing the land surface to tilt slightly westwards. Planation continued into the Late Pliocene, with a major uplift occurring about 2.5 Ma ago. Downcutting and planation continued from the Late Pliocene to the mid Holocene and river terraces formed in response to climatic oscillations and glacio-eustatic sea-level changes (Partridge and Maud, 1987; Boelhouwers, 1988a).

Large deep-seated landslides in KwaZulu-Natal have been associated with increased fluvial incision caused by uplift during the Pliocene (Sumner and Meiklejohn, 2000). Similarly, large palaeo-landslides have been observed in the Giant's Castle area of the UDP (Boelhouwers, 1992) and the Injisuthi Valley (Bijker, 2001), as well at various locations in KwaZulu-Natal (Singh, 2008). Changes in drainage pattern and localised damming have been related to large relict mass movement features (Sumner and Meiklejohn, 2000; Singh, 2008), however more detailed research relating to the contribution and environmental effects of these relict mass movements on landform development in the Drakensberg is still needed. Basalt terraces represent another noticeable geomorphological landform in the UDP, particularly at high altitudes (above 2 900m a.s.l). Basalt terraces are most likely the result the result of preferential or differential weathering of thinly layered lava flows which occurred during the Late Jurassic (Grab et al., 2005).

Periglacial landforms in the Drakensberg have been described by numerous authors (e.g. Hastenrath and Wilkinson, 1973; Beckedahl, 1977; Lewis, 1988; Verster and Van Rooyen, 1988; Watson, 1988; Boelhouwers, 1991; Garland and Humphrey, 1992; Grab, 1994, 1996, 1999, 2000, 2001; 2002; 2005a, 2005b; Sumner, 2004; Mills and Grab, 2005; Grab et al., 2009; Mills et al., 2009; Temme et al., 2008), however the debate on the origins of these features is ongoing. Most work has focussed on the identification of relict periglacial

landforms for palaeo-climatic reconstruction or on the role of frost and environmental conditions on weathering (Boelhouwers and Meiklejohn, 2002).

Periglacial landforms that have been identified in the Drakensberg include nivation cirques, blockfields, solifluction lobes, stone-banked lobes and thufur (Sparrow, 1971; Marker, 1989; Boelhouwers, 1991, 1994; Boelhouwers and Sumner, 2003; Grab, 2000). The distribution of these features appears to be influenced by altitude and typical elevations for solifluction forms vary between 1 900-3 300m a.s.l and between 2 900-3 100m a.s.l for thufur (Lewis, 1987; Boelhouwers, 1991; Grab, 1994). Turf and stone-banked lobes and steps have been observed at altitudes from 3 150 and up to 3 400m a.s.l. (Boelhouwers, 1991, 1994; Grab, 2000). Whilst Boelhouwers and Miekeljohn (2002) note that no direct evidence of contemporary permafrost has been recorded, apparent glacial moraine, which may have formed during cooler conditions of the Last Glacial Maximum, have been identified in the southern Drakensberg of eastern Lesotho (Mills and Grab, 2005; Mills et al., 2009). The application of a glacier reconstruction technique suggests that glaciers could have existed in Lesotho at 3 136m a.s.l, which coincides with the locations of observed periglacial landforms (Mills et al., 2009).

Active frost-related processes are associated with needle-ice and diurnal and seasonal freezing. Landforms associated with these processes include lobes and terracettes associated with solifluction and sorted and non-sorted patterned ground (Hastenrath and Wilkinson, 1973; Boelhouwers, 1988a; Boelhouwers and Hall, 1990; Hanvey and Marker, 1992; Grab, 2000). Needle ice may develop and melt within one freeze-thaw cycle as long as ground temperatures are lower than -0.4°C (Grab, 2001). Needle ice of up to 7cm has been observed at Tiffendell, close to the south-eastern border of Lesotho (Kück and Lewis, 2002), and up to 9cm long in the Mashai valley just south of Sani Pass (Grab,

2001). On south-facing slopes above 3 000m a.s.l, ground frost may penetrate to 60cm deep and remain frozen for up to three months (Grab, 2007).

Soil piping has been documented at Kamberg and near the Oliviershoek Pass, and is classified as 'moist area' soil pipes (Beckedahl, 1977; Garland and Humphrey, 1992). Soil pipes can be clearly identified on the slopes of the Little Berg as lines of greener, thicker vegetation, especially during winter when *Themeda traindra* turns yellow (Beckedahl, 1977). The pipe roofs usually occur approximately 30-50cm below the ground surface, whilst floors of soil pipes range from 80-160cm below the surface. Pipe widths widen downslope from about 30cm to over 120cm (personal observations, 2004). Although Garland and Humphrey (1992) found that discharge in the soil pipes was seasonal, moisture and base flow has been observed in soil pipes in the GCSF during recent winter months. Discharge is in response to rainfall events and up to 9% of rainfall is converted to pipe discharge (Garland and Humphrey, 1992). The montane tree fern *Alsophila dregei* may be found growing in soil pipes where there is sufficient moisture, cooler temperatures and protection from wind and frost (Humphreys, 1971).

Diurnal and seasonal variation of incoming solar radiation is a function of slope and aspect and marked differences can be observed between north- and south-facing slopes in the UDP. Comparison of a north (equator)-facing and south (pole)-facing slope of 10° in summer and winter shows that at noon in summer an equator-facing slope receives only slightly more radiation than its pole-facing counterpart (Tyson et al., 1976). In winter, pole-facing slopes receive 50% less radiation and slopes of 30° receive six times less than its opposite slope (Tyson et al., 1976). The asymmetry of incoming solar radiation has a major impact on soil moisture and temperature and is thought to have controlled the pronounced topographic asymmetry that occurs in the Drakensberg (Meiklejohn, 1992; Boelhouwers, 2003). Equator-facing slopes

are generally drier, respond rapidly to changes in temperature and experience more chemical weathering (Boelhouwers, 1988b).

4.3 Climate

A scarcity of climate data exist for the Drakensberg due to the low number of monitoring stations in the UDP and surrounds (Tyson et al., 1976; Sumner, 1995; Grab, 1999). In the southern Drakensberg, climate data are only available from Shaleburn, although some rainfall data have recently been collected at Sani Pass (Nel and Sumner, 2005). The climate of the Drakensberg is characterised by a warm, rainy summer season (November to January) and cool, dry winter season (May to July). Air circulation is controlled by the seasonal movement of pressure cells located along the coast and over the interior. In summer, the Kalahari High Pressure cell rises to allow an influx of humid air from the Indian Ocean, providing moisture for precipitation. In winter, the cell drops and creates an inversion over the interior of South Africa (Tyson, 1988). Precipitation occurs throughout the year in the form of thunderstorms, hail, fog and snow, making the Drakensberg one of the best watered and least drought prone areas in southern Africa (Tyson et al., 1976). Rainfall variability in terms of amount and intensity increases from south to north in the UDP (Nel and Sumner, 2006).

Temperatures for the hottest days in the Drakensberg rarely exceed 35°C and are seldom colder than 2.5°C on the coldest days, whilst nocturnal temperatures may drop to -12.5°C in mid-winter (Tyson et al., 1976). Frosty nights can be expected for more than 3 months of the year and the annual duration of frost varies from 180-200 days in Lesotho (Grab, 1999), but is reduced to 60 days in the Little Berg (Boelhouwers, 1988b). Rock temperatures measured in Lesotho show significant variations in temperature between north- and south-facing

slopes such that north-facing slopes experience 35 times fewer freezing days than south-facing slopes (Grab, 2007).

The Drakensberg receives maximum rainfall in January and February but local variations in rainfall occur due to relief and rain shadow effects. About 13 to 15 raindays can be expected per month in the Little Berg, whereas between 16 and 18 raindays occur in the High Berg (Tyson et al., 1976). Thunderstorms occur on about 100 days per year and regularly produce hail (Tyson et al., 1976). In winter, frontal rainfall during winter gives rise to non-erosive, low-intensity drizzle, whereas in summer, thunderstorms are more common and more erosive (Nel and Sumner, 2008). Fog occurs frequently in the Drakensberg and may contribute up to 31% of the total precipitation received per annum (Tyson et al., 1976; Hilliard and Burt, 1987). About 3 to 8 snowfalls may occur per year and snow may remain for several weeks in well shaded areas. Snowfall in the Little Berg is less frequent but may last up to two weeks in sheltered spots (Granger, 1976).

4.4 Vegetation

Several authors have identified altitudinal vegetation zones for the Drakensberg, but those developed by Killick (1963, 1990) are the most widely used (Boelhouwers, 1988a; Sumner, 1995). The three vegetation belts distinguished by Killick (1963) include the Montane Belt (1 280-1 830m a.s.l.) with *Podocarpus latifolius* Forest as the climax community; the Subalpine Belt (1 830-2 865m a.s.l.) with *Passerine-Phillipa-Widdringtonia* Fynbos as the climax community; and the Alpine Belt (> 2865m a.s.l.) with *Erica-Helichrysum* Heath as the climax community (Killick, 1963).

There are nearly 120 different kinds of grass in the southern Drakensberg and most are tufted. Closely spaced tufts or tussocks give the appearance of

continuous cover but bare ground is observed after burning (Hilliard and Burt, 1987). The following descriptions of each zone have been made by Killick (1990). The Montane Belt is characterised by *Themeda Triandra* grassland, which often serves as an understorey to *Protea* Savanna. With protection from fire, the grass becomes replaced with *Hyparrhenia* grassland which has a patchy distribution and occurs in moist gullies, at the foot of cliffs and in disturbed areas. *Miscanthus-Cymbopogon* grassland is also found in moist areas such as streambanks, gullies and forest margins. Bracken veld generally occurs on deep, moist soil along streambanks, at the edge of pools, in boulder beds and along cliff faces, with *Leucosidea sericea* and *Buddleja saliiifolia* predominating.

The Subalpine Belt is composed primarily of *Themeda triandra* grassland which extends to higher altitudes on warmer and drier slopes. *Rendia altera* grassland is found where soils are thin, black and peaty, whilst tall grassland and scrub characterises streambanks, moist flats and gullies at lower altitudes. Fynbos is limited to areas protected from fire and the greatest variety of species is found on pole-facing slopes (Granger, 1976). The Alpine Belt extends into Lesotho and consists of heath communities dominated by *Helychrisum* and *Erica*, interspersed with short grasslands of *Merxmullera* and *Festuca*. Aquatic, hygrophilous and lithophilous communities occur where bogs and streams form the headwaters of rivers.

The vegetation of the Drakensberg is diverse as it includes both the mesic vegetation of the KwaZulu-Natal escarpment and the vegetation of the drier Eastern Cape Drakensberg and Lesotho interior (Carbutt and Edwards, 2003). Both the floristic and vegetative diversity may be explained on a broad scale by the altitudinal, climatic, topographic and edaphic gradients at a smaller scale, by the multitude of micro-habitats created by various combinations of relief,

aspect, exposure and slope angle). These attributes create suitable ecological niches for prolific species coexistence (Carbutt and Edwards, 2003).

4.5 Soils

Most of the research on soils in the Drakensberg has been undertaken in the northern regions of the UDP (Bijker, 2001). Soil classification was undertaken in the Tugela basin in the late 1960s (van Der Eyk et al., 1969), in Cathedral Peak in the mid 1970s (Schulze, 1974; Granger 1976) and in KwaZulu-Natal in the late 1990s (Turner, 2000). However, as the lithology is relatively homogenous throughout the UDP it is possible to relate some of this information to soils in the southern region, especially as lithology affects the infiltration rate of a residual soil (Garland, 1990). Dominant soils in the Drakensberg that have been identified are the Mispah, Clovelly, Hutton, Griffin and Katspruit Forms (Van Der Eyk et al., 1969). Recently, the soils of the Drakensberg have been described as ‘organic’, occurring from the Low Berg upwards where topographic and bedrock conditions allow water to persist (Fey, 2010). Elsewhere, humic soils with apedal subhorizons overlying weathered saprolite have been observed. The apedal nature of the subsoil is attributed to clay mineral composition which stabilises pore spaces and inhibits expansion and contraction (Fey, 2010).

Garland (1979) argues that better soil and vegetation development can be expected on pole-facing slopes due to the availability of moisture which sustains plant growth, promotes weathering and reduces accidental fire. Skeletal soils that were poor in organic matter and clays, and lacking true profile development, were observed on equator-facing slopes, whilst thicker organically rich soils overlying a clayey, plastic horizon were observed on pole-facing slopes in the Kamberg area (Garland, 1979). In the Drakensberg, stream density was found to be greater on equator-facing slopes where sheet erosion is

dominant, whilst on pole-facing slopes, soil piping, terracettes and occasional sliding movements are prevalent (Boelhouwers, 1988b).

4.6 Anthropogenic activities

4.6.1 Fires

Natural fires occur in the Drakensberg as a result of lightning strikes and rockfalls but the majority of fires occur as controlled burns or arson. Bundles of dry grass are set alight and rolled down the slopes of the Little Berg to distract farmers as part of a cattle rustling scheme, and in other cases areas are set alight in protest to management decisions taken by Ezemvelo KZN Wildlife (Kruger, 2007). The burning policy adopted by the UDP is designed to prevent the accumulation of a heavy fuel load, thus avoiding hotter fires which burn more deeply, and cause slower regrowth (Hilliard and Burt, 1987; Short et al., 2003). Grasslands are divided into blocks and each is separated by a firebreak that follows the watersheds. Blocks are burnt every alternate year on equator-facing slopes and every third year on pole-facing slopes to account for the slower accumulation of biomass (Hilliard and Burt, 1987). Burning may increase soil repellence, however as the degree of repellence is determined by the heat of the fire, it is expected that minimal soil heating occurs as controlled burning is undertaken just after the rain season (Short et al., 2003).

4.6.2 Footpaths

The Drakensberg is relatively susceptible to erosion due to the high kinetic energy of the rainfall and steep local relief (Garland and Humphrey, 1980; Irwin et al., 1980), thus footpaths need to be managed in a way that reduces multiple footpath development and surface erosion. The path networks in the Bushman's Nek region have been classified as river paths (34%), plateau paths (30%), contour paths (10%), and slope paths which exceed gradients of 5°

(26%) (Grab and Kalibbala, 2008). One footpath along the Ngwangwane River is routinely moved and older paths are filled with rocks to discourage multiple path development. Wooden struts have been installed along the Bushman's River footpath and these 'anti-erosion logs' have proven useful in stabilising footpath if installed correctly (Grab and Kalibbala, 2008). Most footpaths in the UDP are located between 1 300 to 2 500 m a.s.l, in fine-grained Tarkastad Sandstones and coarse-grained Molteno Sandstones (Grab and Kalibbala, 2008). Burning, as well as variations in rainfall have been associated with increased footpath erosion in the Kamberg area of the Drakensberg (Garland, 1987) and footpath erosion has been referred to as one of the most serious problems facing conservation planners in the UDP (Garland, 1990).

5 Methodology

5.1 Introduction

Field investigation was undertaken to identify the range of mass movement types and the possible environmental factors that are related to mass movement activity in the southern Drakensberg. Fieldwork forms the basis of most landslide hazard analyses as the field survey provides important information relating to the location and morphometric attributes of mass movement features (Brardinoni et al., 2003; Abdullah et al., 2005; Fall et al., 2006). API was used to produce a mass movement inventory and to map rock deposits, and ArcGIS (9.0) was used to create eight environmental variables which were then sampled for each mass movement type and for the random datasets. Univariate and multivariate statistical modelling was then undertaken. The discussion of the method adopted for this dissertation therefore falls into two broad categories; namely a fieldwork and desktop component.

5.2 Fieldwork methods

Seven visits were made to the Bushman's Nek area between 2004 and 2006 and twelve landslide sites were investigated. The autumn/winter period is the most suitable for site visits as the weather is usually clear and the vegetation less dense than during the summer period. Veld burning is also undertaken during this period, which provides a good opportunity to compare the masking effect that vegetation has on mass movement feature identification. A preliminary site visit revealed that a large number of mass movement features occur in the study area, but that not all are easily accessible. Thus, detailed fieldwork was only possible for sites within 5km of the Bushman's Nek border post. A field survey form (Table 5.1) was developed and then amended, given that some components were too difficult to determine and/or not applicable once in the field.

5.2.1 Field survey

Mass movement locations and elevations were determined using a Garmin GPSmap 60C. Although this GPS does not provide the same accuracy as a differential GPS, it was adequate for the purpose of this study. Detailed oblique photographs were taken at each site to compare the visual appearance of the mass movement feature in the field to that on the orthophotos. These photographs were important for documenting the appearance of the mass movement features, particularly when producing geomorphological maps.

The mass movement field survey form (Table 5.1) was divided into sections that were qualitatively assessed, and a brief description and sketch of the site was written on the back of the form. Morphometric attributes were measured for each feature using the indices suggested by Brunsden (1993) and the width, length and depth of the three main zones of the mass movement feature (depletion zone, transport zone and deposition zone) were measured using a 30m and 50m measuring tape. The slope gradient for each zone was measured using an Abney level and range rod. Mass movement type, style and state of activity were described using the terms suggested by the Multilingual Landslide Glossary (Dikau et al., 1996) where possible. Descriptive statistics were generated for each mass movement using Microsoft Excel 2003. Terraced mass movement features were not included in the field survey for two reasons. Firstly, at the time of the field visits, terrace type mass movements were not included in the analysis as the extent and influence of the terraced fields had not been established and secondly, due to the inaccessibility of most of the terraced field sites.

Geology							
Bedrock				Slope History			
Formation				Past mm activity	Absent	Present	
Dolerite	Present	Absent		Creep activity	Absent	Present	
Joint density	Low	V High		Footpath/ road	Absent	Present	
Joint openings	Tight	Wide		Burnt	Absent	Recovering	Present
Dip	Away from slope	Towards slope		Vegetation			
Degree of weathering	None	High		Type	Grass	Shrubs	Trees
Character of weathering	Mechanical	Chemical	Solution	Major species			
Depth of weathering	Uniform	Variable		% Cover/ square meter			
Competent over incom strata	Absent	Present		Mm effects	Removed	Established	
Regolith				Vegetation islands	Present	Absent	
Tension cracks	Absent	Present		Topography			
Coherent over incoh beds	Absent	Present		Slope shape above crown	Concave	Convex	Linear
Depth	Shallow (cm)	Deep (m)		Rupture surface	Not visible	L>W	W>L
Dessication cracks	Absent	Present		Scarps	Absent	Main scarp	Terraces
Permeable over imperm beds	Absent	Present		Depletion zone c/s	No form	Linear	Curved
Nature of reg/rock contact	Gradual	Abrupt		Depletion zone shape	Indistinct	U/Crescent	Bowl/spoon
Drainage				Transfer zone	Absent	L>W	W>L
Surface				Transfer zone channel	Absent	Incised	Surficial
Density	Low	V High		Accumulation zone	Absent	L>W	W>L
River gradient	Gentle	V Steep		Accumulation shape	Indistinct	Fan	Lobe
Undercutting	None	Severe		Accumulation slope	Concave	Convex	Linear
Mm connected to drainage	None	Indirectly	Directly	Nature of deposit	Sand/Clay/Silt	Debris/Boulders	Rocks
Mm effects	Formed stream head	Obstructed flow		Levees	Absent	Vegetated	Bare
Subsurface				Topo hollows	Absent	Mm confined to	Mm between
Springs	Absent	Present		Limits			
Seeps/ damp areas	Absent	Present		Exposed bedrock	Absent	Above feature	Below feature
Moist veg	Absent	Present		Fluvial base level	Absent	Present	
Pipes/ holes	Absent	Present		Planation surface	Absent	Above feature	Below feature

Table 5.1 Field survey form used to describe the mass movement features. Items in grey were not assessed in the field.

5.2.2 Geomorphological field maps

Geomorphological maps were generated in ArcGIS 9.2 as this program has the same drawing utilities as software packages such as AutoCAD but can incorporate spatial information, such as contour data. A geomorphological legend was developed for each site, which includes information obtained from the field survey form, such as for example zones of future expansion and tension cracks. Legend styles were based on those used for geomorphological mapping of landslides by Terhorst and Kirschhausen (2001) and Ertek and Erginal (2006).

5.3 Desktop methods

A multi-method assessment methodology was developed for mapping mass movement potential in the southern Drakensberg. The method is composed of five steps (Figure 5.1). Firstly, a DEM was developed at a scale appropriate for representing topographic attributes. The DEM was also used to create catchments which partitioned the study area into smaller areas. Secondly, the environmental variables considered important for causing mass movements were collected and either digitised or extracted from the DEM. A shapefile representing lithology (1:250 000) was obtained from the Council for Geoscience. Thirdly, a mass movement inventory was prepared which included mass movement features identified by API techniques and those that had been surveyed in the field. The fourth step involved sampling the environmental variables for each mass movement type and the randomly generated point shapefiles which represent the absence of mass movement activity. Univariate and multivariate statistical analyses were then performed for each dataset. Finally, five mass movement potential maps were produced for each mass movement type and compared using the variables selected by the logistic regression model. A final mass movement potential map for each type was then produced.

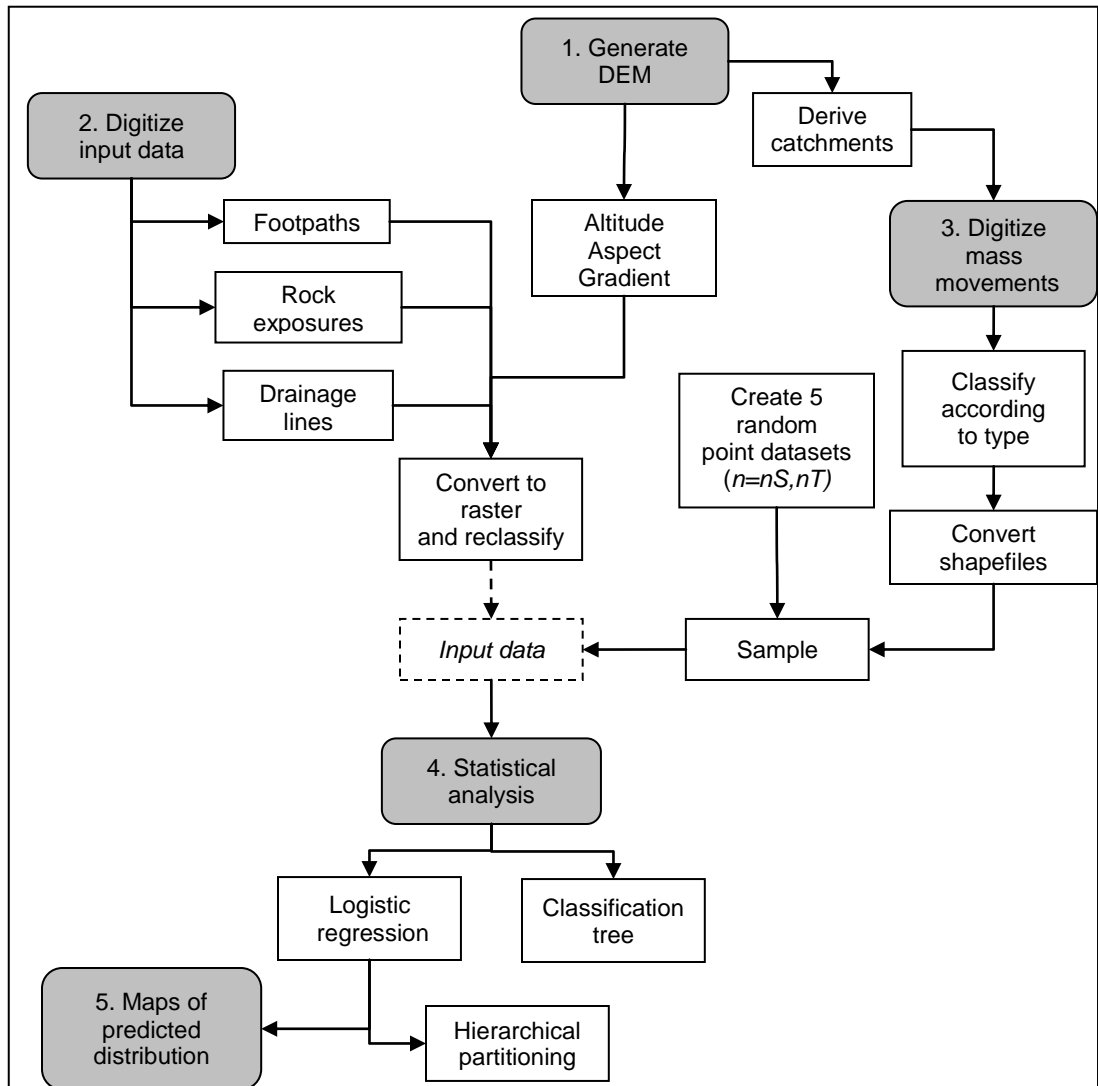


Figure 5.1 Flow diagram illustrating the desktop method.

5.3.1 Generating a digital elevation model

Ezemvelo KZN Wildlife provided a 20m DEM for the Drakensberg region that was produced by GIMS. The DEM was interpolated from 1: 50 000 topographic vector data using spot height elevations and 20m contours. In order to assess the accuracy and applicability of the KZN DEM, a second DEM was developed using the Topo to Raster tool in ArcGIS 9.0 Spatial Analyst. Topo to Raster uses an iterative finite difference interpolation technique that allows for

the production of a hydrologically correct DEM (ESRI, 2008). Sinks are conservatively removed from the output DEM and drainage lines can be imposed onto the DEM, however the process will not impose drainage conditions in locations that would contradict the input elevation data. The drainage enforcement can be turned off, in which case the sink clearing process is ignored. For comparison of the two interpolated DEMs, no drainage enforcement was undertaken as the KZN DEM did not include this aspect of the interpolation process.

Topo to Raster uses a combination of vector lines, points and polygons in the form of a contour line shapefile, boundary and lake polygons, an elevation point shapefile and a stream line shapefile to interpolate a raster surface. These are available from the NGI as uncorrected 1:50 000 topographic vector data. Given that the contour intervals are 20m, the output DEM has a cell size of 25m. Although a smaller cell size can be selected, the resolution of the DEM is determined by the scale of the input data. If the cell size is smaller than the minimum size of the input layers, no new data will be created. Cells are interpolated using nearest-neighbour resampling and the result is as precise as the coarsest input. Contours and spot heights were used to interpolate a 25m DEM (hereafter referred to as the TTR [Topo To Raster] DEM) and no drainage, sink or boundary information was included in the process. Although the KZN DEM is supposed to have included trigonometrical beacon elevations, this information was not available for the study area.

5.3.2 Comparison of the KZN DEM and TTR DEM

Contour data and spot height data were used to generate the TTR DEM. The first run of Topo to Raster produced erroneous results, so the input layers were checked and corrected. Inconsistencies within each dataset were tested by comparing the sample distributions for the spot heights and contours (Figure

5.2). Spot height values had a reasonable range of altitudinal values (minimum = 1 430m a.s.l, maximum = 3 401m a.s.l) but the contour data had missing altitudinal values and an overly large range (minimum = 0, maximum = 15 803m a.s.l). The contour data were then investigated further and different types of error were identified.

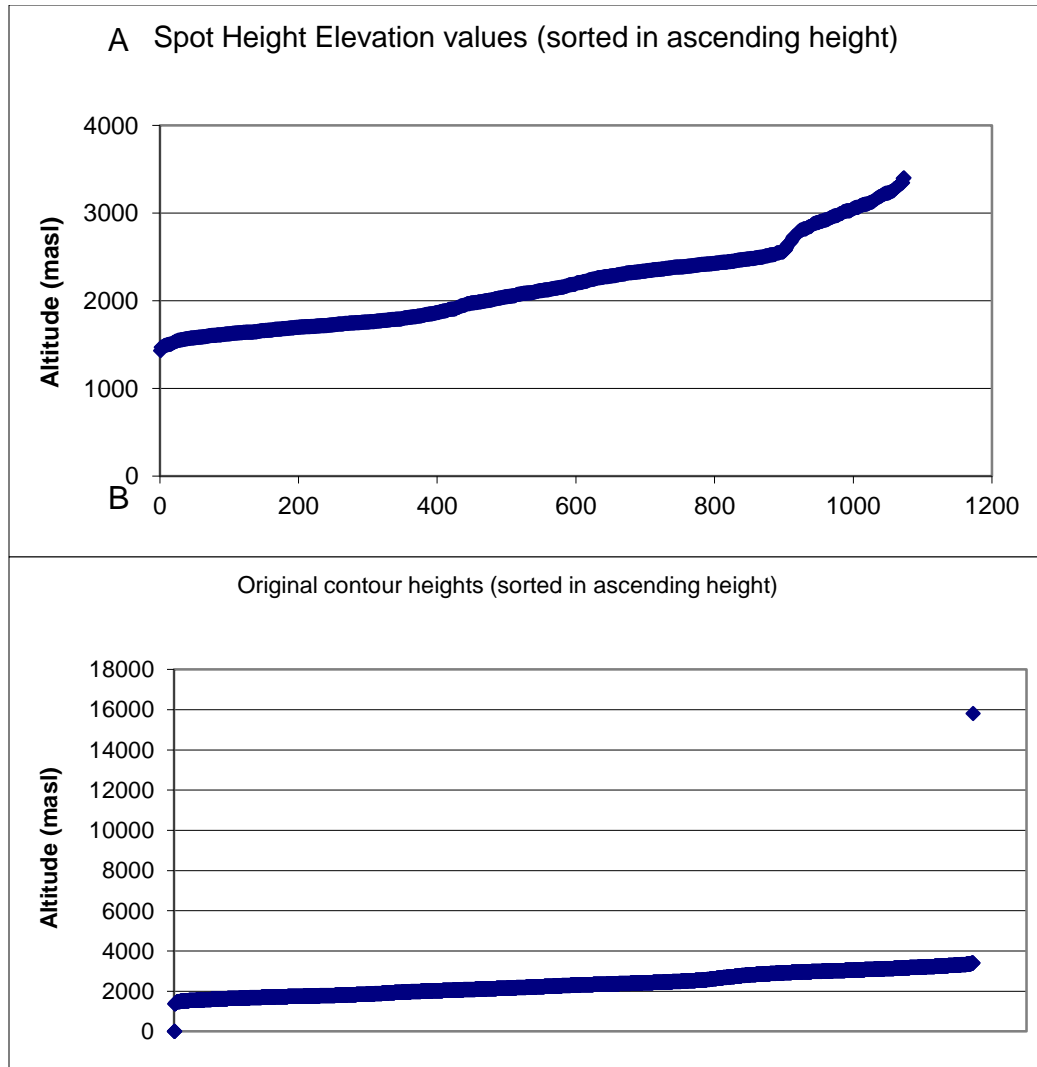


Figure 5.2 A) Spot heights (m a.s.l.) showing no outliers. B) Contour heights (m a.s.l.) showing outliers.

The first type of error is a labelling error which occurs where a contour line spans two mapsheets and has different elevation values. Errors have also arisen

due to the scanning procedure used to convert the paper maps to vector shapefiles so that along the edge of the mapsheet contour lines are produced that do not align with one another or arcs are missing or contours have become closed polygons instead of joined polylines (Figure 5.3). Most of the error occurred between sheets 2929CB and 2929CD and are probably due to a datum error that was not accounted for in the scanning process. Fixing the contour dataset resulted in a more accurate contour dataset (n increased from 4687 to 4699).

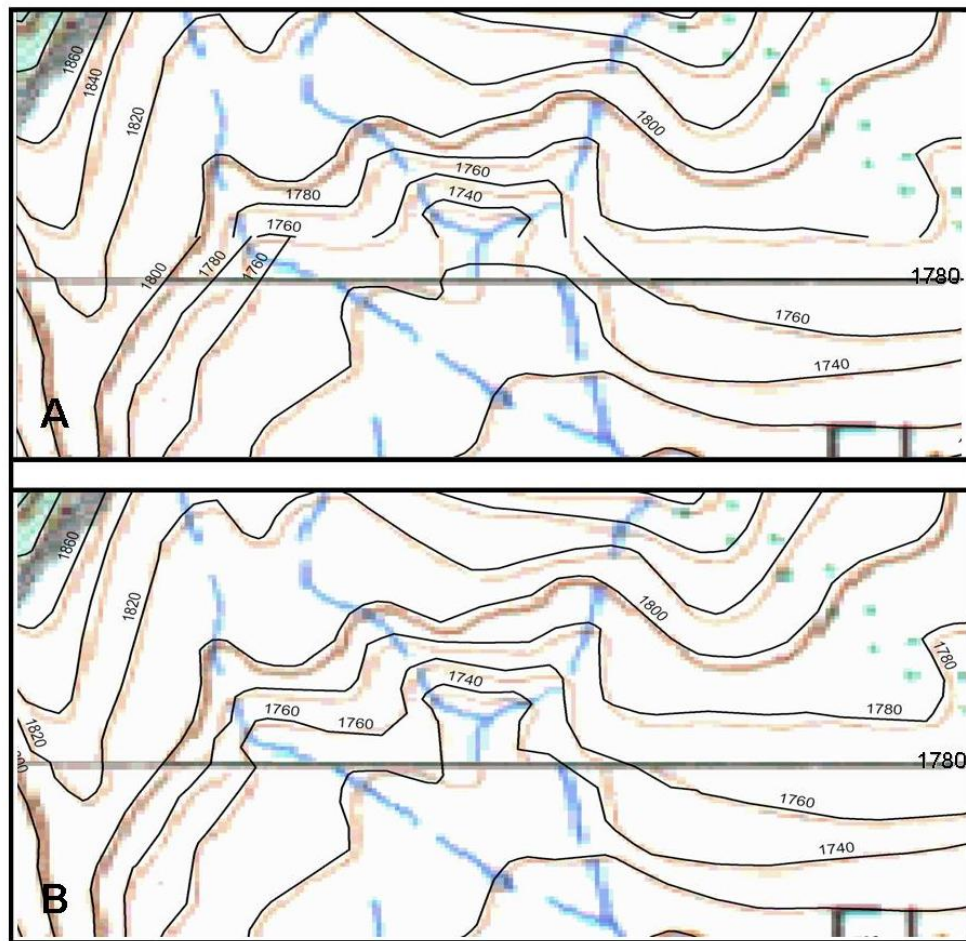


Figure 5.3 A) Examples of error created during the scan digitizing between map sheets and B) the corrected contours.

Consecutive runs of Topo to Raster were generated and the output TTR DEM was compared to the KZN DEM by calculating the altitudinal difference using

Raster Calculator. Cells with the greatest difference were identified in the TTR DEM, the contour height and spot heights were then compared and the contour heights were reclassified to better match the spot height data. This technique established another type of error; namely where slope gradients are steep and the contours are closely spaced, the contour lines have been dropped and connected to adjacent lines. An attempt was made to correct this by digitising the missing arcs to create continuous contour lines.

A comparison in the ranges of altitudinal values for the KZN and final TTR DEM was made by selecting the cells with the highest altitudinal difference (>80m) from the TTR DEM, selecting the same cells from the KZN DEM and then subtracting these values from the altitudinal value of the closest contour. This technique showed that in areas where there was large variation in altitude which was not attributable to errors in the contour dataset, the TTR DEM had altitudinal values that were closer in elevation value to the input contour data than the KZN DEM. This suggests that the KZN DEM was generated using uncorrected contour data and that the TTR DEM is more accurate. The TTR DEM was therefore adopted for further analyses.

5.3.3 Photogrammetric techniques for DEM generation

As the resolution of the DEM was considered quite coarse, an attempt was made to use photogrammetric techniques to produce a more detailed DEM. Leica Photogrammetric Suite (LPS) 9.0 software was used and a total of 61 aerial images scanned at 25 microns were acquired from the NGI, with the camera calibration certificate and GPS coordinates of the flight plan. The camera which is an RC30 and the average flying height was 7 200m. Each image was rotated to the correct orientation using a standard photo editing package. Pyramids were built for each image, and the interior orientation of the images was set by locating the eight fiducial marks for each image (RMSE <0.5

pixels). The images were dark and locating the fiducial marks was problematic, otherwise the Autolocate tool could have been used.

Tie points and ground control points (GCPs) had to be manually added and points were selected that occurred on more than one pair of images, due to the 60% image overlap between images in the horizontal and 30% overlap in the vertical. As the study area falls predominantly within a conservation area, it was difficult to use standard techniques for tie-point collection. Only a relatively small portion of the study area has infrastructure, so tributary intersections, high spots in vlei areas and isolated rocks had to be used as tie points.

The aerial triangulation tool establishes the mathematical relationship that exists between the tie points, GCPs and the exterior orientation. Once this relationship has been established, the RMSE between the control and check points is given, which serves as an estimation of accuracy. The final output of the process is a continuous representation of the ground surface, however the final DEM that was generated was questionable and therefore not used for the study. Over 220 hours were committed to this component of the project with little to no effect on quality of the final DEM output (also see Nichol et al., 2006).

5.4 Environmental variables

A review of the input variables used by previous authors provided an indication of the input layers best suited for the analysis (Gupta and Joshi, 1990; Carrara et al., 1991, 2003; Guzzetti et al., 1999, 2005; Baeza and Corominas, 2001; Lineback Gritzner et al., 2001; Clerici et al., 2002; Jordan, 2003; Santacana et al., 2003; Ayalew et al., 2004; D'Amato Avanzi et al., 2004; Fernandes et al.,

2004; Liu et al., 2004; Ermini et al., 2005; Gokceoglu et al., 2005; Singh et al., 2005; Yesilnacar and Topal, 2005; Nadim et al., 2006).

Three environmental variables were identified from the literature that were associated with mass movement activity in the field; namely, proximity to a rock exposure, drainage line and footpaths/roads. Each of these was digitised from the orthophotos as polylines, however the coverages are not exhaustive due to shadow effects and distortion caused by the orthorectification process (Figure 5.4). The NEAR tool was used to establish proximity of a mass movement feature to each variable. Drainage lines were identified by their appearance on the orthophotos and represent the presence of a topographic, rather than hydrologic feature. Therefore no inference is made on presence or seasonality of flow. Drainage lines were ordered according to Strahler’s method (Strahler, 1952). Table 5.2 shows the percentage of river length for each stream order within the 461km² study area.

Stream order	Length (km)	% length
1	1128.35	49.93
2	528.73	23.40
3	291.30	12.89
4	155.42	6.88
5	72.30	3.20
6	60.70	2.69
7	23.17	1.03

Table 5.2 Total and percentage length of drainage line by stream order.

The distance to footpath variable was included after digitising the mass movements as some mass movement features, particularly terraces, were observed in close proximity to footpaths. Although the distribution of footpaths is relatively concentrated in the GCSF, including this variable improved the performance of the logit models. The variable was therefore included in all of the analyses for the sake of continuity and consistency. Buffers were created

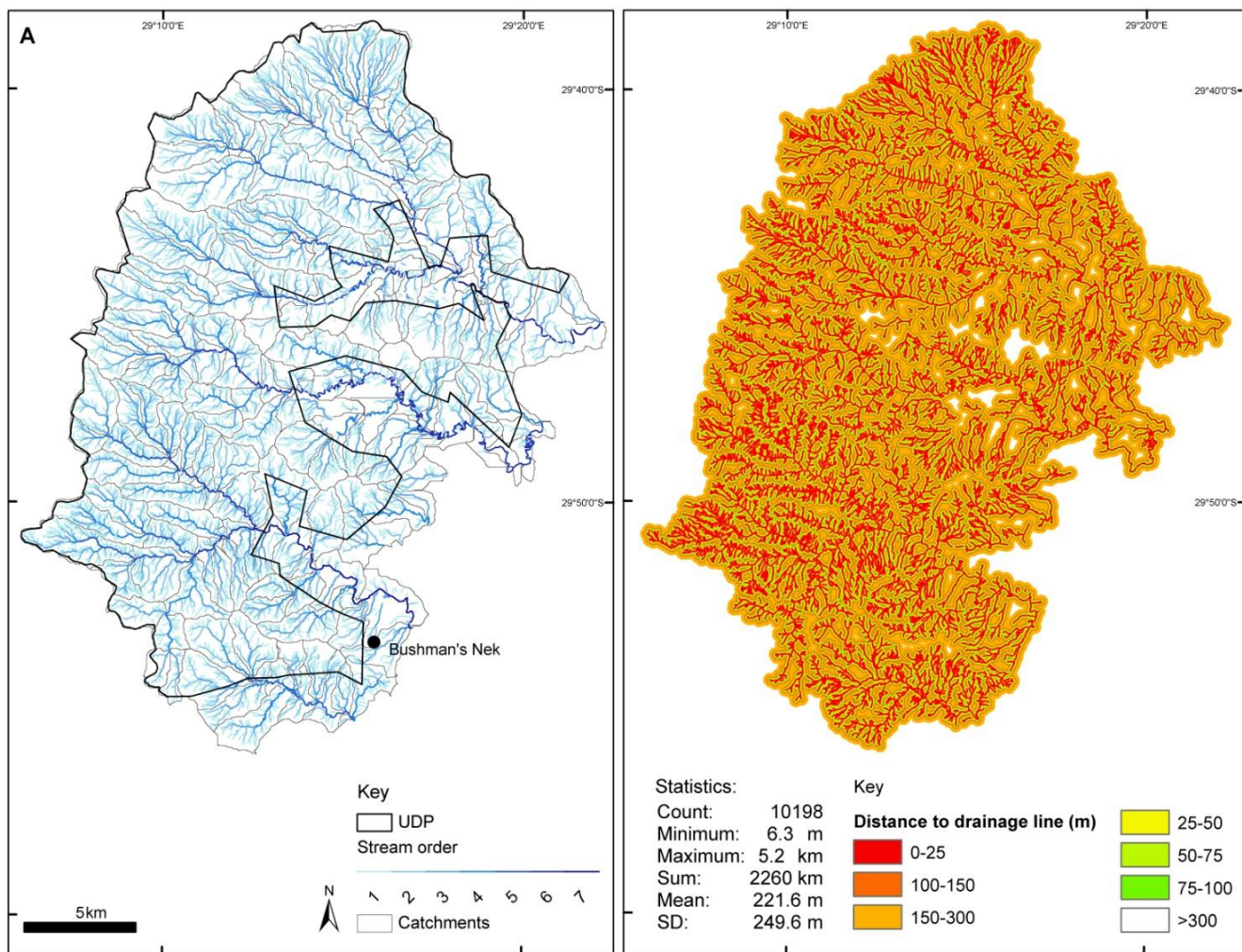


Figure 5.4 Vector data of drainage lines and the buffered raster used for the statistical analyses

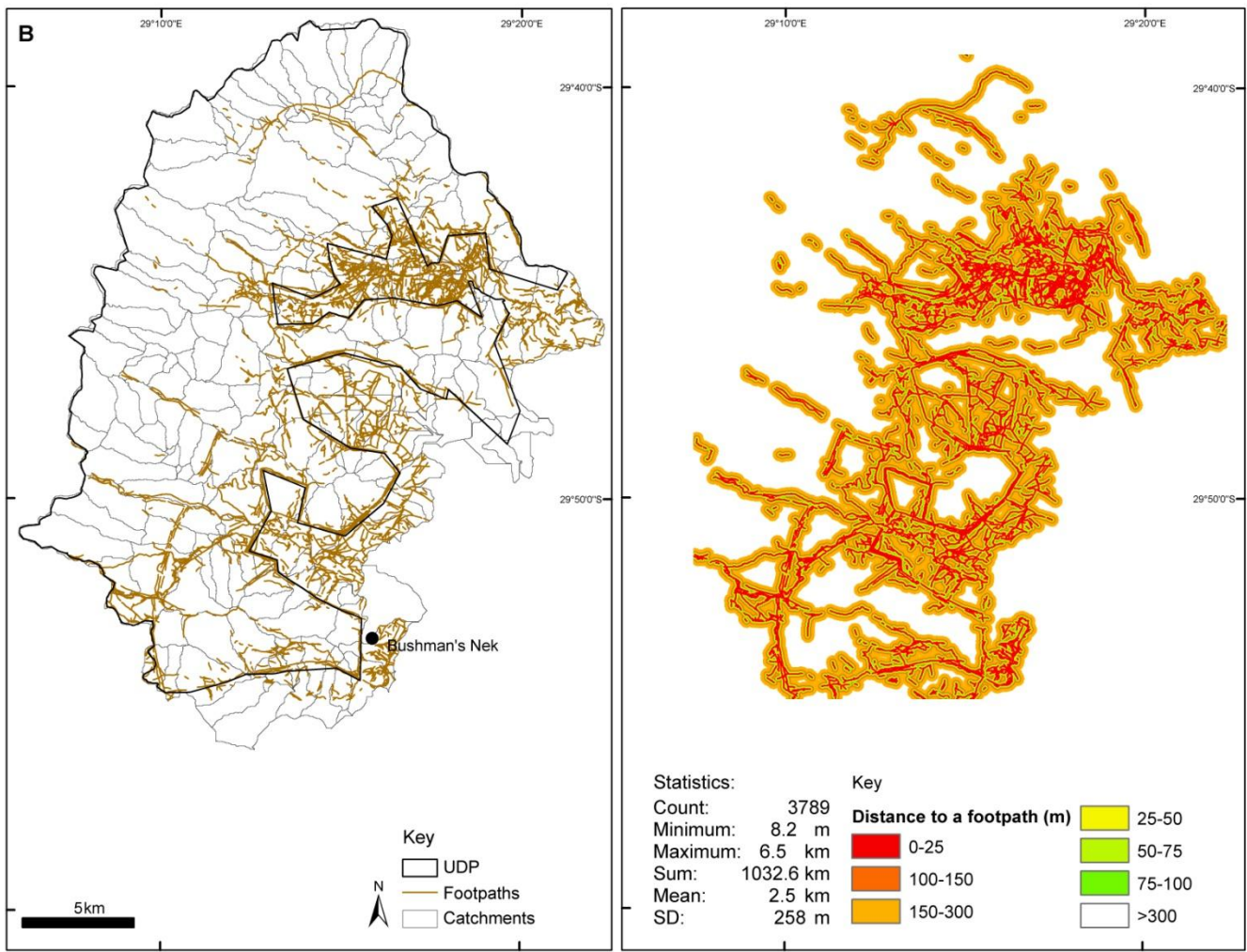


Figure 5.5 Vector data of footpaths and the buffered raster used for the statistical analyses.

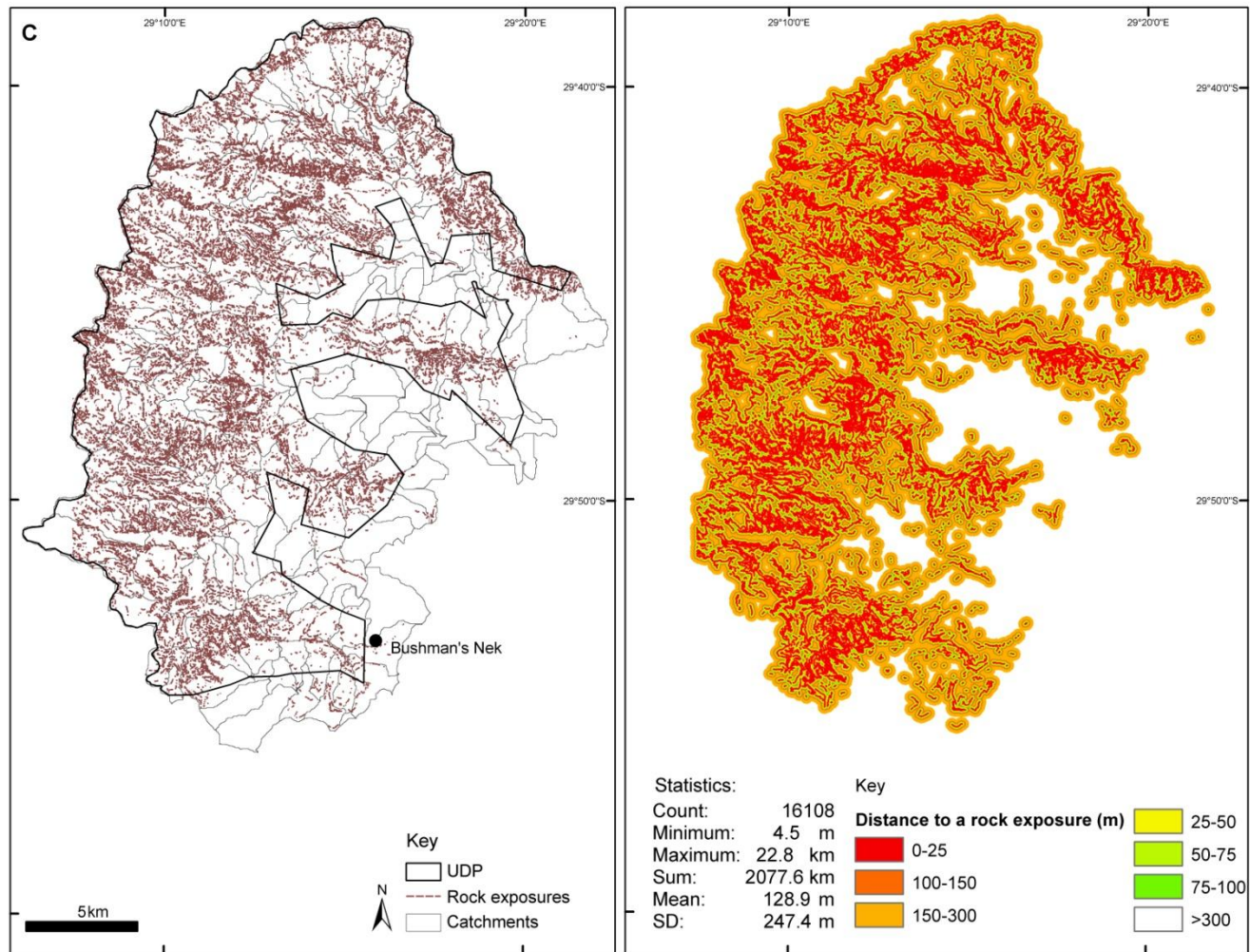


Figure 5.6 Vector data of rock exposures and the buffered raster used for the statistical analyses.

around the polylines in each shapefile so that the distance from a mass movement feature could be represented as pixels of the DEM (Figure 5.4-5.6). This facilitated the interpretation of the statistical results and made all of the dependent variables categorical. Mass movement frequency apparently peaks from about 50m of a drainage line (Abdallah et al., 2005) and declines from about 300m (Yesilnacar and Topal, 2005). The buffers were then converted to rasters for sampling.

Geological data describing the lithology of the southern Drakensberg were provided by the Council for Geoscience at 1: 250 000 scale (Figure 5.7). The polygon shapefile was converted to a 25m cell size raster for sampling. Minimum and maximum elevation ranges for the Clarens Formation are greater than expected for the southern Drakensberg (Table 4.1). The Clarens Formation dips slightly along the Drakensberg and this expands the altitudinal range relative to the thickness of the unit (G. Botha, pers. comm.).

Topographic variables associated with mass movement activity include altitude, aspect, slope gradient and curvature, which represent second derivatives of a DEM as they are constructed from algorithms within a GIS environment. Altitude was generated by reclassifying the TTR DEM into classes with ranges of 200m (Figure 5.8). Altitude values derived from the DEM range from 1 527 to 3 296m a.s.l.

The Aspect algorithm (ESRI, 2008) uses a moving 3x3 window to calculate the rate of change in height from one cell to each of its eight neighbours. The rate of change in the x direction is defined as:

$$[dz / dx] = ((c + f + i) - (a + 2d + g)) / 8$$

Whilst the rate of change in the y direction is:

$$[dz / dy] = ((g + 2h + i) - (a + 2b + c)) / 8$$

Where: dz/dx is the rate of change in the x direction (delta)

dz/dy is the rate of change in the y direction (delta)

and a to i are constants which represent the position of a 3x3 grid stack.

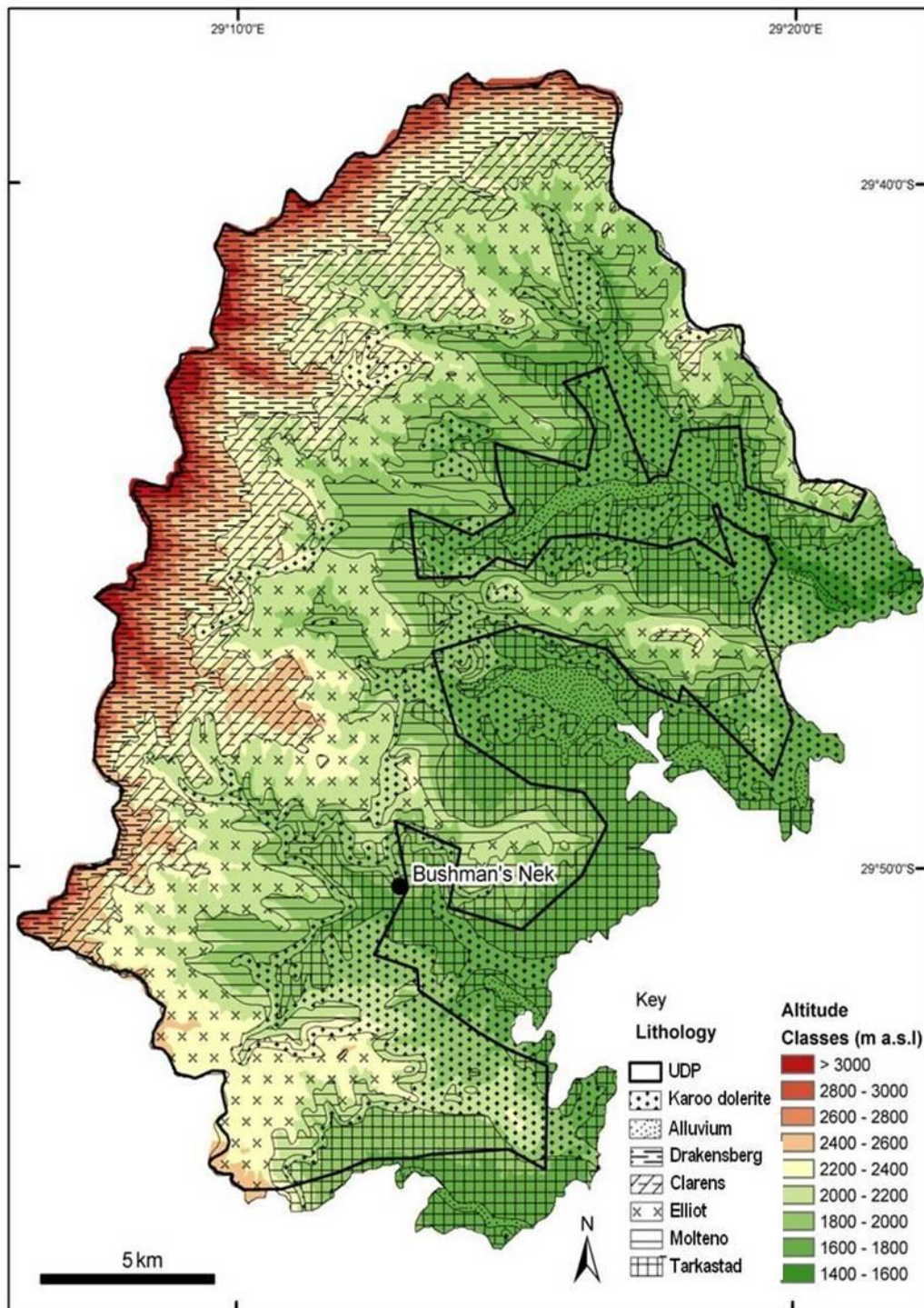


Figure 5.7 Lithology of the southern Drakensberg and altitudinal classes from the TTR DEM.

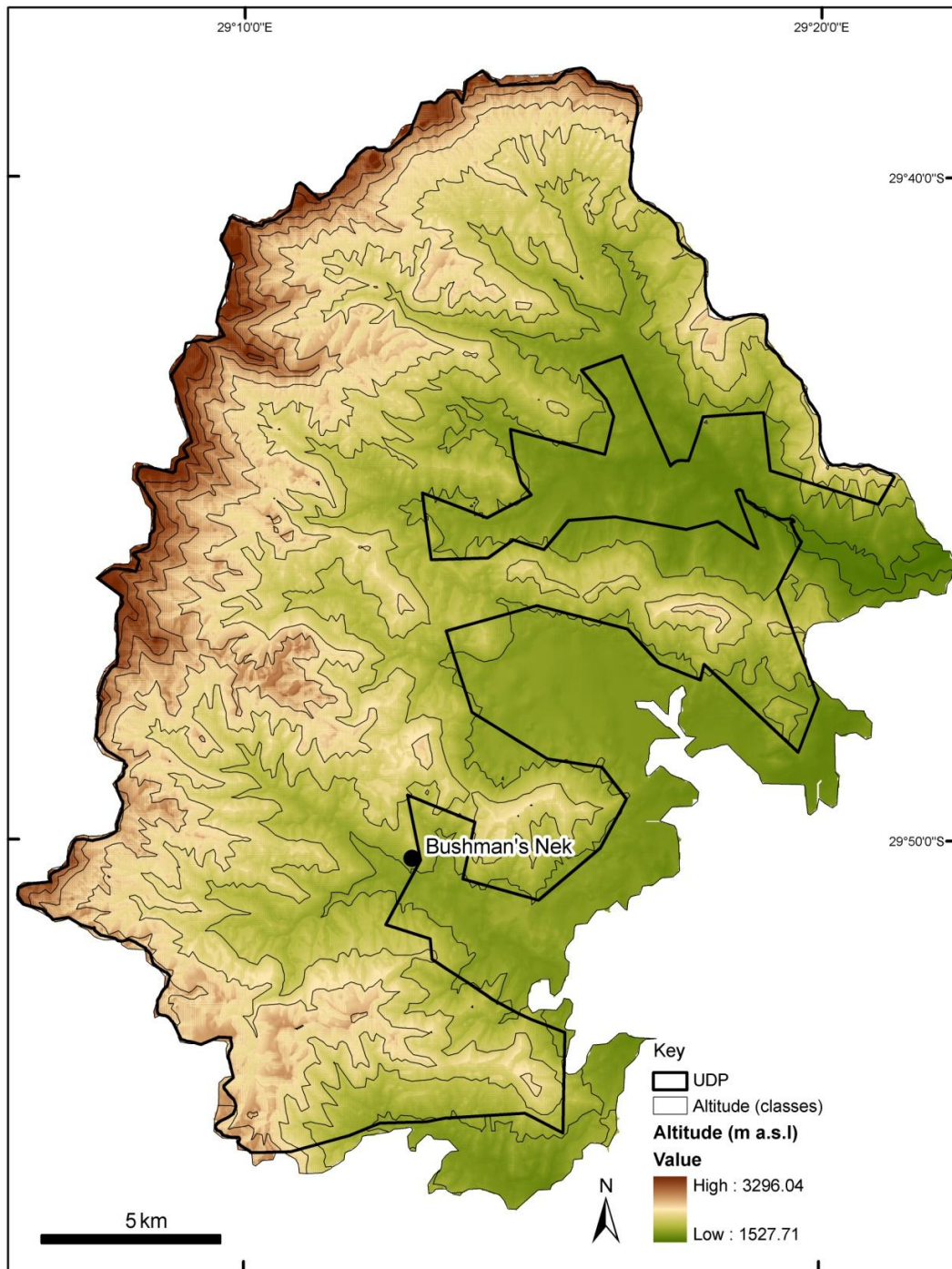


Figure 5.8 Altitude raster in the background and classed altitudinal values in the foreground.

The rate of change for a given cell is then calculated as:

$$\text{Aspect} = 57.29578 * \text{atan2} ([dz/dy] - [dz/dx]).$$

The aspect value is converted to a compass bearing from 0° - 360° and aspect values were then reclassified into categories corresponding to cardinal points (Figure 5.9).The software automatically generates a rendered layer which

separates north-facing slopes into 2 groups (0° - 22.5° and 337.5° - 360°) to match the number of degrees in a circle. These groups both represent north-facing slopes and are grouped into one category or left separate where necessary depending on the type of statistic being performed. Aspect is an important factor controlling mass movement distribution because aspect influences soil moisture conditions, temperature and weathering. In Japan, mass movements tend to be concentrated on north to north-east facing slopes (Ayalew and Yamagishi, 2004), whilst in Hong Kong mass movement distributions are concentrated on south-facing slopes (Dai and Lee, 2002).

Gradient is calculated using the SLOPE function which also uses a 3x3 moving window to compare the rate of change of the surface in the horizontal and vertical directions. Slope measured in degrees uses the algorithm:

$$\text{Slope_degrees} = \text{ATAN} (\sqrt{([\text{dz} / \text{dx}]^2 + [\text{dz} / \text{dy}]^2)}) * 57.29578.$$

Slope values were reclassified into classes of 10° intervals. Slope gradients for the study area range from 0° to 61° , based on the derived slope gradient raster (Figure 5.10). This may appear to be an underestimate of the actual slope gradients for the Drakensberg, given that vertical and near vertical rock exposures occur extensively throughout the study area. However, as slope is calculated along the extent of a 25m x 25m cell, the gradient represents an average. The number of categories and size of intervals that some studies have used varies (c.f. Dhakal et al., 1999; Ayalew et al., 2004; Ayalew and Yamagishi, 2004) from as few as four to as many as eight classes (Wachal and Hudak, 2000; Dai and Lee, 2002; Bai et al., 2010).

Plan and profile curvature rasters were calculated using the CURVATURE function. This is determined on a cell by cell basis and a fourth-order polynomial is fit to a surface composed of a 3x3 moving window. To better understand how slope form affects mass movement distribution, the plan and profile curvature rasters were multiplied to produce nine layers that matched the nine landforms identified by Ayalew and Yamagishi (2004) (Figure 5.11). Four slope units were

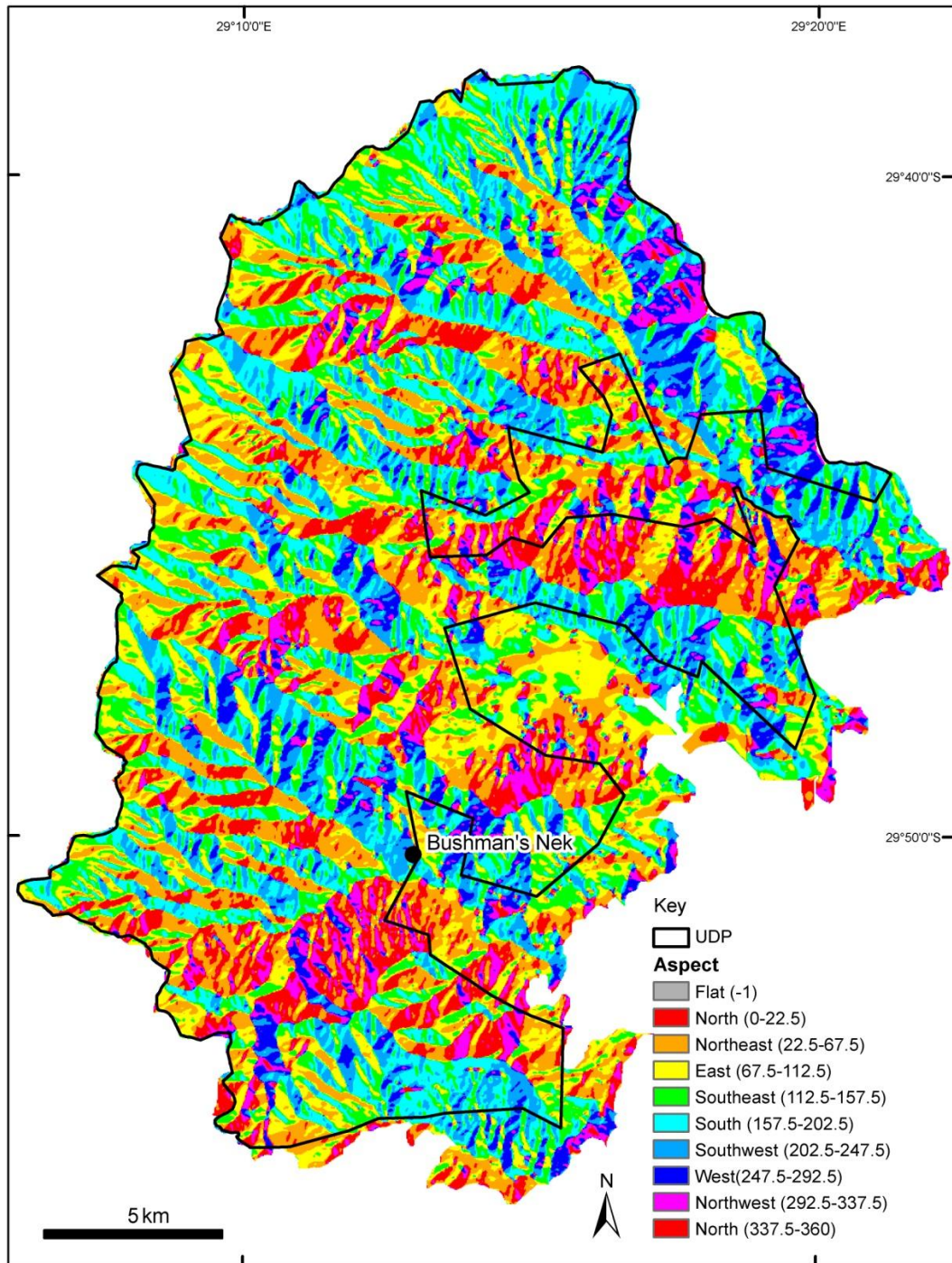


Figure 5.9 Aspect according to cardinal directions. The two values for north (0-22.5 and 337.5-360) are equivalent.

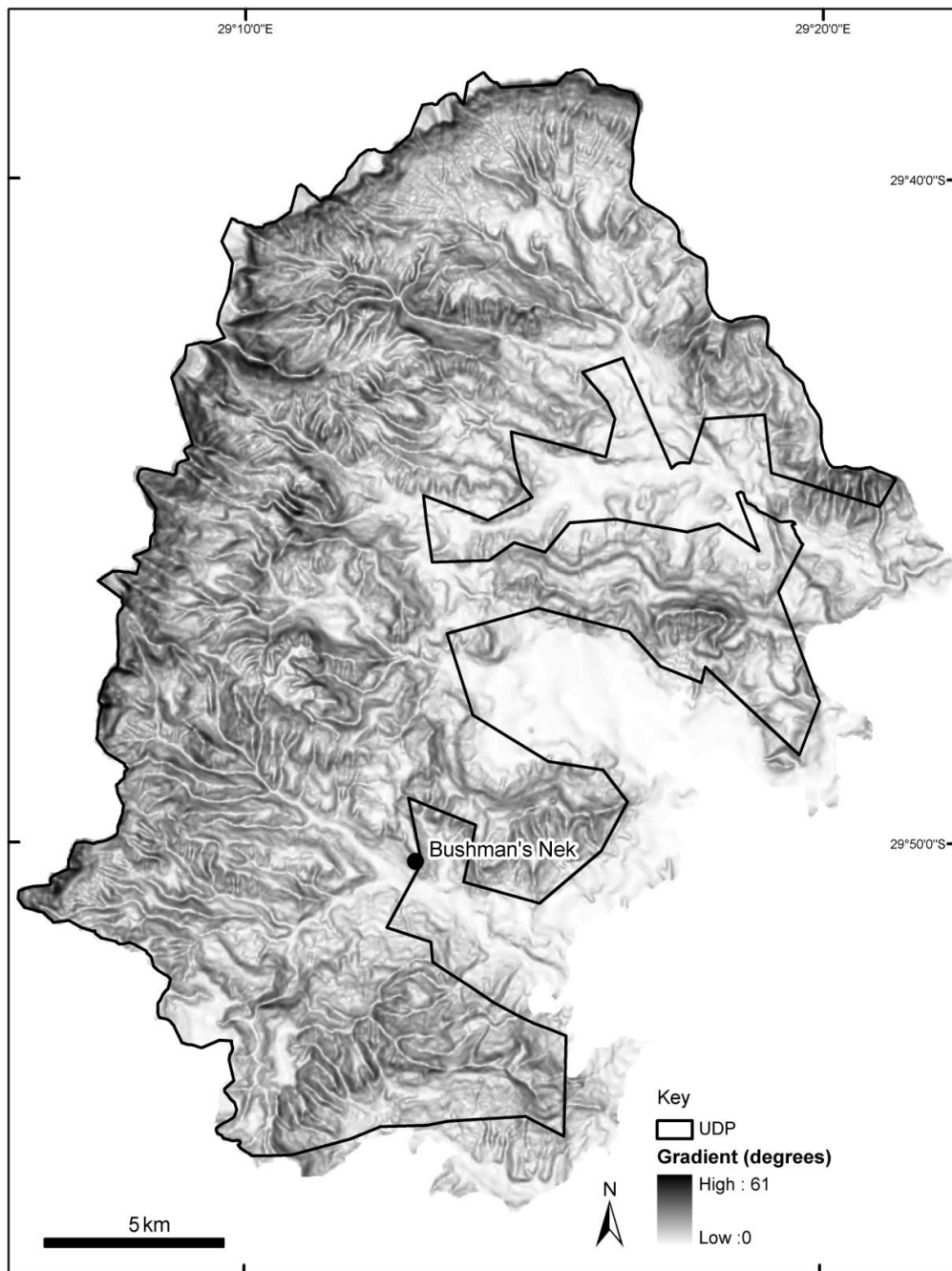


Figure 5.10 Gradient in degrees.

associated with mass movement activity in the southern Drakensberg; namely sloping closed basins which have a concave lateral and vertical profile (CC), sloping inflated hills which have a convex lateral and vertical profile (CxCx), sloping protuberant basins that have a convex lateral profile and concave vertical profile (Cx C) and sloping recessing hills which have a concave lateral profile and convex vertical profile (CCx) (Figure 5.12).

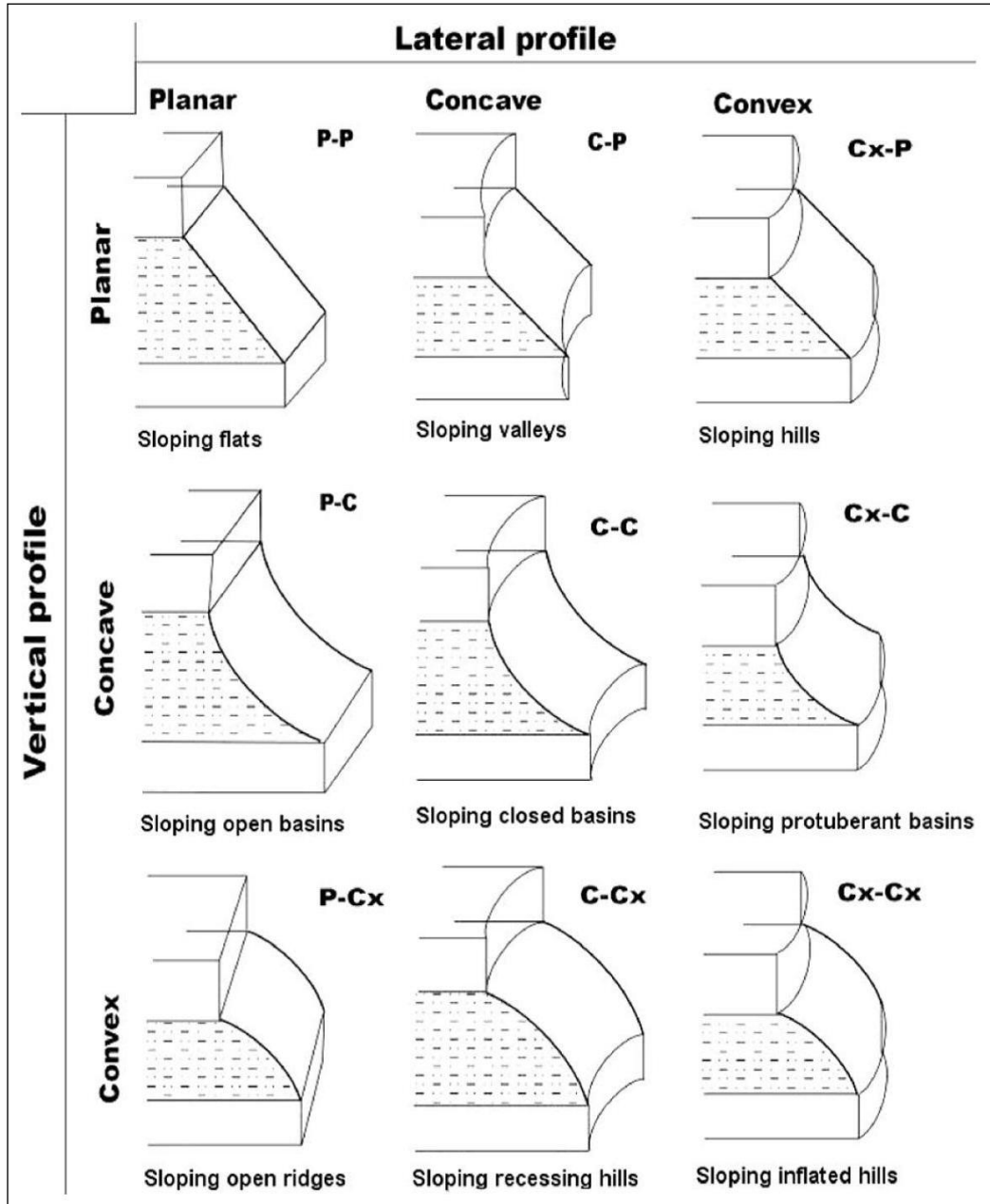


Figure 5.11 The hypothetical landscape model (after Ayalew and Yamagishi, 2004).

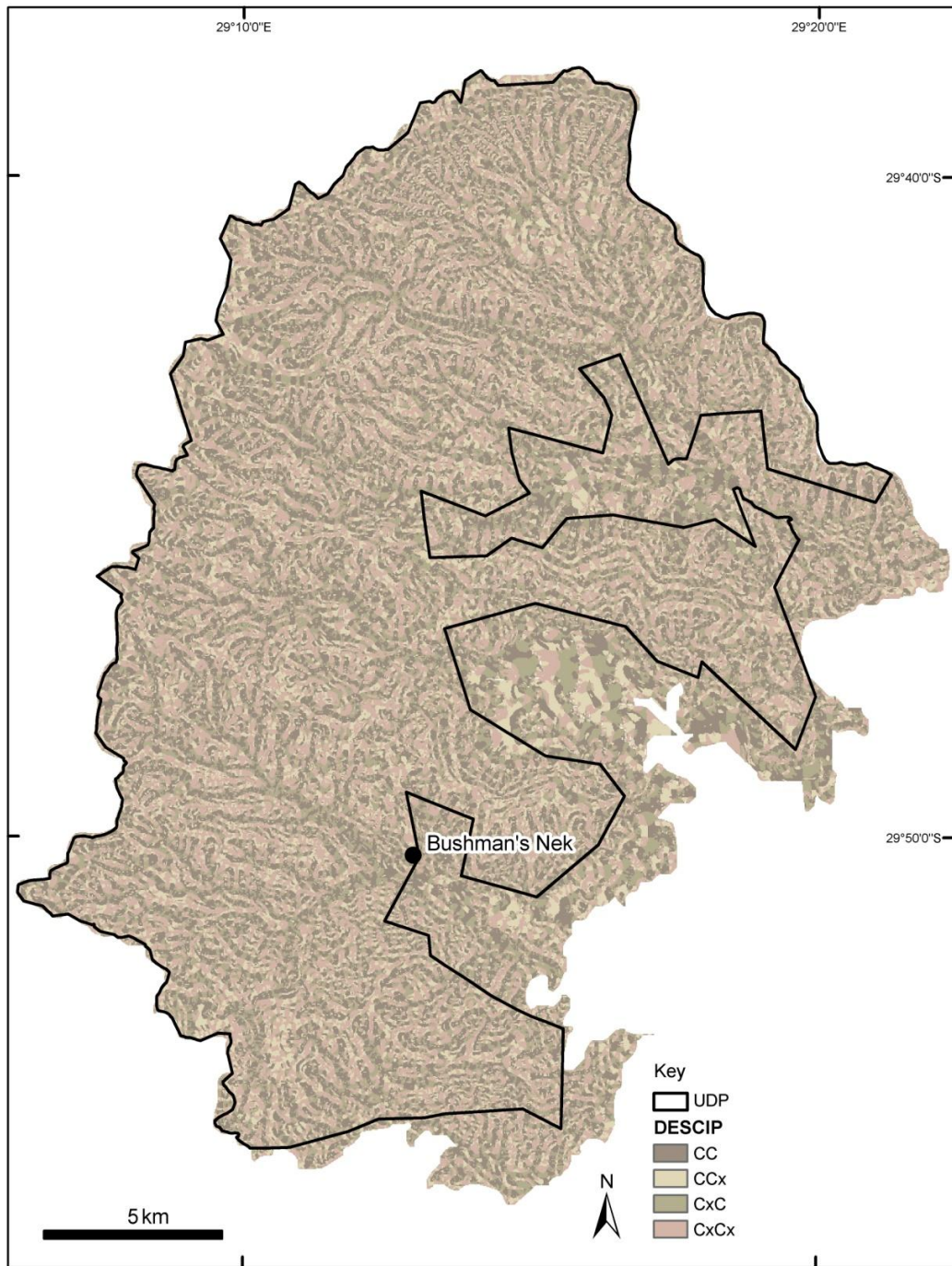


Figure 5.12 A composite raster of the four landscape units present in the southern Drakensberg, derived after Ayalew and Yamagishi's (2004) nine-unit landscape model.

Data describing the frequency and nature of fires in the area over the past 14 years were provided by Ezemvelo KZN Wildlife. However, this information was later discarded because no time/date information exists for mass movement events in the southern Drakensberg, so mass movement activity could not be correlated to

burn regularity. Time series analyses would need to be undertaken to relate the frequency of fires to mass movement events. A summary of the final variables selected for input into the statistical models is presented in Table 5.3. All input data were categorized and converted to rasters with a cell size of 25m.

Data	Source	Scale	Format	Derived dataset	Raster format	# of classes
Drainage lines	Digitized	1:50 k	Polyline	Distance to drainage line	Categorical	7
Footpaths	Digitized	1:50 k	Polyline	Distance to footpath	Categorical	7
Rock exposures	Digitized	1:50 k	Polyline	Distance to rock exposure	Categorical	7
Lithology	Geoscience	1:250 k	Polygon	Lithology	Categorical	8
DEM	Topo to Raster	25m	Raster	Altitude	Continuous	9
				Aspect	Continuous	9
				Gradient	Continuous	6
				Slope unit -	Categorical	5
				Plan curvature	Continuous	-
				Profile curvature	Continuous	-
Total number of classes						58

Table 5.3 Layers representing the environmental variables used to compare mass movement types.

5.5 The mass movement inventory

Hardcopy black and white aerial photographs and digital orthophotos (1:50 000) for the period from 2000/2001 (Job 1047) were obtained from the NGI. The aerial photographs were not used for consequent analyses as the scanned images could not be orthorectified. All digitising was therefore completed using the 1:50 000 orthophotos at a scale of 1:2 835. Mass movements were identified by API based on their morphological form, the presence of bare surfaces that show as lighter colours on the image, and by hummocky topography which represent standard techniques for API (c.f Sowers and Royster, 1978). Mass movements were digitized as polygons and the rock deposits were digitized as points using the shape and difference in colouration between the rocks and the surrounding vegetation (Antoniou and Lekkas, 2010).

195 Catchments were delineated using the TTR DEM and ArcHydro 8.3, with a stream initiation threshold of 1.5 km or 2 400 cells. The total catchment area (461

km²) represents the final study area which extends beyond the boundary of the UDP (351 km²). Mass movement features and rock movement deposits were digitised per catchment to ensure that the study area was exhaustively sampled. Where possible, the whole mass movement feature (from crown to toe) was digitised, given that in some cases multiple mass movements were observed within the displaced mass of the original mass movement. No prior mass or rock movement inventory exists for the GCSF, thus no historical information could be included, such as frequency or scale of events

The mass movement inventory shapefile contained all the mass movement feature types identified by API and in the field. Each type was allocated a 'Class' (S for slide scar, T for terrace) and 'Type' (SA, SB, SC, SD, SE, T1, T2, T3). Class S represents shear scars caused by slides, flows and slides/falls and Class T represents terracettes, terraces and solifluction lobes which were not digitised individually, but rather captured as 'fields', given that these features are best represented as a collective (Table 5.4). No attribute data was captured for the rock movement deposits.

Most rockfalls occur along exposed bedrock outcrops and are caused by weathering processes, although some composite slide/falls occur along vertical slope faces that have eroded by stream incision. The shadow effects associated with steep slopes make identifying the rockfall source areas on aerial photographs difficult. It is however possible to map the displaced blocks and surface areas of rock movement deposits, and this technique has been used in previous studies to identify potential source areas (Antoniou and Lekkas, 2010). The rock movement deposits are located within centimeters to metres of the source area, depending on the velocity of the displaced rock. The environmental variables sampled in the GIS using the rock movement point data therefore represent information about the depositional conditions of the slope. Duplicate points were identified using the `v.clean` command in GRASS (6.4.1RC1), which creates an output shapefile of the duplicated points. A total of 595 points were then manually removed in ArcMap.

Mass movement type	Description	Appearance	Number digitised
T1	Terracettes	Regularly spaced, groups of linear steps / treads that run parallel to the contour of the slope.	677
T2	Solifluction lobes	Terraces that have lobate fronts, generally more distinct than terracettes and wider in areal extent.	200
T3	Terraces	Irregularly shaped single linear steps / treads occurring over a short horizontal distance.	337
SA	Shear scar	Elliptical to u-shaped concave depression of varying sizes. Slide scar surfaces may be vegetated or exposed. Slide scar scarps form a distinct boundary. Examples are sites E and F.	1 900
SB	Shear scar and incised flow path	Shear scar as described in SA but has a clearly identifiable incised flow path. The flow track tapers downslope and the deposit at the toe is relatively prominent. Incised flow paths are easily identifiable even after the track has been vegetated due to the new substrate usually being colonised by trees and shrubs rather than grass. Incised flow tracks may develop into drainage lines. Examples are sites B and D.	480
SC	Shear scar and surficial deposit	Shear scar as described in SA but a surficial deposit is easily identifiable. The flow path and associated deposit is slightly sinuous and widens in the downslope direction. The deposit runs the length of the flow path and may form a fan at the base of the slope or taper to a point. As the vegetation along the flow path is covered rather than removed, it is only possible to identify these features if the surficial deposit has not been eroded by surface wash. Examples are sites G and H.	385
SD	Sheet slide in solifluction lobe fields	Irregularly shaped shear surface that has a larger areal extent than type SA. Deposits are composed of scree and are bare of vegetation. These features only occur in solifluction lobe fields.	108
SE	Slide/fall	Shear scar associated with a near-vertical slope gradient in the downslope direction, usually the result of a fall or topple. Examples are sites A and J.	49

Table 5.4 Classification used to create the mass movement inventory.

Each mass movement polygon shapefile was converted to a point shapefile using ArcGIS 9.0 so that the environmental variables could be sampled for each point. The resulting point is located at the centre of gravity of the polygon. Five random point shapefiles were then generated using a modelling protocol created using Model Builder in the ArcGIS Toolbox. Each random point shapefile has a population equivalent to the number of mass movements observed for that type. The aim of the random sampling was to test the robustness of the statistical techniques. The SAMPLE tool in Spatial Analyst was used to extract the values of the input raster variables to points in the mass movement and random shapefiles.

5.6 Statistical analyses

Numerous techniques have been developed for predicting mass movement occurrence and a thorough examination of methodologies and examples pre-2000 can be found in Carrara et al. (1995), Soeters and van Westen (1996) and Guzzetti et al. (1999). Most probability models are deterministic and based on the concept that mass movements in the future are more likely to occur under the conditions which caused mass movement in the past and present (Carrara et al., 1995). Typical prediction models include Conditional Analysis (Clerici et al., 2002; Donati and Turrini, 2002; Gokceoglu et al., 2005; Havenith et al., 2006; Conoscenti et al., 2008), calculating weights (Gupta and Joshi, 1990; Ayalew et al., 2004; Lan et al., 2004; Saha et al., 2005; Neuhäuser and Terhorst, 2007; Thierry et al., 2007; Ruff and Czurda, 2008; Song et al., 2008), Discriminant Analysis (Carrara et al., 1991; Baeza and Corominas, 2001; Santacana et al., 2003; Guzzetti et al., 2006), and Logistic Regression and Neural Networks (Catani et al., 2005; Ermini et al., 2005; Mathew et al., 2009; Pradhan, 2010; Dong et al., 2011).

5.6.1 Multivariate techniques: logistic regression, hierarchical partitioning and CLT

Logistic regression appears to be an increasingly popular method for producing probability maps of mass movement and has recently been applied in the

Americas (Ohlmacher and Davis, 2003; Gorsevski et al., 2006; Chang et al., 2008; García-Rodríguez et al., 2008), Europe (Yesilnacar and Topal, 2005; Begueria, 2006; van Den Eeckhaut et al., 2006; Akgun and Bulut, 2007; Federici et al., 2007; Greco et al., 2007; Marques et al., 2007; Nefeslioglu et al., 2008) and Asia (Lee, 2004, 2005, 2007; Chau and Chan, 2005; Lee and Sambath, 2006; Lee and Pradhan, 2007; Lee et al., 2007; Wang et al., 2007; Yao et al., 2008). Logistic regression creates a multivariate regression between a dependent variable and several independent variables. The independent variables may be categorical or continuous and they do not need to be normally distributed, making logistic regression a more robust technique to use than linear regression. The goal of a regression model is to find the best-fitting model to describe the relationship between the independent and dependent variables, and step-wise techniques can be used to determine which independent variables are redundant.

Logistic regression can be used to spatially represent areas of increasing susceptibility to mass movement, however one of the major drawbacks of this technique is that multi-collinearity between the independent variables means that using a combination of the 'largest' coefficients to infer causality between independent and dependent variables provides little valid explanatory power (Mac Nally and Horrocks, 2002). The individual coefficients of a multiple regression model can only be interpreted for direct effects on the response variable when the other predictor variables are held constant (James & McCulloch, 1990). Thus, logistic regression cannot be used to conclude, for example, that terracettes are most likely to occur within 25 – 50 m of a rock exposure on south-facing slopes, based on the evidence that these are the highest coefficients. However, logistic regression can provide enough information to make comparative statements about variables, such as for example that there is a greater probability that terracettes will occur on south facing slopes (coefficient = 0.031) rather than on south-east facing slopes (coefficient = 0.000).

Hierarchical partitioning (Chevan and Sutherland, 1991) is a possible solution to the dilemma of identifying the most likely causal factors of a particular

phenomenon. The hierarchical partitioning method has been used by conservation biologists to predict habitat types and species distributions (Mac Nally, 1996, 2000; Townsend Peterson and Cohoon, 1999; Mac Nally and Horrocks, 2002; Gibson et al., 2004; Pont et al., 2005), whilst Hjort (2006) used hierarchical partitioning to identify environmental factors associated with periglacial landforms. Hierarchical partitioning is based on the theorem of hierarchies in which all possible models in a regression are jointly considered so that the most likely causal factors can be identified (Pont et al., 2005). The impact of a variable X is determined by comparing the goodness-of-fit statistics for all models that include the variable X, so that if variable X has strong independent effects, model XU will have an improved goodness-of-fit statistic than for model U alone (Mac Nally, 2000).

Another multivariate method that has been developed for the purpose of classifying data is classification and regression trees (CART). CART is a statistical technique that distinguishes mutually exclusive and exhaustive subgroups of a population whose members share characteristic attributes (Lemon et al., 2003). CART evaluates all of the possible splits for a selection of predictor variables and selects the best single split overall, based on the impurity of a node (Berk, 2008). Ideally, the best split is one that has the least impurity, and is defined as a nonnegative function of the probability that $y=1$. The Gini Index is commonly used to calculate impurity and will partition the data so that there is one homogenous node with few cases and other relatively homogenous nodes with many cases. Entropy tends to partition the data until all of the nodes contain relatively equal numbers of cases and homogeneity (Berk, 2008).

CART is relatively easy to use and generates a graphical output that is simple to interpret (De'ath and Fabricius, 2000). However, classification trees may produce splitting decisions that are unstable because a few observations can dramatically affect which variables are selected. Trees may also become complex, which makes them difficult to interpret and may create associations between variables that do not exist in reality. Thus, expert knowledge is required to distinguish

which associations are representative. CART was therefore used to identify possible subcategories which may exist within the classification used for API.

5.6.2 Univariate statistics: histograms and the InfoVal

Interpretation of univariate techniques, such as histograms, which are used to predict or weight independent variables, is as complicated as the multivariate methods. A frequency distribution can only provide information on one of the independent variables and therefore fails to show the influence of a range of input variables. This is particularly problematic if some input variables are known to increase the likelihood of a mass movement, whilst others are known to reduce it. Compounding this problem is that classes within an input variable will have different influences on the dependent variable, and that the relationship between classes within a category is not always linear. Another problem encountered when relying on frequency distributions for information, is that the frequency is not normalised for area. Various weighting approaches exist (for example the Information Value (InfoVal) and Weights of Evidence [WofE] methods), which determine the ratio of the number of mass movement features within a class to the area of that particular class. This means that a class that covers a small surface area will have a higher weighting than another class with the same number of mass movement features but encompassing a greater surface area. However, although this method better represents the distribution of mass movement features than a frequency distribution, it cannot be used to describe causality between the variables.

Frequency statistics for each mass movement type were generated using XLStat 2009. An InfoVal was calculated for each class of the independent variables as follows (Saha et al., 2005):

$$W_i = \ln \left(\frac{\text{Densclas}}{\text{Densmap}} \right) = \ln \frac{N_{\text{pix}}(S_i)/N_{\text{pix}}(N_i)}{\sum_{i=1}^n N_{\text{pix}}(S_i) / \sum_{i=1}^n N_{\text{pix}}(N_i)}$$

Densclas is the landslide density within a thematic class and Densmap is the landslide density within the entire thematic layer. $N_{\text{pix}}(S_i)$ is the number of

landslide pixels in a certain thematic class, $N_{pix}(N_i)$ is the total number of pixels in a certain thematic class, and n is the number of classes in a thematic map. The natural logarithm is used to take care of the large variation in the weights. The frequency distributions and Infoval were ranked and the highest values were then compared.

A classification tree was created for each random iteration per mass movement type using XLStat 2009. The classification tree produces divisions based on the Gini coefficient, which calculates the amount of homogeneity within a leaf and represents the purity of that leaf. The classification tree was used to identify whether subcategories existed within a defined mass movement type. For example, summarising the classification trees for terrace mass movements indicates that terraces may be further categorized based on lithology. The classification trees for each mass movement type were summarised by selecting the nodes that had the highest membership of mass movement ($Typemm > Type0$) and by comparing the overall frequency (n_{Leaf} ; n_{Sample}) and purity. Subdivision beyond the fifth node produced meaningless results because nodes either represent cases where $Typemm < Type0$ or had a frequency of $<10\%$ of the total sample size (n_{Sample}). These nodes were pruned from the tree and a summarised tree was created which represents the most division (greatest purity) and the highest frequency of actual mass movement features ($Typemm$).

Logistic regression modelling and hierarchical partitioning was undertaken using the R Statistical package which is an open-source software product operating under the GNU license. The extensions used to undertake the analysis are called 'mass' and 'heir.part'. Further information on the logistic function is provided by Ohlmacher and Davis (2003). Forward and backward stepwise regression was used and model performance was assessed using the Akaike's Information Criteria (AIC) goodness-of-fit estimate. The model with the lowest AIC represents the model that best fits the logit curve and minimises the number of independent variables used. The Bayes Information Criterion (BIC) is also used to assess model goodness-of-fit, but includes a higher penalty for the number of

independent variables used in the model. The BIC therefore consistently selected a model with less parameters than were selected by the AIC. A misclassification matrix which estimates the overall predictive accuracy of the model was also used to compare models. Failure to converge errors occurred for almost all of the mass movement types (T1, T2, T3, SC, SD and SE). This type of error occurs if there is more than one class within a dataset that contains no Type=1 cases and only Type=0. Thus, the model cannot fit the data to the curve and the intercept value of the model is infinite. In this situation the classes that contain no Type=1 are collapsed until all the classes contain at least one instance of Type=1. The highest number of collapsed classes was for the solifluction lobes (16/58 classes collapsed) and for sheet slides (20/50 classes collapsed).

Five iterations of logistic regression and hierarchical partitioning were undertaken for each type and the number of variables selected. The AIC, BIC and percentage correctly predicted as well as the variable with the highest independent contribution and the first node from the CART analysis were compared. Conclusions could then be made about the number of independent variables which best predict a mass movement type and the variable which has the greatest independent effect (%I) on the model. The highest %I contribution was also compared to the highest frequency distribution identified by histograms and the highest InfoVal. The results do not compare well due to the underlying nature of the statistical techniques.

Technique	Type	Area weighted?	Predictive?	Infers causality?	Sub-classifies?
Histograms	Univariate	No	No	No	No
InfoVal	Univariate	Yes	Heuristic	No	No
CART	Multivariate	No	No*	Limited	Yes
Logistic regression	Multivariate	No	Yes	No	No
Hierarchical partitioning	Multivariate	No	No	Yes	No

Table 5.5 The various techniques and their applications for statistical analysis. No* represents that predictive modelling can be undertaken with CART but this requires further analysis. CART was not used for predicting mass movement distribution for this study.

Table 5.5 shows how each of the statistical techniques were applied in this study. These techniques were selected because they are appropriate for modelling categorical data and do not require that the input data be normally distributed.

5.6.3 Probability mapping

Five maps representing the probability of a particular type of mass movement were generated using the intercepts and beta coefficients produced by each logistic regression model. The calculated beta coefficient is added in a field to the attribute tables of the input variables per class. If a model's classes were collapsed to create convergence, the logistic regression was rerun and a proxy value of 10-8 was used. This was done so that all of the classes could be used in the models and be allocated a coefficient. All of the input rasters were then summed using the field containing the beta coefficients. Raster Calculator was used to calculate the negative exponent of the weighted sum and the probability as:

$$\text{Probability} = 1 / (1 + \{\text{negative exponent of the weighted sum}\}).$$

The five maps for each mass movement type were then compared using a cut and fill operation to determine where the greatest variation between probabilities occurred, as most of the models had relatively similar misclassification values. This provided complimentary information to support a final model selection and a composite mass movement probability map was then generated for each mass movement type.

5.6.4 Spatial Point pattern analysis

Spatial point pattern studies are useful for exploring the underlying structure of a dataset and has application in a wide variety of scientific and engineering disciplines (Su and Chou, 2001; Hirzel et al., 2002). A number of techniques exist to establish the degree of randomness of the distribution of a series of points and most compare area or quadrat counts to a Poisson distribution (Cressie, 1993). A Poisson distribution expresses the probability of a given number of events occurring in a fixed area of time or space if these events occur at an average known rate or independently of each other (Su and Chou, 2001). Complete spatial randomness (csr) is synonymous with a homogenous Poisson process and has the

property that the events of a process in a bounded region are equally likely to occur anywhere within that region and that the events do not interact with each other (Cressie, 1993). Two methods exist for determining csr, namely statistics based on distances between events, and descriptive statistics based on quadrat counts.

The Average Nearest Neighbour ratio (ANN) was calculated to determine whether the point data is clustered or dispersed. If the point data are statistically clustered, more detailed models can be developed. The function measures the distance between each feature centroid and its nearest neighbour's centroid location. If the average distance is less than the average for a hypothetical random distribution, the distribution of the features being analyzed is considered clustered, whereas if the average distance is greater than a hypothetical random distribution, the features are considered dispersed. The ANN is given as:

$$ANN = \frac{\bar{D}_O}{\bar{D}_E}$$

Where \bar{D}_O is the observed mean distance between each feature and their nearest neighbour:

$$\bar{D}_O = \sum_{i=1}^n d_i$$

And \bar{D}_E is the expected mean distance for the features given a random pattern:

$$\bar{D}_E = \frac{0.5}{\sqrt{n/A}}$$

d_i equals the distance between feature i and its nearest feature, n corresponds to the total number of features and A is the total study area. If the index (average nearest neighbour ratio) is less than 1, the pattern exhibits clustering. If the index is greater than 1, the trend is toward dispersion (ESRI, 2011). The ANN is different to the average distance between N th neighbours which is a summary

statistic determined by measuring the distance between a feature and all of its Nth nearest neighbours. The average distance is a useful summary statistic for determining neighbourhood threshold distances (ESRI, 2011).

Quadrat sampling involves counting the number of events in subsets or sample areas within a study region (Cressie, 1993). The shape of the quadrats is traditionally rectangular, although any sample shape is possible. Quadrats may be placed randomly or contiguously. Rectangular contiguous quadrats of various sizes were created using the Vector Grid tool in QGIS, which is available in the fTools plugin. The numbers of events per quadrat were calculated using the Points in Polygon tool which is also part of the fTools package. Descriptive statistics were calculated for the quadrats in Excel, with the number of quadrats and the mean, standard deviation, maximum number and number of unique values of points for each layer calculated. The mean, excluding quadrats which contained no points (frequency, or number of points in polygon [PIP] equals 0), the percentage of quadrats containing values greater than zero, and the average deviation from the mean, were also calculated. These values highlight the effect that quadrat size has on identifying clusters within the layer, as larger quadrats have fewer rectangles containing no points but much higher deviations from the mean.

The Point and Kernel Density function in ArcGIS were used to calculate a magnitude per unit area. The Point Density function calculates the density of point features around each output raster cell. Conceptually, a neighbourhood is defined around each raster cell centre, and the number of points that fall within the neighbourhood is totalled and divided by the area of the neighbourhood (ESRI, 2011). Neighbourhoods may be circular, rectangular, annulus or wedge. The Kernel Density function calculates the density from each point feature using a kernel function based on the quadratic kernel function described in Silverman (1986). The function calculates the density of a number of points within a defined neighbourhood or search radius by adding the values of all the kernel surfaces where they overlay the raster cell centre. Only a circular search area is possible

within the kernel density function (ESRI, 2011). The difference between the Point and Kernel density functions is that the Kernel function spreads the known quantity of the population for each point out from the point location, creating a smoother continuous surface. Increasing the radius will not greatly change the calculated density values (ESRI, 2011).

The Kernel Density function produces a raster grid of intensity values that were converted into contours using the Contour tool in the Spatial Analyst toolbox. Contours of 5 000 events/km² were generated and then compared to the digitized rock movement points. Whilst the contours identified areas with highly clustered points, the density function could not differentiate between clusters in close proximity to one another. The Hot Spot and Cluster Analysis tools in the Statistical analyst toolbox were then used to confirm this. The results suggest that point clusters cannot be statistically identified using statistical tools available in standard software packages, and therefore further analysis on the morphology of rock movement deposits was not undertaken. However, the point data can still be used to identify environmental variables associated with their location and to produce probability maps using hierarchical partitioning and logistic regression.

A stratified sampling technique was developed to sample the rock movement point data, as logistic regression over-estimates the significance of co-variables when the dependent variable dataset is too large. Hsieh et al. (1998) have developed calculations for selecting adequate sample sizes from datasets which range from 119 – 3 060 depending on the research design and the statistical properties of the input data, although larger sample populations of up to 176 857 can be used for univariate regression models (Hsieh, 1989). Traditionally, the number of landslide events which have been used to model landslide probability lies within this range [e.g. 30 (Akgun, 2012), 43 (Dong et al., 2011), 142 (Bai et al., 2010), 253 (Mathew et al., 2009), 324 (Pradhan, 2010) and 492 (Falaschi et al., 2010)]. The stratified samples representing the rock deposits were created by randomly selecting a percentage of points (1%, 5% and 15%) within different class densities to preserve the spatial pattern of the event data (Hengl et al., 2009),

and then merging the selections from each class into one shapefile (Figure 5.13). The absence data was created by randomly selecting a number of points equivalent to the presence data where no rock movement deposits had been digitized. All of the environmental variables, excluding distance to a footpath, were then sampled for each stratified 'presence' layer and the 'absence' point layers and the same statistical techniques used for the mass movement modeling were adopted. Probability maps were then generated for each sample set. Similar techniques have been adopted for producing rockfall hazard maps in Greece (Antoniou and Lekkas, 2010) and New Zealand (Allen et al., 2011).

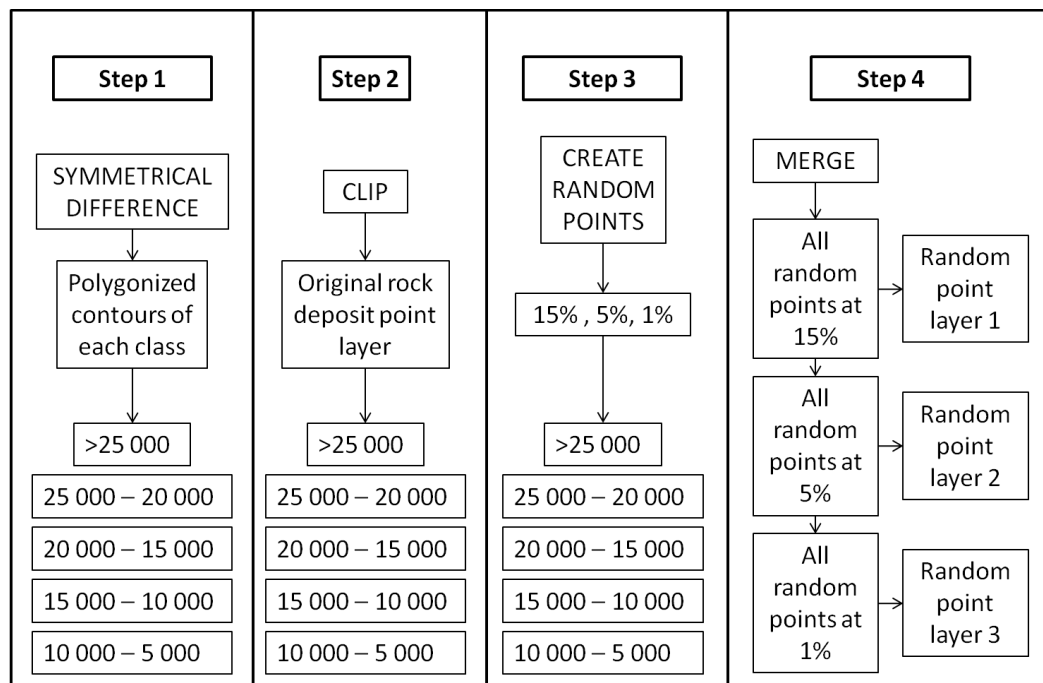


Figure 5.13 Flow diagram of the process used for generating the stratified samples of the rock movement point data

6 Field-based assessment of mass movement landforms in the southern Drakensberg

6.1 Introduction

Chapter 6 presents the results of the fieldwork component in sub-sections which provide information about each mass movement feature observed in the field. The results of the field assessment include a classification of the type of movement using the proposed classification and the terminology of Varnes (1978) (Figure 6.1), a description of the topographic location and associated environmental conditions, and photographs and geomorphological maps of the mass movement features. A brief summary of the vegetation types found at the sites is given [using Pooley (2003)], however as the majority of fieldwork was undertaken during the dry winter months, some of the grasses could not be identified. The descriptions of the mass movement features are based on observations made in the field, the inventory forms and detailed oblique photographs (Figure 6.2). Table 6.1 summarizes the morphometric attributes measured at each site.

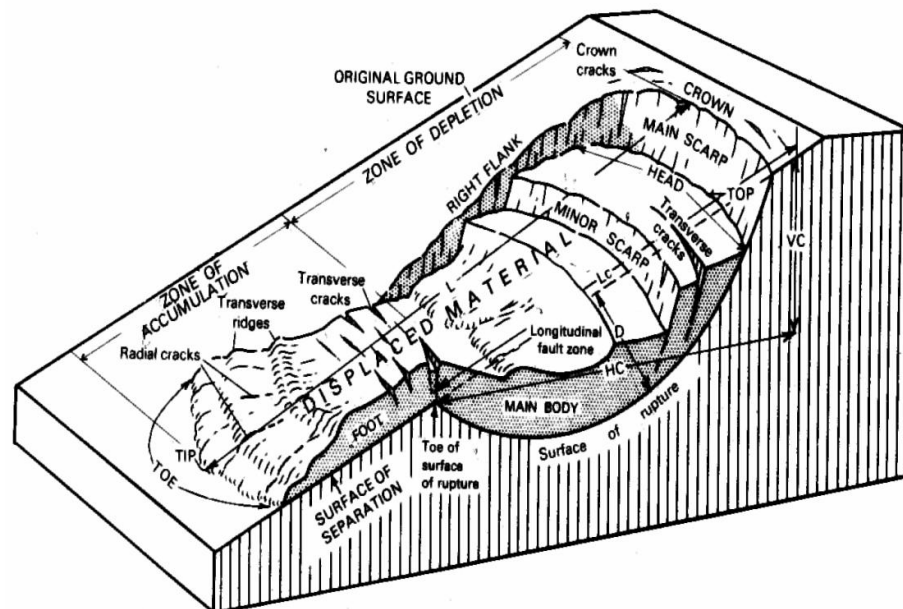


Figure 6.1 Idealised block diagram of a landslide showing the terminology used to describe the components of the slide (after Varnes, 1978).

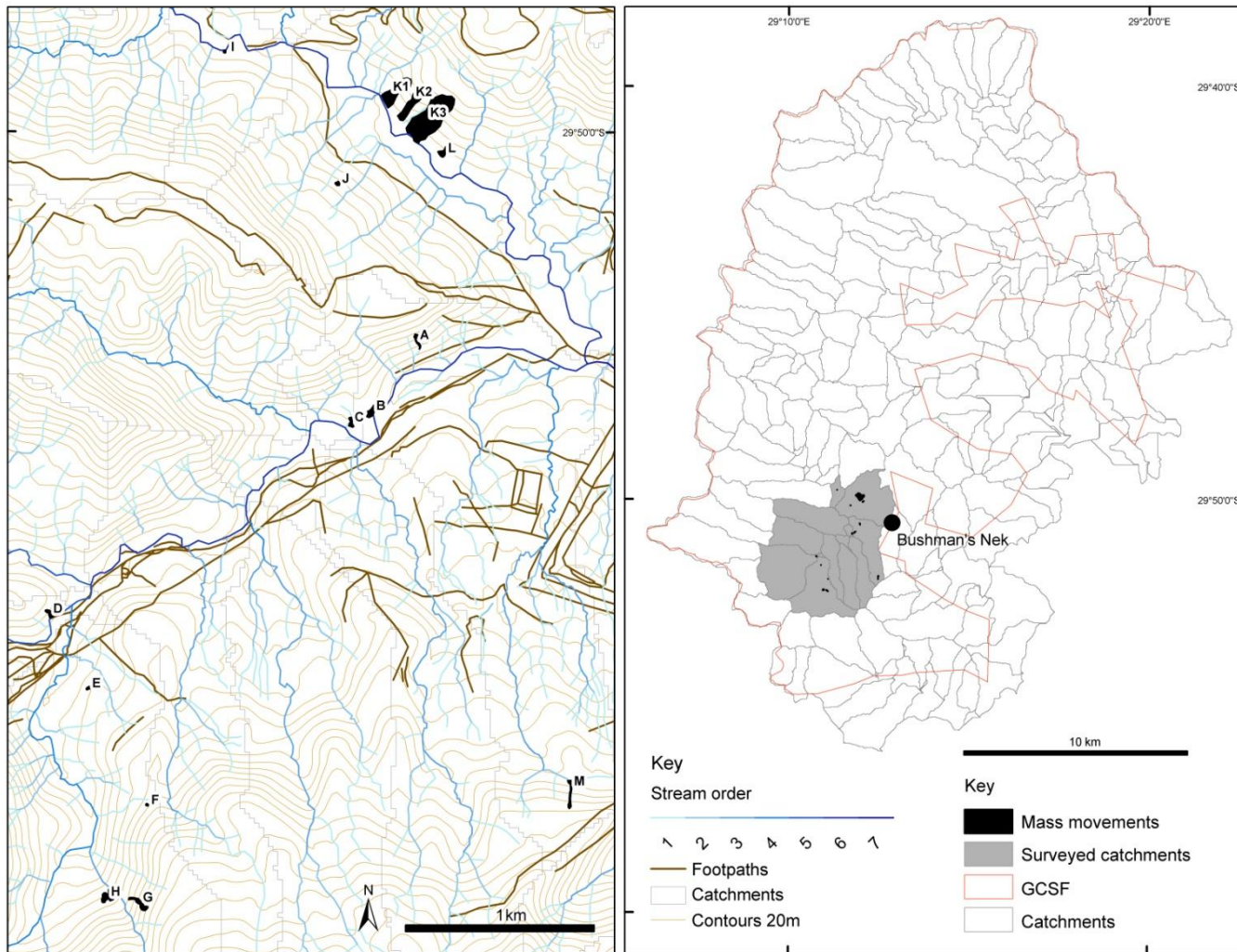


Figure 6.2 Locations of sites which were measured in the field in relation to the GCSF.

Site	MM type	SMh	STh	Sw	SI	Sdg	Th	Tw	TI	Tdg	Dw	DI	Ddg	Aspect
A	Slide/flow	0.4-1.2	0.5-0.32	20.7	27.6	32	0.3-0.5	6.8-13.5	47.6	41	15.6	23	20.7	South
A	Consequent slide	0.4	-	4.3	6.2	15	-	-	-	-	-	-	-	South
B	Fall	-	-	87	3-11.7	90	-	-	-	-	10.8-18	2.7-5.6	14-19	Southeast
B	Consequent slide	0.34	-	4.6	5.1	23	-	-	-	-	-	-	-	Southeast
C	Slide/flow	0.8	0.3	22	10.9	15	-	14.4	18.5	18	32	27.8	12	Southeast
D	Incised flow	0.8-1.8	0.5-0.8; 1.2-1.8	20.5	29.2	37	1.1	9.3	33.7	28	21	8.9	17	Southeast
E	Slide	0.5-0.8	-	23	8.8	28	-	-	-	-	-	-	-	Northwest
F	Slide	0.8	-	22.1	13.3	21	-	-	-	-	-	-	-	West
G	Surficial slide/flow	0.58	-	12.2	8.2	68	-	16.7	66.1	47	3.8	16.2	25	Northwest
H	Surficial slide/flow	0.3-1.7	-	10.3	8.2	30	0.35	4.9	29.6	29	3.2	8.7	10	North
H	Surficial slide/flow	0.3-1.7	-	10.3	8.2	30	0.35	5.6	33.4	35	11.8	5.8	10	North
I	Slide	0.9-1.7	1.1	12.2	9.2	34	-	-	-	-	-	-	-	North
J	Slide	2.85	0.7	24.7	21.3	30	-	-	-	-	-	-	-	Northeast
L	Slide/flow	1.6	0.9	27	42.2	40	-	14.5	11.8	24	43	41.5	20	Southwest
	Average	1.02	0.76	21.49	14.70	35.21	0.60	10.90	34.39	31.71	18.63	18.84	16.39	
M	Slide/flow/soil pipe?	2.6	-	14	29.3	34	1.2	6.5	95.8	26	37	26.7	3	North
SMh	Main scarp height (m)						Tw	Width of transport zone parallel to contour (m)						
STh	Secondary terrace height (m)						TI	Length of transport zone perpendicular to contour (m)						
Sw	Scar width parallel to contour (m)						Tdg	Gradient of transport zone (degrees)						
SI	Scar length perpendicular to contour (m)						Dw	Width of deposit parallel to contour (m)						
Sdg	Gradient of scar (degrees)						DI	Length of deposit perpendicular to contour (m)						
Th	Height of transport zone (m)						Ddg	Gradient of deposit (degrees)						

Table 6.1 Morphometric measurements were obtained in the field for all sites except K. Average values exclude site M which was not classified.

6.2 Site A: Slide, Ngwangwane River

Site A is located at 29°11'58.53" E; 29°50'34.43"S; at 1 868m a.s.l (Figure 6.2). The slide is located on a south-facing slope along the Ngwangwane River. The style of movement is complex, although there is evidence of consequent and composite mass movement around the slide scar. Zonation is distinct and the source, transport and depositional zones can be identified (Figure 6.3). Movement type appears to progress from slide to flow. The slide was originally classified as a rotational movement due to the terraced state of the displaced material, however on closer inspection the slide was reclassified as translational. These movement types have also been referred to as 'roto-translational' or 'semi-translational' (Hart, 2008; Dahal et al., 2009). The displaced material breaks up into small 'islands' that are held together by clumps of grass which have been referred to as 'rafted islands' (Geertsema and Pojar, 2007). The 'islands' appear to be moving independently, suggesting that a number of events have led to their development rather than a single event. Loose sediment from the scarp and shear surface have accumulated in rills on the shear surface and are progressively confined into a single transport channel.

The main scarp which forms the back wall of the slide is vertical and appears to be composed of colluvial material which overlies a weathered and crumbly purple-yellowish mudstone, possibly of the Elliot Formation. The contact between the two zones is relatively distinct and can be identified in the profile of the main scarp (Figure 6.4). Tension cracking parallel to the crown area has created joints and cracks in the soil that have progressed in places to become soil pillars. The main scarp is between 0.4 and 1.2m high and the terraces below the scarp become shallower downslope (from 0.51-0.32m). The slide is 20.7m in width and 27.6m in length. The average slope angle for the depletion zone is 32° (Table 6.1).

When viewed from the opposite valley side and from the 1: 50 000 orthophotos, the slide identified at site A appears to be a secondary movement upon the shear surface of a larger inactive mass movement feature. Levees are present on both sides of the slide; the left levee is up to 31m wide and about 85m long and the

right levee is up to 19m wide and 74m long (Figure 6.5). These levees are too large and well vegetated to have been created by the recent movements observed at the site. A large, well-vegetated debris lobe of 58m in width and 70m in length occurs downslope of the shear surface at site A. Examination of the aerial and oblique photographs showed another two potential slide scars to the left and right of site A whose morphological boundaries have been smoothed by erosion. All of the inactive features appear to have originated as slides and progressed to incised flows (Figure 6.6). The general topography of the area is hummocky and this site presents a possible association between inactive, large, palaeo-mass movements and contemporary mass movement activity.

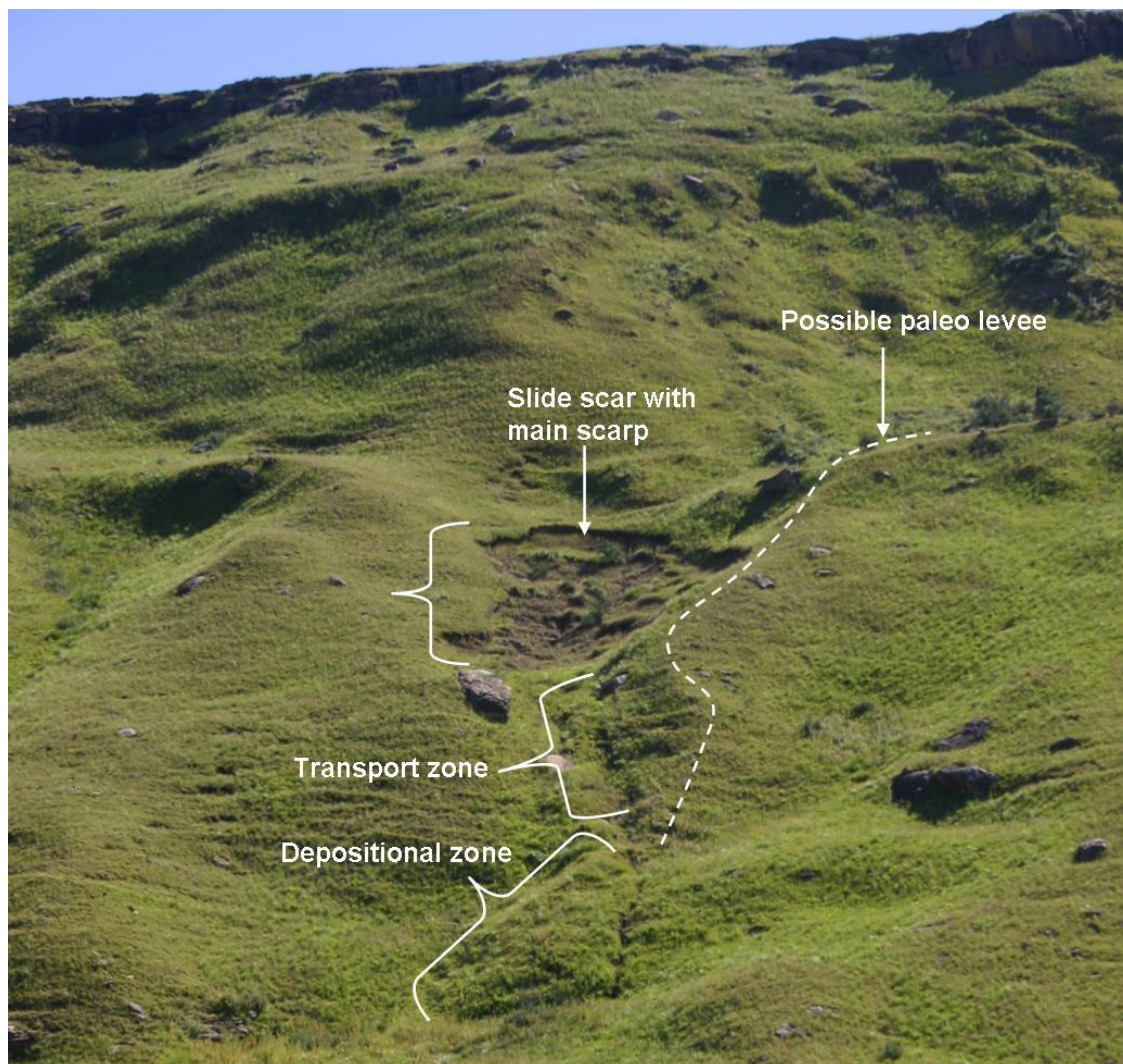


Figure 6.3 Oblique photograph of site A showing main scarp and the transport and depositional zones.



Figure 6.4 (A) The contact between the colluvium and mudstone and (B) a tension crack at the crown of the slide scar which has developed into a soil pillar.

Below the shear scar, the slope angle of the transport channel is about 41° and the flow channel tapers from 13.5m to 6.8m. The channel is confined by lateral ridges on either side. A number of rills on the shear surface coalesce into a single channel just above the transport zone and the presence of *Merxmeullera macowanii* and *Morella pilulifera* in the channel suggest either that moisture is present at the site or that the channel serves as a drainage line. No seepage zones were observed at Site A, although the soil on the right flank of the feature appeared wetter than the soil on the left flank, as this area was shadowed by the surrounding terrain. The slope angle decreases to 20.7° at the foot of the site where the deposit is fan-shaped and measures 23m in length and 15.6m in width. Sediments consisting of small particles to boulders are transported in the channel and some of the larger blocks appear to have originated from a rock exposure about 100m upslope. The deposit is composed of both new and stabilised material and it appears that the depositional process is slow, allowing grasses to grow which stabilise the deposit.

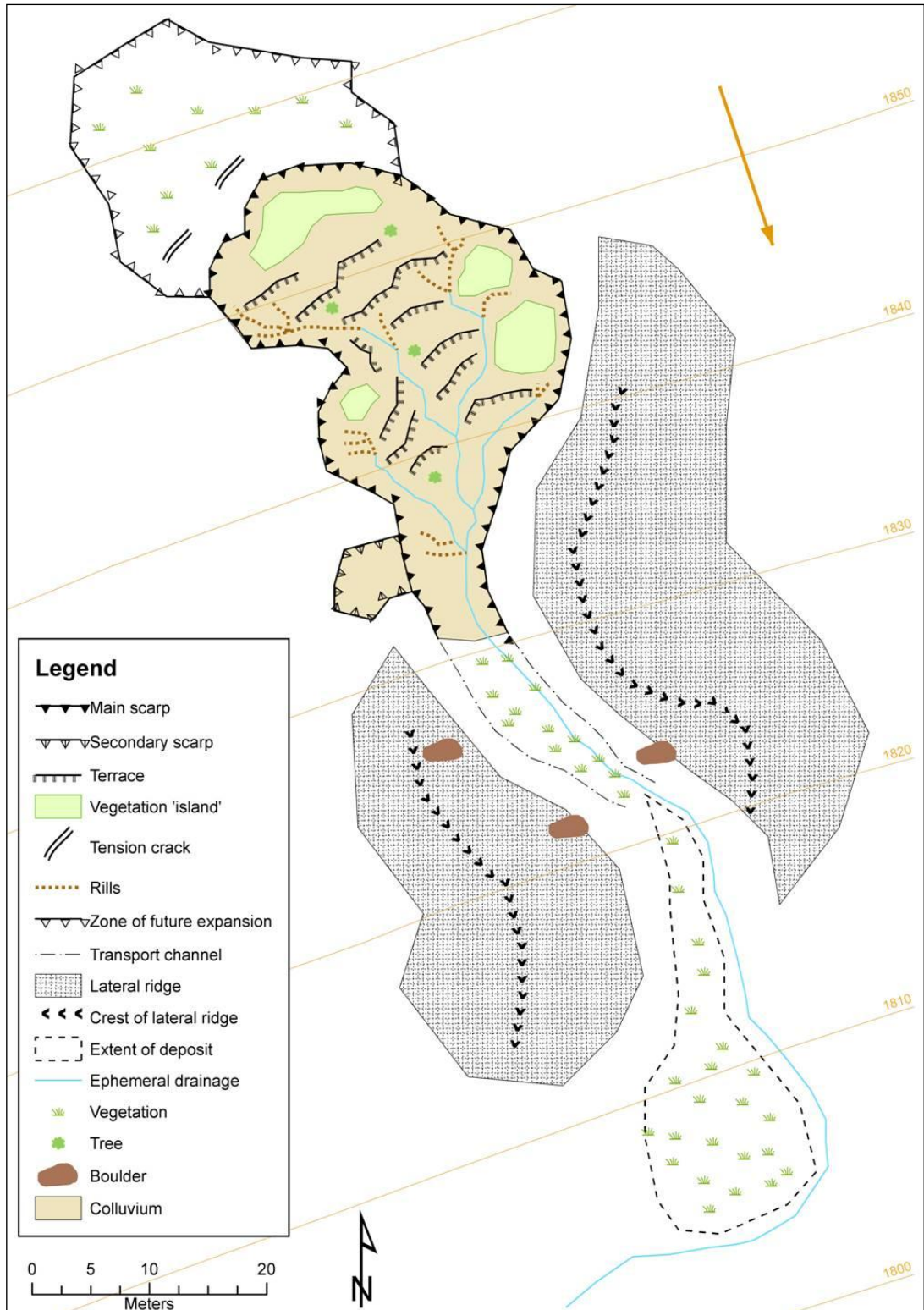


Figure 6.5 Geomorphological map of the complex mass movement feature at site A.

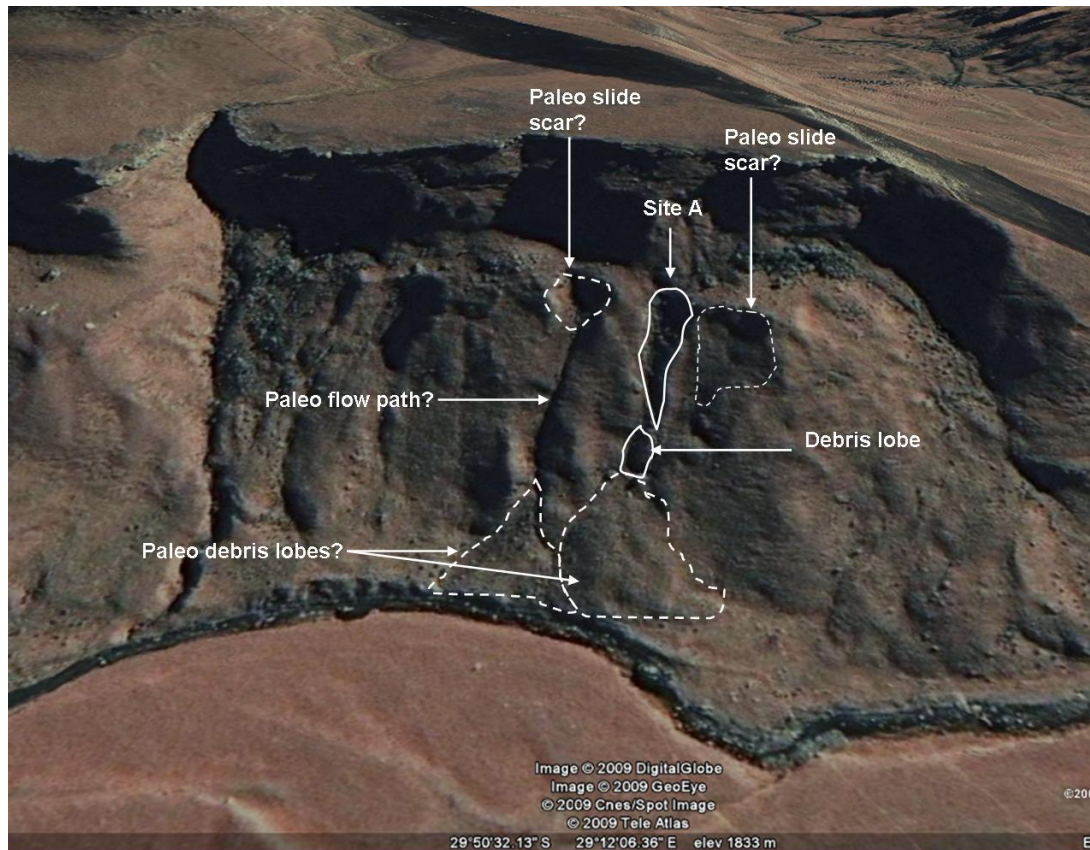


Figure 6.6 Oblique view of site A using Google Earth (2009). Two possible palaeo-mass movement features can be observed. Note the hummocky terrain on the surrounding slopes.

A small translational slide can be observed on the left flank of the depletion zone. The shear surface is 4.3m wide and 6.2m long and inclined at 15° , dipping towards the main slide scar. The material mobilised by the slide would have been transported to the shear surface of site A, incorporated into the flow channel and deposited on the fan. Similar small ‘slumps’ could be observed around the main scarp suggesting that the feature is slowly expanding laterally and upslope. The main scarp of site A is roughly in line with the scarps of the inactive features on both sides, and a small planation surface can be observed above this zone. Thus, although retrogressive movement seems active, it is limited by the slope angle above the slide scar. Lateral extension below the depletion zone is limited by the levees and it is unlikely that the debris fan at the base of the feature will increase in size, especially given the small quantity of material that is currently being mobilised from the shear surface.

6.3 Site B: Slide, Ngwangwane River

Site B is located on the southeast-facing bank of the Ngwangwane River at 29°11'50.18" E; 29°50'47.89"S; at 1 788m a.s.l (Figure 6.2). The feature is classified as a multiple fall/composite slide (Table 2.6) as a number of processes are occurring at the site. A relatively distinct zone of failure exists which is created by a near-vertical exposure of Tarkastad Subgroup sandstones and mud/siltstones (Figure 6.7). Two types of movement can be observed at the site; namely a slide which occurs above the main scarp and falls across the rock face.

Seepage zones are visible across the face of the exposure, even during the dry season, and this constant supply of water has resulted in extensive weathering and discolouration (Figure 6.8). The rock is composed of red and green to grey mudstone and medium grained sandstones that have a sandy white to yellow colour on exposure and become orange-red to purple-grey when weathered. Two lithological units occur; the first comprises most of the depletion zone, is lighter in colour and coarser in texture than the layer beneath it, suggesting that the former is more arenaceous. The lower layer is composed of soft, fine grained sediments that may be more argillaceous in origin, displaying more bedded layers than the overlying strata. The sandstone is more consolidated and contains wider joint spacings and discontinuities, whilst the finely grained sediments below are highly weathered, jointed and crumbly.

The deposits at the base of the exposure are at an angle of repose between 14-19° (Table 6.1). Three separate deposits occur with the largest in the centre of the mass movement feature. This central cone has a maximum width of 18m and is about 5.6m long, with larger blocks (>1m³) forming the front of the deposit. The majority of the material in the deposit appears to come from the sandstone unit and the blocks have diverted the flow of the Ngwangwane River towards the opposite stream bank. The central deposit is asymmetrically distributed and extends downstream and some grading of the deposited material was observed.

This is most likely caused by fluvial transport as smaller material would have been transported downstream during high flows.

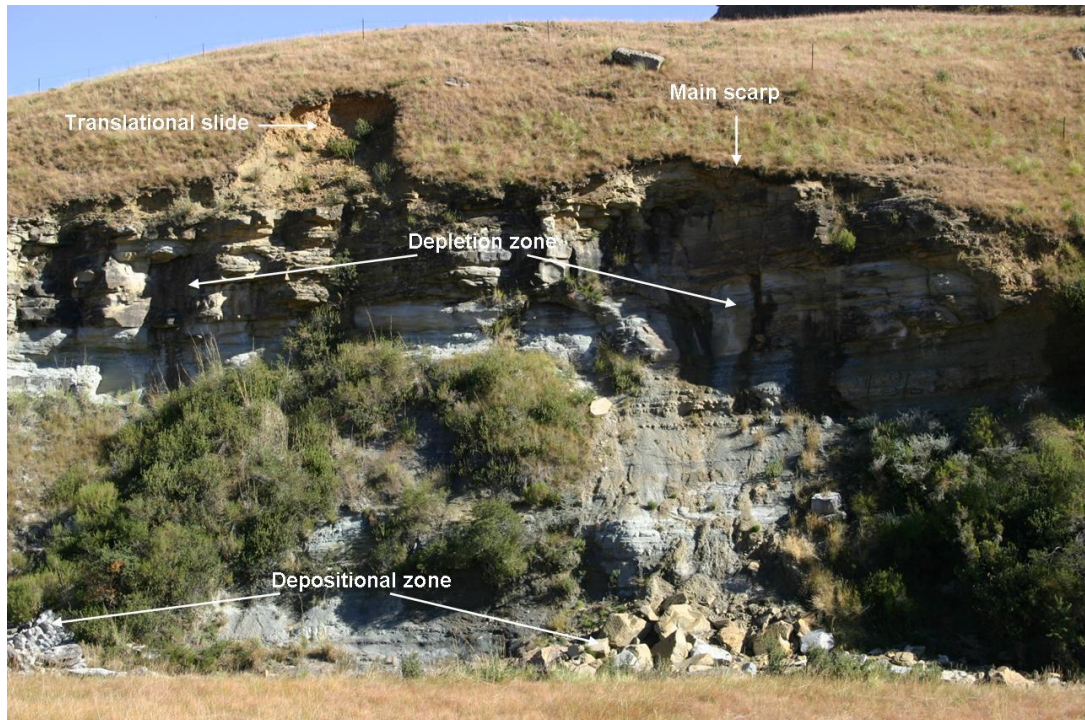


Figure 6.7 Oblique photograph of site B showing the main scarp and zones of activity.

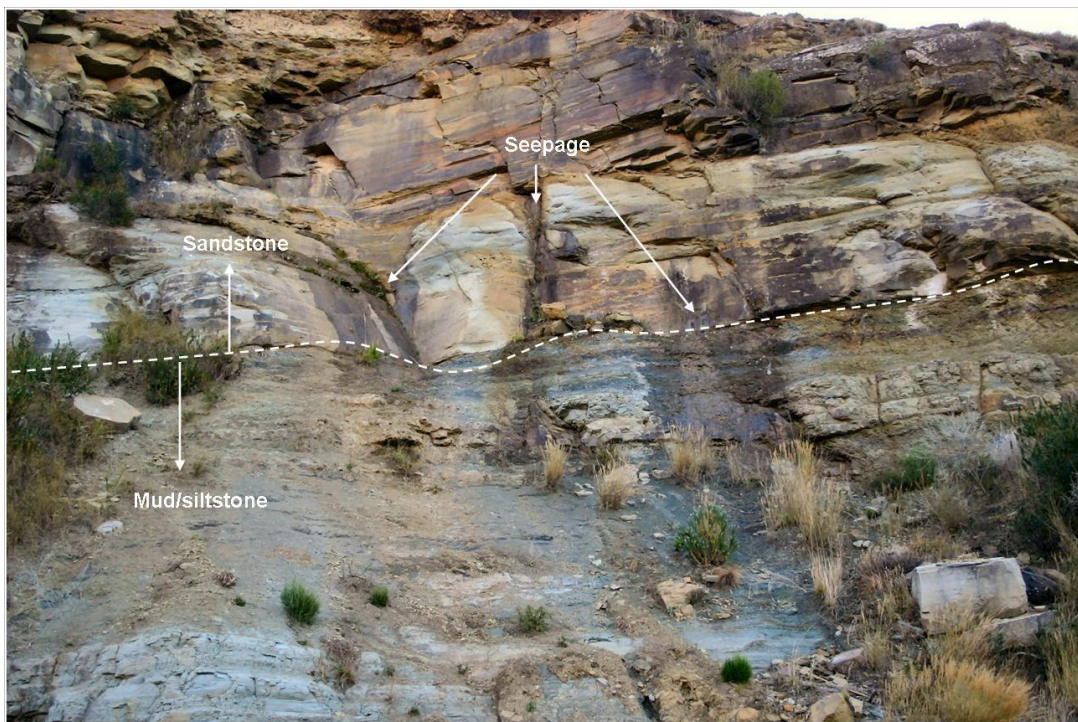


Figure 6.8 Photograph of the depletion zone showing the two lithological units and seepage zones. The scrub vegetation consists mostly of *Lycopodium clavatum*.

Vegetation in the depositional area is relatively thick and typical of riparian vegetation for the southern Drakensberg. *Lycopodium clavatum* which is an evergreen creeping herb that occurs on steep streambanks dominates on the centre and flanks of the fall (Figure 6.7), whilst *Euryops montanus* occurs in the same area in isolated patches. *Phyllica thodei* grows between joints on the vertical face of the feature alongside *Lycopodium clavatum*. *Leucosidea sericea*, *Cliffortia nitidula* subsp. *Pilosa* and *Athrixia pinifolia* grow in close proximity to the river as they favour rocky watercourses and boulder beds.

The translational slide above the main scarp is 5.1m long and 4.6m wide and the average depth of the slide scarp is 34cm. No seepage could be observed along the shear scar of the slide. Small rocks and pebbles ($<8\text{cm}^3$) have accumulated at the base of the shear scar and are likely to contribute to the displaced material that is deposited on the cones. The slide does not appear to be retrogressing and progressive movement is limited by the exposed rock face downslope, however the loose material in the main body of the slide suggests that weathering and erosion processes are active. Vegetation within the slide scar is limited to patches of grasses and the poor vegetation cover may be due to erosion, continued instability of the shear scar or poor soil development. Vegetation on the surrounding slopes is predominantly *Themeda triandra* grassland with small tufts of *Merxmuellera macowani*. Isolated colonies of *Helichrysum krookii*, a perennial herb that favours moist grassland, are observed above the crown area. This and the presence of *Merxmuellera macowani* suggest moist soil conditions upslope of the rock exposure.

Movement of the multiple rockfall/composite slide appears to be a two-fold process. The seepage zones provide water to the deeply weathered, highly jointed argillaceous material which has eroded more quickly than the overlying blocks of arenite. As basal support is removed, the blocks above the arenite become weakened and break off along discontinuities and joints. Movement was probably originally initiated by stream incision into the slope, thereby removing the weathered argillite. Changes in slope equilibrium as a result of the falling blocks

would have resulted in the shallow translational slide. Future extension of the multiple rockfall/composite slide is limited by the Ngwangwane River which provides a downslope barrier to progressive movements and a planation surface that flattens out about 6m above the crown of the translational slide and provides an upslope barrier for retrogressive movements (Figure 6.9).

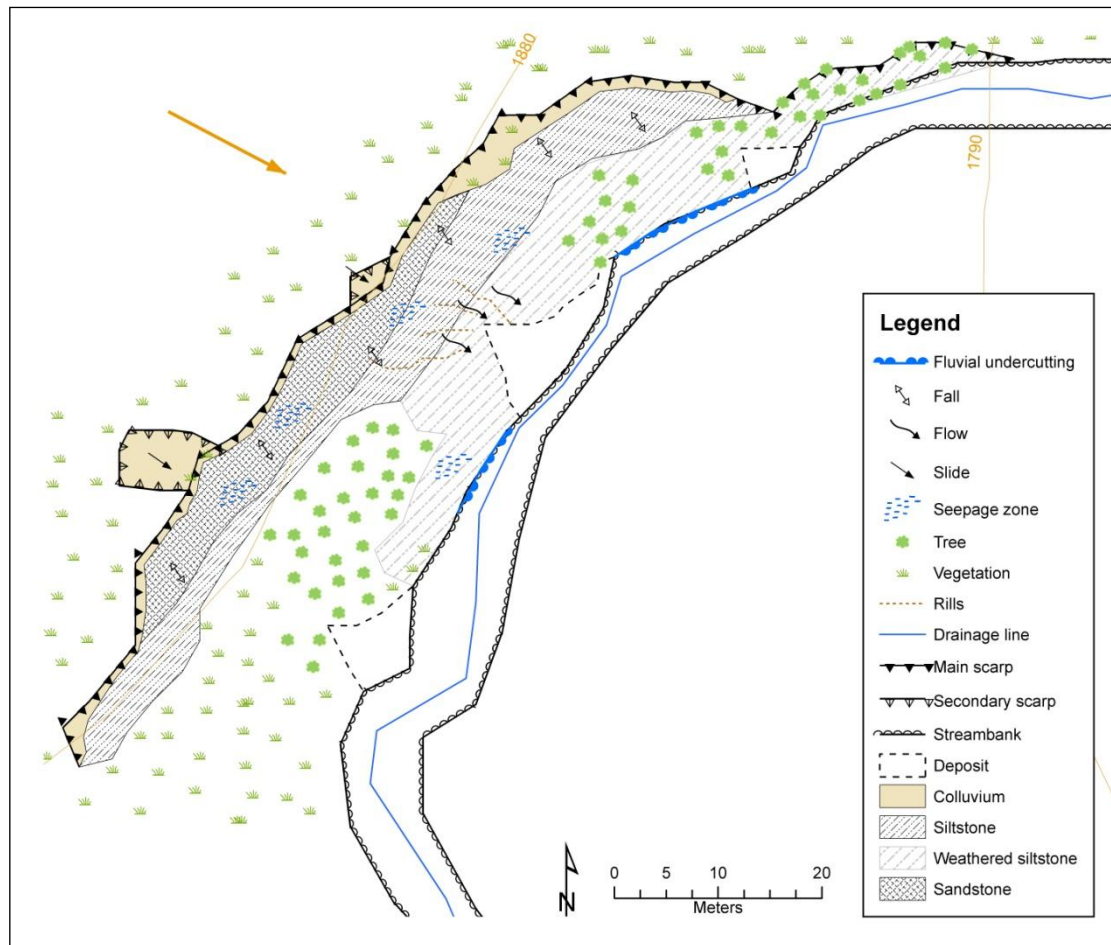


Figure 6.9 Geomorphological map of the rockfall and translational slide at site B.

6.4 Site C: Slide, Ngwangwane River

Site C is located about 150m upstream of site B, on a south-facing bank of the Ngwangwane River at 29°11'46.11" E; 29°50'49.13"S; at 1 807m a.s.l (Figure 6.2). Although the depletion, transport and depositional zones can be identified, only the first shows evidence of recent sliding activity (Figure 6.10). This suggests that current movement in the depletion zone is secondary or that activity

is slow and episodic. The shear scar is 22m wide and 10.9m long and has a gradient of 15° (Table 6.1). Two main vegetated ‘islands’ occur in the depletion zone which host *Themeda triandra* grasses that have been protected from fire by the bare scarp walls and shear surface of the slide. This feature was not identified in the field during two previous trips as dense vegetation obscured the main scarp. The shear surface is composed of regolith and weathered mudstone and is 0.8m high. Material within the depletion zone is unconsolidated and it is likely that erosive processes mobilise sediments downslope (Figure 6.11). Although a transfer zone of 18.5m in width and 14.4m in length, and a depositional zone 32m wide and 27.8m long can be identified, it is difficult to determine whether these are residual forms from previous activity or whether they can be associated with current activity.

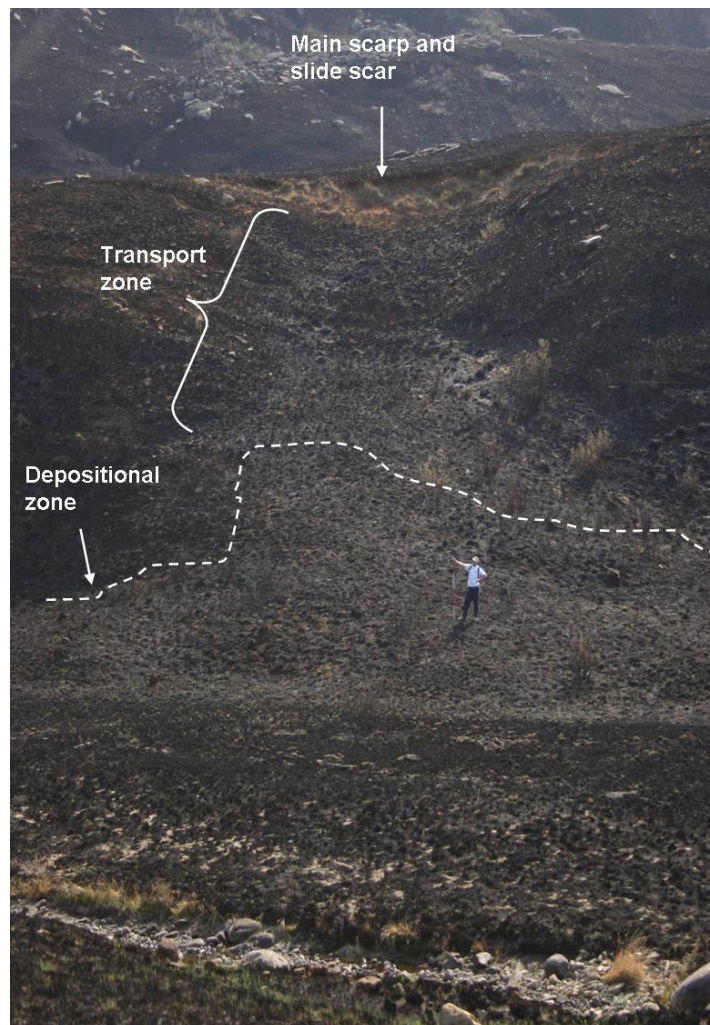


Figure 6.10 Oblique photograph of site C showing the shear scar and zones of movement.

The crown of the slide is at the crest of the slope upon which it occurs and a local planation surface is evident immediately upslope. These planation surfaces are most likely caused by differential or preferential weathering of thinly layered lava flows. It is likely that the deposit formed either during a single period of activity or has accumulated gradually as the shear surface has been eroded. Although the Ngwangwane River flows at the base of the slope, it is currently located on the opposite side of the floodplain to site C. Two possible river terraces/stream banks can be seen on the satellite image (Figure 6.12) which suggests that stream incision may be responsible for removing some of the slide deposit before meandering away from the site. It is therefore likely that movement occurred prior to the river meandering and that consequent movement has not been triggered by fluvial undercutting.

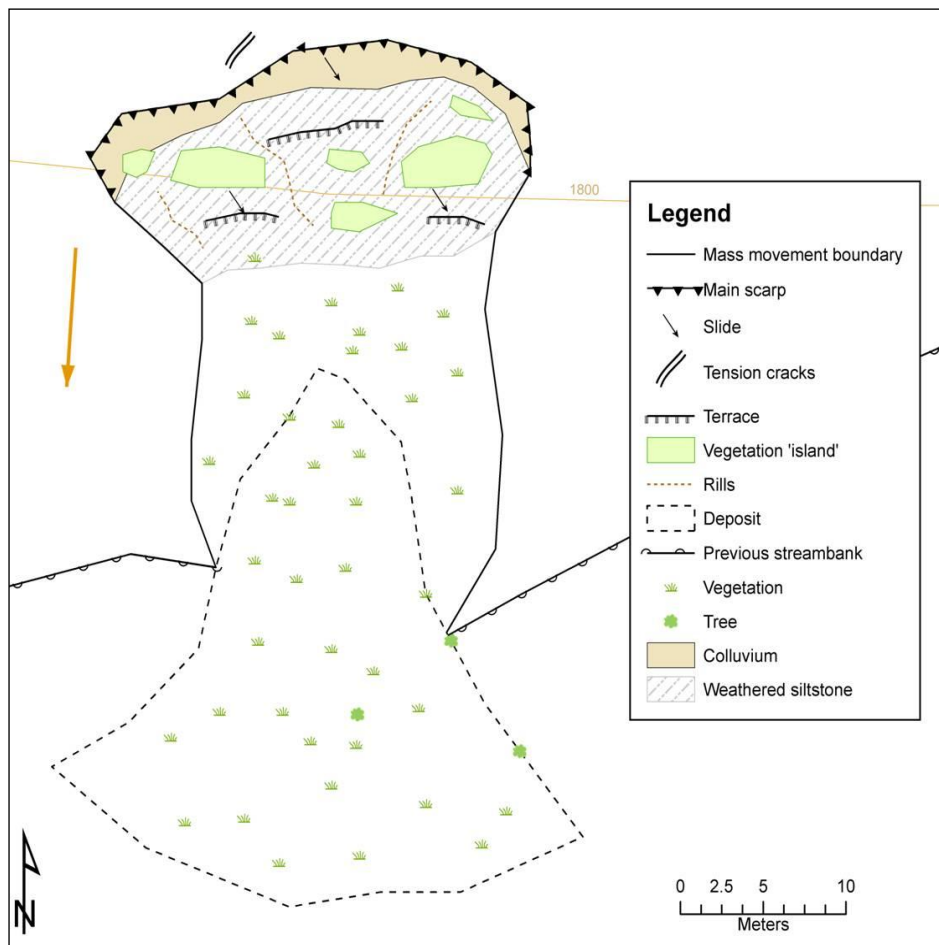


Figure 6.11 Geomorphological map of the translational slide site C.

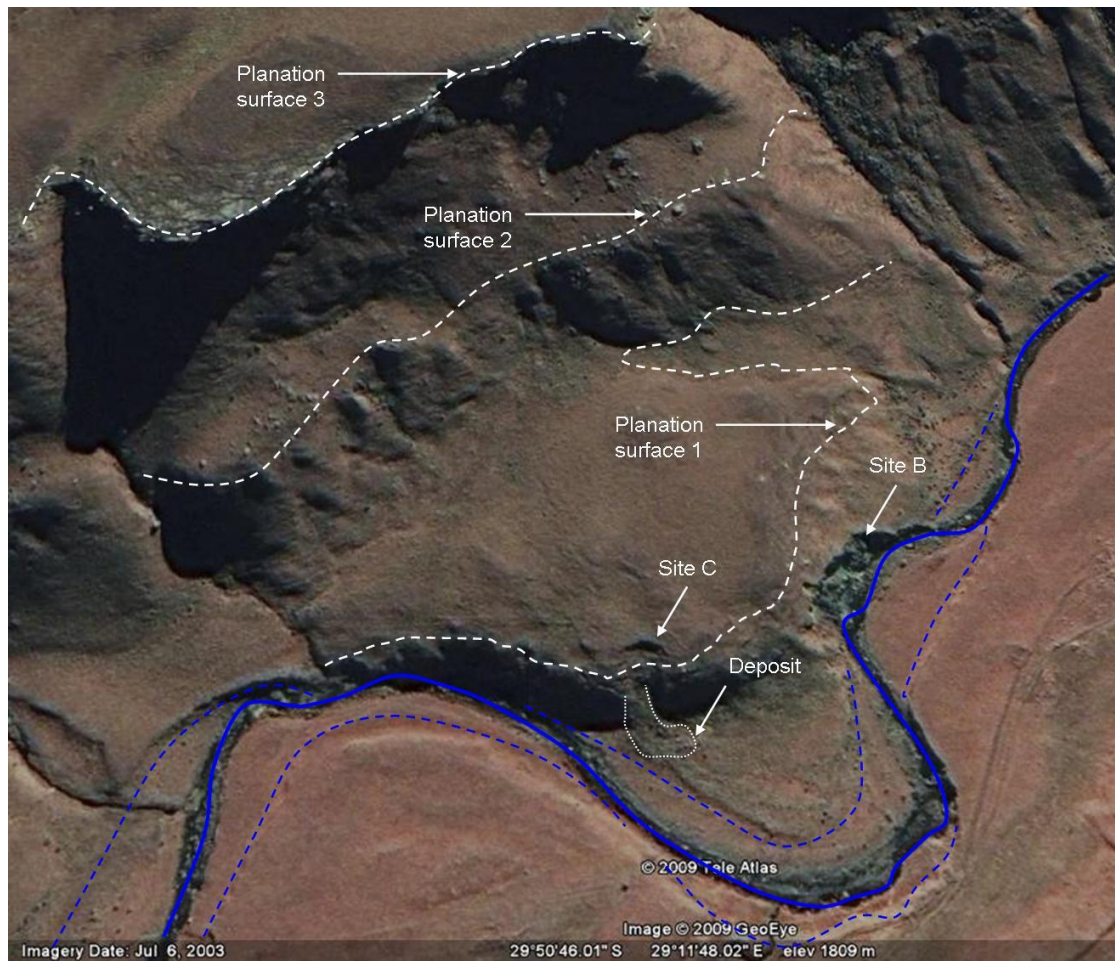


Figure 6.12 Google Earth (2009) image of site B and C showing planation surfaces above each site and the position of the Ngwangwane River. River terraces which may indicate previous positions of the river are represented by the dashed blue line.

6.5 Site D: Incised flow, Ngwangwane River

Site D is located on the southeast-facing bank of the Ngwangwane River, at $29^{\circ}10'46.35''$ E; $29^{\circ}51'22.40''$ S; between 1 874 and 1 841m a.s.l (Figure 6.2) The movement style is been classified as complex as two types of movement appear to have occurred in sequence. The first movement is a slide that has a shear surface which forms the depletion zone of the feature. The second type of movement is a flow that continues from the transport zone to the depositional zone, migrating from the left side of the flow channel to the right. The flow track has incised into the slope forming a transport channel for material removed by the slide (Figure 6.13).

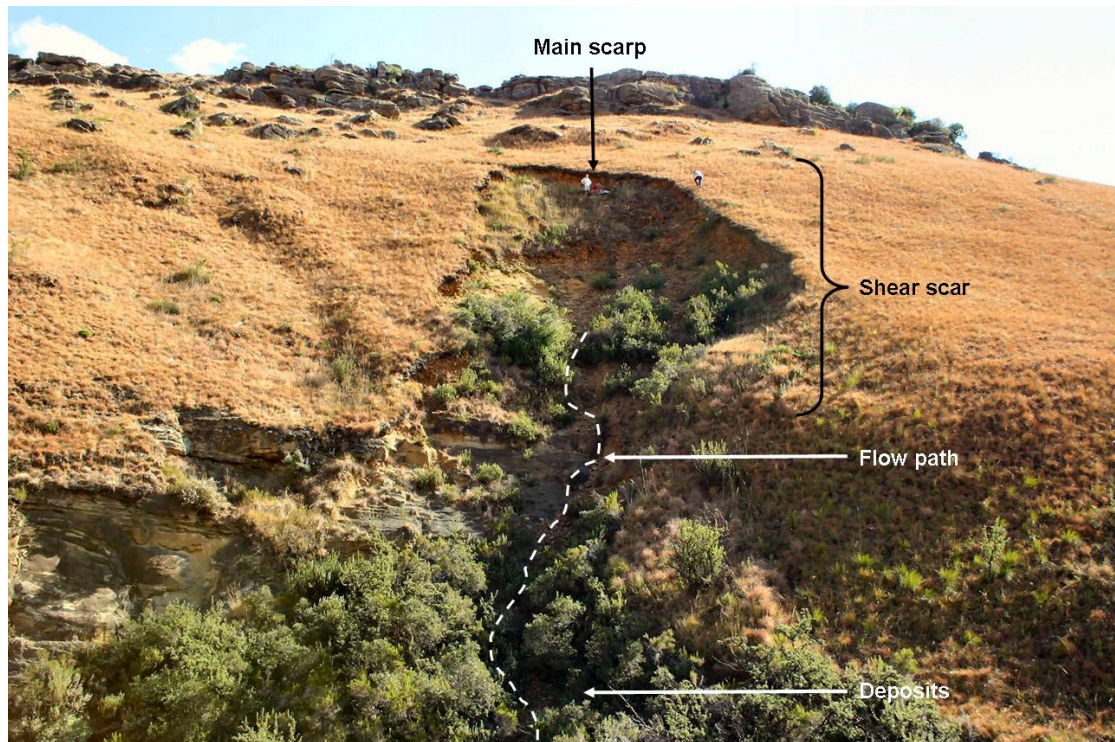


Figure 6.13 Oblique photograph of the slide at site B. The slide is characterised by a flow track which is transporting sediment downstream to the river.

Main and secondary scarps are observed at the site, as well as a tension crack 3.5m long to the left of the crown of the feature. The main scarp of the slide continues from the bedrock face on the left of the feature to the convex slope unit on the right. The main scarp is between 0.8-1.8m high, becoming higher towards the crown and shallower towards the flanks and both scarps are near vertical (Figure 6.14). Small vegetation ‘islands’ occur just below the second scarp on the shear surface, which are composed of single clumps of densely tufted perennial grass, similar to *Tristachya leucothrix*. The secondary scarp is 0.5-0.8m high on the right flank and 1.2-1.8m high on the left flank, becoming less distinguishable from the shear surface. Grass cover is thicker on the right side of the terrace which has formed between the main and secondary scarp, and suggests that the left flank of the feature is more actively eroding than the right. A small translational slide occurs on the left flank of the feature which, when combined with the active erosion on the right side, indicates that the depletion zone is widening laterally.

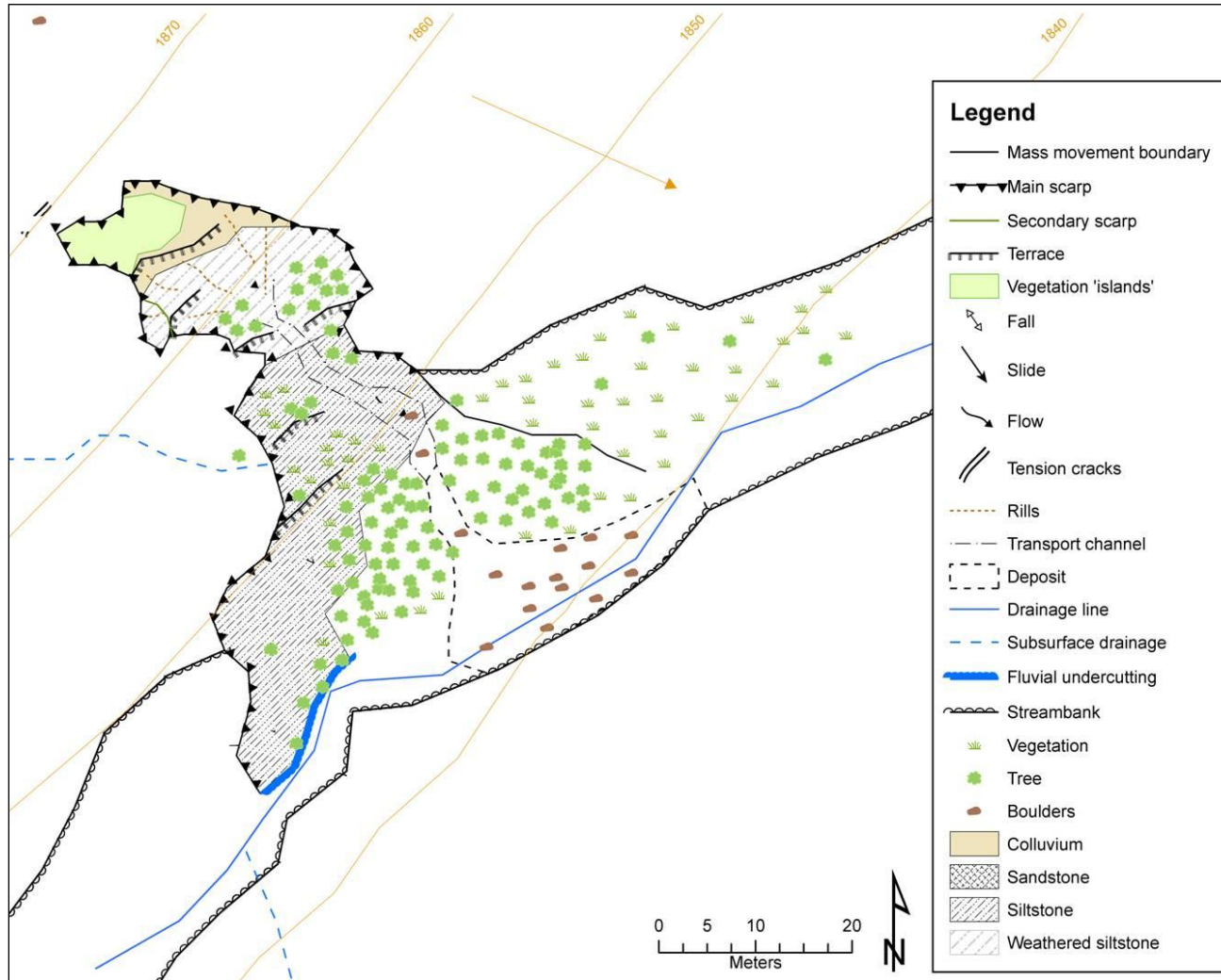


Figure 6.14 Geomorphological map of the incised flow at site D.

The shear surface is composed of weathered, crumbly yellow mudstone that is highly mobile and abruptly overlain by a loosely consolidated colluvial deposit composed of flat, angular blocks of varying sizes (Figure 6.15). The colluvial mantle is the main source of material being transported in the flow channel and deposited at the foot of the flow. A thin organic horizon (38-56cm) covers the regolith and provides a substrate for grass and plant roots. *Eucomis schiffii* and lichen occur on the main scarp in the organic horizon which suggests moist soil conditions; although no surface seepage was observed at the site. The depletion zone has plants characteristic of rocky steep areas, such as *Lycopodium clavatum*, *Euryops montanus* and *Felicia filifolia*. These assemblages are different to the surrounding slopes which are predominantly *Themeda triandra*, and this has been observed when mass movement activity changes local soil conditions and influences habitat (Geertsema and Pojar, 2007).



Figure 6.15 (A) Profile of the main scarp. (B) Angular material that is being transported in the flow channel.

6.6 Site E: Slide

Site E is located at 29°10'54.93" E; 29°51'35.63"S; at 1 868m a.s.l (Figure 6.2). The movement appears to have occurred as a single translational slide. The slide occurs on a northwest-facing convex-linear slope (Figure 6.16). Distinguishing between zones is difficult as the depletion and transport zones overlap and no clear depositional zone was observed. The slide has one main vertical scarp that is 0.5-0.8m high and is composed of consolidated colluvial material. The shear surface is highly weathered yellowish mudstone that flakes and crumbles on touch. No seepage zones were observed within the shear scar and vegetation is limited to short tussock grasses. The depletion zone is 23m wide and 8.8m in length and the average slope gradient is 28° (Table 6.1). The central part of the translational slide is vegetated and loose material is transported around the edges of the vegetated island. Small rills within the shear scar indicate that erosion is active on the shear surface (Figure 6.17).



Figure 6.16 Translational slide occurring at site E. Sites F,G and H can be seen in the background.

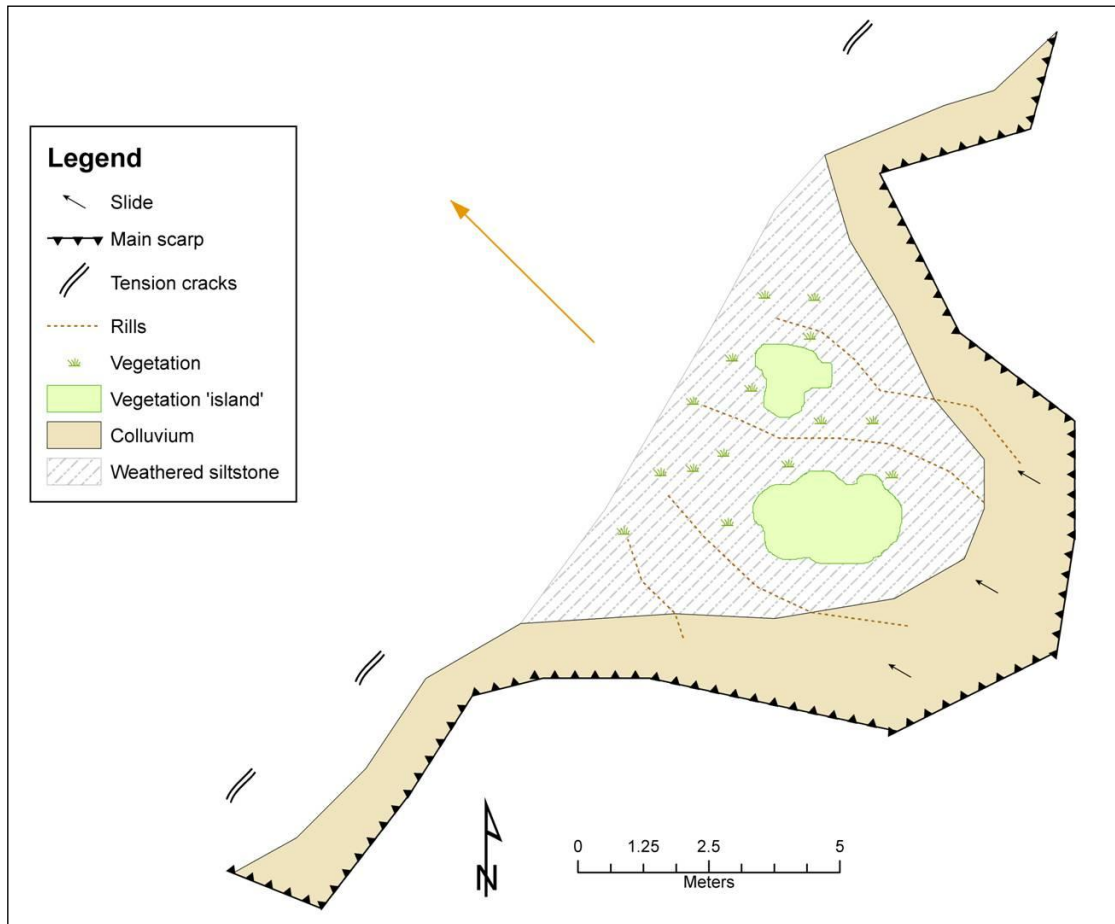


Figure 6.17 Geomorphological map of the translational slide at site E.

Retrogressive movement is unlimited for about 7m upslope after which the slope reaches a crest. Progressive movement is limited downslope as the gradient flattens out about 25m below the translational slide. Although no subsurface drainage or seepage was observed at the site, it is possible that the planation surface upslope of the translational slide creates a perched watertable which leads to saturated soil conditions. A second mass movement feature can be observed to the right of the feature, but as it appears to be stabilised and revegetated, no assessment was undertaken in the field.

6.7 Site F: Slide

Site F is located at 29°11'6.06" E; 29°51'55.65"S on a west-facing slope at 1 987m a.s.l (Figure 6.2). The feature is a shallow translational slide, similar to the

slide that occurred at site E, displaying an arcuate shape of the main scarp, which is typical of shallow translational slides (c.f. Varnes, 1958) (Figure 6.18). The main scarp is 0.8m high and is composed of consolidated regolith and a shallow organic horizon (0.2m), which corresponds to the depth of the grass roots growing on the adjacent slopes. The shear surface of the slide is 22.1m wide, 13.3m long and inclined at 21°, with tension cracks having developed at the base of the scarp in the displaced material (Table 6.1). It is probable that these cracks will widen to form small terraces or vegetated ‘islands’ if downslope movement continues. The extent of the depositional zone could roughly be determined based on the evidence of loose material on the slope, despite there being no distinct depositional lobe or fan. A rock outcrop downslope of the translational slide forms a topographic boundary limiting the downslope movement of the deposit (Figure 6.19). Loose platy, angular blocks originating from rock exposures upslope, have been transported further downslope by the displaced material.

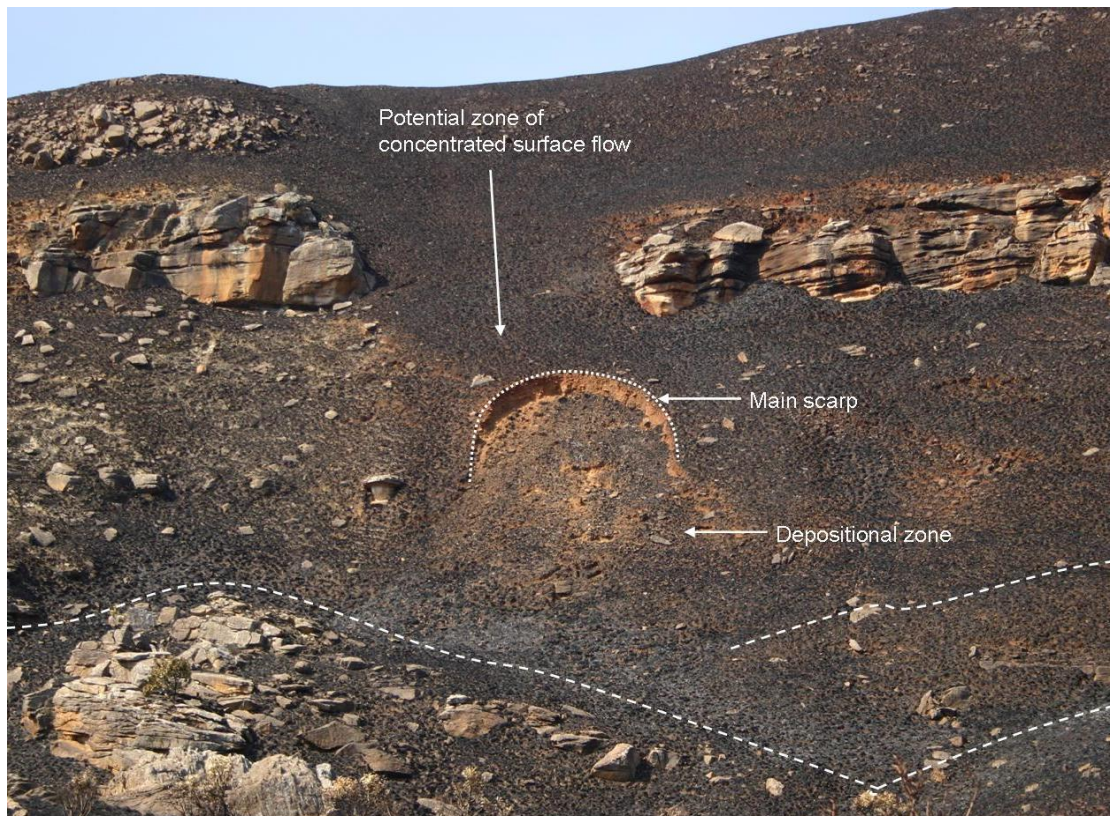


Figure 6.18 Oblique photograph of site F showing the main scarp and zone of deposition. Dashed white lines indicate where slope gradient decreases to create local topographic terraces.

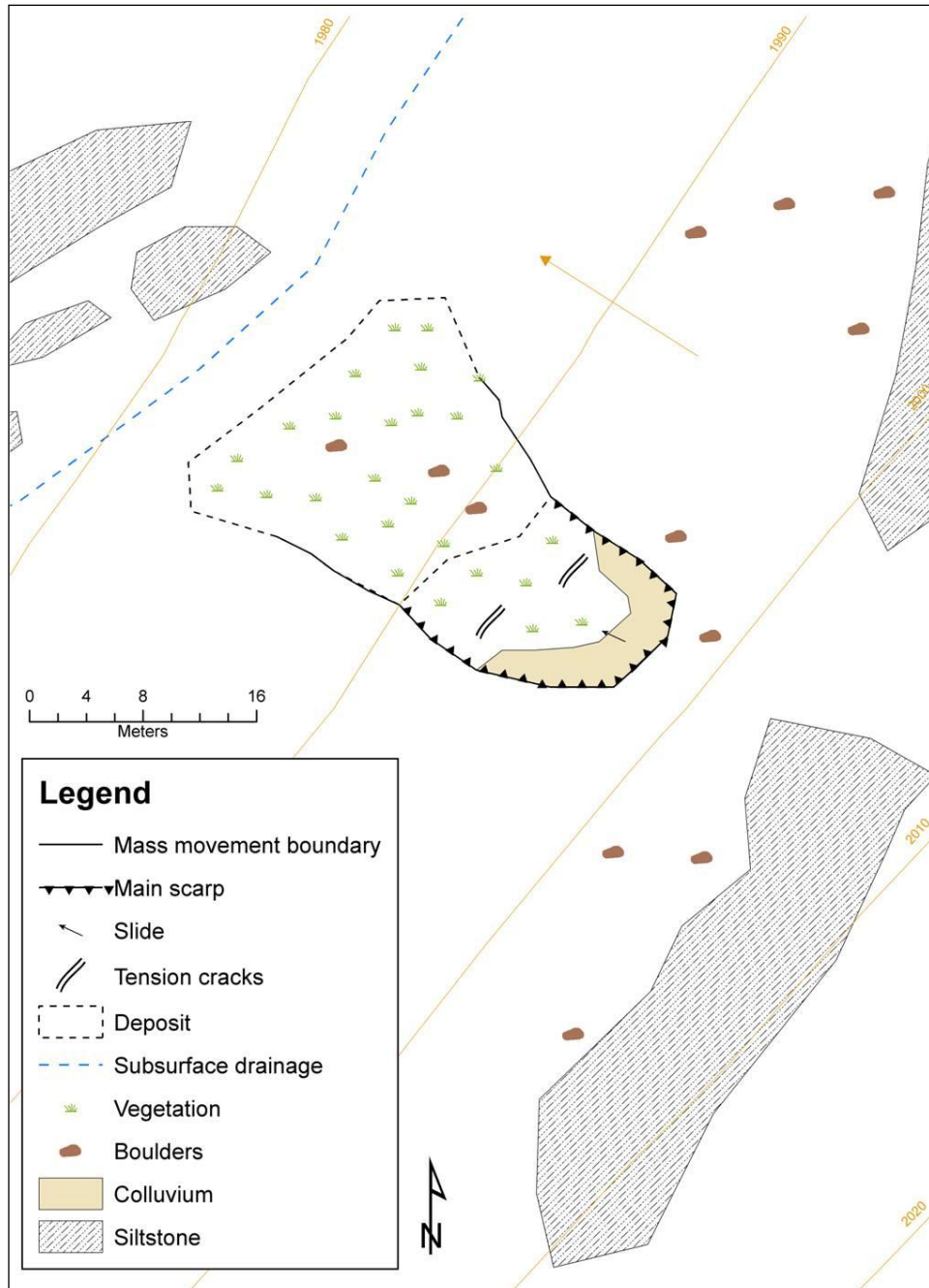


Figure 6.19 Geomorphological map of the translational slide at site F.

The rock exposures are sandstones of the Elliot Formation and the reddish colour of the soils is typical of residual soils in the Drakensberg (Brink, 1984). Of particular interest is the absence of a rock exposure directly above site F. This may potentially channel overland flow and throughflow from the slopes above, however it is also possible that this is a local fault zone. Neither proposition could

be verified in the field and no evidence of seepage, surface or subsurface drainage could be identified from the aerial photos. However, *Hyparrhenia hirta*, *Merxmuellera macowani* and a species of *Protea* were observed growing at the base of the slope, which may indicate that some moisture is available near the site for part of the year.

6.8 Site G: Surficial flow

Site G is located at 29°11'5.03" E; 29°52'13.05"S; at 2 095m a.s.l (Figure 6.20). The feature occurs on a northwest-facing slope above a tributary of the Ngwangwane River. The style of movement is complex, and began as a translational slide that progressed into a surficial flow (Caniani et al., 2008). Aerial photography analysis indicates that initial movement occurred between 2000/2001 and 2004. Zonation is relatively distinct and the depletion, transport and depositional zones are well represented. The shear scar of the translational slide is located about 2.3m below an exposed rock face and is 12.2m in width and 8.2m in length (Table 6.1). The main scarp is shallow (about 0.58m high) and composed of regolith. A weathered yellow mudstone layer is exposed in the lower half of the shear surface and no evidence for seepage was observed in the depletion zone. The shear surface is steeply inclined (68°) and bare of vegetation.

The transport zone widens as the flow progresses downslope and has a maximum width of 16.7m and is about 66.1m in length. The material mobilised by the slide appears to have been transported downslope as a debris flow, over a second rock exposure and deposited at the base of the slope where the slope gradient changes from 47° to 25° (Figure 6.21). Little to no surface incision occurred within the transport zone as the vegetation was flattened within the track, rather than removed. A number of indicators suggest that the flow travelled at high speeds and had possibly reached its liquid limit. Firstly, the deposit lengthened and thinned downslope, which is a characteristic feature of saturated debris flows (Iverson and LaHusen, 1993). Secondly, small clumps of debris were ejected from the main flow body where the track diverted around obstacles, and thirdly, the

planar and longitudinal shape of the deposit suggests that the deposit remained in a fluid-like state until enough water had been removed for the mass to assume a solid state (Iverson, 1997). It is apparent that the liquefied mass flowed into gaps between grass tussocks and around rocks (Figure 6.22B).



Figure 6.20 Oblique photograph of site G showing the shear surface and the main flow path. The levees are shown as dashed lines. The foot of the depositional fan is not visible.

Two distinct levees can be identified on the sides of the flow track which are between 0.4 and 0.6m high, 1.2m wide and between 47 and 53m in length. The levees appear to be poorly sorted although pebbles ($<8\text{cm}^3$) and small boulders ($<20\text{cm}^3$) mantle the sides and top of the levees. The presence of pebbles and small boulders may be due to kinetic sieving which involves large clasts being suspended in the mass due to gravity and boundary drag being insufficient to force the clasts through small voids created during movement (Iverson, 1997). Small, surficial drainage lines can be observed on the surface of the deposit which is relatively flat (Figure 6.23). These small rills would probably have developed whilst the deposit was drying, as declining pore pressure within the mass would have resulted in the material consolidating into a solid, resulting in the remaining fluid draining away from the mass (Iverson, 1997).

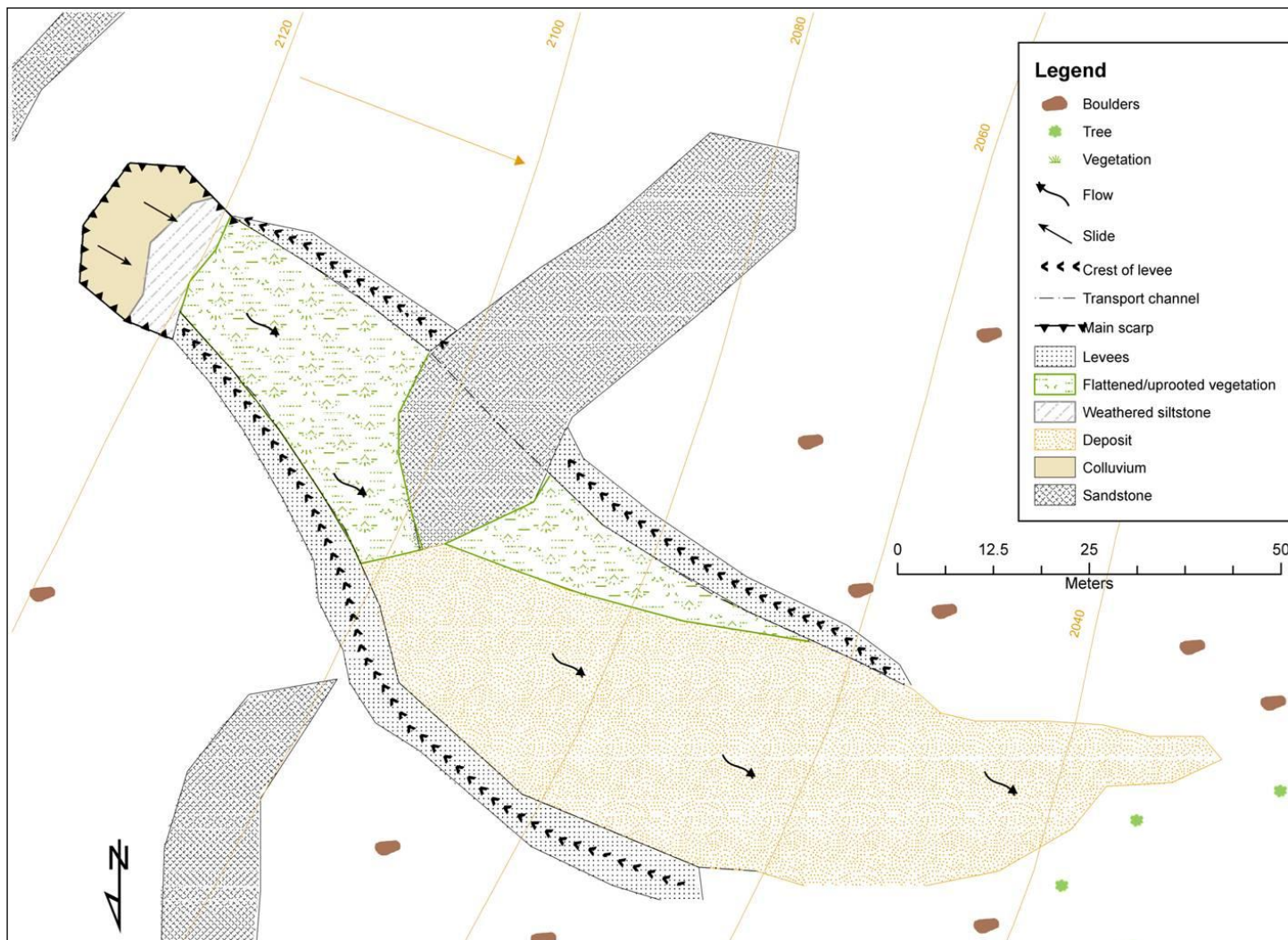


Figure 6.21 Geomorphological map of the surficial flow at site G.



Figure 6.22 The flow deposit at site G indicating (A), how the flow spread around grass tussocks and (B), how vegetation created a cast that moulded the shape of the deposit.



Figure 6.23 Vegetation was flattened as the displaced material flowed over it. (B) Drainage lines developed in the mass as the sediment settled and the fluid drained away.

6.9 Site H: Surficial flows

Site H is located at 29°10'58.27" E, 29°52'11.75" S; at 1 983m a.s.l on a north-facing slope opposite to site G (Figure 6.2). The feature is a complex translational slide which progresses into two surficial flows (Figure 6.24). The main scarp of the slide scar is at the interface of a colluvial layer which overlies a sandstone exposure and the flows are separated by a convex-convex slope unit. The slide scar is 10.3m in width and extends 8.2m downslope (Table 6.1). The east-facing flow is 4.9m in width and 29.6m in length with an average slope gradient of 29°. The west-facing flow is 5.6m in width and 33.4m in length with an average slope gradient of 35°. Both flows have eroded into the colluvium immediately below the shear scar and the collapse of the inner walls of the flow tracks suggests that future failure will occur where the flows diverge. The collapse of these inner walls will result in the shear scar extending downslope.

The flows are classified as surficial rather than incised flows as the erosion is relatively shallow (between 0.1-0.3m of the soil) compared to the slope incision observed at site D. Both of the flows extend laterally downslope, however the degree of extension is limited by the local topography. The west-facing deposit is 8.7m in width and 3.2m in length and the east-facing deposit is 11.8m in width and 5.8m in length. Vegetation has been removed from the slide scar and the flow tracks, and the loosened grass tussocks form mounds in the deposits. A subsequent visit to site H revealed that some of the grass tussocks had become stabilised and had begun growing.

Levees are absent for both of the flows and the depositional fans are more lobate than elongate (Figure 6.25). Large boulders in the vicinity of the deposits appear to originate from exposed rock faces upslope of the site. A visual comparison of the two deposits suggests that the east-facing fan contains less smaller sized material than the west-facing fan and it is likely that smaller particles have been transported downstream by a tributary of the Ngwangwane River, which flows along the toe of the east-facing flow. A planation surface occurs at the foot of the west-facing flow which has a gradient of 10° and has limited the runout length of

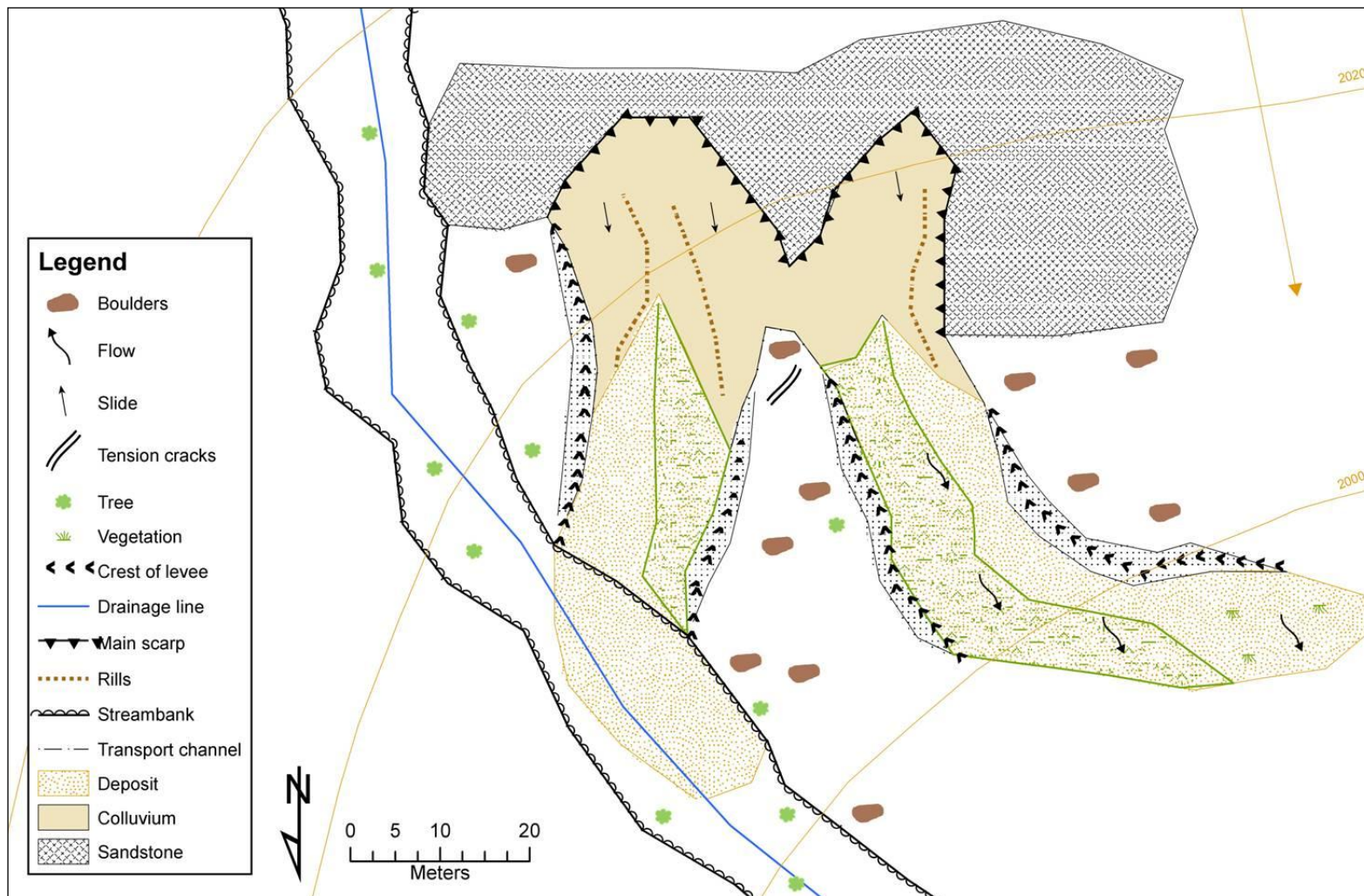


Figure 6.24 Geomorphological map of the surficial flows at site H.

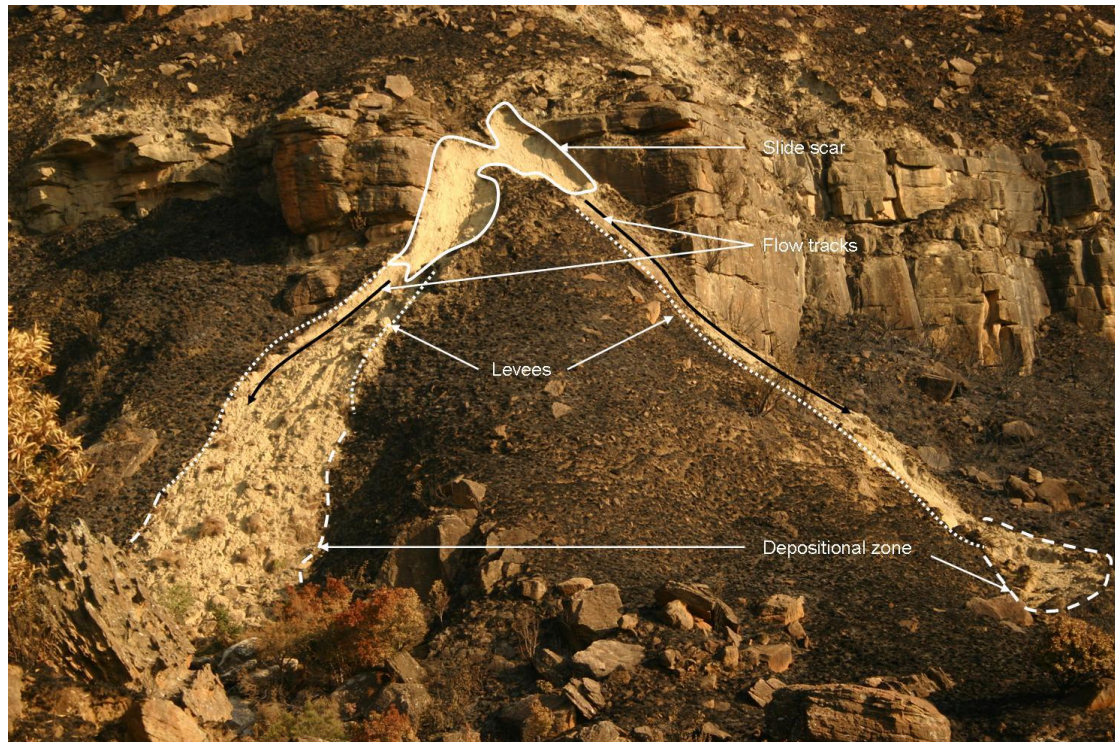


Figure 6.25 Oblique photograph of the two flows at site H showing the main scarp and zones of activity.

the flow. Although the downslope extent of both of the flows is limited, retrogressive and progressive expansion of the shear surface appears to be unrestricted and the slope gradient is steep enough for movement to continue.

6.10 Site I: Slide, Bushman's River

Site I is located at 29°11'21.07" E; 29°49'46.30"S; at 1 823m a.s.l (Figure 6.2). The feature is a translational slide which occurs on the north-facing bank of the Bushman's River, on the thalweg side of a meander bend. The style of movement is simple and movement appears to have occurred as a single translational slide following fluvial undercutting of the bank. No distinction can be made between zones as the distance between the depletion zone and the stream is too small for a significant transport zone to have developed and the stream has removed most of the depositional zone (Figure 6.26). A small depositional remnant composed of large blocks suggests that fluvial transport has removed smaller sized particles from the deposit. A main scarp can be identified that is vertical and between 0.9-

1.7m high and that narrows towards the outer flanks of the slide scar. The scarp is composed of consolidated colluvium that changes in colour from orange to brown down the profile. This colour change suggests that the geochemical or hydraulic properties of the soil layers differ and that the underlying colluvial material has experienced less *in situ* oxidation than the overlying material.



Figure 6.26 Oblique photograph of the translational slide at site I on the Bushman's River.

A small terrace occurs within the displaced material that is about 1.1m high and the slide scar is 12.2m in width, 9.2m in length and has a gradient of 34° (Table 6.1). Vegetation in the depletion zone mostly consists of *Themeda triandra* grass, whilst *Merxmeullera macowanii* and *Cliffortia nitidula* subsp. *Pilosa* grow in the riparian zone at the base of the slide scar. Boulders along the toe of the slide are slope rather than fluvial deposits, as the blocks are angular and not rounded. These blocks possibly originate from a rock exposure 80-100m upslope. Retrogressive movement is limited as the scarp is at the top of the crest of the bank. Progressive movement is limited downslope by the Bushman's River (Figure 6.27). Subsurface drainage lines can be observed about 70m upstream of the feature and meander bend scars are prominent across the floodplain.

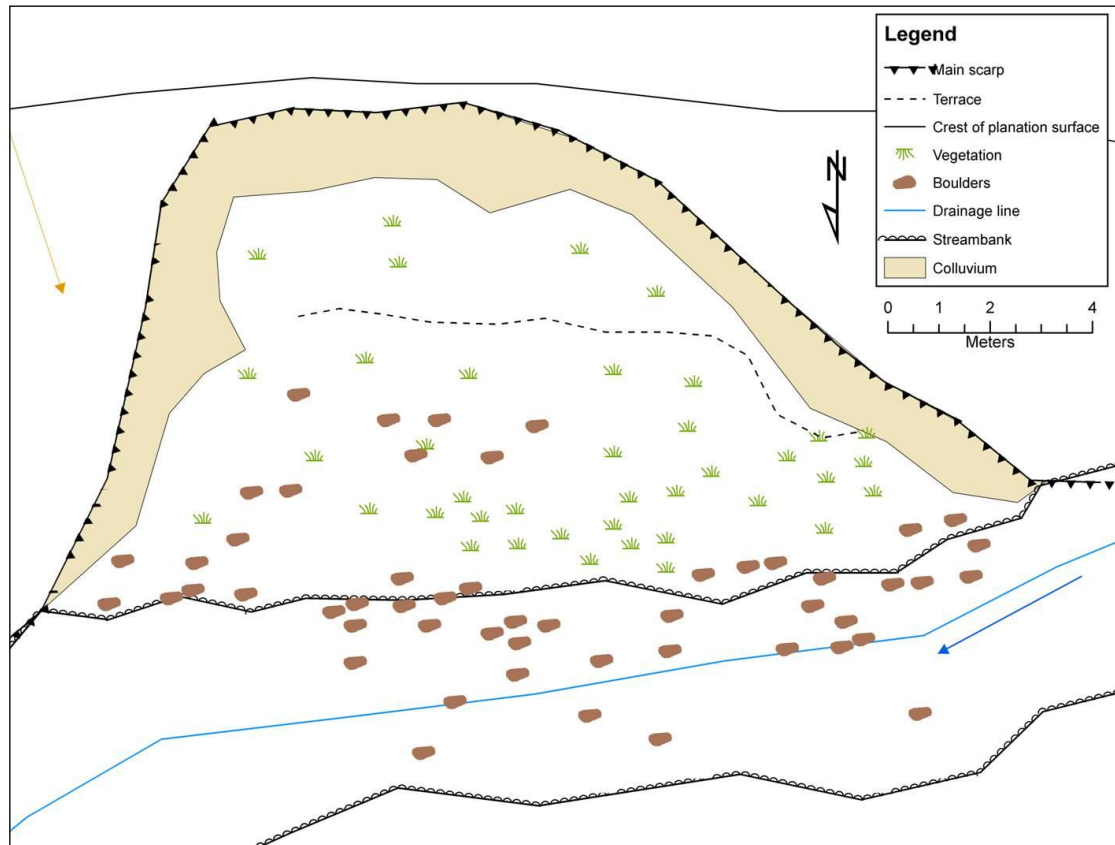


Figure 6.27 Geomorphological map of the translational slide at site I.

6.11 Site J: Slide, Bushman's River

Site J is located at 29°11'43.32" E; 29°50'9.02"S on a northeast-facing slope along the Bushman's River valley at 1 885m a.s.l (Figure 6.2). The type of movement is shallow and translational, however small falls of debris detached from the main scarp are also evident. Site J is located above an outcrop of Elliot Formation mudstone and only the main scarp is visible in Figure 6.28. The slide scar is 24.7m wide and 21.3m long and is occupied by vegetated 'islands' and terraces (Figure 6.29A). The main scarp is 2.85m high and near vertical, whilst the average terrace scarp is 0.7m high (Table 6.1). The slope gradient of the slide scar is 30°, but the rock outcrop near the foot of the slide is near vertical. As sediment becomes detached from the shear surface, gravity and overland flow initiate sediment movement over the exposed rock face which is consequently deposited onto the slope below. Small (<0.08m³) sandstone and dolerite boulders were observed within the displaced material and are also present in the soil profile

exposed at the main scarp (Figure 6.29B). Retrogressive movement is limited as the crown of the translational slide is at the crest of a slope, below a planation surface. Progressive movement is also limited by the bedrock outcrop at the foot of the slide. Lateral extension appears to be unlimited although drainage lines in the vicinity (30-50m) would eventually limit its extension (Figure 6.30).

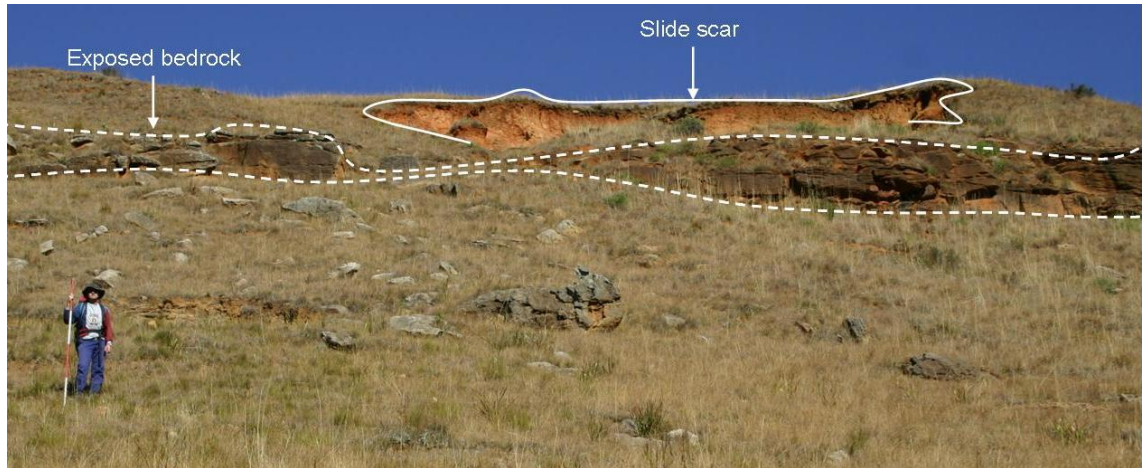


Figure 6.28 Site J displaying the main scarp. Note the exposed bedrock just below the shear surface.



Figure 6.29 (A) Vegetated 'islands' on the shear surface and (B) the gradual transition of the contact between the mobile soil and weathered saprolite.

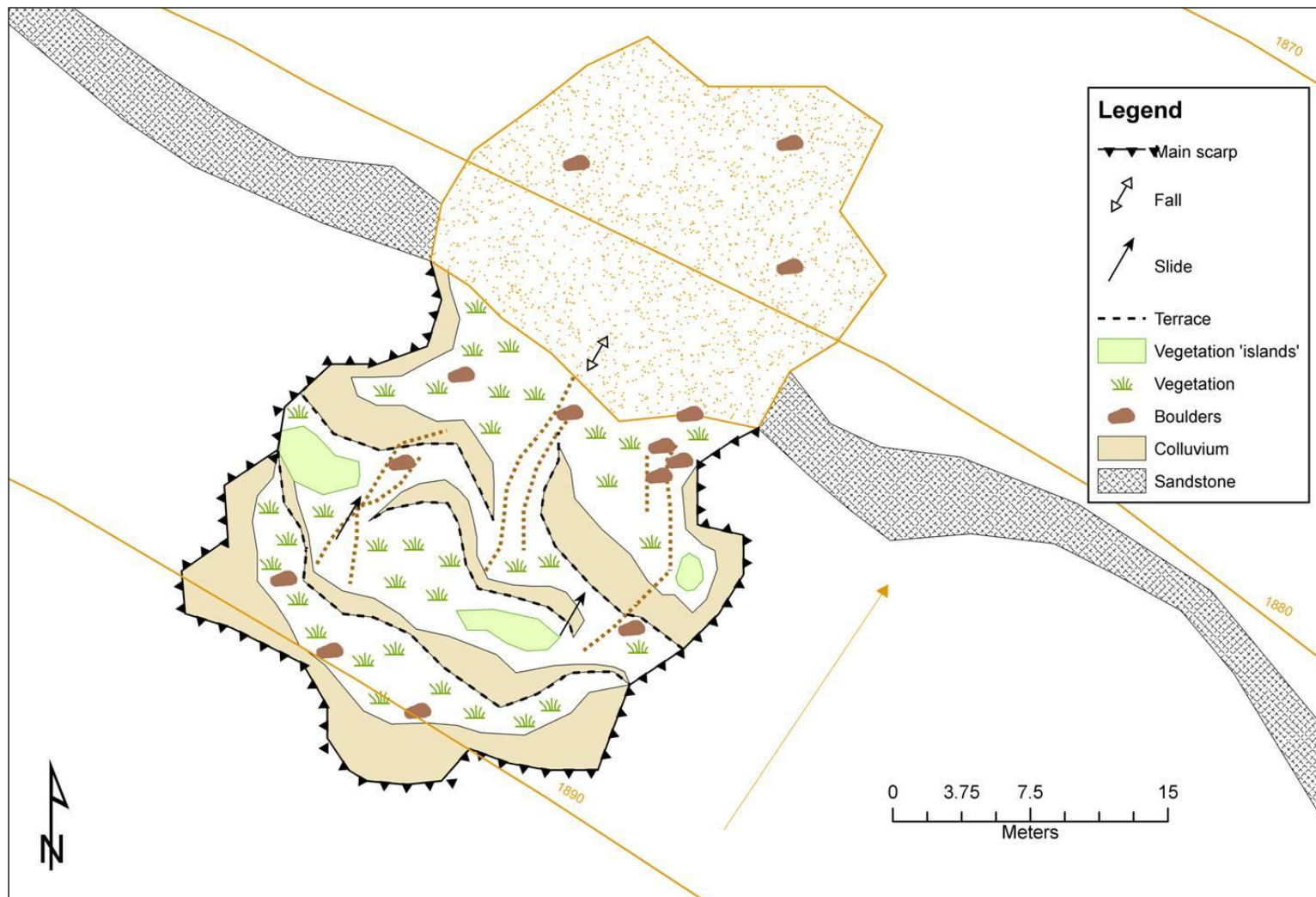


Figure 6.30 Geomorphological map of the translational slide at site J.

6.12 Site K: Landslide complex, Bushman's River

Site K was not measured in the field as the site was difficult to access and the morphometric attributes of the larger mass movements (such as K1 and the relict mass movement scar) were almost impossible to distinguish in the field. This was due to a combination of the large size of the features and the effects of erosion which have smoothed the boundaries within the features. All measurements were therefore made using the aerial photographs in ArcGIS 9.2.

For ease of reference, Site K has been separated into three sites; namely site K1, K2 and K3 (Figure 6.31). Site K1 is located at 29°11'55.95" E; 29°49'51.75"S, site K2 at 29°11'59.57" E; 29°49'53.19"S and site K3 at 29°12'4.34" E; 29°49'55.16"S (Figure 6.2). The depositional zone for all of the features is coincident with the floodplain of the Bushman's River at about 1 796m a.s.l. The main depletion zones for K1, K2 and K3 are at 1 836m a.s.l, 1 882m a.s.l and 1 899m a.s.l. The crowns of all of the mass movement features correspond to a lithological transition from Molteno Formation to Karoo dolerite, which has manifested as a planation surface upslope of the crowns. The planation surface dips slightly backwards into the slope resulting in an increase, rather than a decrease in altitude downvalley.

Site K1 is bowl-shaped, having a large depletion and depositional zone and small transport zone and was probably initiated as a slide which progressed into a flow. The full extent of the depletion zone is about 72m in width and 97m in length, and is composed of a number of shear surfaces. The majority of these surfaces are vegetated except for a few on the flanks of the slide. The individual shear surfaces have created a number of drainage lines within the depletion zone that merge into a main channel that flows through the middle of the transport zone (Figure 6.32). All zones are well vegetated with grasses and *Leucosidea sericea* bushes which commonly form stands in sheltered places. The transport zone is about 30m wide and 41m long, with a number of structural and secondary features visible alongside this zone. A terrace about 40m in width is visible upstream of the

transport zone which is possibly bedrock controlled, whilst a number of shear surfaces are visible immediately downslope of the terrace, ranging from 7m to 30m in width. An eroded scarp downstream of the transport zone, which is possibly a relict translational slide, can be identified that is about 19m wide and 40m long. A lateral ridge separates the two features and the position and size of the ridge suggest that it is bedrock controlled. A levee can be identified within the transport zone of the slide/flow which influences the direction of surface flow originating on the slide scar. The K1 deposit is fan shaped and the Bushman's River is eroding into the toe of the deposit, suggesting that the deposit formed prior to positional meander changes along the Bushman's River.

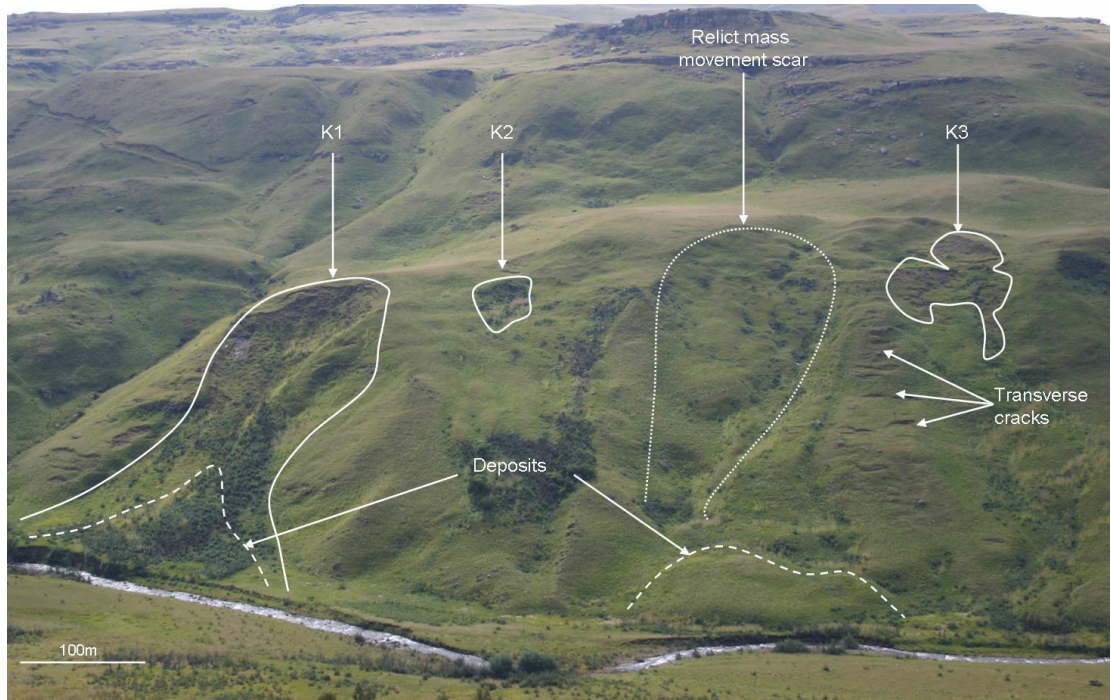


Figure 6.31 Oblique photograph of site K indicating a number of primary and secondary features.



Figure 6.32 Oblique photo of site K1 showing the main scarp and transport channel, slide scars in the immediate vicinity and the location of the Bushman's river in relation to the foot of the flow.

Site K2 is a slide which is about 11m in width and 20m in length. Two large lateral ridges separate site K2 from K1 and K3 and have created a topographic depression. Hummocky topography in the vicinity of the slide scar suggest that this site may have experienced large-scale mass movement activity in the past, however, the absence of the distinguishable zones implies that the period of activity would have preceded the development of the other mass movement features at site K.

Site K3 is a complex feature exhibiting both slide and flow movements and a number of recently active shear surfaces can be identified within the depletion zone; however, these represent only half of the area surrounded by the main scarp (Figure 6.33). The shear surfaces are between 24-32m in width and 15-21m in

length. A flow track can be identified on the right flank of the zone of depletion which is about 21m wide and 173m long, whilst the flow to the left is only 17m wide and 55m long. Three individual debris lobes could be identified which suggests that a number of pulsed flow events may have occurred. Mass movement activity downstream of the flow, together with fluvial undercutting, has reshaped the deposit so that its form is more irregular than has been observed at other slide/flow sites. A lateral ridge occurs between the flow and the recently active shear scars which is approximately 60m wide and 193m long, whilst a number of secondary movements in the form of shallow translational slides can be observed on the ridge.

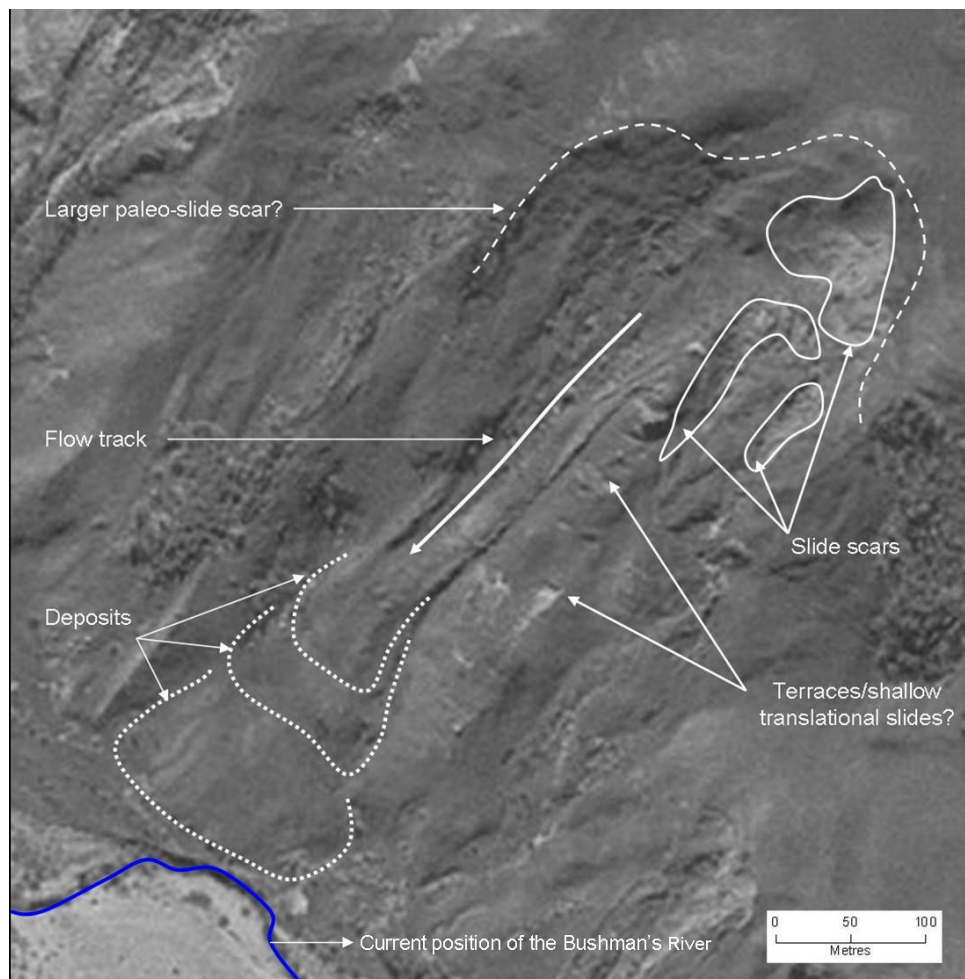


Figure 6.33 Aerial photo of the slide/flow at site K3 showing shear scars, flow track and deposits of the flow.

On several occasions, the Bushman's River has changed its course within the immediate area of site K, as is evidenced by old meander scars and over-

steepened banks along the margins of the floodplain. This floodplain varies in width between 80-300m. It is possible to construct a hypothetical timeline describing the position of the river in relation to the mass movement deposits (Figure 6.34). The river appears to originally have flowed along the base of the south-facing slopes of site K and to have undercut the deposits and lateral ridges of K2 and K3. The event that produced K1 would have diverted the river to the opposite north-facing bank for a period until the river could migrate back to its original position. This migration has caused active undercutting of the deposit at K1.

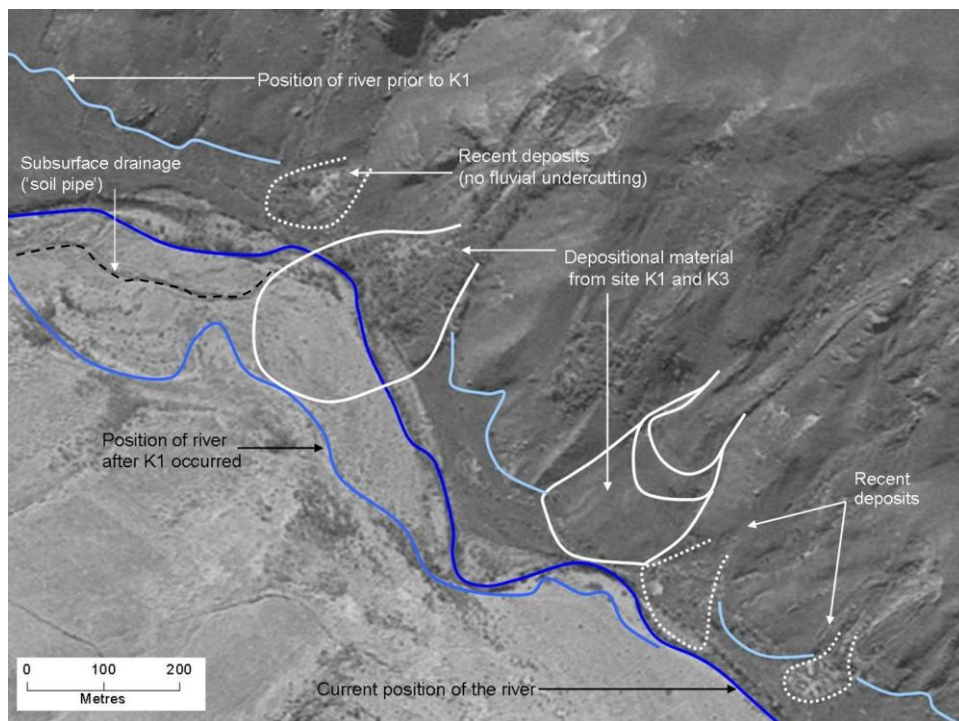


Figure 6.34 Aerial photo of site K showing the hypothetical reconstruction of mass movements events and their effect on the drainage pattern of the Bushman's River.

6.13 Site L: Slide, Bushman's River

Site L is located at 29°12'6.31" E; 29°50'2.67"S at 1 811m a.s.l on a southwest-facing bank of the Bushman's River (Figure 6.2). Mass movement activity appears to have occurred recently as a series of shallow translational slides, however the size of the shear surface and depositional fan suggests that originally a larger slide might have been present which exhibited some flow-like behaviour

(Figure 6.35). Site L is located about 250m downstream of site K and a number of large, active and inactive mass movement features can be identified from the aerial photos between the two sites indicating that the slopes in this area are relatively unstable.



Figure 6.35 Slide/flow at site L showing the main scarp, flow tracks and depositional fan.

The slide has a large depositional zone of 43m in width and 41.5m in length, whilst the depletion zone is 27m wide and 42.2m long (Table 6.1) (Figure 6.36). The transport zone is small in comparison; being only 14.5m wide and 11.8m long. A number of shear surfaces occur within the depletion zone, however all are connected by individual scarps and terraces. The main scarp is 1.6m high and the largest terrace is 0.9m high. The main scarp is composed of weathered, yellow mudstones of the Molteno Formation, whilst the terraces expose a soil profile that is yellow to light brown, having a thin organic horizon and a boulder line about 0.3m deep. *Merxmuellera macowani* grasses are evident in all three zones, whilst *Themeda triandra* and *Leucosidea sericea* grow along the banks of the Bushman's

River, which is about 80m from the foot of the slide. No fluvial undercutting of the deposit is evident from the aerial photos, suggesting that mass movement activity preceded fluvial meandering away from the south-facing bank. The slide is confined laterally by lateral ridges on either side of the surface of rupture. Upslope of the slide crown, the slope gradient flattens to form a planation surface, whilst downslope extension is limited by the local base level of the Bushman's River.

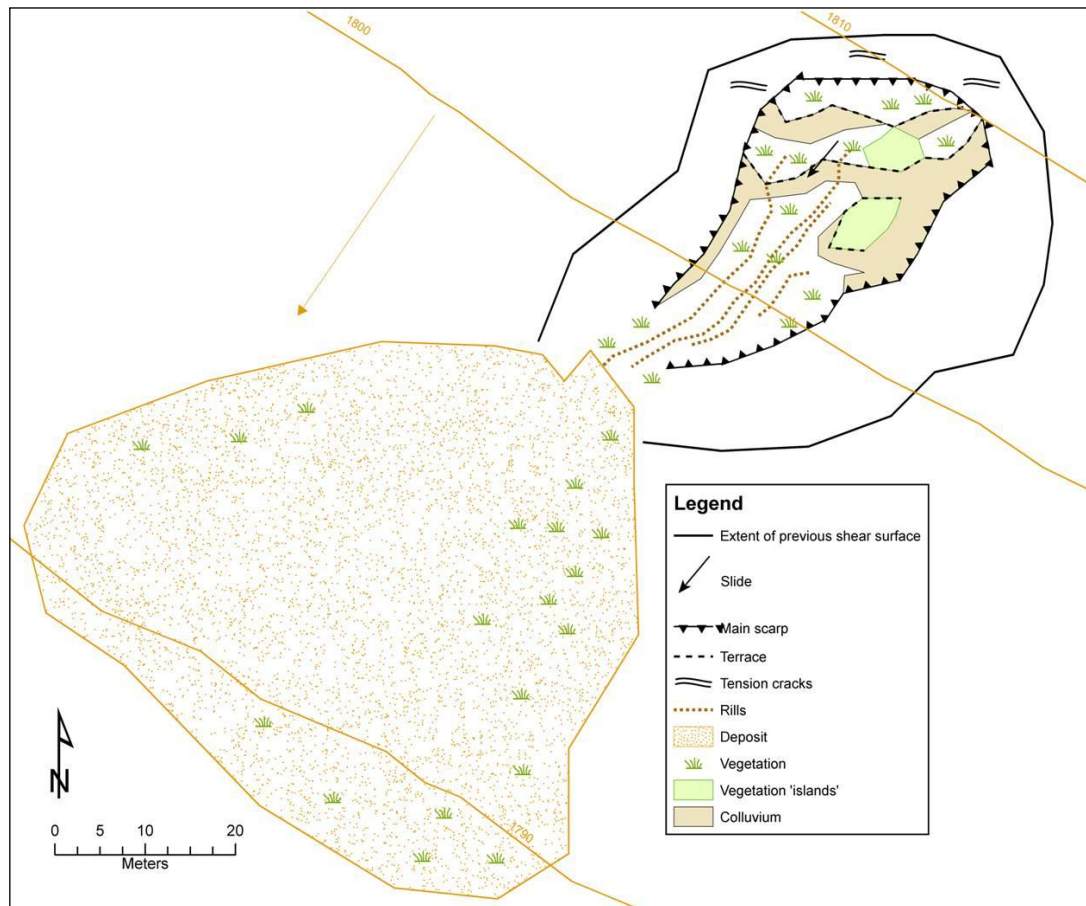


Figure 6.36 Geomorphological map of the slide at site L.

6.14 Site M: Incised flow or collapsed soil pipe?

Site M is located at 29°12'29.44" E; 29°51'55.81"S; 2 097m a.s.l on a north-facing slope (Figure 6.2). The type of movement is difficult to classify as there is no evidence of recent activity which might be used to infer the type of movement which may have occurred. The morphology is similar to an incised flow which is

initiated by a translational slide, however the depression is more bowl-shaped and deeper than the other translational slides observed in the region (Figure 6.37). It is also likely that the landform is a collapsed soil pipe. Soil pipes were observed in the field which generally had straight flow channels that were between 0.3-0.8m deep. No classification has therefore been made for site M.

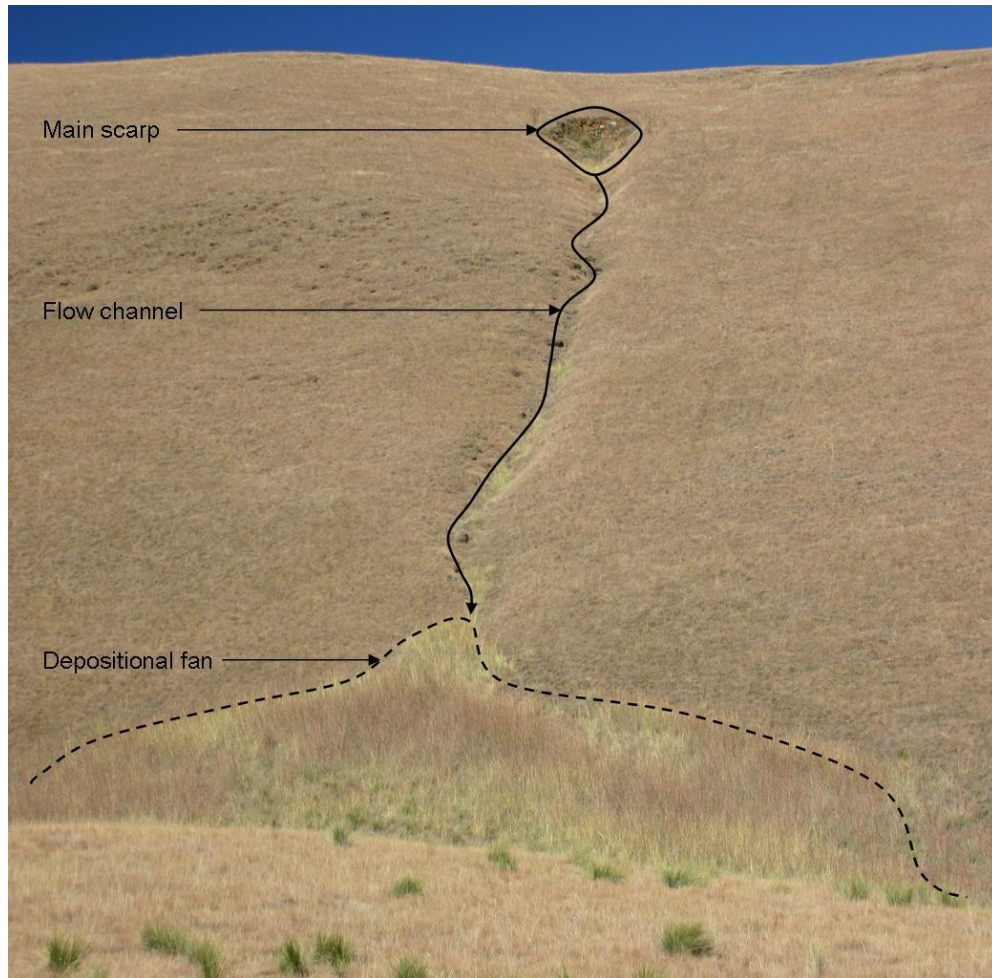


Figure 6.37 Oblique photograph of the main scarp, flow channel and depositional fan at site M.

The landform is characterised by a bowl-shaped depression that is 2.6m high, 14m wide and about 29.3m long (Table 6.1). The depression is composed of bedrock and poorly developed soil, whilst the vegetation is limited to tussocks of *Helichrysum pagophilum*, *Rubus ludwigii* and *Helichrysum nudifolium*. The average gradient along the base of the depression is 34° whilst the main scarp is near vertical. The transport zone is characterised by an incised channel up to 6.5m wide and 95.8m long. The landform is the longest measured in the region and is

over 150m long from crown to foot (Figure 6.38). The flow channel is well-vegetated with *Themeda triandra* and other dense grass species, as well as *Mohria rigida* and it is expected that this channel concentrates surface flow during rainfall events. The average gradient of the flow channel is 26°.

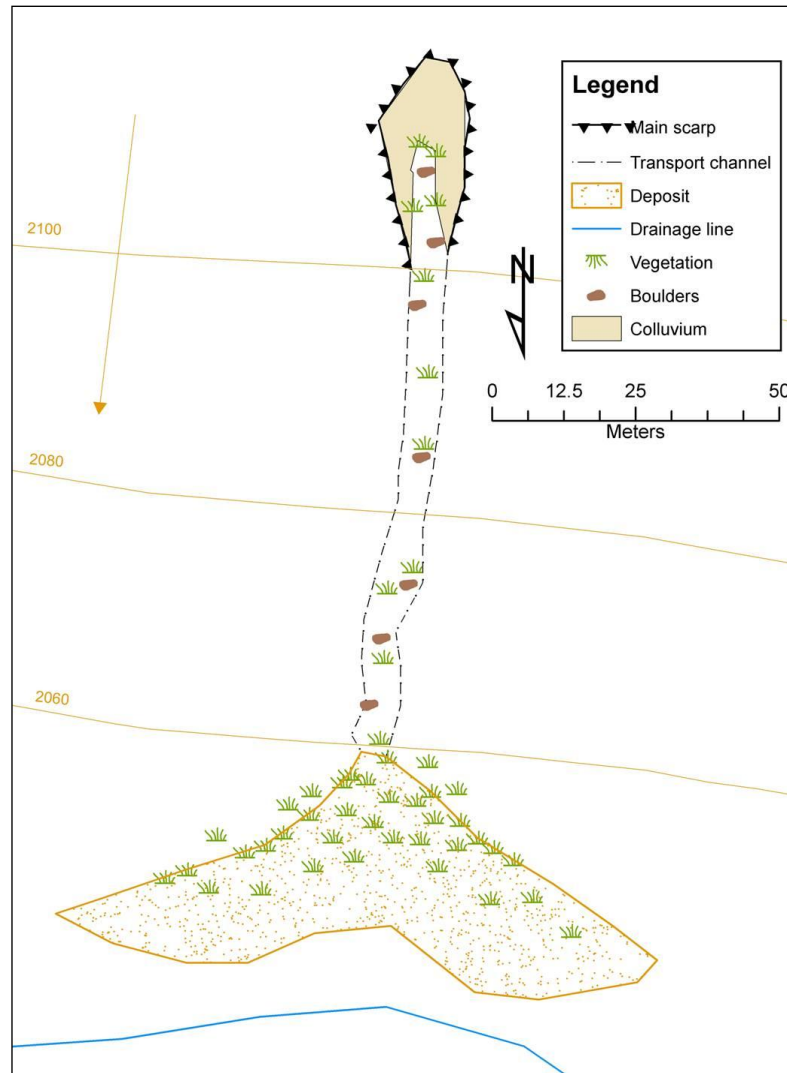


Figure 6.38 Geomorphological map of the landform at site M.

The deposit at the base of the slope is 37m wide and 26.7m long and is fan shaped. The average gradient of the fan from its source to toe is 3°. This change in gradient is caused by the local base level at the foot of the slope, which forms a small tributary valley to the Ngwangwane River. *Hyparrhenia hirta* grow thickly across the apex of the fan and *Merxmullera macowani* grow from the toe of the fan up onto the opposite facing slope. The absence of tension cracks and

secondary mass movement activity suggests that expansion of the feature is unlikely, although sediment and loose rocks have been displaced from the vertical main scarp and fallen into the depression.

6.15 Secondary mass movement features

A number of small translational slides and terraces were observed in the study area. These were generally less than 15m wide with main scarps <0.8m. A number of translational slides were observed on north-facing slopes along the Bushman's River, along footpaths and along drainage lines. The small size of these slides and their abundance made extensive field analysis unfeasible, especially given that all feature types have already been discussed in this chapter. Instead, these features have been included in the mass movement inventory, derived by using API.

6.16 Conclusion

Despite some mass movement forms having a bowl-shaped or curved shear surface, such attributes are not sufficient to classify them as rotational slides. Rotational slides most commonly form in man-made deposits such as berms, which are composed of homogeneous materials (Varnes, 1984; Dikau et al., 1996), which are absent in the study area. Further, rotational slides are usually deep-seated features, which was not the case for the landforms observed in the Bushman's Nek region. Rotational slides in that occur on natural slopes in Belgium have main scarps of about 8m deep and estimated rupture surfaces that range from 30-70m (Dewitte et al., 2008).

Most of the mass movement features observed in the Bushman's Nek region of the southern Drakensberg begin as relatively shallow translational slides (0.3 to <3m deep) which progress to flows or falls. Similar ranges in depth have been observed for translational slides in Japan and most of the slides occur at the contact between slope colluvium and underlying saprolite (Dahal et al., 2009). Comparing the depths of the main scarp for the sites suggests that slides on northerly-facing slopes are slightly deeper than the main scarps on southerly-

facing slopes which compares well with trends in soil depth found by (Garland, 1979).

Type of flow is controlled by the degree of deformation which the displaced material experiences. Shear scars range in size from 4-27m in width and 3-42m in length (Table 6.1). The average width of the transfer zone is 10.9m (range: 4.9-16.7m) and the average length is 34.3m (range: 11.8-95.8m). The average slope gradient of the transport zone is 32° (range: 18°-47°) whilst the depositional zone averages 16°. The shape and size of deposits vary greatly and range from 3.2-43m in width to 2.7-41.5 m in length. In general, mass movement features which appear to have been recently active are smaller and shallower than palaeo-mass movement features which are deep-seated and large. The presence of large palaeo-landslides suggests that the Drakensberg was once more geomorphologically active than at present, however the shear surfaces of the palaeo-landslides appear to strongly influence mass movement activity at present.

The main purpose of the fieldwork was to assess how well the classification developed for mass movements in southern Africa could be applied. Thus far, differentiating between rotational and translational slides has been unnecessary, whilst the distinction between surficial and incised flows appears to be appropriate.

7 GIS-based assessment of mass movement landforms in the southern Drakensberg

7.1 Introduction

The following section describes each of the mass movement categories which were observed from the aerial photographs and which were used to populate the mass movement inventory. Three terrace-type landforms and five shear-scar type mass movements were observed in the field, however only four of the types are discussed. The frequency distributions for each of the mass movement types is presented and then compared with the results of the area-weighting method. This is followed by a discussion on the models selected using the logit function to best predict mass movement activity and the results of the hierarchical partitioning. Further sub-classifications are suggested based on the results of the classification trees. A summary of the spatial variation in prediction models is discussed and a final map of predicted mass movement activity for each type is presented.

7.2 Terrace-type 1: Terracettes

Terracettes represent a form of slope microrelief (Watson, 1988) that are locally small, quasi-parallel, staircase-like, stepped landforms, <1m in height and up to 300m long (Weihs and Shroder, 2011). Terracettes are sometimes the result of solifluction which has been defined as the slow downslope movement of a soil mass caused by cyclical freeze-thaw and frost heave (Matsuoka, 2001; Hjort, 2006). Terracettes in the southern Drakensberg have the appearance of groups of regularly spaced steps in the soil surface that occur parallel to the slope contour. This project has digitized 677 groups or ‘fields’ of terracettes from aerial photos. Terracettes have a relatively distinct appearance on the landscape and their distribution is generally widespread (Figure 7.1). The term ‘terracette’ was first used by King (1944) to describe these types of mass movement features in the Drakensberg, whilst subsequent studies in the region indicate that terracettes are most likely initiated by shear failure and solifluction (Watson, 1988).

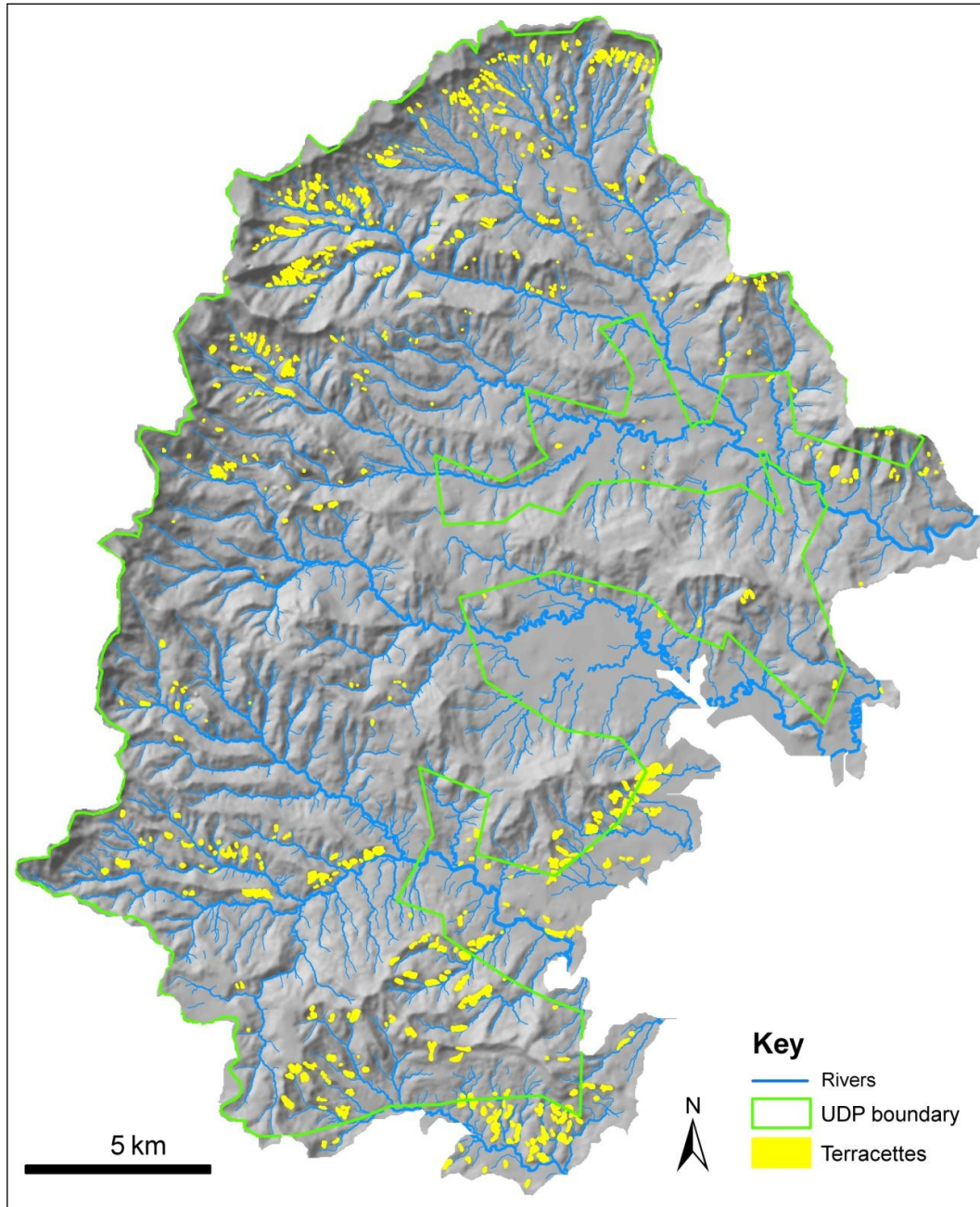


Figure 7.1 Distribution of terracettes digitized from the 1: 50 000 orthophotos.

The morphometric attributes of terracettes appear to differ widely in the southern African literature and this may be due to the geographic locations where landforms have been investigated, or to the classification used by the researcher to identify the landform. Average riser height (0.6m) and tread length (0.35m) measured in the Northern Drakensberg (Watson, 1988) were a third smaller than the mean lengths measured in the central Drakensberg (Garland, 1987), whilst

terraces studied in the Eastern Cape Drakensberg had riser heights of between 0.25-0.55m and an average tread length of 0.7m (Kück and Lewis, 2002). Boelhouwers (1988a) observed terraces in the southern Drakensberg and differentiated between ‘cattle-step’ terraces, which have an average riser height of 0.05-0.25m and tread length of 0.1-0.5m, with ‘slipscar’ terraces which have an average tread riser height and tread length of 0.05-1.3m and 0.4-6.0m respectively. Anderson (1972) proposed a classification for terraces observed in western Britain based on vegetation cover and morphometric data. ‘Normal’ terraces are completely covered in vegetation, whilst ‘tear’ terraces are bare of vegetation. Differences in morphology have been attributed to soil type, with volcanic soils producing narrower terraces than sedimentary soils (Garland, 1987). Soil depth and clay content also influences the distribution and density of terrace features, with higher densities of terraces observed in shallow clay-rich soils (Verster and Van Rooyen, 1988), or deep soil mantles resting directly on the underlying bedrock (Garland, 1987).

Topographic variables such as aspect and gradient also influence the distribution of terraces. In the northern Drakensberg, the density of terraces is apparently substantially greater on drier north-facing slopes than on the surrounding slopes (Watson, 1988). However, Boelhouwers (1988a) observed that high densities of ‘cattle-step’ terraces occur on south-facing slopes and that 46% of the ‘slipscar’ types of terraces occur on southeast-facing slopes in the southern Drakensberg (see Figure 7.2 and 7.3). In the Eastern Cape Drakensberg, terraces occur on south- and south-east facing slopes at gradients between 23° to 26° (Kück and Lewis, 2002), whilst in the Pyrenees, terraces occur on south-facing slopes at gradients between 25°-30° (Gallart et al., 1993).

Aspect is not expected to directly influence terrace development but rather influence soil development and vegetation growth. Grassy vegetation, which has a dense root network, appears to bind the regolith to form a scarp (Granger, 1976; Kück and Lewis, 2002). Slope gradient was attributed to have the greatest



Figure 7.2 Front view of several groups of terracettes (1 – 4) taken in August 2005. A-B are reference points showing the location of the terracettes in Figure 7.3.

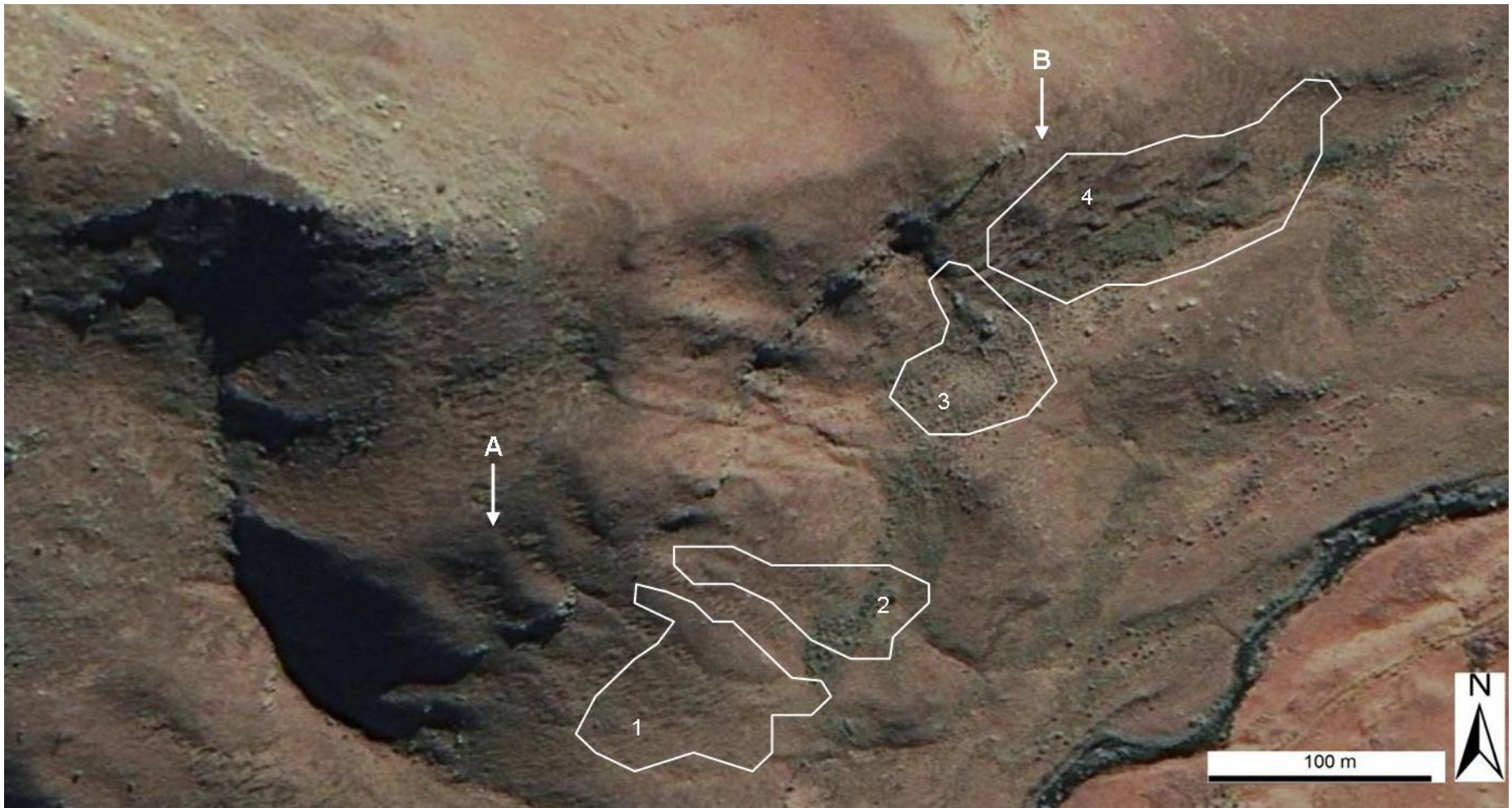


Figure 7.3 Plan view (A – B) of the terracette groups shown in Figure 6.2 (1 – 4) (Google Earth, 2008).

influence on the processes which initiate terracette development and this was confirmed in the northern Drakensberg as the density, overall size and tread width of terracettes increased steadily with increasing slope gradient. Terracettes in the Pyrenees are limited to altitudes between 1 700-2 700m a.s.l (Gallart et al., 1993), and this altitudinal zone corresponds to the location of the winter snowpack. Terracettes in Taiwan have been observed at 3 400m a.s.l, however these landforms are thought to have occurred under different climatic conditions as ground-freezing is not intense enough to initiate development (Klose, 2006). A large number of terracettes in the Eastern Cape Drakensberg were observed between 2 750 and 2 880m a.s.l, which implies that they are climatically sensitive landforms (Kück and Lewis, 2002). However, Boelhouwers (1991) argues that 'cattle-steps' and terracettes in the KwaZulu-Natal Drakensberg are of widespread occurrence, both above and below the frost line.

Terracette formation has sometimes been linked to periglacial processes, such as frost heave, needle ice growth and the presence of interstitial ice lenses associated with diurnal freeze-thaw where sufficient soil moisture is available (Troll, 1944; Killick, 1963; Kück and Lewis, 2002). Other initiating mechanisms have been postulated, such as the movement of water-saturated soil over underlying bedrock, in association with shear failures leading to soil slippage and eventual flow (De Villiers, 1962; Watson, 1988). Terracette development has also been attributed to anthropogenic activities and bioturbation. The introduction of grazing animals to New Zealand, as well as vegetation transformation, has been associated with an increase in terracette development and associated landsliding (Brown, 1983). However, Trimble and Mendel (1993) note that the effects of grazing animals on the geomorphic environment are dichotomous and have been shown to both improve and degrade soil quality.

A frequency distribution of the occurrence of terracettes in relation to the eight variables and their associated class categories is presented in Figure 7.4. The results of the distance variables suggest that the majority of terracettes occur within 25 m of a drainage line (30%), within 25 m of a rock exposure (40%) and

more than 300 m from a footpath (59%). Thus distance to footpath has no geomorphic influence on the formation of terracettes and is not referred to further in this discussion. Interpreting the relationship between terracette formation and the other two distance variables is more difficult as terracette formation is not likely to be dependent on proximity to a drainage line or rock exposure. These variables may have a secondary influence on terracette development, by providing soil moisture or being related to a lithology that produces regolith that is susceptible to deformation. However, it is more likely that the two distance variables are dependent on other variables which have a greater influence on the development of terracettes, such as gradient and altitude.

Terracettes are predominantly associated with south-facing aspects, with over 74% of features occurring on south- and southeast facing slopes (112.5–202.5°), which supports findings by Boelhouwers (1988a) and Kück and Lewis (2002). However, the combination of aspect and gradient is also important for terracette formation. Boelhouwers (1988b) notes that south-facing slopes in the Giant's Castle area of the Drakensberg have slope gradients of $\geq 30^\circ$ and are generally cooler and moister than other slopes. In winter, south-facing slopes with gradients of 30° receive about one-sixth the solar radiation received on north-facing slopes of similar gradient (Boelhouwers, 1988b). Field observations made in winter 2005 confirmed that snow patches were present on steeper south-facing slopes and absent on gentler north-facing slopes. This suggests that aspect and gradient have a noticeable effect on micro-climate and likely terracette formation.

The highest frequency (46%) of terracettes occurs on slope gradients of 20-30°, whilst 30% occur at altitudes between 2 400-2 600m a.s.l. Enough evidence exists in published literature to support the conclusion that gradient is important for terracette formation (Anderson, 1972; Gallart et al., 1993; Kück and Lewis, 2002), however less information is available on the influence of altitude. The high frequency of terracettes between 2 200-2 400m a.s.l is confirmed by Boelhouwers (1988a) for the southern Drakensberg, where 'cattle steps' were observed around 2 300m a.s.l and 'slipscars' observed up to 2 500m a.s.l. In the Eastern Cape

Drakensberg, Kück and Lewis (2002) only observed terracettes between 2 750-2 880m a.s.l, whilst in the French Pyrenees, terracettes have been observed at altitudes between 1 700 to 2 700m a.s.l (Gallart et al., 1993). This suggests that terracettes occur in a wide range of altitudes and it is likely that the presence or absence of permafrost is more influential on terracette development than a specific altitudinal range.

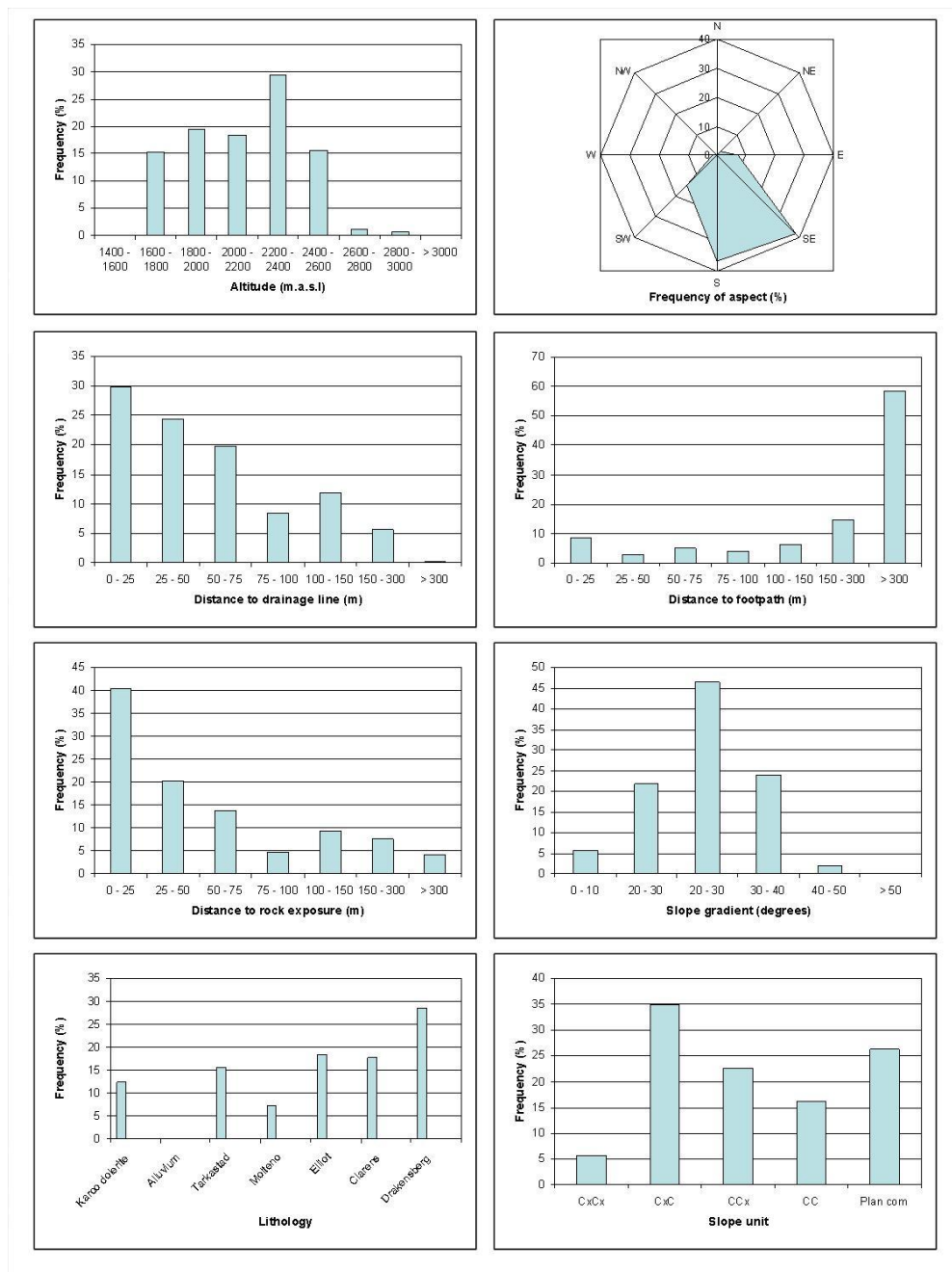


Figure 7.4 Histograms of the independent variables for terracettes.

The highest frequency of terracettes for any given slope unit is the convex–convex or ‘sloping inflated hills’ category (35%). Slope units have not previously been used as a measure in southern African terracette studies. Ayalew and Yamagishi (2004) describe convex–convex units as very stable, as the convex-upward plan and profile shape of the slope drains moisture away from the region. It is not clear how slope unit may therefore influence the formation of terracettes. The Drakensberg Group has the highest frequency of terracettes (29%) for any lithology in the GCSF and is composed of basaltic lava with minor sandstone, tuff and agglomerate in the lower part of the succession (CGS, 2008). According to the 1:250 000 lithological dataset, the Drakensberg Group ranges from 2 129–3 267m a.s.l in the study area and corresponds with soils of the Glenrosa and Mispah forms (van Der Eyk et al, 1969). These soils are generally shallow and consist of topsoil underlain by weathered or hard rock, which would support the contention that terracettes occur when soils become saturated and move along an underlying bedrock layer (De Villiers, 1962; Watson, 1988). Underlying lithology and gradient have been selected as the most influential factors controlling creep-induced terracettes in Slovenia (Komac, 2006)

Ranking the percentage of terracettes that occur within a class suggests that terracettes most frequently occur on slope gradients of 20–30°, within 25 m of a rock exposure, on south- and southeast-facing convex–convex slope units, at altitudes between 2 200–2 400m a.s.l, within 25 m of a drainage line, and in the Drakensberg Group. However, a slightly different ranking is obtained if the variables are normalized using area. The Information Value (InfoVal) is a ratio which can be used to rank the relative frequency of a mass movement feature against the total area of a class within a variable. Therefore, a higher weighting will be ascribed to a class that contains a high number of terracettes in a class that has a small area. In some cases the highest weight (or ratio) corresponds to the highest frequency and this occurs when the frequency/area ratios are similar.

InfoVal weights for aspect, distance to footpath, lithology and slope unit reflect the same patterns as for the frequency distributions (Table 7.1). However, InfoVal

Variable	Class	Area (%)	Frequency (%)	InfoVal	Ratio (F/A)
Altitude	1400-1600	0.77	0	\$	0.00
	1600 - 1800	26.05	15	-0.538	0.58
	1800 - 2000	25.94	19	-0.293	0.75
	2000 - 2200	19.51	18	-0.055	0.95
	2200 - 2400	15.33	30	0.656	1.93
	2400 - 2600	6.46	16	0.876	2.40
	2600 - 2800	2.48	1	-0.742	0.48
	2800 - 3000	2.41	1	-1.183	0.31
> 3000	1.05	0	\$	0.00	
Aspect	N (0 - 22.5)	7.08	0	\$	0.00
	NE (22.5 - 67.5)	17.32	2	-2.279	0.10
	E (67.5 - 112.5)	14.78	7	-0.694	0.50
	SE (112.5 - 157.5)	15.37	38	0.904	2.47
	S (157.5 - 202.5)	15.51	37	0.859	2.36
	SW (202.5 - 247.5)	11.83	14	0.202	1.22
	W (247.5 - 292.5)	6.92	2	-1.449	0.23
	NW (292.5 - 337.5)	6.32	0	-3.756	0.02
N (337.5 - 360)	4.86	0	\$	0.00	
DistDrain	0 - 25	32.64	30	-0.090	0.91
	25 - 50	14.78	24	0.500	1.65
	50 - 75	14.06	20	0.342	1.41
	75 - 100	9.65	8	-0.136	0.87
	100 - 150	14.26	12	-0.188	0.83
	150 - 300	12.22	6	-0.778	0.46
	> 300	2.39	0	-2.782	0.06
DistFoot	0 - 25	14.27	8	-0.527	0.59
	25 - 50	6.06	3	-0.718	0.49
	50 - 75	5.92	5	-0.165	0.85
	75 - 100	4.39	4	-0.059	0.94
	100 - 150	7.96	6	-0.249	0.78
	150 - 300	14.58	15	0.003	1.00
	> 300	46.83	59	0.225	1.25
Dist RockX	0 - 25	31.24	40	0.259	1.30
	25 - 50	11.56	20	0.560	1.75
	50 - 75	10.04	14	0.314	1.37
	75 - 100	6.47	5	-0.346	0.71
	100 - 150	9.80	9	-0.051	0.95
	150 - 300	13.51	8	-0.584	0.56
> 300	17.40	4	-1.436	0.24	
Gradient	0 - 10	31.95	6	-1.739	0.18
	10 - 20	28.45	22	-0.263	0.77
	20 - 30	25.04	46	0.617	1.85
	30 - 40	11.73	24	0.719	2.05
	40 - 50	2.56	2	-0.213	0.81
	> 50	0.27	0	\$	0.00
Lithology	Karoo dolerite	19.86	12	-0.471	0.62
	Alluvium	2.30	0	\$	0.00
	Tarkastad	18.72	16	-0.179	0.84
	Molteno	13.40	7	-0.616	0.54
	Elliot	22.37	18	-0.200	0.82
	Drakensberg	12.93	29	0.796	2.22
	Clarens	10.42	18	0.532	1.70
SlopeUnit	CxCx	28.81	35	0.191	1.21
	CxC	23.14	23	-0.023	0.98
	CCx	17.53	16	-0.076	0.93
	CC	30.50	26	-0.148	0.86
	PlanCom	0.03	0	\$	0.00

Table 7.1 Comparison of the frequency distributions and InfoVal weights for terracettes. Bold indicates highest value in category, colour indicates variable with greatest frequency.

weights for altitude, two of the distance variables, and for gradient, suggest that terracettes are more likely to occur between 2 400-2 600m a.s.l, within 25-50m of a drainage line, within 25-50m of a rock exposure, and on gradients of 30-40°. The ranked InfoVal weights suggest that terracettes are most frequent on southeast-facing slopes, between 2 400-2 600m a.s.l, in the Drakensberg Group, on slope gradients between 30-40 °, within 25-50m of a rock exposure and drainage line, and on convex– convex slopes. Thus, aspect and altitude appear to have a stronger influence on terracette distribution than gradient and distance to rock exposure.

Hierarchical partitioning was undertaken to rank the variables according to their greatest independent contribution (%I) to the logistic regression model. A hierarchical partition was created for each iteration of random points and the resulting %I are presented in Figure 7.5. Gradient consistently has the highest independent contribution and accounts for an average of 54% (2.46 SD) of the model. Distance to a rock exposure (12%) and lithology (10%) have the second and third highest contribution after gradient and this corresponds well with the variable ranking produced for the frequency distributions.

Stepwise forward and backward logistic regression using all of the variables was used to develop a prediction model which could predict the maximum number of terracettes using the smallest number of variables. Akaike's Information Criterion (AIC) and Bayes Information Criterion are given in Table 7.2. The lowest AIC and BIC for the five iterations is for the Random Point 2 (RP2) dataset. Six independent variables are selected using the AIC, whilst 4 are selected using the BIC. Altitude, aspect, gradient and lithology appear in the AIC models for each iteration, whilst aspect and gradient are consistently selected for the BIC models. Random point 4 (RP4) has the highest percentage of terracettes that have been correctly classified, however the RP4 model only classifies 0.53% more than RP2, which has better AIC and BIC values. These results confirm that gradient has a primary influence on the distribution of terracette features and suggests that aspect

may also have some influence despite this variable having a low %I (mean=2.88, SD=1.38).

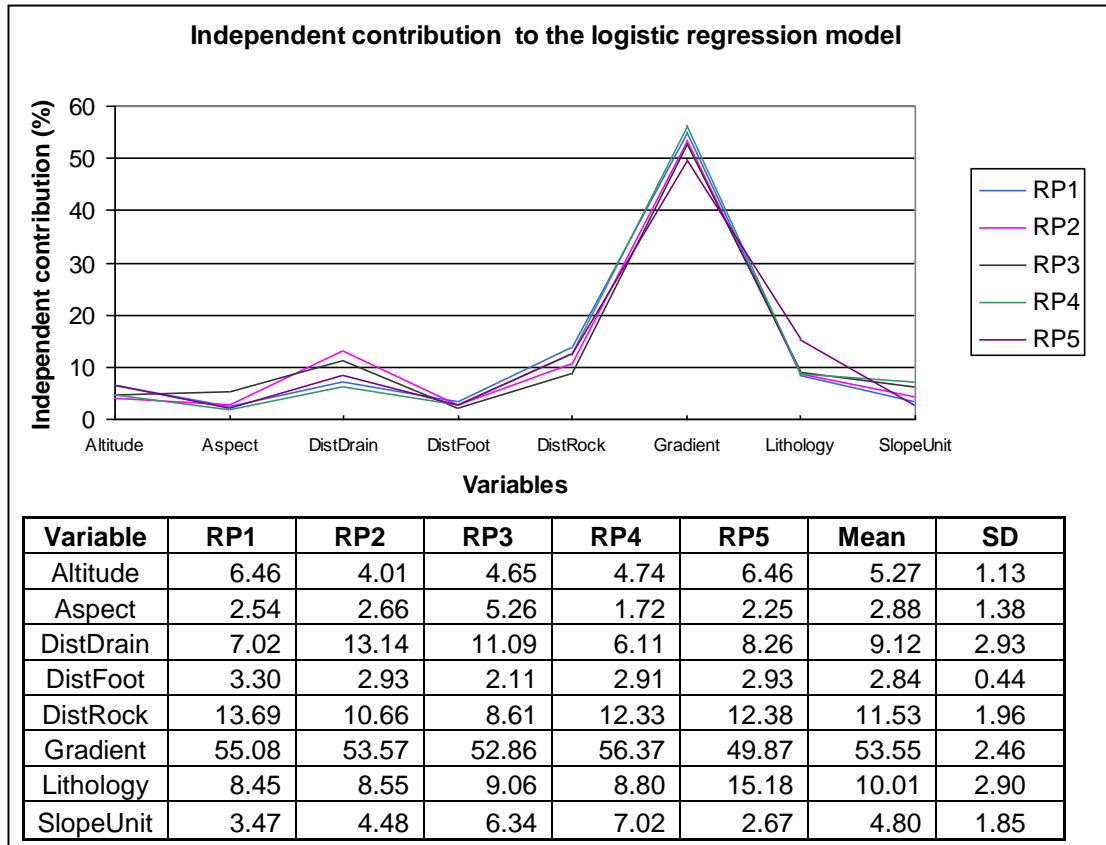


Figure 7.5 Graph representing the percentage contribution of each variable to the logit model. The table shows the mean and standard deviations for each contribution.

Probability maps were created in a GIS environment to spatially compare the predictive ability of each model (Figure 7.6, 7.7 and 7.8). The values of the probability function were classified to reflect differences in the total area for a range of probability values (Table 7.3). It is noteworthy that the areas predicted for a particular probability class are consistently within one standard deviation which confirms that the models perform equally and that any variations observed between datasets is due to the effects of the actual (Type=T1) dataset and not the randomly generated (Type=T0) dataset. Less than 30% of the study area has more than a 50% chance of developing terracettes.

Models	RP 1	RP2	RP3	RP4	RP5
Full AIC	1311	1305	1326	1316	1309
Best AIC	1299	1297	1307	1304	1298
No Var	5	6	5	5	5
Variables	Altitude	Altitude	Altitude	Altitude	Altitude
	Aspect	Aspect	Aspect	Aspect	Aspect
	DistRock	DistDrain	-	DistDrain	DistDrain
	Gradient	Gradient	Gradient	Gradient	Gradient
	Lithology	Lithology	Lithology	Lithology	Lithology
	-	SlopeUnit	SlopeUnit	-	-
Best BIC	1401	1392	1407	1400	1394
No Var	4	4	3	3	3
Variables	Altitude	Altitude	-	Altitude	-
	Aspect	Aspect	Aspect	Aspect	Aspect
	Gradient	Gradient	Gradient	Gradient	Gradient
	Lithology	Lithology	Lithology	-	Lithology
%CorrPred	78.13	79.46	79.39	79.99	79.17

Table 7.2 The AIC, BIC and variables selected for each iteration. Note that the percentage of correctly predicted terracettes is similar for each model.

Numerous classification trees were produced for the five random point datasets to compare the findings of the hierarchical partition (Figure 7.9). Three trees were created for each random dataset, the first included all variables, the second only variables selected by the AIC statistics and the third using only the variables selected by the BIC. The results of a classification tree are relatively easy to interpret and the confusion matrix reported for each tree was used to select the tree with the largest percentage of correctly predicted events. In general, trees which used all 8 variables had a better success rate than trees which used fewer variables, however the trees are also larger and therefore more difficult to interpret. As the logistic regression provided an indication of which variables were the most significant, only the trees which used the least number of variables were included in further analyses.

The first node for all five random datasets is consistently aspect (south, southeast), as these two classes account for almost 75% of the Type=T1. Lithology was selected as the second level node by RP1, RP3 and RP5, whilst altitude was selected as the second level node by RP2 and RP4. RP5 has the highest percentage of correctly predicted events (74.9%) and is represented in Figure 7.9, whilst RP2 had the lowest percentage correctly classified. The classification trees suggest that a sub-classification may exist for terracette mass movement features

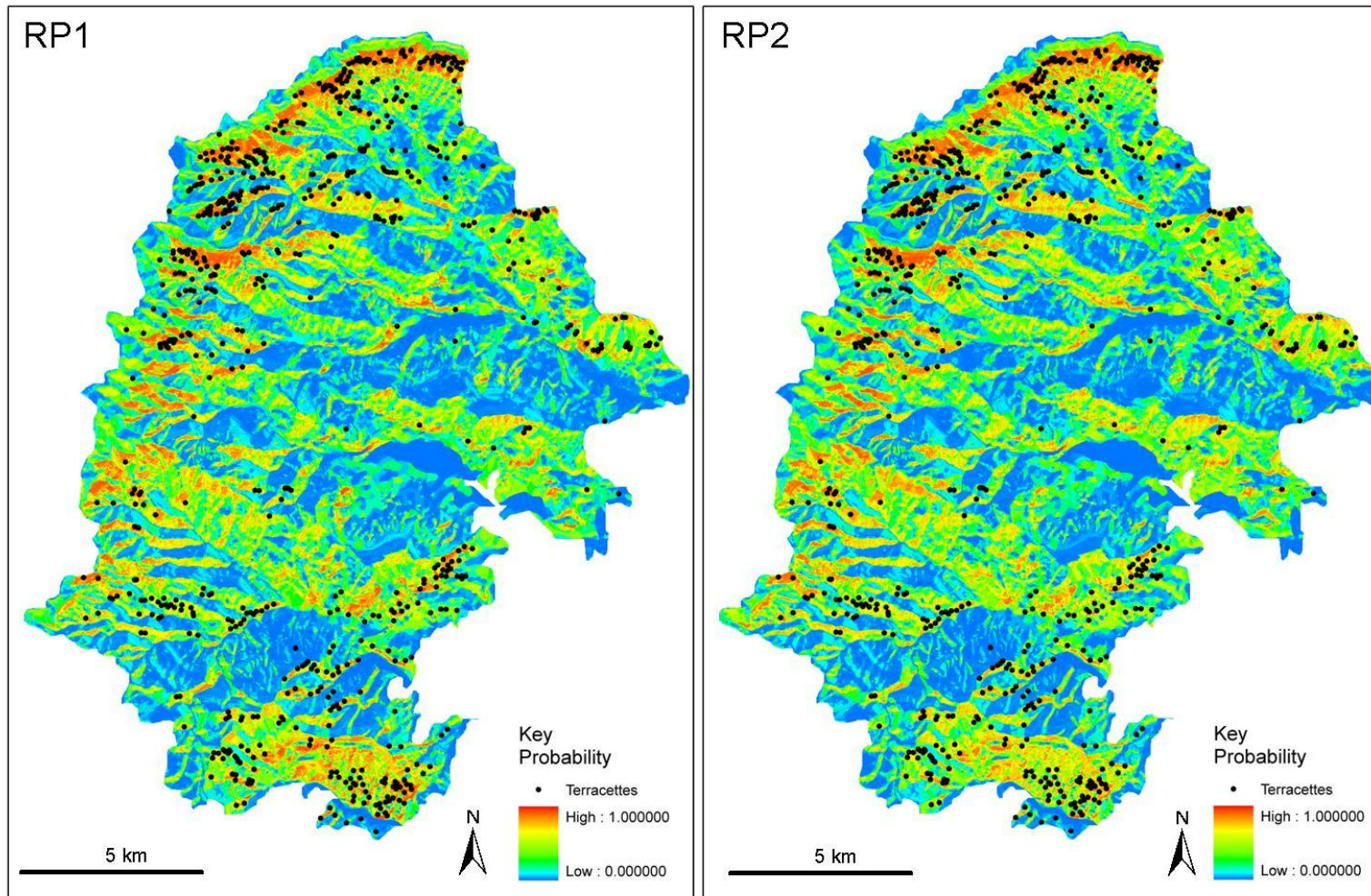


Figure 7.6 Probability maps for terracettes using the RP1 and RP2 datasets.

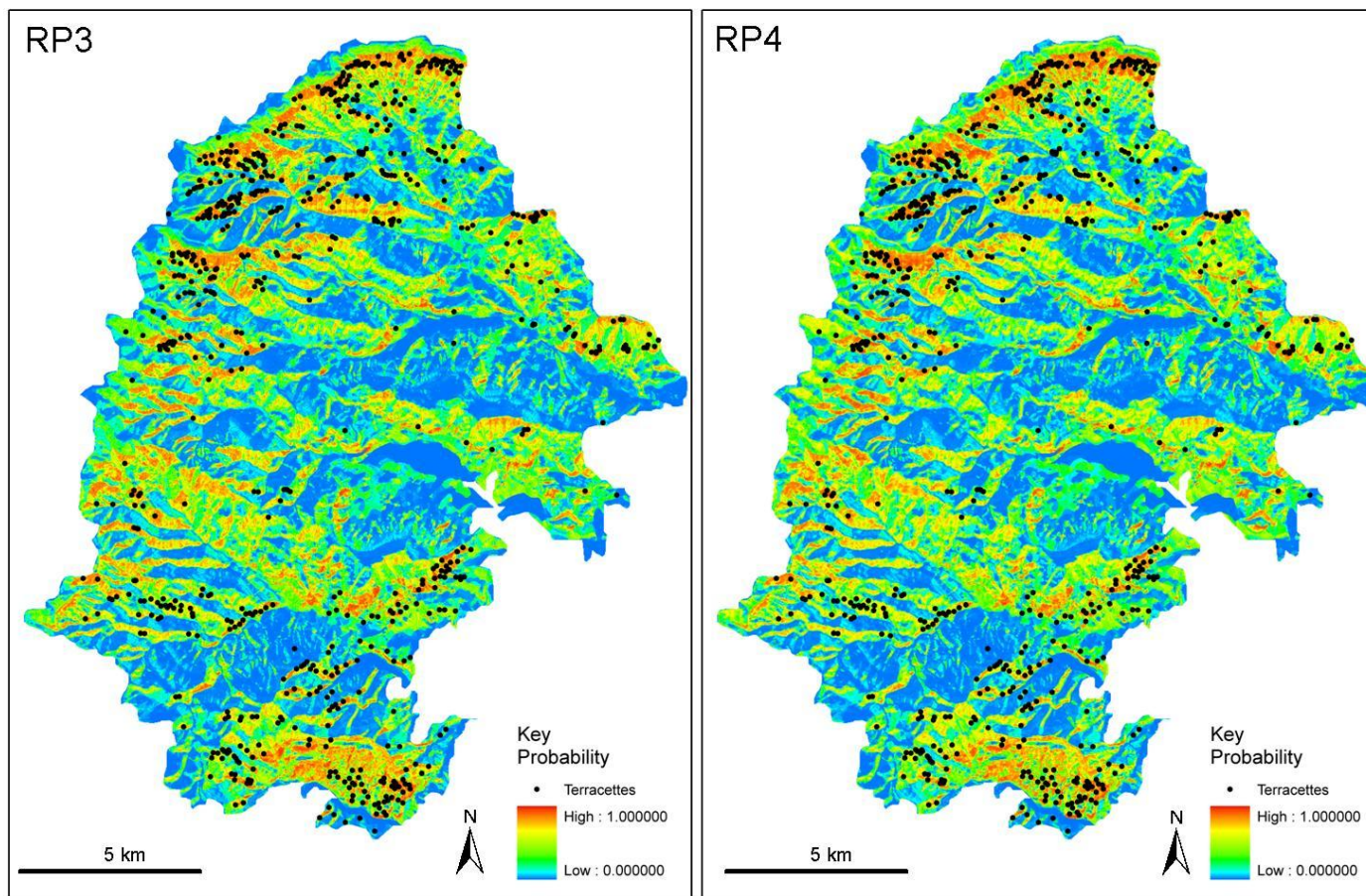


Figure 7.7 Probability maps for terracettes using the RP3 and RP4 datasets.

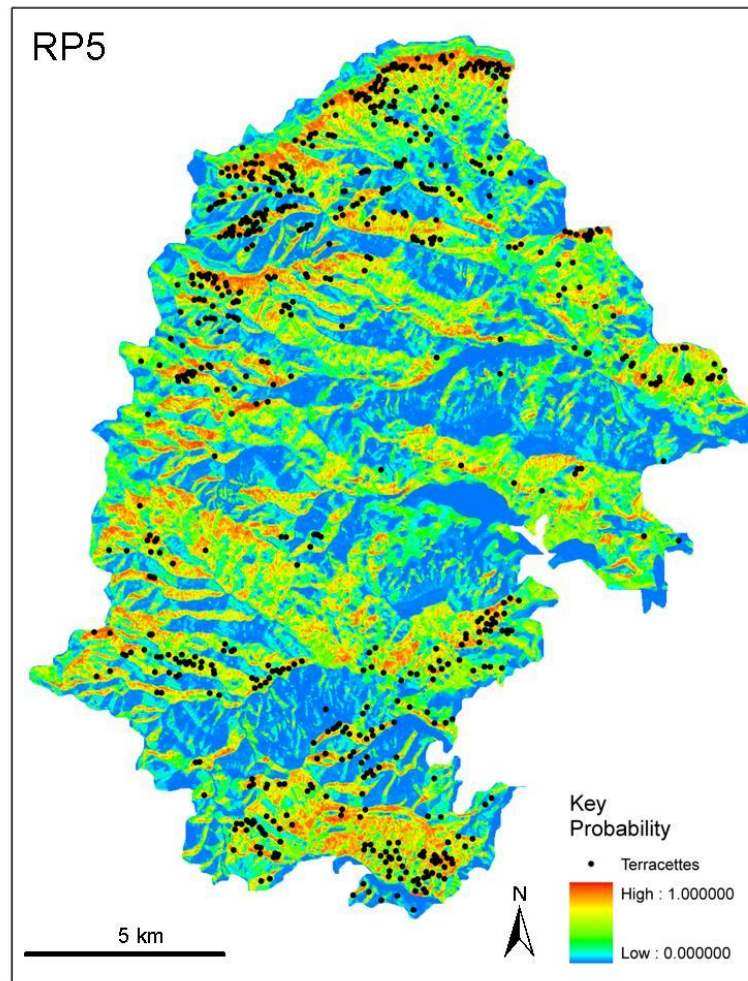


Figure 7.8 Probability maps for terracettes using the RP5 datasets.

based on underlying lithology. Thus, half of the terracettes which occur on south- and southeast-facing slopes will occur on lithologies of the Drakensberg Group, Clarens or Molteno Formations, whilst the other half of terracettes will occur in areas underlain by Karoo dolerite, alluvium, or the Elliot and Tarkastad Subgroups. This is confirmed by altitude, which is the third node of the left-hand branch, because altitude and lithology are closely linked in the Drakensberg due to the horizontal nature of bedding structure. It is also likely that there is a strong link between gradient and the Tarkastad and Elliot Formations, as these are considered to contain more mudstones and shale than the Clarens or Molteno Formations (Brink, 1982). Thus, slope gradient, which is dependent on the internal strength properties of the underlying bedrock, is the third node of the right-hand branch.

Probability	RP1			RP2			RP3			RP4			RP5			Mean	
	Area	%	SD	Area	%	SD	Area	%	SD	Area	%	SD	Area	%	SD	Area	%
0 - 0.5	338.3	73.4	0.6	335.5	72.8	0.2	332.6	72.2	0.3	330.4	71.7	0.6	334.8	72.7	0.1	334.3	72.6
0.5 - 0.6	30.7	6.7	0.0	27.9	6.0	0.4	31.0	6.7	0.1	32.6	7.1	0.3	31.4	6.8	0.1	30.7	6.7
0.6 - 0.7	33.0	7.2	0.0	31.8	6.9	0.2	34.2	7.4	0.2	34.5	7.5	0.2	32.0	6.9	0.2	33.1	7.2
0.7 - 0.8	25.8	5.6	0.9	32.1	7.0	0.1	32.9	7.1	0.2	32.4	7.0	0.1	34.1	7.4	0.4	31.5	6.8
0.8 - 0.9	24.7	5.4	0.1	29.1	6.3	0.5	25.1	5.4	0.1	26.2	5.7	0.1	22.9	5.0	0.4	25.6	5.6
0.9 - 1.00	8.3	1.8	0.4	4.4	1.0	0.2	4.9	1.1	0.1	4.8	1.0	0.1	5.5	1.2	0.0	5.6	1.2
> 0.5		26.6			27.2			27.8			28.3			27.3			27.4

Table 7.3 Total area (km² and percent) of probability values for each iteration of random points for terracette type mass movements.

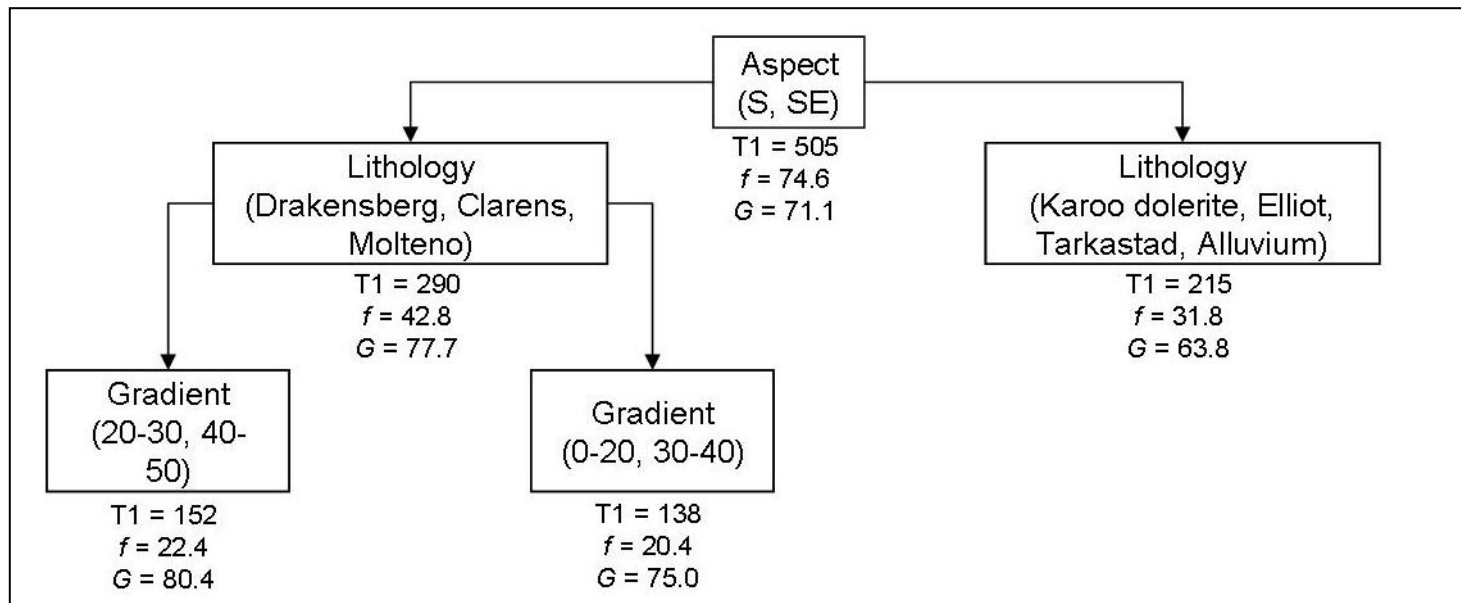


Figure 7.9 Summarized and pruned classification tree for terracette type mass movement features (*f*: frequency, *G*: Gini coefficient).

The frequency distribution and hierarchical partitioning suggest that gradient has the largest influence on terracette distribution, whilst the InfoVal and classification tree suggest that aspect also has an influence. Both variables appear consistently in the logistic regression models which perform equally well. It is therefore suggested that whilst gradient has the largest independent influence on the ability of a logit model to predict terracette distribution, aspect is also important. It is also suggested that although aspect has a weak independent influence on the predictive ability of the logit model, aspect could be used to create a sub-classification for the terracettes. However, the validity of a sub-classification would need to be confirmed by future research in the field.

7.3 Terrace-type 2: Solifluction lobes

Solifluction has been defined as the slow downslope flow of saturated unfrozen earth materials caused by freeze-thaw action (Ridefelt and Boelhouwers, 2006). Solifluction lobes are the second largest group of terrace-type mass movements which have been observed in the southern Drakensberg and have the appearance of groups of overlapping terraces with lobate fronts (Figure 7.10). These landforms are generally more distinct in appearance than terracettes and tend to extend over a greater surface area. Solifluction lobes have been subdivided into turf-banked and stone-banked forms (Matsuoka, 2001), and examples of each have been observed in the Drakensberg (Dardis and Granger, 1986; Lewis, 1987, 1988; Boelhouwers, 1991; Grab, 2000). However the resolution of the aerial photographs was too poor to make the distinction between turf- and stone-banked lobes during the API.

Solifluction lobes are usually the result of freeze-thaw processes and are generally found in periglacial environments in the Arctic, mid-latitude mountain ranges (c.f. Matsuoka, 2001), and the Antarctic (Boelhouwers et al., 2003). Solifluction lobes in southern Africa have been observed in the mountains of the Eastern Cape, High Drakensberg and Maluti, and have been studied since the 1960's (Harper, 1969; c.f.

Boelhouwers and Meiklejohn, 2002). This project has digitised 200 solifluction lobe fields in the southern Drakensberg (Figure 7.11), however the distribution of these landforms seems relatively limited when compared to the other terrace-type mass movements in the region (Figure 7.12).

The occurrence of solifluction lobes in the Drakensberg has been attributed to palaeo-periglacial conditions and present-day freeze-thaw activity (Boelhouwers, 1994). Frost occurs on about 120 days per year in the Little Berg and an average of 2-8 snowfalls occur in winter (Schulze, 1965), however snowfalls in summer have also been observed on occasion (Boelhouwers and Meiklejohn, 2002). Strong diurnal heating and large daily, temperature fluctuations characterize the Drakensberg in the winter months and needle ice activity has been observed above 2 300m a.s.l (Boelhouwers, 1991). Soil surface minima temperatures of -3°C and -2.1°C have been recorded for the winters of 2003-2004 at Sani Pass (Nel and Sumner, 2008). Although the longest period of continuous soil freeze recorded during this period was only 4 days, these results suggest that freeze-thaw processes may still be active in the GCSF. Grab (2002) notes that the contemporary environment in the Drakensberg is conducive to marginal periglacial conditions. Solifluction lobe development is most likely related to diurnal frost creep in the upper layer of the soil material and factors such as freeze-thaw depth, water availability and sediment thickness are expected to influence the growth of solifluction lobes (Matsuoka et al., 2005).

Solifluction lobes have been reported from altitudes ranging from 1 500-1 900m a.s.l on slope gradients from 5° - 23° in the Yukon Territory, Canada, between 2 200-2 800m a.s.l in the Swiss Alps (Matsuoka et al., 2005) and between 800-1 100m a.s.l on slope gradients of 12° to 20° in Sweden (Ridefelt and Boelhouwers, 2006). In New Zealand, solifluction lobes are best developed on north- and northeast-facing slopes as snow persists for longer on these slopes (Soons and Price, 1990).



Figure 7.10 Front view of several fields of solifluction lobes. A – large sheet slide, B – smaller sheet slide, C – translational slide along a drainage line.

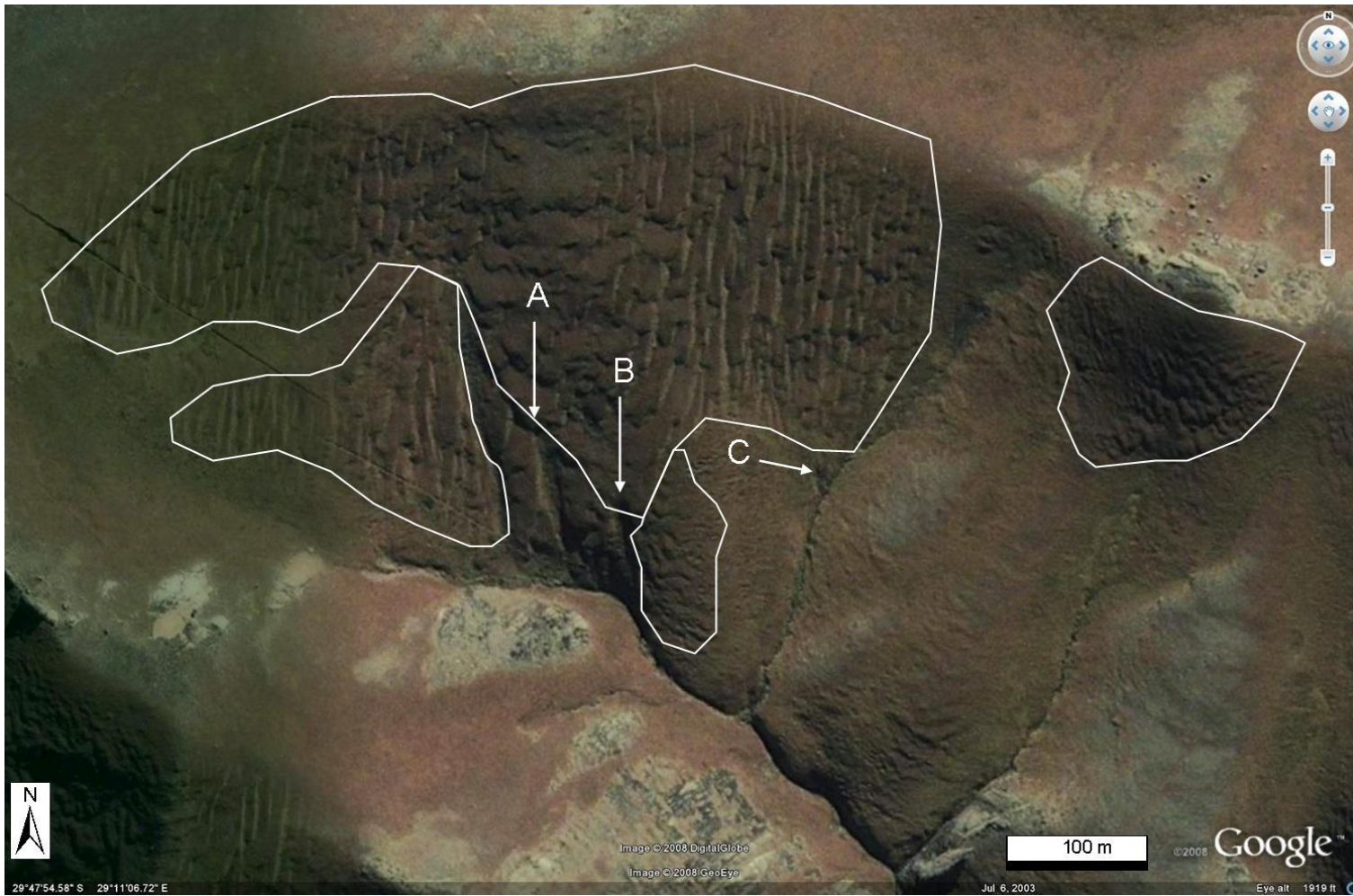


Figure 7.11 Plan view of the solifluction fields as shown in Figure 7.10 (A – large sheet slide, B – smaller sheet slide, C – translational slide along drainage line) (Google Earth, 2009).

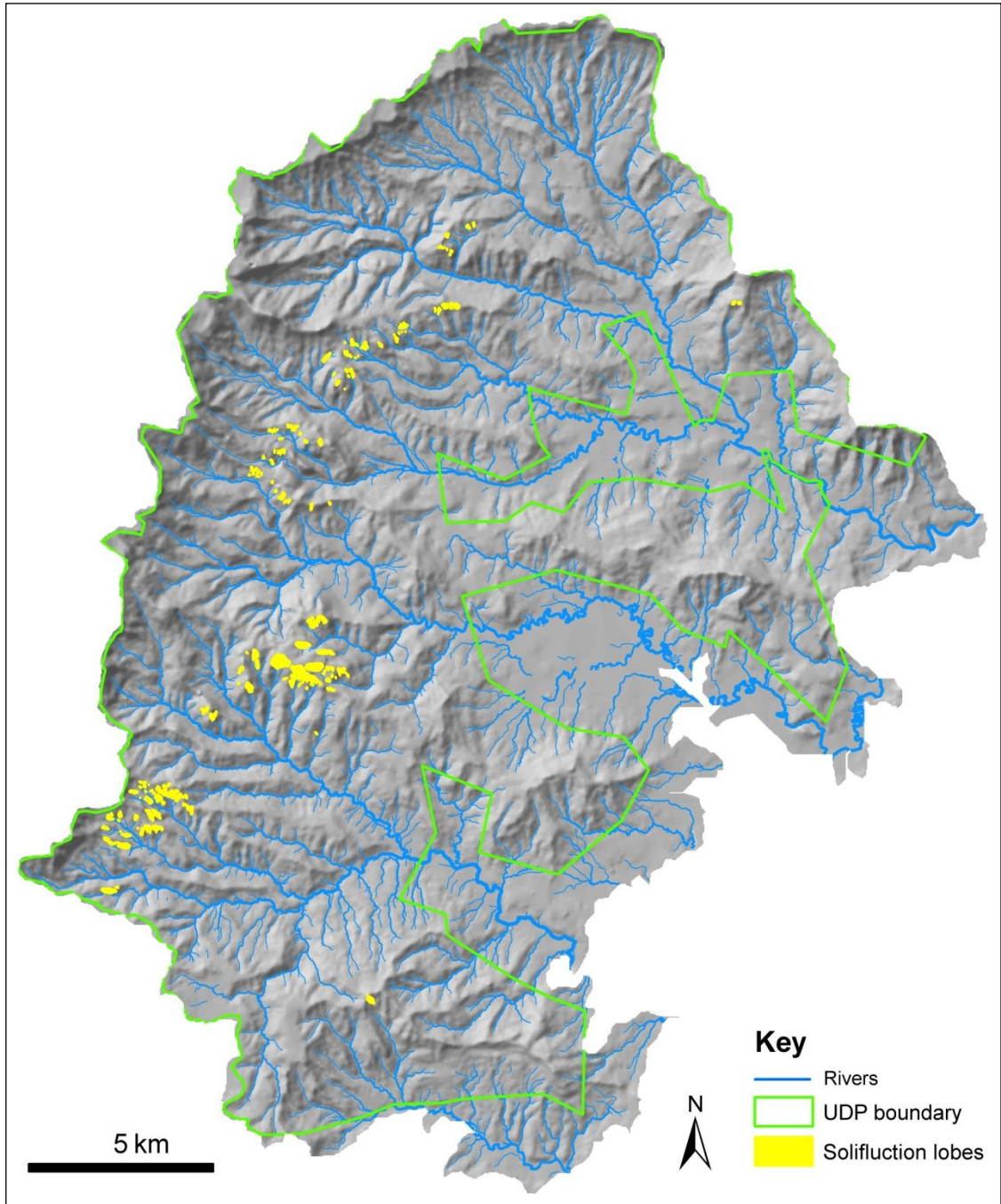


Figure 7.12 Distribution of solifluction lobes digitized from the 1: 50 000 orthophotos.

A frequency distribution of the occurrence of the solifluction lobes in relation to the eight variables and their associated class categories is presented in Figure 7.13. The results show that the highest overall frequency is for lithology, with over 80% of

solifluction lobe fields occurring in the Clarens Formation. The second highest frequency is for altitude, with >70% of lobes occurring in the 2 200–2 400m a.s.l category. Lewis (1987) suggests that an altitudinal boundary exists for stone- and turf-banked lobes and that the lower boundary is at 2 550m a.s.l, which is slightly above the range suggested by this category. The third highest frequency occurs for the distance to footpath variable, with >65% of solifluction lobes occurring more than 300m from a footpath. This variable therefore is unlikely to have a geomorphic influence on solifluction lobe development. South-facing slopes have the next highest-frequency (>50%), followed by gradient (20°–30°), distance to a drainage line (0–25m), distance to a rock exposure (0–25m) and then slope unit (CxCx, CCx).

A comparison of the hierarchy of the highest frequency per class for each variable with the InfoVal for each class shows that lithology and altitude remain the first two highest variables (Table 7.4). However, aspect, rather than distance to a footpath is the third highest variable using the InfoVal, due to the effect of area for each variable (almost 47% of the study area is >300m from a footpath, whilst only 16% is south-facing). The high frequency of solifluction lobes on south-, southeast- and southwest-facing slopes (95%) supports the finding by Boelhouwers (1988b) that south-facing slopes of >30° gradients will be cooler and wetter for longer periods of time, making them more susceptible to freeze-thaw activity. Boelhouwers and Meiklejohn (2002) note that the absence of soil moisture is the main limiting factor to more widespread frost-induced soil disturbance in the Drakensberg, especially in the winter months (Meiklejohn et al., 2009). Thus, topographic conditions which prolong the existence of soil moisture will support the development of solifluction lobes and may explain why their distribution is more limited than terracettes, which are less dependent on freeze-thaw processes for their development. Gradient has the fourth highest InfoVal after aspect, and the 30-40° class is selected as having a higher InfoVal than the 20-30° class, which has the highest frequency. Once again, this is due to area which is reflected in the area/frequency ratio (0.54 for the 30-40° class, 0.45 for the 20-30°

class). The variables with the next highest InfoVal in descending order are distance to a rock exposure, distance to a drainage line, slope unit and distance to a footpath.

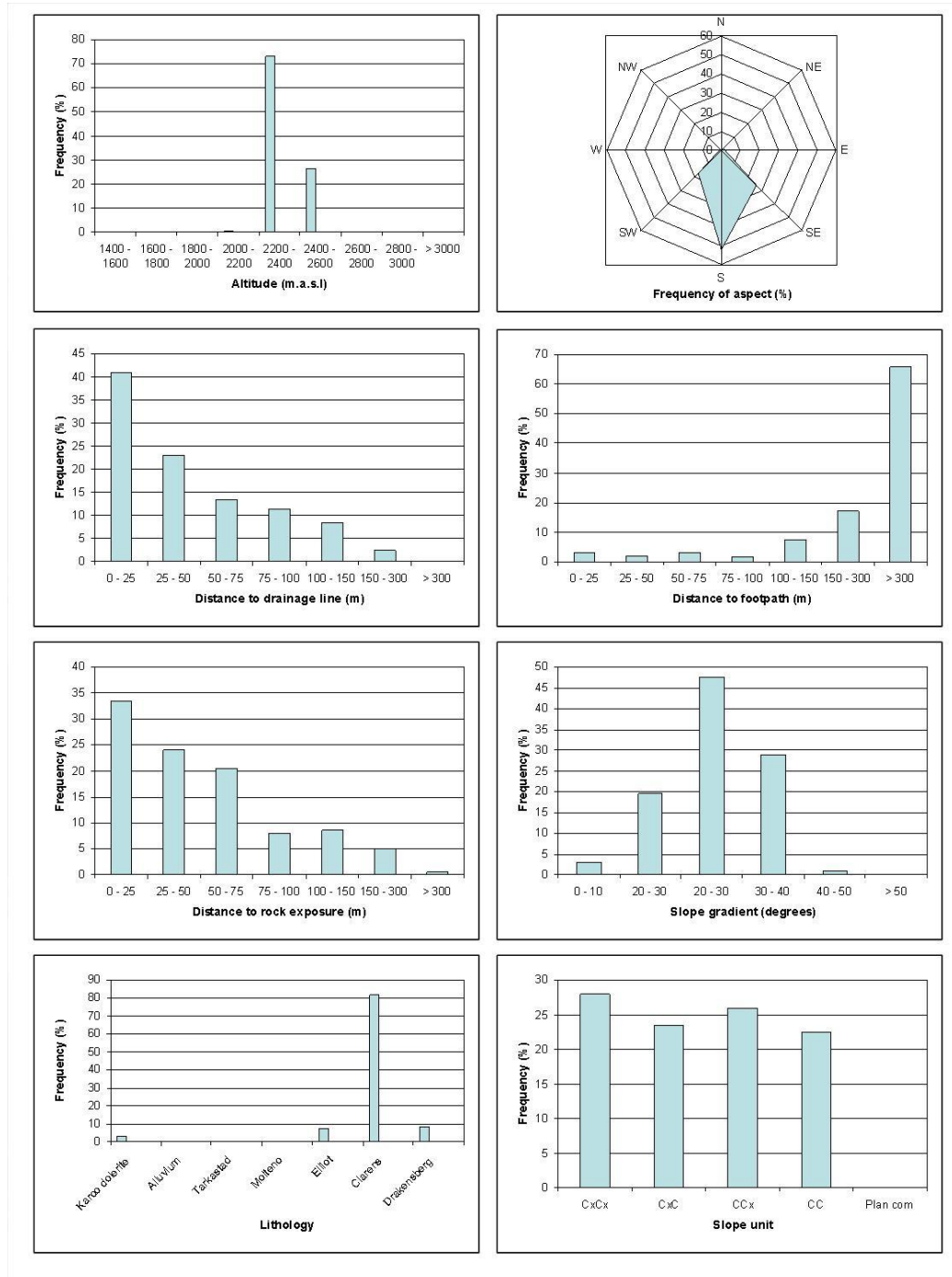


Figure 7.13 Histogram of the independent variables for solifluction lobes.

The results of the hierarchical partition are presented in Figure 7.14. Lithology has the highest %I (mean=47%, SD=3.47) followed by altitude (mean=24.5%, SD=3.57) and this compares well with the results of the frequency distribution and InfoVal. Gradient has the third highest %I contribution to the logit model, followed by the three distance variables, whilst slope unit has the smallest independent contribution (<1%). The solifluction lobes occur almost exclusively in Clarens Formation sandstones which have been found to weather into angular clastic deposits (Sumner et al., 2009). Sandy, feldspathic residual soils are associated with the disintegration of Clarens Formation sandstones, and an increase in moisture content causes a rapid decrease in the volume of the material which facilitates instability (Brink, 1982).

Solifluction lobes observed in the high Drakensberg have been classified as ‘inactive’ under present climatological conditions (Grab, 2000), however sheet slides which occur within the solifluction lobe fields show signs of activity over the last 50 years. These slides are similar in description to thin stone-banked lobes described by Matsuoka (2001) which occur in warmer environments that are characterized by diurnal freeze-thaw. Therefore, it is possible that the development of solifluction lobes is not dependent on the presence of permafrost (which would be related to altitude), but rather underlying lithology.

An analysis of the relationship between lithology, altitude, gradient and aspect was undertaken for the study area to determine to what degree these variables are linked. Contingency tables were created for each combination of variables and chi-square tests (χ^2) were used to determine whether the variables are independent of one another or contingent (Table 7.5). Further statistics were performed on the data (Pearson’s Phi [ϕ], Contingency Co-efficient [C] and Cramer’s V, [V]) to show the strength of the relationship if one should exist.

Variable	ClassDescrip	Area (%)	Frequency (%)	InfoVal	Ratio (F/A)
Altitude	1400-1600	0.77	0	\$	0.00
	1600 - 1800	26.05	0	\$	0.00
	1800 - 2000	25.94	0	\$	0.00
	2000 - 2200	19.51	1	-3.664	0.01
	2200 - 2400	15.33	73	1.561	1.03
	2400 - 2600	6.46	27	1.412	0.89
	2600 - 2800	2.48	0	\$	0.00
	2800 - 3000	2.41	0	\$	0.00
	> 3000	1.05	0	\$	0.00
Aspect	N (0 - 22.5)	7.08	0	\$	0.00
	NE (22.5 - 67.5)	17.32	2	-2.446	0.02
	E (67.5 - 112.5)	14.78	2	-2.000	0.03
	SE (112.5 - 157.5)	15.37	26	0.526	0.37
	S (157.5 - 202.5)	15.51	52	1.210	0.73
	SW (202.5 - 247.5)	11.83	17	0.362	0.31
	W (247.5 - 292.5)	6.92	1	-1.934	0.03
	NW (292.5 - 337.5)	6.32	1	-2.537	0.02
	N (337.5 - 360)	4.86	0	\$	0.00
DistDrain	0 - 25	32.64	41	0.228	0.27
	25 - 50	14.78	23	0.442	0.34
	50 - 75	14.06	14	-0.040	0.21
	75 - 100	9.65	12	0.176	0.26
	100 - 150	14.26	9	-0.518	0.13
	150 - 300	12.22	3	-1.587	0.04
		> 300	2.39	0	\$
DistFoot	0 - 25	14.27	3	-1.559	0.05
	25 - 50	6.06	2	-1.108	0.07
	50 - 75	5.92	3	-0.680	0.11
	75 - 100	4.39	2	-1.073	0.07
	100 - 150	7.96	8	-0.059	0.20
	150 - 300	14.58	17	0.154	0.25
		> 300	46.83	66	0.343
Dist RockX	0 - 25	31.24	34	0.070	0.23
	25 - 50	11.56	24	0.731	0.45
	50 - 75	10.04	21	0.714	0.44
	75 - 100	6.47	8	0.212	0.27
	100 - 150	9.80	9	-0.142	0.19
	150 - 300	13.51	5	-0.994	0.08
		> 300	17.39	1	-3.549
Gradient	0 - 10	31.95	3	-2.366	0.02
	10 - 20	28.45	20	-0.378	0.15
	20 - 30	25.04	48	0.640	0.41
	30 - 40	11.73	29	0.905	0.54
	40 - 50	2.56	1	-0.939	0.08
		> 50	0.27	0	\$
Lithology	Karoo dolerite	19.86	3	-1.890	0.03
	Alluvium	2.30	0	\$	0.00
	Tarkastad	18.72	0	\$	0.00
	Molteno	13.40	0	\$	0.00
	Elliot	22.37	7	-1.162	0.07
	Drakensberg	12.93	8	-0.480	0.13
	Clarens	10.42	82	2.063	1.71
SlopeUnit	CxCx	28.81	28	-0.028	0.21
	CxC	23.14	24	0.016	0.22
	CCx	17.53	26	0.394	0.32
	CC	30.50	23	-0.304	0.16
	PlanCom	0.03	0	\$	0.00

Table 7.4 Comparison of the frequency distributions and InfoVal weights. Bold indicates highest value in each category, colour indicates variable with greatest frequency.

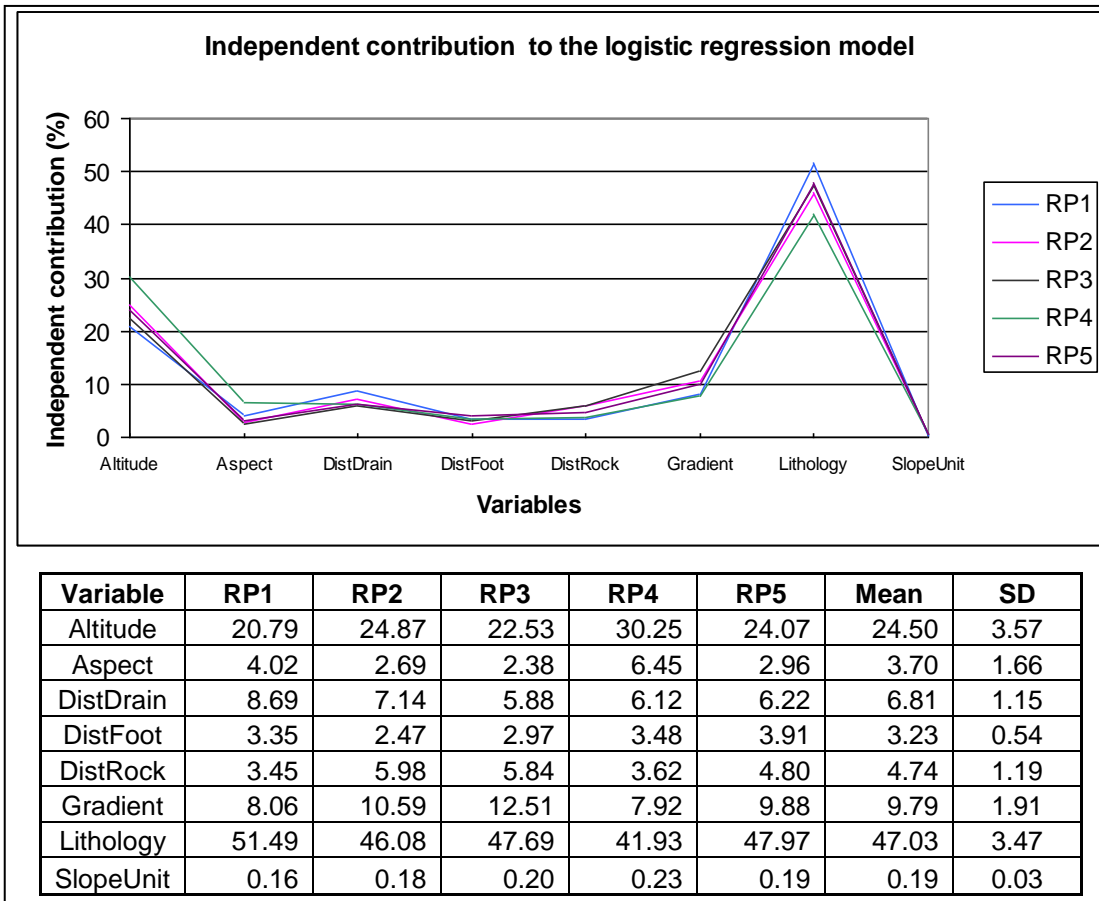


Figure 7.14 Graph representing the percentage contribution of each variable to the logit model. The table shows the mean and standard deviations for each contribution.

Variable combination	χ^2 (Observed)	χ^2 (Critical)	DF	p-value	ϕ	C	C(con)	V	Relationship
Aspect - Gradient	11.031	49.802	35	1.000	0.155	0.153	0.167	0.069	Independent
Aspect - Altitude	19.675	74.468	56	1.000	0.207	0.202	0.216	0.078	Independent
Aspect - Lithology	32.841	58.124	42	0.843	0.267	0.258	0.279	0.109	Independent
Lithology - Gradient	143.902	43.773	30	< 0.0001	0.559	0.488	0.534	0.250	Linked
Altitude - Gradient	222.860	55.758	40	< 0.0001	0.695	0.571	0.625	0.311	Linked
Lithology - Altitude	703.635	65.171	48	< 0.0001	1.236	0.777	0.840	0.504	Linked

Table 7.5 Summary of the contingency table statistics used to compare relationships between topographic variables. Tests are significant at the 95% confidence interval.

The strongest link exists between lithology and altitude, which is most likely due to the horizontally bedded layers which characterize sedimentary rocks of the Karoo Supergroup. Thus, each lithological group will occur at a specific altitudinal range (see Table 7.13). Altitude and gradient have the second strongest link, followed by lithology and gradient. The altitude–gradient linkage can be described by the lithology–gradient linkage as lithology will determine the gradient at which a slope is in equilibrium. Karoo dolerite, alluvium and the Tarkastad Formation occur most frequently in the 0-10° slope gradient range, whilst the Elliot and Clarens Formations and Drakensberg Group dominate in the 20-30° gradient range (Table 7.6). The Molteno Formation has equally high frequencies in the 10-20° and 20-30° slope gradient range. Of all the lithological groups, the Drakensberg Group has the highest frequency of area in the >40° slope gradient range. Although lithology has the highest %I contribution, altitude and gradient are expected to have some influence on solifluction lobe development. Aspect has no links to lithology, altitude or gradient, and is the only independent variable.

Initial attempts to predict solifluction lobe distribution with logistic regression were problematic as the models consistently failed to converge. Convergence errors occur because of complete or quasi-separation of the variables. Complete separation occurs when one predictor or a linear combination of predictor variables perfectly predict the dependent variable. Then a linear function rather than the logit function can predict the event, with the result that the logit model cannot converge to a maximum likelihood estimate and the model is infinite. Quasi-separation occurs when only a few values of the predictor yield the same response in the dependent variable. As the distribution of the solifluction lobes is very limited in terms of lithology, altitude and aspect, classes which contained no frequencies of Type=T2 were grouped into classes with at least 1 instance of Type=T2.

Pivot tables were created for all of the variables in each random dataset in order to create cross-tabulation tables with no zero frequencies. This helped the logit models

to converge but as the random (Type=T0) datasets differ with each iteration, the number of classes collapsed in each dataset also varies accordingly. This resulted in less similarity between models than for the terracettes. However, the overall percentage of correctly predicted events is much higher (92% for solifluction lobes versus 72% for terracettes). Aspect, distance to a rock exposure, gradient and lithology were chosen as significant variables for all five models according to the AIC, whilst aspect and lithology were chosen for all five models when using the BIC (Table 7.7). The minimum number of variables selected was for RP2 (AIC: 4 variables, BIC: 3 variables) and the highest percentage of events correctly predicted was for RP4 (AIC: 6 variables, BIC: 4 variables).

Gradient	0 - 10	10 - 20	20 - 30	30 - 40	40 - 50	> 50
Karoo dolerite	8.98	5.93	3.65	1.19	0.11	0.00
Alluvium	2.22	0.07	0.01	0.00	0.00	0.00
Tarkastad	10.96	5.43	2.10	0.22	0.00	0.00
Molteno	3.26	4.46	4.20	1.41	0.07	0.00
Elliot	4.17	6.47	7.59	3.63	0.47	0.03
Clarens	1.31	3.33	3.59	1.92	0.24	0.01
Drakensberg	1.05	2.75	3.88	3.35	1.66	0.23
Total	32	28	25	12	3	0

Table 7.6 Comparison of the percentage area of each lithological unit to ranges in gradient.

The relationships between distance to a rock exposure and altitude, lithology and gradient were also compared as distance to a rock exposure appeared consistently in all five logistic regression models (Table 7.8). Distance to a rock exposure is significantly linked to each of the topographic variables which would explain why this variable is selected by the logit model. This is also confirmed by the distribution of areas of each lithological type against distance to a rock exposure (Table 7.9). The Molteno, Elliot and Clarens Formations and Drakensberg Group have the largest percentage areas within 25m of a rock exposure, which contrasts with the Tarkastad Subgroup, Quaternary alluvium and dolerite in the study area, which all peak >300m from a rock exposure. This implies that the Molteno, Elliot and Clarens Formations and Drakensberg Group are lithologically more suited to developing prominent vertical bedrock scarps than the Tarkastad Subgroup, Quaternary alluvium and

dolerite. Overall, the results of the contingency tables highlights that a close link exists between altitude, lithology, gradient and distance to a rock exposure, and all of these variables are selected by the logit models.

Models	RP1	RP2	RP3	RP4	RP5
Full AIC	188	183	216	188	218
Best AIC	176	172	205	181	212
No Var	5	4	5	6	7
Variables	Altitude	-	Altitude	Altitude	Altitude
	Aspect	Aspect	Aspect	Aspect	Aspect
	-	-	-	DistDrain	DistDrain
	DistRock	DistRock	DistRock	DistRock	DistRock
	Gradient	Gradient	Gradient	Gradient	Gradient
	Lithology	Lithology	Lithology	Lithology	Lithology
	-	-	-	-	SlopeU
Best BIC	238	233	266	254	287
No Var	3	3	4	4	4
Variables	-	-	Altitude	Altitude	Altitude
	Aspect	Aspect	Aspect	Aspect	Aspect
	-	DistRock	DistRock	DistRock	DistRock
	Gradient	-	-	-	-
	Lithology	Lithology	Lithology	Lithology	Lithology
%CorrPred	92.5	92.25	90.75	93.25	92.5

Table 7.7 The AIC, BIC and variables selected for each iteration. Variations in predictive ability are caused by dissolving some of the classes.

Variable combination	X² (Observed)	X² (Critical)	DF	p-value	ø	C	C(con)	V	Relationship
Dist RockX - Gradient	162.812	43.773	30	< 0.0001	0.594	0.511	0.560	0.266	Linked
Dist RockX - Lithology	184.131	50.998	36	< 0.0001	0.632	0.534	0.577	0.258	Linked
Dist RockX - Altitude	198.849	65.171	48	< 0.0001	0.657	0.549	0.593	0.268	Linked

Table 7.8 Summary of the contingency table statistics used to compare relationships between topographic variables and distance to a rock exposure. Tests are significant at the 95% confidence interval.

Dist RockX	Karoo dolerite	Alluvium	Tarkastad	Molteno	Elliot	Clarens	Drakensberg
0-25	2.7	0.0	1.8	5.4	11.8	4.1	5.4
25-50	1.3	0.0	1.0	2.1	3.7	1.6	1.9
50-75	1.4	0.0	1.2	1.8	2.7	1.4	1.5
75-100	1.2	0.0	1.0	1.1	1.4	0.8	0.9
100-150	2.2	0.0	2.0	1.6	1.5	1.1	1.3
150-300	4.3	0.3	4.5	1.2	1.1	1.0	1.1
>300	6.7	2.0	7.3	0.1	0.2	0.4	0.8

Table 7.9 Cross-tabulation of the percentage area of each lithological class compared to the distance to a rock exposure (m). Highest percentage is in bold.

Probability maps were produced for each of the logistic regression models to determine whether there were spatial variations in the predictive ability of the models (Figure 7.15-7.17). Variations in the location of the high susceptibility cells are due to the beta coefficients which are calculated by the logit model. However, it is difficult to compare the beta coefficients as classes were grouped differently for each dataset. A comparison of the probability maps produced by the logit models and the ranges of probabilities (Table 7.10) also shows how dissolving classes affects the overall logit model. RP4, which predicts the highest percentage of Type=T2 correctly, also has the highest percentage of cells with a probability of 0.9–1.00. RP3 has the highest percentage of cells with a probability of 0.5–1.00, which is visible in the map as a greater presence of yellow-orange cells. This suggests that RP3 is not as efficient at predicting solifluction lobe occurrence as the other models as RP3 has the lowest percentage of correctly predicted events of Type=T2. Only 17.3% of the study area is classified as being >50% likely to develop solifluction lobes, which is almost half the size of the area that is likely to develop terracettes.

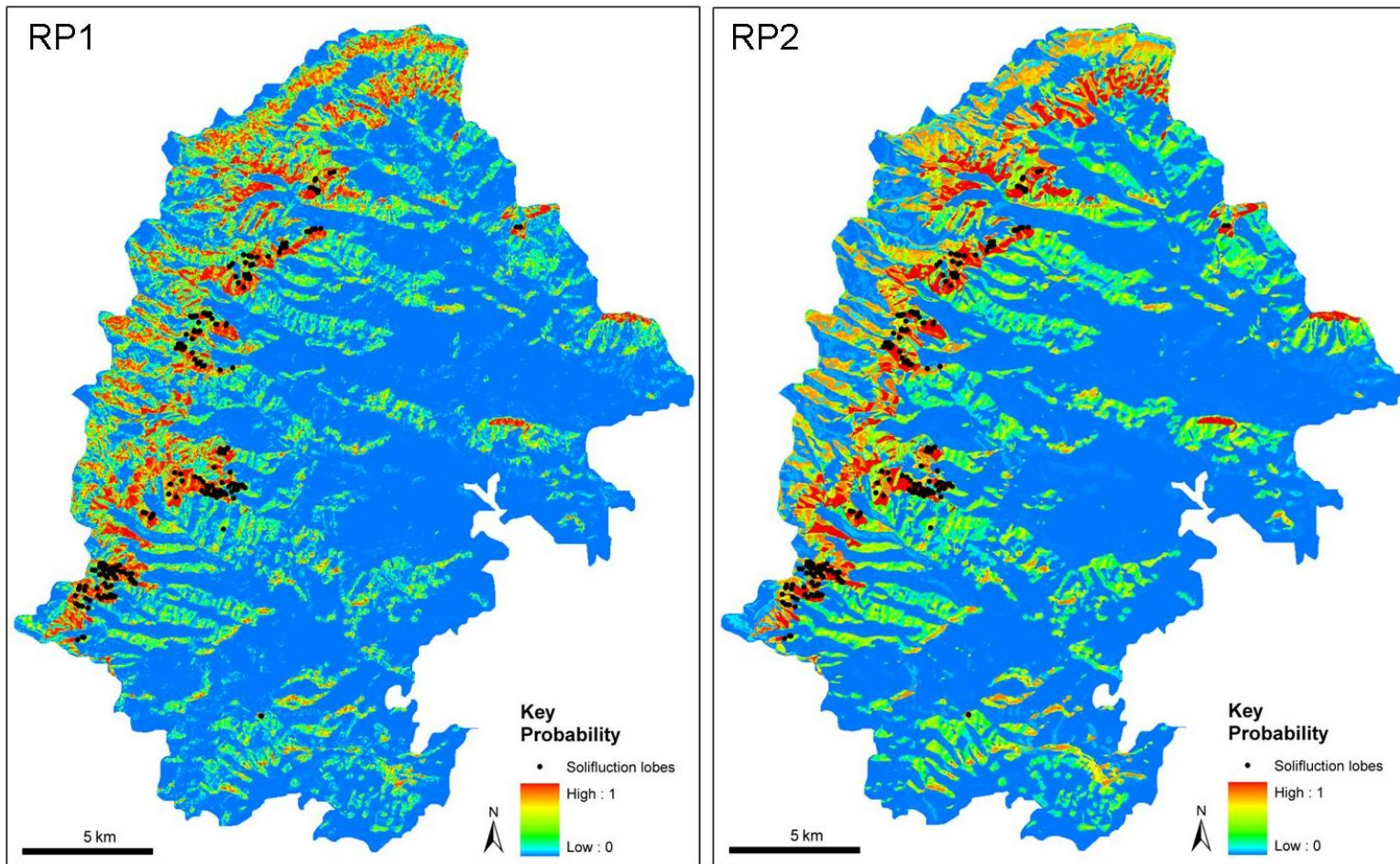


Figure 7.15: Probability maps for solifluction lobes using the RP1 and RP2 datasets.

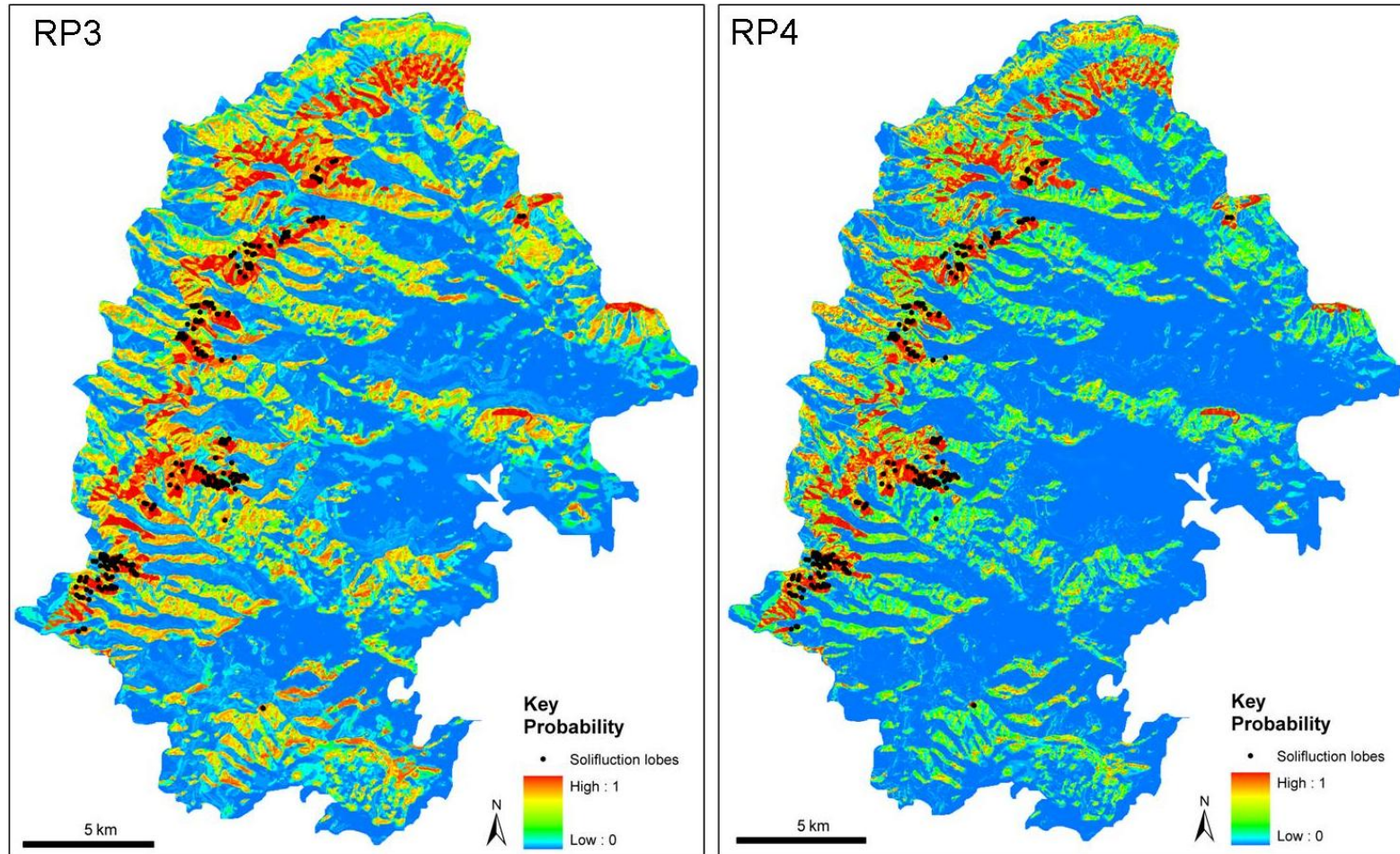


Figure 7.16: Probability maps for solifluction lobes using the RP3 and RP4 datasets.

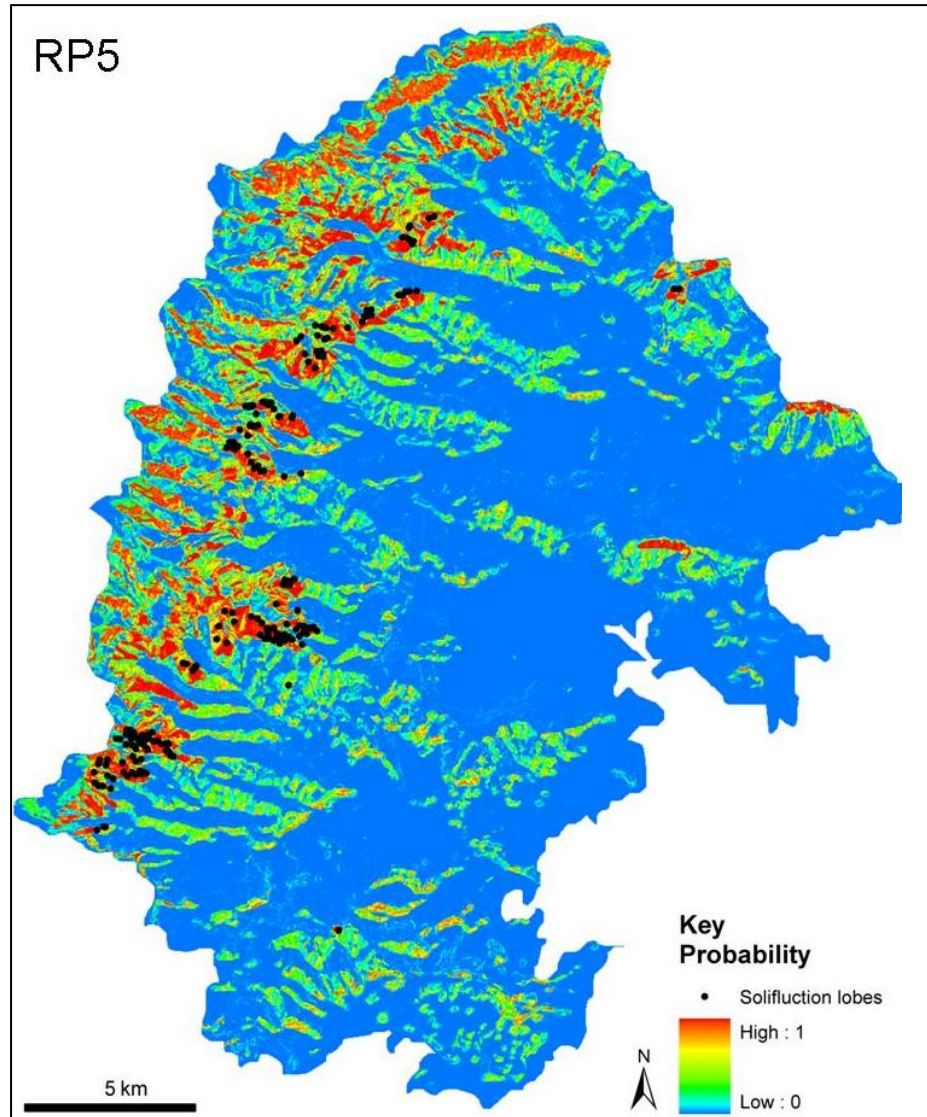


Figure 7.17: Probability maps for solifluction lobes using the RP5 dataset.

Classification trees were created for each of the random point iterations, however the trees showed little consensus in node selection. All of the trees select lithology (Clarens) as the first node, however RP1, RP2 and RP5 select aspect as the second node, whilst RP3 and RP4 select distance to a rock exposure as the second level node. The trees that selected distance to a rock exposure as the second level node created a split for distances of 0–25m, 75–100m and 150–300m and a second split for distances of 25–75m, 100–150m and >300m from a rock exposure. It is difficult to interpret these categories in terms of geomorphic influence as the splits do not represent

Probability	RP1			RP2			RP3			RP4			RP5			Mean	
	Area	%	SD	Area	%	SD	Area	%	SD	Area	%	SD	Area	%	SD	Area	%
0 - 0.5	389.7	84.6	1.3	386.5	83.9	0.8	337.6	73.3	6.7	393.2	85.3	1.9	398.3	86.4	2.6	381.1	82.7
0.5 - 0.6	14.2	3.1	0.2	19.3	4.2	1.0	11.6	2.5	0.2	10.8	2.3	0.3	9.1	2.0	0.6	13.0	2.8
0.6 - 0.7	12.0	2.6	0.1	4.9	1.1	0.9	21.7	4.7	1.6	7.8	1.7	0.5	8.7	1.9	0.4	11.0	2.4
0.7 - 0.8	10.2	2.2	0.9	14.1	3.1	0.3	38.5	8.4	3.5	8.5	1.9	1.1	8.7	1.9	1.1	16.0	3.5
0.8 - 0.9	9.4	2.0	0.7	14.5	3.1	0.1	24.4	5.3	1.6	10.2	2.2	0.6	10.6	2.3	0.5	13.8	3.0
0.9 - 1.00	25.4	5.5	0.1	21.5	4.7	0.7	27.0	5.9	0.2	30.2	6.5	0.7	25.4	5.5	0.1	25.9	5.6
>0.5		15.4			16.1			26.7			14.7			13.6			17.3

Table 7.10 Total area (km² and percent) of probability values for each iteration of random points for the solifluction lobe fields.

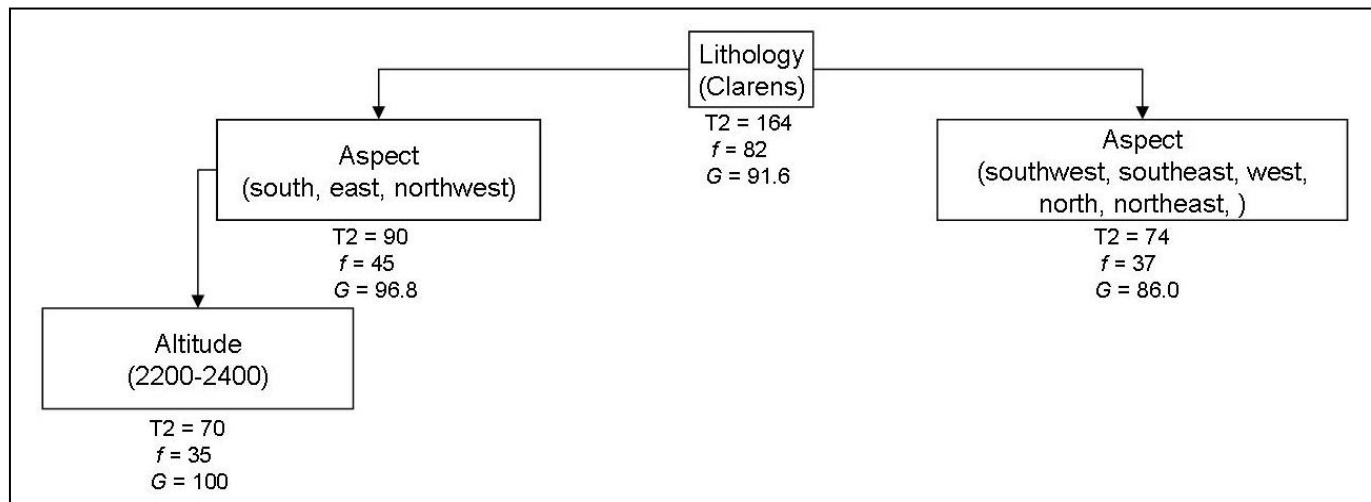


Figure 7.18: Summarized and pruned classification tree for solifluction lobe fields (*f*: frequency, *G*: Gini coefficient).

logical groups (i.e. nodes from 0–75m versus a node with all distances >75m). The remaining trees which selected aspect as the second level node, selected different variations of values as predicting the highest frequency of Type=T2 events (classes of aspect with the highest frequency for RP1:S, E, NW; RP2:S, W, NE; RP5:S, E, W). A comparison of the confusion matrix produced for each dataset suggests that RP1 produces the tree with the highest percentage of correctly predicted events (96.5%), whereas the other datasets predict between 94-95% correctly.

The tree presented in Figure 7.18 is a pruned tree of the RP1 dataset. The tree was pruned to three levels as nodes produced beyond this level, selected classes that were previously used as nodes (which implies over-fitting). The first level node (lithology: Clarens) predicts 82% of Type=2 and aspect provides a clear second level split with no overlap (45% and 37% of the data). Altitude is selected as the third level node and further subdivisions which use the Clarens Formation as the third node are based on combinations of individual classes from those which have previously been selected. The third level node accounts for 32% of Type=T2 (Gini: 100%) with only three variables.

An inspection of GoogleEarth Quickbird satellite imagery of the solifluction lobes suggests that a subdivision based on morphology may exist, as the solifluction lobes show some variation in form from lobate shaped to more elongate. However, as the lobes were digitized together from the orthophotos as ‘fields’, the sampling procedure used would not have yielded enough information to contrast lobes within a field and further research should be undertaken to confirm the existence of a sub-classification based on morphology using the techniques identified by Ridefelt et al.(2009).

7.4 Terrace-type 3: Terraces

Terraces are the third category of terrace-type mass movements which have been observed in the southern Drakensberg and have the appearance of groups of

irregularly shaped linear steps/treads (Figure 7.19 and 7.20). Although terraces occur in groups, the surface area of the group is generally smaller than the surface area of terracette and solifluction lobe fields. These landforms are relatively distinct in appearance due to contrasting shades of light and dark (Figure 7.21), and are more frequent along major footpaths which represent transport routes between Lesotho and the South African border post at Bushman's Nek, or in areas close to human habitation along the boundary of the UDP. This project has digitized 337 groups of terrace fields in the southern Drakensberg (Figures 7.22).

Terraces in the field have the appearance of long undulating steps with unvegetated vertical risers (up to 0.5 m in height) that are generally longer (5.75-1518.44m, average=67.53m) than they are wide (2.00-405.91m, average=33.03m). Field investigation did not offer more information on the possible initiating mechanism of terrace development and the vertical scarps of the terraces give these landforms the appearance of shallow translational slides. It is possible that these terraces are similar to the 'stepped microrelief' and 'crescentic terracettes' referred to by Killick (1963), Garland (1987) and Boelhouwers (1988). However, when the morphologies of terraces and known translational slides are compared in the orthophotos, obvious differences are observed. Firstly, translational slides mostly occur in isolation, whilst terraces are clearly discernible in groups. Secondly, terraces have a more defined colour contrast and appear as alternating dark and light stripes. Thirdly, translational slides in the southern Drakensberg tend to have a u-shaped scarp, whereas terraces have much longer, more undulating scarps. Photographs taken in the field do not show the terraces in great detail as the scarps are very shallow and long, and the base of the scarp is usually flat, but the striping effect and close proximity is notable (Figure 7.19).



Figure 7.19 View of a terrace on a northeast-facing slope along the Bushman's River.

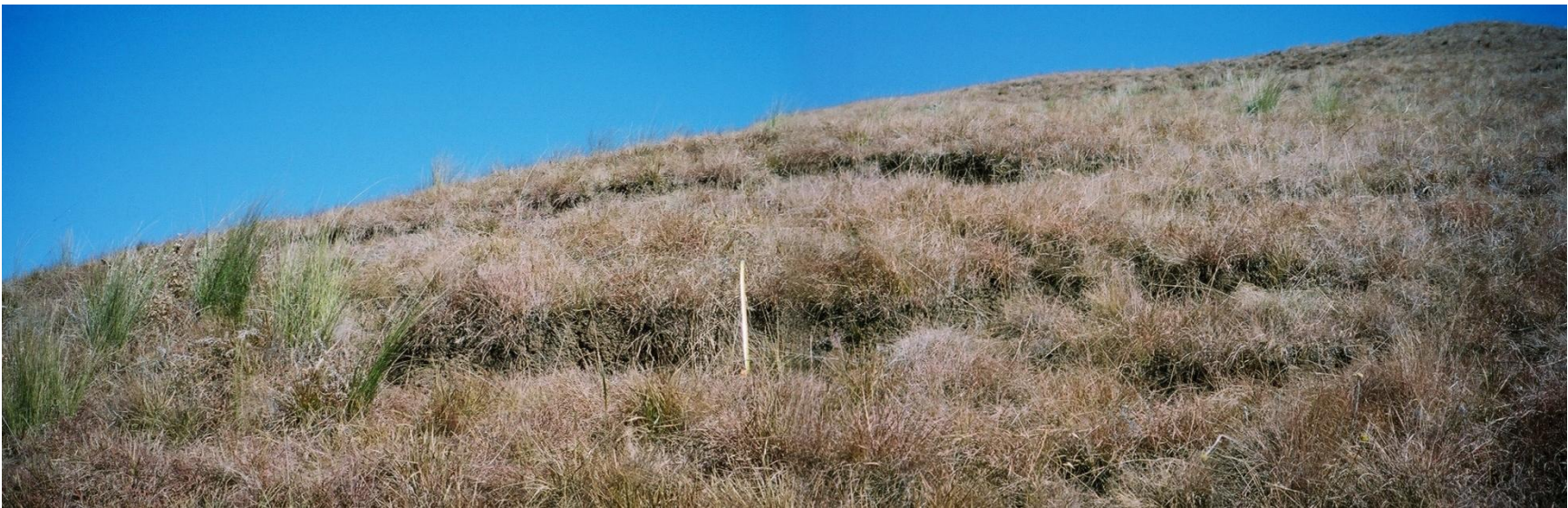


Figure 7.20 Group of terraces long the Bushman's River. Measuring tape (50 cm) shows the height of the step.

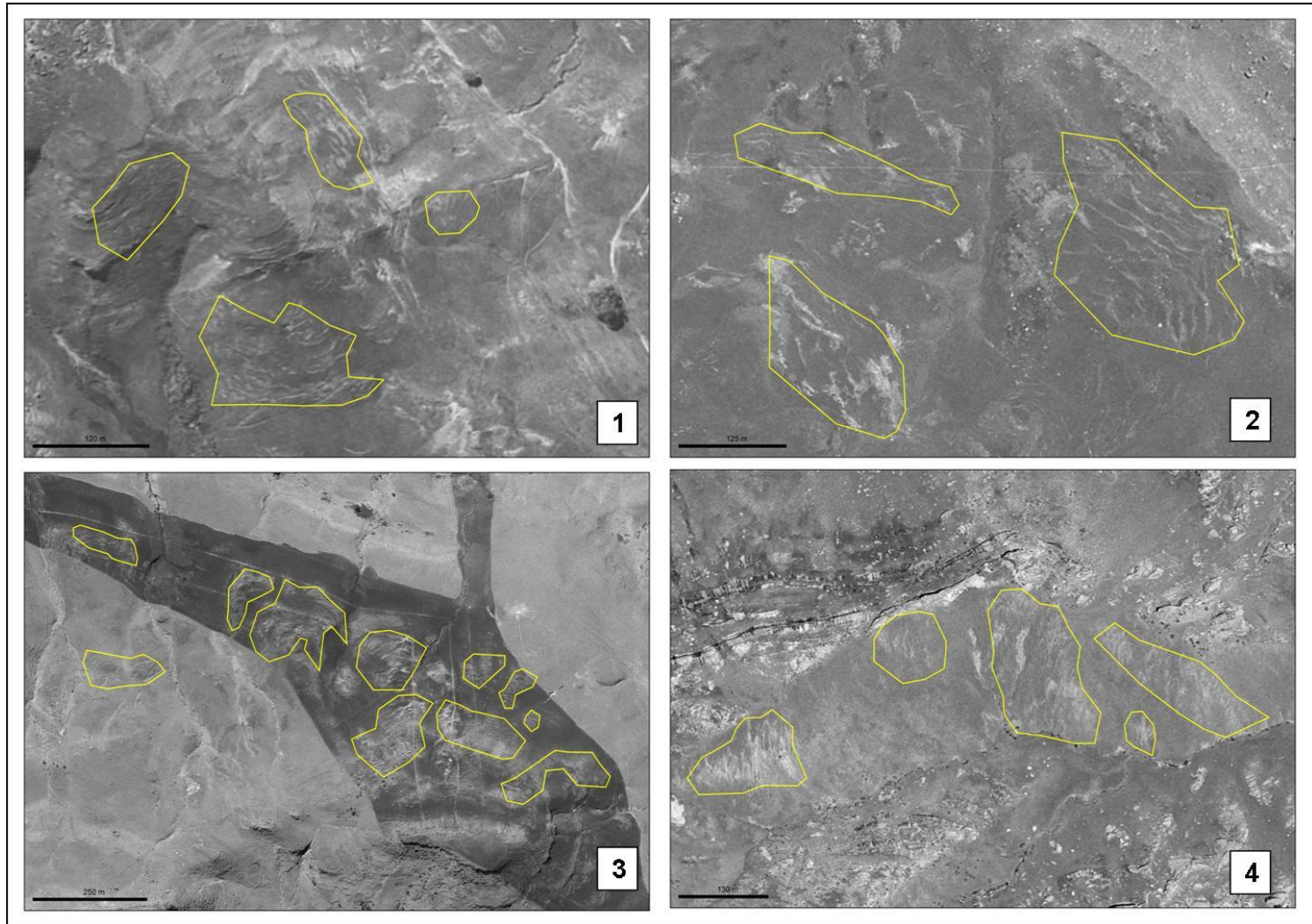


Figure 7.21 Aerial view of several fields of terraces that occur in the study area. Locations of photos 1-4 are provided in Figure 7.22.

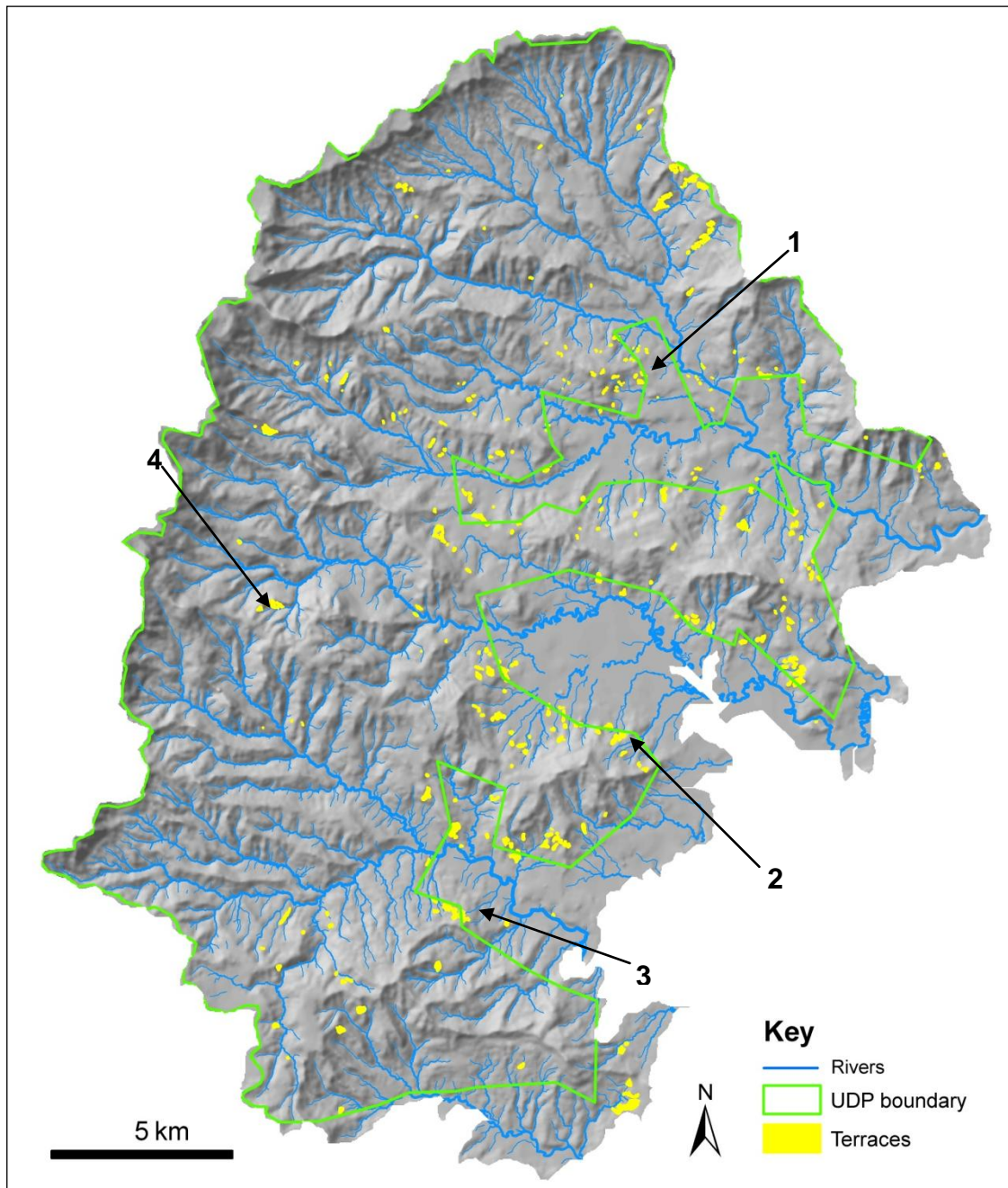


Figure 7.22 Distribution of terraces digitized from the 1: 50 000 orthophotos. 1-4 refers to images in Figure 7.21.

The occurrence of terraces in the Drakensberg has not been well documented, probably because terraces have been classified as terracettes in the literature (c.f Boelhouwers and Meiklejohn, 2002). Grab et al. (2005) studied the origin of ‘terrace

pediments' in the High Drakensberg (>3 000m a.s.l), however these terraces are geological in nature rather than geomorphological, as each terrace corresponds to an individual lava flow. Differential weathering across the lithologies has also enhanced the layered effect of the basalt flows. 'Turf-banked terraces' have been identified in the Eastern Cape Drakensberg between 2 765-2 880m a.s.l on west- and south-facing slopes with gradients between 15^o-28^o (Kück and Lewis, 2002).

A frequency distribution of the occurrence of terraces in relation to the eight variables and their associated class categories is presented in Figure 7.23. The results show that the highest overall frequency is for altitude, with 50% of terrace fields occurring between 1 800-2 000m a.s.l. The second highest frequency is for gradient, with almost 40% of terraces occurring on slopes with gradients between 10-20^o. Terraces occur at a lower altitudinal range and on flatter slopes than either terracettes or solifluction lobes. The third highest frequency is for slope unit, with 36% of terraces occurring on convex-convex slopes, or sloping inflated hills. The frequencies for the remaining variables in descending order are distance to a footpath (> 300m), lithology (Tarkastad Subgroup), distance to a drainage line (0-25 m), distance to a rock exposure (0-25 m) and aspect (northeast). It is noteworthy that terraces are the only terrace-type mass movement features to have a higher frequency of occurrence on north-facing rather than south-facing slopes. This suggests that it is unlikely that terrace formation is influenced by freeze-thaw activity to the same extent as terracettes and solifluction lobes.

Comparing the frequency distribution per class for each variable with the InfoVal for each class, shows that altitude remains the variable with the highest relative frequency (Table 7.11). The InfoVal in descending order of relative frequency is lithology (Molteno Formation), distance to a drainage line (50-75m), distance to a footpath (25-50m), distance to a rock exposure (100-150m), north-facing aspect, gradient (20-30^o) and slope unit (CxC). This is the only category of terrace-type mass movements which has selected the 25-50m class for the distance to footpath variable,

which may confirm that some of the terraces were incorrectly identified. Once again, the influence of area on frequency is apparent as an interpretation of the histograms would suggest that distance to a drainage line and rock exposure influence terrace distribution as the highest frequencies occur within 50m of each variable. However, the area weighted values suggest that distance to a drainage line and rock exposure have less influence, and that distance to a footpath is more important.

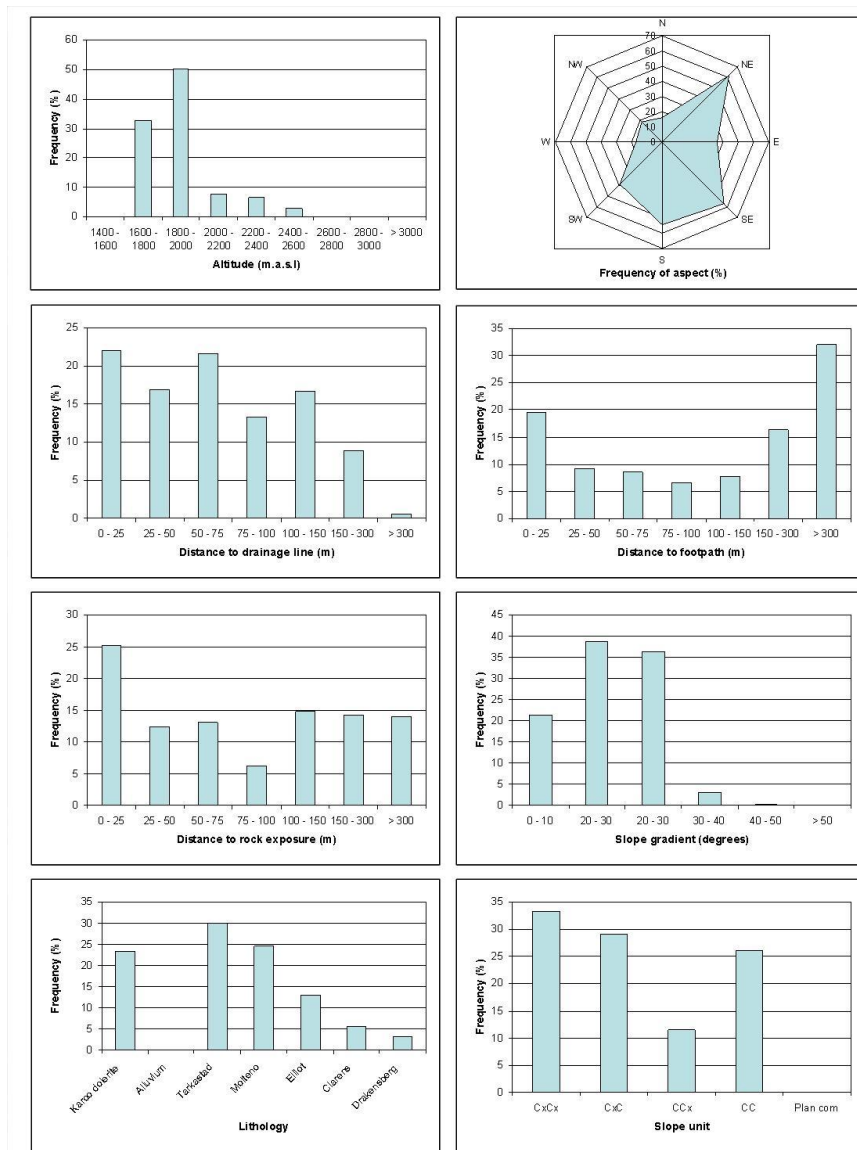


Figure 7.23 Histograms of the independent variables for terrace-type mass movement features.

Variable	Class	Area (%)	Frequency (%)	InfoVal	Ratio (F/A)
Altitude	1400 - 1600	0.77	0.0	\$	0.00
	1600 - 1800	26.05	32.6	0.225	1.25
	1800 - 2000	25.94	50.1	0.659	1.93
	2000 - 2200	19.51	7.7	-0.928	0.40
	2200 - 2400	15.33	6.5	-0.854	0.43
	2400 - 2600	6.46	3.0	-0.777	0.46
	2600 - 2800	2.48	0.0	\$	0.00
	2800 - 3000	2.41	0.0	\$	0.00
	> 3000	1.05	0.0	\$	0.00
Aspect	NE (22.5 - 67.5)	17.32	18.4	0.060	1.06
	E (67.5 - 112.5)	14.78	10.7	-0.325	0.72
	SE (112.5 - 157.5)	15.37	16.9	0.096	1.10
	S (157.5 - 202.5)	15.51	16.0	0.033	1.03
	SW (202.5 - 247.5)	11.83	11.6	-0.022	0.98
	W (247.5 - 292.5)	6.92	5.0	-0.316	0.73
	NW (292.5 - 337.5)	6.32	5.6	-0.114	0.89
	N (337.5 - 22.5)	11.94	15.7	0.275	1.32
DistDrain	0 - 25	32.64	22.0	-0.396	0.67
	25 - 50	14.78	16.9	0.135	1.14
	50 - 75	14.06	21.7	0.432	1.54
	75 - 100	9.65	13.4	0.325	1.38
	100 - 150	14.26	16.6	0.153	1.17
	150 - 300	12.22	8.9	-0.317	0.73
	> 300	2.39	0.6	-1.391	0.25
DistFoot	0 - 25	14.27	19.6	0.317	1.37
	25 - 50	6.06	9.2	0.418	1.52
	50 - 75	5.92	8.6	0.374	1.45
	75 - 100	4.39	6.5	0.397	1.49
	100 - 150	7.96	7.7	-0.031	0.97
	150 - 300	14.58	16.3	0.113	1.12
	> 300	46.83	32.0	-0.379	0.68
Dist RockX	0 - 25	31.24	25.2	-0.214	0.81
	25 - 50	11.56	12.5	0.075	1.08
	50 - 75	10.04	13.1	0.263	1.30
	75 - 100	6.47	6.2	-0.037	0.96
	100 - 150	9.8	14.8	0.415	1.51
	150 - 300	13.51	14.2	0.053	1.05
	> 300	17.4	13.9	-0.221	0.80
Gradient	0 - 10	31.95	21.4	-0.403	0.67
	10 - 20	28.45	38.9	0.312	1.37
	20 - 30	25.04	36.5	0.377	1.46
	30 - 40	11.73	3.0	-1.374	0.25
	40 - 50	2.56	0.3	-2.154	0.12
	> 50	0.27	0.0	\$	0.00
Lithology	Karoo dolerite	19.86	23.4	0.060	1.18
	Alluvium	2.3	0.0	\$	0.00
	Tarkastad	18.72	30.0	0.365	1.60
	Molteno	13.4	24.6	0.503	1.84
	Elliot	22.37	13.1	-0.644	0.58
	Clarens	12.93	5.6	-0.719	0.44
	Drakensberg	10.42	3.3	-1.481	0.31
SlopeUnit	CxCx	28.81	33.2	0.143	1.15
	CxC	23.14	29.1	0.229	1.26
	CCx	17.53	11.6	-0.415	0.66
	CC	30.5	26.1	-0.155	0.86
	PlanCom	0.03	0.0	\$	0.00

Table 7.11 Comparison of the frequency distributions and InfoVal weights. Bold indicates highest value in each category, colour indicates variable with the greatest frequency.

Gradient is similarly affected by area and the 20-30° class is selected as having the highest InfoVal rather than the 10-20° class. The InfoVal for slope unit selected the convex-concave class rather than the convex-convex class and the Molteno Formation, rather than Tarkastad Subgroup is selected. Of the three terrace-type mass movements, terraces show the most discrepancies between the frequency distributions and InfoVal. This is mostly because there is no individual class with a much greater frequency than the adjacent classes, such as is the case with the solifluction lobes, so the influence of area is greater.

The results of the hierarchical partition are presented in Figure 7.24. Altitude was consistently selected as the variable having the highest %I (mean=58%, SD=6.43) contribution, followed by lithology (mean=12%, SD=2.23) and distance to a footpath (mean=11%, SD=1.89). Terraces in the Eastern Cape Drakensberg have been observed to occur at slightly lower altitudes than terracettes in the same region (Kück and Lewis, 2002), and it is noteworthy that the class of altitude with the highest InfoVal is the 1 800-2 000m a.s.l. This is the lowest altitudinal range selected for any of the terrace-type mass movement features.

The results of the logistic regression confirm the findings of the hierarchical partitioning as altitude is consistently selected as a variable by both the AIC and BIC (Table 7.12). RP3 and RP4 have a similar percentage of correctly predicted events (Type=T3), although the models are based on different variables, with RP4 using two more variables than RP3. RP2 achieves a relatively high percentage of correctly classified events with the least number of variables and therefore the AIC and BIC values are the lowest of all the models. The logit models for the original datasets failed to converge, and thus individual classes within altitude, gradient and lithology were collapsed. Tests on the effect of collapsing classes showed that the predictions of the models increased by less than 2% on average. The average percentage of correctly predicted events is the lowest of the three terrace-type mass movements (72% for terracettes, 92% for solifluction lobes, 70% for terraces).

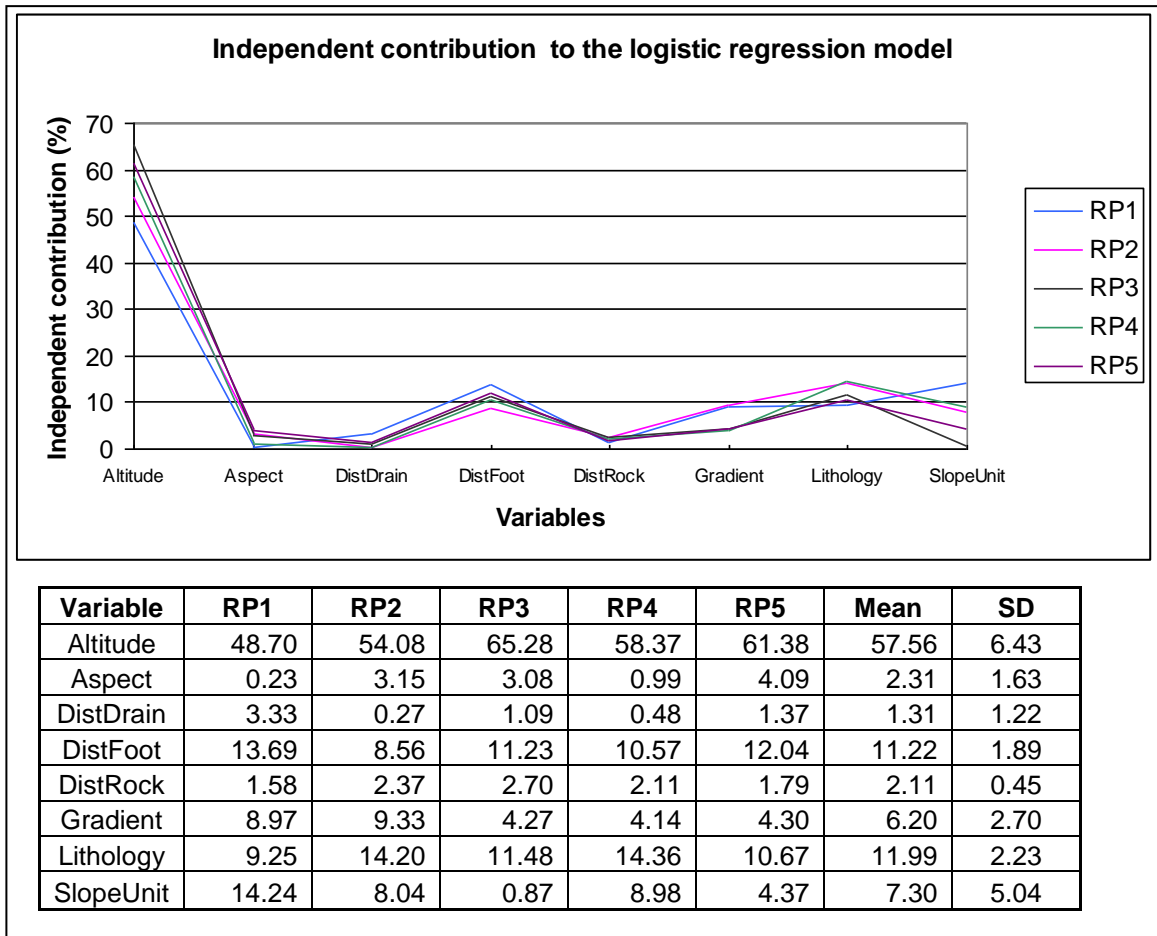


Figure 7.24 Graph representing the percentage contribution of each variable to the logit model. The table shows the mean and standard deviations for each contribution.

The results of the histograms, InfoVal, hierarchical partitioning and logistic regression suggest that the distribution of terraces is most strongly influenced by altitude. The influence of lithology, which appears to have some influence according to the hierarchical partitioning, is most likely due to the close relationship which exists between altitude and lithology and it is worth noting that lithology is not selected by any of the logit models. The highest InfoVal for altitude is for the 1 800-2 000m a.s.l class, whilst the highest InfoVal for lithology is the Molteno Formation. Table 7.13 shows that the highest percentage of Molteno formation occurs in this altitudinal range. Gradient has the second highest overall frequency of the variables

and is consistently selected by the logit models, yet gradient has a low %I contribution. Distance to a footpath has the third greatest %I, yet the variable has not been selected by any of the logit models nor does the variable appear to have much influence according to the frequency distribution or InfoVal (highest frequency is >300 m, whilst the highest InfoVal is for the 25-50m class).

Models	RP1	RP2	RP3	RP4	RP5
Full AIC	859	801	827	818	815
Best AIC	835	785	804	805	796
No Var	3	3	3	5	4
Variables	-	-	Aspect	Aspect	-
	Altitude	Altitude	Altitude	Altitude	Altitude
	-	-	-	DistDrain	DistDrain
	-	-	-	-	DistRockX
	Gradient	Gradient	Gradient	Gradient	Gradient
	SlopeUnit	SlopeUnit	-	SlopeUnit	-
Best BIC	878	822	840	856	847
No Var	2	2	2	2	2
Variables	Altitude	Altitude	Altitude	Altitude	Altitude
	Gradient	Gradient	Gradient	Gradient	Gradient
%CorrPred	68.1	71.7	70.9	70.4	72.1

Table 7.12 The AIC, BIC and variables selected for each iteration. Variations in predictive ability are caused by dissolving some of the classes.

	1400 - 1600	1600 - 1800	1800 - 2000	2000 - 2200	2200 - 2400	2400 - 2600	2600 - 2800	2800 - 3000	> 3000
Karoo dolerite	0.6	9.3	6.6	2.4	0.9	0.0	0.0	0.0	0.0
Alluvium	0.1	2.2	0.0	0.0	0.0	0.0	0.0	0.0	0.0
Tarkastad	0.1	13.3	5.2	0.2	0.0	0.0	0.0	0.0	0.0
Molteno	0.0	1.2	9.2	2.8	0.1	0.0	0.0	0.0	0.0
Elliot	0.0	0.0	5.0	11.2	5.7	0.5	0.0	0.0	0.0
Clarens	0.0	0.0	0.0	2.8	6.0	1.6	0.0	0.0	0.0
Drakensberg	0.0	0.0	0.0	0.1	2.6	4.4	2.5	2.4	1.0

Table 7.13 Cross-tabulation of the percentage area of each lithological class compared to altitude (m.a.s.l). Highest percentage is in bold.

A comparison of the probability maps produced by the logit models (Figure 7.25-7.27) and the ranges of probabilities (Table 7.14) shows that RP5 has the highest percentage of cells with a probability of 0.9-1.0, as well as having the highest percentage of correctly classified events (Type=T3). RP4 and RP5 are the only logit models that are able to identify cells with a probability of >0.9. RP2, which shows the largest separation of data, has the largest percentage of cells in the 0-0.5 probability and the highest percentage in the 0.8-0.9 probability range. Only 35% of the study area has a >50% probability of developing terraces, however this represents a greater proportion of area that is susceptible to either terracette or solifluction lobe development.

Classification trees for terrace-type mass movements were less able to discriminate between variables than the other terrace-types and the majority of the models (RP1, RP3 and RP4) selected three classes of lithology (Clarens, Molteno and Tarkastad) as the first node (number of events of Type=T3 is 203). However, only 5% of the terrace-type mass movements occur in the Clarens Formation, hence lithology was not used to create a pruned tree. Of the three trees which are separated on lithology, RP1 and RP4 use distance to a rock exposure as the second level split with one node at 0-50m, 150-300m and >300m and the second node from 25-150m. RP1 then separated on aspect, whilst RP4 separated using distance to a footpath. Distance to a footpath was selected as the first split by RP5 with the highest number of events (Type=T3: 203) in the 0-150m class. As none of the models selected the same level one node, it was not possible to create a combined tree, thus the results of the confusion matrix of Type=T3 and Type=T0 were compared. Model performance ranged from 89.17% (RP3) correctly predicted events, to 90.8% (RP2) respectively. The tree presented in Figure 7.28 is a summary of the tree created using the RP2 dataset.

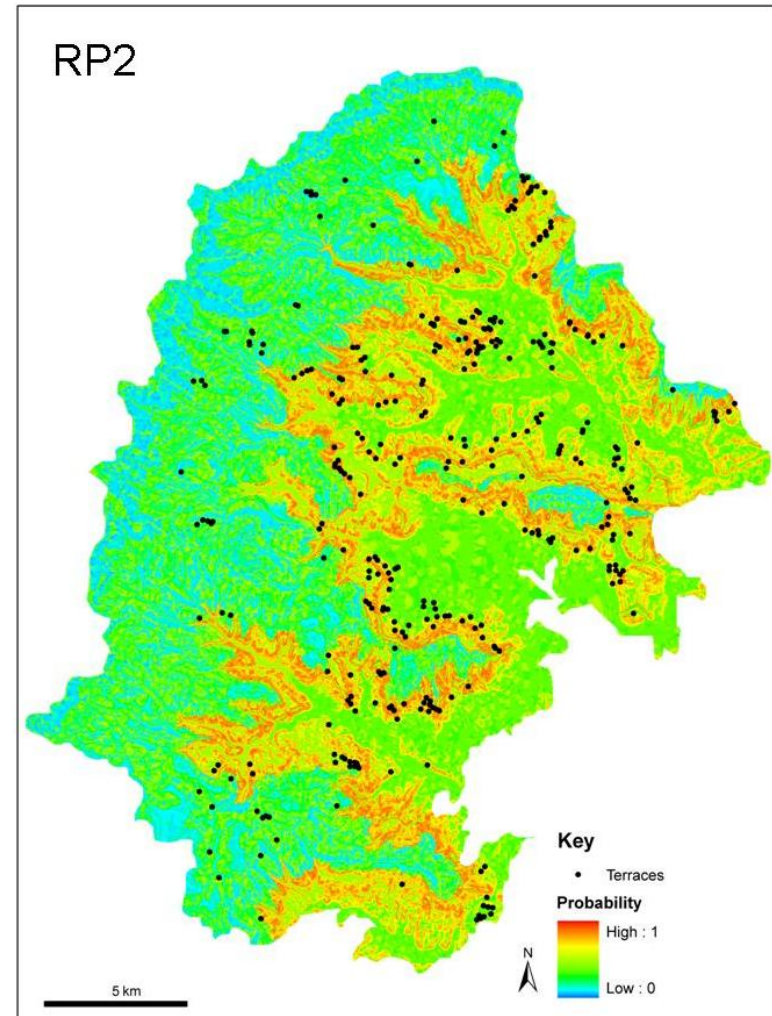
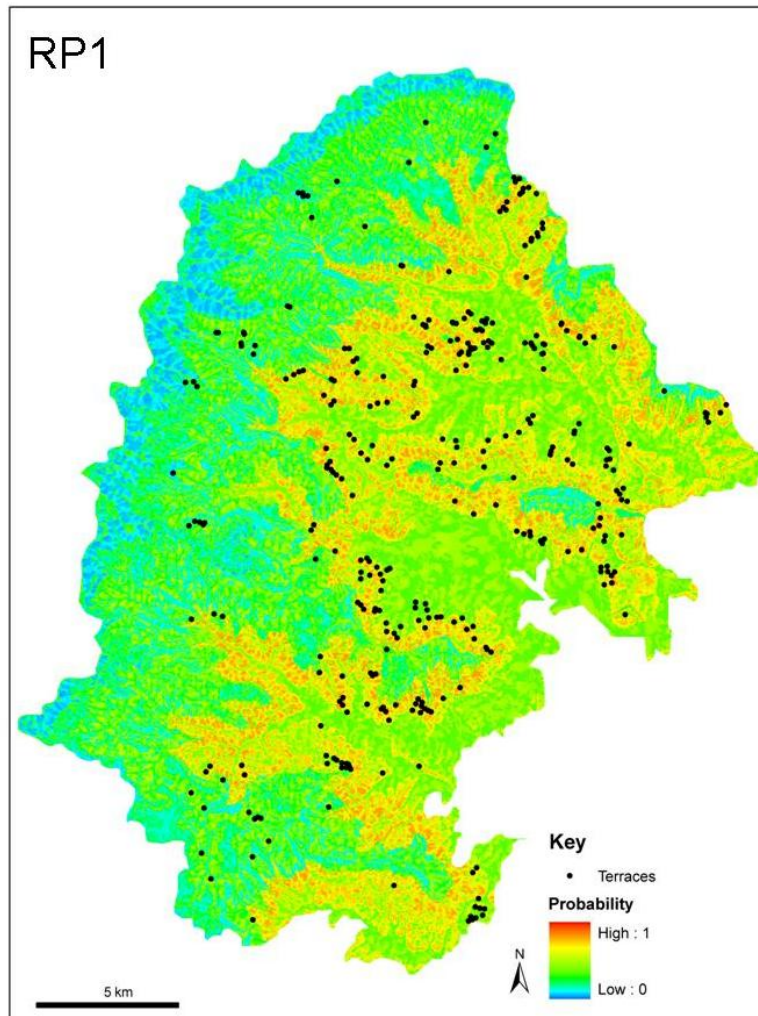


Figure 7.25 Probability maps for terraces using the RP1 and RP2 datasets.

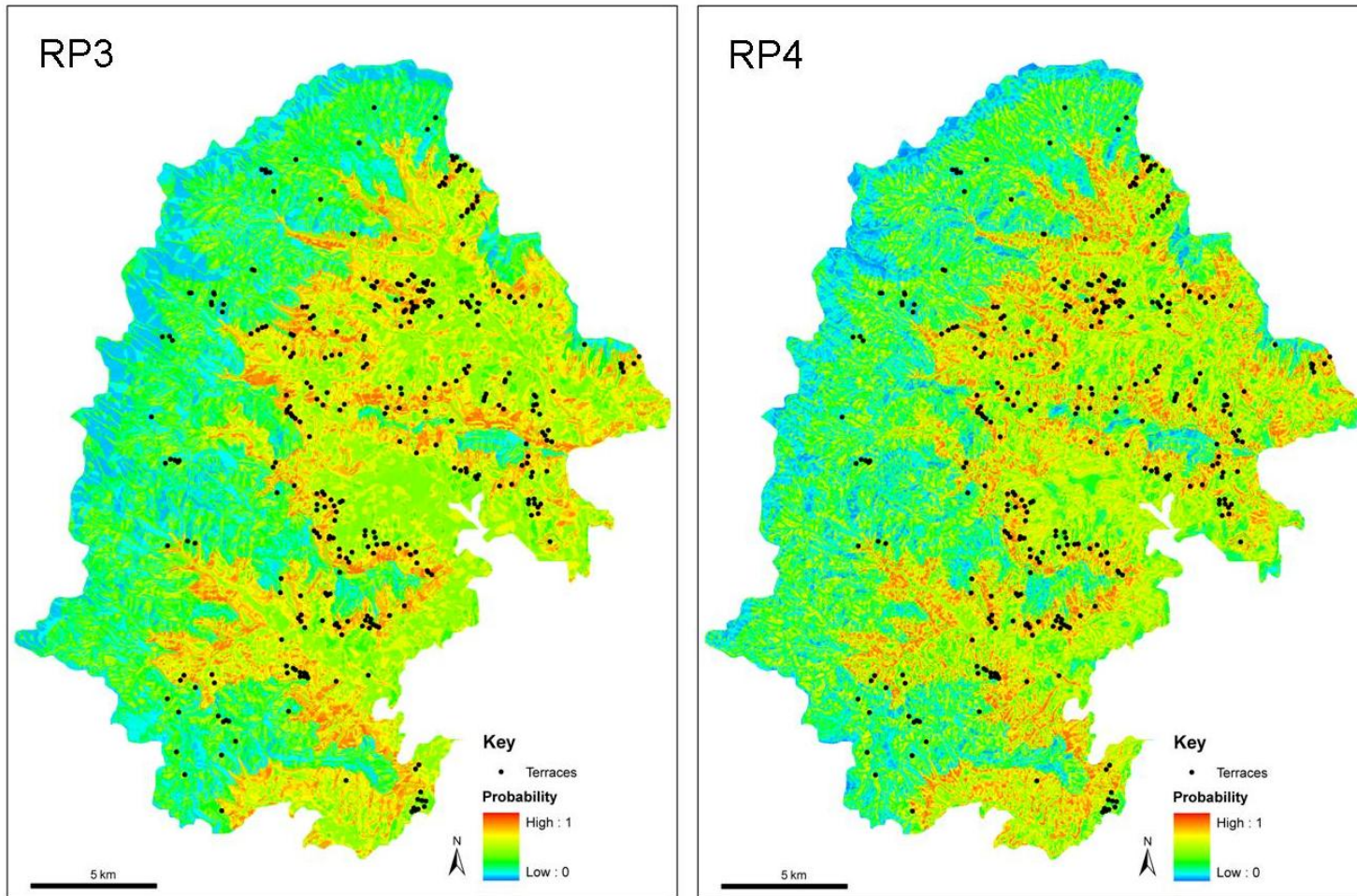


Figure 7.26 Probability maps for terraces using the RP3 and RP4 datasets.

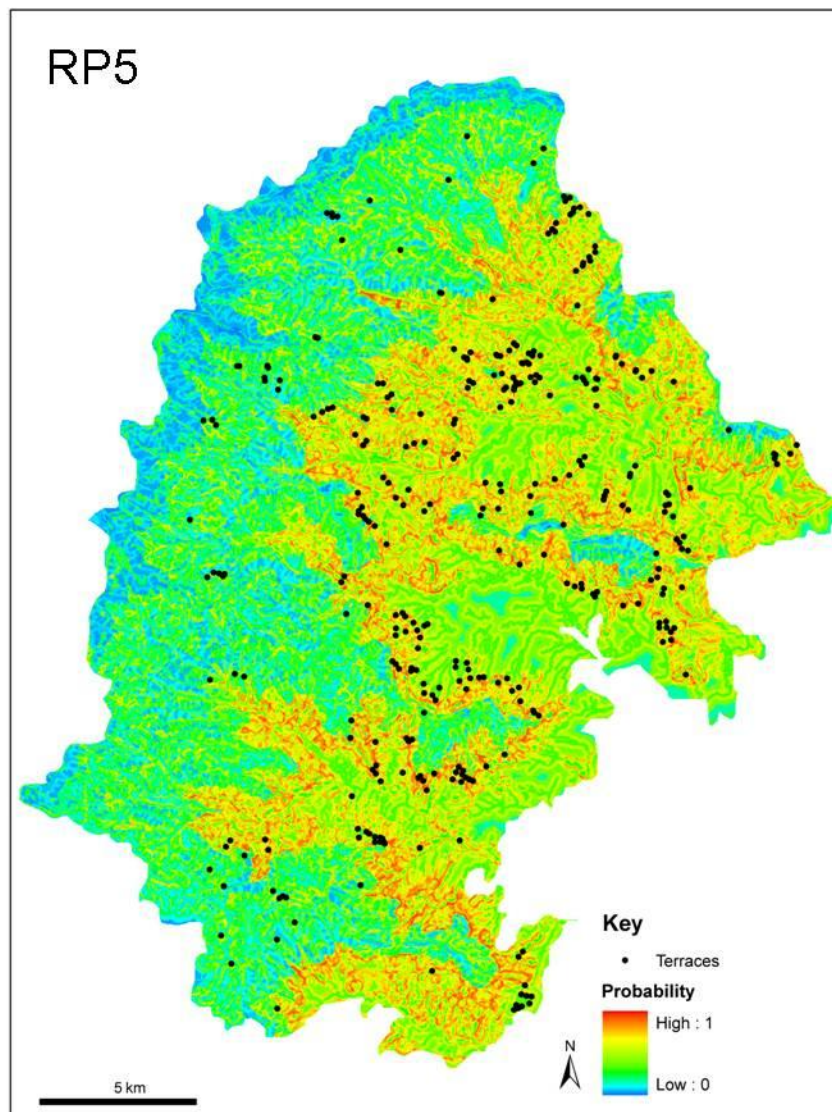


Figure 7.27 Probability maps for terraces using the RP5 dataset.

A comparison of the predicted frequencies and Gini coefficient's (G) of the terraces to the terracette and solifluction lobes shows that the terrace category is not as well defined as the other two terrace-type mass movements. The predicted frequency for terraces using aspect, identified almost 75% of Type=T1 (G : 70.7), whilst lithology predicted 82% (G : 90) of solifluction lobes. Using altitude, lithology or distance to a footpath as the first node predicts only 30% of Type=T3. This suggests that either not all of the Type=T3 are terraces or that terraces are not influenced by the variables used in the analysis to the degree that they can be clearly distinguished. As the logit

models appear to perform relatively well, it is not likely that poor discrimination is caused by the variables. It is more likely that some of the mass movement features that were classified as Type=T3 may be representative of terracettes rather than terraces due to the effects of distortion in some of the orthophotos. At the time of digitizing, terrace-type features were classified as Type=T3 if they could not be categorically identified as terracettes. It is also possible that footpaths which were in close proximity to one another were included in the classification as the footpaths had a similar appearance on the orthophotos as terraces. Footpaths are generally linear and semi-continuous and areas that have multiple footpaths have a similar appearance on the orthophotos to terraces. The only major difference between footpaths and terraces is that the terraces occur in 'fields' whilst the footpaths generally occur as single linear features.

The classification tree produced by the RP2 dataset suggests that a sub-classification based on aspect may exist for the terrace-type mass movements. The majority of correctly predicted events (Type=T3) occur in the 1 800-2 200m a.s.l altitudinal range, in the Tarkastad and Molteno Formations and no further sub-divisions were identified for the alternate lithology split (Karoo dolerite, Elliot and Clarens Formations). However, the aspect split separates the remaining Type=T3 events almost equally with 10% of terraces occurring on E-N-W-facing slopes and the remaining 8% occurring on predominantly south-facing slopes. A small percentage of terraces therefore may be influenced by aspect, but this would need to be established in the field.

	RP1			RP2			RP3			RP4			RP5			Mean	
	Area	%	SD	Area	%	SD	Area	%	SD	Area	%	SD	Area	%	SD	Area	%
0 - 0.5	124.6	67.0	21.2	315.7	68.5	8.2	303.9	66.0	6.3	281.3	61.0	2.9	287.5	62.4	3.8	299.4	65.0
0.5 - 0.6	111.8	12.4	8.2	24.3	5.3	5.2	31.4	6.8	4.1	61.5	13.3	0.5	62.2	13.5	0.6	47.3	10.3
0.6 - 0.7	94.7	10.6	5.8	34.7	7.5	3.4	69.6	15.1	2.0	47.9	10.4	1.4	36.7	8.0	3.1	47.5	10.3
0.7 - 0.8	94.3	8.0	6.6	42.6	9.2	1.3	31.6	6.9	3.0	41.0	8.9	1.5	45.2	9.8	0.9	39.5	8.6
0.8 - 0.9	35.4	2.1	0.8	43.4	9.4	2.0	24.3	5.3	0.9	25.3	5.5	0.8	23.3	5.1	1.1	25.2	5.5
0.9 - 1.00	0.0	0.0	0.3	0.0	0.0	0.3	0.0	0.0	0.3	3.7	0.8	0.3	5.8	1.3	0.6	1.9	0.4
>0.5		33.0			31.5			34.0			39.0			37.6			35.0

Table 7.14 Total area (km² and percent) of probability values for each iteration of random points for the terrace type mass movement features.

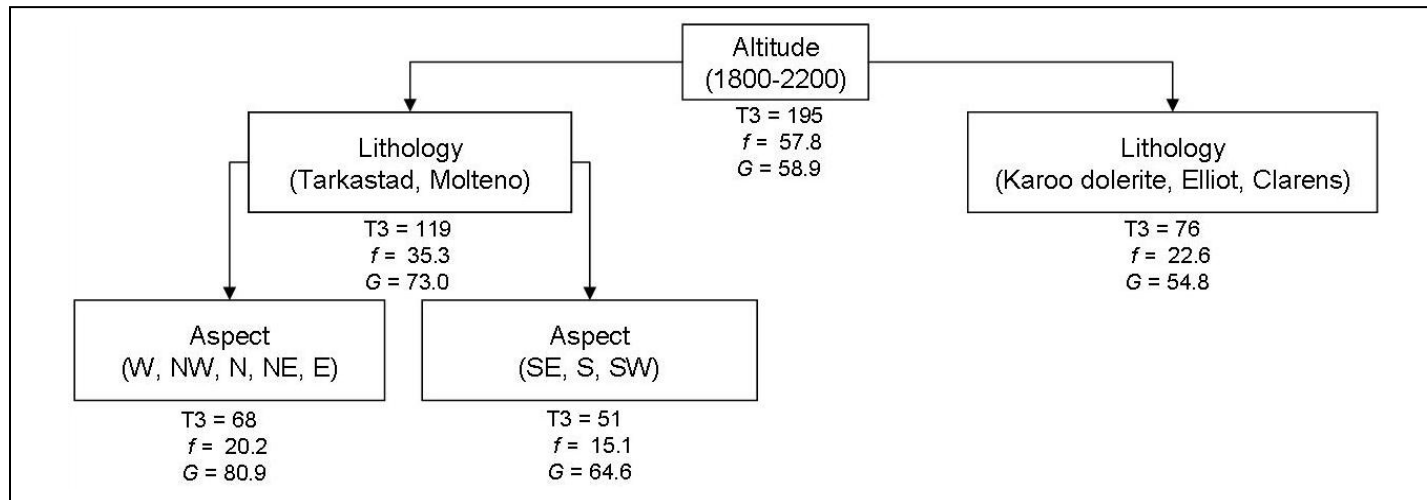


Figure 7.28 Summarized and pruned classification tree for terrace mass movement features (*f*: frequency, *G*: Gini coefficient).

7.5 Shear-type 1: Shear scars

Landslide hazard analyses are usually undertaken for all of the mass movement types which occur in a given area and few studies have examined the variation in variables between types. However, Greco et al. (2007) provide an example of a hazard analysis undertaken on a variety of mass movements in Calabria, Italy. It is therefore difficult to compare the range of variable values calculated for the three different slide types, particularly because most studies do not differentiate between incised and surficial flows. In some cases, poor representation of some types of mass movement has resulted in the flow types being excluded from the analysis (Santacana et al., 2003; Yesilnacar and Topal, 2005; van Den Eeckhaut et al., 2006). The following discussion is focused on slides in general but applies to both of the flow categories as well.

The shear scar category of mass movements contains all slide scars regardless of the degree of activity or rate of movement. Slide scars which did not have the diagnostic characteristics of any of the other four types were included in this category and it is expected that some scars are relict or stabilized scars of the incised and surficial flow mass movement types. This project has digitized 1 900 individual slide scars from aerial photos.

The term 'slide' is used for mass movements which occur along a recognizable shear plane (Goudie, 2004). Debris slides usually involve the movement of colluvium and the displaced mass tends to break into smaller parts as it advances downslope (Goudie, 2004). In the GCSEF, slide scars are elliptical to u-shaped concave depressions of varying sizes with surfaces that may be vegetated or exposed. Slide scar scarps form a distinct boundary line which can be identified on the orthophotos. Slide scars are relatively easy to identify as their morphological shape is not removed quickly (five decades of aerial photos show that a selection of scars remain visible from the 1950's to present); and even when the scar becomes revegetated, the scarp wall remains bare. Once the scarp has been smoothed by vegetation, a slight depression may still be observed from the

orthophotos (Figure 7.29). Figure 7.30 is a good example of high relief creating shadows which mask the presence of a mass movement feature.

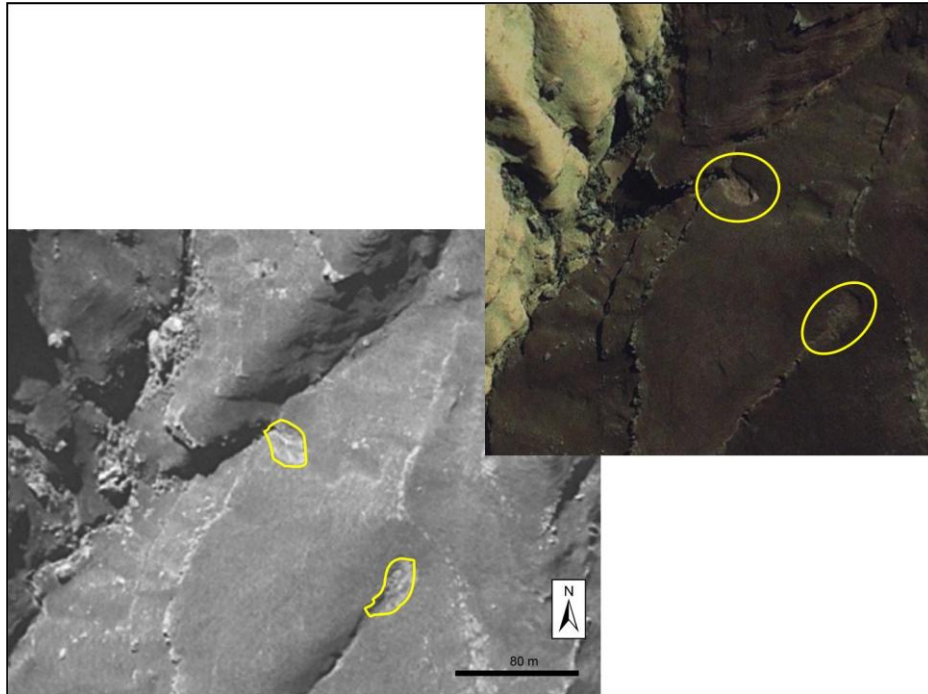


Figure 7.29 Photographs of slide scars on the orthophotos and in satellite images (Google Earth, 2008). Examples (in yellow) are similar to Site J.

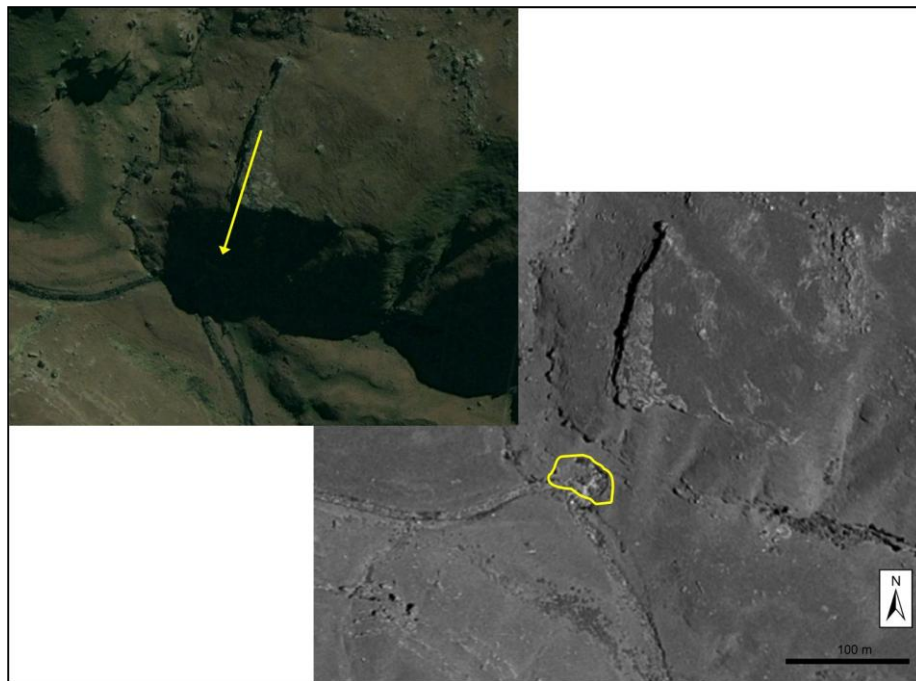


Figure 7.30 Orthophoto of a slide scar along the Bushman's river. The slide scar is obscured in the satellite image due to orographic shadow (Google Earth, 2008). The appearance of the slide scar in the orthophotos is similar to the slide scar at Site I.

Slide scar distribution in the UDP is relatively widespread (Figure 7.31) although clusters of slide scars occur on the surfaces of relict palaeo-landslides. The surface areas of the slide scars in the UDP range from 12m^2 to 15km^2 (average of 292m^2) (Table 7.29) with larger slide scars being associated with relict, possibly fossil rotational slides which were initiated under different climatic conditions (Singh, 2008). Surface areas of 31.6km^2 and 88.1km^2 have been recorded for palaeo-landslides studied in KwaZulu-Natal (Singh, 2008). The area of slide scars in the GCSF is variable due to the difficulties associated with separating the scar from the displaced mass, and similarly wide ranges of scar areas have been measured in Nepal (150m^2 - 2km^2) (Saha et al., 2005), Italy (100m^2 - $4\times 10^6\text{m}^2$) (Catani et al., 2005) and Austria (2.5km^2 - 15km^2) (Ruff and Czurda, 2008). All of the large rotational slides show evidence of more recent slide activity in the form of smaller translational slides. The mean Circularity Ratio of slide scars is 0.69, which is tending towards circular (CR=1), with the highest frequency of slides occurring in the CR range of 0.6-0.8 (Table 7.30).

Slides are most commonly caused by events which increase the moisture content of the slope material, or with events that cause shear stress, such as earthquakes (Goudie, 2004). It is most likely that the slides which have been digitized in the GCSF are triggered by intense precipitation rather than by seismic activity (Garland, 1978; Paige-Green, 1989; van Schalkwyk and Thomas, 1991; Singh, 2008), however seismic activity may have been responsible for palaeo-landsliding during the Quaternary (Singh, 2008). Likewise, Bijker (2001) found that over 80% of slides in the Injisuthi Valley were on inherently unstable slopes and did not require further rainfall to increase instability, whilst 8% of slides required up to 143mm/day to become unstable. The presence of palaeo-landslides had a greater role to play on the instability of slopes than rainfall duration or intensity, whilst palaeo-slide distribution has been related to the presence of dolerite dykes in the Drakensberg (Bijker, 2001; Singh, 2008).

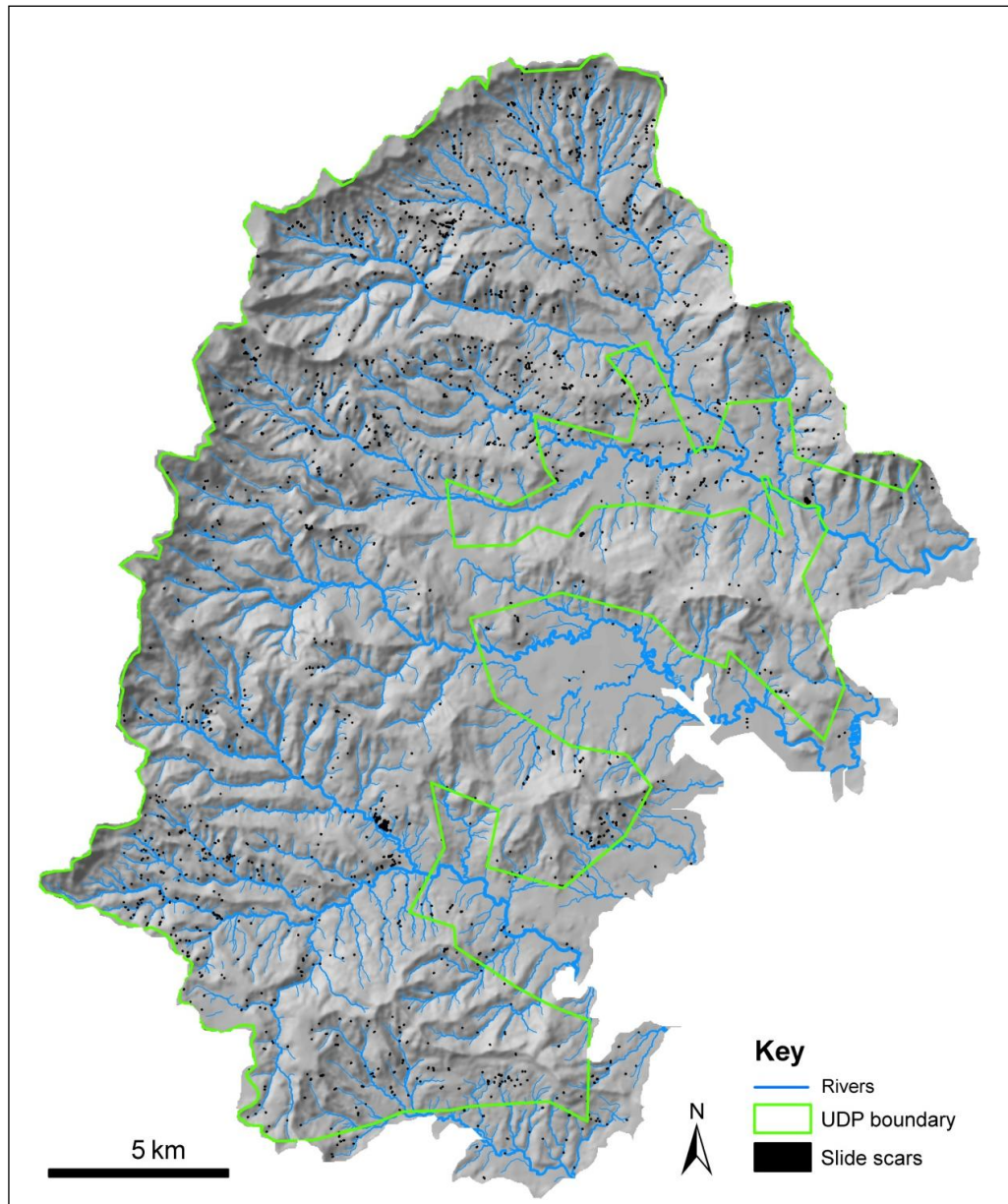


Figure 7.31 Distribution of slide scars digitized from the 1: 50 000 orthophotos.

Slope gradient has a strong influence on slide and flow development and is argued to be the most important factor for modeling landslide occurrence (Brardinoni et al., 2003; Ohlmacher and Davis, 2003; Komac, 2006). Slope gradients between 25°-30° in Hong Kong (Zhou et al., 2003), 30°-40 in British Columbia (Brardinoni et al., 2003), 20°-29° in Brazil (Fernandes et al., 2004), 30°-40° in Japan (Wang et al., 2007); 21°-40° in Austria (Ruff and Czurda, 2008) and from 28° in Lebanon (Abdallah et al., 2005) have been associated with increased mass movement activity. In Italy, slide frequency increased to a critical limit between 36°-40°, then

diminished on slopes $>45^\circ$, which is due to the smaller proportion of study area with steep gradients and reduced soil cover on steep slopes (D'Amato Avanzi et al., 2004). In Portugal, slope gradient influences the type of slide, as shallow translational slides occur on slope gradients between 22° - 26° , whereas deeper translational slides occur on slope gradients which range from 11° - 22° (Zêzere et al., 1999).

Aspect is also commonly used to compare mass movement frequency, although the causal role that aspect plays in slide development is not always clear, which has led to this variable being excluded in some slide risk assessments (Ohlmacher and Davis, 2003, Wang et al., 2008). Increased slide activity has been noted on south-facing slopes in Austria and British Columbia; these are dominated by extensive colluvium and till which are more exposed to wind (Brardinoni et al., 2003; Ruff and Czurda, 2008). The aspect argument is problematic as both drier slopes (which receive more insolation) and wetter, cooler slopes are cited as having increased slide activity (Moreiras, 2004; Abdallah et al., 2005). The interpretation of the role that aspect plays on soil conditions and slide activity is therefore probably very site specific.

Lithological type is almost always used in landslide risk assessments in conjunction with distance to geological features. Sandstones have been associated with increased slide activity in Japan (Ayalew et al., 2004) and in KwaZulu-Natal (Singh, 2008), however, whilst sandstones were associated with the highest frequency of landslides in the Du Toit's Kloof, the frequency/ratios indicated that slides were more likely to develop in weathered granite (Gupta, 2001). This highlights the importance of normalizing frequency distributions by area.

A frequency distribution of the occurrence of slide scars in relation to the eight variables and their associated class categories is presented in Figure 7.32. The results suggest that the majority of slide scars occur within 25m of a drainage line (54%) and within 25m of a rock exposure (40%). Almost half of the slide scars occur >300 m from a footpath, so this variable is excluded from further discussion.

A large number of the shear scars occur within close proximity to a rock exposure, usually above the rock face, and it is likely that the bedrock layer acts as an impermeable surface which leads to saturated soil conditions and reduced shear strength of the colluvial material (Site J). Geological boundaries and contacts have been associated with an abundance of springs and increased soil moisture which may increase slide activity (Sumner, 1993; Komac, 2006; Singh, 2008).

Shear scars associated with drainage lines usually occur because stream incision undercuts the stream banks, which causes a collapse of the slope (Site I). The distance to drainage variable also has the second highest InfoVal (both for the 0-25m category) after lithology. Proximity to a drainage line has been associated with increased mass movement activity in Lebanon, where over 30% of mass movements occur within 50m of a drainage line (Abdallah et al., 2005), and in Slovenia where drainage lines are associated with the presence of groundwater and stream bank erosion (Komac, 2006).

The slope unit variable accounts for the fourth greatest frequency (40%) of shear scars after the three distance variables, followed by gradient (36%), altitude (27%), lithology (26%) and aspect (25%). Concave-concave slopes or 'sloping-closed basins' are described as topographic hollows which concentrate surface flow and have generally moister soil conditions (Ayalew and Yamagishi, 2004). In Ethiopia, 'sloping-closed basins' are associated with retrogressive upslope-propagating landslides that develop into multiple slides which are limited in extent by the slope gradient and the underlying geology (Ayalew and Yamagishi, 2004). Site A in the study area is a good example of a multi-tiered shear scar (Figure 6.3). Concave slope units have been associated with increased slide activity in Slovenia as these slope units are areas of increased pore water (Komac, 2006). Ohlmacher (2007) notes that increasing plan curvatures should be associated with an increasing susceptibility to slope failure.

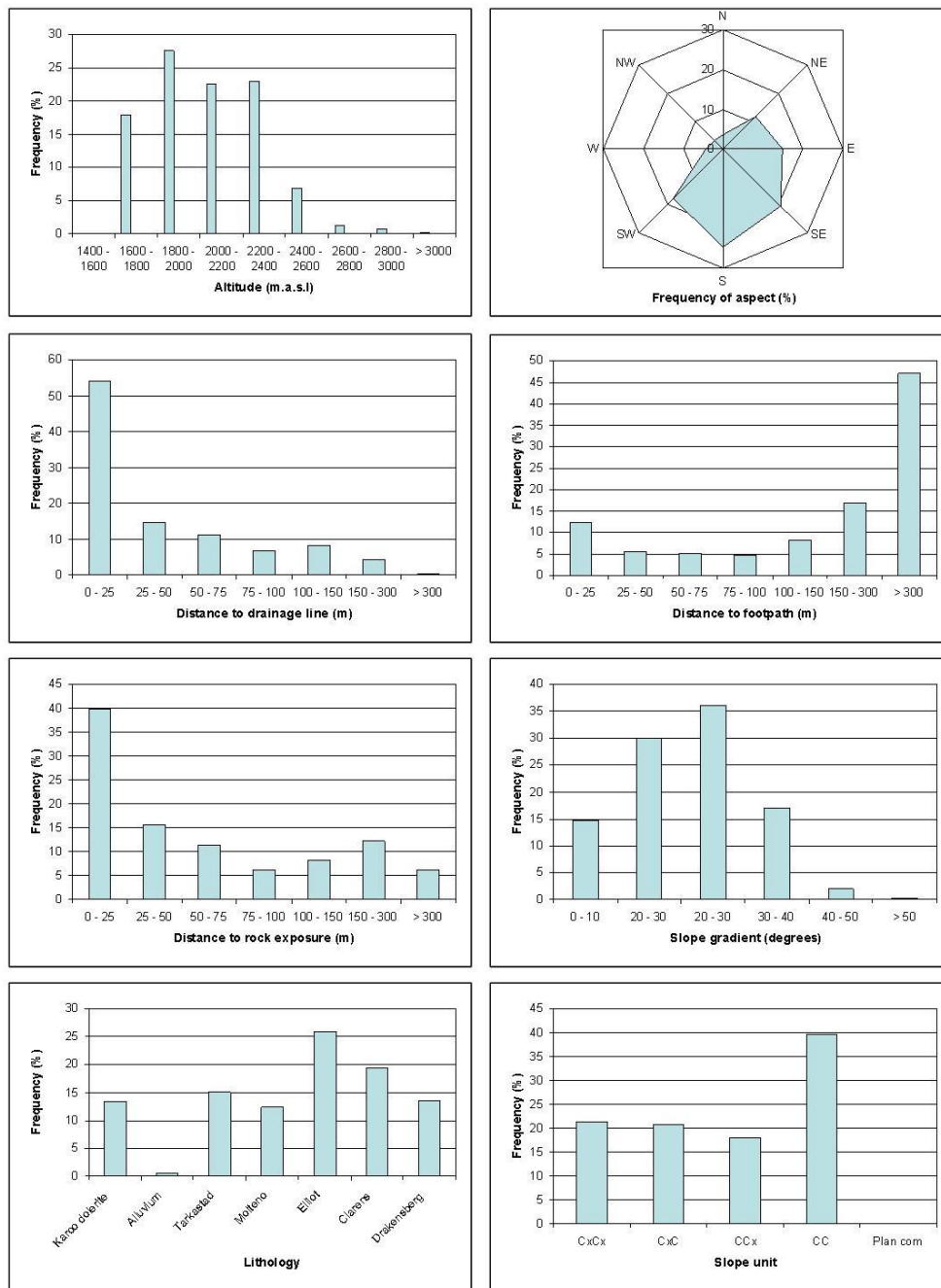


Figure 7.32 Histograms of the independent variables for shear scars.

Shear scars occur predominantly on slopes with gradients of 20-30°, which compares well with observations in the Du Toit’s Kloof, Western Cape where landslides occur on slope gradients between 21°-30° (Gupta, 2001). However, this range of gradient was also associated with the highest degree of anthropogenic activity represented by the presence of road cuts, so the causal influence of gradient could not be determined. Correlating soil depth and slope gradient shows

that slides can develop in relatively shallow soils (<0.8m) on steeper slopes (>20°) and in deeper soils (2m) on gentler slopes (<15°) (Bijker, 2001). Soil depth influences the development of shallow translational slides as depth determines the amount of water that can percolate through the soil profile. The depth of shallow translational slides (average of 0.5m) in the Drakensberg correlates with alternating soil types (from orthic A to plinthic B) (Bijker, 2001) and with transitions from colluvium to saprolite (Sumner, 1993).

The highest frequency distribution of slide scars occurs between 1 800-2 000m a.s.l, in the Elliot Formation, whilst the highest InfoVal for altitude is between 2 200-2 400m a.s.l and in the Clarens Formation. The relationship that exists between altitude and lithology has previously been discussed, however it should be reiterated that the largest proportion of Clarens Formation lies between 2 200-2 400m a.s.l. Thus, it is likely that lithology has a greater influence on slide distribution than altitude, which is supported by the InfoVal weighting for lithology.

Residual material of the Clarens Formation has been associated with a collapsible fabric consisting of a quartz framework that is loosely held together by clay minerals (Brink, 1982). Increases in moisture content may cause a rapid reduction in density, thus making residual soils of the Clarens Formation susceptible to sliding, particularly where the sandstones overlie mudstones of the Elliot Formation (Blight et al., 1970). Almost 60% of shear scars occur on southerly-facing slopes (SE, S, SW), however it is difficult to compare this result for slide scars as landslide risk assessments in southern Africa have not used aspect as an input variable. Nonetheless, the high frequency of slide scars on south-facing slopes is supported by a high InfoVal weighting (Table 7.15). Garland and Humphrey (1980) confirm a higher frequency of shallow translational slides on south-facing slopes in the Kamberg district of the Drakensberg compared to north, east or west-facing slopes.

Variable	Class	Area (%)	Frequency (%)	InfoVal	Ratio (A/F)
Altitude	1400-1600	0.77	0.0	\$	0.00
	1600 - 1800	26.05	17.9	-0.376	0.69
	1800 - 2000	25.94	27.5	0.058	1.06
	2000 - 2200	19.51	22.6	0.146	1.16
	2200 - 2400	15.33	23.0	0.406	1.50
	2400 - 2600	6.46	6.9	0.073	1.08
	2600 - 2800	2.48	1.3	-0.675	0.51
	2800 - 3000	2.41	0.7	-1.259	0.28
	> 3000	1.05	0.2	-1.895	0.15
Aspect	N (0 - 22.5)	7.08	2.4	-1.096	0.33
	NE (22.5 - 67.5)	17.32	11.5	-0.407	0.67
	E (67.5 - 112.5)	14.78	14.8	0.004	1.00
	SE (112.5 - 157.5)	15.37	20.4	0.284	1.33
	S (157.5 - 202.5)	15.51	24.7	0.467	1.59
	SW (202.5 - 247.5)	11.83	17.5	0.393	1.48
	W (247.5 - 292.5)	6.92	4.3	-0.484	0.62
	NW (292.5 - 337.5)	6.32	3.2	-0.677	0.51
	N (337.5 - 360)	4.86	1.1	-1.482	0.23
DistDrain	0 - 25	32.64	54.2	0.506	1.66
	25 - 50	14.78	14.8	0.004	1.00
	50 - 75	14.06	11.2	-0.226	0.80
	75 - 100	9.65	6.8	-0.351	0.70
	100 - 150	14.26	8.4	-0.527	0.59
	150 - 300	12.22	4.3	-1.041	0.35
		> 300	2.39	0.3	-2.204
DistFoot	0 - 25	14.27	12.2	-0.156	0.86
	25 - 50	6.06	5.5	-0.091	0.91
	50 - 75	5.92	5.2	-0.128	0.88
	75 - 100	4.39	4.7	0.065	1.07
	100 - 150	7.96	8.3	0.037	1.04
	150 - 300	14.58	16.9	0.147	1.16
		> 300	46.83	47.2	0.008
Dist RockX	0 - 25	31.24	39.9	0.246	1.28
	25 - 50	11.56	15.6	0.299	1.35
	50 - 75	10.04	11.4	0.129	1.14
	75 - 100	6.47	6.3	-0.032	0.97
	100 - 150	9.80	8.3	-0.170	0.84
	150 - 300	13.51	12.2	-0.101	0.90
		> 300	17.40	6.3	-1.013
Gradient	0 - 10	31.95	14.8	-0.767	0.46
	10 - 20	28.45	30.1	0.057	1.06
	20 - 30	25.04	36.1	0.365	1.44
	30 - 40	11.73	17.0	0.371	1.45
	40 - 50	2.56	1.9	-0.273	0.76
		> 50	0.27	0.1	-1.653
Lithology	Karoo dolerite	19.86	13.3	-0.400	0.67
	Alluvium	2.30	0.5	-1.474	0.23
	Tarkastad	18.72	15.1	-0.218	0.80
	Molteno	13.40	12.4	-0.080	0.92
	Elliot	22.37	25.9	0.148	1.16
	Clarens	10.42	19.3	0.615	1.85
	Drakensberg	12.93	13.5	0.045	1.05
SlopeUnit	CxCx	28.81	21.4	-0.296	0.74
	CxC	23.14	20.9	-0.099	0.91
	CCx	17.53	18.0	0.027	1.03
	CC	30.50	39.6	0.262	1.30
	PlanCom	0.03	0.0	\$	0.00

Table 7.15 Comparison of the frequency distributions and InfoVal weights. Bold indicates highest value in category, colour indicates variable with greatest frequency.

Ranking the frequency of shear scars that occur within a class suggests that the scars occur within 25m of a drainage line and rock exposure, on concave-concave

slopes, on slopes with gradients between 20-30°, between 1 800-2 000m a.s.l, in the Elliot Formation and on south-facing slopes. The ranking of the InfoVal weights is lithology (Clarens Formation), distance to a drainage line (0-25m), aspect (south-facing), altitude (2 200-2 400m a.s.l), gradient (30-40°), distance to a rock exposure (25-50m) and slope unit (CC).

Only three variables have InfoVal weights and frequency distributions that select the same class within each variable as having the greatest influence, and these are aspect, distance to a drainage line and slope unit. The InfoVal selects different classes than the frequency distributions when area is accounted for. Lithology becomes the variable with the highest InfoVal and the Clarens Formation rather than Elliot Group is selected. Distance to a drainage line and aspect have the second and third highest InfoVal weights followed by altitude, however the class with the highest InfoVal is 2 200-2 400m a.s.l. The gradient variable is ranked next (30-40°), followed by distance to a rock exposure (0-25m). The last two variables are slope unit and distance to a footpath.

Hierarchical partitioning was undertaken to rank the variables according to their greatest independent contribution (%I) to the logistic regression model. A hierarchical partition was created for each iteration of random points and the resulting %I are presented in Figure 7.33. Distance to a drainage line consistently has the highest independent contribution and accounts for an average of 45% (3.02 SD) of the model. Gradient (14%), lithology (12%) and distance to a rock exposure (12%) contribute equally to the model but to a much smaller extent, however only the distance to drainage line compares well to the frequency distribution and InfoVal.

Stepwise forward and backward logistic regression with all of the variables was used to develop a prediction model which could predict the maximum number of slide scars using the smallest number of variables. Akaike's Information Criterion (AIC) and Bayes Information Criterion are given in Table 7.16. Distance to a footpath was selected as a variable by RP5 (based on the BIC) so a second logistic

regression was performed to determine whether the distance to a footpath variable improved the logit fit. From Table 7.16 it can be seen that including the distance to a footpath variable improves the model fit as the AIC scores are higher (and therefore better) than when the variable is excluded. This highlights that statistical significance and geomorphic significance are not necessarily the same and reinforces the notion that the beta coefficients should not be used to explain causality.

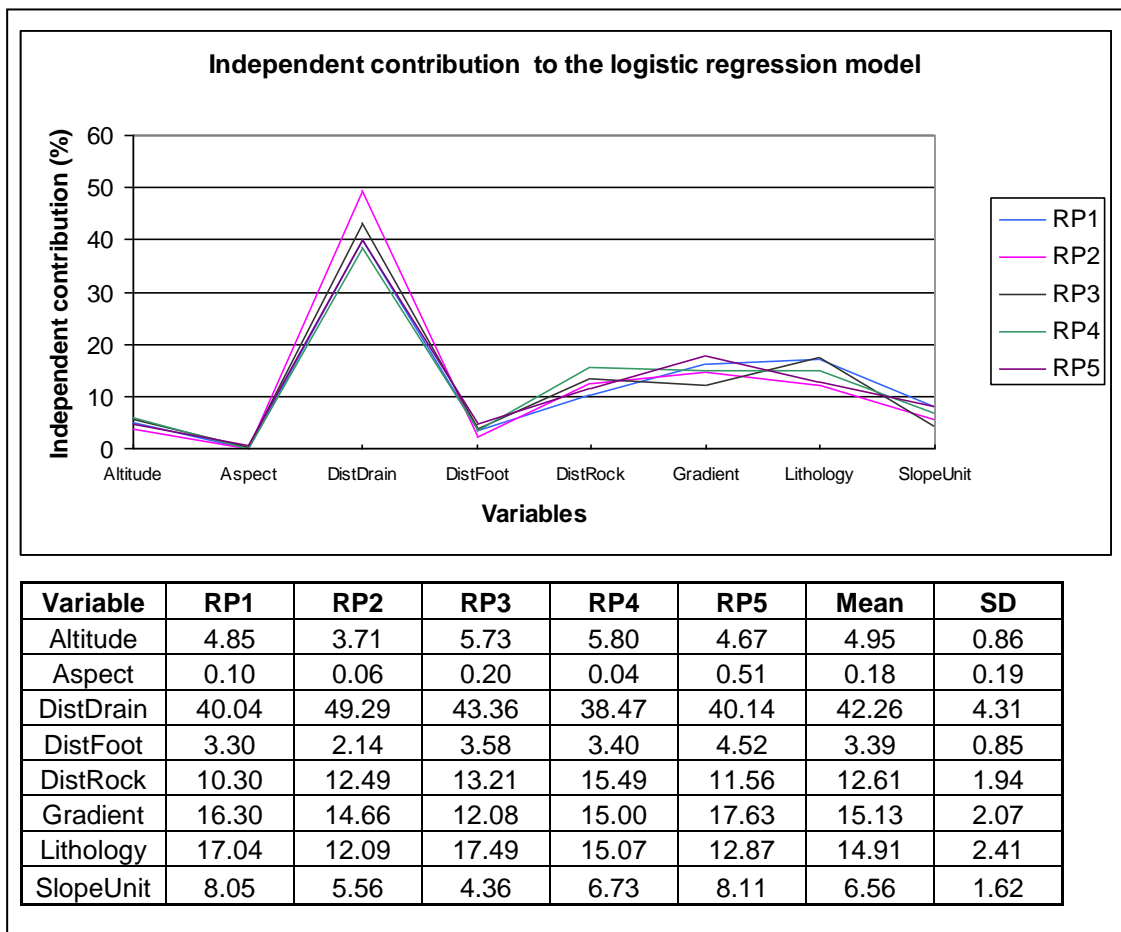


Figure 7.33 Graph representing the percentage contribution of each variable to the logit model. The table shows the mean and standard deviations for each contribution.

The lowest AIC and BIC for the five iterations is for the RP2 dataset. Seven independent variables are selected using the AIC, whilst 3 are selected using the BIC. All of the variables (except slope unit) were selected for this model using the AIC, whilst aspect, gradient and distance to a drainage line were selected using the BIC. These results confirm that gradient and distance to a drainage line

influences the distribution of slide scars and suggests that aspect may also have some influence despite this variable having a low %I (mean = 0.18, SD = 0.19). The predictive power of RP2 is the same as RP4, however RP2 uses less variables to produce the same percentage of correctly identified events.

Models	Random Point 1	Random Point 2	Random Point 3	Random Point 4	Random Point 5
Full AIC	4646	4636	4647	4638	4676
Full AIC (exl. DistFoot)	4677	4655	4676	4669	4724
Best AIC	4645.6	4634.04	4647.46	4638.34	4675.73
No Var	8	7	8	8	8
Variables	Altitude	Altitude	Altitude	Altitude	Altitude
	Aspect	Aspect	Aspect	Aspect	Aspect
	DistDrain	DistDrain	DistDrain	DistDrain	DistDrain
	DistFoot	DistFoot	DistFoot	DistFoot	DistFoot
	DistRock	DistRock	DistRock	DistRock	DistRock
	Gradient	Gradient	Gradient	Gradient	Gradient
	Lithology	Lithology	Lithology	Lithology	Lithology
	SlopeUnit	-	SlopeUnit	SlopeUnit	SlopeUnit
Best BIC	4880	4807.16	4873.74	4865.74	4881.47
No Var	4	3	4	3	4
Variables	Altitude	-	Altitude	-	-
	Aspect	Aspect	Aspect	Aspect	Aspect
	DistDrain	DistDrain	DistDrain	DistDrain	DistDrain
	-	-	-	-	DistFoot
	Gradient	Gradient	Gradient	Gradient	Gradient
%CorrPred	67.58	67.86	67.47	67.86	67.57

Table 7.16 The AIC, BIC and variables selected for each iteration. Note that the percentage of correctly predicted terracettes is similar for each model.

The probability maps for each model are shown in Figures 7.34-7.36. Given that most of the models used all eight variables, it is not surprising that the probability maps look similar. Likewise, the standard deviations of the probability ranges are very low (Table 7.17). It is noteworthy that RP4 and RP5 predict slightly more cells in the 0.8-1.00 probability range than the other models. Only 36% of the study area has a >50% probability for slide occurrence. Relatively high probabilities are predicted in the central region of the study area, which is not reflected in the distribution of the digitized slide scars. This is due either to digitizing error (where slide scars have not been included) or prediction error (the logit model is over-performing).

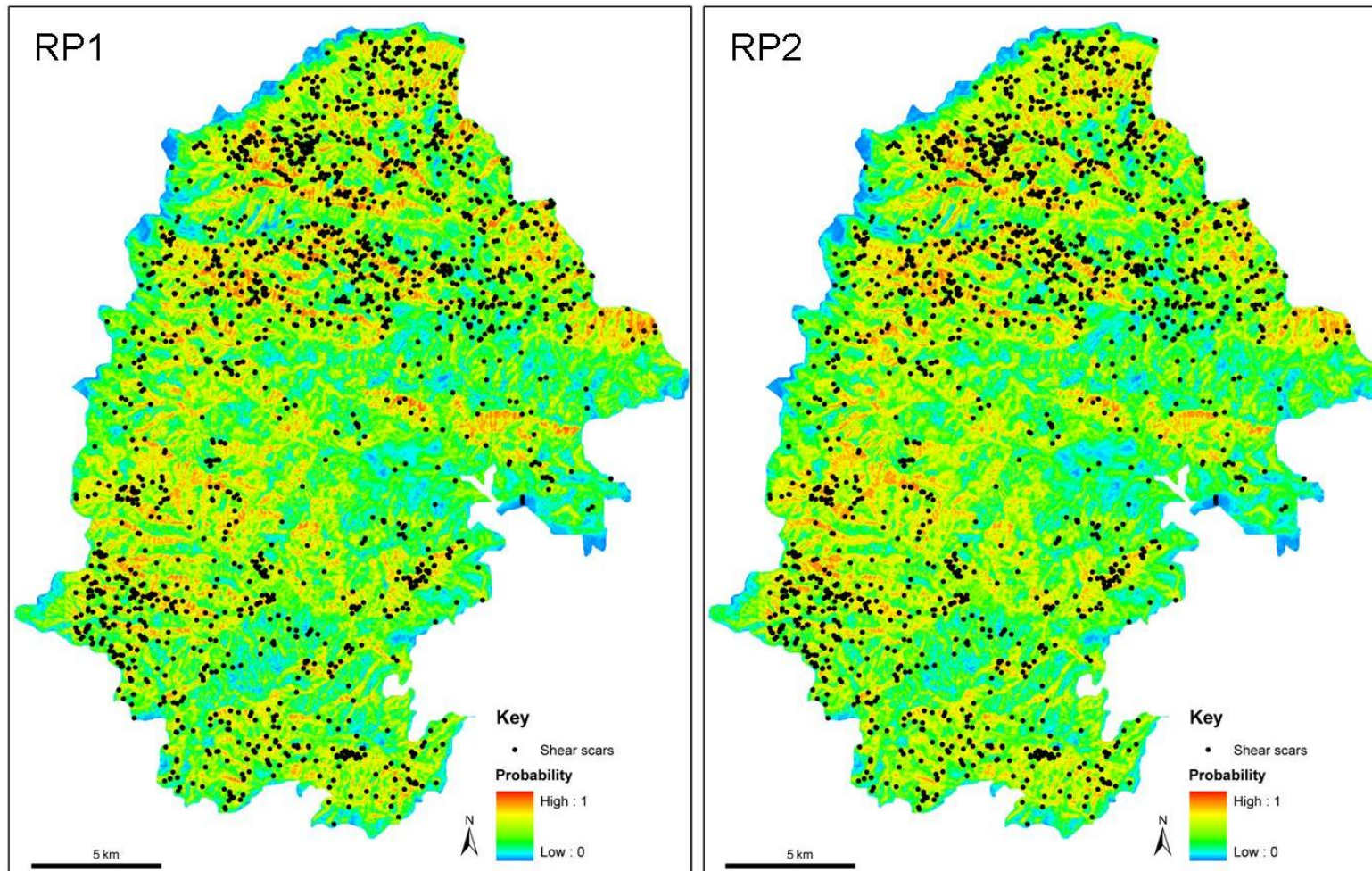


Figure 7.34 Probability maps of shear scars for the RP1 and RP2 datasets.

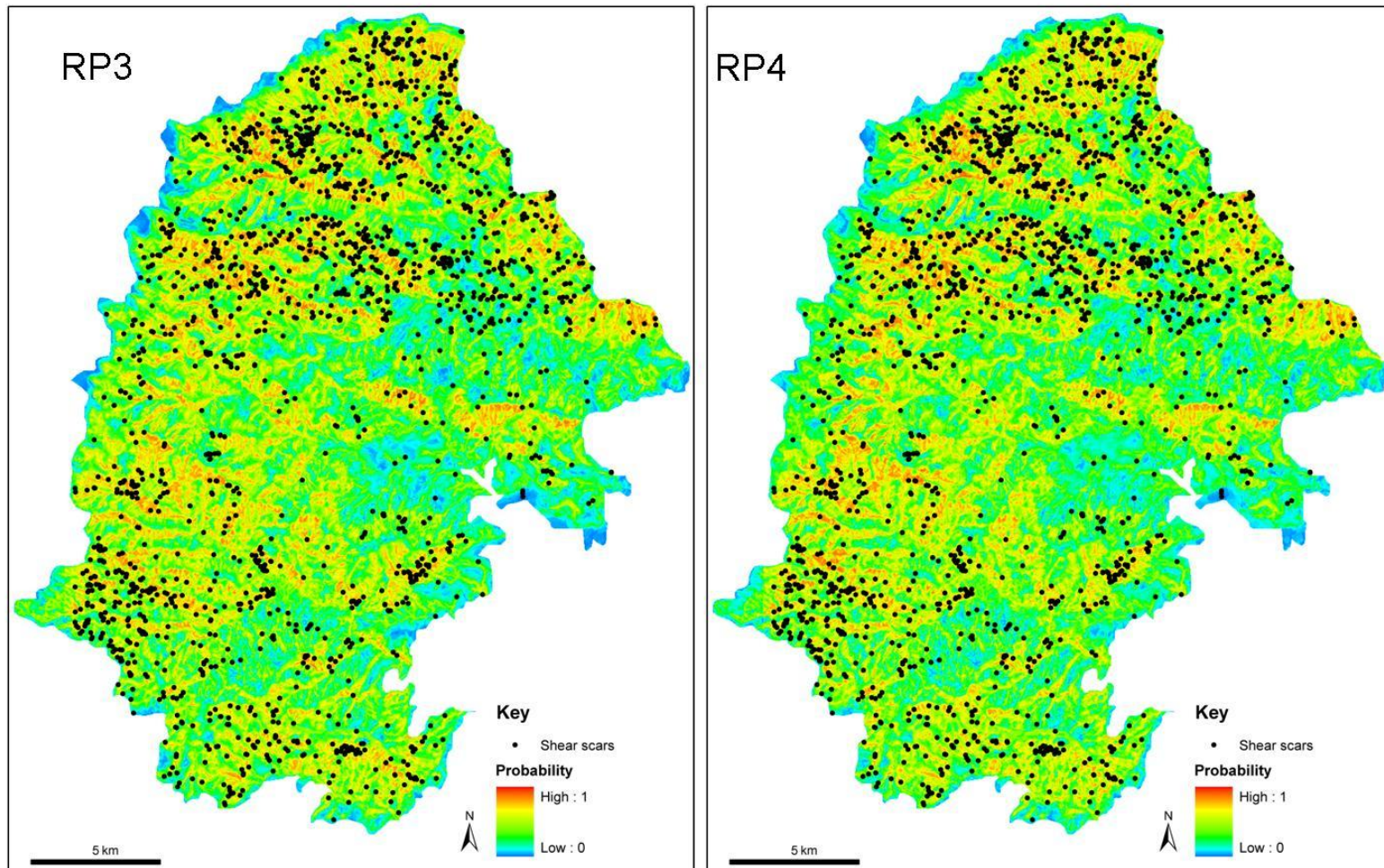


Figure 7.35 Probability maps of shear scars for the RP3 and RP4 datasets.

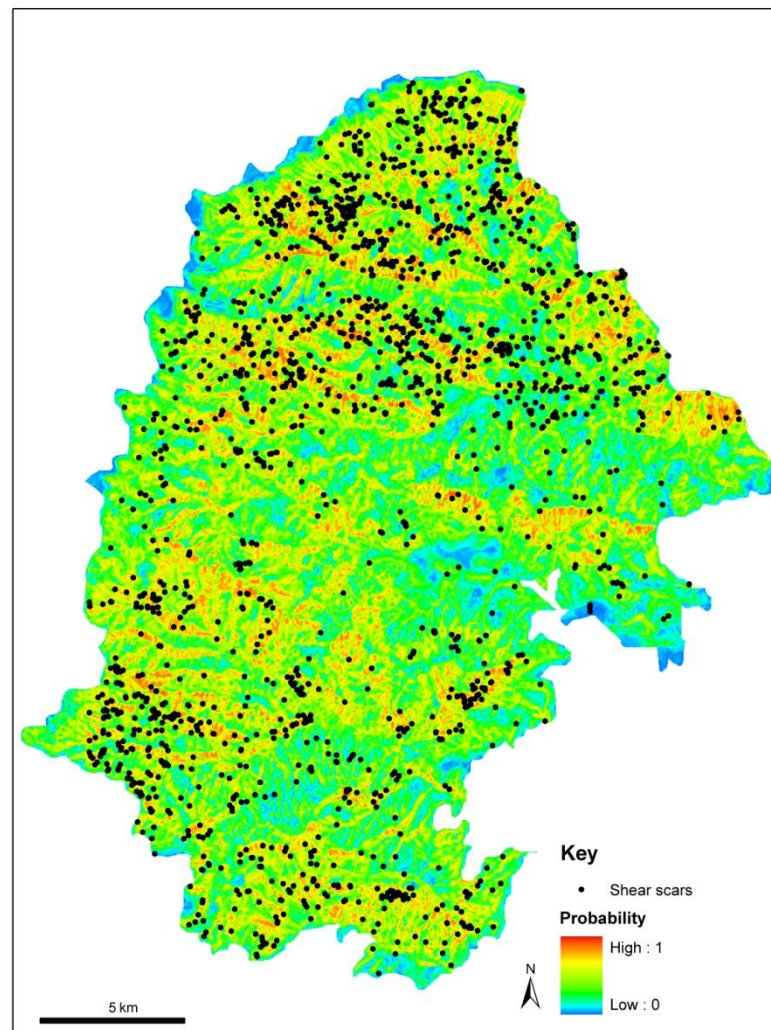


Figure 7.36 Probability maps of shear scars for the RP5 dataset.

Classification trees for each of the random iterations were produced and the confusion matrices compared to select the best tree. RP2 predicted the highest number of events (Type=SA) correctly and is represented in Figure 7.37. Three of the trees used distance to a drainage line as the first node (RP1, RP2 and RP5), whilst the remaining two trees used aspect. The distance to drainage categories (0-25, 75-100), selected by the first node, are quite disparate and may represent a sub-classification for slide scars that are caused by stream undercutting or increased moisture levels. Gradient is the second-level node with the 2 000-2 600m a.s.l category containing 5% more events of Type=SA.

Probability	RP1			RP2			RP3			RP4			RP5			Mean	
	Area	%	SD	Area	%	SD	Area	%	SD	Area	%	SD	Area	%	SD	Area	%
0 - 0.5	294.0	63.8	0.2	289.9	62.9	0.5	292.6	63.5	0.1	294.5	63.9	0.2	293.9	63.8	0.1	293.0	63.6
0.5 - 0.6	62.2	13.5	0.0	63.4	13.8	0.2	63.3	13.7	0.1	60.6	13.1	0.3	62.4	13.6	0.0	62.4	13.5
0.6 - 0.7	53.6	11.6	0.0	53.6	11.6	0.0	55.5	12.1	0.3	52.3	11.4	0.2	52.3	11.4	0.2	53.5	11.6
0.7 - 0.8	38.4	8.3	0.0	41.2	8.9	0.4	37.4	8.1	0.2	38.7	8.4	0.0	37.4	8.1	0.2	38.6	8.4
0.8 - 0.9	12.4	2.7	0.1	12.6	2.7	0.1	11.8	2.6	0.2	14.1	3.1	0.2	14.2	3.1	0.2	13.0	2.8
0.9 - 1.00	0.2	0.0	0.0	0.1	0.0	0.0	0.1	0.0	0.0	0.6	0.1	0.0	0.5	0.1	0.0	0.3	0.1
>0.5	166.8	36.1	0.1	170.9	37.0	0.7	168.1	36.5	0.8	166.3	36.1	0.7	166.8	36.3	0.6	167.8	36.4

Table 7.17 Total area (km² and percent) of probability values for each iteration of random points.

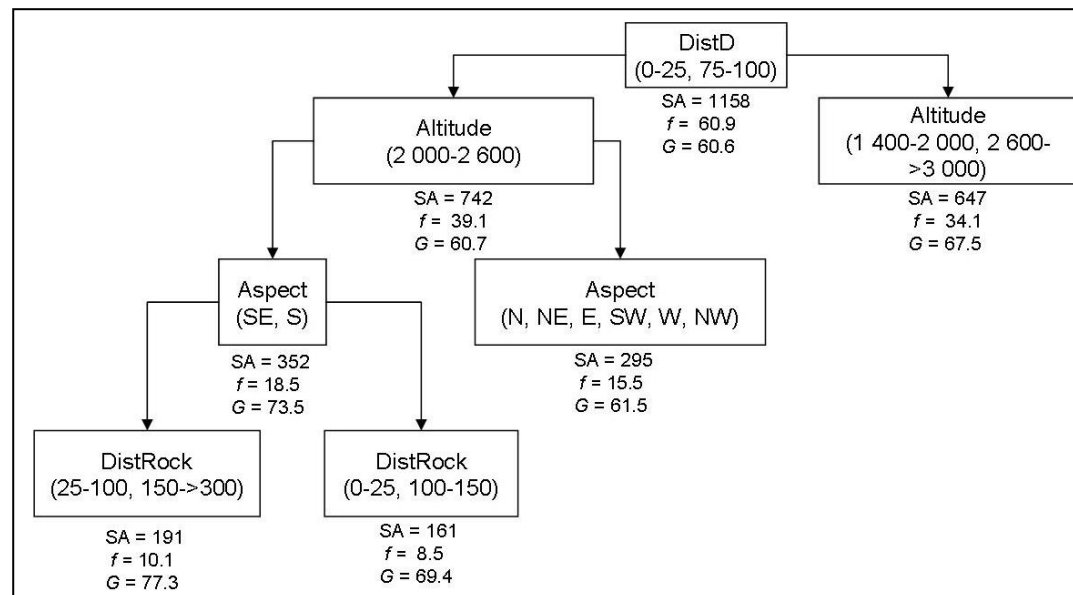


Figure 7.37 Summarized and pruned classification tree for shear scars (*f*: frequency, *G*: Gini coefficient).

The frequency distribution, hierarchical partitioning and classification tree suggest that distance to a drainage line has the largest influence on slide scar development, whilst the InfoVal suggests that lithology, particularly the Clarens Formation sandstones, also has an important influence. However, only aspect and distance to a drainage line appear in all of the BIC models. The distance to a drainage line category that has been selected (0-25m) is statistically and geomorphologically meaningful, as slide scars were observed to occur in close proximity to drainage lines. However, the overall importance that this variable plays is difficult to determine as slides caused by stream bank undercutting and scars associated with debris flows were included in this mass movement type.

7.6 Shear-type 2: Incised flows

Shear scars that have an incised flow track may also be defined as ‘channelised’ or ‘confined’ debris flows (Hungre et al., 2001) which usually consist of a mixture of fine to coarse material and a variable amount of water which combines to form muddy slurry that moves downslope (Coussot and Meunier, 1996; Goudie, 2004). This type of mass movement appears as a slide scar on the orthophotos with the addition of a clearly identifiable incised flow path created by the gouging out and transport of slope materials. The flow track tapers downslope and the deposit is relatively prominent. Incised flow paths are easily identifiable even after the track has been revegetated as the new substrate is usually colonised by trees and shrubs, rather than grass (Figure 7.38). Incised flow tracks may develop into drainage lines and examples of incised tracks are visible at site D (Figure 6.13). This project has digitized 480 slide scars with incised flow tracks from aerial photos (Figure 7.39).

Debris flows are commonly triggered by unusually intense rainfall or by events which increase the amount of available moisture, such as rapid snowmelt or lake overflows (Goudie, 2004; Glade, 2005). Surface runoff and upslope contributing area influence debris flow development as they promote saturated soil conditions in steep environments (Berti and Simoni, 2005). Movement is rapid and flows

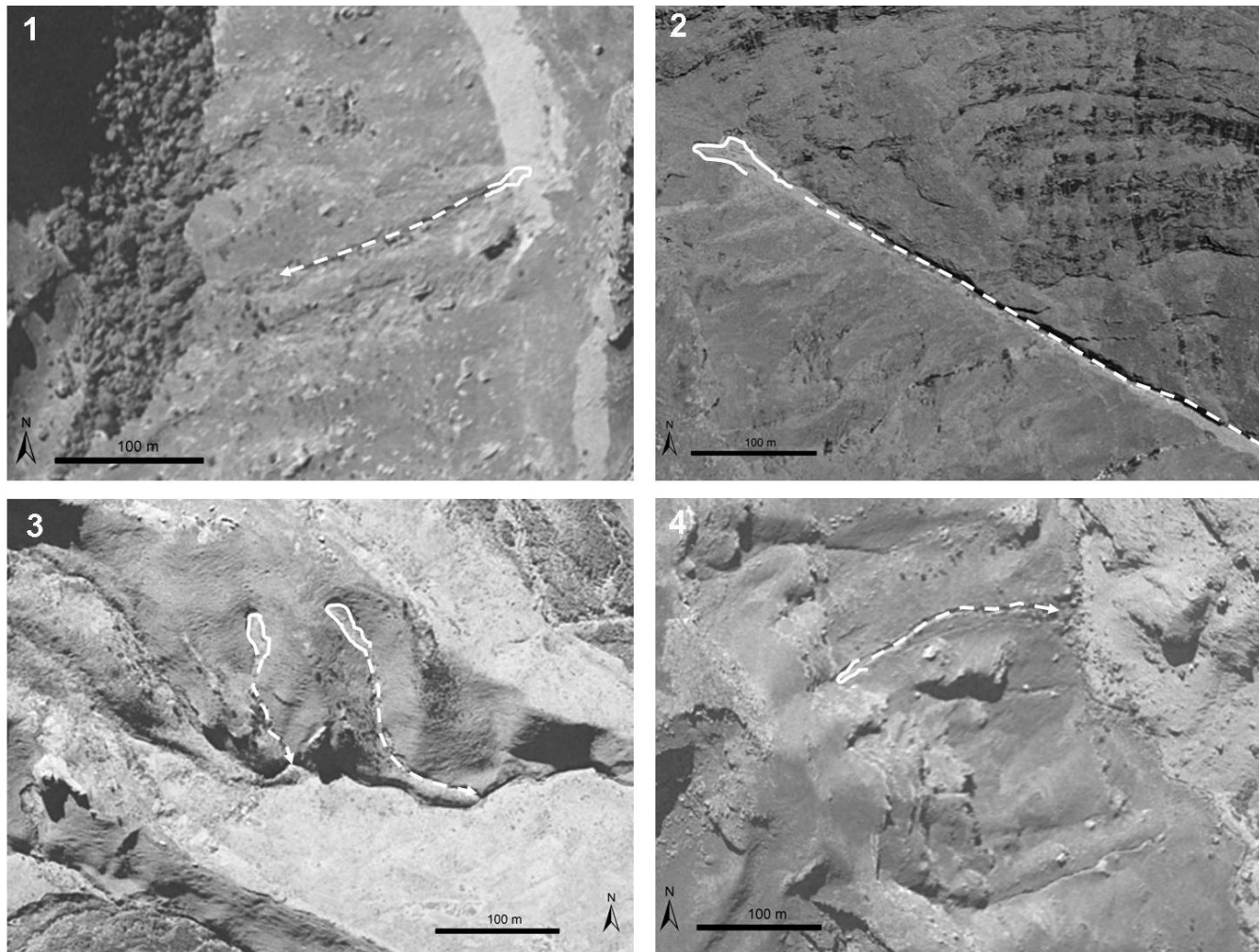


Figure 7.38 Aerial view of slide scars with incised flow tracks (locations of images 1-4 are shown in Figure 7.39) .

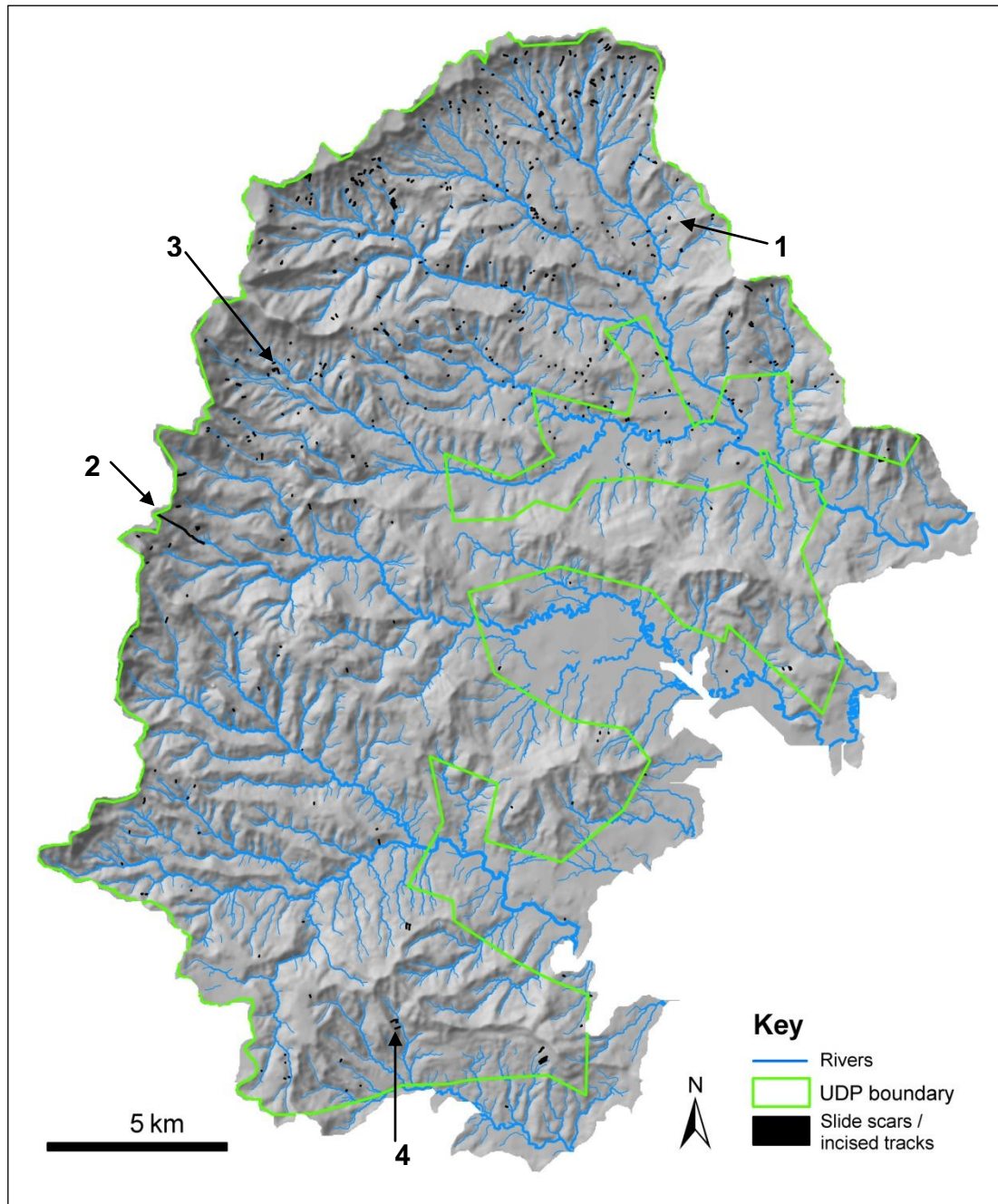


Figure 7.39 Distribution of shear scars with incised flow tracks digitized from the 1: 50 000 orthophotos.

typically begin as shallow translational slides (Guthrie and Evans, 2004; Berti and Simoni, 2005), which explains why the features are characterized by a shear scar. Debris slide/flows studied in the Du Toit's Kloof begin as shallow translational slides and then disintegrate into debris flows, with all shallow translational slides having a shear surface at the contact between the colluvium and underlying

bedrock (Boelhouwers et al., 1998). Incised debris flow tracks observed in the UDP are relatively shallow (<2.5m deep) but are generally longer than they are wide (Table 7.29). Estimated widths for incised flows range between 3.2m to 77.9m (average=15.8m), whilst the lengths range between 7.8m to 1 518m (average = 58.3). This elongated form is confirmed by an average Circularity Ratio of 0.46 (Table 7.30).

Debris flow deposits differ from stream flows, or hyper-concentrated flows, in that the flow deposits contain a wide range of particle sizes, from clays to large boulders with little or minimum grading (Coussot and Meunier, 1996), as has been observed in the current study for all of the flow deposits. Deposits generally form lobes which have steeper fronts and flanks than the deposits formed by surficial flows (Cenderelli and Kite, 1998). Incised flows generally contain larger boulders and rocks than surficial flows and are the likely cause of slope scour. Incised flows with erosion depths of up to 2m have been recorded at North Fork Mountain in the USA (Cenderelli and Kite, 1998), as well as at Vancouver Island in Canada (Guthrie and Evans, 2004), and in Iceland (Decaulne et al., 2005). These types of flows commonly occur along existing drainage lines or become drainage lines after the failure occurs, as slope scour removes vegetation and concentrates surface flow (Hung et al., 2001; May and Gresswell, 2004).

The frequency distribution of the occurrence of incised flows in relation to the eight variables and their associated class categories is presented in Figure 7.40. The results of the distance variables suggest that the majority of incised flows occur >300m from a footpath. The same approach used for slide scars is adopted and this variable is not discussed further. The second highest frequency is the distance to drainage variable with 54% of features occurring within 25 m of a drainage line. Slope unit has the next highest frequency in the CC category (48%), followed by distance to a rock exposure (0-25m) and gradient (20^o-30^o). The hierarchy of the remaining variables is lithology (Drakensberg Group), aspect (south-facing) and altitude (2 000-2 200m a.s.l). Similarly, aspect and proximity

to a rock exposure have been related to increased debris flow activity in the Du Toit's Kloof (Boelhouwers et al., 1998).

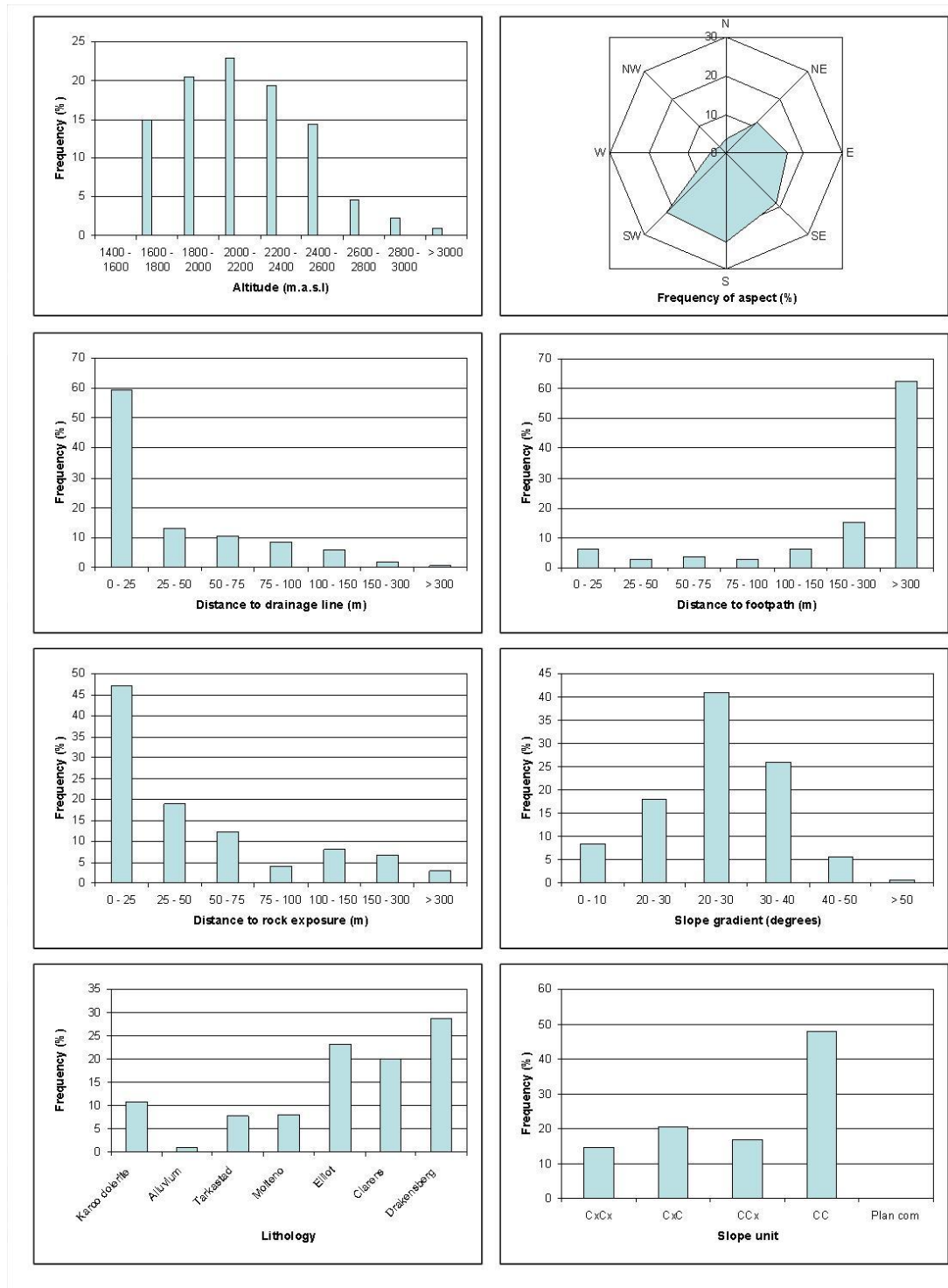


Figure 7.40 Histograms of the independent variables for incised flows.

Variable	Class	Area (%)	Frequency (%)	InfoVal	Ratio (A/F)
Altitude	1400-1600	0.77	0.0	\$	0.00
	1600 - 1800	26.05	15.0	-0.552	0.58
	1800 - 2000	25.94	20.4	-0.239	0.79
	2000 - 2200	19.51	22.9	0.161	1.17
	2200 - 2400	15.33	19.4	0.234	1.26
	2400 - 2600	6.46	14.4	0.800	2.23
	2600 - 2800	2.48	4.6	0.613	1.85
	2800 - 3000	2.41	2.3	-0.050	0.95
> 3000	1.05	1.0	-0.008	0.99	
Aspect	N (0 - 22.5)	7.08	3.1	-0.818	0.44
	NE (22.5 - 67.5)	17.32	11.0	-0.450	0.64
	E (67.5 - 112.5)	14.78	15.8	0.069	1.07
	SE (112.5 - 157.5)	15.37	18.3	0.177	1.19
	S (157.5 - 202.5)	15.51	23.1	0.399	1.49
	SW (202.5 - 247.5)	11.83	21.7	0.605	1.83
	W (247.5 - 292.5)	6.92	4.0	-0.559	0.57
	NW (292.5 - 337.5)	6.32	2.5	-0.928	0.40
N (337.5 - 360)	4.86	0.4	-2.457	0.09	
DistDrain	0 - 25	32.64	59.4	0.598	1.82
	25 - 50	14.78	13.1	-0.119	0.89
	50 - 75	14.06	10.6	-0.280	0.76
	75 - 100	9.65	8.5	-0.122	0.89
	100 - 150	14.26	5.8	-0.894	0.41
	150 - 300	12.22	1.9	-1.875	0.15
	> 300	2.39	0.6	-1.339	0.26
DistFoot	0 - 25	14.27	6.3	-0.825	0.44
	25 - 50	6.06	2.9	-0.731	0.48
	50 - 75	5.92	3.8	-0.457	0.63
	75 - 100	4.39	2.9	-0.408	0.66
	100 - 150	7.96	6.3	-0.242	0.79
	150 - 300	14.58	15.4	0.056	1.06
	> 300	46.83	62.5	0.289	1.33
Dist RockX	0 - 25	31.24	47.1	0.410	1.51
	25 - 50	11.56	19.0	0.495	1.64
	50 - 75	10.04	12.3	0.203	1.22
	75 - 100	6.47	4.0	-0.491	0.61
	100 - 150	9.80	8.1	-0.187	0.83
	150 - 300	13.51	6.7	-0.706	0.49
	> 300	17.40	2.9	-1.786	0.17
Gradient	0 - 10	31.95	8.5	-1.319	0.27
	10 - 20	28.45	18.1	-0.451	0.64
	20 - 30	25.04	41.0	0.494	1.64
	30 - 40	11.73	26.0	0.798	2.22
	40 - 50	2.56	5.6	0.788	2.20
	> 50	0.27	0.6	0.822	2.27
Lithology	Karoo dolerite	19.86	10.8	-0.606	0.55
	Alluvium	2.30	1.0	-0.791	0.45
	Tarkastad	18.72	7.9	-0.861	0.42
	Molteno	13.40	8.1	-0.501	0.61
	Elliot	22.37	23.3	0.042	1.04
	Drakensberg	12.93	28.8	0.799	2.22
	Clarens	10.42	20.0	0.652	1.92
SlopeUnit	CxCx	28.81	14.6	-0.681	0.51
	CxC	23.14	20.6	-0.115	0.89
	CCx	17.53	16.7	-0.050	0.95
	CC	30.50	48.1	0.456	1.58
	PlanCom	0.03	0.0	\$	0.00

Table 7.18 Comparison of the frequency distributions and InfoVal weights. Bold indicates highest value in category, colour indicates variable with greatest frequency.

Ranking of the InfoVal weights places altitude (2 400-2 600m a.s.l) first, followed by lithology (Drakensberg Group) and gradient (30°-40°) (Table 7.18). The combination of altitude and lithology is expected, given that the Drakensberg Group occurs between 2 400-2 600m a.s.l. Moore and Blenkinsop (2006) note that the slopes below the vertical cliffs of the Drakensberg Group are composed of thinly-bedded lava flows which have brecciated upper and lower surfaces. These act as aquifers which are susceptible to chemical weathering and are more readily eroded than the massive lava flows. Aspect (SW), distance to a drainage line (0-25m) and to a rock exposure (50-75m) are the next variables in the hierarchy, followed by slope unit (CC) and distance to a footpath (>300m).

Hierarchical partitioning was undertaken to rank the variables according to their greatest independent contribution (%I) to the logistic regression model. A hierarchical partition was created for each iteration of random points and the resulting %I are presented in Figure 7.41. Gradient has the highest independent contribution and accounts for an average of 31% (3.35 SD) of the model. Distance to a drainage line has the next highest contribution (25%, 3.15 SD) and this is the first mass movement type that is characterized by two independent variables with similar percentage contributions.

Incised debris flows usually occur on steeper slope gradients than surficial debris flows, which would explain why gradient has a greater percentage contribution (May and Gresswell, 2004). However, most incised flows occur along existing drainage lines or develop into drainage lines. These drainage lines represent areas where surface flow has become concentrated, hence the upslope contributing area and the presence of a rock exposure are also important variables to use when predicting debris flow development (Wilford et al., 2004; Berti and Simoni, 2005).

Debris flows associated with drainage lines usually follow first or second order drainage channels (Hungr et al., 2001). A calculation of the average stream order of drainage lines within 5m of an incised flow shows that 73% are first order

channels (Table 7.32). The distance to a rock exposure variable has the third highest independent contribution (15%), whilst slope unit has the fourth highest (12%), which suggests that rock exposures, more particularly joints in rock exposures, can concentrate surface flow, whilst topographic hollows can retain soil moisture until saturated soil conditions exist and failure occurs.

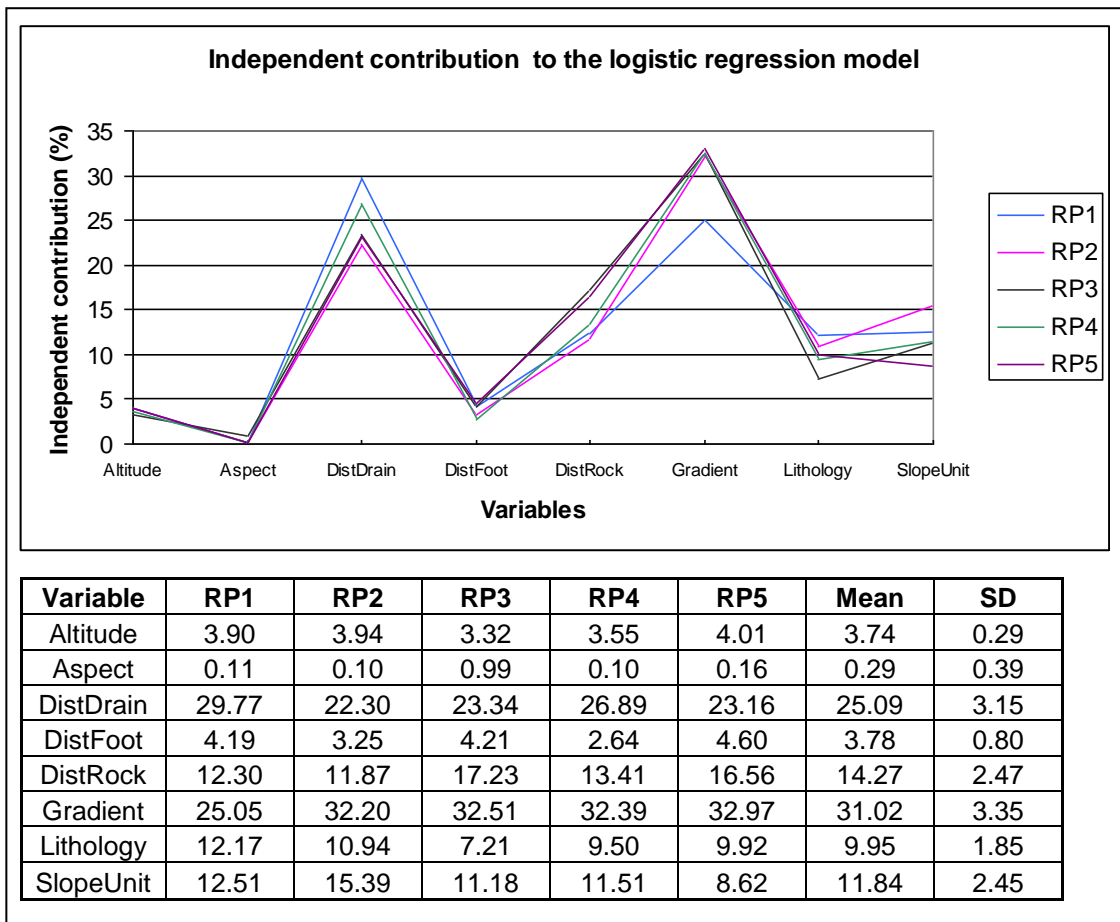


Figure 7.41 Graph representing the percentage contribution of each variable to the logit model. The table shows the mean and standard deviations for each contribution.

Stepwise forward and backward logistic regression using all of the variables was used to develop a prediction model. Akaike’s Information Criterion (AIC) and Bayes Information Criterion (BIC) are presented in Table 7.19. The lowest AIC and BIC for the five iterations is for the Random Point 1 (RP1) dataset. Seven of the available eight variables were selected (distance to a footpath was not selected by any of the models). The BIC models selected two to three variables, however RP1 and RP5 achieved the lowest BIC values with only two variables, gradient

and distance to a drainage line. This confirms the findings of the hierarchical partitioning and helps establish that the incised flows are a distinguishable mass movement type. The RP1 model predicted 76% of Type=SB correctly, compared to the slide scar model, which was only able to predict 67% of the dataset correctly.

Probability maps were created in a GIS environment to spatially compare the predictive ability of each model (Figure 7.42-44). As the beta co-efficients produced by the models are similar (given that the same variables were selected for each random iteration), it is not surprising that the maps are very similar in appearance. Noteworthy from the probability maps is that the northern and western section of the study area is characterized as having higher probabilities. This is most likely because these areas are at a higher altitude than the eastern and southern portions of the study area (Figure 5.7).

Models	RP 1	RP2	RP3	RP4	RP5
Full AIC	1038	1085	1085	1076	1054
Best AIC	1035	1076	1083	1062	1046
No Var	7	7	7	6	7
Variables	Altitude	Altitude	Altitude	Altitude	Altitude
	Aspect	Aspect	Aspect	-	Aspect
	DistDrain	DistDrain	DistDrain	DistDrain	DistDrain
	-	-	-	-	-
	DistRock	DistRock	DistRock	DistRock	DistRock
	Gradient	Gradient	Gradient	Gradient	Gradient
	Lithology	Lithology	Lithology	Lithology	Lithology
	SlopeUnit	SlopeUnit	SlopeUnit	SlopeUnit	SlopeUnit
Best BIC	1159	1177	1181	1168	1155
No Var	2	3	3	2	2
Variables	DistDrain	DistDrain	DistDrain	DistDrain	DistDrain
	Gradient	Gradient	Gradient	Gradient	Gradient
	-	SlopeUnit	SlopeUnit	-	-
%CorrPred	76.14	75.1	74.58	75.0	75.52

Table 7.19 The AIC, BIC and variables selected for each iteration. Note that the percentage of correctly predicted incised flows is similar for each model.

The values of the probability function were classified to reflect differences in the total area for a range of probability values (Table 7.20). It is noteworthy that the areas predicted for a particular probability class are consistently within one

standard deviation which confirms that the models perform equally and that any variations observed between datasets is due to the effects of the randomly generated (Type=S0) dataset not the actual (Type=SB) dataset. The RP1 model predicts the highest percentage of area with a high probability (>0.9) which might indicate slight overfitting of the model. The presence of slides in these areas which may have not been included in the original inventory would need to be ascertained, but it is likely that not all of the mass movement features were captured as these areas correspond with areas in shadow on the orthophotos (Figure 7.45). About 29% of the study area has a $>50\%$ chance of developing a shear scar with incised flow.

Confusion matrices for each classification tree were produced to compare the predictive ability of each tree. The tree produced by the RP5 dataset had an 88% success rate compared to RP4, which had the lowest percentage (83%) of correctly identified events (Type=SB) (Figure 7.46). All of the trees used gradient as the first node and RP5 selected three classes of gradient (classes 20° - 30° , 30° - 40° and $>50^{\circ}$), however three of the models only used two (20° - 30° and 30° - 40°). Including the $>50^{\circ}$ class only adds three more events (Type=SB is 325 rather than 322) to the node. The second node is lithology, with the Tarkastad and Clarens Formations and Drakensberg Group having the highest number of events ($f=39$, $G=76$) which compares well with the univariate statistics. The third node is distance to a drainage line and the 0-25m class predicts 23% of the incised flows. This means that almost 25% of incised flows occur on slope gradients between 20° - 40° , within 25m of a drainage line and in either Tarkastad or Clarens Formation sandstones or Drakensberg Group basalts.

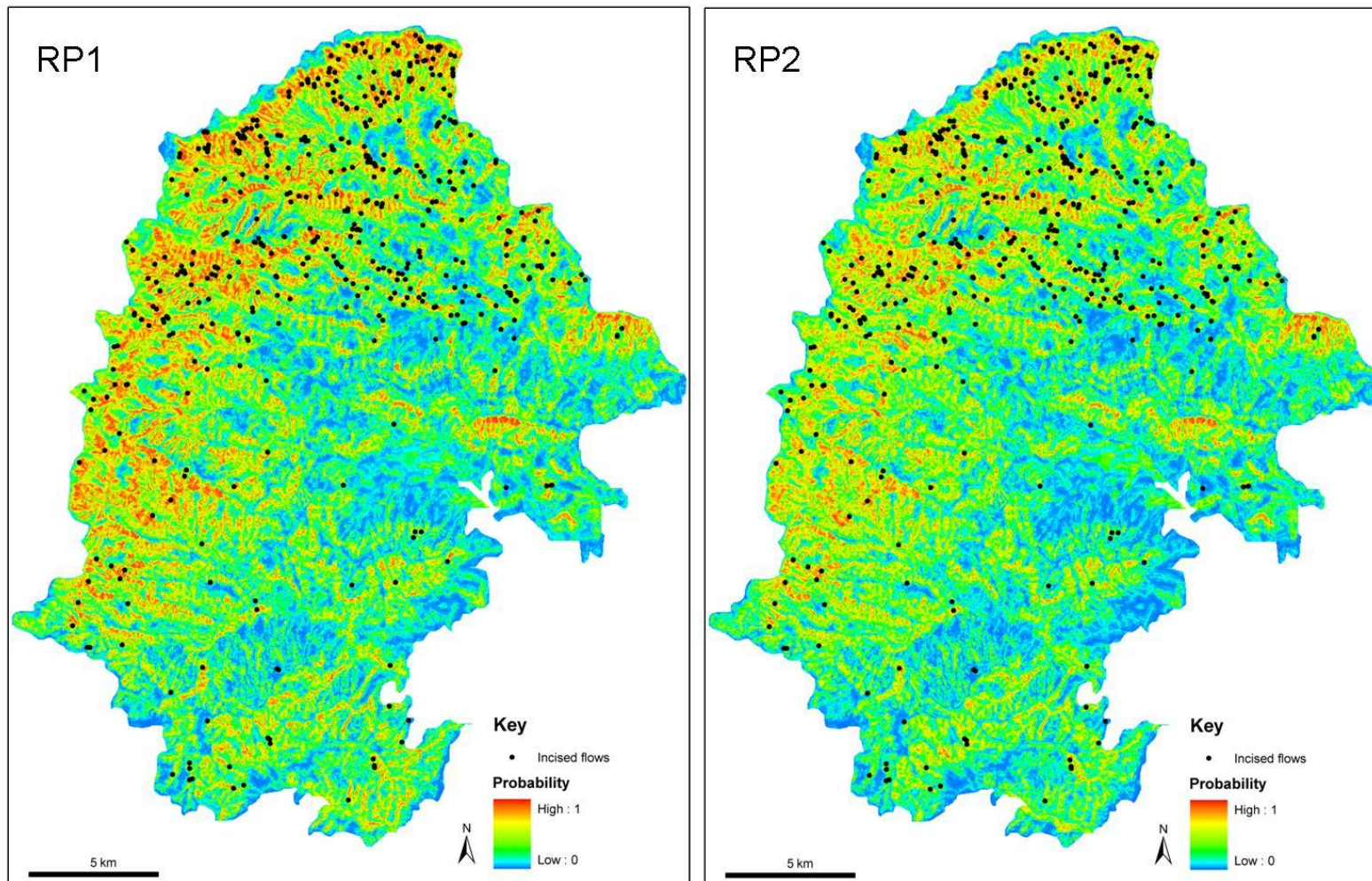


Figure 7.42 Probability maps for incised flows for the RP1 and RP2 datasets.

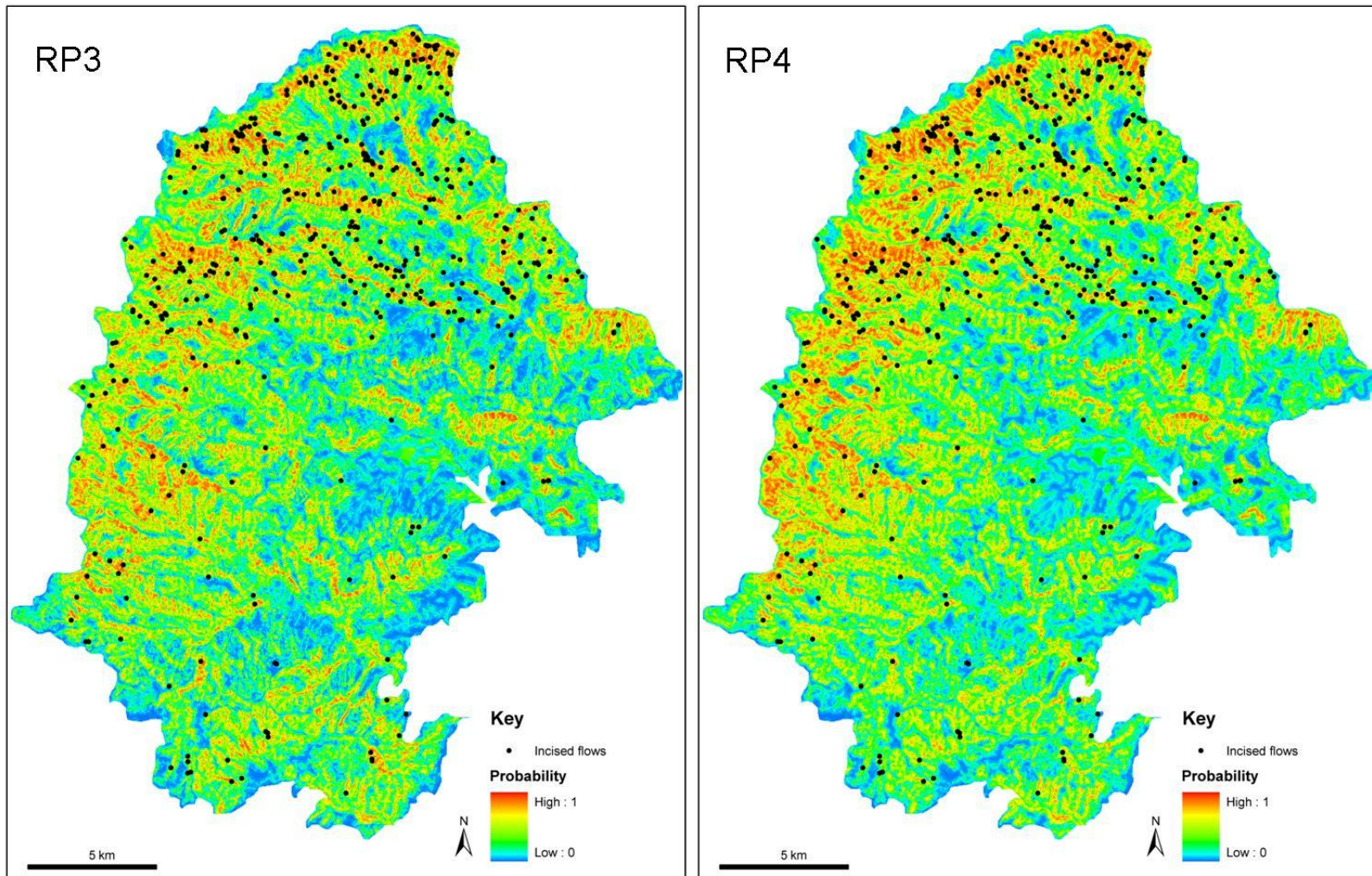


Figure 7.43 Probability maps for incised flows for the RP3 and RP4 datasets.

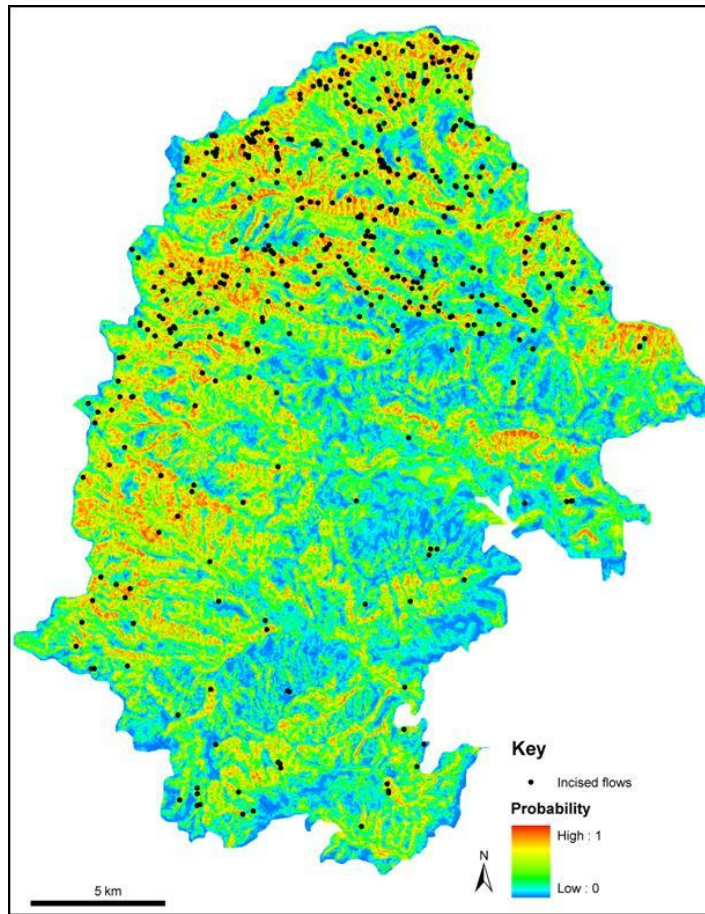


Figure 7.44 Probability maps for incised flows for the RP5 dataset.

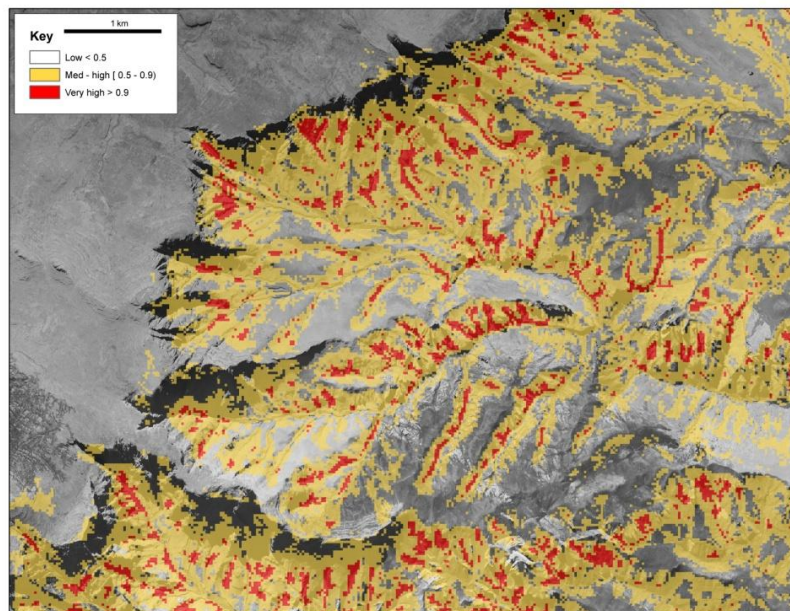


Figure 7.45 Overlay of the prediction surface produced using RP1 onto the orthophotos. Areas predicted as medium to very high probability occur in shadows (black areas) caused by high relief and flying angle.

Probability	RP1			RP2			RP3			RP4			RP5			Mean	
	Area	%	SD	Area	%	SD	Area	%	SD	Area	%	SD	Area	%	SD	Area	%
0 - 0.5	319.4	69.3	0.9	345.7	75.0	3.1	320.7	69.6	0.7	314.6	68.3	1.7	326.8	70.9	0.2	325.4	70.6
0.5 - 0.6	36.6	7.9	0.5	37.6	8.2	0.3	42.0	9.1	0.4	41.7	9.0	0.3	40.6	8.8	0.1	39.7	8.6
0.6 - 0.7	35.1	7.6	0.2	32.2	7.0	0.6	37.0	8.0	0.1	40.4	8.8	0.6	36.3	7.9	0.0	36.2	7.9
0.7 - 0.8	32.5	7.1	0.2	25.4	5.5	0.9	32.1	7.0	0.1	34.3	7.4	0.5	31.3	6.8	0.0	31.1	6.8
0.8 - 0.9	27.3	5.9	0.6	17.1	3.7	0.9	24.0	5.2	0.1	25.0	5.4	0.3	22.3	4.8	0.1	23.1	5.0
0.9 - 1.00	9.8	2.1	0.7	2.8	0.6	0.4	5.0	1.1	0.0	4.9	1.1	0.0	3.6	0.8	0.2	5.2	1.1
>0.5	141.3	30.6	2.2	115.1	25.0	3.1	140.1	30.4	0.7	146.3	31.7	1.7	134	29.1	0.4	135	29.4

Table 7.20 Total area (km² and percent) of probability values for each iteration of random points.

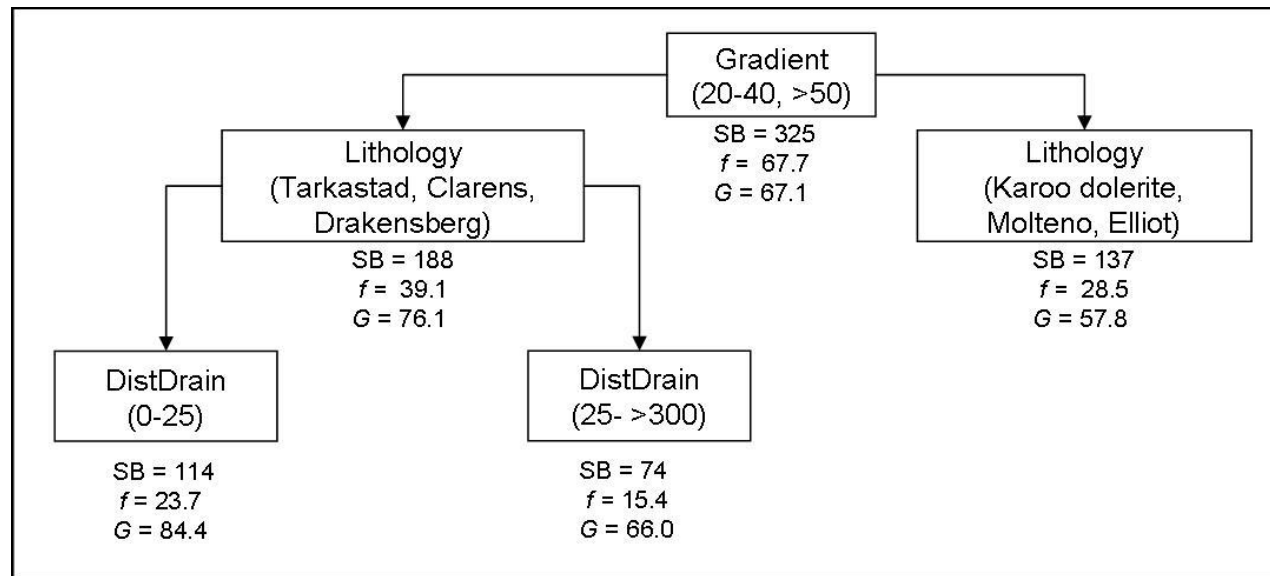


Figure 7.46 Summarized and pruned classification tree for slide scars with incised flow tracks (f : frequency; G : Gini coefficient).

7.7 Shear-type 3: Surficial flows

Slide scars associated with a surficial deposit may also be defined as wet soil- or mud-flows (Hungre et al., 2001), and are a type of debris flow that is composed of high proportions of finer colluvial material, rather than coarse clasts (Goudie, 2004). This type of mass movement also appears as a slide scar on the orthophotos but with a clearly identifiable deposit. The flow path is slightly sinuous and widens in the downslope direction (Varnes, 1978). The deposit travels the length of the flow path and may form a fan at the base of the slope or taper to a point. These features look similar to eroded surfaces on the orthophotos because the displaced material is deposited on the slope covering the vegetation, rather than removing it. Examples of surficial flows can be seen at site G (Figure 6.20) and site H (Figure 6.24). This project has digitized 385 slide scars with surficial deposits from aerial photos (Figure 7.47).

Surficial flows are also initiated by shallow translational slides and have been associated with soils that have high clay contents, as the displaced mass will completely collapse and behave like a viscous fluid (Varnes, 1978; Iverson, 1997; Hungre et al., 2005; Gabet and Mudd, 2006). Vegetation on the scar is usually completely removed and the shear surface generally occurs at the contact between the colluvium and underlying bedrock (Wieczorek et al., 2004; Gabet and Mudd, 2006). The deposit begins almost immediately downslope of the scar and is relatively shallow (Crozier, 1996). Flows can have multiple source areas which either separate into diverging flow paths or converge into a single flow path (Guthrie and Evans, 2004; Wieczorek et al., 2004).

Larger material and vegetation is pushed to the sides of the deposit due to increased friction along the edge of the flow and this forms levees along the steeper portions of the flow track (Harris and Gustafson, 1993) (Figure 7.48). As the gradient flattens out, the material in the flow is deposited, whilst increased water content (and decreasing shear strength) promotes the development of a flat fan rather than a rounded lobe shape (Harris and Gustafson, 1993; Crozier, 1996;

Malet et al., 2005). This type of flow has also been referred to as an ‘earthflow’ (Crozier, 1996) and ‘open-faced’ debris slide (Guthrie and Evans, 2004).

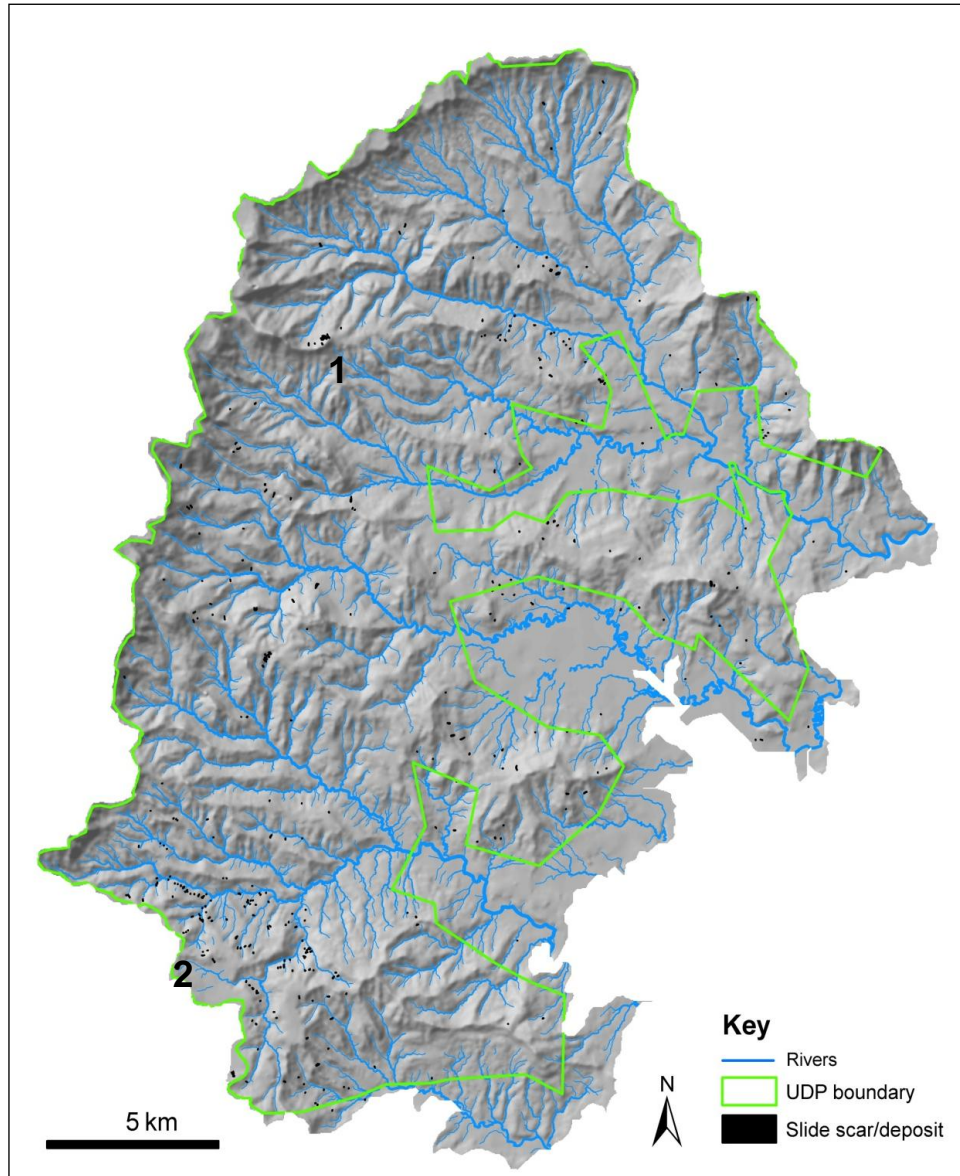


Figure 7.47 Distribution of slide scars with surficial deposits digitized from the 1: 50 000 orthophotos.

Surficial slides in the GCSF are not as long as incised flows, with lengths between 7m to 150m (average=38m) and widths between 2.85 to 67m wide (average=13m), and as a result are not as elongated (CR=0.5) (Table 7.29 and 7.30). A comparison of flows in California, USA, showed that flows which occurred on grassy slopes were more likely to travel further than flows occurring

on slopes covered with scrub (Gabet and Mudd, 2006). However, as the majority of slopes in the UDP are grass-covered, variations in runout length are likely to be more attributable to terrain conditions than vegetation or rainfall (Crozier, 2005). Gradient therefore, is expected to be an important variable for characterizing surficial flows, as these types of flows usually originate on slopes with relatively steep gradients, whilst deposition is associated with a sharp decrease in slope gradient (Harris and Gustafson, 1993; Crozier, 1996; Cannon et al., 2001).

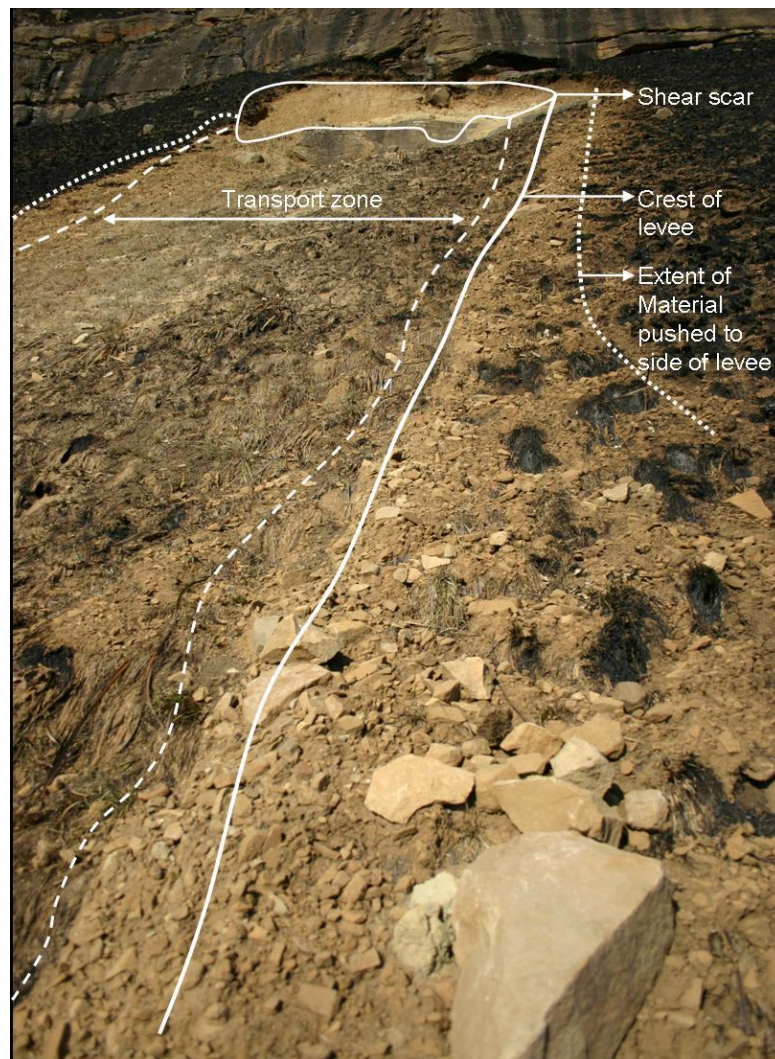


Figure 7.48 An example of a levee associated with the surficial flow at site G. larger material and vegetation has been pushed to the outer flank of the levee.

The lithology of the Drakensberg is horizontally bedded and the foothills are composed of a series of steps and terraces (Bordy et al., 2005). These lithological

terraces, which represent topographic breaks in the slope, act as flat zones or geomorphic barriers and slow the progression of surficial flows downslope (Guthrie and Evans, 2004) (Figure 7.49). The flows spread out across the slope and around rocks and vegetation forming a layer of silt to clay-sized material at the foot of the slope. Over a period of a few years, the deposit will be removed by surface wash and the vegetation along the track and under the deposit will recover relatively quickly. However, surficial flow deposits have been associated with boreal forest degradation in the United States, as the sediments on the depositional fans dry out to form a dense, hard layer with little void spaces which prevent oxygen from reaching the root stock (Harris and Gustafson, 1993).

Increased surficial flows have been noted in areas that experience regular fires in the USA (Cannon et al., 2001). The causality between burning and mud flows has been attributed to reduced evapo-transpiration and root decay which encourages increased soil moisture and these processes are expected to continue for a few years after the main fire events (Cannon et al., 2001). As discussed in the Methodology, it was not possible to relate the frequency and intensity of fires in the GCSF to mass movement as there are no temporal data for the mass movements, but as fires are an important component of grassland management, it may be of interest to explore this relationship in future.

The frequency distribution of the occurrence of surficial flows in relation to the eight variables and their associated class categories is presented in Figure 7.50. The variable with the highest frequency per class is distance to a footpath (>300m), so the variable is not included in further discussions. The variable with the next highest frequency is distance to a rock exposure (41% within 25m), followed by distance to a drainage line (38% within 25m). Mud flows in the USA have been observed to occur downslope of topographic lows, and in close proximity to low-order channels where surface flow has been concentrated (Cannon et al., 2001). A comparison of the locations of surficial flows in relation to digitized rock exposures is presented in Table 7.21.

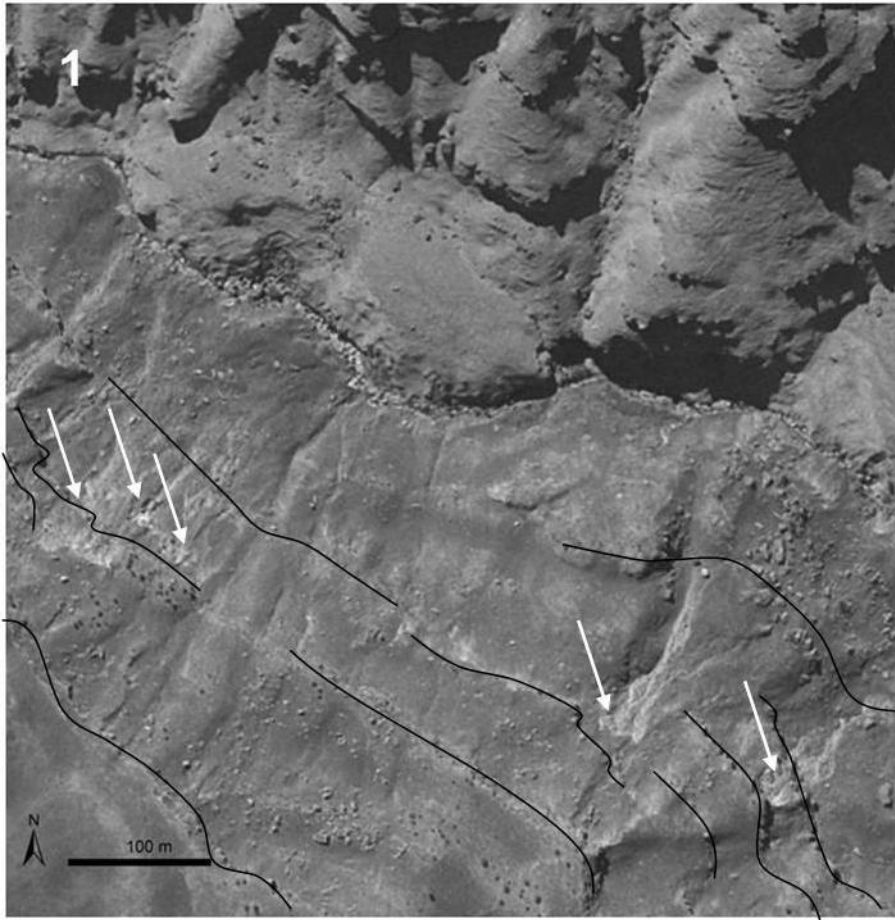


Figure 7.49 Aerial view of slide scars with surficial deposits (location of 1-2 is shown in Figure 7.47). Note how the slides generally occur below a rock exposure (black lines) and how the deposit flows onto the planation surfaces below.

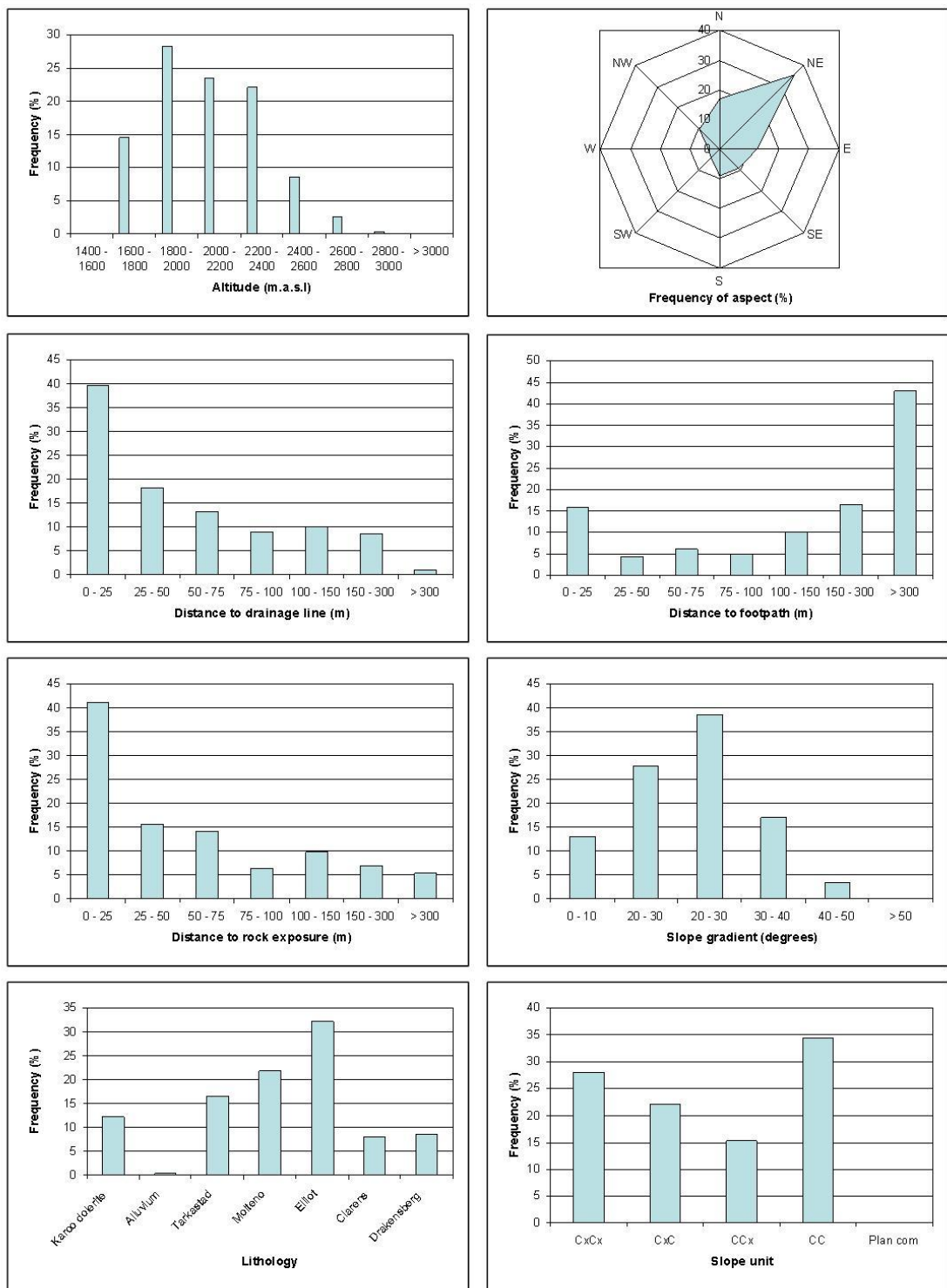


Figure 7.50 Histograms of the independent variables for surficial flows.

Only surficial flows within 10m of a rock exposure were selected and then classified according to whether the flow occurred upslope or downslope of a rock exposure or between two rock exposures. Almost 75% of surficial flows occur

downslope of a rock exposure (if the ‘between’ category is included), which confirms that rock exposures exert considerable influence on surficial flow development. Gradients between 20°-30° have the next highest frequencies followed by aspect (NE). These are the only types of slide scar mass movement features which are concentrated on north-, rather than south-facing slopes. Slope unit (CC) is the next variable in the hierarchy, followed by lithology (Elliot Formation) and altitude (1 800-2 000m a.s.l).

Location relative to rock exposure	Number (n=76)	Percentage (%)
Upslope	19	25
Between rock exposures	14	18
Downslope	43	57

Table 7.21 Comparison of the number of surficial scars in relation to rock exposures.

The highest InfoVal weights for aspect, gradient and slope unit reflect the same patterns as for the frequency distributions (Table 7.22). Aspect (NE) has the highest InfoVal making it the variable with the greatest weighting, followed by lithology (in this case the Molteno Formation rather than the Elliot Formation). The combination of Molteno Formation, north-facing slopes and gradients between 20°-30° based on the highest InfoVal, has been observed for the terrace category of mass movements (T3). Valley asymmetry in the Drakensberg has been attributed to variations in incoming solar radiation caused by slope aspect and variations in temperature have been used to explain differences in slope gradient between north- and south-facing slopes (Garland, 1979; Boelhouwers, 1998; 2003). It has been hypothesized that north-facing slopes are drier, have less dense vegetation cover, shallower soils and experience more chemical weathering.

Increased chemical weathering rates may also explain why surficial slides and terraces occur more frequently on north-facing slopes as these types of flows are

Variable	Class	Area (%)	Frequency (%)	InfoVal	Ratio (A/F)
Altitude	1400-1600	0.77	0.0	\$	0.00
	1600 - 1800	26.05	14.5	-0.583	0.56
	1800 - 2000	25.94	28.3	0.088	1.09
	2000 - 2200	19.51	23.6	0.192	1.21
	2200 - 2400	15.33	22.1	0.365	1.44
	2400 - 2600	6.46	8.6	0.283	1.33
	2600 - 2800	2.48	2.6	0.045	1.05
	2800 - 3000	2.41	0.3	-2.228	0.11
> 3000	1.05	0.0	\$	0.00	
Aspect	N (0 - 22.5)	7.08	8.6	0.191	1.21
	NE (22.5 - 67.5)	17.32	35.3	0.713	2.04
	E (67.5 - 112.5)	14.78	12.5	-0.170	0.84
	SE (112.5 - 157.5)	15.37	8.8	-0.554	0.57
	S (157.5 - 202.5)	15.51	9.1	-0.534	0.59
	SW (202.5 - 247.5)	11.83	4.2	-1.046	0.35
	W (247.5 - 292.5)	6.92	3.9	-0.574	0.56
	NW (292.5 - 337.5)	6.32	9.4	0.392	1.48
N (337.5 - 360)	4.86	8.3	0.536	1.71	
DistDrain	0 - 25	32.64	39.7	0.197	1.22
	25 - 50	14.78	18.2	0.207	1.23
	50 - 75	14.06	13.2	-0.059	0.94
	75 - 100	9.65	9.1	-0.059	0.94
	100 - 150	14.26	10.1	-0.342	0.71
	150 - 300	12.22	8.6	-0.355	0.70
> 300	2.39	1.0	-0.831	0.44	
DistFoot	0 - 25	14.27	15.8	0.105	1.11
	25 - 50	6.06	4.2	-0.377	0.69
	50 - 75	5.92	6.0	0.009	1.01
	75 - 100	4.39	4.9	0.117	1.12
	100 - 150	7.96	9.9	0.215	1.24
	150 - 300	14.58	16.4	0.116	1.12
> 300	46.83	42.9	-0.089	0.92	
Dist RockX	0 - 25	31.24	41.3	0.279	1.32
	25 - 50	11.56	15.6	0.299	1.35
	50 - 75	10.04	14.3	0.353	1.42
	75 - 100	6.47	6.5	0.004	1.00
	100 - 150	9.80	9.9	0.008	1.01
	150 - 300	13.51	7.0	-0.656	0.52
> 300	17.40	5.5	-1.160	0.31	
Gradient	0 - 10	31.95	13.0	-0.900	0.41
	10 - 20	28.45	27.8	-0.023	0.98
	20 - 30	25.04	38.7	0.436	1.55
	30 - 40	11.73	17.1	0.380	1.46
	40 - 50	2.56	3.4	0.278	1.32
	> 50	0.27	0.0	\$	0.00
Lithology	Karoo dolerite	19.86	12.2	-0.487	0.61
	Alluvium	2.30	0.5	-1.487	0.23
	Tarkastad	18.72	16.6	-0.119	0.89
	Molteno	13.40	21.8	0.487	1.63
	Elliot	22.37	32.2	0.364	1.44
	Clarens	10.42	8.1	-0.258	0.77
	Drakensberg	12.93	8.6	-0.411	0.66
SlopeUnit	CxCx	28.81	28.1	-0.027	0.97
	CxC	23.14	22.1	-0.047	0.95
	CCx	17.53	15.3	-0.134	0.87
	CC	30.50	34.5	0.125	1.13
	PlanCom	0.03	0.0	\$	0.00

Table 7.22 Comparison of the frequency distributions and InfoVal weights. Bold indicates highest value in category, colour indicates variable with greatest frequency.

characterized by high water contents. If chemical weathering predominates on north-facing slopes and the soils are thin and poor in organic content (Garland,1979), it is likely that relatively small amounts of rainfall would be required for soils to become saturated. Linked to this is the occurrence of surficial flows in close proximity to rock exposures, which would act as impermeable surfaces that concentrate precipitation and surface runoff, supplying soils immediately downslope with enough water to initiate failure. It is also worth noting that the Elliot and Molteno Formations have the highest percentage of area within 25m of a rock exposure (Table 7.9). The variable with the next highest InfoVal is altitude (2 200-2 400m a.s.l), followed by distance to a rock exposure (50-75m), distance to a drainage line (25-50m), then slope unit (CC). The CC category of slope unit is consistently selected for all of the slide mass movement types, which emphasizes the importance that topographic curvature has on slide development.

Hierarchical partitioning was undertaken to rank the variables according to their greatest independent contribution (%I) to the logistic regression model. A hierarchical partition was created for each iteration of random points and the resulting %I are presented in Figure 7.51. This is the second of the mass movement types which has two independent variables with a similar contribution, as gradient and distance to a rock exposure each account for an average of 37% of the model. Distance to a drainage line has the third highest independent contribution (8%), followed by distance to a footpath and aspect (both 5%). Altitude, lithology and slope unit contribute the remaining 8%.

The gradient class selected by the InfoVal with the highest weighting is 20°-30°, which is one category (10°) less than the gradient class selected for either the shear scars or incised flows and compares well with slope gradients observed in the literature. Gradients between 26° to 33° in the USA (Harris and Gustafson, 1993; Cannon et al., 2001; Gabet and Mudd, 2006) and average slope gradients of 28° in New Zealand (Crozier, 1996) and 25° in France (Malet et al., 2005) have been related to surficial flow activity. Lower slope gradients are probably related

to the occurrence of surficial flows on north-facing, rather than south-facing slopes.

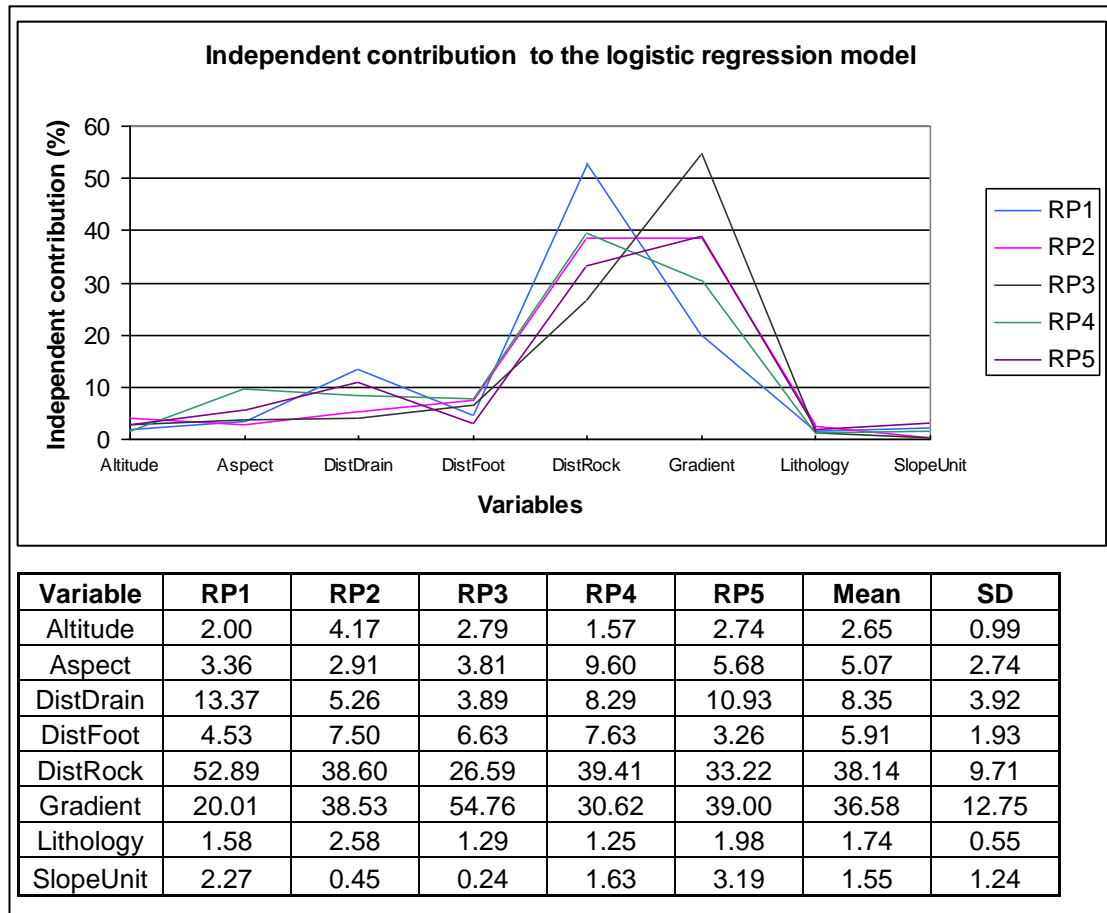


Figure 7.51 Graph representing the percentage contribution of each variable to the logit model. The table shows the mean and standard deviations for each contribution.

The distance to a rock exposure category selected by the InfoVal is 50-75m, which would suggest a statistical rather than geomorphic relationship. However, both of the surficial slides observed in the field (Sites G and H) occurred almost at the contact between a rock exposure and the slope colluvium. The scars appear to occur in mudstones of the Elliot Formation, which disintegrate into small, blocky fragments upon weathering (Groenewald, 1986). Contingency tables presented in section 7.3 show that distance to a rock exposure is related to altitude, gradient and lithology, which may therefore have influenced the selection of this variable. Lithology has been associated with an increased distribution of surficial flows, especially in thin colluvial soils developed from mudstones (Crozier, 1996) and

with lithological types which weather to plastic silts and clays (Guthrie and Evans, 2004). Recent studies on the mineralogical composition of Karoo volcanic rocks and sandstones suggest that mineralogy strongly influences the degree and type of weathering which will occur (Sumner et al., 2009).

Stepwise forward and backward logistic regression using all of the variables was used to develop a prediction model which could predict the maximum number of surficial flows using the smallest number of variables. Only aspect and gradient are selected by all of the models. Akaike's Information Criterion (AIC) and Bayes Information Criterion (BIC) are given in Table 7.23. The lowest AIC and BIC for the five iterations is for the Random Point 5 (RP5) dataset. Five independent variables are selected using the AIC, whilst 3 are selected using the BIC. The variables using the AIC are altitude, aspect, gradient, lithology and slope unit, whilst the variables selected by the BIC are aspect, gradient and lithology. RP5 is the only dataset to select three variables using the BIC, although this model combination only produces a marginally lower BIC value. RP5 also predicts the highest percentage of surficial flows.

Models	RP 1	RP2	RP3	RP4	RP5
Full AIC	957	971	944	943	901
Best AIC	946	957	927	938	893
Best AIC (excl DistFoot)	955	979	947	-	-
No Var	4	4	5	6	5
Variables	-	-	Altitude	Altitude	Altitude
	Aspect	Aspect	Aspect	Aspect	Aspect
	-	-	-	DistDrain	-
	DistFoot	DistFoot	DistFoot	-	-
	DistRock	DistRock	-	DistRock	-
	Gradient	Gradient	Gradient	Gradient	Gradient
	-	-	Lithology	Lithology	Lithology
	-	-	-	-	SlopeUnit
Best BIC	1014	1035	1000	1034	996
No Var	2	2	2	2	3
Variables	Aspect	Aspect	Aspect	Aspect	Aspect
	Gradient	Gradient	Gradient	Gradient	Gradient
	-	-	-	-	Lithology
%CorrPred	70.51	69.87	72.21	71.95	73.51

Table 7.23 The AIC, BIC and variables selected for each iteration. Note that the percentage of correctly predicted surficial slides is relatively similar for each model.

Distance to a footpath was selected by three of the logistic regression models, so these models were rerun and the footpath variable was excluded. Note that the AICs of the full models are lower when the footpath variable is included. However, the implications of including the distance variables can be seen in Table 7.24 which shows the percentage area for ranges of probability values. RP1, RP2 and RP3, which include the distance to footpath variable and RP4, which uses distance to a drainage line and distance to a rock exposure, predict almost 10% more of the study area as having >50% chance of developing surficial flows.

The InfoVal weights rank aspect, lithology and gradient in descending order, and hierarchical partitioning selects gradient as one of the largest independent variables, and this suggests that gradient strongly influences the distribution of surficial flows. It has been hypothesized that gentler gradients in the Drakensberg are associated with north-facing slopes which experience more chemical weathering (Garland, 1979; Boelhouwers, 1998; 2003), so it is possible that the translational slides which lead to surficial slides are generated by different processes to those that generate incised flows.

Probability maps were created in a GIS environment to spatially compare the predictive ability of each model (Figure 7.52-54). The values of the probability models were classified to reflect differences in the total area for a range of probability values (Table 7.24). The probability map produced by RP5 has a higher proportion of areas with low probabilities (73% of the area has <50% chance of developing surficial flows) and only 0.4% of the area has a high risk of developing surficial flows. Whilst RP3 and RP4 predict greater proportions of area as having a high risk (0.9-1.0), the results of the confusion matrix suggest that the model may be over-predicting. However, the relatively low standard deviations (<5%) confirm that differences in the models are the results of the randomly generated (Type=S0) dataset rather than the actual (Type=SC) dataset. About 33% of the study area is predicted to have >50% chance of developing surficial slides.

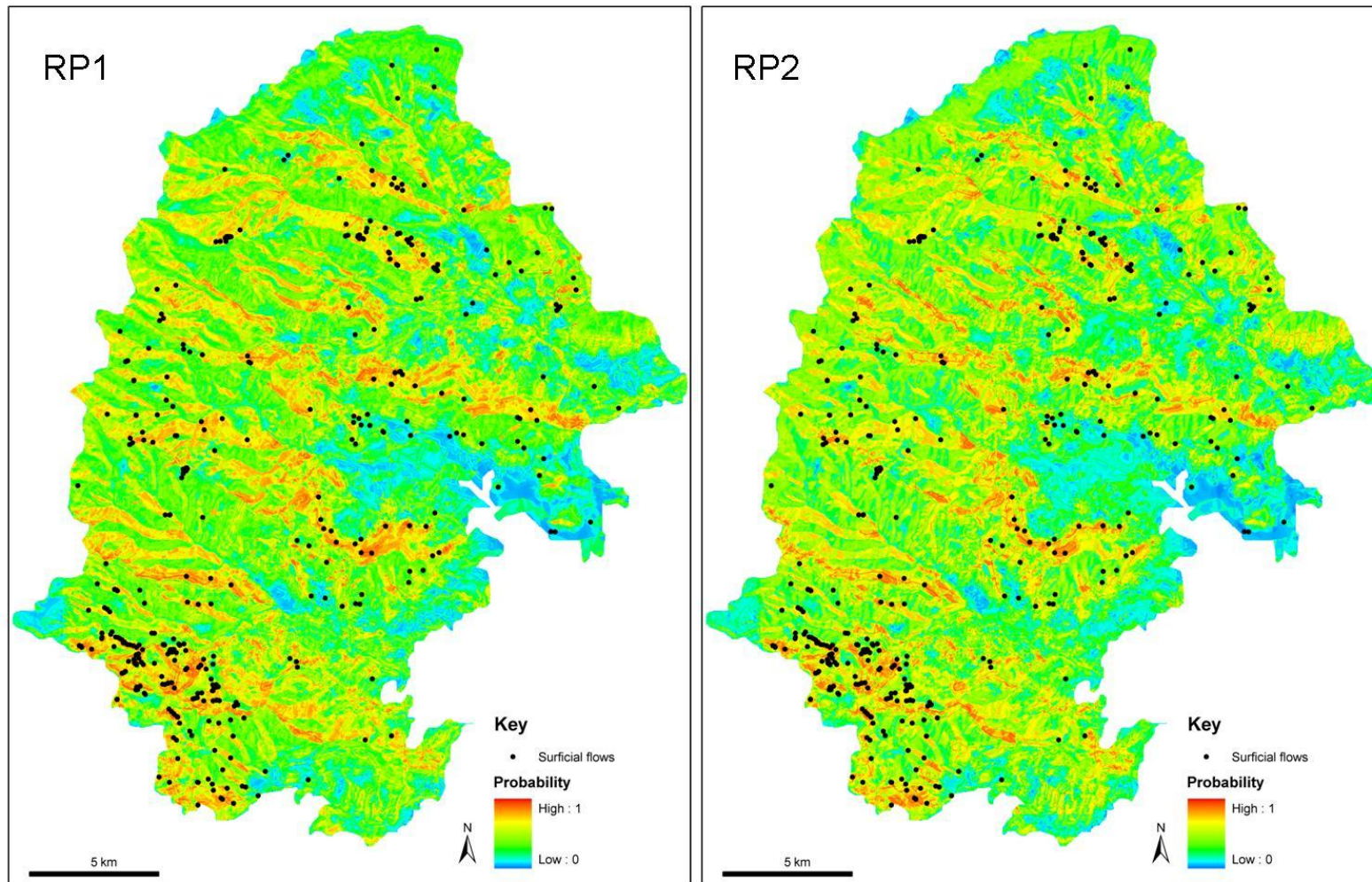


Figure 7.52 Prediction maps of surficial flows for the RP1 and RP2 datasets.

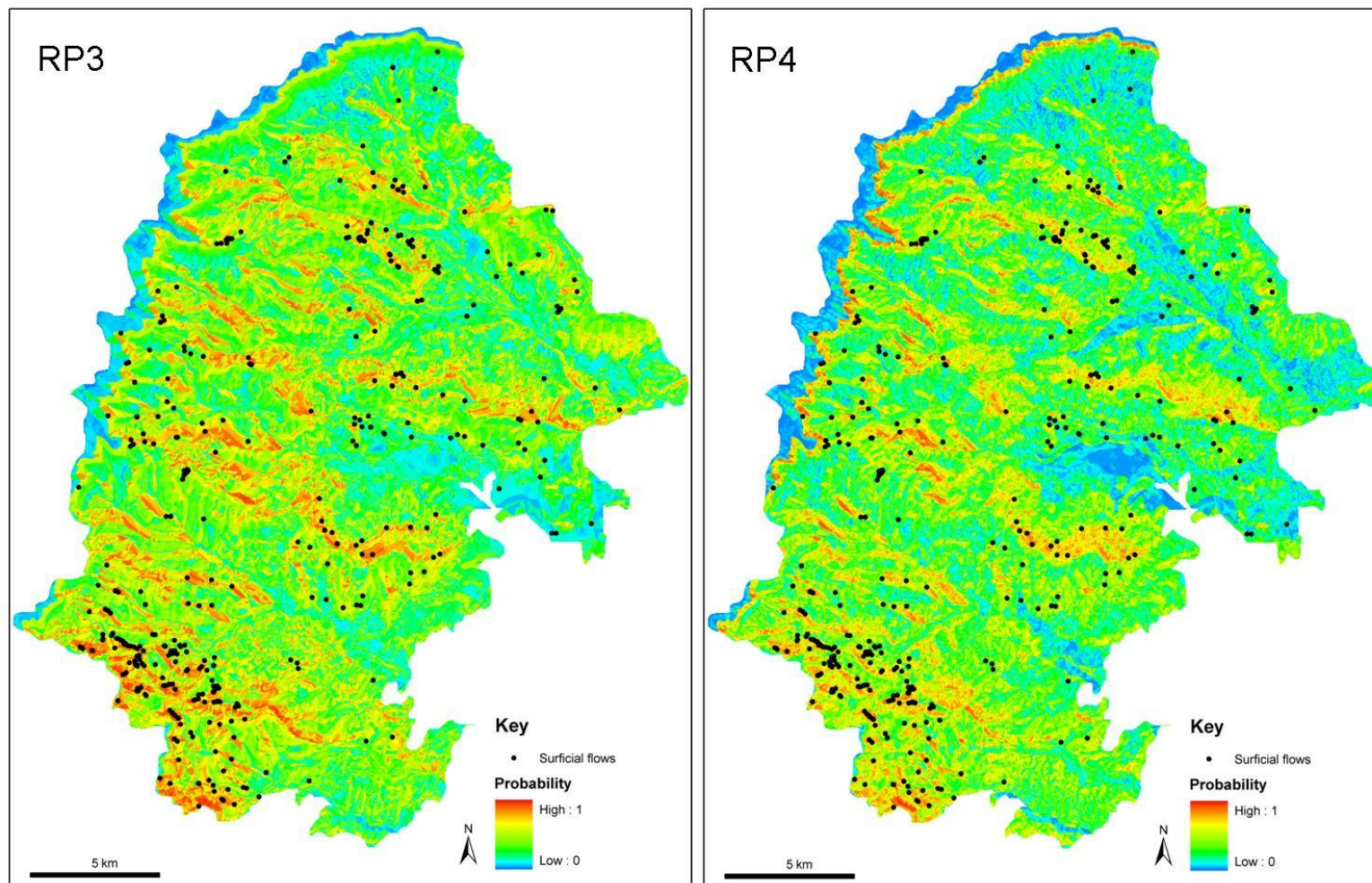


Figure 7.53 Prediction maps of surficial flows for the RP3 and RP4 datasets.

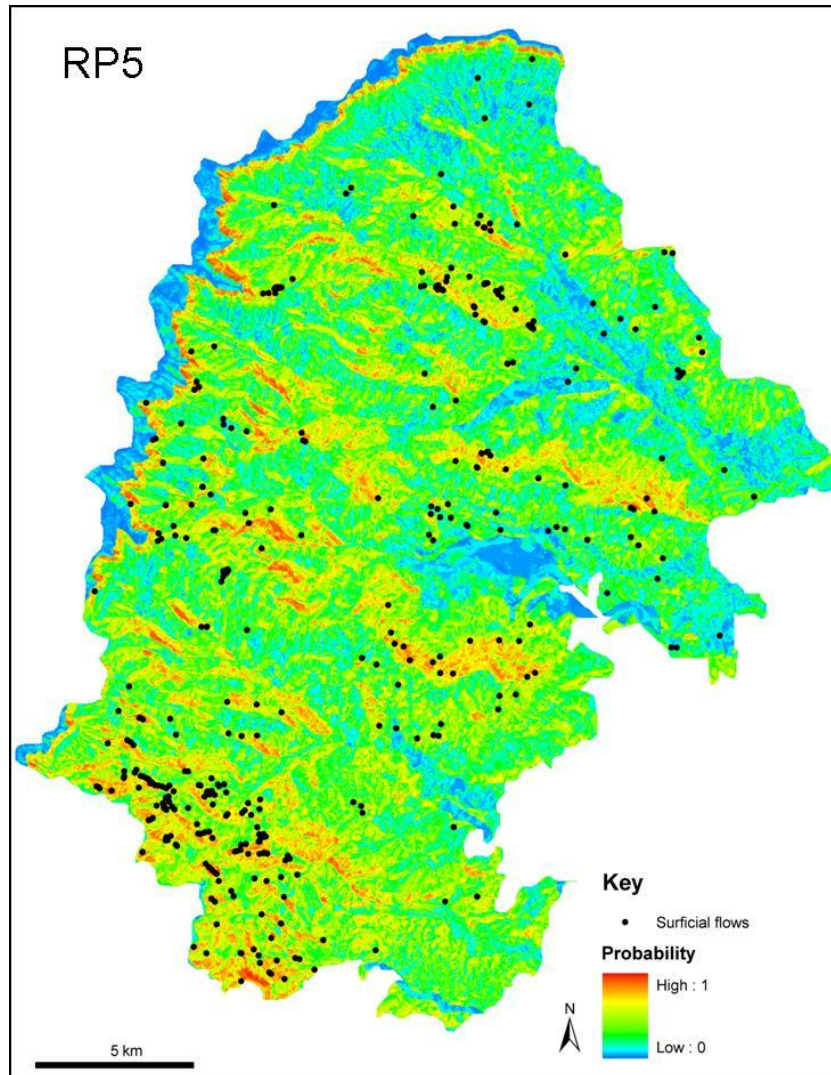


Figure 7.54 Prediction maps of surficial flows for the RP5 dataset.

Classification trees were produced using each of the five datasets and the tree with the highest percentage of correctly classified features was selected (Figure 7.56). The classification trees predicted between 79-86% of the actual events (Type=SC). All of the models use aspect as the first node with splits created between aspects that are predominantly north-facing (NW, N, NE) rather than south-facing. Three of the models selected gradient as the second node (RP2, RP3 and RP5), however all of these models proceeded to create random splits based on sub-groups of the classes selected by the second level node. The selection of aspect and gradient by the classification trees corresponds well with the use of both variables in the logistic regression models.

Probability	RP1			RP2			RP3			RP4			RP5			Mean	
	Area	%	SD	Area	%	SD	Area	%	SD	Area	%	SD	Area	%	SD	Area	%
0 - 0.5	303.2	65.8	0.8	302.1	65.6	1.0	302.8	65.7	0.9	296.9	64.4	1.8	338.5	73.5	4.6	308.7	67.0
0.5 - 0.6	44.8	9.7	0.9	55.8	12.1	0.8	55.7	12.1	0.8	49.9	10.8	0.1	46.2	10.0	0.7	50.5	11.0
0.6 - 0.7	47.6	10.3	0.5	53.8	11.7	1.4	39.0	8.5	0.8	45.6	9.9	0.2	36.2	7.9	1.3	44.4	9.6
0.7 - 0.8	48.6	10.5	1.9	33.0	7.2	0.5	35.8	7.8	0.1	38.4	8.3	0.3	25.3	5.5	1.7	36.2	7.9
0.8 - 0.9	15.8	3.4	0.4	13.9	3.0	0.7	23.4	5.1	0.8	25.7	5.6	1.1	12.8	2.8	0.8	18.3	4.0
0.9 - 1.00	0.9	0.2	0.3	2.2	0.5	0.1	4.1	0.9	0.2	4.3	0.9	0.3	1.8	0.4	0.1	2.6	0.6
> 0.5	157.7	34.1	4	158.7	34.5	3.5	158	34.4	2.7	163.9	35.5	2	122.3	26.6	4.6	152	33.1

Table 7.24 Total area (km² and percent) of probability values for each iteration of random points.

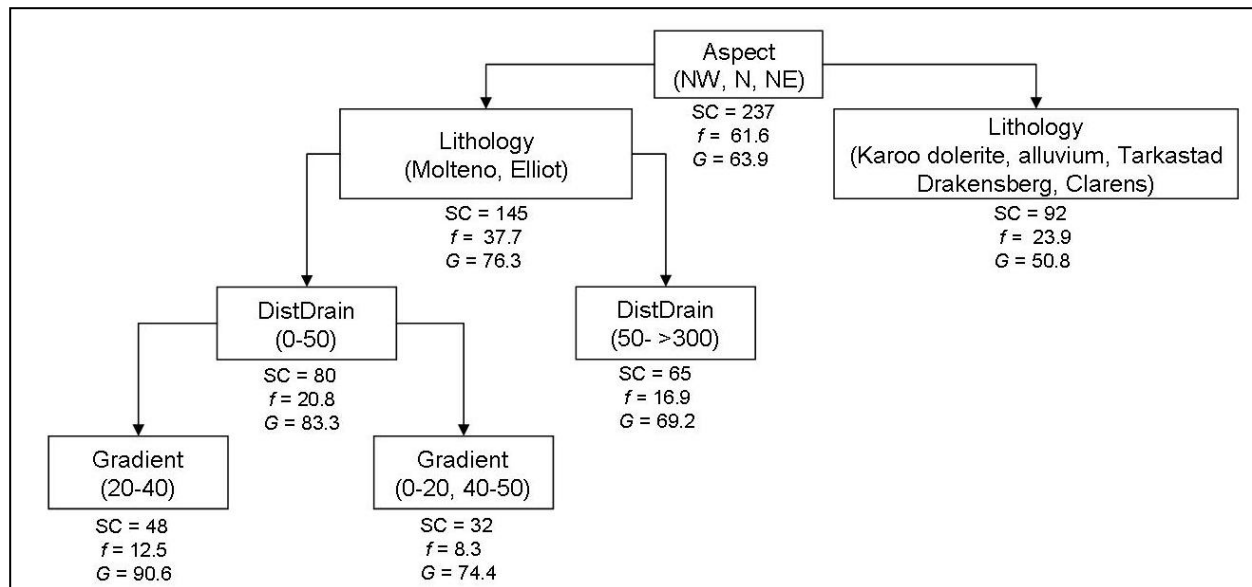


Figure 7.55 Summarized and pruned classification tree for surficial flows (f : frequency, G : Gini coefficient).

7.8 Shear-type 4: Sheet slides

This category of landform has been termed a sheet slide and almost always occurs in close proximity to solifluction lobe fields in the GCSF. Terms which have been used to describe slides within a solifluction landform are ‘stone banked sheets’ (Boelhouwers, 1994), ‘stony debris slides’ (Nyssen et al., 2003) and ‘shallow planar slides’ (Swanger and Marchant, 2007). The slides tend to modify the shape of the solifluction lobes, and mudslides in solifluction lobes have been observed in Germany (Chandler, 1972). The development of slides within solifluction lobes has been described as a successive process. As the lobes enlarge and reach a maximum size, constant downslope movement of the material on the tread causes over-steepening of the slowly advancing riser, which eventually leads to instability (Hugenholtz and Lewkowicz, 2002). A study on solifluction lobes in the Swiss Alps identified mudflow-affected solifluction lobes which occur when soils become supersaturated by meltwater from late-lying snow patches and fail (Matsuoka et al., 2005).

On the orthophotos the sheet slides appear as irregularly shaped surfaces composed of scree which are bare of vegetation. Inspection of oblique photographs of one of the solifluction lobe fields suggests that the sheet slides form depressions on the slope but it is not known whether the depressions represent a shear surface. The mean areal extents of the surfaces of the sheet slides are larger than any of the other slide-type mass movement features, and have widths of between 2 to 110m and lengths of between 17 to 198m (Table 7.29). The Circularity Ratio is 0.47, which suggests that the landforms are more elongated than circular (Table 7.30) and the slides tend to taper in the downslope direction (Figure 7.56). Sheet slides were not studied in the field and all observations are made using API. The API technique was relatively robust as indicated by a cross-check which was performed for the area shown in Figure 7.56 using oblique photographs provided by Prof. Stefan Grab at the University of the Witwatersrand. Two of the landforms originally digitized as sheet slides were consequently removed as the oblique photographs suggested that the landforms

were topographic hollows associated with drainage lines. This project has digitized 408 sheet slides from the orthophotos.

As the sheet slides occur almost exclusively within close proximity to a solifluction lobe field (Figure 7.57), it is assumed that the processes which caused the solifluction lobes are also responsible for the development of the sheet slides. Thus, sheet slides may represent an end-member of solifluction lobe forms as suggested by Hugenholtz and Lewkowicz (2002).

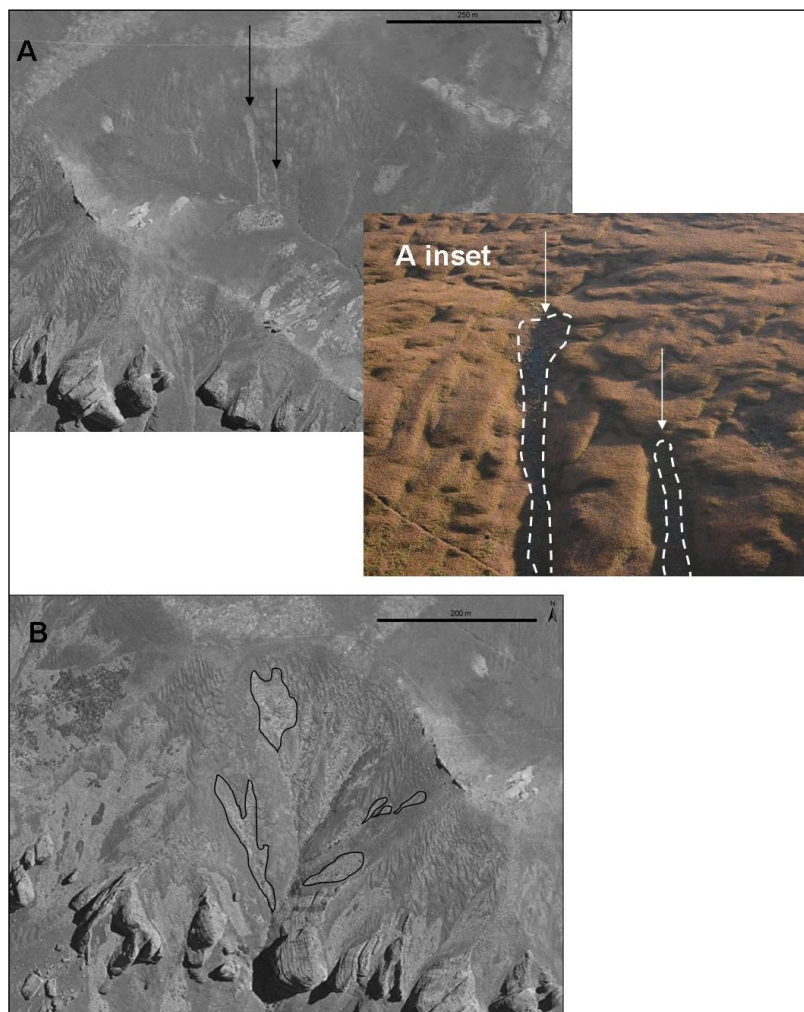


Figure 7.56 Aerial views of sheet slides within the solifluction lobe fields (locations of A and B are shown in Figure 7.57). A Inset-oblique photograph of two sheet slides, arrows indicate location in A.

The frequency distribution of the sheet slides in relation to the eight variables and their associated class categories is presented in Figure 7.58. Almost 94% of sheet

slides occur within Clarens Formation sandstones whilst 66% occur between 200-2 400m a.s.l. The distance to a footpath variable has the third highest frequency, with almost 64% of sheet slides occurring >300m from a footpath, so this variable is assumed to have no geomorphic influence on sheet slide development. Distance to a drainage line is the variable with the next highest frequency (52% in the 0-25m category), followed by gradient (30°-40°), aspect (south-facing), concave-concave slope units and finally, distance to a rock exposure (25-50m). The frequency distribution for the solifluction lobes also had the highest number of features in the Clarens Formation at altitudes between 200-2 400m a.s.l (Table 7.4). Ranking of the InfoVal weights places lithology (Clarens Formation) first, followed by altitude (2 400-2 600m a.s.l) and then gradient (30°-40°) (Table 7.25). The combination of altitude and lithology is expected as the InfoVal of the solifluction lobes also weighted these two variables highest, however the altitudinal range selected for sheet slides is 200m higher than for the solifluction lobes. Aspect (south-facing) is the third ranked variable for the solifluction lobes followed by gradient (30°-40), however the InfoVal rankings for the sheet slides are gradient followed by aspect (southwest-facing). This suggests that although sheet slides only occur in solifluction lobe fields, slightly different environmental factors may lead to sheet slide development.

Hierarchical partitioning was undertaken to rank the variables according to their greatest independent contribution (%I) to the logistic regression model. A hierarchical partition was created for each iteration of random points and the resulting %I are presented in Figure 7.59. Lithology has the highest independent contribution and accounts for an average of 51% (4.9 SD) of the model. Altitude is the variable with the second highest independent contribution (19%, 4.63 SD), followed by gradient (13%, 2.85 SD), distance to a drainage line (6%, 2.15 SD) and aspect (5%, 3.63 SD). The hierarchy of ranking of these first four variables is the same as for the solifluction lobes. The remaining variables are distance to a footpath (3%), rock exposure (1%) and slope unit (<1%), however the percentage contributions are minimal.

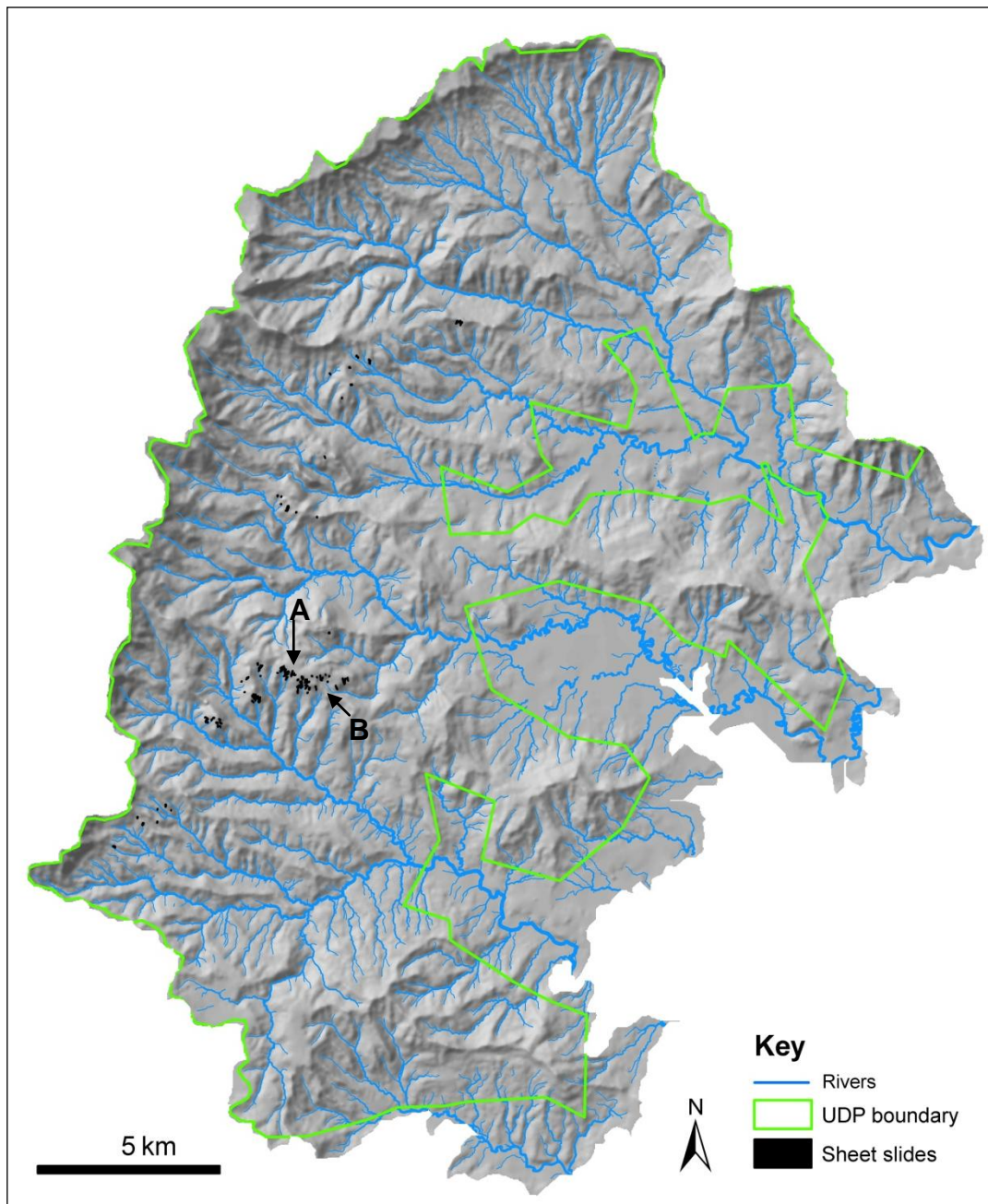


Figure 7.57 Distribution of sheet slides digitized from the 1:50 000 orthophotos. Distribution is confined to areas where solifluction occurs.

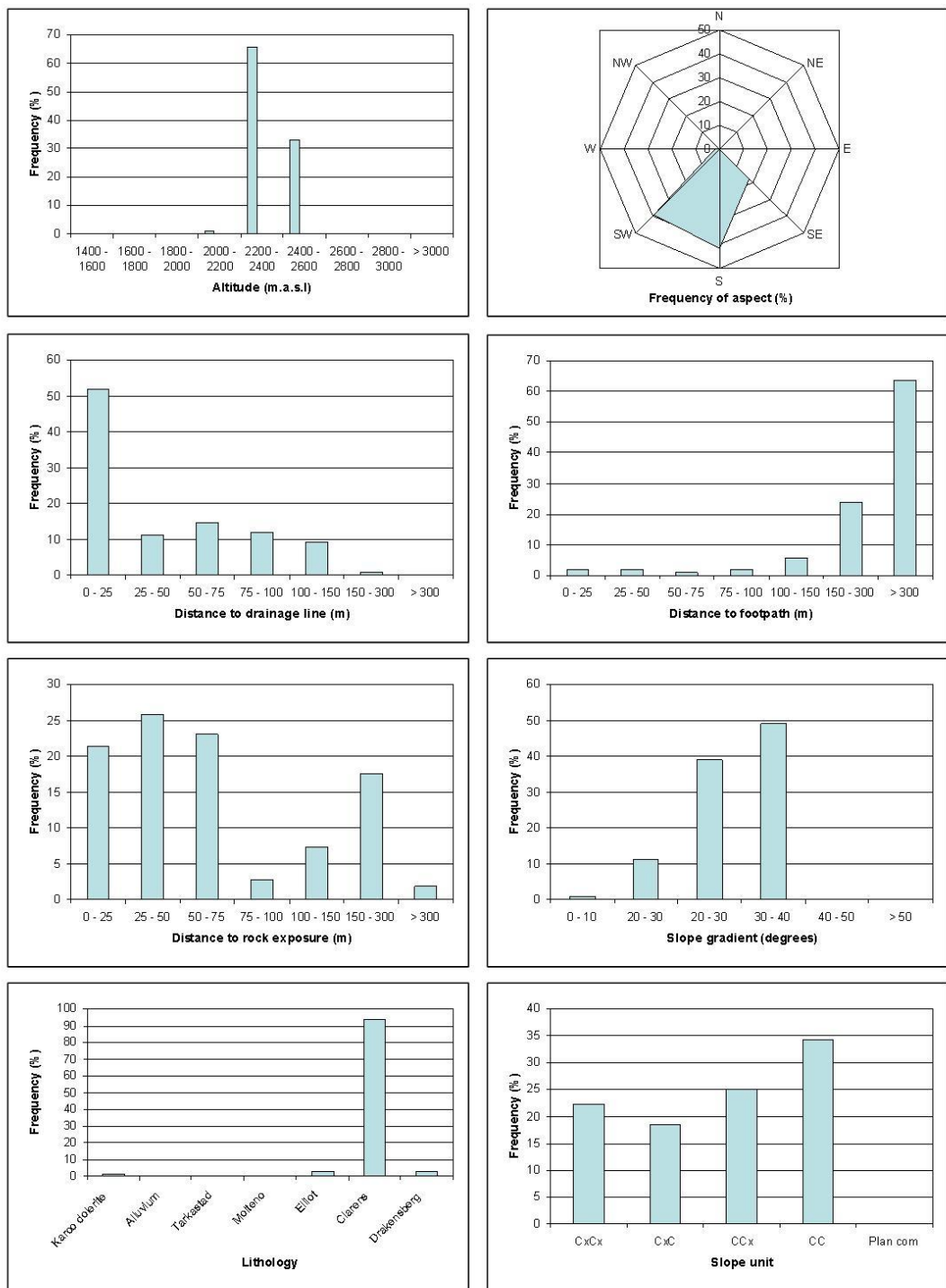


Figure 7.58 Histograms of the independent variables for sheet slides.

Variable	Class	Area (%)	Frequency (%)	InfoVal	Ratio (A/F)
Altitude	1400-1600	0.77	0.0	\$	0.00
	1600 - 1800	26.05	0.0	\$	0.00
	1800 - 2000	25.94	0.0	\$	0.00
	2000 - 2200	19.51	0.9	-3.048	0.05
	2200 - 2400	15.33	65.7	1.456	4.29
	2400 - 2600	6.46	33.3	1.642	5.16
	2600 - 2800	2.48	0.0	\$	0.00
	2800 - 3000	2.41	0.0	\$	0.00
> 3000	1.05	0.0	\$	0.00	
Aspect	N (0 - 22.5)	7.08	0.0	\$	0.00
	NE (22.5 - 67.5)	17.32	0.0	\$	0.00
	E (67.5 - 112.5)	14.78	0.0	\$	0.00
	SE (112.5 - 157.5)	15.37	17.6	0.135	1.14
	S (157.5 - 202.5)	15.51	41.7	0.988	2.69
	SW (202.5 - 247.5)	11.83	38.9	1.190	3.29
	W (247.5 - 292.5)	6.92	1.9	-1.318	0.27
	NW (292.5 - 337.5)	6.32	0.0	\$	0.00
N (337.5 - 360)	4.86	0.0	\$	0.00	
DistDrain	0 - 25	32.64	51.9	0.463	1.59
	25 - 50	14.78	11.1	-0.285	0.75
	50 - 75	14.06	14.8	0.052	1.05
	75 - 100	9.65	12.0	0.221	1.25
	100 - 150	14.26	9.3	-0.432	0.65
	150 - 300	12.22	0.9	-2.580	0.08
	> 300	2.39	0.0	\$	0.00
DistFoot	0 - 25	14.27	1.9	-2.042	0.13
	25 - 50	6.06	1.9	-1.185	0.31
	50 - 75	5.92	0.9	-1.856	0.16
	75 - 100	4.39	1.9	-0.863	0.42
	100 - 150	7.96	5.6	-0.360	0.70
	150 - 300	14.58	24.1	0.502	1.65
	> 300	46.83	63.9	0.311	1.36
Dist RockX	0 - 25	31.24	21.3	0.279	-0.38
	25 - 50	11.56	25.9	0.299	0.81
	50 - 75	10.04	23.1	0.353	0.84
	75 - 100	6.47	2.8	0.004	-0.85
	100 - 150	9.80	7.4	0.008	-0.28
	150 - 300	13.51	17.6	-0.656	0.26
	> 300	17.40	1.9	-1.160	-2.24
Gradient	0 - 10	31.95	0.9	-3.541	0.03
	10 - 20	28.45	11.1	-0.940	0.39
	20 - 30	25.04	38.9	0.440	1.55
	30 - 40	11.73	49.1	1.431	4.18
	40 - 50	2.56	0.0	\$	0.00
	> 50	0.27	0.0	\$	0.00
Lithology	Karoo dolerite	19.86	0.9	-3.066	0.05
	Alluvium	2.30	0.0	\$	0.00
	Tarkastad	18.72	0.0	\$	0.00
	Molteno	13.40	0.0	\$	0.00
	Elliot	22.37	2.8	-2.086	0.12
	Clarens	10.42	93.5	2.195	7.24
	Drakensberg	12.93	2.8	-1.538	0.27
SlopeUnit	CxCx	28.81	22.2	-0.260	0.77
	CxC	23.14	18.5	-0.223	0.80
	CCx	17.53	25.0	0.355	1.43
	CC	30.50	34.3	0.116	1.12
	PlanCom	0.03	0.0	\$	0.00

Table 7.25 Comparison of the frequency distributions and InfoVal weights. Bold indicates highest value in category, colour indicates variable with greatest frequency.

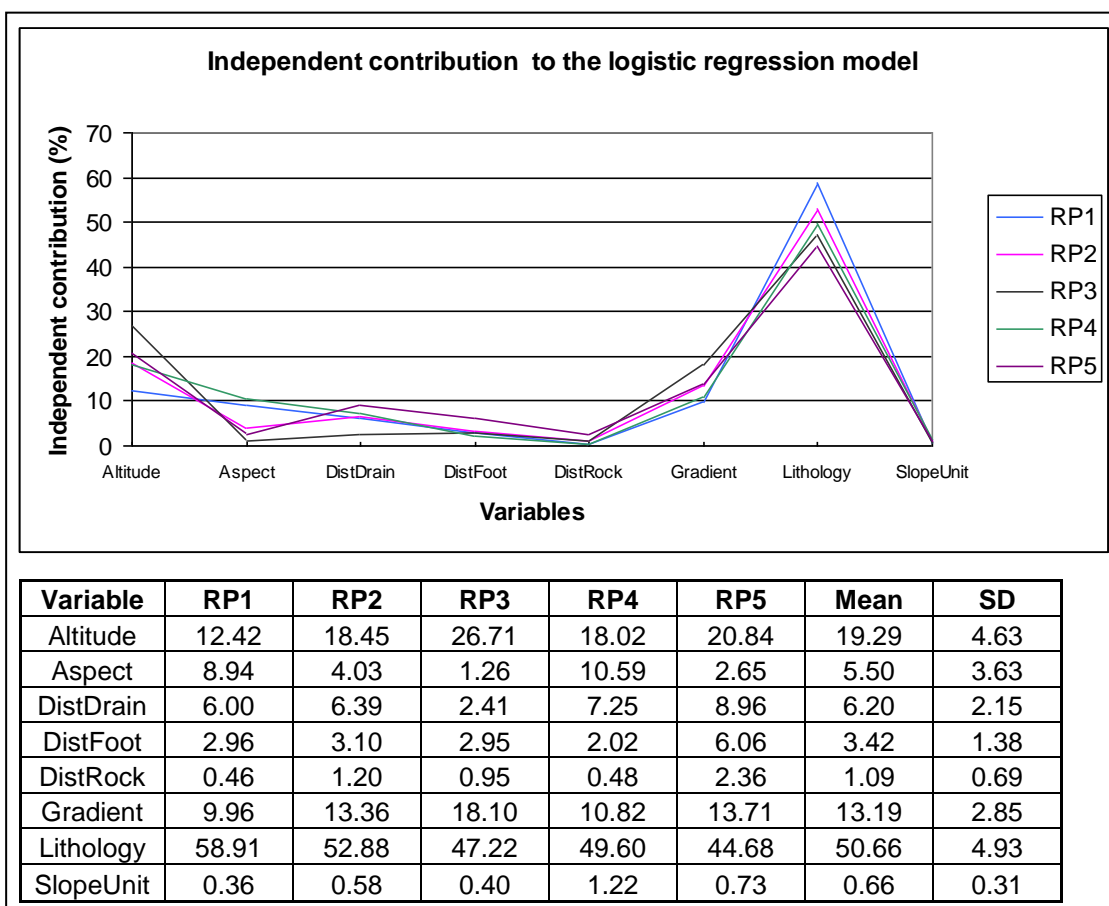


Figure 7.59 Graph representing the percentage contribution of each variable to the logit model. The table shows the mean and standard deviations for each contribution.

Stepwise forward and backward logistic regression using all of the variables was used to develop a prediction model. The AIC and BIC are given in Table 7.26. However, most of the models failed to converge so almost all of the variables had to be grouped in order to get at least one event (Type=SD) into a class. The lowest AIC and BIC for the five iterations is for the Random Point 2 (RP2) dataset. Five of the available eight variables were selected (distance to a footpath was not selected by any of the models). Lithology and aspect are the only variables selected by all of the models. The BIC models selected three variables for each model, although RP1 and RP2 use aspect whilst RP3, RP4 and RP5 use gradient. The RP2 model predicted almost 96% of the Type=SD events correctly.

Models	RP 1	RP2	RP3	RP4	RP5
Full AIC	121	99	126	104	112
Best AIC	102	79	106	90	103
No Var	4	5	4	5	5
Variables	Altitude	Altitude	-	-	-
	Aspect	Aspect	Aspect	Aspect	Aspect
	DistDrain	DistDrain	DistDrain	-	DistDrain
	-	-	-	-	DistRock
	-	Gradient	Gradient	Gradient	Gradient
	Lithology	Lithology	Lithology	Lithology	Lithology
				SlopeUnit	
Best BIC	128	105	131	112	126
No Var	3	3	3	3	3
Variables	Altitude	Altitude	-	-	
	Aspect	Aspect	Aspect	Aspect	Aspect
	-	-	Gradient	Gradient	Gradient
	Lithology	Lithology	Lithology	Lithology	Lithology
%CorrPred	93.51	95.83	93.98	93.98	93.51

Table 7.26 The AIC, BIC and variables selected for each iteration.

Probability maps were created in a GIS environment to spatially compare the predictive ability of each model (Figure 7.60-7.62). As the beta co-efficients produced by the models are different (given that different variables are selected per random iteration and that the classes are not always collapsed into the same groups), it is not surprising that the maps are varied in appearance. The probability maps for RP1, RP3 and RP5 show the pattern of the distance to drainage variable whilst RP4 shows the pattern of slope unit. RP2 shows the highest degree of separation of values between very low and very high, however this is masked in Table 7.27 because the probability values from 0 to 0.5 have been grouped.

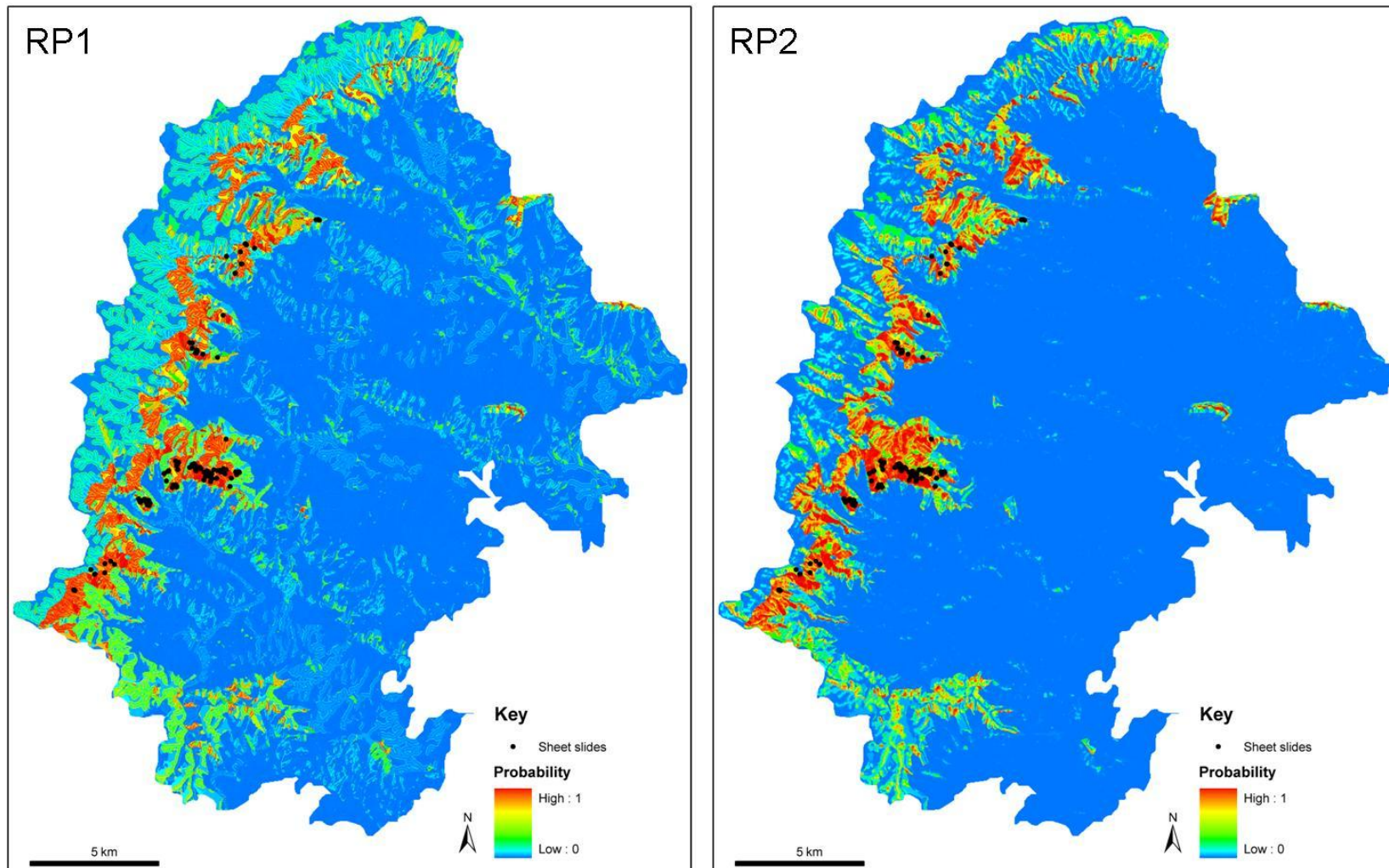


Figure 7.60 Probability maps for the random point 1 and random point 2 models.

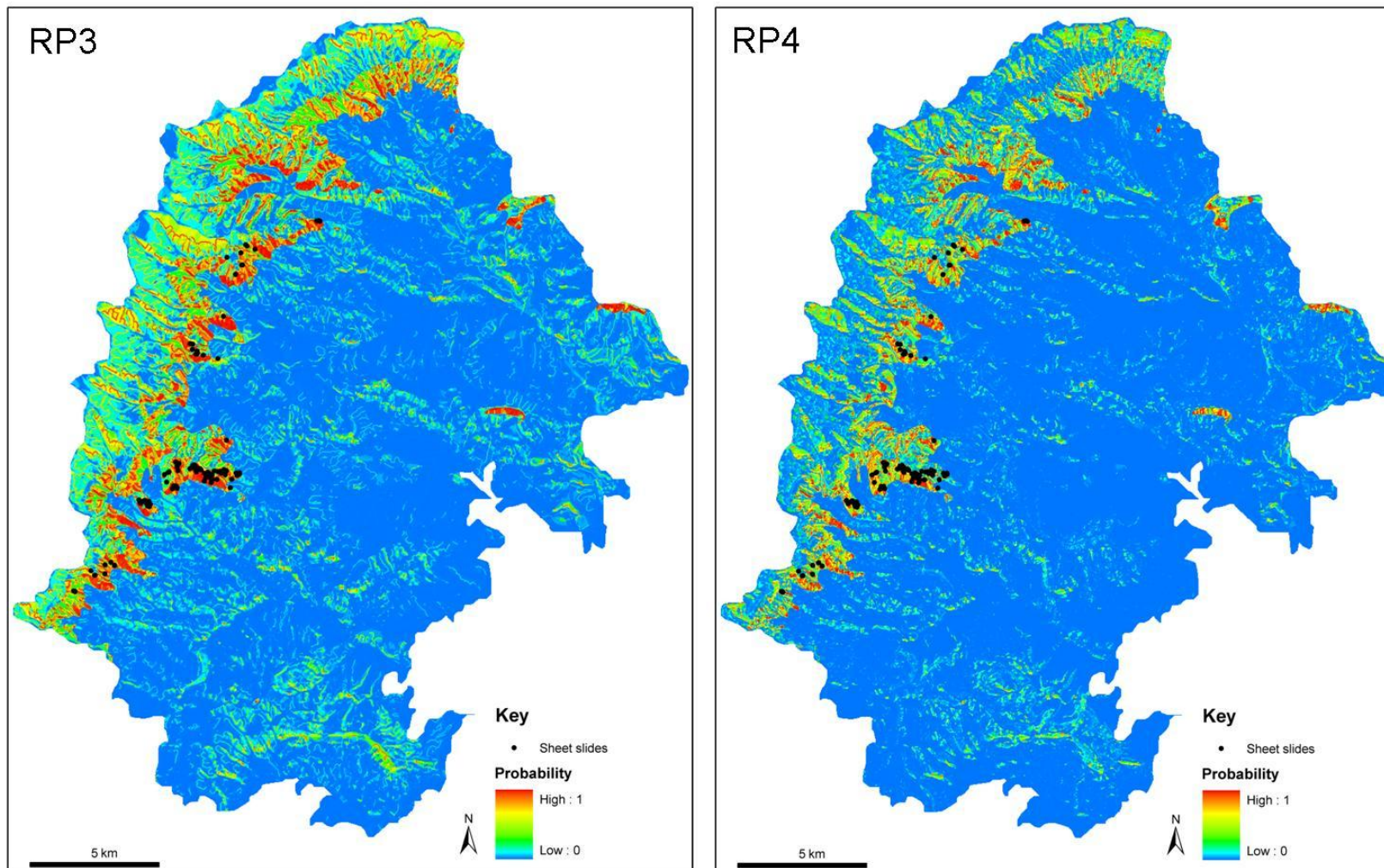


Figure 7.61 Probability maps for the random point 3 and random point 4 models.

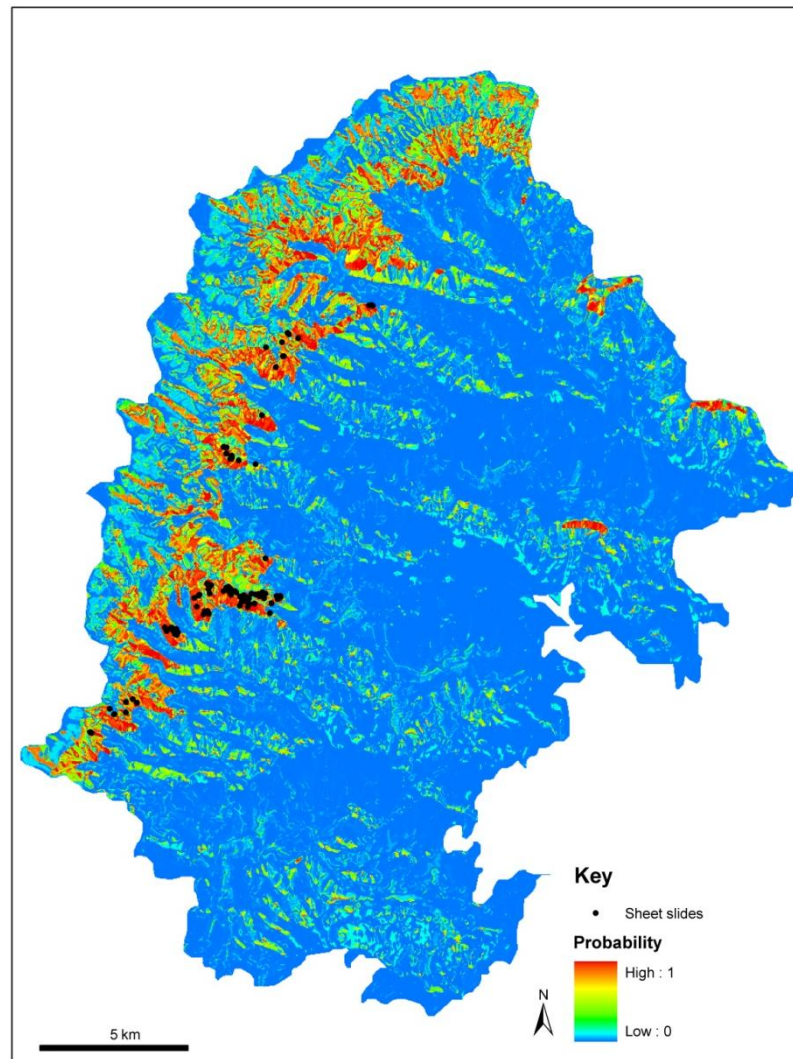


Figure 7.62 Probability maps for random point dataset 5.

The values of the probability function were classified to reflect differences in the total area for a range of probability values (Table 7.27). Although RP2 has the highest number of correctly predicted events of Type=SD, it does not have the highest proportion of probability values <0.5 or >0.9 . RP3 and RP5 predict the highest proportion of study area as having a very high probability (>0.9) However, if the number of cells having <0.1 probability for RP2 and RP4 (which has the highest proportion of area with a <0.5 probability) are compared, RP2 classifies almost 9% of the study area as very low, whilst RP4 classifies 6% as very low. This highlights how important it is for a model not to overfit the data. An average of 9% of the study area is likely to develop sheet slides.

Probability	RP1			RP2			RP3			RP4			RP5			Mean	
	Area	%	SD	Area	%	SD	Area	%	SD	Area	%	SD	Area	%	SD	Area	%
0 - 0.5	419.7	91.1	0.2	419.6	91.1	0.1	410.7	89.1	1.2	432.6	93.9	2.1	410.9	89.2	1.2	418.7	90.9
0.5 - 0.6	3.0	0.6	0.2	3.7	0.8	0.1	6.9	1.5	0.4	1.7	0.4	0.4	6.1	1.3	0.3	4.3	0.9
0.6 - 0.7	8.1	1.8	0.2	5.3	1.2	0.2	7.5	1.6	0.1	8.4	1.8	0.2	5.0	1.1	0.3	6.9	1.5
0.7 - 0.8	7.4	1.6	0.0	6.4	1.4	0.1	11.2	2.4	0.6	3.8	0.8	0.5	6.9	1.5	0.0	7.1	1.6
0.8 - 0.9	1.8	0.4	0.6	6.9	1.5	0.2	6.6	1.4	0.1	4.4	1.0	0.2	9.7	2.1	0.6	5.9	1.3
0.9 - 1.00	20.8	4.5	0.4	18.9	4.1	0.1	17.8	3.9	0.0	9.9	2.2	1.2	22.2	4.8	0.7	17.9	3.9
>0.5	41.1	8.9	1.4	41.2	9	0.7	50	10.8	1.2	28.2	6.2	2.5	49.9	10.8	1.9	42.1	9.2

Table 7.27 Total area (km² and percent) of probability values for each iteration of random points.

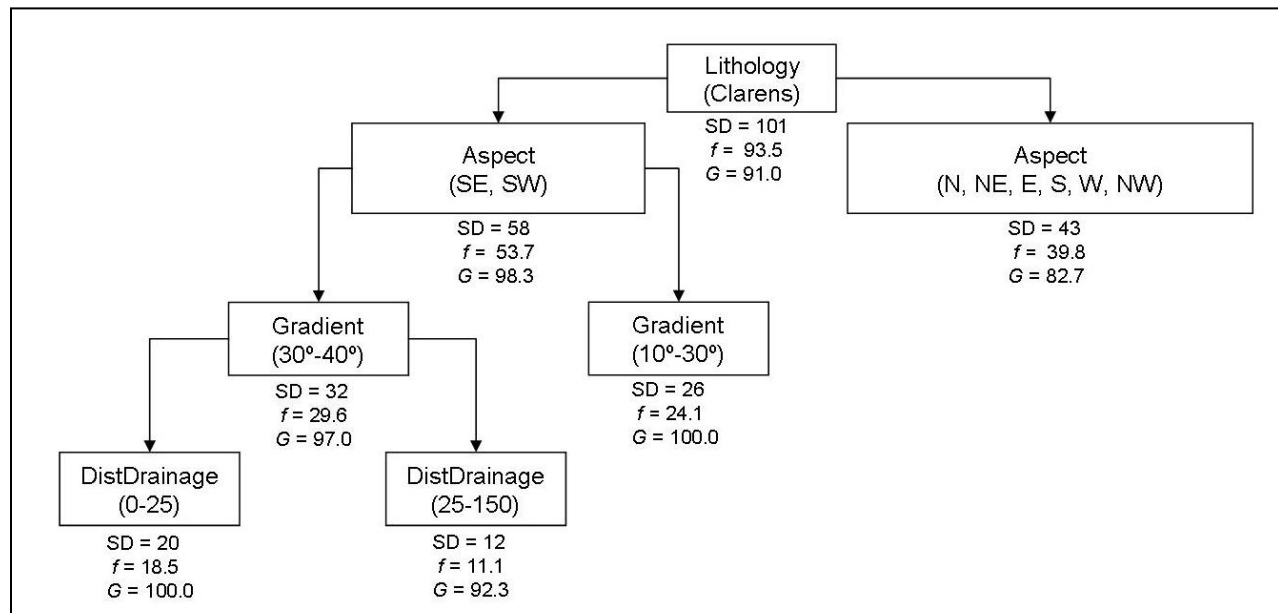


Figure 7.63 Summarized and pruned classification tree for sheet slides (*f*: frequency, *G*: Gini coefficient).

Classification trees were developed for each random iteration and confusion matrices for each tree were produced to compare the predictive ability of the models (Figure 7.63). The tree produced by the RP2 dataset had a success rate of almost 97% (minimum=RP4: 94%). All of the trees used lithology (Clarens) as the first node and four of the trees selected aspect as the second level node. The aspect class with the highest frequency is a combination of south, southeast and southwest. Gradient was selected as the third level node, with one group splitting at 30°-40° (29%) and the second at 10°-30° (24%). Distance to a drainage line is the fourth node and a logical separation was created with 195 of Type=SD events occurring within 25m of a drainage line and 11% occurring 25-150m from a drainage line. Kück and Lewis (2002) also noted that solifluction lobes occur in close proximity to drainage lines in the Eastern Cape Drakensberg. As the sheet slides create topographic depressions, it is not clear whether these landforms create drainage lines or if the sheet slides merely occur in close proximity to drainage lines which help create saturated soil conditions.

7.9 Comparison of the mass movement landforms observed in the GCSF

The techniques used to identify environmental variables which can be used to classify each of the mass movement types appear to be able to discriminate between most of the landforms. It should be noted however, that these variables are probably representative of conditioning rather than initiating mechanisms. Of the three terrace-type mass movements, terraces appear to be the most disparate. Whilst terracettes and solifluction lobes are visually very different, the variables which influence their development are relatively similar and are presented in Table 7.28., which compares the results of the frequency distributions, InfoVals and the hierarchical partitioning.

The variable with the highest independent contribution for terracettes is gradient and the highest InfoVal value for gradient is the 30°-40° category. Increased terracette

Frequency	Terracettes (T1)	Solifluction lobes (T2)	Terraces (T3)
Altitude	2 200-2 400m a.s.l	2 200-2 400m a.s.l	1 800-2 000m a.s.l
Aspect	Southeast	South	Northeast
Distance to a drainage line	0-25m	0-25m	0-25m
Distance to a footpath	>300m	>300m	>300m
Distance to a rock exposure	0-25m	0-25	0-25m
Gradient	20-30°	20-30°	10-20°
Lithology	Drakensberg	Clarens	Tarkastad
Slope unit	CxCx	CxCx	CxCx
InfoVal			
Altitude	2 400-2 600m a.s.l	2 200-2 400m a.s.l	1 800-2 000m a.s.l
Aspect	Southeast	South	Northwest
Distance to a drainage line	25-50m	25-50m	50-75m
Distance to a footpath	>300m	>300m	25-50m
Distance to a rock exposure	25-50m	25-50m	100-150m
Gradient	30-40°	30-40°	20-30°
Lithology	Drakensberg	Clarens	Molteno
Slope unit	CxCx	CCx	CxC
Hierarchical partitioning	Gradient (53%)	Lithology (47%)	Altitude (58%)
Area with >50% probability of	30%	17%	35%

Table 7.28 Comparison of the frequency distributions, InfoVal and hierarchical partitioning for the terrace-type mass movement features.

activity is also associated with the Drakensberg Group at altitudes between 2 400-2 600m a.s.l, however this does not suggest that terracette development is limited to these zones. Kück and Lewis (2002) observed high concentrations of terracettes on the slopes of the Drakensberg Group, so this finding compares well with others made in the Eastern Cape Drakensberg. It is possible that the terracettes are caused by processes related to free-thaw activity or by saturated soil conditions caused by an impermeable sub-surface horizon, as the terracettes are concentrated on southeast-facing slopes (Troll, 1944; Killick, 1963; Watson, 1988, Kück and Lewis, 2002). However, the occurrence of terracettes on convex-convex slopes which are associated

with drier, more stable soil conditions (Ayalew and Yamagishi, 2004), suggests that other processes may initiate movement. Bioturbation may be responsible for the initiation of terracettes, however Bielecki and Mueller (2002) concluded that terracettes in California, USA, were caused by mass movement processes rather than anthropogenic factors or grazing. Grazing animals tend to follow one another which rules out the development of multiple, stepped micro-relief which has been observed in the study area.

Lithology was selected as the variable with the biggest independent contribution for the solifluction lobes. According to the InfoVal, a large proportion of the solifluction lobe fields occur in the Clarens Formation sandstones. Studies on the weathering properties of the Clarens Formation suggests that the sandstones are susceptible to weathering, caused mainly by the alternation of wetting and drying, which forms platy material (Sumner et al., 2009). Matsuoka et al. (2005) note that such platy material is commonly associated with solifluction lobes in the Swiss Alps. Because the solifluction lobes have higher frequencies in the Clarens Formation, which occurs at lower altitudes in the southern Drakensberg, a lower class of altitude was selected for the solifluction lobes in comparison to the terracettes. Altitude is also related to the distribution of solifluction lobes, however, this is most probably due to the altitudinal zonation of the lithological layers than to climatic factors associated with altitude.

Terraces are the most environmentally different of the three terrace-type landforms. Terraces are the only type to occur predominantly on north-facing slopes, at lower altitudes and on gentler slope gradients. This may largely be due to the distribution of terraces on north-facing slopes which have been classified as longer, gentler slopes than their south-facing counterparts (Boelhouwers, 1988). Hierarchical partitioning selected altitude as the variable with the largest independent contribution, and the InfoVal selected the 1 800-2 000m a.s.l, which roughly corresponds to the altitudinal range of the Molteno Formation. A larger proportion of the study area is predicted as

being susceptible to terrace development than for either of the other terrace-type landforms, with solifluction lobes predicted to only affect 17% of the study area. The environmental variables associated with the terraces suggest that the area where terraces are likely to develop are most likely those that will be used by tourists as footpaths so this particular type of mass movement landform may be of interest to conservation managers in the UDP.

A comparison of the average widths, lengths and areas of the landforms is shown in Table 7.29. The morphometric attributes of the terrace-type landforms has not been discussed as the measurements are representative of the fields that the features occupy, rather than the landforms themselves. However, it is worth noting that the area occupied by solifluction lobes is much greater than the average area of terraced fields. A comparison of the Circularity Ratios in Table 7.30 highlights that the fields are generally the same shape, being more circular than elongated, however this may be an artifact of the digitizing rather than a true representation of form.

The results produced for the shear scars also suggest that environmental variables can be used to classify each type. The morphometric attributes of the shear scars show some variation in form, with sheet slides on average having the longest widths and slide scars the shortest, whilst incised flows have the longest lengths and slide scars have the shortest. Sheet slides have the greatest surface area of the shear scar landforms and a comparison of the Circularity Ratios shows how the landforms vary in shape. Incised flows have the highest frequency of landforms tending toward elongation, followed by sheet slides. The shear scars have the highest frequency tending towards circularity. This is most likely because once the displaced material has been eroded, all that remains is a circular shaped depression.

Terrace landforms	T1			T2			T3			Legend		
Statistic	ShAx	LoAx	Area	ShAx	LoAx	Area	ShAx	LoAx	Area	T1:	T2:	T3:
No. of observations	677	677	677	200	200	200	337	337	337	T1:	T2:	T3:
Minimum	13.81	19.28	0.197	15.66	22.25	0.335	7.89	15.71	0.135	SA:	SB:	SC:
Maximum	405.91	727.73	136.2	343.88	492.13	85.281	281.23	441.88	54.565	SD:		
Range	392.11	708.45	136.003	328.22	469.87	84.945	273.34	426.17	54.43			
1st Quartile	44.06	85.61	2.788	36.03	75.3	1.855	45.92	78.11	2.499			
Median	64.98	126.28	5.665	56.96	111.53	3.887	68.62	116.86	5.833			
3rd Quartile	100.47	203.08	12.81	90.5	173.76	10.373	95.29	172.45	11.217			
Mean	78.58	156.32	10.639	67.95	136.57	8.544	77.4	136.91	8.926			
Standard deviation (n)	50.03	105.08	14.216	46.31	89.77	12.25	46.45	81.39	9.546			
Skewness (Pearson)	1.91	1.87	3.753	1.99	1.46	3.379	1.43	1.14	2.133			
Kurtosis (Pearson)	5.63	5.1	20.772	6.5	2.22	14.725	2.57	1.2	5.132			
Lower bound on mean (95%)	74.8	148.39	9.565	61.48	124.02	6.832	72.41	128.18	7.902			
Upper bound on mean (95%)	82.36	164.26	11.712	74.42	149.12	10.256	82.38	145.65	9.951			
Slide/flow forms	SA			SB			SC			SD		
Statistic	ShAx	LoAx	Area	ShAx	LoAx	Area	ShAx	LoAx	Area	ShAx	LoAx	Area
No. of observations	1900	1900	1900	480	480	480	385	385	385	108	108	108
Minimum	2	5.75	0.012	3.27	7.79	0.018	2.85	7.49	0.024	2.4	16.97	0.059
Maximum	112.91	249.78	15.023	77.94	1518.44	27.881	67.26	150.14	4.291	110.04	198.3	9.808
Range	110.91	244.03	15.011	74.67	1510.65	27.862	64.41	142.65	4.266	107.64	181.33	9.748
1st Quartile	10.06	16.72	0.127	9.75	28.95	0.205	8.85	20.07	0.13	10.88	31.14	0.241
Median	12.76	21.96	0.205	13.49	43.68	0.339	11.95	28.74	0.221	15.75	46.18	0.429
3rd Quartile	16.33	29.78	0.318	19.01	67.76	0.677	15.53	47.88	0.412	24.46	85.83	0.974
Mean	13.94	25.5	0.292	15.79	58.3	0.645	13.29	38.04	0.371	19.52	60.3	0.825
Standard deviation (n)	6.84	15.73	0.595	9.02	77.63	1.423	7.07	26.55	0.483	13.78	39.19	1.142
Skewness (Pearson)	4.43	5.18	16.286	2.12	14.1	14.942	2.87	1.69	4.469	3.12	1.23	4.932
Kurtosis (Pearson)	42.61	51.46	330.99	7.32	258.24	277.588	13.86	2.91	25.615	15.88	0.86	33.544
Lower bound on mean (95%)	13.63	24.79	0.266	14.98	51.33	0.518	12.58	35.37	0.322	16.88	52.79	0.606
Upper bound on mean (95%)	14.25	26.21	0.319	16.6	65.27	0.773	14	40.7	0.419	22.16	67.81	1.044

Table 7.29 Length (km) and area statistics (km²) for each of the mass movement types. ShAx is the shortest axis of a bounding rectangle representing the polygon of the shape and LoAx is the longest axis of the same rectangle.

Hierarchical partitioning selected the distance to drainage variable as having the highest independent contribution to the prediction of shear scars (Table 7.31). The InfoVal category of the distance to a drainage line variable with the highest weighting is 0-25m, which implies that the variable may have a geomorphic effect on shear scar development. Table 7.32 shows the frequency of mass movement features that occur within 5m of a drainage line and their distribution according to Strahler stream order. Thirty-one percent of shear scars occur within 5m of a drainage line and the distribution of shear scars is relatively well dispersed across the various stream orders. The incised flow category has a far greater percentage of mass movement features within 5m of a drainage line and the majority (73%) occurs within 5m of a first order stream. This highlights that whilst more incised flows are associated with a drainage line, it is most likely because the incised flows become topographic hollows and act as channels for surface flow becoming first order drainage lines, whereas drainage lines, regardless of order, cause shear scar development. The most likely initiating mechanism is fluvial undercutting as observed at site I.

MM Type	0.2	0.4	0.6	0.8	1	Total	Average CR
1		50	179	299	149	677	0.657691
2		13	57	96	34	200	0.646779
3		15	76	150	96	337	0.691101
A	2	59	378	950	511	1900	0.695483
B	34	163	158	98	27	480	0.467539
C	15	77	126	124	43	385	0.549751
D	8	36	33	27	4	108	0.476069
Total	64	421	1029	1758	864	4136	

Table 7.30 Frequency of landforms with CR in range intervals of 0.2. The average Circularity Ratio is also given.

Hierarchical partitioning selected gradient as the variable with the single largest contribution for predicting shear scars with an incised flow track. The InfoVal with the highest weighting for gradient is 30°-40° and it is noteworthy that this class of gradient is given the largest weighting for all of the mass movement types besides terraces and surficial flows. It has already been noted that steep gradients are associated with incised flows as gradient provides the momentum for flow. Whilst gradient accounts for 31% of the model, distance to a drainage line

accounts for 25%, and the relationship between this variable and incised flows has been discussed previously. Higher frequencies of incised flows are associated with the Drakensberg Group basalts, which deteriorate when swelling clay minerals within the rock mass such as montmorillonite, expand. Changes in the volume of the minerals occur as soon as they are exposed to moisture and jointing and fissuring will cause an incremental increase in rock porosity, which ultimately results in failure (Sumner et al., 2009). It has already been observed that almost all of the landslides observed in the study area have a shear surface at the contact between the colluvium and underlying bedrock.

Frequency	Shear scars (SA)	Incised flows (SB)	Surficial flows (SC)	Sheet slides (SD)
Altitude	1 800-2 000m a.s.l	2 000-2 200m a.s.l	1 800-2 000m a.s.l	2 200-2 400m a.s.l
Aspect	South	South	Northeast	South
Distance to a drainage line	0-25m	0-25m	0-25m	0-25m
Distance to a footpath	>300m	>300m	>300m	>300m
Distance to a rock exposure	0-25m	0-25	0-25m	25-50m
Gradient	20-30°	20-30°	20-30°	30-40°
Lithology	Elliot	Drakensberg	Elliot	Clarens
Slope unit	CC	CC	CC	CC
InfoVal				
Altitude	2 200-2 400m a.s.l	2 400-2 600m a.s.l	2 200-2 400m a.s.l	2 400-2 600m a.s.l
Aspect	South	Southwest	Northeast	Southwest
Distance to a drainage line	0-25m	0-25m	50-75m	0-25m
Distance to a footpath	150-300m	>300m	25-50m	150-300m
Distance to a rock exposure	25-50m	25-50m	100-150m	50-75
Gradient	30-40°	30-40°	20-30°	30-40°
Lithology	Clarens	Drakensberg	Molteno	Clarens
Slope unit	CC	CC	CC	CCx
Hierarchical partitioning	DistDrain (42%)	Gradient (31%)	DistRock (38%)	Lithology (51%)
Area with >50% probability of occurrence	36%	29%	33%	9.2%

Table 7.31 Comparison of the frequency distributions, InfoVal and hierarchical partitioning for the shear-type mass movement features.

Hierarchical partitioning of the surficial flows selected distance to a rock exposure as the variable with the greatest independent contribution (38%) followed by gradient (32%). That gradient has an almost equal contribution to surficial flow distribution is not surprising given that it has been selected by the hierarchical partitioning for the previous two shear-scar types, however the range of gradient selected the 20°-30° rather than 30°-40° category. The surficial flow category is the only shear scar type to occur predominantly on north, rather than south-facing slopes. Field investigation of sites G and H showed that the shear scars of the surficial slides were relatively shallow and that the morphological form of the slide was related to the degree of liquefaction of the deposit. It may therefore be likely that surficial flows develop on relatively shallow soils which saturate and fail quicker than deeper colluvial mantles. However, this would need to be verified through further research.

Stream order (Strahler)	A		B		C	
	<i>n</i>	%	<i>n</i>	%	<i>n</i>	%
1	370	62.82	201	73.09	55	14.29
2	125	21.22	48	17.45	13	3.38
3	55	9.34	20	7.27	4	1.04
4	22	3.74	4	1.45	4	1.04
5	15	2.55	2	0.73	2	0.52
6	1	0.17	-		-	
7	1	0.17	-		-	
Total number of slides	1900		480		385	
Total number within 5m of a drainage line	589	31.00	275	57.29	78	20.26

Table 7.32 A comparison of the number of shear scars for each type which are within 5m of a drainage line and the percentage of those scars according to stream order.

Hierarchical partitioning selected lithology as the variable with the greatest independent contribution for sheet slides and the category of lithology with the highest InfoVal weight is Clarens Formation sandstones. The distribution of sheet slides is limited to areas affected by solifluction lobes, whose distribution is in turn affected by lithology and altitude and it is suggested that sheet slides represent an end-member of solifluction lobe development, rather than that sheet slides are a different type of shear scar mass movement landform (Soons and Price, 1990). Unfortunately the resolution of the orthophotos and the sampling

technique used were not suitable to undertake a detailed classification of the solifluction lobes, particularly to determine whether differences in gradient, slope unit, aspect and altitude influence the form of the solifluction lobes.

7.10 Rock movement deposits

Rockfalls are primary processes which determine the evolution of mountain slopes (Selby, 1982; Whalley, 1984; Antoniou and Lekkas, 2010). However, quantifying the incidence and geomorphological context of rockfalls is difficult (Menéndez Duarte and Marquínez, 2002). Integrated analysis of spatial, temporal and magnitude effects, together with a knowledge of rock mechanics is necessary to understand rockfall behaviour (Whalley, 1984). Traditionally, rockfall activity has been measured by gathering data from the clasts detached from cliffs, whilst rockfall modelling studies have focused on assessing the envelope of trajectories of displaced blocks, the maximum runout distance of rockfall deposits, the distribution of kinematic parameters along a fall path and the probability that blocks will stop at specific distances from a starting point (Agliardi and Crosta, 2003; Bigot et al., 2009). Modelling rockfall behaviour using clasts collected at a regional scale is a time- and resource-consuming activity which requires many samples collected across a large geographic area using specialist equipment over a long period of time, given the rate of rockfall activity in the area (Menéndez Duarte and Marquínez, 2002; Copons et al., 2009).

Some of the major problems associated with modeling rockfall behavior is that source areas are often not well known (Agliardi and Crosta, 2003) and that the behaviour of rockfall fragments is largely uncertain as most of the important parameters are difficult to measure (Frattini, et al., 2008; Straub and Schubert, 2008). The energy lost by blocks as they impact or roll downslope is a complex function of the morphology and geomechanical properties of the block, and of the surface roughness and contour of the slope. Additionally, rockfalls undergo lateral dispersion, which may further complicate modelling runout behaviour (Crosta and Agliardi, 2004).

This project has digitized 827 887 points representing the location of a rock or boulder and no attribute information was captured for the points, thus the points represent rocks and boulders of various sizes and orientations. This may influence the analyses of the results as smaller rockfalls, characterized by smaller rocks and shorter runout distances, may have a higher density of points than rockfalls consisting of large boulders. The points appear to be concentrated along rock exposures parallel to the contour of the slope, or along drainage lines, which act as topographic hollows (Figure 7.64).



Figure 7.64 Rockfall deposits in the GCSF. Rock movement types include toppling and falling.

The Average Nearest Neighbour (ANN) for the 827 292 digitised points using Euclidean distance is 0.499705 (z-score: -870.535016). An ANN value of less than 1 suggests that the data exhibit clustering and the z-score suggests that there is less than 1% likelihood that clustering is the result of random chance. It is therefore likely that the points are clustered in response to various environmental

variables. The average distance between each feature and its nearest neighbour (N=1) is 7.23 m.

The descriptive statistics for the quadrats are shown in Table 7.33. The largest quadrats (1000x1000m) have the smallest number of quadrats but the highest average deviation around the mean and the largest percentage of quadrats with a frequency greater than zero. The smallest quadrats (20x20m) have a small deviation from the mean but only 14% have a frequency greater than zero. This highlights that the frequency of events for larger quadrats is more variable, which results in the structure of the spatial pattern being lost. Using a smaller quadrat preserves the spatial pattern but disguises the intensity of the pattern. Density functions are therefore used to model intensity.

Size of quadrats (m)	1000	100	50	25	20
Number of quadrats	768	75048	301301	1200768	1875020
Mean	1077.20	11.02	2.75	0.69	0.44
Mean (excl zero values)	1634.96	25.63	8.77	4.36	2.43
Average deviation from mean	1290.55	15.04	4.01	1.53	0.59
Std Deviation	1878.18	23.94	6.59	1.91	1.30
Max	11180	249	75	29	19
Number of unique values	445	215	75	27	20
% of values >0	66	43	31	23	14

Table 7.33 Descriptive statistics of the quadrats

Figure 7.65 and 7.66 represent the values of the point and kernel density functions respectively, whilst Table 7.44 highlights that the summary statistics for each function are relatively similar. The analysis settings for the point and kernel density functions are the same (cell size: 25m; search neighbourhood: circular; search radius 100m) and were selected to show the effect of the quadratic kernel function which produces a density which better follows the spatial pattern of the point data. The point density function produces a more generalised density pattern which does not clearly differentiate between clusters.

	Kernel density	Point density
Cell size	25	25
Radius	100	100
Range	0 – 24 513	0 – 22 090
Mean	1 092	1 092
Std Deviation	2 325	2 240

Table 7.34: Summary statistics for the density values produced using the kernel and point density functions (number of events per square km)

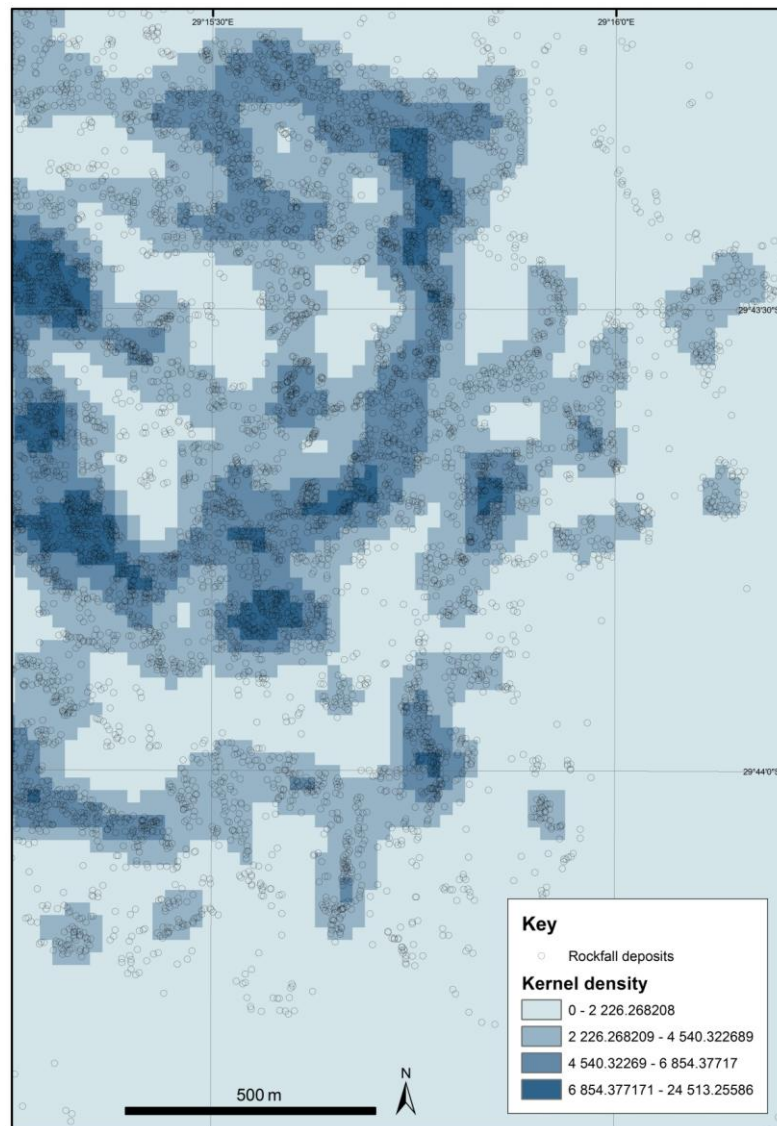


Figure 7.65 Kernel density. Density classified using the standard deviation.

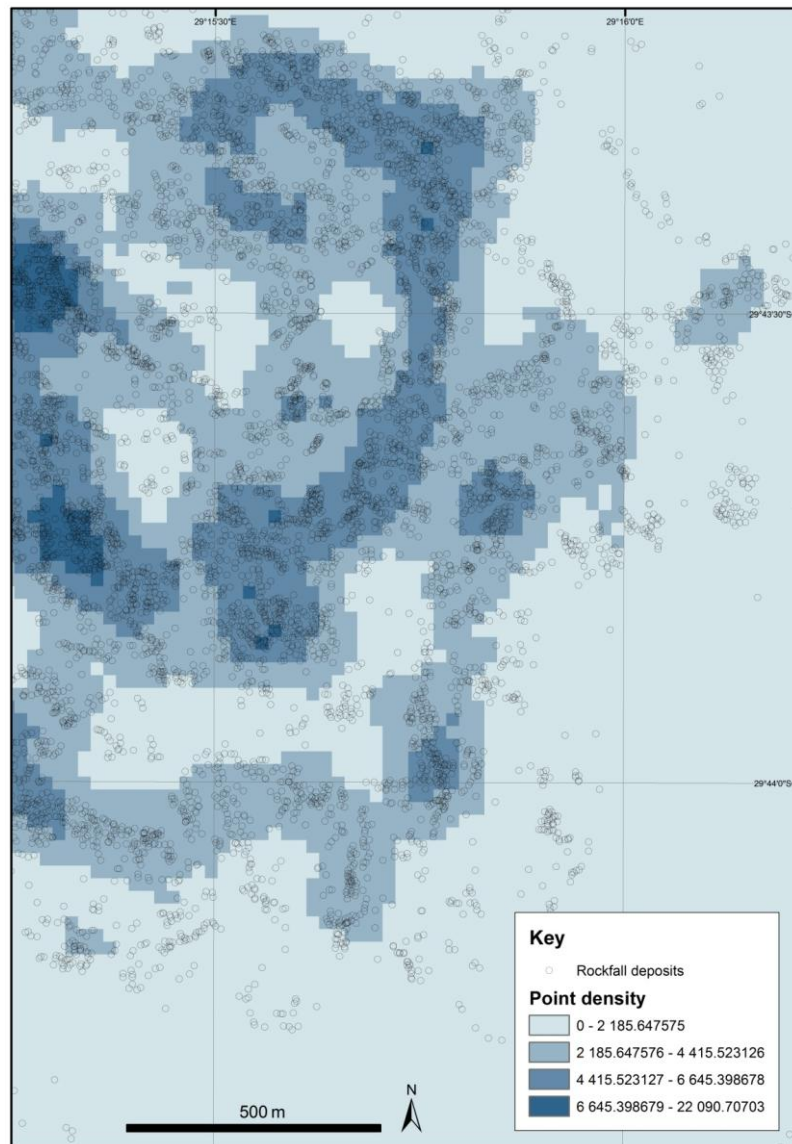


Figure 7.66 Point density. Density classified using the standard deviation.

A number of combinations of cell size and search radius were compared to test the effect that cell size and search radius has on delineating clusters. If the cell size is too large, the shape of the clusters is lost (Figure 7.67a), if the cell size is smaller, a more realistic cluster shape can be identified (Figure 7.67b). If the search radius is too large, clusters of events are aggregated and information is lost (Figure 7.68a), whereas the radius is too small, the resultant output becomes increasingly ‘noisy’ (Figure 7.69b). A change in grid resolution implies a change in the ‘scale’ of the model so that decreasing grid resolution results in a coarser description of the data (Agliardi and Crosta, 2003).

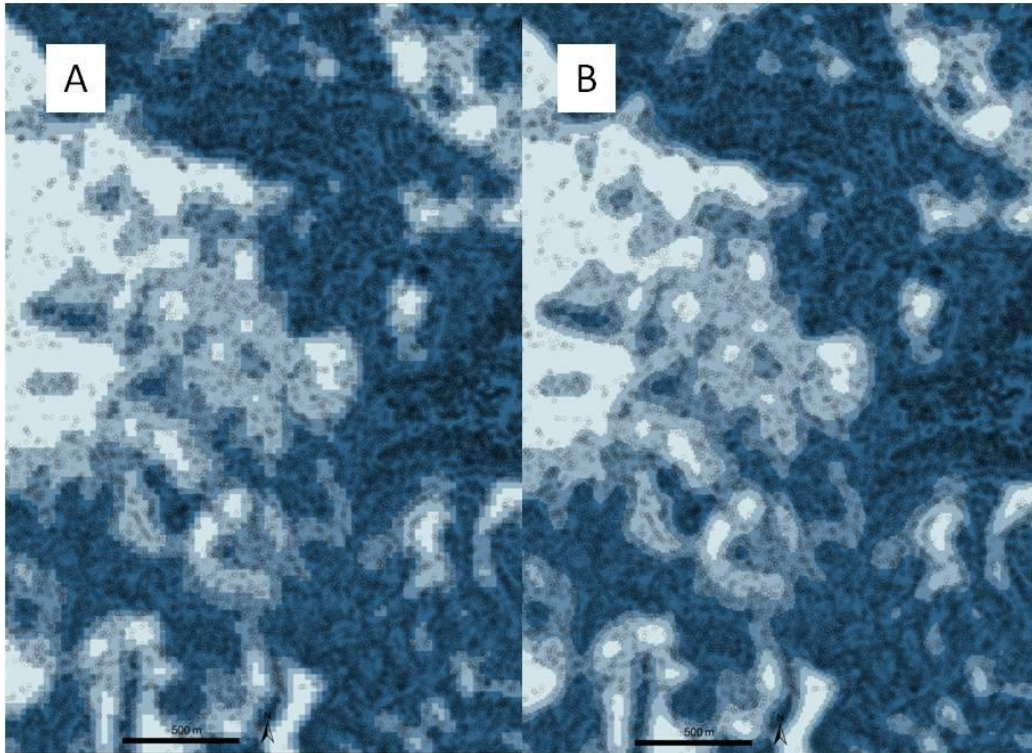


Figure 7.67: A comparison of the affect of cell size on the kernel density function, search radius is 100m. A: 25m, B: 10m

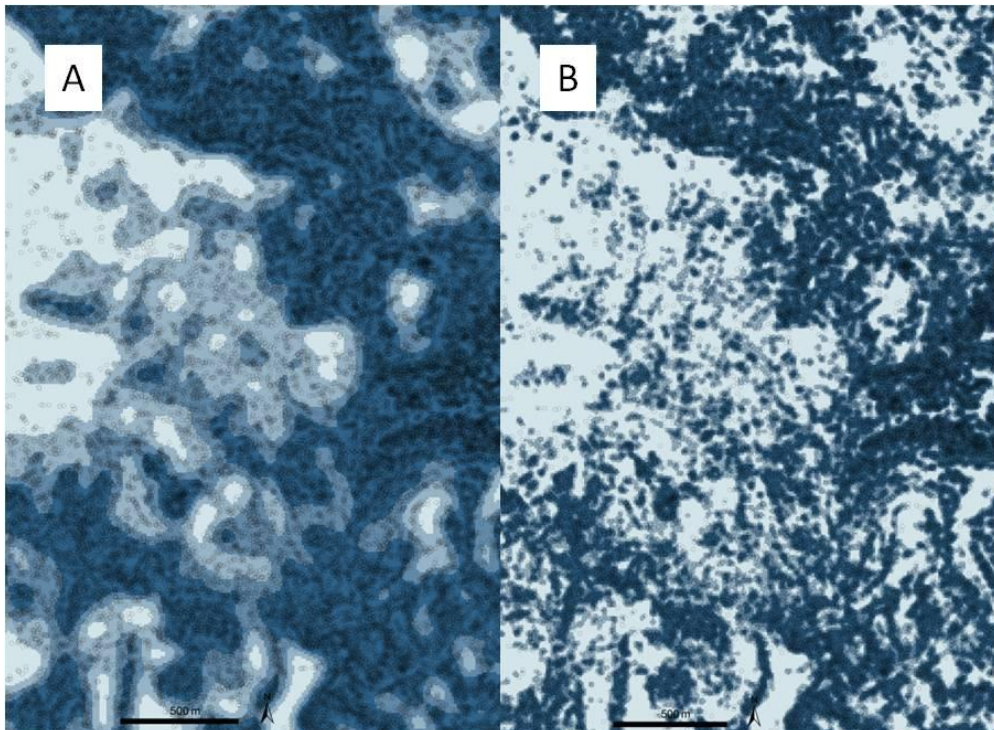


Figure 7.68: A comparison of the affect of the size of the search radius on the kernel density function, cell size is 10m. A: 100m, B: 25m

All further analyses were undertaken using a pixel size of 10m as the raster surface best represents the shape of the clusters. The density rasters generated using a search radius of 50m and 25m were converted to contours to determine which size search radius could identify clusters most effectively in terms of the number of points included in a class and the number and size of the delineated density categories. Initially, contours with intervals of 5000 events/km² were used and the highest category (25 000 – 40 000 events/km²) was selected and then converted to polygons. Descriptive statistics for the polygons are presented in Table 7.35. The number of points occurring in each polygon was also calculated using QGIS.

Although the number of polygons generated using the 25m search radius is much greater than that produced using the 50m radius, the average intensity of the points is the same. Using a smaller search radius does not appear to influence the average density of the points. However, as the main emphasis of this research is on identifying clusters from a point dataset with no marks, using a smaller search radius generates more, smaller, discrete high density areas.

Search radius	No of polygons (density > 25 000)	Average area (sq.m)	Min area (sq.m)	Max area (sq.m)	Mean no. points	Min no. points	Max no. points	Mean no points/ mean area
25m	451	526.06	< 1	8747.21	17	1	269	0.032
50m	33	1295.33	40	6224.32	41	1	196	0.032

Table 7.35: Descriptive statistics of the area and number of points associated with the highest density class created using two different search radii

A series of SQL queries were used to select contours at various intervals (5, 10, 15, 20, 25 x10³/km²) and convert the contour areas to polygons. The Point in Polygon tool was used to count the number of points occurring on each polygon and polygons containing zero points were deleted. Location-based SQL queries were then used to select which polygons contained a respective polygon at a higher level (ie. select from 20 000 contour shapefile those features that intersect with selected features in 25 000 contour shapefile) in order to identify the polygons with the highest density and the associated contours at lower densities.

Quantifying the number of points within each density class provides a useful indication of the exponential increase in the number of points associated with each class (Figure 7.69), however using the density classes to identify individual events is problematic. Firstly, the kernel function is cumulative which smoothes areas of less dense points. Thus the edges of a cluster will have the same density value as individual events in close proximity, and are consequently difficult to determine. Secondly, highly clustered points that are isolated, have lower density values than slightly less clustered points which are in close proximity to one another. It would therefore be incorrect to use the highest density category to identify clusters, as isolated clusters are excluded at this level. At lower density values, more isolated clusters are identified but at the cost of high density clusters in close proximity to one another being grouped into one unit. Figure 7.70A shows the grouping of high density clusters in close proximity to one another and the effect that using a lower density has on delineating events in the same category, are indicated in Figure 7.70B.

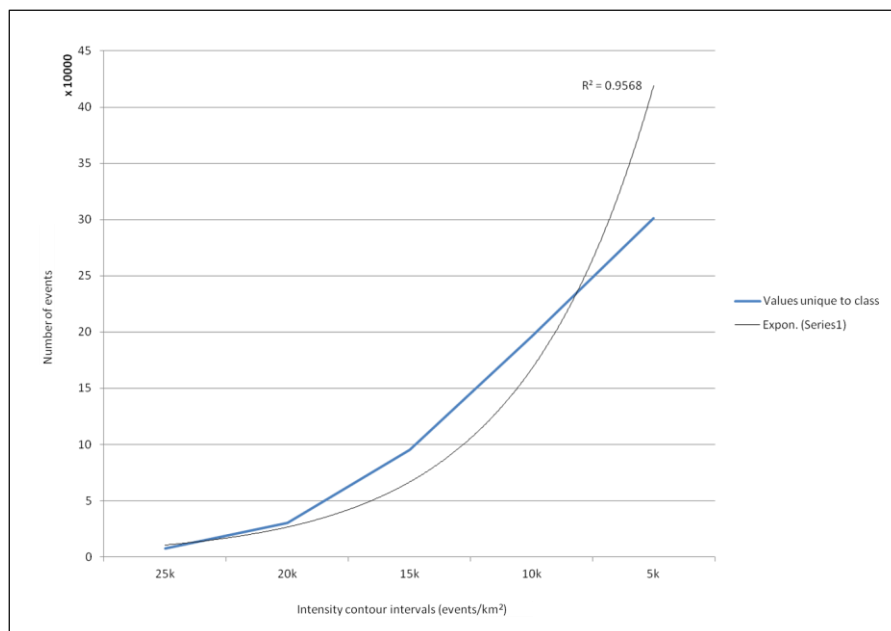


Figure 7.69 Exponential increase in the number of points which are unique to the class interval in which they occur.

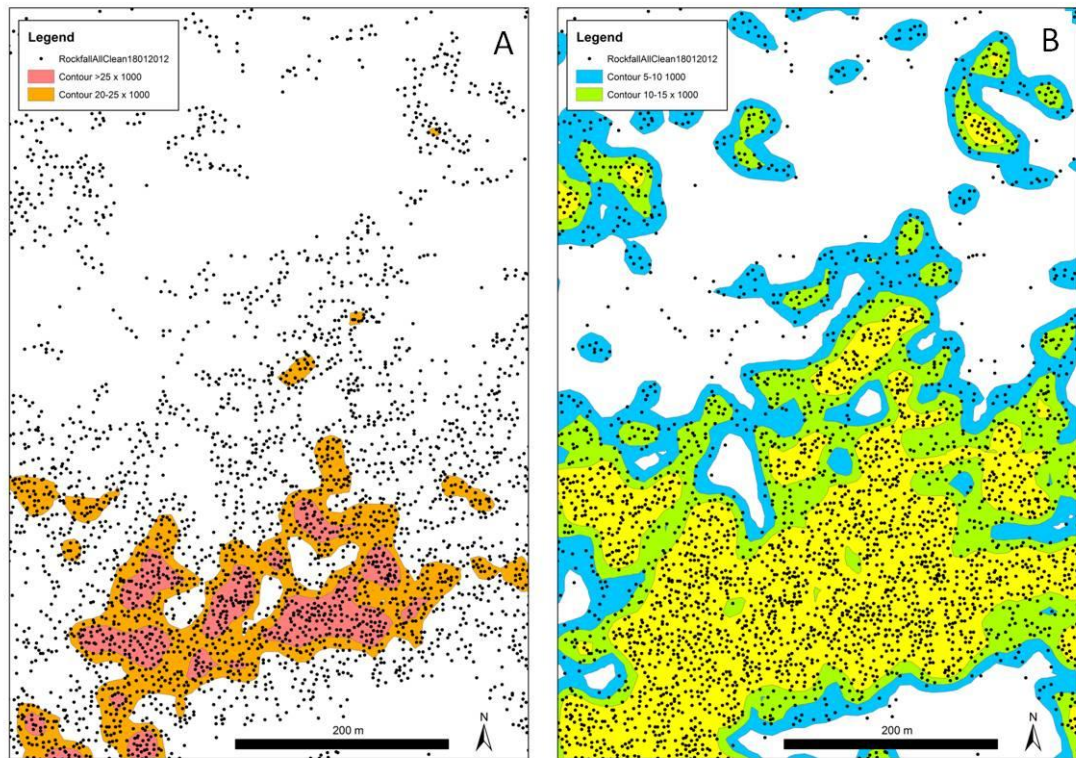


Figure 7.70 A comparison of the polygons created from the kernel density function. **Figure A:** contour intervals of higher density, **B:** contour intervals of lower density.

The Hot Spot Analysis tool calculates the Getis-Ord G_i^* statistic for each feature in a dataset. The resultant z-scores and p-values indicate where features with either high or low values cluster spatially. A statistically significant hot spot is calculated by proportionally comparing the local sum for a feature and its neighbours to the sum of all features. A hotspot is therefore a feature that has a high value and is surrounded by other features with high values as well (ESRI, 2011). The Hot Spot Analysis tool was used to determine whether the existing cluster analysis tool within ArcGIS could identify clusters at all levels. Figure 7.71 highlights that the output of the Getis-Ord G_i^* produces a very similar output to that achieved using the kernel density contours (contour interval of greater than and equal to 5 000 events per km^2).

The Cluster and Outlier Analysis tool identifies spatial clusters of features with attribute values similar in magnitude. As with the Hot Spot Analysis tool, the number of events in a grid cell was used as the attribute data. The tool calculates a

local Moran's I value, a z-score, a p-value, and a code representing the cluster type for each feature and the z-scores and p-values represent the statistical significance of the computed index values (ESRI, 2011). Figure 7.72 illustrates how the local Moran's I statistic is able to identify clusters statistically significant clusters of high values (HH), resulting in the same 'grouping' effect as the kernel density and hot spot analyses.

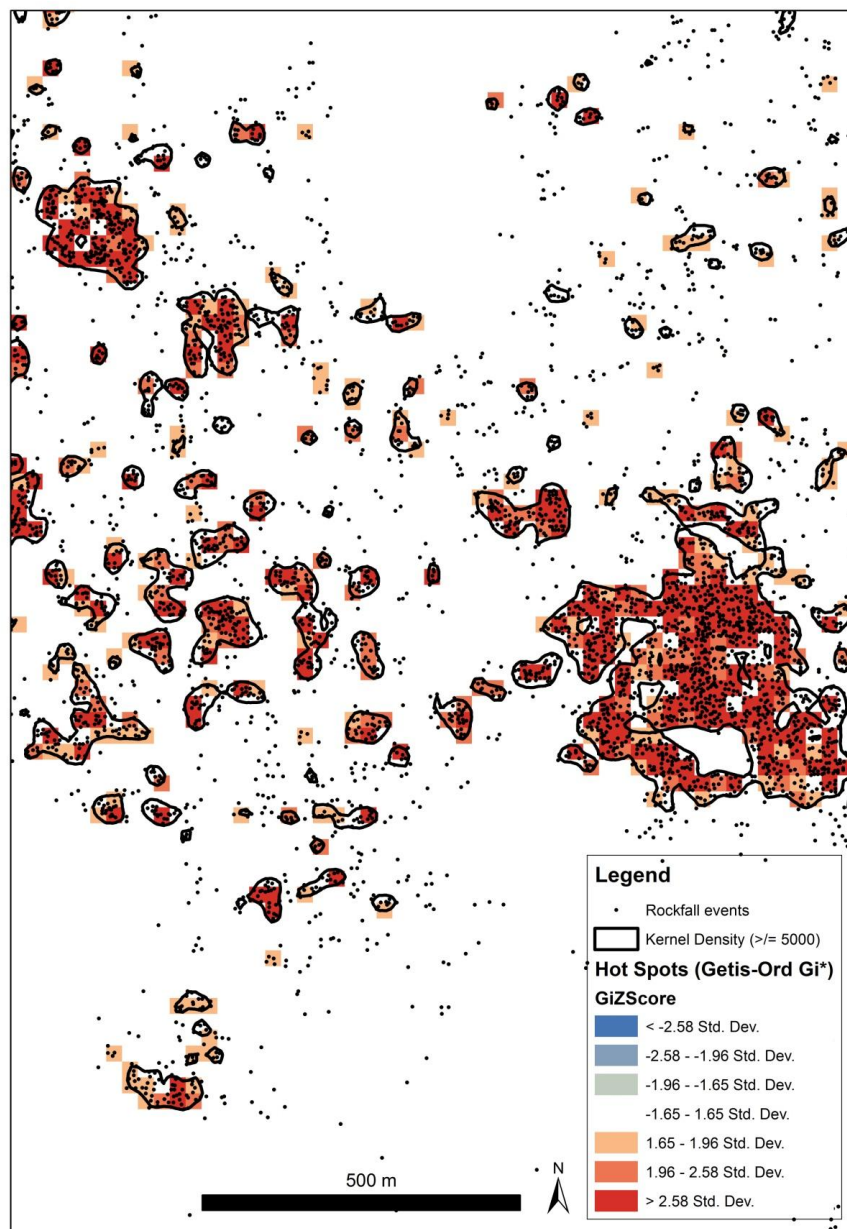


Figure 7.71 Comparison of the kernel density (black) and the Getis-Ord Gi* statistic

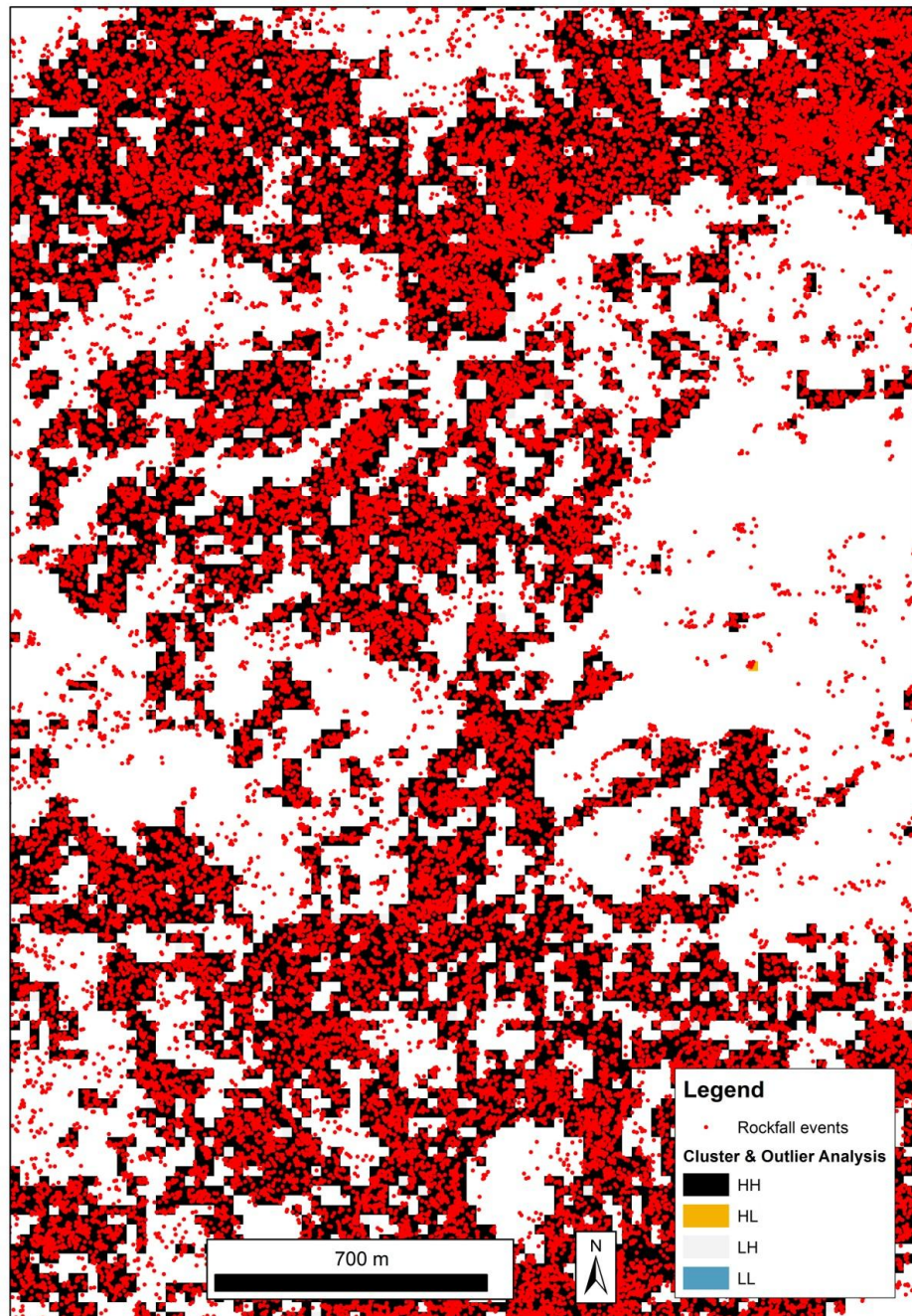


Figure 7.72 Cluster and Outlier analysis (Anselin Local Morans I).

These results suggest that it is not possible to use statistical techniques to identify rockfall clusters at a regional scale when the clusters occur in close proximity or are superimposed on one another. It is thus not possible to generate bounding containers which represent rock movement deposits. Having no boundary to use to delineate the deposits means that further analyses on the length and orientation

of the rockfalls cannot be undertaken. Future research using these data should aim to use the events as input into a 3D rockfall modeling tool, such as Rockfall Analyst (Lan et al., 2007), to identify potential source areas. Another research opportunity would be to undertake manual scaled analyses of each group of clusters and then attempt to identify individual cluster events, which would be achieved by shrinking the search radius until every cluster has a unique polygon.

A stratified sampling technique was developed for sampling the rock movement deposit data in order to identify the environmental variables associated with the deposits. Presence data was calculated by selecting 1%, 5% and 15% of the total data points within each class and then merging the layers. The first stratified sample (SS01) contains 6 302 points, the second stratified sample (SS05) contains 31 508 points and the third sample (SS15) contains 94 524 points. The Kernel Density function was calculated for each sample to check that spatial pattern was preserved (Figure 7.73). Figure 7.73A is the original Kernel Density function with all 827 887 points and it would appear that the stratified samples maintain the same general spatial pattern. Absence data was generated by using the 20x20m grid and selecting all polygons with a Point in Polygon (PIP) value of zero. The full rectangular extent was then clipped to the study area boundary and the Create Random Points tool in ArcGIS was used to generate 6 302 (SS01A), 31 508 (SS05A) and 94 524 (SS15A) random points in three layers.

The frequency distributions of SS01, SS05 and SS15 in relation to the seven variables and their associated class categories are presented in Figure 7.74, 7.75 and 7.76. It should be noted that the distributions for the stratified samples are similar.

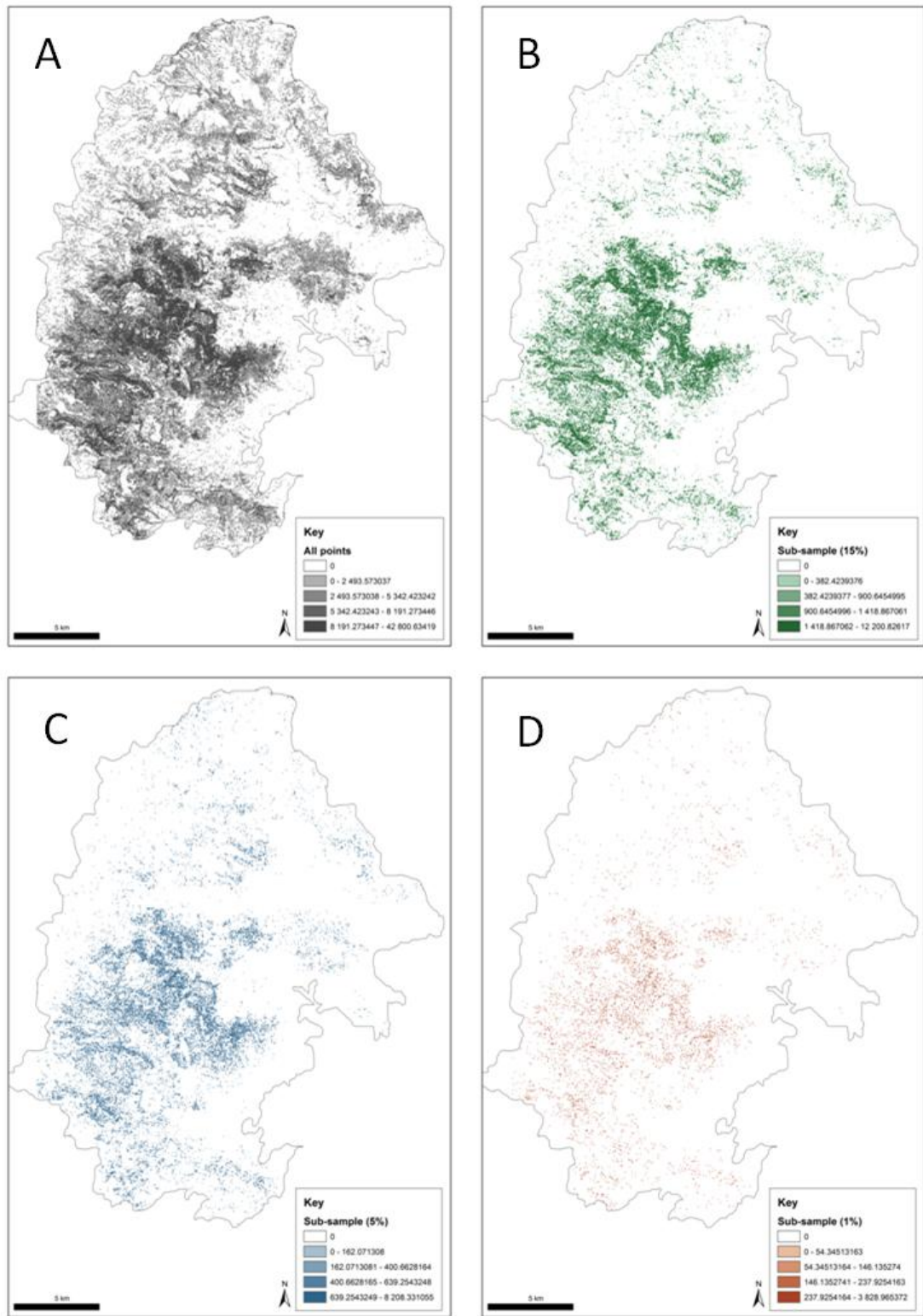


Figure 7.73 Comparison of the kernel density function for the full dataset, 1%, 5% and 15%.

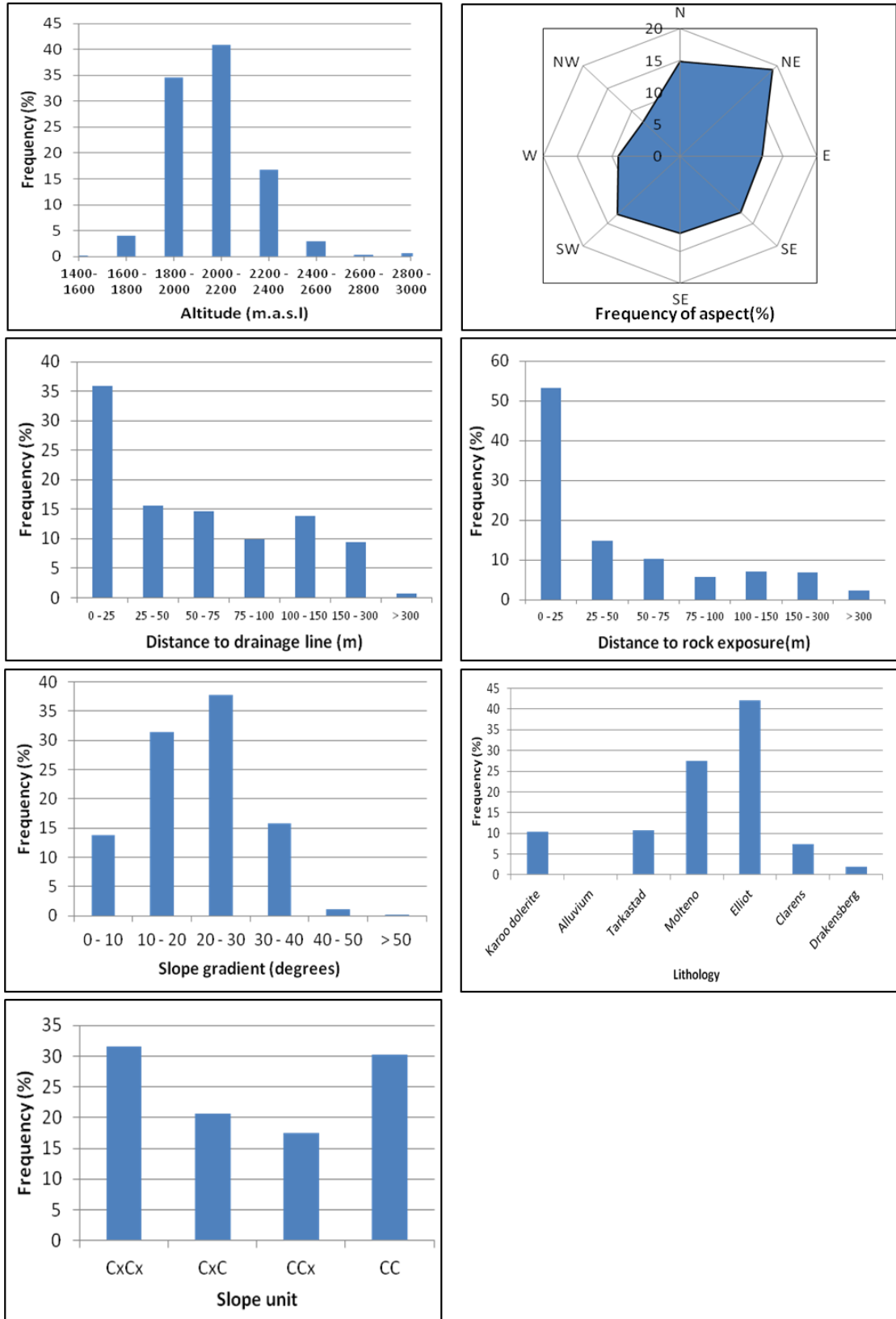


Figure 7.74 Histograms of the independent variables for SS01.

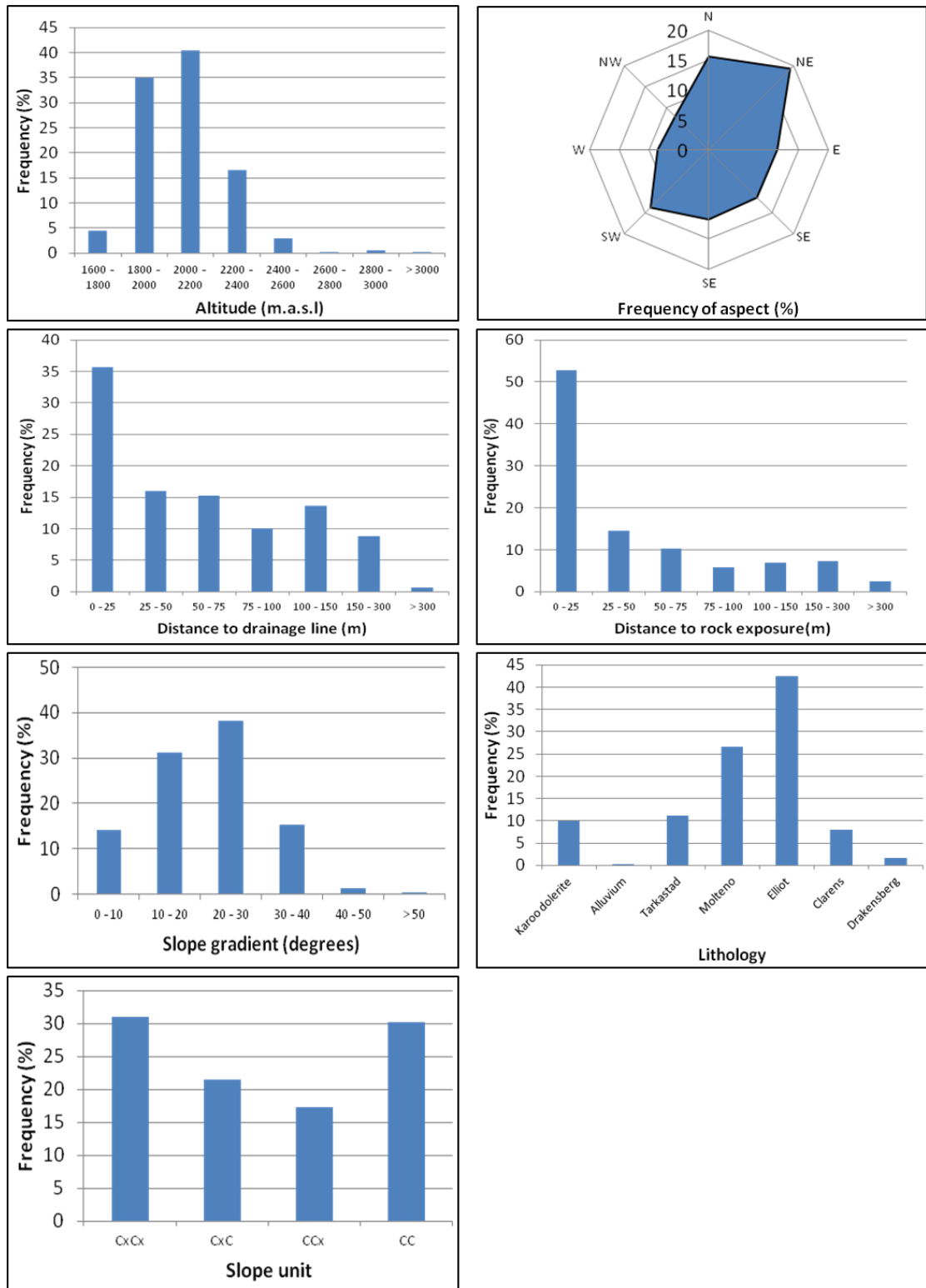


Figure 7.75 Histograms of the independent variables for SS05.

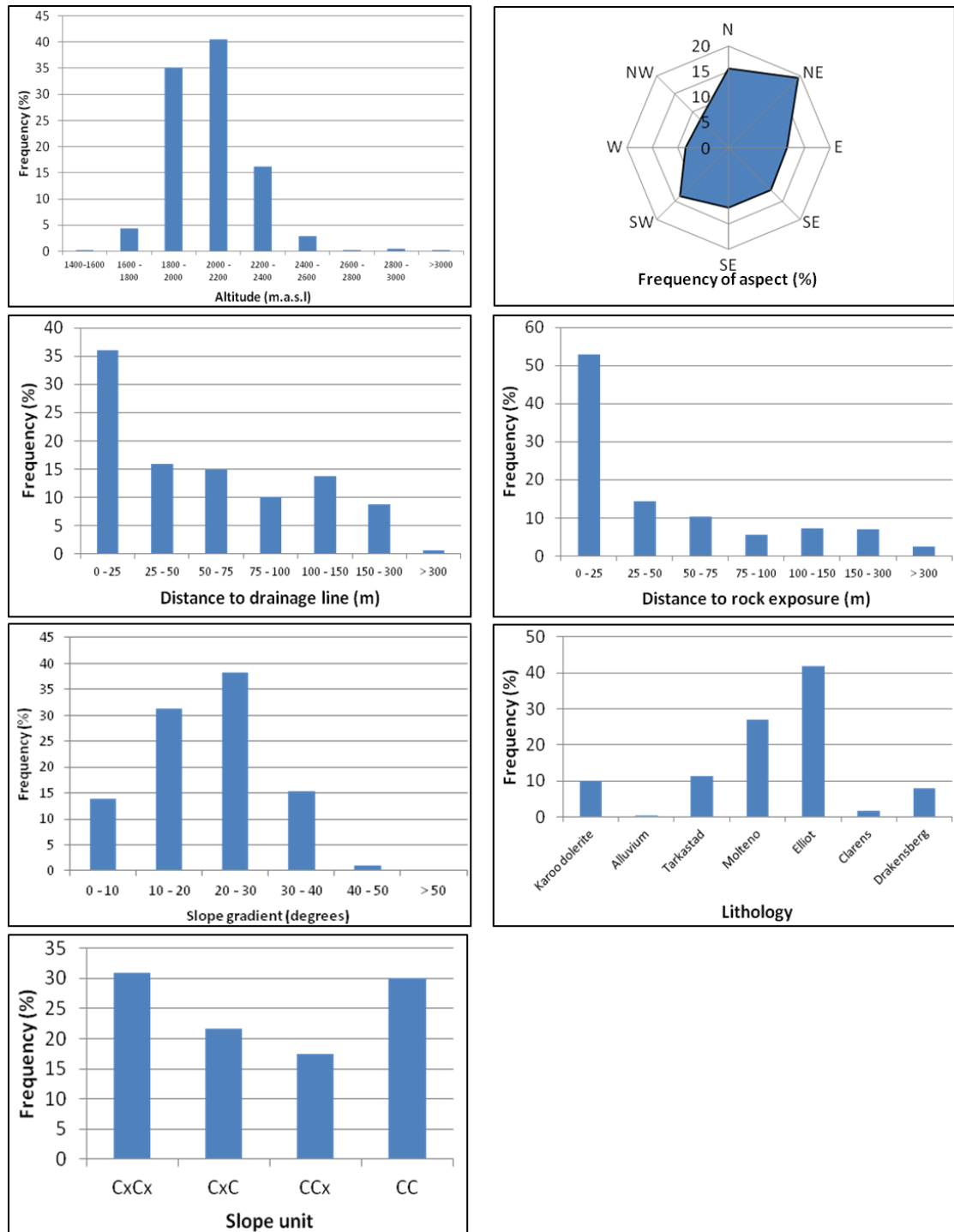


Figure 7.76 Histograms of the independent variables for SS15.

Rock movement deposits are predominantly found within 25m of a drainage line and rock exposure between 1 800 and 2 200 m.a.s.l. The linear directional mean of the digitized rock exposures for the study area is 98°-351°, which is approximately north-west to south-east. A comparison of the linear directional

mean and the frequency distribution of the rock movement deposits suggests that the deposits are orientated perpendicularly to the rock exposures. This compliments the observation that most rockfalls originate from the horizontally bedded rock exposures which are orientated parallel to the slope contour, thus the aspect histogram shows the orientation of average runout perpendicular to the slope contour.

The highest frequency of rock movement deposits is in the Elliot and Molteno Formations respectively. Preliminary investigation in the field suggests that most of the displaced blocks are from the Clarens Formation. The high frequency of deposits in these lithologies may indicate that blocks displaced from the Clarens Formation settle on the gentler slopes of the Elliot and Molteno Formations which are downslope. It may also suggest that the Elliot and Molteno Formations are more susceptible to rock weathering, due to higher concentrations of silt- and mudstones and that more rockfalls occur in these layers.

The high frequency of rock movement deposits within 25 m of a rock exposure supports the observation that most displaced blocks do not travel far from their source areas. The high frequency of rock movement deposits within 25 m of a drainage line suggests that the drainage lines function as topographic lows and collect displaced material. Most rock movement deposits occur on slopes with gradients between 20°-30° which compares well with values for shadow angles provided in the literature (c.f. Copons et al., 2009). The shadow angle is defined as the dipping of the energy line which connects the apex of the talus slope to the furthest fallen boulder (Copons et al., 2009). Reach angles range from 28°-30°, although the exact angle is site-specific. The slope gradients of the rock movement deposits model the shadow angle as the deposits represent the furthest runout distance of the rockfalls.

Variable	Class	Area (%)	Frequency (%)	InfoVal	Ratio (F/A)
Altitude	1400-1600	0.77	0.0	\$	0.02
	1600 - 1800	26.05	4.1	1.410	0.16
	1800 - 2000	25.94	34.5	3.541	1.33
	2000 - 2200	19.51	40.9	3.710	2.09
	2200 - 2400	15.33	16.8	2.819	1.09
	2400 - 2600	6.46	2.9	1.061	0.45
	2600 - 2800	2.48	0.3	-1.310	0.11
	2800 - 3000	2.41	0.6	-0.480	0.26
	> 3000	1.05	0.0	\$	0.00
Aspect	N (337.5 - 22.5)	7.45	14.8	0.680	1.98
	NE (22.5 - 67.5)	18.20	19.1	0.039	1.05
	E (67.5 - 112.5)	15.54	12.0	-0.248	0.77
	SE (112.5 - 157.5)	16.15	12.5	-0.249	0.77
	S (157.5 - 202.5)	16.30	12.1	-0.230	0.74
	SW (202.5 - 247.5)	12.44	12.9	0.081	1.04
	W (247.5 - 292.5)	7.27	9.0	0.112	1.24
	NW (292.5 - 337.5)	6.64	7.6	0.066	1.14
DistDrain	0 - 25	32.64	35.9	3.582	1.10
	25 - 50	14.78	15.6	2.749	1.06
	50 - 75	14.06	14.7	2.685	1.04
	75 - 100	9.65	9.9	2.288	1.02
	100 - 150	14.26	13.9	2.633	0.98
	150 - 300	12.22	9.4	2.237	0.77
	> 300	2.39	0.6	-0.455	0.27
Dist RockX	0 - 25	31.24	53.2	3.974	1.70
	25 - 50	11.56	14.8	2.694	1.28
	50 - 75	10.04	10.3	2.334	1.03
	75 - 100	6.47	5.6	1.729	0.87
	100 - 150	9.80	7.1	1.955	0.72
	150 - 300	13.51	6.8	1.913	0.50
	> 300	17.40	2.3	0.812	0.13
Gradient	0 - 10	31.95	13.8	-0.760	0.43
	10 - 20	28.45	31.5	0.092	1.11
	20 - 30	25.04	37.8	0.397	1.51
	30 - 40	11.73	15.7	0.262	1.34
	40 - 50	2.56	1.1	-0.647	0.45
	> 50	0.27	0.0	\$	0.17
Lithology	Karoo dolerite	22.81	10.3	2.337	0.45
	Alluvium	2.64	0.1	-2.757	0.02
	Tarkastad	21.50	10.7	2.370	0.50
	Molteno	15.39	27.5	3.314	1.79
	Elliot	25.69	42.1	3.739	1.64
	Clarens	11.96	7.4	1.996	0.62
	Drakensberg	14.84	2.0	0.677	0.13
SlopeUnit	CxCx	28.81	31.6	3.454	1.10
	CxC	23.14	20.6	3.024	0.89
	CCx	17.53	17.5	2.861	1.00
	CC	30.50	30.3	3.411	0.99
	PlanCom	0.03	0.0	\$	0.51

Table 7.36 Comparison of the frequency distributions and InfoVal weights for SS01. Bold indicates highest value in category, colour indicates variable with greatest frequency.

Variable	Class	Area (%)	Frequency (%)	InfoVal	Ratio (F/A)
Altitude	1400-1600	0.77	0.0	\$	0.00
	1600 - 1800	26.05	4.4	1.486	0.17
	1800 - 2000	25.94	34.9	3.553	1.35
	2000 - 2200	19.51	40.4	3.698	2.07
	2200 - 2400	15.33	16.5	2.804	1.08
	2400 - 2600	6.46	3.0	1.090	0.46
	2600 - 2800	2.48	0.2	-1.462	0.09
	2800 - 3000	2.41	0.5	-0.641	0.22
	> 3000	1.05	0.0	\$	0.02
Aspect	N (337.5 - 22.5)	7.45	15.7	0.680	2.11
	NE (22.5 - 67.5)	18.20	19.3	0.039	1.06
	E (67.5 - 112.5)	15.54	11.5	-0.248	0.74
	SE (112.5 - 157.5)	16.15	11.4	-0.249	0.71
	S (157.5 - 202.5)	16.30	11.7	-0.230	0.72
	SW (202.5 - 247.5)	12.44	13.8	0.081	1.11
	W (247.5 - 292.5)	7.27	8.6	0.112	1.18
	NW (292.5 - 337.5)	6.64	8.0	0.066	1.20
DistDrain	0 - 25	32.64	35.6	3.574	1.09
	25 - 50	14.78	16.0	2.773	1.08
	50 - 75	14.06	15.3	2.725	1.09
	75 - 100	9.65	10.0	2.306	1.04
	100 - 150	14.26	13.6	2.612	0.96
	150 - 300	12.22	8.8	2.173	0.72
	> 300	2.39	0.7	-0.430	0.27
Dist RockX	0 - 25	31.24	52.8	3.966	1.69
	25 - 50	11.56	14.5	2.674	1.25
	50 - 75	10.04	10.3	2.331	1.03
	75 - 100	6.47	5.8	1.757	0.90
	100 - 150	9.80	7.0	1.944	0.71
	150 - 300	13.51	7.3	1.983	0.54
	> 300	17.40	2.4	0.869	0.14
Gradient	0 - 10	31.95	14.0	-0.760	0.44
	10 - 20	28.45	31.3	0.092	1.10
	20 - 30	25.04	38.2	0.397	1.53
	30 - 40	11.73	15.2	0.262	1.30
	40 - 50	2.56	1.2	-0.647	0.47
	> 50	0.27	0.0	\$	0.15
Lithology	Karoo dolerite	22.81	10.1	2.316	0.44
	Alluvium	2.64	0.1	-2.403	0.03
	Tarkastad	21.50	11.4	2.436	0.53
	Molteno	15.39	27.0	3.296	1.75
	Elliot	25.69	43.2	3.767	1.68
	Clarens	11.96	8.1	2.092	0.68
	Drakensberg	14.84	1.7	0.550	0.12
SlopeUnit	CxCx	28.81	31.0	3.433	1.07
	CxC	23.14	21.4	3.065	0.93
	CCx	17.53	17.3	2.853	0.99
	CC	30.50	30.3	3.410	0.99
	PlanCom	0.03	0.0	\$	0.10

Table 7.37 Comparison of the frequency distributions and InfoVal weights for SS05. Bold indicates highest value in category, colour indicates variable with greatest frequency.

Variable	Class	Area (%)	No	Frequency (%)	InfoVal	Ratio (F/A)
Altitude	1400-1600	0.77	5	0.0	-5.242	0.01
	1600 - 1800	26.05	4166	4.4	1.483	0.17
	1800 - 2000	25.94	33205	35.1	3.559	1.35
	2000 - 2200	19.51	38298	40.5	3.702	2.08
	2200 - 2400	15.33	15349	16.2	2.787	1.06
	2400 - 2600	6.46	2790	3.0	1.082	0.46
	2600 - 2800	2.48	241	0.3	-1.367	0.10
	2800 - 3000	2.41	448	0.5	-0.747	0.20
> 3000	1.05	22	0.0	-3.760	0.02	
Aspect	N (337.5 - 22.5)	7.45	14722	15.6	2.746	2.09
	NE (22.5 - 67.5)	18.20	18349	19.4	2.966	1.07
	E (67.5 - 112.5)	15.54	10909	11.5	2.446	0.74
	SE (112.5 - 157.5)	16.15	11156	11.8	2.468	0.73
	S (157.5 - 202.5)	16.30	11178	11.8	2.470	0.73
	SW (202.5 - 247.5)	12.44	12793	13.5	2.605	1.09
	W (247.5 - 292.5)	7.27	8013	8.5	2.137	1.17
	NW (292.5 - 337.5)	6.64	7404	7.8	2.058	1.18
DistDrain	0 - 25	32.64	33978	35.9	3.582	1.10
	25 - 50	14.78	15021	15.9	2.766	1.08
	50 - 75	14.06	14147	15.0	2.706	1.06
	75 - 100	9.65	9552	10.1	2.313	1.05
	100 - 150	14.26	12997	13.7	2.621	0.96
	150 - 300	12.22	8319	8.8	2.175	0.72
	> 300	2.39	510	0.5	-0.617	0.23
Dist RockX	0 - 25	31.24	49946	52.8	3.967	1.69
	25 - 50	11.56	13549	14.3	2.663	1.24
	50 - 75	10.04	9799	10.4	2.339	1.03
	75 - 100	6.47	5328	5.6	1.729	0.87
	100 - 150	9.80	6799	7.2	1.973	0.73
	150 - 300	13.51	6704	7.1	1.959	0.52
	> 300	17.40	2399	2.5	0.931	0.15
Gradient	0 - 10	31.95	13201	14.0	2.637	0.44
	10 - 20	28.45	29644	31.4	3.446	1.10
	20 - 30	25.04	36141	38.2	3.644	1.53
	30 - 40	11.73	14468	15.3	2.728	1.31
	40 - 50	2.56	1040	1.1	0.096	0.43
	> 50	0.27	30	0.0	-3.450	0.12
Lithology	Karoo dolerite	22.81	9547	10.1	2.313	0.44
	Alluvium	2.64	89	0.1	-2.363	0.04
	Tarkastad	21.50	10760	11.4	2.432	0.53
	Molteno	15.39	25485	27.0	3.294	1.75
	Elliot	25.69	39631	41.9	3.736	1.63
	Clarens	11.96	1643	1.7	0.553	0.15
	Drakensberg	14.84	7369	7.8	2.054	0.53
SlopeUnit	CxCx	28.81	29229	30.9	3.431	1.07
	CxC	23.14	20408	21.6	3.072	0.93
	CCx	17.53	16458	17.4	2.857	0.99
	CC	30.50	28429	30.1	3.404	0.99
	PlanCom	0.03	0	0.0	\$	0.00

Table 7.38 Comparison of the frequency distributions and InfoVal weights for SS15. Bold indicates highest value in category, colour indicates variable with greatest frequency.

Ranking the percentage of rock movement deposits suggests that the deposits most frequently occur within 25 m of a rock exposure, between 2 000-2 200 m.a.s.l, on slope gradients between 20-30, in the Elliot Formation. The InfoVal weights suggest a similar trend, however the Area-Weighted frequency suggests that altitude and aspect (North) might be more important.

Hierarchical partitioning was undertaken to rank the variables according to their greatest independent contribution (%I) to the logistic regression model. A hierarchical partition was created for each stratified sample and the resulting %I are presented in Figure 7.77. Distance to a rock exposure consistently has the highest independent contribution and accounts for an average of 74% (1.38 SD) of the model. Gradient is the second highest contributor, with an average of 12% (1.35). The frequency statistics, InoVal and hierarchical partitioning all suggest that the most important influence of rock movement deposits is distance to a rock exposure, which is not surprising, given that the rockfalls supply the material for the deposits.

Stepwise forward and backward logistic regression using all of the variables was used to develop a prediction model which could predict the maximum number of terracettes using the smallest number of variables. SS05 and SS01 failed to converge so only the logistic regression values for SS01 are reported. Akaike's Information Criterion (AIC) for the full model is 12 820 and Bayes Information Criterion 13 070. The lowest BIC (13 020) selected five independent variables for the model, namely distance to a drainage line, distance to a rock exposure, lithology, altitude and slope gradient, and this compares well with the results of the frequency distributions, InfoVal and hierarchical partitioning.

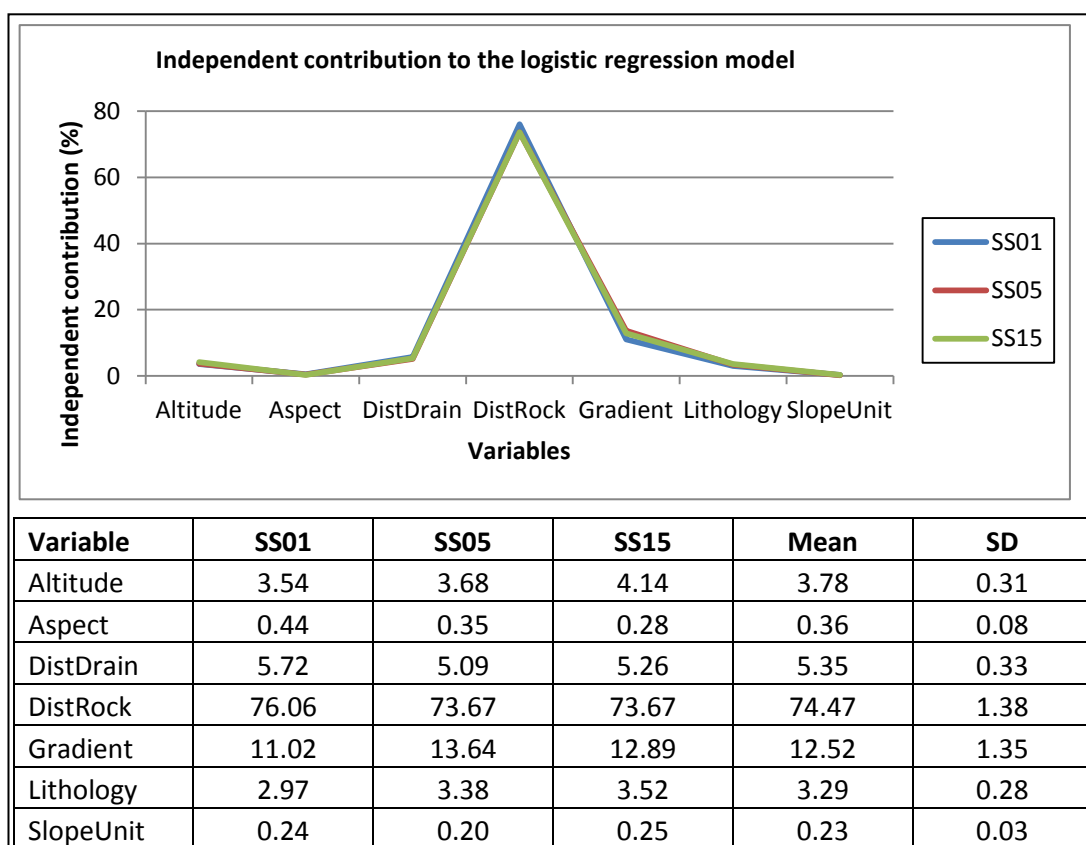


Figure 7.77 Graph representing the percentage contribution of each variable to the logit model. The table shows the mean and standard deviations for each contribution.

A probability map was created in a GIS environment to identify areas with a high probability of having rock movement deposits (Figure 7.78). More than 80% of the study area has >50% probability for having rock movement deposits which is expected given that rock exposures are observed throughout the GCSF (Table 39).

Of the variables used in the study, altitude, gradient and lithology were selected as strong predictors most often. This compares well with a similar study by van Den Eeckhaut et al. (2010) which found that gradient and lithology were strong predictors. Distance to a drainage line and distance to a rock exposure were selected for some types of landforms, mostly of the shear scar variety. Distance to a footpath was not a useful variable for describing anthropogenic effects on the environment, possibly because the footpaths are so limited in extent, however this variable did have some influence on the logistic regression models. Distance to a rock exposure was the strongest predictor variable for rock movement deposits,

however this is not a surprising result given that the bedrock outcrops provide the material for the rock movement deposits. The result does confirm the use of logistic regression and hierarchical partitioning for characterizing mass movement processes.

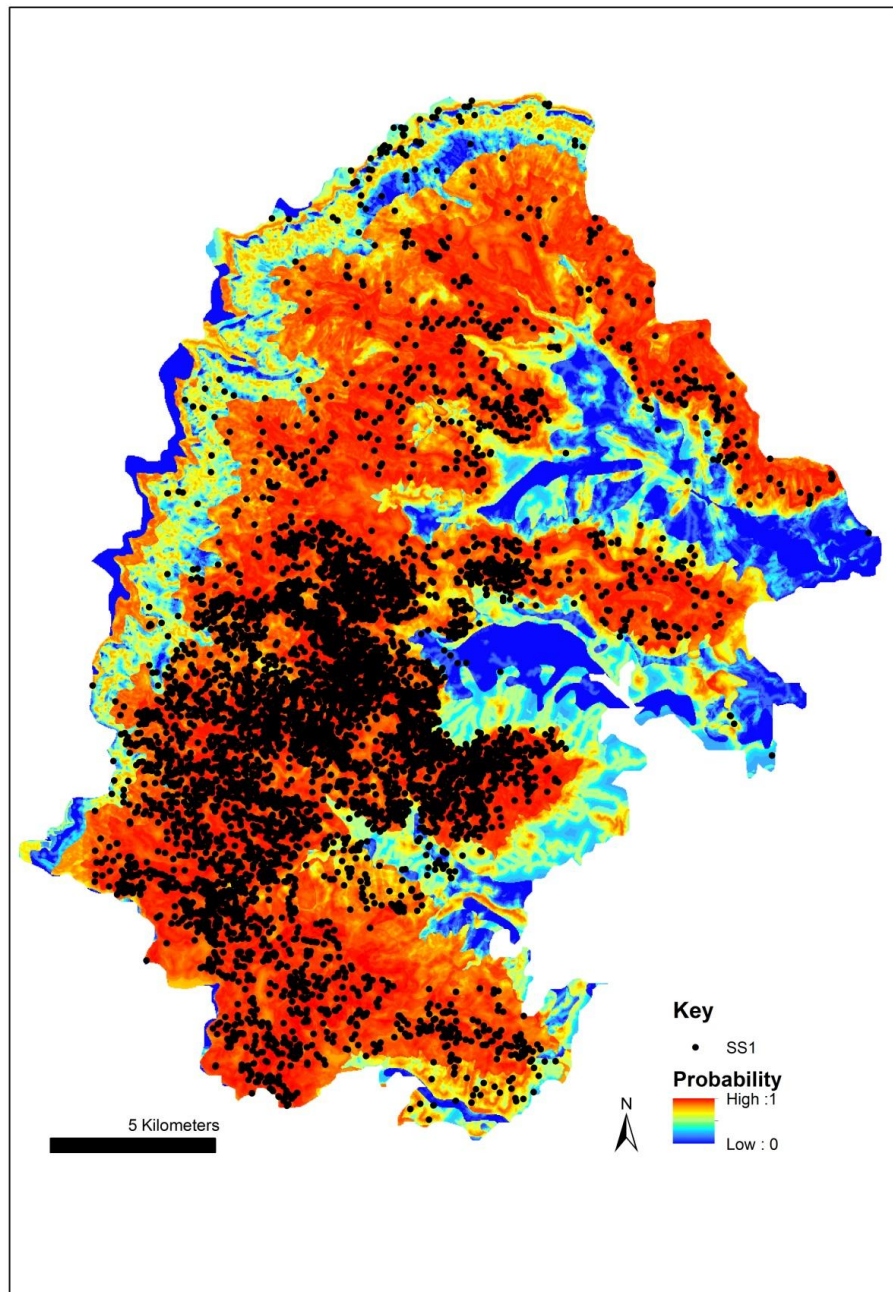


Figure 7.78 Probability maps for rock movement deposits using SS01.

Probability	Area	%
0 - 0.5	56.0	12.2
0.5 - 0.6	27.1	5.9
0.6 - 0.7	34.6	7.5
0.7 - 0.8	36.1	7.8
0.8 - 0.9	52.4	11.4
0.9 - 1.00	254.6	55.3
>0.5		88.0

Table 7.39 Total area (km² and percent) of probability values for SS1.

Aspect, which was assumed to have a strong influence in predicting mass movement activity, was not selected as a strong independent contributor by the hierarchical partitioning for any of the landforms, which was surprising given that it was the only variable which was not contingent on any of the other variables. The role of aspect in geomorphic processes is therefore uncertain with the context of the southern Drakensberg. Valley asymmetry in the Drakensberg has been ascribed to the effects of aspect on micro-climate and weathering, however these results would suggest that aspect either does not play as significant role as previously assumed or that the role of aspect is masked by other, more dominant processes and cannot be quantified by the techniques applied in this study.

8 Conclusion

In this study, a mass movement classification was developed for the southern Drakensberg, based on the work of Varnes (1958), which was used for the identification of mass movement landforms on orthophotos. A mass movement inventory was developed based on a combination of field and GIS-based methods and statistical modeling; univariate statistics, a weighting method (InfoVal), hierarchical partitioning and classification and regression trees. These techniques proved useful for identifying environmental variables associated with each type of mass movement feature. Predictive mapping using the beta-coefficients of the logistic regression models was undertaken and the proportion of area most likely to experience a particular type of mass movement activity was identified. On average, about 30% of the study area has conditions conducive to the development of at least one of the mass movement types identified.

8.1 Methodological considerations

Fieldwork allowed for the testing of the proposed classification and most of the mass movement landforms which the classification was developed for could be identified using aerial photograph interpretation. The exceptions were mass movements which were not well defined in the classification, specifically terrace-type mass movements as API techniques are not suited to identifying the initiating mechanism of movement. It was therefore difficult to describe the terrace-type landforms identified by the API in terms of the classification. Terracettes may equally be caused by sliding or flowing motions depending on the mechanisms of initiation, whilst solifluction lobes are most likely flow features. Terraces may be a type of translational slide that experience little forward displacement, or are purely controlled by underlying lithology. As no fieldwork was undertaken on these landforms, it is difficult to draw further conclusions about their origins.

The second type of mass movement which was excluded from the mass movement inventory are large, relict palaeo-landslides. Whilst a number of these landforms were observed in the study area, the morphology of the landforms has

consequently been modified by more recent processes, such as erosion and shallow translational slides, which further complicated doing morphometric analyses on these larger, palaeo-features. Singh (2008) estimates that the majority of these large palaeo-landslides formed during the Holocene and suggests that hazard-based assessments should be focused on shallower mass movement landforms which have had negative anthropogenic impacts over the last few decades.

Statistical analyses required the generation of a number of input layers and the most important of these was the generation of a digital elevation model. The 25m DEM developed for the study area uses cartographic data in the form of spot heights and contours and these had to be extensively quality checked to ensure the final output DEM would be accurate. Photogrammetric techniques used to develop a DEM from the orthophotos proved unfeasible and unnecessarily complex. The DEM was used to create second derivative data such as gradient and aspect and the technique described by Ayalew and Yamagishi (2004) was used to create a slope unit raster. Distance variables were digitized from the orthophotos and the quality and coverage of the variables is almost entirely dependent on the resolution of the orthophotos. There are no set universal criteria for the selection of input variables (Guisan and Zimmermann, 2000; Akgun, 2012) and the decision to include a variable was determined more by data accessibility than by a confirmed geomorphic relationship.

Sampling techniques available in a GIS environment were then used to sample the input data. The process of data sampling assumed that the landforms were small enough that sampling the gravimetric centre of the DEM would provide a realistic value of the environmental variables of the landform. From the results, it appears that the sampling technique was successful, however, future research should be undertaken to determine how variations in the position of the point within the mass movement landform affect the sampled values. One of the limitations created by the resolution of the orthophotos was that, in most cases, it was not possible to identify only the shear scar, and the entire mass movement feature was

therefore digitized. This suggests that the attribute data which were extracted from the points do not necessarily represent the conditions of the slope at the point of failure. The creation of five random datasets and the three stratified datasets was therefore used in an attempt to 'randomise' the random sample so that any statistically significant variables that emerged could be more realistically related to the mass movement data.

Univariate statistical techniques were originally adopted to compare the mass movement types and at face value, they appeared to be able to describe patterns in distribution relatively well. However, when the frequency of mass movement landforms within a category was normalized using area, it became apparent that the frequency distributions were not reliable. A weighting method, called the Information Value was therefore adopted to compare the weights of each variable and to compare the categories within each variable. Logistic regression has traditionally been used to identify areas that are prone to a particular hazard and often, the beta-coefficients produced by the model are used to infer causality. However, the beta-coefficients are relative values which are not normalized for area and as logistic regression is a multivariate technique, the influence of one variable cannot be separated from the combined influence of all the variables in the model. Thus, the InfoVal weights proved useful for comparing classes within the variables.

Hierarchical partitioning was therefore adopted to determine what the individual contribution of a variable was to the logistic regression model. Hierarchical partitioning proved useful for highlighting one variable, or at most two, which could be used to describe the mass movement type. However, the technique could not identify the class within a variable that has the greatest independent contribution. Although other methods were suggested for performing this analysis, such as Weights of Evidence, it was not clear whether it would be possible to identify the effects of classes within categories. Classification and regression trees were therefore adopted to compare the results of the hierarchical partitioning and the weights of the InfoValue. Overall, the classification trees

supported the findings of the hierarchical partitioning and InfoVal, although the classification trees use frequency, rather than area-weighted frequency, to build a classification. The central objective of statistical modeling is accurate prediction and explanation but few analytical techniques are able to do both and there is always likely to be a trade-off in one of these outcomes (Hjort and Marmion, 2009; Akgun, 2012)

Gradient, altitude and lithology were the most frequently selected variables by all of the techniques, whilst distance to a drainage line and a rock exposure were selected for at least two of the mass movement types. Distance to a rock exposure was the strongest predictor for rock movement deposits. Aspect was not selected as a variable with a high independent contribution, despite the variable being independent of any of the other input data. Issues of collinearity were not explored in this study as part of the assumption of working with data from the natural world is that collinearity exists, especially as the DEM was used to derive the other input layers. The distance to a footpath variable had more of a statistical influence than a causal influence as most landforms occurred >300m from a footpath.

Spatial point pattern statistics, as they exist in software packages such as ArcGIS 9 and 10 and QGIS are not sophisticated enough to identify clusters within spatial datasets. Whilst the existing tools can identify the pattern (random, clustered or dispersed) no tool is able to locate and extract clusters. Ideally, a statistical tool should be developed to facilitate the identification of clusters within point patterns at various user-defined thresholds.

8.2 Geomorphological considerations

Probability maps were produced for each of the mass movement types and it is estimated that 30% of the GCSF has a medium to high probability of experiencing some form of mass movement, whilst more than 80% will have rock movement deposits. Sheet slides have the smallest area of likely probability, whilst shear scars have the highest. Within the context of geotourism, the implications of this

study are twofold. Firstly, the variety and aerial extent of the mass movement landforms identified in the GCSF are much greater than was anticipated at the beginning of this study. This suggests that mass movement dynamics may be underestimated in the Drakensberg, which has an impact on the management policies of the UDP, particularly in the context of global environmental change. Changes in rainfall quantity and intensity may result in increased slope instability with associated increases in sediment loads to the hydrological system. This, combined with development pressure, declining access to rangelands for grazing in the surrounding rural areas, and increasing numbers of tourists, poses interesting problems for conservation managers in the UDP. However, the diversity of mass movement landforms in the UDP increases its attractiveness to tourists interested in the geomorphological character of the area.

The second implication for geotourism is that whilst mass movement is a naturally occurring process, there exists a misconception that landslides are entirely caused by anthropogenic factors and represent environmental degradation. This may impact adversely on geotourism in the UDP as the area is viewed as a pristine conservation area. However, once again, the opportunity arises to use the diversity of mass movement landforms as an educational tool. As the landforms have been mapped and classified, it may be possible to select 'representative' sites which could be formatted into a geomorphological field guide, along with information about the geological characteristics of the site.

8.3 Contribution to international and local mass movement studies

Within an international context, this study adopts some relatively unique approaches. Van Westen et al. (2008) have appealed to geomorphologists to start sub-dividing landslide inventories into subsets that relate to a particular failure mechanism, which is linked to a specific combination of causal factors, in order to avoid generating hazard maps which are too general. Whilst there is an emerging trend for inventories to identify various mass movement types, this study

represents one of the few attempts which has done so, and which has classified mass movement landforms using a statistical approach. This study also attempts to show the limitations of some of the approaches that have been adopted for landslide prediction, and suggests alternate ways for comparing data using a variety of statistical methods. Hierarchical partitioning was developed within an ecological context and few geomorphological studies have adopted the method, particularly within the context of mass movement classification. Thus, hierarchical partitioning may represent an alternative or complimentary approach to quantitatively classifying mass movement types. This also represents a shift away from simply locating mass movement landforms, and rather works towards gaining a better understanding of the spatial conditioning factors which lead to mass movement development (Alexander, 2008; Mathew, 2009; Bai et al., 2010).

This study adopts a particularly unique approach for creating the dataset which represents 'no mass movement activity'. Logistic regression relies on a binary data input, typically characterized as 'presence/absence' in landslide prediction. Sampling strategies for hazard analysis typically convert the study area into a matrix of grid cells where each value is coded with 0/1. One of the problems with this approach occurs when a cell is misclassified as having no mass movement activity. This represents a false negative and will influence the predictive ability of the logistic regression model. Whilst the method adopted in this study does not avoid this risk, or the risk of a false positive (random point representing 'absence' is located on a mass movement feature), it is less sensitive to incorrectly classified values as new random points are created for each iteration, thus reducing the influence of a single misclassified point. The success of this approach can be seen in the relative robustness of the logistic regression models.

Within a local context, this study represents a medium scale assessment when compared to the works of Bijker (2001) and Singh (2008), and is one of the first regional studies to compare a range of mass movement types, rather than focus on a particular type or site, as has traditionally been undertaken in the UDP. This study also provides a hazard assessment framework which could be adopted by

landuse planners or engineers proficient in GIS techniques. Internationally, the number and intensity of natural disasters has increased dramatically over the last few years and landslides represent 9% of natural disasters that occurred worldwide in the 1990's (Yilmaz, 2009). This trend is expected to continue due to increased urbanization and development, unsustainable landuse practices, and increased regional precipitation in landslide-prone areas due to climate change. The techniques described in this study could therefore be adopted for hazard assessment in other parts of southern Africa where previous catastrophic mass movements have occurred. Whilst hazard maps represent a snap shot of risk based on the input data used to calculate probability, they are a fundamental tool to understanding slope stability dynamics and have been adopted into land use planning frameworks in some countries (van Westen et al., 2008).

Future research on mass movement features in the GCSF should include more detailed field measurements on the terrace-type landforms, as well as a produce a separate inventory of the palaeo-slide mass movement features in relation to major drainage systems. Although palaeo-slides have been mapped in KwaZulu-Natal, no assessment was made on the impacts of the slide deposits on local drainage. Another area of significant interest is the link between rockfall events and mass movement activity in the GCSF. A large number of rockslides and topples appear to have occurred as isolated events. Nearest neighbour and cluster analyses could be used to test the reality of this, and a variety of rockfall models exist which can be used in a GIS environment to model the runout behaviour of rockfalls. This information could then be used to understand the environmental factors that are associated with rockfalls, and it is likely that there is some overlap between areas which experience rockfalls and areas which are susceptible to other types of regolith-based mass movements.

9 References:

- Abdallah, C., Chorowicz, J., Bou Kheir, R., Khawlie, M., 2005: Detecting major terrain parameters relating to mass movements' occurrence using GIS, remote sensing and statistical correlations, case study Lebanon, *Remote Sensing of Environment*, 99 (4), 448-461.
- Agliardi, F. and Crosta, G.B., 2003: High resolution three-dimensional numerical modelling of rockfalls, *International Journal of Rock Mechanics and Mining Sciences*, 40 (4), 455-471.
- Akgun, A., 2012: A comparison of landslide susceptibility maps produced by logistic regression, multi-criteria decision, and likelihood ratio methods: a case study at İzmir, Turkey, *Landslides*, 9 (1), 93-106.
- Akgun, A. and Bulut, F., 2007: GIS-based landslide susceptibility for Arsin-Yomra (Trabzon, North Turkey) region, *Environmental Geology*, 51 (8), 1377-1387.
- Akgun, A., Dag, S., Bulut, F., 2008: Landslide susceptibility mapping for a landslide-prone area (Findikli, NE of Turkey) by likelihood-frequency ratio and weighted linear combination models, *Environmental Geology*, 54 (6), 1127-1143.
- Aleotti, P., 2004: A warning system for rainfall-induced shallow failures, *Engineering Geology*, 73 (3-4), 247-265.
- Alexander, D.E., 2008: A brief survey of GIS in mass-movement studies, with reflections on theory and methods, *Geomorphology*, 94 (3-4), 261-267.
- Allen, S., Cox, S., Owens, I., 2011: Rock avalanches and other landslides in the central Southern Alps of New Zealand: a regional study considering possible climate change impacts, *Landslides*, 8 (1), 33-48.
- Allison, R.J., 1995: Slopes and slope processes, *Progress in Physical Geography*, 19 (2), 265-279.

- Allison, R.J., 1994: Slopes and slope processes, *Progress in Physical Geography*, 18 (3), 425-435.
- Allison, R.J., 1993: Slopes and slope processes, *Progress in Physical Geography*, 17 (1), 92-101.
- Almagia, R., 1910: Studi geografici sulle frane in Italia [Geographical studies on landslides in Italy], *Memorie della Società Geografica Italiana*, 14 (2), 4-433.
- Anderson, E.W., 1972: Terracettes: a suggested classification, *Area*, 4 (1), 17-20.
- Anderson, M.G. and Howes, S., 1985: Development and application of a combined soil water-slope stability model, *Quarterly Journal of Engineering Geology and Hydrogeology*, 18 (3), 225-236.
- Antoniou, A.A. and Lekkas, E., 2010: Rockfall susceptibility map for Athinios port, Santorini Island, Greece, *Geomorphology*, 118 (1-2), 152-166.
- Arrowsmith, J.R. and Zielke, O., 2009: Tectonic geomorphology of the San Andreas Fault zone from high resolution topography: An example from the Cholame segment, *Geomorphology*, 113 (1-2), 70-81.
- Avian, M., Kellerer-Pirklbauer, A., Bauer, A., 2009: LiDAR for monitoring mass movements in permafrost environments at the cirque Hinteres Langtal, Austria, between 2000 and 2008, *Natural Hazards and Earth System Science*, 9, 1087-1094.
- Ayalew, L., Kasahara, M., Yamagishi, H., 2011: The spatial correlation between earthquakes and landslides in Hokkaido (Japan), a GIS-based analysis of the past and the future, *Landslides*, 8 (4), 433-448.
- Ayalew, L. and Yamagishi, H., 2004: Slope failures in the Blue Nile basin, as seen from landscape evolution perspective, *Geomorphology*, 57 (1-2), 95-116.

- Ayalew, L., Yamagishi, H., Ugawa, N., 2004: Landslide susceptibility mapping using GIS-based weighted linear combination, the case in Tsugawa area of Agano River, Niigata Prefecture, Japan, *Landslides*, 1 (1), 73-81.
- Ayeneu, T. and Barbieri, G., 2005: Inventory of landslides and susceptibility mapping in the Dessie area, northern Ethiopia, *Engineering Geology*, 77 (1-2), 1-15.
- Baeza, C. and Corominas, J., 2001: Assessment of shallow landslide susceptibility by means of multivariate statistical techniques, *Earth Surface Processes and Landforms*, 26 (12), 1251-1263.
- Bai, S., Wang, J., Lü, G., Zhou, P., Hou, S., Xu, S., 2010: GIS-based logistic regression for landslide susceptibility mapping of the Zhongxian segment in the Three Gorges area, China, *Geomorphology*, 115 (1-2), 23-31.
- Bajgier-Kowalska, M., 2008: Lichenometric dating of landslide episodes in the Western part of the Polish Flysch Carpathians, *Catena*, 72 (2), 224-234.
- Baldo, M., Bicocchi, C., Chiocchini, U., Giordan, D., Lollino, G., 2009: LIDAR monitoring of mass wasting processes: The Radicofani landslide, Province of Siena, Central Italy, *Geomorphology*, 105 (3-4), 193-201.
- Ballantyne, C.K., 2002: Paraglacial geomorphology, *Quaternary Science Reviews*, 21 (18-19), 1935-2017.
- Baltzer, A., 1875: Über einen neuerlichen Felssturz am Rossberg, nebst einigen allgemeinen bemerkungen über derartige Erscheinungen in den Alpen, *Neues Jahrbuch für Mineralogie*, 15-26.
- Barlow, J., Martin, Y., Franklin, S., 2009: Evaluating debris slide occurrence using digital data: paraglacial activity in Chilliwack Valley, British Columbia, *Canadian Journal of Earth Sciences*, 46 (3), 181-191.
- Barnard, P.L., Owen, L.A., Sharma, M.C., Finkel, R.C., 2001: Natural and human-induced landsliding in the Garhwal Himalaya of northern India, *Geomorphology*, 40 (1-2), 21-35.

- Baroni, C., Bruschi, G., Ribolini, A., 2000: Human-induced hazardous debris flows in Carrara marble basins (Tuscany, Italy), *Earth Surface Processes and Landforms*, 25 (1), 93-103.
- Basile, A., Mele, G., Terribile, F., 2003: Soil hydraulic behaviour of a selected benchmark soil involved in the landslide of Sarno 1998, *Geoderma*, 117 (3-4), 331-346.
- Baum, R. and Godt, J., 2010: Early warning of rainfall-induced shallow landslides and debris flows in the USA, *Landslides*, 7 (3), 259-272.
- Beckedahl, H.R., 1977: Subsurface erosion near the Oliviershoek Pass, Drakensberg, *South African Geographical Journal*, 59 (2), 130-138.
- Beckedahl, H.R., Hanvey, P.M., Dardis, G.F., 1988: Geomorphology of the Esikhaleni mass movement complex, Transkei, southern Africa: preliminary observations, in G.F. Dardis, B.P. Moon (Eds.), *Geomorphological Studies in Southern Africa*, Balkema, Rotterdam, 457-471.
- Beguería, S., 2006: Changes in land cover and shallow landslide activity: A case study in the Spanish Pyrenees, *Geomorphology*, 74 (1-4), 196-206.
- Bell, F.G. and Maud, R.R., 2000: Landslides associated with the colluvial soils overlying the Natal Group in the greater Durban region of Natal, South Africa, *Environmental Geology*, 39 (9), 1029-1038.
- Bell, F.G. and Maud, R.R., 1995: Expansive clays and construction, especially of low-rise structures: a viewpoint from Natal, South Africa, *Environmental and Engineering Geoscience*, 1, 41-59.
- Benz, U.C., Hofmann, P., Willhauck, G., Lingenfelder, I., Heynen, M., 2004: Multi-resolution, object-oriented fuzzy analysis of remote sensing data for GIS-ready information, *ISPRS Journal of Photogrammetry and Remote Sensing*, 58 (3-4), 239-258.

- Berk, R., 2008: Forecasting methods in crime and justice, *Annual Review of Law and Social Science*, 4, 219-238.
- Berti, M. and Simoni, A., 2005: Experimental evidences and numerical modelling of debris flow initiated by channel runoff, *Landslides*, 2 (3), 171-182.
- Bichler, A., Bobrowsky, P., Best, M., Douma, M., Hunter, J., Calvert, T., Burns, R., 2004: Three-dimensional mapping of a landslide using a multi-geophysical approach: the Quesnel Forks landslide, *Landslides*, 1 (1), 29-40.
- Bielecki, A.E. and Mueller, K.J., 2002: Origin of terraced hillslopes on active folds in the southern San Joaquin Valley, California, *Geomorphology*, 42 (1-2), 131-152.
- Bieniawski, I, 1989: *The Geomechanics of Classification in Rock Engineering Applications*, Wiley, New York.
- Bigot, C., Dorren, L., Berger, F., 2009: Quantifying the protective function of a forest against rockfall for past, present and future scenarios using two modelling approaches, *Natural Hazards*, 49 (1), 99-111.
- Bijker, H.J. , 2001: A Hydrological-Slope Stability Model for Shallow Landslide Prediction in the Injisuthi Valley, KwaZulu-Natal Drakensberg, MSc dissertation, University of Pretoria, Pretoria.
- Blahut, J., van Westen, C.J., Sterlacchini, S., 2010: Analysis of landslide inventories for accurate prediction of debris-flow source areas, *Geomorphology*, 119 (1-2), 36-51.
- Blight, G.E., Van Heerden, A., Brackley, I.J., 1970: Landslides at Amsterdamhoek and Bethlehem: an examination of the mechanics of stiff fissured clays, *Civil Engineer in South Africa*, June, 129-140.
- Blong, R.J., 1973: A numerical classification of selected landslides of the débris slide-avalanche-flow type, *Engineering Geology*, 7 (2), 99-114.

- Blong, R.J., 1973: Relationships between morphometric attributes of landslides, *Zeitschrift für Geomorphologie, Supplement*, 18, 66-77.
- Boelhouwers, J.C., 2003: Quaternary slope developments in the Lesotho highlands: review and alternative model, *South African Journal of Science*, 99, 44-46.
- Boelhouwers, J.C., 1999: Relict periglacial slope deposits in the Hex River Mountains, South Africa: observations and palaeoenvironmental implications, *Geomorphology*, 30 (3), 245-258.
- Boelhouwers, J.C., 1998: *The Present-Day Frost Action Environment and its Geomorphological Significance in the Western Cape Mountains, South Africa*, University of the Western Cape, Cape Town.
- Boelhouwers, J.C., 1992: Field Guide to the Geomorphology of the Giant's Castle Game Reserve, Natal Drakensberg, Southern African Association of Geomorphologists, Durban.
- Boelhouwers, J.C., 1991: Present-day periglacial activity in the Natal Drakensberg, Southern Africa: A Short Review, *Permafrost and Periglacial Processes*, 2 (1), 5-12.
- Boelhouwers, J.C. , 1988: Geological Mapping of Part of the Giant's Castle Game Reserve, Natal Drakensberg, MSc dissertation, University of Natal, Pietermaritzburg.
- Boelhouwers, J.C., Duiker, J.M.C., van Duffelen, E.A., 1998: Spatial, morphological and sedimentological aspects of recent debris flow activity in the Du Toitskloof Valley, Western Cape mountains, *South African Journal of Geology*, 101, 73-89.
- Boelhouwers, J.C., Hall, K., 1990: Active soil frost phenomena and glaciation of the Lesotho Plateau, in P.M. Hanvey (Ed.), *Guide to the Geocryological Features in the Drakensberg*, UNESCO, Grahamstown, 57-70.

- Boelhouwers, J.C. and Meiklejohn, K.I., 2002: Quaternary periglacial and glacial geomorphology of southern Africa: review and synthesis, *South African Journal of Science*, 98, 47-55.
- Boelhouwers, J.C., Sumner, P.D., 2003: The palaeoenvironmental significance of southern African blockfields and blockstreams, in M. Phillips, S.M. Springman, L.U. Arenson (Eds.), *Permafrost*, Swets and Zeitlinger, Lisse, 73-78.
- Boelhouwers, J.C., Holness, S., Sumner, P., 2000: Geomorphological characteristics of small debris flows on Junior's Kop, Marion Island, maritime sub - Antarctic, *Earth Surface Processes and Landforms*, 25 (4), 341-352.
- Boelhouwers, J.C., 1994: Periglacial landforms at Giant'S Castle, Natal Drakensberg, South Africa, *Permafrost and Periglacial Processes*, 5 (3), 129-136.
- Boelhouwers, J., C., Holness, S., Meiklejohn, I., Sumner, P., 2002: Observations on a blockstream in the vicinity of Sani Pass, Lesotho highlands, Southern Africa, *Permafrost and Periglacial Processes*, 13 (4), 251-257.
- Boelhouwers, J., C., Holness, S., Sumner, P., 2003: The maritime Subantarctic: a distinct periglacial environment, *Geomorphology*, 52 (1-2), 39-55.
- Booth, A.M., Roering, J.J., Perron, J.T., 2009: Automated landslide mapping using spectral analysis and high-resolution topographic data: Puget Sound lowlands, Washington, and Portland Hills, Oregon, *Geomorphology*, 109 (3-4), 132-147.
- Bordy, E.M., Hancox, P.J., Rubidge, B.S., 2005: The contact of the Molteno and Elliot formations through the main Karoo Basin, South Africa: a second-order sequence boundary, *South African Journal of Geology*, 108 (3), 351-364.

- Borgatti, L. and Soldati, M., 2010: Landslides as a geomorphological proxy for climate change: A record from the Dolomites (northern Italy), *Geomorphology*, 120 (1–2), 56-64.
- Borghuis, A.M., Chang, K., Lee, H.Y., 2007: Comparison between automated and manual mapping of typhoon - triggered landslides from SPOT - 5 imagery, *International Journal of Remote Sensing*, 28 (8), 1843-1856.
- Bovenga, F., Nutricato, R., Refice, A., Wasowski, J., 2006: Application of multi-temporal differential interferometry to slope instability detection in urban/peri-urban areas, *Engineering Geology*, 88 (3–4), 218-239.
- Brabb, E.E. , 1984: Innovative Approaches to Landslide Hazard Mapping. Proceedings of the 4th International Symposium on Landslides, Toronto, 307-324.
- Brardinoni, F. and Church, M., 2004: Representing the landslide magnitude-frequency relation: Capilano River basin, British Columbia, *Earth Surface Processes and Landforms*, 29 (1), 115-124.
- Brardinoni, F., Hassan, M.A., Rollerson, T., Maynard, D., 2009: Colluvial sediment dynamics in mountain drainage basins, *Earth and Planetary Science Letters*, 284 (3–4), 310-319.
- Brardinoni, F., Slaymaker, O., Hassan, M.A., 2003: Landslide inventory in a rugged forested watershed: a comparison between air-photo and field survey data, *Geomorphology*, 54 (3–4), 179-196.
- Braun, G., 1909: Uber Bodenbewegungen, *Geographische Gesellschaft in Greifswald*, 11, 17-35.
- Brien, D.L. and Reid, M.E., 2008: Assessing deep-seated landslide susceptibility using 3-D groundwater and slope-stability analyses, southwestern Seattle, Washington, *Reviews in Engineering Geology*, 20, 83-101.
- Brink, A.B.A., 1984: *Engineering Geology of Southern Africa, Volume 4*, Building Publications, Pretoria.

- Brink, A.B.A., 1983: *Engineering Geology of Southern Africa, Volume 3*, Building Publications, Pretoria.
- Brink, A.B.A., 1982: *Engineering Geology of Southern Africa, Volume 2*, Building Publications, Pretoria.
- Bromhead, E.N. and Ibsen, M.L., 2004: Bedding-controlled coastal landslides in Southeast Britain between Axmouth and the Thames Estuary, *Landslides*, 1 (2), 131-141.
- Brooks, S.M., Anderson, M.G., Collison, A.J.C., 1995: Modelling the role of climate, vegetation and pedogenesis in shallow translational hillslope failure, *Earth Surface Processes and Landforms*, 20 (3), 231-242.
- Brooks, S.M. and Richards, K.S., 1994: The significance of rainstorm variations to shallow translational hillslope failure, *Earth Surface Processes and Landforms*, 19 (1), 85-94.
- Brown, W.J., 1983: The changing imprint of the landslide on rural landscapes of New Zealand, *Landscape Planning*, 10, 173-204.
- Brown, R.W., Summerfield, M.A., Gleadow, A.J.W., 2002: Denudational history along a transect across the Drakensberg Escarpment of southern Africa derived from apatite fission track thermochronology, *Journal of Geophysical Research*, 107, 2350-2367.
- Brunsden, D., 1993: Mass movement: the research frontier and beyond, *Geomorphology*, 7, 85-128.
- Brunsden, D., Chandler, J.H., 1995: Development of an episodic landform change model based upon the Black Ven mudslide, 1946-1995, in M.G. Anderson, S.M. Brooks (Eds.), *Advances in Hillslope Processes*, Wiley, Chichester, 869-896.
- Brunsden, D., Ibsen, M.L., 1996: Mudslide, in R. Dikau, D. Brunsden, L. Schrott, M.L. Ibsen (Eds.), *Landslide Recognition: Identification, Movement and Causes*, Wiley, Chichester, 103-119.

- Brunsdon, D. and Lee, E.M., 2004: Behaviour of coastal landslide systems: an inter-disciplinary view, *Zeitschrift für Geomorphologie*, 134, 1-112.
- Buma, J., 2000: Finding the most suitable slope stability model for the assessment of the impact of climate change on a landslide in southeast France, *Earth Surface Processes and Landforms*, 25, 565-582.
- Buma, J., van Asch, T.W.J., 1996: Slide Rotational, in R. Dikau, D. Brunsdon, L. Schrott, M. Ibsen (Eds.), *Recognition: Identification, Movement and Causes*, Wiley, Chichester, 43-61.
- Busoni, E., Salvador Sanchis, P., Calzolari, C., Romagnoli, A., 1995: Mass movement and erosion hazard patterns by multivariate analysis of landscape integrated data: the Upper Orcia River Valley (Siena, Italy) case, *Catena*, 25 (1-4), 169-185.
- Bye, A.R. and Bell, F.G., 2001: Stability assessment and slope design at Sandsloot open pit, South Africa, *International Journal of Rock Mechanics and Mining Sciences*, 38 (3), 449-466.
- Caniani, D., Pascale, S., Sdao, F., Sole, A., 2008: Neural networks and landslide susceptibility: a case study of the urban area of Potenza, *Natural Hazards*, 45 (1), 55-72.
- Cannon, S.H., Kirkham, R.M., Parise, M., 2001: Wildfire-related debris-flow initiation processes, Storm King Mountain, Colorado, *Geomorphology*, 39 (3-4), 171-188.
- Carbutt, C. and Edwards, T.J., 2003: The flora of the Drakensberg Alpine Centre, *Edinburgh Journal of Botany*, 60 (3), 581-607.
- Carrara, A., Cardinali, M., Guzzetti, F., Reichenbach, P., 1995: GIS technology in mapping landslide hazard, in A. Carrara, F. Guzzetti (Eds.), *Geographical Information Systems in Assessing Natural Hazards*, Kluwer Academic Press, Dordrecht, 135-175.

- Carrara, A., Catalano, E., Sorriso-Valvo, M., Roali, C., Osso, I., 1978: Digital terrain analysis for land evaluation, *Geology and Applied Hydrogeology*, 13, 69-127.
- Carrara, A., 1989: Landslide hazard mapping by statistical methods: a 'black-box' model approach, in F. Siccardi, R.L. Bras (Eds.), *International Workshop on Natural Disasters in European-Mediterranean Countries*, Perugia, 205-224.
- Carrara, A., 1988: Drainage and divide networks derived from high-fidelity digital terrain models, in C.F. Chung, A.G. Fabbri, R. Sinding-Larsen (Eds.), *Quantitative Analysis of Mineral and Energy Resources*, Reidel, Dordrecht, 581-597.
- Carrara, A., 1983: Multivariate models for landslide hazard evaluation, *Mathematical Geology*, 15 (3), 403-426.
- Carrara, A., Cardinali, M., Detti, R., Guzzetti, F., Pasqui, V., Reichenbach, P., 1991: GIS techniques and statistical models in evaluating landslide hazard, *Earth Surface Processes and Landforms*, 16 (5), 427-445.
- Carrara, A., Crosta, G., Frattini, P., 2003: Geomorphological and historical data in assessing landslide hazard, *Earth Surface Processes and Landforms*, 28 (10), 1125-1142.
- Carrara, A. and Pike, R.J., 2008: GIS technology and models for assessing landslide hazard and risk, *Geomorphology*, 94 (3-4), 257-260.
- Casadei, M., Dietrich, W.E., Miller, N.L., 2003: Testing a model for predicting the timing and location of shallow landslide initiation in soil-mantled landscapes, *Earth Surface Processes and Landforms*, 28 (9), 925-950.
- Casagli, N., Dapporto, S., Ibsen, M., Tofani, V., Vannocci, P., 2006: Analysis of the landslide triggering mechanism during the storm of 20th-21st November 2000, in Northern Tuscany, *Landslides*, 3, 13-21.

- Cascini, L., Cuomo, S., Della Sala, M., 2011: Spatial and temporal occurrence of rainfall-induced shallow landslides of flow type: A case of Sarno-Quindici, Italy, *Geomorphology*, 126 (1–2), 148-158.
- Catani, F., Casagli, N., Ermini, L., Righini, G., Menduni, G., 2005: Landslide hazard and risk mapping at catchment scale in the Arno River basin, *Landslides*, 2 (4), 329-342.
- Cenderelli, D.A. and Kite, J.S., 1998: Geomorphic effects of large debris flows on channel morphology at North Fork Mountain, eastern West Virginia, USA, *Earth Surface Processes and Landforms*, 23 (1), 1-19.
- Cendrero, A. and Dramis, F., 1996: The contribution of landslides to landscape evolution in Europe, *Geomorphology*, 15 (3–4), 191-211.
- Chandler, R.J., 1972: Periglacial mudslides in Vestpitsbergen and their bearing on the origin of fossil “solifluction” shears in low angled clay slopes, *Quaternary Journal of Engineering Geology*, 5, 223-241.
- Chang, F., Chiang, Y., Lee, W., 2009: Investigating the impact of the Chi-Chi earthquake on the occurrence of debris flows using artificial neural networks, *Hydrological Processes*, 23 (19), 2728-2736.
- Chang, K. and Chiang, S., 2009: An integrated model for predicting rainfall-induced landslides, *Geomorphology*, 105 (3–4), 366-373.
- Chang, K., Chiang, S., Lei, F., 2008: Analysing the relationship between typhoon-triggered landslides and critical rainfall conditions, *Earth Surface Processes and Landforms*, 33 (8), 1261-1271.
- Chau, K. and Chan, J., 2005: Regional bias of landslide data in generating susceptibility maps using logistic regression: Case of Hong Kong Island, *Landslides*, 2 (4), 280-290.
- Chen, C., 2009: Sedimentary impacts from landslides in the Tachia River Basin, Taiwan, *Geomorphology*, 105 (3–4), 355-365.

- Chen, H. and Lee, C.F., 2004: Geohazards of slope mass movement and its prevention in Hong Kong, *Engineering Geology*, 76 (1–2), 3-25.
- Chen, R., Chang, K., Angelier, J., Chan, Y., Deffontaines, B., Lee, C., Lin, M., 2006: Topographical changes revealed by high-resolution airborne LiDAR data: The 1999 Tsaoling landslide induced by the Chi–Chi earthquake, *Engineering Geology*, 88 (3–4), 160-172.
- Chevan, A. and Sutherland, M., 1991: Hierarchical Partitioning, *The American Statistician*, 45 (2), 90-96.
- Chigira, M., Duan, F., Yagi, H., Furuya, T., 2004: Using an airborne laser scanner for the identification of shallow landslides and susceptibility assessment in an area of ignimbrite overlain by permeable pyroclastics, *Landslides*, 1 (3), 203-209.
- Chigira, M. and Yagi, H., 2006: Geological and geomorphological characteristics of landslides triggered by the 2004 Mid Niigata prefecture earthquake in Japan, *Engineering Geology*, 82 (4), 202-221.
- Claessens, L., Schoorl, J.M., Veldkamp, A., 2007: Modelling the location of shallow landslides and their effects on landscape dynamics in large watersheds: An application for Northern New Zealand, *Geomorphology*, 87 (1–2), 16-27.
- Clerici, A., Perego, S., Tellini, C., Vescovi, P., 2002: A procedure for landslide susceptibility zonation by the conditional analysis method, *Geomorphology*, 48 (4), 349-364.
- Coates, D.R., 1977: Landslide perspectives, in D.R. Coates (Ed.), *Landslides*, Geological Society of America, Colorado, 3-28.
- Coelho-Netto, A.L., Avelar, A.S., Fernandes, M.C., Lacerda, W.A., 2007: Landslide susceptibility in a mountainous geocosystem, Tijuca Massif, Rio de Janeiro: The role of morphometric subdivision of the terrain, *Geomorphology*, 87 (3), 120-131.

- Colesanti, C. and Wasowski, J., 2006: Investigating landslides with space-borne Synthetic Aperture Radar (SAR) interferometry, *Engineering Geology*, 88 (3–4), 173-199.
- Colombo, A., Lanteri, L., Ramasco, M., Troisi, C., 2005: Systematic GIS-based landslide inventory as the first step for effective landslide-hazard management, *Landslides*, 2, 291-301.
- Comegna, L., Picarelli, L., Urciuoli, G., 2007: The mechanics of mudslides as a cyclic undrained–drained process, *Landslides*, 4 (3), 217-232.
- Conoscenti, C., Di Maggio, C., Rotigliano, E., 2008: GIS analysis to assess landslide susceptibility in a fluvial basin of NW Sicily (Italy), *Geomorphology*, 94 (3–4), 325-339.
- Cooper, J.A.G., 1993: Sedimentation in the cliff-bound, microtidal Mtamvuna Estuary, South Africa, *Marine Geology*, 112, 237-256.
- Copons, R., Vilaplana, J.M., Linares, R., 2009: Rockfall travel distance analysis by using empirical models, *Natural Hazards and Earth System Sciences*, 9, 2107-2118.
- Corominas, J., 1996: The angle of reach as a mobility index for small and large landslides, *Canadian Geotechnical Journal*, 33 (2), 260-271.
- Corominas, J. and Moya, J., 2010: Contribution of dendrochronology to the determination of magnitude–frequency relationships for landslides, *Geomorphology*, 124 (3–4), 137-149.
- Corsini, A., Borgatti, L., Caputo, G., De Simone, N., Sartini, G., Trufelli, G., 2006: Investigation and monitoring in support of the structural mitigation of large slow moving landslides: an example from Ca' Lita (Northern Apennines, Reggio Emilia, Italy), *Natural Hazards and Earth System Sciences*, 6, 55-61.
- Council for Geoscience, 2008: Drakensberg 2829. Geological Map Sheet 1:250 000.

- Coussot, P. and Meunier, M., 1996: Recognition, classification and mechanical description of debris flows, *Earth-Science Reviews*, 40 (3–4), 209-227.
- Cressie, N.A.C. , 1993: *Statistics for Spatial Data*, John Wiley and Sons, New York.
- Crosta, G.B. and Agliardi, F., 2004: Parametric evaluation of 3D dispersion of rockfall trajectories, *Natural Hazards and Earth System Science*, 4 (4), 583-598.
- Crozier, M.J., 1997: The climate landslide couple: a Southern Hemisphere perspective, in A. Matthews, D. Brunsten, B. Frenzel, B. Glasser, M.M. Weis (Eds.), *Rapid Mass Movement as a Source of Climatic Evidence for the Holocene*, Gustav Fischer, Stuttgart, 333-354.
- Crozier, M.J., 1996: Runout behavior of shallow, rapid earthflows, *Zeitschrift für Geomorphologie, Supplement*, 105, 35-48.
- Crozier, M.J., 1986: *Landslides: Causes, Consequences and Environment*, Croom Helm, Sydney.
- Crozier, M.J., 1973: Techniques for the morphometric analysis of landslips, *Zeitschrift für Geomorphologie*, 17 (1), 78-101.
- Crozier, M.J. and Glade, T., 1999: Frequency and magnitude of landsliding: fundamental research issues, *Zeitschrift für Geomorphologie, Supplement*, 115, 141-155.
- Crozier, M.J., 2005: Multiple-occurrence regional landslide events in New Zealand: Hazard management issues, *Landslides*, 2 (4), 247-256.
- Cruden, D.M., 1991: A simple definition of a landslide, *Bulletin International Association of Engineering Geology*, 43, 27-29.
- Cruden, D.M., 1988: Thresholds for catastrophic instabilities in sedimentary rock slopes, some examples from the Canadian Rockies, *Zeitschrift für Geomorphologie, Supplement*, 67, 67-76.

- Cruden, D.M., Varnes, D.J., 1996: Landslide types and processes, in A.K. Turner, R.L. Schuster (Eds.), *Landslides: Investigation and Mitigation*, National Academy Press, Washington, 36-75.
- Dahal, R., Hasegawa, S., Nonomura, A., Yamanaka, M., Masuda, T., Nishino, K., 2009: Failure characteristics of rainfall-induced shallow landslides in granitic terrains of Shikoku Island of Japan, *Environmental Geology*, 56 (7), 1295-1310.
- Dai, F.C. and Lee, C.F., 2002: Landslide characteristics and slope instability modeling using GIS, Lantau Island, Hong Kong, *Geomorphology*, 42 (3–4), 213-228.
- Dai, F.C., Lee, C.F., Deng, J.H., Tham, L.G., 2005: The 1786 earthquake-triggered landslide dam and subsequent dam-break flood on the Dadu River, southwestern China, *Geomorphology*, 65 (3–4), 205-221.
- Dalrymple, J.B., Blong, R.J., Conacher, A.J., 1968: A hypothetical nine-unit landsurface model, *Zeitschrift für Geomorphologie*, 12, 60-76.
- D'Amato Avanzi, G., Giannecchini, R., Puccinelli, A., 2004: The influence of the geological and geomorphological settings on shallow landslides. An example in a temperate climate environment: the June 19, 1996 event in northwestern Tuscany (Italy), *Engineering Geology*, 73 (3–4), 215-228.
- Dardis, G.F. and Granger, J.E., 1986: Contemporary periglacial phenomena in the Natal Drakensberg, South Africa, *Palaeoecology of Africa*, 17, 89-93.
- de Villiers, J.M. , 1962: A Study of Soil Formation in Natal, PhD thesis, University of Natal, Pietermaritzburg.
- De'ath, G. and Fabricius, K.E., 2000: Classification and regression trees: a powerful yet simple technique for ecological data analysis, *Ecology*, 81 (11), 3178-3192.
- Decaulne, A., SÆmundsson, P., Petursson, O., 2005: Debris Flow Triggered by Rapid Snowmelt: A Case Study in The Gleisárhjalli Area, Northwestern

- Iceland, *Geografiska Annaler: Series A, Physical Geography*, 87 (4), 487-500.
- Delparte, D., Jamieson, B., Waters, N., 2008: Statistical runout modeling of snow avalanches using GIS in Glacier National Park, Canada, *Cold Regions Science and Technology*, 54 (3), 183-192.
- Demoulin, A., Glade, T., 2004: Recent landslide activity in Manaihan, East Belgium, *Landslides*, 1, 305-310.
- Devoli, G., Morales, A., Høeg, K., 2007: Historical landslides in Nicaragua—collection and analysis of data, *Landslides*, 4 (1), 5-18.
- Dewitte, O., Jasselette, J.C., Cornet, Y., van Den Eeckhaut, M., Collignon, A., Poesen, J., Demoulin, A., 2008: Tracking landslide displacements by multi-temporal DTMs: A combined aerial stereophotogrammetric and LIDAR approach in western Belgium, *Engineering Geology*, 99 (1–2), 11-22.
- Dhakal, A.S., Amada, T., Aniya, T.A., 1999: Landslide hazard mapping and the application of GIS in the Kulekhani Watershed, Nepal, *Mountain Research and Development*, 19 (1), 3-16.
- Dhakal, A.S. and Sidle, R.C., 2003: Long-term modelling of landslides for different forest management practices, *Earth Surface Processes and Landforms*, 28 (8), 853-868.
- Dikau, R., Brabb, E.E., Mark, R.M., 1991: Landform Classification of New Mexico by Computer, U.S. Department of the Interior, U.S. Geological Survey.
- Dikau, R., Brunsden, D., Schrott, L., Ibsen, M.L., 1996: *Landslide Recognition: Identification, Movement and Causes*, Wiley, Chichester.
- Dill, H.G., Ludwig, R.R., Kathewera, A., Mwenelupembe, J., 2005: A lithofacies terrain model for the Blantyre Region: Implications for the interpretation of palaeosavanna depositional systems and for environmental geology and

- economic geology in southern Malawi, *Journal of African Earth Sciences*, 41 (5), 341-393.
- Dingle, R.V., Siesser, W.G., Newton, A.R., 1983: *Mesozoic and Tertiary Geology of Southern Africa*, Balkema, Rotterdam.
- Diop, S., Forbes, C., Chiliza, G., 2010: Landslide inventorization and susceptibility mapping in South Africa, *Landslides*, 7 (2), 207-210.
- Dixon, N. and Brook, E., 2007: Impact of predicted climate change on landslide reactivation: case study of Mam Tor, UK, *Landslides*, 4 (2), 137-147.
- Donati, L. and Turrini, M.C., 2002: An objective method to rank the importance of the factors predisposing to landslides with the GIS methodology: application to an area of the Apennines (Valnerina; Perugia, Italy), *Engineering Geology*, 63 (3-4), 277-289.
- Dong, J., Tung, Y., Chen, C., Liao, J., Pan, Y., 2011: Logistic regression model for predicting the failure probability of a landslide dam, *Engineering Geology*, 117 (1-2), 52-61.
- Dore, G. , 2005: Performance of the Beaver Creek Section of the Alaska Highway, *Yukon Highways and Public Works*, Transportation and Engineering Branch, Alaska.
- Doyle, M.W. and Julian, J.P., 2005: The most-cited works in Geomorphology, *Geomorphology*, 72 (1-4), 238-249.
- Du Toit, A.L., 1954: *Geology of South Africa*, Oliver and Boyd, London.
- Duncan, J.M. and Wright, S.G., 2005: *Soil Strength and Slope Stability*, John Wiley and Sons, New Jersey.
- Dunning, S.A., Massey, C.I., Rosser, N.J., 2009: Structural and geomorphological features of landslides in the Bhutan Himalaya derived from Terrestrial Laser Scanning, *Geomorphology*, 103 (1), 17-29.

- Dykes, A.P. and Warburton, J., 2007: Mass movements in peat: A formal classification scheme, *Geomorphology*, 86 (1–2), 73-93.
- Enderton, H.B., 1977: *Elements of Set Theory*, Academic Press, New York.
- Erginal, A., Öztürk, B., Ekinçi, Y., Demirci, A., 2009: Investigation of the nature of slip surface using geochemical analyses and 2-D electrical resistivity tomography: a case study from Lapseki area, NW Turkey, *Environmental Geology*, 58 (6), 1167-1175.
- Eriksson, P.G. , 1983: A Paleoenvironmental Study of the Molteno, Elliot and Clarens Formations in the Natal Drakensberg and the Northeastern Orange Free State, PhD thesis, University of Natal, Pietermaritzburg.
- Ermini, L., Catani, F., Casagli, N., 2005: Artificial Neural Networks applied to landslide susceptibility assessment, *Geomorphology*, 66 (1–4), 327-343.
- Ertek, T.A. and Erginal, A.E., 2006: Anthropogenetically triggered landslide factors of the Varyant landslide area at Büyükçekmece, NW Turkey, *Zeitschrift für Geomorphologie*, 50 (2), 177-191.
- ESRI, 2011: ArcMap, Environmental Systems Resource Institute 9.3.
- ESRI, 2008: ArcMap, Environmental Systems Resource Institute 9.2.
- ESRI, 2004: ArcMap, Environmental Systems Resource Institute 8.3.
- Esterhuizen, G.S. and Streuders, S.B., 1998: Rockfall hazard evaluation using probabilistic keyblock analysis, *Journal of the South African Institute of Mining and Metallurgy* (2), 59-64.
- Falaschi, F., Giacomelli, F., Federici, P., Puccinelli, A., D'Amato Avanzi, G., Pochini, A., Ribolini, A., 2009: Logistic regression versus artificial neural networks: landslide susceptibility evaluation in a sample area of the Serchio River valley, Italy, *Natural Hazards*, 50 (3), 551-569.

- Fall, M., Azzam, R., Noubactep, C., 2006: A multi-method approach to study the stability of natural slopes and landslide susceptibility mapping, *Engineering Geology*, 82 (4), 241-263.
- Federici, P.R., Puccinelli, A., Cantarelli, E., Casarosa, N., D'Amato Avanzi, G., Falaschi, F., Giannecchini, R., Pochini, A., Ribolini, A., Bottai, M., Salvati, N., Testi, C., 2007: Multidisciplinary investigations in evaluating landslide susceptibility—An example in the Serchio River valley (Italy), *Quaternary International*, 171, 52-63.
- Fell, R., Corominas, J., Bonnard, C., Cascini, L., Leroi, E., Savage, W.Z., 2008: Guidelines for landslide susceptibility, hazard and risk zoning for land-use planning, *Engineering Geology*, 102 (3–4), 99-111.
- Fernandes, N.F., Guimarães, R.F., Gomes, R.A.T., Vieira, B.C., Montgomery, D.R., Greenberg, H., 2004: Topographic controls of landslides in Rio de Janeiro: field evidence and modeling, *Catena*, 55 (2), 163-181.
- Finaly, P.J., Fell, R., Maguire, P.K., 1997: The relationship between the probability of landslide occurrence and rainfall, *Canadian Geotechnical Journal*, 34, 811-824.
- Fiorillo, F., 2003: Geological features and landslide mechanisms of an unstable coastal slope (Petacciato, Italy), *Engineering Geology*, 67 (3–4), 255-267.
- Flageollet, J., 1996: The time dimension in the study of mass movements, *Geomorphology*, 15 (3–4), 185-190.
- Flageollet, J., Malet, J.P., Maquaire, O., 2000: The 3D structure of the super-sauze earthflow: A first stage towards modelling its behaviour, *Physics and Chemistry of the Earth, Part B: Hydrology, Oceans and Atmosphere*, 25 (9), 785-791.
- Flageollet, J., Maquaire, O., Martin, B., Weber, D., 1999: Landslides and climatic conditions in the Barcelonnette and Vars basins (Southern French Alps, France), *Geomorphology*, 30 (1–2), 65-78.

- Flageollet, J., Weber, D., 1996: Fall, in R. Dikau, D. Brunsten, L. Schrott, M.L. Ibsen (Eds.), *Landslide Recognition: Identification, Movement and Causes*, Wiley, Chichester, 13-28.
- Floris, M. and Bozzano, F., 2008: Evaluation of landslide reactivation: A modified rainfall threshold model based on historical records of rainfall and landslides, *Geomorphology*, 94 (1–2), 40-57.
- Foote, K.E., Huebner, D.J., 1995: Error, Accuracy and Precision. The Geographers Craft Project, 5 December 2004.
- Frattini, P., Crosta, G., Carrara, A., Agliardi, F., 2008: Assessment of rockfall susceptibility by integrating statistical and physically-based approaches, *Geomorphology*, 94 (3–4), 419-437.
- Fukuoka, H., Wang, G., Sassa, K., Wang, F., Matsumoto, T., 2004: Earthquake-induced rapid long-traveling flow phenomenon: May 2003 Tsukidate landslide in Japan, *Landslides*, 1 (2), 151-155.
- Gabet, E.J., 2007: A theoretical model coupling chemical weathering and physical erosion in landslide-dominated landscapes, *Earth and Planetary Science Letters*, 264 (1–2), 259-265.
- Gabet, E.J. and Mudd, S.M., 2006: The mobilization of debris flows from shallow landslides, *Geomorphology*, 74 (1–4), 207-218.
- Gallart, F., Puigdefabregas, J., del Barrio, G., 1993: Computer simulation of high mountain terraces as interaction between vegetation growth and sediment movement, *Catena*, 20 (6), 529-542.
- Galli, M., Ardizzone, F., Cardinali, M., Guzzetti, F., Reichenbach, P., 2008: Comparing landslide inventory maps, *Geomorphology*, 94 (3–4), 268-289.
- García-Rodríguez, M.J., Malpica, J.A., Benito, B., Díaz, M., 2008: Susceptibility assessment of earthquake-triggered landslides in El Salvador using logistic regression, *Geomorphology*, 95 (3–4), 172-191.

- García-Ruiz, J.M., Beguería, S., Alatorre, L.C., Puigdefábregas, J., 2010: Land cover changes and shallow landsliding in the flysch sector of the Spanish Pyrenees, *Geomorphology*, 124 (3–4), 250-259.
- Garland, G.G., 1979: Asymmetry in the Drakensberg valleys: an alternative point of view, *South African Journal of Science*, 75, 138-140.
- Garland, G.G., 1978: An embankment landslide in Berea Red Sands, Durban, *African Geographical Journal*, 60 (1), 63-70.
- Garland, G.G. and Humphrey, B., 1992: Field measurements of discharge and sediment yield from a soil pipe in the Natal, *Zeitschrift für Geomorphologie*, 36 (1), 15-23.
- Garland, G.G., 1990: Technique for assessing erosion risk from mountain footpaths, *Environmental Management*, 14 (6), 793-798.
- Garland, G.G. and Humphrey, B., 1980: Assessment and mapping of land erosion potential in mountainous recreational areas, *Geoforum*, 11 (1), 63-70.
- Garland, G.G., 1987: Rates of soil loss from mountain footpaths: an experimental study in the Drakensberg Mountains, South Africa, *Applied Geography*, 7 (1), 41-54.
- Geertsema, M., Clague, J.J., Schwab, J.W., Evans, S.G., 2006: An overview of recent large catastrophic landslides in northern British Columbia, Canada, *Engineering Geology*, 83 (1–3), 120-143.
- Geertsema, M. and Pojar, J.J., 2007: Influence of landslides on biophysical diversity — A perspective from British Columbia, *Geomorphology*, 89 (1–2), 55-69.
- Gerrard, A.J. and Gardner, A.M., 2000: The role of landsliding in shaping the landscape of the Middle Hills, Nepal, *Zeitschrift für Geomorphologie, Supplement*, 122, 47-62.

- Gers, E., Florin, N., Gartner, H., Glade, T., Dikau, R., Schweingruber, F.H., 2001: Application of shrubs for dendrogeomorphological analysis to reconstruct spatial and temporal landslide movement patterns: a preliminary study, *Zeitschrift für Geomorphologie, Supplement*, 125, 163-175.
- Gerstell, M.F., Aharonson, O., Schorghofer, N., 2004: A distinct class of avalanche scars on Mars, *Icarus*, 168 (1), 122-130.
- Gibson, L.A., Wilson, B.A., Cahill, D.M., Hill, J., 2004: Spatial prediction of rufous bristlebird habitat in a coastal heathland: a GIS-based approach, *Journal of Applied Ecology*, 41 (2), 213-223.
- Glade, T., 2000: Modelling landslide triggering rainfall thresholds at a range of complexities, in E. Bromhead, N. Dixon, M.L. Ibsen (Eds.), *Landslides in Research, Theory and Practice*, Thomas Telford, Cardiff, 633-640.
- Glade, T., 2005: Linking debris-flow hazard assessments with geomorphology, *Geomorphology*, 66 (1-4), 189-213.
- Glenn, N.F., Streutker, D.R., Chadwick, D.J., Thackray, G.D., Dorsch, S.J., 2006: Analysis of LiDAR-derived topographic information for characterizing and differentiating landslide morphology and activity, *Geomorphology*, 73 (1-2), 131-148.
- Göçtürkler, G., Balkaya, C., Erhan, Z., Yurdakul, A., 2008. Investigation of a shallow alluvial aquifer using geoelectrical methods: a case from Turkey. *Environmental Geology* 54, 1283-1290.
- Godt, J.W., Baum, R.L., Chleborad, A.F., 2006: Rainfall characteristics for shallow landsliding in Seattle, Washington, USA, *Earth Surface Processes and Landforms*, 31 (1), 97-110.
- Gokceoglu, C., Sonmez, H., Nefeslioglu, H.A., Duman, T.Y., Can, T., 2005: The 17 March 2005 Kuzulu landslide (Sivas, Turkey) and landslide-susceptibility map of its near vicinity, *Engineering Geology*, 81 (1), 65-83.

- González-Díez, A., Remondo, J., Díaz de Terán, J.R., Cendrero, A., 1999: A methodological approach for the analysis of the temporal occurrence and triggering factors of landslides, *Geomorphology*, 30 (1–2), 95-113.
- Goodchild, M.F., 2001: Metrics of scale in remote sensing and GIS, *International Journal of Applied Earth Observation and Geoinformation*, 3 (2), 114-120.
- Gordon, A.D., 1987: A review of hierarchical classification, *Journal of the Royal Statistical Society*, 150, 119-137.
- Gorsevski, P.V., Gessler, P.E., Foltz, R.B., Elliot, W.J., 2006: Spatial Prediction of Landslide Hazard Using Logistic Regression and ROC Analysis, *Transactions in GIS*, 10 (3), 395-415.
- Goudie, A.S., 2004: *Encyclopedia of Geomorphology*, Routledge, London.
- Grab, S.W., 1996: Slope deposits in the high Drakensberg, South Africa: possible indicators for plateau, niche and cirque glaciation, *Zeitschrift für Geomorphologie, Supplement*, 103, 389-403.
- Grab, S.W., 2007: Near-surface rockwall temperatures in the high Drakensberg basalt: spatio-temporal differences and possible implications for weathering, *Zeitschrift für Geomorphologie, Supplement*, 51, 103-113.
- Grab, S.W., Mulder, N.A., Mills, S.C., 2009: Spatial associations between longest-lasting winter snow cover and cold region landforms in the High Drakensberg, southern Africa , *Geografiska Annaler: Series A, Physical Geography*, 91 (2), 83-97.
- Grab, S.W., 2005a: Aspects of the geomorphology, genesis and environmental significance of earth hummocks (thúfur, pounus): miniature cryogenic mounds, *Progress in Physical Geography*, 29 (2), 139-155.
- Grab, S.W., 2005b: Earth hummocks (thúfur): new insights to their thermal characteristics and development in eastern Lesotho, southern Africa, *Earth Surface Processes and Landforms*, 30 (5), 541-555.

- Grab, S.W., 2002: Characteristics and palaeoenvironmental significance of relict sorted patterned ground, Drakensberg plateau, southern Africa, *Quaternary Science Reviews*, 21 (14–15), 1729-1744.
- Grab, S.W., 2001: Needle ice observations from the high Drakensberg, Lesotho, *Permafrost and Periglacial Processes*, 12 (2), 227-231.
- Grab, S.W., 2000: Stone-banked lobes and environmental implications, high Drakensberg, southern Africa, *Permafrost and Periglacial Processes*, 11 (3), 177-187.
- Grab, S.W., 1999: Block and Debris Deposits in the High Drakensberg, Lesotho, Southern Africa: Implications for High Altitude Slope Processes, *Geografiska Annaler: Series A, Physical Geography*, 81 (1), 1-16.
- Grab, S.W., 1994: Thufur in the Mohlesi Valley, Lesotho, southern Africa, *Permafrost and Periglacial Processes*, 5 (2), 111-118.
- Grab, S.W. and Kalibbala, F., 2008: ‘Anti-erosion’ logs across paths in the southern uKhahlamba–Drakensberg Transfrontier Park, South Africa: Cure or curse?, *Catena*, 73 (1), 134-145.
- Grab, S.W., van Zyl, C., Mulder, N., 2005: Controls on basalt terrace formation in the eastern Lesotho highlands, *Geomorphology*, 67 (3–4), 473-485.
- Granger, J.E. , 1976: The Vegetated Changes, some Related Factors in the Water Balance Following 20 Years of Fire Exclusion in Catchment IX, Cathedral Peak Forestry Station, PhD thesis, University of Natal, Pietermaritzburg.
- GRASS Development Team, 2011: Geographic Resources Analysis Support System (GRASS), Users manual 6.4, 1-425.
- Greco, R., Sorriso-Valvo, M., Catalano, E., 2007: Logistic Regression analysis in the evaluation of mass movements susceptibility: The Aspromonte case study, Calabria, Italy, *Engineering Geology*, 89 (1–2), 47-66.

- Green, R.W.E. and Bloch, S., 1971: The Ceres, South Africa, earthquake of September 29, 1969: Report on some aftershocks, *Bulletin of the Seismological Society of America*, 61 (4), 851-859.
- Groenewald, G.H., 1986: Geology of the Golden Gate Highlands National Park, *Koedoe*, 29, 165-181.
- Gruber, S. and Haeberli, W., 2007: Permafrost in steep bedrock slopes and its temperature-related destabilization following climate change, *Journal of Geophysical Research*, 112, 2-19.
- Guisan, A. and Zimmermann, N.E., 2000: Predictive habitat distribution models in ecology, *Ecological Modelling*, 135 (2-3), 147-186.
- Gupta, R.P. and Joshi, B.C., 1990: Landslide hazard zoning using the GIS approach—A case study from the Ramganga catchment, Himalayas, *Engineering Geology*, 28 (1-2), 119-131.
- Gupta, V., 2001: Geomorphological controls on landslide activity in the Du Toitskloof, Western Cape mountains, South Africa, *South African Geographical Journal*, 83 (3), 258-262.
- Guthrie, R.H. and Evans, S.G., 2004: Analysis of landslide frequencies and characteristics in a natural system, coastal British Columbia, *Earth Surface Processes and Landforms*, 29 (11), 1321-1339.
- Guzzetti, F., Cardinali, M., Reichenbach, P., Carrara, A., 2000: Comparing landslide maps: a case study in the Upper Tiber River Basin, Central Italy, *Environmental Management*, 25 (3), 247-263.
- Guzzetti, F., Peruccacci, S., Rossi, M., Stark, C.P., 2007: Rainfall thresholds for the initiation of landslides in central and southern Europe, *Meteorology and Atmospheric Physics*, 98 (3), 239-267.
- Guzzetti, F., Ardizzone, F., Cardinali, M., Rossi, M., Valigi, D., 2009: Landslide volumes and landslide mobilization rates in Umbria, central Italy, *Earth and Planetary Science Letters*, 279 (3-4), 222-229.

- Guzzetti, F., Carrara, A., Cardinali, M., Reichenbach, P., 1999: Landslide hazard evaluation: a review of current techniques and their application in a multi-scale study, Central Italy, *Geomorphology*, 31 (1–4), 181-216.
- Guzzetti, F., Peruccacci, S., Rossi, M., Stark, C., 2008: The rainfall intensity–duration control of shallow landslides and debris flows: an update, *Landslides*, 5 (1), 3-17.
- Guzzetti, F., Reichenbach, P., Ardizzone, F., Cardinali, M., Galli, M., 2006: Estimating the quality of landslide susceptibility models, *Geomorphology*, 81 (1–2), 166-184.
- Guzzetti, F., Reichenbach, P., Cardinali, M., Galli, M., Ardizzone, F., 2005: Probabilistic landslide hazard assessment at the basin scale, *Geomorphology*, 72 (1–4), 272-299.
- Hancox, G.T. and Perrin, N.D., 2009: Green Lake Landslide and other giant and very large postglacial landslides in Fiordland, New Zealand, *Quaternary Science Reviews*, 28 (11–12), 1020-1036.
- Hansen, M.J., 1984: Strategies for the classification of landslides, in D. Brunsten, B.P. Prior (Eds.), *Slope Instability*, Wiley, New York, 1-25.
- Hanvey, P.M., Lewis, C.A., Lewis, G.E., 1986: Periglacial slope deposits in Carlisle's Hoek, near Rhodes, Eastern Cape Province, *South African Geographical Journal*, 68, 164-174.
- Hanvey, P.M. and Marker, M.E., 1992: Present-day periglacial microforms in the Lesotho Highlands: Implications for present and past climatic conditions, *Permafrost and Periglacial Processes*, 3 (4), 353-361.
- Hardenbicker, U. and Grunert, J.M., 2001: Temporal occurrence of mass movements in the Bonn area, *Zeitschrift für Geomorphologie, Supplement* (125), 13-24.
- Harper, G., 1969: Periglacial evidence in southern Africa during the Pleistocene epoch, *Palaeoecology of Africa*, 4, 71-101.

- Harris, S.A. and Gustafson, C.A., 1993: Debris flow characteristics in an area of continuous permafrost, St. Elias Range, Yukon Territory, *Zeitschrift für Geomorphologie, Supplement*, 37, 41-56.
- Harris, S.A. and Gustafson, C.A., 1988: Retrogressive slumps, debris flows and river valley development in icy, unconsolidated sediments on hills and mountains, *Zeitschrift für Geomorphologie, Supplement*, 32, 441-455.
- Harris, S.A. and McDermid, G., 1998: Frequency of debris flows on the Sheep Mountain Fan, Kluane Lake, Yukon Territory, *Zeitschrift für Geomorphologie, Supplement*, 42, 159-175.
- Harris, C., Smith, J.S., Davies, M.C.R., Rea, B., 2008: An investigation of periglacial slope stability in relation to soil properties based on physical modelling in the geotechnical centrifuge, *Geomorphology*, 93 (3–4), 437-459.
- Harris, P.D., Branney, M.J., Storey, M., 2011: Large eruption-triggered ocean-island landslide at Tenerife: Onshore record and long-term effects on hazardous pyroclastic dispersal, *Geology*, 39 (10), 951-954.
- Harrison, K.P. and Grimm, R.E., 2003: Rheological constraints on martian landslides, *Icarus*, 163 (2), 347-362.
- Hart, M.W., May, 2008: Structural and Geomorphic Characteristics of Landslides at Coyote Mountain, Anza-Borrego Desert State Park, California, *Environmental & Engineering Geoscience*, 14 (2), 81-96.
- Harvey, D. , 1969: *Explanation in Geography*, E. Arnold, London.
- Hastenrath, S. and Wilkinson, J., 1973: A contribution to the periglacial morphology of Lesotho, southern Africa, *Biuletyn Peryglacjalny*, 22, 157-167.
- Haughton, S.H., 1969: *Geological History of Southern Africa*, Geological Society of South Africa, Cape Town.

- Havenith, H., Strom, A., Caceres, F., Pirard, E., 2006: Analysis of landslide susceptibility in the Suusamyr region, Tien Shan: statistical and geotechnical approach, *Landslides*, 3 (1), 39-50.
- Heim, A., 1932: *Bergsturz Und Menschenleben*, Fretz and Wasmuth, Zurich.
- Heim, A., 1882: Der Bergsturz von Elm, *Zeitschrift der Deutschen Geologischen Gesellschaft*, 34, 74-115.
- Helsen, M.M., Koop, P.J.M., Van Steijn, H., 2002: Magnitude-frequency relationship for debris flows on the fan of the Chalance torrent, Valgaudemar (French Alps), *Earth Surface Processes and Landforms*, 27 (12), 1299-1307.
- Hencher, S.R., 2010: Preferential flow paths through soil and rock and their association with landslides, *Hydrological Processes*, 24 (12), 1610-1630.
- Hengl, T., Sierdsema, H., Radović, A., Dilo, A., 2009: Spatial prediction of species' distributions from occurrence-only records: combining point pattern analysis, ENFA and regression-kriging, *Ecological Modelling*, 220 (24), 3499-3511.
- Hewitt, K., 1993: The altitudinal distribution of Karakoram geomorphic processes and depositional environments, in J.F. Shroder (Ed.), *Himalaya to the Sea: Geology, Geomorphology and the Quaternary*, Routledge, New York, 159-183.
- Hewitt, K., Clague, J.J., Orwin, J.F., 2008: Legacies of catastrophic rock slope failures in mountain landscapes, *Earth-Science Reviews*, 87 (1-2), 1-38.
- Hilliard, O.M. and Burt, B.L., 1987: *the Botany of the Southern Natal Drakensberg*, National Botanic Gardens, Cape Town.
- Hirzel, A.H., Hausser, J., Chessel, D., Perrin, N., 2002: Ecological-niche factor analysis: how to compute habitat-suitability maps without absence data?, *Ecology*, 83 (7), 2027-2036.

- Hjort, I. , 2006: *Environmental Factors Affecting the Occurrence of Periglacial Landforms in Finnish Lapland: A Numerical Approach*, Shaker Verlag, Aachen.
- Hjort, J. and Marmion, M., 2009: Periglacial distribution modelling with a boosting method, *Permafrost and Periglacial Processes*, 20 (1), 15-25.
- Holm, K. and Jakob, M., 2009: Long rockfall runout, Pascua Lama, Chile, *Canadian Geotechnical Journal*, 46 (2), 225-230.
- Howe, E., 1909: *Landslides in the San Juan Mountains, Colorado, U.S. Geological Survey Professional Paper 67*, U.S. Geological Survey, Colorado.
- Hsieh, F.Y., Bloch, D.A., Larsen, M.D., 1998: A simple method for sample size calculation for linear and logistic regression regression, *Statistics in Medicine*, 17, 1623-1634.
- Huabin, W., Gangjun, L., Weiya, X., Gonghui, W., 2005: GIS-based landslide hazard assessment: an overview, *Progress in Physical Geography*, 29 (4), 548-567.
- Hughenoltz, C.H. and Lewkowicz, A.G., 2002: Morphometry and environmental characteristics of turf-banked solifluction lobes, Kluane Range, Yukon Territory, Canada, *Permafrost and Periglacial Processes*, 13 (4), 301-313.
- Huggel, C., Schneider, D., Miranda, P.J., Delgado Granados, H., Kääh, A., 2008: Evaluation of ASTER and SRTM DEM data for lahar modeling: A case study on lahars from Popocatepetl Volcano, Mexico, *Journal of Volcanology and Geothermal Research*, 170 (1–2), 99-110.
- Humphreys, A.J.B., 1971: Age determination of the rock art of southern Africa, *South African Journal of Science*, 2, 86-90.
- Hungr, O., Evans, S.G., Bovis, M.J., Hutchinson, J.N., 2001: A review of the classification of landslides of the flow type, *Environmental & Engineering Geoscience*, 7 (3), 221-238.

- Hungr, O., McDougall, S., Bovis, M.J., 2005: Entrainment of material by debris flows, in M. Jakob, O. Hungr (Eds.), *Debris-Flow Hazards and Related Phenomena*, Springer-Praxis, Berlin, 135-158.
- Hungr, O., McDougall, S., Wise, M., Cullen, M., 2008: Magnitude–frequency relationships of debris flows and debris avalanches in relation to slope relief, *Geomorphology*, 96 (3–4), 355-365.
- Hürlimann, M., Ledesma, A., Martí, J., 2001: Characterisation of a volcanic residual soil and its implications for large landslide phenomena: application to Tenerife, Canary Islands, *Engineering Geology*, 59 (1–2), 115-132.
- Hutchinson, J.N., 1988: Morphological and Geotechnical Parameters of Landslides in Relation to Geology and Hydrogeology. Proceedings of the Proceedings of the 5th International Symposium on Landslides, Lausanne, Switzerland, 3-36.
- Hutchinson, J.N., 1968: Mass movement, in R.W. Fairbridge (Ed.), *Encyclopaedia of Earth Sciences*, Reinhold, New York, 688-695.
- Hutchinson, J.N., 1983: A pattern in the incidence of major coastal mudslides, *Earth Surface Processes and Landforms*, 8 (4), 391-397.
- Hutchinson, M.F., 1989: A new procedure for gridding elevation and stream line data with automatic removal of spurious pits, *Journal of Hydrology*, 106 (3–4), 211-232.
- Ibsen, M.L. , 1994: Evaluation of the Temporal Distribution of Landslide Events Along the South Coast of Britain between Straight Point and St, Margaret's Bay, PhD, University of London, London.
- Irwin, P., Ackhurst, J., Irwin, D. , 1980: *A Field Guide to the Natal Drakensberg*, Wildlife Society of South Africa, Durban.
- Iverson, R.M., 1997: The physics of debris flows, *Reviews of Geophysics*, 35 (3), 245-296.

- Iverson, R.M., LaHusen, R.G., 1993: Friction in Debris Flows: Inferences from Large-Scale Flume Experiments. Proceedings of the Hydraulic Engineering, American Society of Civil Engineers, San Francisco, California, 1604-1609.
- Ivy-Ochs, S., Poschinger, A.v., Synal, H.A., Maisch, M., 2009: Surface exposure dating of the Flims landslide, Graubünden, Switzerland, *Geomorphology*, 103 (1), 104-112.
- Jaboyedoff, M. and Labiouse, V., 2011: Technical note: preliminary estimation of rockfall runout zones, *Natural Hazards and Earth System Sciences*, 11, 819-828.
- Jakob, M. and Friele, P., 2010: Frequency and magnitude of debris flows on Cheekye River, British Columbia, *Geomorphology*, 114 (3), 382-395.
- Jakob, M., 2005: A size classification for debris flows, *Engineering Geology*, 79 (3-4), 151-161.
- Jakob, M. and Lambert, S., 2009: Climate change effects on landslides along the southwest coast of British Columbia, *Geomorphology*, 107 (3-4), 275-284.
- James, F.C. and McCulloch, C.E., 1990: Multivariate analysis in Ecology and Systematics: Panacea or Pandora's Box?, *Annual Review of Ecology and Systematics*, 21, 129-166.
- Jongmans, D. and Garambois, S., 2007: Geophysical investigation of landslides : a review, *Bulletin de la Societe Geologique de France*, 178 (2), 101-112.
- Jordan, G., 2003: Morphometric analysis and tectonic interpretation of digital terrain data: a case study, *Earth Surface Processes and Landforms*, 28 (8), 807-822.
- Kääb, A., 2008: Remote sensing of permafrost-related problems and hazards, *Permafrost and Periglacial Processes*, 19 (2), 107-136.

- Kandel, A., 1986: *Fuzzy Mathematical Techniques with Applications*, Addison-Wesley Longman, Boston.
- Kasai, M., Ikeda, M., Asahina, T., Fujisawa, K., 2009: LiDAR-derived DEM evaluation of deep-seated landslides in a steep and rocky region of Japan, *Geomorphology*, 113 (1–2), 57-69.
- Katz, O. and Aharonov, E., 2006: Landslides in vibrating sand box: What controls types of slope failure and frequency magnitude relations?, *Earth and Planetary Science Letters*, 247 (3–4), 280-294.
- Kawagoe, S., Kazama, S., Ranjan Sarukkalige, P., 2009: Assessment of snowmelt triggered landslide hazard and risk in Japan, *Cold Regions Science and Technology*, 58 (3), 120-129.
- Keefer, D.K., 1984: Landslides caused by earthquakes, *Bulletin of the Geological Society of America*, 95, 406-421.
- Kenny, F. and Matthews, B., 2005: A methodology for aligning raster flow direction data with photogrammetrically mapped hydrology, *Computers & Geosciences*, 31 (6), 768-779.
- Keqiang, H., Xiangran, L., Xueqing, Y., Dong, G., 2008: The landslides in the Three Gorges Reservoir Region, China and the effects of water storage and rain on their stability, *Environmental Geology*, 55 (1), 55-63.
- Khaldoun, A., Moller, P., Fall, A., Wegdam, G., De Leeuw, B., Méheust, Y., Otto Fossum, J., Bonn, D., 2009: Quick clay and landslides of clayey soils, *Physical Review Letters*, 103 (18), 188-301.
- Killick, D.J.B., 1990: *A Field Guide - the Flora of the Natal Drakensberg*, Jonathan Ball and Ad Donker, Johannesburg.
- Killick, D.J.B., 1963: An Account of the Plant Ecology of the Cathedral Peak Area of the Natal Drakensberg, *Memoirs of the Botanical Society*, Botanical Research Institute, Pretoria.

- King, L.C., 1982: *The Natal Monocline*, University of Natal Press, Pietermaritzburg.
- King, L.C., 1944: Geomorphology of the Natal Drakensberg, *Transactions of the Geological Society of southern Africa*, 47, 255-282.
- Kirschbaum, D.B., Adler, R., Hong, Y., Hill, S., Lerner-Lam, A., 2010: A global landslide catalogue for hazard applications: method, results and limitations, *Natural Hazards*, 52, 561-575.
- Klose, C., 2006: Climate and geomorphology in the uppermost geomorphic belts of the Central Mountain Range, Taiwan, *Quaternary International*, 147 (1), 89-102.
- Knight, K., Everitt, P.R., Sudgen, M.B. , 1977: Stability of Shale Slopes on the Natal Coastal Belt. Proceedings of the Fifth South -East Asian Conference on Soil Engineering, Bangkok, 201-212.
- Ko Ko, C., Flentje, P., Chowdhury, R., 2004: Interpretation of probability of landsliding triggered by rainfall, *Landslides*, 1 (4), 263-275.
- Komac, M., 2006: A landslide susceptibility model using the Analytical Hierarchy Process method and multivariate statistics in perialpine Slovenia, *Geomorphology*, 74 (1-4), 17-28.
- Korup, O., 2004: Landslide-induced river channel avulsions in mountain catchments of southwest New Zealand, *Geomorphology*, 63 (1-2), 57-80.
- Kovanen, D.J. and Slaymaker, O., 2008: The morphometric and stratigraphic framework for estimates of debris flow incidence in the North Cascades foothills, Washington State, USA, *Geomorphology*, 99 (1-4), 224-245.
- Kruger, S., 2007: Wilderness stewardship challenges in the uKhahlamba Drakensberg Park World Heritage Site, in A. Watson, J. Sproull, L. Dean (Eds.), *Science and Stewardship to Protect and Sustain Wilderness Values, Proceedings RMRS-P-49*, Department of Agriculture, Rocky Mountain Research Station, 326-330.

- Kück, K.M. and Lewis, C.A., 2002: Terracettes and active gelifluction terraces in the Drakensberg of the Province of the Eastern Cape, South Africa: a process study, *South African Geographical Journal*, 84 (2), 214-225.
- Ladd, G.E., 1935: Landslides, subsidence and rock-falls, *American Railway Engineering Association Proceedings*, 36, 1091-1162.
- Lamb, P.J., 1982: The persistence of Sub-Saharan drought, *Nature*, 299, 46-48.
- Lan, H.X., Zhou, C.H., Wang, L.J., Zhang, H.Y., Li, R.H., 2004: Landslide hazard spatial analysis and prediction using GIS in the Xiaojiang watershed, Yunnan, China, *Engineering Geology*, 76 (1-2), 109-128.
- Lan, H., Derek Martin, C., Lim, C.H., 2007: RockFall Analyst: A GIS extension for three-dimensional and spatially distributed rockfall hazard modeling, *Computers & Geosciences*, 33 (2), 262-279.
- Lan, H., Martin, C.D., Zhou, C., Lim, C.H., 2010: Rockfall hazard analysis using LiDAR and spatial modeling, *Geomorphology*, 118 (1-2), 213-223.
- Lang, A., Moya, J., Corominas, J., Schrott, L., Dikau, R., 1999: Classic and new dating methods for assessing the temporal occurrence of mass movements, *Geomorphology*, 30 (1-2), 33-52.
- Lavigne, F., Thouret, J.C., Voight, B., Suwa, H., Sumaryono, A., 2000: Lahars at Merapi volcano, Central Java: an overview, *Journal of Volcanology and Geothermal Research*, 100 (1-4), 423-456.
- Le Roux, O., Schwartz, S., Gamond, J.F., Jongmans, D., Bourles, D., Braucher, R., Mahaney, W., Carcaillet, J., Leanni, L., 2009: CRE dating on the head scarp of a major landslide (Séchilienne, French Alps), age constraints on Holocene kinematics, *Earth and Planetary Science Letters*, 280 (1-4), 236-245.
- Lee, K.T. and Ho, J., 2009: Prediction of landslide occurrence based on slope-instability analysis and hydrological model simulation, *Journal of Hydrology*, 375 (3-4), 489-497.

- Lee, S., 2007: Application and verification of fuzzy algebraic operators to landslide susceptibility mapping, *Environmental Geology*, 52 (4), 615-623.
- Lee, S., 2005: Application of logistic regression model and its validation for landslide susceptibility mapping using GIS and remote sensing data, *International Journal of Remote Sensing*, 26 (7), 1477-1491.
- Lee, S., 2004: Application of likelihood ratio and logistic regression models to landslide susceptibility mapping using GIS, *Environmental Management*, 34 (2), 223-232.
- Lee, S. and Pradhan, B., 2007: Landslide hazard mapping at Selangor, Malaysia using frequency ratio and logistic regression models, *Landslides*, 4 (1), 33-41.
- Lee, S., Ryu, J., Kim, I., 2007: Landslide susceptibility analysis and its verification using likelihood ratio, logistic regression, and artificial neural network models: case study of Youngin, Korea, *Landslides*, 4 (4), 327-338.
- Lee, S., Ryu, J., Min, K., Won, J., 2003: Landslide susceptibility analysis using GIS and artificial neural network, *Earth Surface Processes and Landforms*, 28 (12), 1361-1376.
- Lee, S. and Sambath, T., 2006: Landslide susceptibility mapping in the Damrei Romel area, Cambodia using frequency ratio and logistic regression models, *Environmental Geology*, 50 (6), 847-855.
- Legros, F., 2002: The mobility of long-runout landslides, *Engineering Geology*, 63 (3-4), 301-331.
- Lemon, S., Roy, J., Clark, M., Friedmann, P., Rakowski, W., 2003: Classification and regression tree analysis in public health: Methodological review and comparison with logistic regression, *Annals of Behavioral Medicine*, 26 (3), 172-181.

- Lewis, C.A., 1996: Periglacial features, in C.D. Lewis (Ed.), *The Geomorphology of the Eastern Cape*, Grocott and Sherry, Grahamstown, 103-119.
- Lewis, C.A., 1988: Periglacial landforms, in B.P. Moon, G.F. Dardis (Eds.), *The Geomorphology of Southern Africa*, Southern Book Publishers, Johannesburg, 325-335.
- Lewis, C.A., 1987: Periglacial features in southern Africa: an assessment, *Palaeoecology of Africa*, 19, 357-370.
- Lewis, C.A., 2005: Late Glacial and Holocene palaeoclimatology of the Drakensberg of the Eastern Cape, South Africa, *Quaternary International*, 129 (1), 33-48.
- Li, C., Ma, T., Zhu, X., Li, W., 2011: The power-law relationship between landslide occurrence and rainfall level, *Geomorphology*, 130 (3-4), 221-229.
- Lin, G., Chen, H., Hovius, N., Horng, M., Dadson, S., Meunier, P., Lines, M., 2008: Effects of earthquake and cyclone sequencing on landsliding and fluvial sediment transfer in a mountain catchment, *Earth Surface Processes and Landforms*, 33 (9), 1354-1373.
- Linde, J. and Grab, S.W., 2008: Regional contrasts in mountain tourism development in the Drakensberg, South Africa, *Mountain Research and Development*, 28 (1), 65-71.
- Lineback Gritzner, M., Marcus, W.A., Aspinall, R., Custer, S.G., 2001: Assessing landslide potential using GIS, soil wetness modeling and topographic attributes, Payette River, Idaho, *Geomorphology*, 37 (1-2), 149-165.
- Liu, J.G., Mason, P.J., Clerici, N., Chen, S., Davis, A., Miao, F., Deng, H., Liang, L., 2004: Landslide hazard assessment in the Three Gorges area of the Yangtze river using ASTER imagery: Zigui-Badong, *Geomorphology*, 61 (1-2), 171-187.

- Mac Nally, R., 1996: Hierarchical partitioning as an interpretative tool in multivariate inference, *Australian Journal of Ecology*, 21 (2), 224-228.
- Mac Nally, R., 2000: Regression and model-building in conservation biology, biogeography and ecology: The distinction between – and reconciliation of – ‘predictive’ and ‘explanatory’ models, *Biodiversity and Conservation*, 9 (5), 655-671.
- Mac Nally, R. and Horrocks, G., 2002: Relative influences of patch, landscape and historical factors on birds in an Australian fragmented landscape, *Journal of Biogeography*, 29 (3), 395-410.
- Malamud, B.D., Turcotte, D.L., Guzzetti, F., Reichenbach, P., 2004: Landslide inventories and their statistical properties, *Earth Surface Processes and Landforms*, 29 (6), 687-711.
- Malczewski, J., 2006: GIS - based multicriteria decision analysis: a survey of the literature, *International Journal of Geographical Information Science*, 20 (7), 703-726.
- Malet, J.P., Laigle, D., Remaître, A., Maquaire, O., 2005: Triggering conditions and mobility of debris flows associated to complex earthflows, *Geomorphology*, 66 (1–4), 215-235.
- Malin, M.C. and Edgett, K.S., 2000: Evidence for recent groundwater seepage and surface runoff on Mars, *Science*, 288 (5475), 2330-2335.
- Mangold, N., 2005: High latitude patterned grounds on Mars: Classification, distribution and climatic control, *Icarus*, 174 (2), 336-359.
- Mantovani, F., Soeters, R., Van Westen, C.J., 1996: Remote sensing techniques for landslide studies and hazard zonation in Europe, *Geomorphology*, 15 (3–4), 213-225.
- Margielewski, W. and Urban, J., 2003: Crevice-type caves as initial forms of rock landslide development in the Flysch Carpathians, *Geomorphology*, 54 (3–4), 325-338.

- Marker, M.E., 1989: Periglacial geomorphology at Golden Gate Highlands National Park: a note on its fieldwork potential, *South African Geographer*, 16 (1/2), 147-153.
- Marquez, R., Zêzere, J.L., Queiroz, G., Coutinho, R., 2007: GIS-based logistic regression method for susceptibility assessment of earthquake-triggered landslides: a case study from Fogo Volcano (S. Miguel, Azores), *Geophysical Research Abstracts*, 9, 1-17.
- Marston, R.A., 2010: Geomorphology and vegetation on hillslopes: Interactions, dependencies, and feedback loops, *Geomorphology*, 116 (3–4), 206-217.
- Martelloni, G., Segoni, S., Fanti, R., Catani, F., 2011: Rainfall thresholds for the forecasting of landslide occurrence at regional scale, *Landslides*, 1-11.
- Martha, T.R., Kerle, N., Jetten, V., van Westen, C.J., Kumar, K.V., 2010: Characterising spectral, spatial and morphometric properties of landslides for semi-automatic detection using object-oriented methods, *Geomorphology*, 116 (1–2), 24-36.
- Martin, Y., 2000: Modelling hillslope evolution: linear and nonlinear transport relations, *Geomorphology*, 34 (1–2), 1-21.
- Mathew, J., Jha, V., Rawat, G., 2009: Landslide susceptibility zonation mapping and its validation in part of Garhwal Lesser Himalaya, India, using binary logistic regression analysis and receiver operating characteristic curve method, *Landslides*, 6 (1), 17-26.
- Matsuoka, N., 2001: Solifluction rates, processes and landforms: a global review, *Earth-Science Reviews*, 55 (1–2), 107-134.
- Matsuoka, N., Ikeda, A., Date, T., 2005: Morphometric analysis of solifluction lobes and rock glaciers in the Swiss Alps, *Permafrost and Periglacial Processes*, 16 (1), 99-113.

- May, C.L. and Gresswell, R.E., 2004: Spatial and temporal patterns of debris-flow deposition in the Oregon Coast Range, USA, *Geomorphology*, 57 (3–4), 135-149.
- McCarthy, T. and Rubidge, B., 2005: *Earth and Life*, Struik, Cape Town.
- McDougall, S. and Hungr, O., 2004: A model for the analysis of rapid landslide motion across three-dimensional terrain, *Canadian Geotechnical Journal*, 41 (6), 1084-1097.
- McKean, J. and Roering, J., 2004: Objective landslide detection and surface morphology mapping using high-resolution airborne laser altimetry, *Geomorphology*, 57 (3–4), 331-351.
- Meiklejohn, K.I., 1997: The role of moisture in the weathering of the Clarens Formation of the KwaZulu-Natal Drakensberg: Implications for the preservation of indigenous rock art, *South African Geographical Journal*, 79 (3), 199-206.
- Meiklejohn, K.I., 1992: Some aspects of valley asymmetry in the high Drakensberg, *South African Geographical Journal*, 74, 49-53.
- Meiklejohn, K.I., Hall, K., Davis, J.K., 2009: Weathering of rock art at two sites in the KwaZulu-Natal Drakensberg, southern Africa, *Journal of Archaeological Science*, 36 (4), 973-979.
- Menéndez Duarte, R. and Marquínez, J., 2002: The influence of environmental and lithologic factors on rockfall at a regional scale: an evaluation using GIS, *Geomorphology*, 43 (1–2), 117-136.
- Metternicht, G., Hurni, L., Gogu, R., 2005: Remote sensing of landslides: An analysis of the potential contribution to geo-spatial systems for hazard assessment in mountainous environments, *Remote Sensing of Environment*, 98 (2–3), 284-303.

- Migoñ, P., 2010: Landslide geomorphology in weathered terrains, in D. Calcaterra, M. Parise (Eds.), *Weathering as a Predisposing Factor to Slope Movements*, The Geological Society, Bath, 33-46.
- Miles, S.B. and Keefer, D.K., 2009: Evaluation of CAMEL — comprehensive areal model of earthquake-induced landslides, *Engineering Geology*, 104 (1–2), 1-15.
- Mills, S.C. and Grab, S.W., 2005: Debris ridges along the southern Drakensberg escarpment as evidence for Quaternary glaciation in southern Africa, *Quaternary International*, 129 (1), 61-73.
- Mills, S.C., Grab, S.W., Carr, S.J., 2009: Recognition and palaeoclimatic implications of late Quaternary niche glaciation in eastern Lesotho, *Journal of Quaternary Science*, 24 (7), 647-663.
- Mitchell, P.J., 1996: The late Quaternary of the Lesotho highlands, southern Africa: preliminary results and future potential of ongoing research at Sehonghong shelter, *Quaternary International*, 33, 35-43.
- Miyabe, N., 1935: A study of landslides, *Bulletin of the Earthquake Research Institute*, 13, 85-113.
- Molitor, D., 1894: Landslides, *Journal of the Association of Engineering Societies*, 13, 12-32.
- Möller, R., Glade, T., Dikau, R., 2001: Application of Soil Mechanical Response Units (SMRU) in regional landslide hazard assessment, *Zeitschrift für Geomorphologie, Supplement*, 125, 139-151.
- Molnar, P., Densmore, A.L., McArdell, B.W., Turowski, J.M., Burlando, P., 2010: Analysis of changes in the step-pool morphology and channel profile of a steep mountain stream following a large flood, *Geomorphology*, 124 (1–2), 85-94.
- Montgomery, D.R., Massong, T.M., Hawley, S.C.S., January, 2003: Influence of debris flows and log jams on the location of pools and alluvial channel

reaches, Oregon Coast Range, *Geological Society of America Bulletin*, 115 (1), 78-88.

Montgomery, D.R., Schmidt, K.M., Dietrich, W.E., McKean, J., 2009: Instrumental record of debris flow initiation during natural rainfall: Implications for modeling slope stability, *Journal of Geophysical Research*, 114, 1-16.

Moon, B.P. and Selby, M.J., 1983: Rock mass strength and scarp forms in southern Africa, *Geografiska Annaler, Series A, Physical Geography*, 65 (1/2), 135-145.

Moore, A. and Blenkinsop, T., 2006: Scarp retreat versus pinned drainage divide in the formation of the Drakensberg escarpment, southern Africa, *South African Journal of Geology*, 109 (4), 599-610.

Moore, D.P. and Mathews, W.H., 1978: The Rubble Creek landslide, southwestern British Columbia, *Canadian Journal of Earth Sciences*, 15 (7), 1039-1052.

Moore, J.M., Asphaug, E., Morrison, D., Spencer, J.R., Chapman, C.R., Bierhaus, B., Sullivan, R.J., Chuang, F.C., Klemaszewski, J.E., Greeley, R., Bender, K.C., Geissler, P.E., Helfenstein, P., Pilcher, C.B., 1999: Mass Movement and Landform Degradation on the Icy Galilean Satellites: Results of the Galileo Nominal Mission, *Icarus*, 140 (2), 294-312.

Mora, P., Baldi, P., Casula, G., Fabris, M., Ghirotti, M., Mazzini, E., Pesci, A., 2003: Global Positioning Systems and digital photogrammetry for the monitoring of mass movements: application to the Ca' di Malta landslide (northern Apennines, Italy), *Engineering Geology*, 68 (1-2), 103-121.

Moreiras, S.M., 2005: Landslide susceptibility zonation in the Rio Mendoza Valley, Argentina, *Geomorphology*, 66 (1-4), 345-357.

- Moreiras, S.M., 2004: Landslide incidence zonation in the Rio Mendoza valley, Mendoza Province, Argentina, *Earth Surface Processes and Landforms*, 29 (2), 255-266.
- Moya, J., Corominas, J., Pérez Arcas, J., Baeza, C., 2010: Tree-ring based assessment of rockfall frequency on talus slopes at Solà d'Andorra, Eastern Pyrenees, *Geomorphology*, 118 (3–4), 393-408.
- Msilimba, G. and Holmes, P., 2010: Landslides in the Rumph District of Northern Malawi: characteristics and mechanisms of generation, *Natural Hazards*, 54 (3), 657-677.
- Msilimba, G.G. and Holmes, P.J., 2005: A landslide hazard assessment and vulnerability appraisal procedure: Vunguvungu/Banga Catchment, Northern Malawi, *Natural Hazards*, 34 (2), 199-216.
- Mugagga, F., Kakembo, V., Buyinza, M., 2012: Land use changes on the slopes of Mount Elgon and the implications for the occurrence of landslides, *Catena*, 90 (0), 39-46.
- Nadim, F., Kjekstad, O., Peduzzi, P., Herold, C., Jaedicke, C., 2006: Global landslide and avalanche hotspots, *Landslides*, 3 (2), 159-173.
- Naudet, V., Lazzari, M., Perrone, A., Loperte, A., Piscitelli, S., Lapenna, V., 2008: Integrated geophysical and geomorphological approach to investigate the snowmelt-triggered landslide of Bosco Piccolo village (Basilicata, southern Italy), *Engineering Geology*, 98 (3–4), 156-167.
- Nefeslioglu, H.A., Gokceoglu, C., Sonmez, H., 2008: An assessment on the use of logistic regression and artificial neural networks with different sampling strategies for the preparation of landslide susceptibility maps, *Engineering Geology*, 97 (3–4), 171-191.
- Nel, W. and Sumner, P.D., 2005: First rainfall data from the KZN Drakensberg escarpment edge (2002 and 2003), *Water SA*, 31, 399-402.

- Nel, W. and Sumner, P.D., 2008: Rainfall and temperature attributes on the Lesotho-Drakensberg escarpment edge, southern Africa, *Geografiska Annaler: Series A, Physical Geography*, 90 (1), 97-108.
- Nel, W. and Sumner, P.D., 2006: Trends in rainfall total and variability (1970-2000) along the KwaZulu-Natal Drakensberg foothills, *South African Geographical Journal*, 88 (2), 130-137.
- Neuhäuser, B. and Terhorst, B., 2007: Landslide susceptibility assessment using “weights-of-evidence” applied to a study area at the Jurassic escarpment (SW-Germany), *Geomorphology*, 86 (1–2), 12-24.
- Ng, C.W.W. and Shi, Q., 1998: A numerical investigation of the stability of unsaturated soil slopes subjected to transient seepage, *Computers and Geotechnics*, 22 (1), 1-28.
- Ng, K.Y., 2006: Landslide locations and drainage network development: A case study of Hong Kong, *Geomorphology*, 76 (1–2), 229-239.
- Nichol, J.E., Shaker, A., Wong, M., 2006: Application of high-resolution stereo satellite images to detailed landslide hazard assessment, *Geomorphology*, 76 (1–2), 68-75.
- Noetzli, J., Huggel, C., Hoelzle, M., Haeberli, W., 2006: GIS-based modelling of rock-ice avalanches from Alpine permafrost areas, *Computational Geosciences*, 10 (2), 161-178.
- Noferini, L., Pieraccini, M., Mecatti, D., Macaluso, G., Luzi, G., Atenzi, C., 2007: DEM by ground-based SAR interferometry, *IEEE Geoscience and Remote Sensing Letters*, 4 (4), 659-663.
- Nyssen, J., Moeyersons, J., Poesen, J., Deckers, J., Mitiku Haile, 2003: The environmental significance of the remobilisation of ancient mass movements in the Atbara–Tekeze headwaters, Northern Ethiopia, *Geomorphology*, 49 (3–4), 303-322.

- Ohlmacher, G.C., 2007: Plan curvature and landslide probability in regions dominated by earth flows and earth slides, *Engineering Geology*, 91 (2–4), 117-134.
- Ohlmacher, G.C. and Davis, J.C., 2003: Using multiple logistic regression and GIS technology to predict landslide hazard in northeast Kansas, USA, *Engineering Geology*, 69 (3–4), 331-343.
- Ohmori, H. and Hirano, M., 1988: Magnitude, frequency and geomorphological significance of rocky mud flows and the collapse of steep slopes, *Zeitschrift für Geomorphologie, Supplement*, 67, 55-65.
- Ouimet, W.B., Whipple, K.X., Royden, L.H., Sun, Z., Chen, Z., 2007: The influence of large landslides on river incision in a transient landscape: Eastern margin of the Tibetan Plateau (Sichuan, China), *Geological Society of America Bulletin*, 119 (11-12), 1462-1476.
- Owen, L.A., 1991: Mass movement deposits in the Karakoram Mountains: their sedimentary characteristics, recognition and role in Karakoram landform evolution, *Zeitschrift für Geomorphologie*, 35 (4), 401-424.
- Paige-Green, P., 1989: Landslides: extent and economic significance in southern Africa, in E.E. Brabb, B.L. Harrod (Eds.), *Landslides: Extent and Economic Significance*, Balkema, Rotterdam, 261-269.
- Paige-Green, P. and Leyland, R., 2009: Structural Failures of the Road Environment, *PG Technical Report*, CSIR, Pretoria.
- Pallàs, R., Vilaplana, J.M., Guinau, M., Falgàs, E., Alemany, X., Muñoz, A., 2004: A pragmatic approach to debris flow hazard mapping in areas affected by Hurricane Mitch: example from NW Nicaragua, *Engineering Geology*, 72 (1–2), 57-72.
- Pandey, A., Dabral, P., Chowdary, V., Yadav, N., 2008: Landslide Hazard Zonation using Remote Sensing and GIS: a case study of Dikrong river

- basin, Arunachal Pradesh, India, *Environmental Geology*, 54 (7), 1517-1529.
- Pánek, T., Hradecký, J., Smolková, V., Šilhán, K., 2008: Gigantic low-gradient landslides in the northern periphery of the Crimean Mountains (Ukraine), *Geomorphology*, 95 (3–4), 449-473.
- Pantelidis, L., 2009: Rock slope stability assessment through rock mass classification systems, *International Journal of Rock Mechanics and Mining Sciences*, 46 (2), 315-325.
- Partridge, T.C. and Maud, R.R., 1987: Geomorphic evolution of southern Africa since the Mesozoic, *South African Journal of Geology*, 90 (2), 179-205.
- Parvaiz, I., Champatiray, P.K., Bhat, F.A., Dadhwal, V.K., 2012: Earthquake-induced landslide dam in the Kashmir Himalayas, *International Journal of Remote Sensing*, 33 (2), 655-660.
- Penck, A., 1904: Der Drakensberg und der Quathlambaruch, *Sitzung Koniglicher Preussischer Akademie der Wissenschaften*, 11, 320-358.
- Penck, A., 1894: *Morphologie Der Erdoberfläche*, J. Englehorn, Stuttgart.
- Perrone, A., Zeni, G., Piscitelli, S., Pepe, A., Loperte, A., Lapenna, V., Lanari, R., 2006: Joint analysis of SAR interferometry and electrical resistivity tomography surveys for investigating ground deformation: the case-study of Satriano di Lucania (Potenza, Italy), *Engineering Geology*, 88 (3–4), 260-273.
- Petley, D.N., 2008: The global occurrence of landslides in 2007, *Quarterly Journal of Engineering Geology and Hydrogeology*, 43, 487-496.
- Petley, D.N., 2010: On the impact of climate change and population growth on the occurrence of fatal landslides in South, East and SE Asia, *Quarterly Journal of Engineering Geology and Hydrogeology*, 43 (4), 487-496.

- Peyret, M., Djamour, Y., Rizza, M., Ritz, J.-., Hurtrez, J.-., Goudarzi, M.A., Nankali, H., Chéry, J., Le Dortz, K., Uri, F., 2008: Monitoring of the large slow Kahrod landslide in Alborz mountain range (Iran) by GPS and SAR interferometry, *Engineering Geology*, 100 (3–4), 131-141.
- Picarelli, L., Olivares, L., Comegna, L., Damiano, E., 2008: Mechanical aspects of flow-like movements in granular and fine grained soils, *Rock Mechanics and Rock Engineering*, 41 (1), 179-197.
- Piegari, E., Cataudella, V., Di Maio, R., Milano, L., Nicodemi, M., Soldovieri, M.G., 2009: Electrical resistivity tomography and statistical analysis in landslide modelling: A conceptual approach, *Journal of Applied Geophysics*, 68 (2), 151-158.
- Pike, R., 1988: The geometric signature: Quantifying landslide-terrain types from digital elevation models, *Mathematical Geology*, 20 (5), 491-511.
- Pirulli, M., Colombo, A., Scavia, C., 2011: From back-analysis to run-out prediction: a case study in the Western Italian Alps, *Landslides*, 8 (2), 159-170.
- Pont, D., Hugueny, B., Oberdorff, T., 2005: Modelling habitat requirement of European fishes: do species have similar responses to local and regional environmental constraints?, *Canadian Journal of Fisheries and Aquatic Sciences*, 62 (1), 163-173.
- Pooley, E. , 2003: *Mountain Flowers: A Field Guide to the Flora of the Drakensberg and Lesotho*, Flora Publications Trust, Durban.
- Popov, I.V., 1946: A scheme for the natural classification of landslides, *Doklady USSR Academy of Sciences*, 54, 157-159.
- Porkess, R. , 2004: *Collins Dictionary of Statistics*, Harper Collins, Glasgow.
- Pradhan, B., 2010: Remote sensing and GIS-based landslide hazard analysis and cross-validation using multivariate logistic regression model on three test areas in Malaysia, *Advances in Space Research*, 45 (10), 1244-1256.

- Pradhan, B., Chaudhari, A., Adinarayana, J., Buchroithner, M., 2012: Soil erosion assessment and its correlation with landslide events using remote sensing data and GIS: a case study at Penang Island, Malaysia, *Environmental Monitoring and Assessment*, 184 (2), 715-727.
- Prager, C., Ivy-Ochs, S., Ostermann, M., Synal, H.A., Patzelt, G., 2009: Geology and radiometric ¹⁴C, ³⁶Cl and Th/U dating of the Fernpass rockslide (Tyrol, Austria), *Geomorphology*, 103 (1), 93-103.
- Rapp, A. and Nyberg, R., 1981: Alpine debris flows in Northern Scandinavia: morphology and dating by lichenometry, *Geografiska Annaler, Series A*, 63, 183-196.
- Reidel, B. and Walther, A., 2008: InSAR processing for the recognition of landslides, *Advances in Geosciences*, 14, 189-194.
- Restrepo, C. and Alvarez, N., 2006: Landslides and Their Contribution to Land-cover Change in the Mountains of Mexico and Central America, *Biotropica*, 38 (4), 446-457.
- Rib, H.T., Liang, T., 1978: Recognition and identification, in R.L. Schuster, R.J. Krizek (Eds.), *Landslides: Analysis and Control*, Transportation Research Board, Washington, 34-81.
- Ridefelt, H. and Boelhouwers, J., 2006: Observations on regional variation in solifluction landform morphology and environment in the Abisko region, northern Sweden, *Permafrost and Periglacial Processes*, 17 (3), 253-266.
- Ridefelt, H., Boelhouwers, J., Eiken, T., 2009: Measurement of solifluction rates using multi-temporal aerial photography, *Earth Surface Processes and Landforms*, 34 (5), 725-737.
- Rocchini, D., 2004: Misleading information from direct interpretation of Geometrically Incorrect aerial photographs, *The Photogrammetric Record*, 19 (106), 138-148.

- Roering, J.J., Stimely, L.L., Mackey, B.H., Schmidt, D.A., 2009: Using DInSAR, airborne LiDAR, and archival air photos to quantify landsliding and sediment transport, *Geophysical Research Letters*, 36 (19), 19402.
- Romana, M., 1988: Practice of SMR classifications for slope appraisal, in C. Bannard (Ed.), *Landslides: Glissements De Terrain*, Balkema, Rotterdam, 1227-1231.
- Roper, H., 1960: Volume changes of concrete affected by aggregate type, *Journal of the Portland Cement Association Research and Development Laboratories*, 2, 1-19.
- Rott, H. and Nagler, T., 2006: The contribution of radar interferometry to the assessment of landslide hazards, *Advances in Space Research*, 37 (4), 710-719.
- Rowbotham, D., Scally, F.D., Louis, J., 2005: The identification of debris torrent basins using morphometric measures derived within a GIS, *Geografiska Annaler: Series A, Physical Geography*, 87 (4), 527-537.
- Ruff, M. and Czurda, K., 2008: Landslide susceptibility analysis with a heuristic approach in the Eastern Alps (Vorarlberg, Austria), *Geomorphology*, 94 (3-4), 314-324.
- Saha, A.K., Gupta, R.P., Sarkar, I., Arora, M.K., Csaplovics, E., 2005: An approach for GIS-based statistical landslide susceptibility zonation—with a case study in the Himalayas, *Landslides*, 2 (1), 61-69.
- Sanchez, G., Rolland, Y., Corsini, M., Braucher, R., Bourlès, D., Arnold, M., Aumaître, G., 2010: Relationships between tectonics, slope instability and climate change: Cosmic ray exposure dating of active faults, landslides and glacial surfaces in the SW Alps, *Geomorphology*, 117 (1-2), 1-13.
- Santacana, N., Baeza, B., Corominas, J., De Paz, A., Marturiá, J., 2003: A GIS-Based Multivariate Statistical Analysis for Shallow Landslide

- Susceptibility Mapping in La Pobla de Lillet Area (Eastern Pyrenees, Spain), *Natural Hazards*, 30 (3), 281-295.
- Sass, O., Bell, R., Glade, T., 2008: Comparison of GPR, 2D-resistivity and traditional techniques for the subsurface exploration of the Öschingen landslide, Swabian Alb (Germany), *Geomorphology*, 93 (1–2), 89-103.
- Sato, H., Sekiguchi, T., Kojiroi, R., Suzuki, Y., Iida, M., 2005: Overlaying landslides distribution on the earthquake source, geological and topographical data: the Mid Niigata prefecture earthquake in 2004, Japan, *Landslides*, 2 (2), 143-152.
- Scheidegger, A.E., 1984: A review of recent work on mass movements on slopes and on rock falls, *Earth-Science Reviews*, 21 (4), 225-249.
- Schmidt, K. and Beyer, I., 2001: Factors controlling mass movement susceptibility on the Wellenkalk-scarp in Hesse and Thuringia, *Zeitschrift für Geomorphologie, Supplement*, 125, 43-63.
- Schulz, W.H., 2007: Landslide susceptibility revealed by LIDAR imagery and historical records, Seattle, Washington, *Engineering Geology*, 89 (1–2), 67-87.
- Schulze, R.E., 1974: Catchment Evapotranspiration in the Natal Drakensberg, MSc dissertation, University of Natal, Pietermaritzburg.
- Schulze, R.E., 1965: *Climate of South Africa*, Weather Bureau, Pretoria.
- Schuster, R.L., 1996: Introduction, in R.L. Schuster, R.J. Krizek (Eds.), *Landslides: Analysis and Control*, Transportation Research Board, Washington, 1-10.
- Schwab, M., Rieke-Zapp, D., Schneider, H., Liniger, M., Schlunegger, F., 2008: Landsliding and sediment flux in the Central Swiss Alps: A photogrammetric study of the Schimbrig landslide, Entlebuch, *Geomorphology*, 97 (3–4), 392-406.

- Schweigl, J., Ferretti, C., Nössing, L., 2003: Geotechnical characterization and rockfall simulation of a slope: a practical case study from South Tyrol (Italy), *Engineering Geology*, 67 (3–4), 281-296.
- Selby, M.J., 1993: *Hillslope Materials and Processes*, Oxford University Press, Oxford.
- Selby, M.J., 1982: Rock mass strength and the form of some inselbergs in the central Namib desert, *Earth Surface Processes and Landforms*, 7 (5), 489-497.
- Sharpe, C.F.S., 1938: *Landslides and Related Phenomena*, Columbia University Press, New York.
- Shaw, A., Holmes, P., Rogers, J., 2001: Depositional landforms and environmental change in the headward vicinity of Dias Beach, Cape Point, *South African Journal of Geology*, 104 (2), 101-114.
- Short, A.D., O'Connor, T.G., Hurt, C.R., 2003: Medium-term changes in grass composition and diversity of Highland Sourveld grassland in the southern Drakensberg in response to fire and grazing management, *African Journal of Range & Forage Science*, 20 (1), 1-10.
- Shroder, J.F.J., 1976: Mass movement on the Nyika Plateau, Malawi, *Zeitschrift für Geomorphologie, Supplement*, 2, 56-77.
- Shroder, J., J., Cvercková, L., Mulhern, K., 2005: Slope-failure Analysis and Classification: Review of a Century of Effort, *Physical Geography*, 26 (3), 216-247.
- Shroder, J.F., Schettler, M.J., Weihs, B.J., 2011: Loess failure in northeast Afghanistan, *Physics and Chemistry of the Earth, Parts A/B/C*, 36 (16), 1287-1293.
- Shroder, J.F. and Weihs, B.J., 2010: Geomorphology of the Lake Shewa landslide dam, Badakhshan, Afghanistan, using remote sensing data, *Geografiska Annaler: Series A, Physical Geography*, 92 (4), 469-483.

- Shroder, J.F., Weihs, B.J., Schettler, M.J., 2011: Mass movement in northeast Afghanistan, *Physics and Chemistry of the Earth, Parts A/B/C*, 36 (16), 1267-1286.
- Silverman, B.W., 1986: *Density Estimation for Statistics and Data Analysis*, Chapman and Hall, New York.
- Singh, B. and Goel, R.K., 1999: *Rock Mass Classification: A Practical Approach in Civil Engineering*, Elsevier Science, Oxford.
- Singh, R.G., 2008: Landslide Classification, Characterization and Susceptibility Modeling in KwaZulu-Natal, MSc dissertation, University of the Witwatersrand, Johannesburg.
- Singh, L., van Westen, C., Champati Ray, P., Pasquali, P., 2005: Accuracy assessment of InSAR derived input maps for landslide susceptibility analysis: a case study from the Swiss Alps, *Landslides*, 2 (3), 221-228.
- Singh, R.G., Botha, G.A., Richards, N.P., McCarthy, T.S., 2008: Holocene landslides in KwaZulu-Natal, South Africa, *South African Journal of Geology*, 111 (1), 39-52.
- Skempton, A.W., 1953: Soil mechanics in relation to geology, *Proceedings of the Yorkshire Geological Society*, 29, 33-62.
- Smedley, M.I. and Nowlan, P.H., 1978: A geotechnical investigation of a landslide on the Broodsnersplaas to Richard's Bay coal line, *The Civil Engineer in South Africa*, 20 (7), 169-173.
- Smith, R.M.H., Eriksson, P.G., Botha, W.J., 1993: A review of the stratigraphy and sedimentary environments of the Karoo-aged basins of Southern Africa, *Journal of African Earth Sciences (and the Middle East)*, 16 (1-2), 143-169.
- Soeters, R., van Westen, C.J., 1996: Slope instability recognition, analysis, and zonation, in A.K. Turner, R.L. Schuster (Eds.), *Landslides: Investigation and Mitigation*, National Academy Press, Washington, 129-177.

- Song, R., Hiromu, D., Kazutoki, A., Usio, K., Sumio, M., 2008: Modeling the potential distribution of shallow-seated landslides using the weights of evidence method and a logistic regression model: a case study of the Sabae Area, Japan, *International Journal of Sediment Research*, 23 (2), 106-118.
- Soons, J.M. and Price, L.W., 1990: Periglacial phenomena in New Zealand, *Permafrost and Periglacial Processes*, 1 (2), 145-159.
- Sorriso-Valvo, M., Gulla, G., 1996: Rock slide, in R. Dikau, D. Brunsten, L. Schrott, M.L. Ibsen (Eds.), *Landslide Recognition: Identification, Movement and Causes*, Wiley, Chichester, 89-102.
- Sorriso-Valvo, M., Gullà, G., Antronico, L., Tansi, C., Amelio, M., 1999: Mass-movement, geologic structure and morphologic evolution of the Pizzotto-Greci slope (Calabria, Italy), *Geomorphology*, 30 (1-2), 147-163.
- Sowers, G.F., Royster, D.L., 1978: Field investigation, in R.L. Schuster, R.J. Krizek (Eds.), *Landslides: Analysis and Control*, Transportation Research Board, Washington, 81-111.
- Sparrow, G.W.A., 1971: Some Pleistocene studies in southern Africa, *Journal of Geography*, 3, 809-814.
- Stengel, I., 2001: Fossil landslides in the Schwarzrand, Huib and Huns escarpment areas - a contribution to the Quaternary morphostratigraphy of southern Namibia, *Palaeoecology of Africa*, 27, 221-238.
- Stengel, I., 1997: Fossil landslides in southern Namibia - first results, *Würzburger Geographische Arbeiten*, 92, 269-284.
- Sterling, S. and Slaymaker, O., 2007: Lithologic control of debris torrent occurrence, *Geomorphology*, 86 (3-4), 307-319.
- Stiny, J., 1910: *Muren, Versuch Einer Monographie Mit Besonderer Berücksichtigung Der Verhältnisse in Den Tiroler Alpen*, Wagner, Innesbruck.

- Strahler, A.N., 1952: Hypsometric (area-altitude) analysis of erosional topography, *Geological Society of America Bulletin*, 63 (11), 1117-1142.
- Straub, D. and Schubert, M., 2008: Modeling and managing uncertainties in rock-fall hazards, *Georisk: Assessment and Management of Risk for Engineered Systems and Geohazards*, 2 (1), 1-15.
- Su, M.C. and Chou, C.H., 2001: A modified version of the K-means algorithm with a distance based on cluster symmetry, *IEEE Transactions on Pattern Analysis and Machine Intelligence*, 23 (6), 1117-1142.
- Suess, E., 1904: *Das Antlitz Der Erde [the Face of the Earth]*, Clarendon Press, Oxford.
- Sumner, P.D., 1995: Comments on the article: Cutbacks in the Natal Drakensberg Escarpment: comments on a hypothesis on their origin, *South African Journal of Science*, 91, 285-286.
- Sumner, P.D., 1993: A landslide complex near Sani Pass, Natal Drakensberg, South Africa, *Geokodynamik*, 14, 93-104.
- Sumner, P.D., Meiklejohn, K.I., 2000: Landscape evolution in a changing environment, in R. Fox, K. Rowntree (Eds.), *The Geography of South Africa in a Changing World*, Oxford University Press, Cape Town, 304-325.
- Sumner, P.D., Hall, K.J., van Rooy, J.L., Meiklejohn, K.I., 2009: Rock weathering on the eastern mountains of southern Africa: Review and insights from case studies, *Journal of African Earth Sciences*, 55 (5), 236-244.
- Sumner, P., 2004: Relict sorted patterned ground in Lesotho, *Permafrost and Periglacial Processes*, 15 (1), 89-93.
- Sumner, P.D. and Nel, W., 2006: Surface-climate attributes at Injisuthi Outpost, Drakensberg, and possible ramifications for weathering, *Earth Surface Processes and Landforms*, 31 (11), 1445-1451.

- Swanger, K.M. and Marchant, D.R., 2007: Sensitivity of ice-cemented Antarctic soils to greenhouse-induced thawing: Are terrestrial archives at risk?, *Earth and Planetary Science Letters*, 259 (3–4), 347-359.
- Tarolli, P. and Tarboton, D.G., 2006: A new method for determination of most likely landslide initiation points and the evaluation of digital terrain model scale in terrain stability mapping, *Hydrology and Earth System Sciences Discussions*, 10 (5), 663-677.
- Temme, A.J.A.M., Baartman, J.E.M., Botha, G.A., Veldkamp, A., Jongmans, A.G., Wallinga, J., 2008: Climate controls on late Pleistocene landscape evolution of the Okhombe valley, KwaZulu-Natal, South Africa, *Geomorphology*, 99 (1–4), 280-295.
- Terhorst, B., 2001: Mass movements of various ages on the Swabian Jurassic escarpment: geomorphologic processes and their causes, *Zeitschrift für Geomorphologie, Supplement*, 125, 105-127.
- Terhorst, B. and Kirschhausen, D., 2001: Legends for mass movements in the MABIS-Project, *Zeitschrift für Geomorphologie, Supplement*, 125, 105-127.
- Terzaghi, K., 1950: Mechanism of landslides, in S. Paige (Ed.), *Application of Geology to Engineering Practice*, Geological Society of America, New York, 83-123.
- Terzaghi, K., 1925: *Erdbaumechanik Auf Bodenphysikalischer Grundlage*, Deuticke, Vienne.
- Terzaghi, K. and Peck, R.B., 1948: *Soil Mechanics in Engineering Practice*, Wiley, New York.
- Thiery, Y., Malet, J.P., Sterlacchini, S., Puissant, A., Maquaire, O., 2007: Landslide susceptibility assessment by bivariate methods at large scales: Application to a complex mountainous environment, *Geomorphology*, 92 (1–2), 38-59.

- Thomas, M.A. and van Schalkwyk, A., 1993: Geological hazards associated with intense rain and flooding in Natal, *Journal of African Earth Sciences (and the Middle East)*, 16 (1–2), 193-204.
- Tiranti, D., Bonetto, S., Mandrone, G., 2008: Quantitative basin characterisation to refine debris-flow triggering criteria and processes: an example from the Italian Western Alps, *Landslides*, 5 (1), 45-57.
- Townsend Peterson, A. and Cohoon, K.P., 1999: Sensitivity of distributional prediction algorithms to geographic data completeness, *Ecological Modelling*, 117 (1), 159-164.
- Trauth, M.H., Bookhagen, B., Marwan, N., Strecker, M.R., 2003: Multiple landslide clusters record Quaternary climate changes in the northwestern Argentine Andes, *Palaeogeography, Palaeoclimatology, Palaeoecology*, 194 (1–3), 109-121.
- Trimble, S.W. and Mendel, A.C., 1995: The cow as a geomorphic agent — A critical review, *Geomorphology*, 13 (1–4), 233-253.
- Troll, C., 1944: Strukturböden, Solifluktion und Frostklimate der Erde, *Geologische Rundschau*, 34, 545-694.
- Turner, D.P., 2000: Soils of KwaZulu-Natal and Mpumalanga: Recognition of Natural Soil Bodies, PhD thesis, University of Pretoria, Pretoria.
- Twidale, C.R., 1976: *Analysis of Landforms*, Wiley, Sydney.
- Tyson, P.D., 1988: *the Atmosphere and Weather of Southern Africa*, Oxford University Press, Oxford.
- Tyson, P.D., Preston-Whyte, R.A., Schulze, R.E. , 1976: *the Climate of the Drakensberg, Natal Town and Regional Planning Reports, 31*, Natal Town and Regional Planning Commission, Pietermaritzburg.
- UNEP-WCMC, 2006: Strategic Plan, 2006-2011, UNEP World Conservation Monitoring Centre, Cambridge.

- van Asch, T.W.J., van Beek, L.P.H., Bogaard, T.A., 2007: Problems in predicting the mobility of slow-moving landslides, *Engineering Geology*, 91 (1), 46-55.
- van Den Eeckhaut, M., Poesen, J., Verstraeten, G., Vanacker, V., Moeyersons, J., Nyssen, J., van Beek, L.P.H., 2005: The effectiveness of hillshade maps and expert knowledge in mapping old deep-seated landslides, *Geomorphology*, 67 (3-4), 351-363.
- Van Den Eeckhaut, M., Vanwalleghem, T., Poesen, J., Govers, G., Verstraeten, G., Vandekerckhove, L., 2006: Prediction of landslide susceptibility using rare events logistic regression: A case-study in the Flemish Ardennes (Belgium), *Geomorphology*, 76 (3-4), 392-410.
- van Den Eeckhaut, M., Verstraeten, G., Poesen, J., 2007: Morphology and internal structure of a dormant landslide in a hilly area: The Collinabos landslide (Belgium), *Geomorphology*, 89 (3-4), 258-273.
- van Den Eeckhaut, M.V., Marre, A., Poesen, J., 2010: Comparison of two landslide susceptibility assessments in the Champagne-Ardenne region (France), *Geomorphology*, 115 (1-2), 141-155.
- van Den Eeckhaut, M.V., Reichenbach, P., Guzzetti, F., Rossi, M., Poesen, J., 2009: Combined landslide inventory and susceptibility assessment based on different mapping units: an example from the Flemish Ardennes, Belgium, *Natural Hazards and Earth System Science*, 9 (2), 507-521.
- van Der Eyk, J.J., MacVicar, C.N., de Villiers, J.M. , 1969: *Soils of the Tugela Basin: A Study in Subtropical Africa with a Soil Association Map 1:100 000*, Town and Regional Planning Commission, Pietermaritzburg.
- van Rooy, J.L. and van Schalkwyk, A., 1993: The geology of the Lesotho Highlands Water Project with special reference to the durability of construction materials, *Journal of African Earth Sciences (and the Middle East)*, 16 (1-2), 181-192.

- van Schalkwyk, A., Thomas, M.A., 1991: Slope failures associated with the floods of September 1987 and February 1988 in Natal and KwaZulu, Republic of South Africa, in G.E. Blight (Ed.), *Geotechnics in the African Environment*, Balkema, Rotterdam, 57-64.
- van Steijn, H., 1996: Debris-flow magnitude—frequency relationships for mountainous regions of Central and Northwest Europe, *Geomorphology*, 15 (3–4), 259-273.
- van Westen, C.J., Castellanos, E., Kuriakose, S.L., 2008: Spatial data for landslide susceptibility, hazard, and vulnerability assessment: An overview, *Engineering Geology*, 102 (3–4), 112-131.
- van Westen, C.J., Soeters, R., Sijmons, K., 2000: Digital geomorphological landslide hazard mapping of the Alpa area, Italy, *International Journal of Applied Earth Observation and Geoinformation*, 2 (1), 51-60.
- van Zijl, J.S.V., 2006: A review of the resistivity structure of the Karoo Supergroup, South Africa, with emphasis on the dolerites: A study in anisotropy, *South African Journal of Geology*, 109 (3), 315-328.
- Varnes, D.J., 1984: *Landslides Hazard Zonation: A Review of Principles and Practice*, UNESCO Press, Paris.
- Varnes, D.J., 1978: Slope movement types and processes, in R.L. Schuster, R.J. Krizek (Eds.), *Landslides: Analysis and Control*, Transportation Research Board, Washington, 11-33.
- Varnes, D.J., 1958: Landslide types and processes, in E.B. Eckel (Ed.), *Landslides and Engineering Practice*, Highway Research Board, Washington, 20-47.
- Verster, E., van Rooyen, T.H., 1988: Measurement of soil movement on two hillslopes displaying terracettes in humid South Africa, in G.F. Dardis, B.P. Moon (Eds.), *Geomorphological Studies in Southern Africa*, Balkema, Rotterdam, 311-320.

- Visser, J.N.J., 1989: The Permo-Carboniferous Dwyka Formation of southern Africa: deposition by a predominantly subpolar marine ice sheet, *Palaeogeography, Palaeoclimatology, Palaeoecology*, 70 (4), 377-391.
- Visser, J.N.J. and Botha, B.J.V., 1980: Meander channel, point bar, crevasse splay and aeolian deposits from the Elliot Formation, Barkly Pass, north-eastern Cape, *Transactions of the Geological Society of South Africa*, 83, 55-62.
- Wachal, D.J. and Hudak, P.F., 2000: Mapping landslide susceptibility in Travis County, Texas, USA, *GeoJournal*, 51 (3), 245-253.
- Walsh, S.J., Butler, D.R., Malanson, G.P., 1998: An overview of scale, pattern, process relationships in geomorphology: a remote sensing and GIS perspective, *Geomorphology*, 21 (3-4), 183-205.
- Walsh, S.J., Butler, D.R., Malanson, G.P., Crews-Meyer, K.A., Messina, J.P., Xiao, N., 2003: Mapping, modeling, and visualization of the influences of geomorphic processes on the alpine treeline ecotone, Glacier National Park, MT, USA, *Geomorphology*, 53 (1-2), 129-145.
- Walstra, J., Dixon, N., Chandler, J.H., 2007: Historical aerial photographs for landslide assessment: two case histories, *Quarterly Journal of Engineering Geology and Hydrogeology*, 40 (4), 315-332.
- Wang, F., Zhang, Y., Huo, Z., Peng, X., Wang, S., Yamasaki, S., 2008: Mechanism for the rapid motion of the Qianjiangping landslide during reactivation by the first impoundment of the Three Gorges Dam reservoir, China, *Landslides*, 5 (4), 379-386.
- Wang, H.B. and Sassa, K., 2006: Rainfall-induced landslide hazard assessment using artificial neural networks, *Earth Surface Processes and Landforms*, 31 (2), 235-247.
- Wang, H.B., Sassa, K., Xu, W.Y., 2007: Assessment of landslide susceptibility using multivariate logistic regression: a case study in southern Japan, *Environmental & Engineering Geoscience*, 13 (2), 183-192.

- Ward, W.H., 1945: The stability of natural slopes, *Geographical Journal*, 105, 170-197.
- Watson, H.K., 1988: Terracettes in the Natal Drakensberg, South Africa, in G.F. Dardis, B.P. Moon (Eds.), *Geomorphological Studies in Southern Africa*, Balkema, Rotterdam, 299-310.
- Watson, H.K., 1988: Terracettes in the Natal Drakensberg, South Africa, in G.F. Dardis, B.P. Moon (Eds.), *Geomorphological Studies in Southern Africa*, Balkema, Rotterdam, 299-310.
- Weihs, B.J. and Shroder, J.F., 2011: Mega-terraces and related ungulate activities in Loess Hills, Iowa, USA, *Zeitschrift für Geomorphologie*, 55 (1), 45-61.
- Weirich, F. and Blesius, L., 2007: Comparison of satellite and air photo based landslide susceptibility maps, *Geomorphology*, 87 (4), 352-364.
- Wen, B., Wang, S., Wang, E., Zhang, J., 2004: Characteristics of rapid giant landslides in China, *Landslides*, 1 (4), 247-261.
- Whalley, W.B., 1984: Rockfalls, in D. Brunsten, B.P. Prior (Eds.), *Slope Instability*, Wiley and Sons, Chichester, 217-256.
- Wieczorek, G.F., 1996: Landslide triggering mechanisms, in A.K. Turner, R.L. Schuster (Eds.), *Landslides: Investigation and Mitigation*, National Academy Press, Washington, 76-90.
- Wieczorek, G.F., Mossa, G.S., Morgan, B.A., 2004: Regional debris-flow distribution and preliminary risk assessment from severe storm events in the Appalachian Blue Ridge Province, USA, *Landslides*, 1 (1), 53-59.
- Wilford, D.J., Sakals, M.E., Innes, J.L., Sidle, R.C., Bergerud, W.A., 2004: Recognition of debris flow, debris flood and flood hazard through watershed morphometrics, *Landslides*, 1 (1), 61-66.

- Wilkinson, P.L., Anderson, M.G., Lloyd, D.M., 2002: An integrated hydrological model for rain-induced landslide prediction, *Earth Surface Processes and Landforms*, 27 (12), 1285-1297.
- Wu, W. and Sidle, R.C., 1995: A distributed slope stability model for steep forested basins, *Water Resources Research*, 31 (8), 2097-2110.
- Xu, C., Xu, X., Lee, Y., Tan, X., Yu, G., Dai, F., 2012: The 2010 Yushu earthquake triggered landslide hazard mapping using GIS and weight of evidence modeling, *Environmental Earth Sciences*, 66 (6), 1603-1616.
- Yalcin, A., Reis, S., Aydinoglu, A.C., Yomralioglu, T., 2011: A GIS-based comparative study of frequency ratio, analytical hierarchy process, bivariate statistics and logistics regression methods for landslide susceptibility mapping in Trabzon, NE Turkey, *Catena*, 85 (3), 274-287.
- Yalcin, A., 2008: GIS-based landslide susceptibility mapping using analytical hierarchy process and bivariate statistics in Ardesen (Turkey): Comparisons of results and confirmations, *Catena*, 72 (1), 1-12.
- Yao, X., Tham, L.G., Dai, F.C., 2008: Landslide susceptibility mapping based on Support Vector Machine: A case study on natural slopes of Hong Kong, China, *Geomorphology*, 101 (4), 572-582.
- Yesilnacar, E. and Topal, T., 2005: Landslide susceptibility mapping: A comparison of logistic regression and neural networks methods in a medium scale study, Hendek region (Turkey), *Engineering Geology*, 79 (3-4), 251-266.
- Yilmaz, I., 2009: Landslide susceptibility mapping using frequency ratio, logistic regression, artificial neural networks and their comparison: A case study from Kat landslides (Tokat—Turkey), *Computers & Geosciences*, 35 (6), 1125-1138.
- Yin, Y., Wang, F., Sun, P., 2009: Landslide hazards triggered by the 2008 Wenchuan earthquake, Sichuan, China, *Landslides*, 6 (2), 139-152.

- Young, T.Y.andCalvert, T.W. , 1974: *Classification, Estimation and Pattern Recognition*, Elsevier, New York.
- Zaruba, Q.andMencl, V., 1969: *Landslides and their Control*, Elsevier, Amsterdam.
- Zêzere, J.L., de Brum Ferreira, A., Rodrigues, M.L., 1999: The role of conditioning and triggering factors in the occurrence of landslides: a case study in the area north of Lisbon (Portugal), *Geomorphology*, 30 (1–2), 133-146.
- Zhou, G., Esaki, T., Mitani, Y., Xie, M., Mori, J., 2003: Spatial probabilistic modeling of slope failure using an integrated GIS Monte Carlo simulation approach, *Engineering Geology*, 68 (3–4), 373-386.
- Zimmer, V.L., Collins, B.D., Stock, G.M., Sitar, N., 2012: Rock fall dynamics and deposition: an integrated analysis of the 2009 Ahwiyah Point rock fall, Yosemite National Park, USA, *Earth Surface Processes and Landforms*, 37 (6), 680-691.
- Zinck, J.A., Lopez, J., Metternicht, G.I., Shresta, D.P., Vazquez-Selem, L., 2001: Mapping and modeling mass movements and gullies in mountainous areas using remote sensing and GIS techniques, *Journal of Applied Earth Observation and Geoinformatics*, 31 (1), 43-53.